Feasibility of residential solar air-conditioning in Australia, including space heating and hot water

Inga Doemland

A thesis submitted for the degree of
Doctor of Philosphy (PhD)
The Australian National University

May 2015

This work is an account of research undertaken between September 2010 and December 2014 through the College of Engineering and Computer Science at the Australian National University.

Except where otherwise indicated, this thesis is my own original work. No material in this thesis has been previously submitted for the purpose of obtaining a degree in any university or other tertiary education institution.

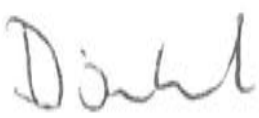

Inga Doemland
Wednesday 20th May, 2015

Acknowledgments

The person I would like to thank most is Dr Mike Dennis. He supported my work from start to finish and his valuable suggestions, professional judgment and time invested improved the outcome on all levels.

Furthermore, I would like to thank Dr Stephen White and Dr John Pye for their support.

I am also grateful that I met Dr Christian Holter on a conference in Australia in 2012. His experiences with absorption chillers and solar cooling systems proved to be a very valuable input to my work. In 2014 I was able to gain practical experience in Singapore, while working for his company SOLID for 6 months. The knowledge exchange within the Singapore team was excellent and the experience strongly helped to increase my own judgment of my work. Next to Sabine Putz, I want to thank all other team members involved who made this project possible.

In 2013 I published a conference paper together with Jan Albers who's input to my absorption chiller modeling approach I greatly appreciate.

I would also like to thank Phil Wilkinson for nominating me as a representative of AIRAH to be a part of the Australian Standard committee CS-028, solar water heaters. In thanking the panel chair Ken Guthrie, I thank the entire panel for the excellent work experience.

Dr José Zapata I would like to thank for his support on any topic. His general knowledge is remarkable and his tips and hints proved most valuable for the generation of my results. He is one great colleague amongst others I would like to thank, Jeff Cumpston, Xiaolin Wang, Liangzhuo Hou, Tom Cochrane, Ash Kearton, Dr Arnold McKinley, Dr Angelika Basch and Lawrence McIntosh. Rebecca Dunn deserves particular mentioning as she is a key figure for me having settled in Canberra and started a PhD at the ANU.

I would also like to thank my Australian relatives, the family's of Vaughn Fisher and Jenny Sheppard for their support in my early days in Australia.

And I would like to thank my dear flatmate Hugh Hartigan. I owe much of my strength over the last 4 years to his great advise and personal support. Furthermore, I would like to thank my friend Bradley O'Shea for partially reviewing this work.

And last but not least...

... möchte ich mich bei meinen Eltern und meinem Bruder für deren langjährige Unterstützung und ihr Verständnis bedanken. In Tatendrang, Ehrlichkeit, Gewissenhaftigkeit und Großzügigkeit werden sie mir immer ein Vorbild sein.

Abstract

In Australia residential air-conditioning has been claimed as one of the main drivers for peak electricity demand problems in the years from 2007 until 2012. Expensive network infrastructure upgrades have been required to maintain legislated reliability of electricity supply. This electricity grid augmentation has translated to increased cost of electricity for residences by around 70% until 2012 and 100% until 2014.

This thesis investigates the potential for residential solar cooling to ease stress on the electricity grid while providing electricity cost savings to consumers and reductions in greenhouse gas emissions due to building energy services. A modeling approach is chosen using TRNSYS 16 as the software environment.

The modeling examines residential solar cooling performance in seven different climates in Australia, reviewing solar electric as well as solar thermal cooling options. Space heating and domestic hot water are included throughout this work as both provide the means to utilize solar thermal collectors fully, also in winter. It strongly contributes to the cost-effectiveness of solar thermal systems and colder climates benefit most. The solar collector array for electricity and heat is sized to a cooling and heating solar fraction of 60%. The performances are compared from an environmental, financial and human comfort perspective using a new overall performance measure.

In the first part of this work reference models are established to represent a residential building typical for each climate. In these models, the building is cooled and heated by a reverse cycle air-conditioner and domestic hot water is provided by a hot water system with an electric heating element.

The first investigation involves addition of photovoltaic modules to offset grid electricity consumption of the reverse cycle air conditioner. In this configuration, the electricity grid acts as an energy supply buffer to supplement fluctuations in solar energy. The cost-effectiveness of this option depends strongly on the value of solar electricity export, which can be very low or non-existent in some areas of Australia. In the very hot climates the break even electricity price is low enough to be exceeded by the retail price already. In the colder climates the electricity break even price is \$0.60 to \$0.90 kWh^{-1} if no value is placed on the solar export of surplus electricity. Nevertheless, the photovoltaic driven system design is very simple and proved to be the most cost-effective one. This investigation was extended to include options for electricity storage and a diesel electricity back up rather than the grid.

The next investigation involved modeling a solar thermal system consisting of a single effect absorption chiller and an evacuated tube solar collector, following European examples. Initially, a sensitivity study was performed to better understand the model behavior and to size components correctly. The main parameters in the sensitivity analysis were chiller capacity, collector and tank sizes, dehumidification strategies and control set point temperatures. The absorption chiller model is based on the characteristic equation and is controlled via the hot water inlet temperature in a load following manner. The cooling system is scaled in a unique way to match the cooling load of each climate and to normalize energy consumption and cost. The absorption chiller uses gas as its backup energy source.

The thermal solar cooling system model is extended by inclusion of options for a latent storage and a sensible chilled water storage tank.

The results of the solar thermal system simulations are rather disheartening for the case of residential solar cooling using absorption chillers. Unless domestic hot water and space heating are included in the calculations, the levelized cost of space cooling and heating is too high to be acceptable when comparing it to the solar electric option. Without domestic hot water the break even electricity price is \$0.70 kWh^{-1} in the cooler climates to \$1.70 kWh^{-1} in the very hot and humid climate. The inclusion of domestic hot water service in the system strongly contributes to the cost-effectiveness of solar thermal systems, predominantly in colder climates. The break even price including domestic hot water comes down to \$0.30 to \$0.60 kWh^{-1}.

Including cold storage increases this cost even more, but additional greenhouse gases can be saved due to lower auxiliary gas consumption. The analysis would be expected to be different for large scale solar cooling installations, where absorption chillers can operate under base load conditions backed up by conventional chillers with good part load performance.

Contents

List of Figures

List of Tables

Nomenclature

Abbreviations

AC	Air-conditioning
AEMO	Australian Electricity Market Operator
AER	Australian Energy Regulator
AIRAH	Australian Institute for Refrigeration, Air-conditioning and Heating
ANU	Australian National University
AusSCIG	Australian Solar Cooling Interest Group
BOM	Bureau of Meteorology
CS	(1) Conditioned space (floor area). (2) Cold storage
CSIRO	The Commonwealth Scientific and Industrial Research Organization
DHW	Domestic hot water
DNI	Direct normal irradiation
GDP	Gross domestic product
GFC	Gloabl Financial Crisis
GHI	Global horizontal irradiation
HCFC	Hydrochlorofluorocarbon
HFC	Hydrofluorocarbon
HVAC(&R)	Heating, Ventilation and Air-conditioning (& Refrigeration)
IEA	International Energy Agency
NEM	National Electricity Market including the jurisdictions QLD, NSW, ACT, SA, VIC and since 2005 TAS
NER	National Electricity Rules

NSW	New South Wales (Australian state)
NT	Northern Territory (Australian state)
OECD	The Organisation for Economic Co-operation and Development
PCM	Phase change material
PMV	Predictive mean vote
PPD	Percentage of people dissatisfied
PV	Photovoltaic
QLD	Queensland (Australian state)
SA	South Australia (Australian state)
SHGC	Solar heat gain coefficient
TAS	Tasmania (Australian state)
VBA	Visual basic for applications
VIC	Victoria (Australian state)
WA	Western Australia (Australian state)

Indices

0	design/rated conditions
AC	Subscript to capital cost of reverse cycle air-conditioner
air	(1) Air flow. (2) Ambient temperature in chapter 3
amb	Ambient air condition (temperature or humidity)
aux	Auxiliary energy or auxiliary equipment, here gas
avg	Average conditions
bat	Battery
BatReg	Battery regulator
BE	Subscript "break even" indicating break even price of electricity
c	Cooling
CC, HC	Cooling coil (CC) and heating coil (HC)
chb	Chilled beams

chiller $\rightarrow$ *coils*	Cooling supplied to the fan coils directly from the absorption chiller
chiller	Absorption chiller
chw	Chilled water, chilled water through the evaporator of the absorption chiller
circ	One circuit of N_{circ} circuits, which contain the heat transfer medium in the latent cold storage tank
climate	Climates 1 to 7
CO2, *CO2* – *eq*	Subscript to units, both indicating greenhouse gas emissions expressed as carbon dioxide equivalent
coll	(1) Subscript to area indicating solar collector area. (2) Subscript to solar radiation indicating radiation normal to the collector surface
CS $\rightarrow$ *coils*	Cooling released from the cold storage tank to supply the fan coils
CS	(1) cold storage tank when subscript to variables, (2) conditioned space when subscript to units
CT	Refers to the cooling tower
CTdry	Dry cooling tower
cw	Cooling water for heat rejection through absorber and condenser of absorption chiller
design	Design conditions
dhw	DHW is included or the hot water system is concerned
el	Energy in form of electricity
f	Fluid (here water)
fix	Subscript for capacity charge
gas	gas consumption (e.g. for back-up heating)
h	Heating
H2O	Water as subscript to units
HVAC	Referring to the HVAC system including cooling and heating, but excluding DHW

hw	Hot water through the desorber/ generator of the absorption chiller
i, o	Inner/outer diameter of a pipe
in, out	Inlet/outlet condition of fluid circuit
inv	Inverter
l	Liquid state
lat	Subscript to heat indicating latent heat removal
LCov	Subscript to solar fraction meaning "load coverage", which is the time when solar electricity supply and HVAC (and DHW) demand coincide. As opposed to the index "tot".
loss	Subscript to heat indicating heat loss
max	Maximum condition
n	(1) Annual. (2) The n^{th} of N circles in section 9.1.2
non − el	Subscript to operating cost for everything but electricity
PCM	Phase change material
peak	Energy consumption during peak hours from 16:00 to 20:00
PInst	Indicating planning and installation
PV	Photovoltaic
r	Room
rated	Rated conditions
ref	Concerning the reference system as described in section 5
req	Required condition (equation 7.16 to 7.18)
s	Solid state
scaled	Scaled from design or rated conditions
sens	Subscript to heat indicating sensible heat removal
set	Set point
sol → bat	Solar electricity stored in the battery
sol → grid	Solar electricity exported to the grid
sol → lost	Solar electricity lost to the environment

sol	Energy from the solar collectors
t	Tank
$t = 0$	Initial conditions as subscript to capital cost
th	Energy in form of heat (at low or high temperature) as subscript to units
tot	Subscript to solar fraction meaning that total solar energy generated is considered, as opposed to the index *"LCov"*
wall	(1) Wall of building in section 4.3. (2) Wall of tube/ pipe in chapter 9
water	Concerning water or water consumption
z_i	Zone i = 1 to 3
$bat \rightarrow HVAC(\&DHW)$	Indicating battery electricity supply to HVAC (and DHW) system
$grid \rightarrow HVAC(\&DHW)$	Indicating grid electricity supply to HVAC (and DHW) system
$sol \rightarrow HVAC(\$DHW)$	Solar energy supplied to HVAC (and DHW) system
AC	Absorber and condenser
D	Desorber
E	Evaporator
X	The component within the absorption chiller (D,AC,E)

Logical symbols

( )	Containing groups of mathematical operations on signals which are in the interval $[0, 1]$, using the operators $\cdot$ and $+$
$+$	Adding control signals in the interval $[0, 1]$
$\cdot$	Mathematical operator to multiply signals of the form 1 or 0 corresponding to the logical statement "and"; or multiplying signals in the interval $[0, 1]$
$\neg$	Not
$\vee$	Logical operator "or"
{ }	Containing logical expressions which are either 0 or 1, e.g. the expression $\{T > 20\,°C\}$ can be "true" or "false" which corresponds to 1 or 0

$AuxStatus$	Indicator if auxiliary heater is on or off	[0 or 1]
$charging$	Signal to charge the cold storage tank	[0 or 1]
$ChillerReq$	Request to switch chiller on or off	[0 or 1]
$ChillerStatus$	Indication if chiller is on or off	[0 or 1]
$CoolingReq$	$HVAC_c$	[0 or 1]
$disch_{1,zones}$	Discharging signal for the cold storage tank in mode 1. Each zone's individual signal is $disch_{1,z_i}$ (equation 9.37) and they are connected through an "or" statement	[0 or 1]
$disch_{2,zones}$	Discharging signal to prevent the zones from cooling down below the set point for heating. Each zone's individual signal is $disch_{2,z_i}$ (equation 9.39) and they are connected through an "or" statement	[0 or 1]
$discharging$	Discharging signal for the tank if $discharging_1$ or $discharging_2$ is "true"	[0 or 1]
$discharging_1$	Discharging of the cold storage tank while chiller is in operation	[0 or 1]
$discharging_2$	Discharging of the cold storage tank while chiller is not in operation	[0 or 1]
$HeatingReq$	$HVAC_h$	[0 or 1]
$HVAC_{c/h}$	Control signal requesting either heating "h" or cooling "c"	[0 or 1]
$HVAC_{sched}$	Control signal triggered by schedule for heating or cooling	[0 or 1]
$HVAC_{therm}$	Control signal triggered by thermostat for heating or cooling	[0 or 1]
$prediction$	Resembling a forecasting algorithm and indicating that the temperature of the following day at midday is larger than the indoor set point temperature for cooling	[0 or 1]
$signal_{chb}$	Signal for discharging the cold storage tank over the chilled beams in zone z_i (equation 9.46)	[0 or 1]
$signal_{chw}$	Chilled water pump signal (equation 9.40)	

Variables

α, β, γ	(1) Weighting coefficients of the overall performance factor indicating preference for specific cost, greenhouse gas emissions or comfort (equation 4.30). (2) Regression coefficients for the prediction of absorption chiller performance (equation 7.6)
$\bar{\epsilon}$	Average error of regression analysis in section 7.2.2
$\bar{c}_{m,ref}$	Population weighted average specific cost of the reference system [$\$\,kWh^{-1}$]
$\bar{t}$	Arithmetic mean temperature of each of the three external flow circuits of the absorption chiller [°C]
χ	Re-heating air flow set point temperature (equation 7.27) [°C]
$\Delta\Delta t$	Characteristic temperature difference. Superscrip ′ indicates modifications [°C]
$\Delta\dot{E}_{el}$	Rate of electricity saved [kW]
Δc_m	Difference in cost specific to the cooling and heating energies supplied, comparing the reference system to the solar system [$\$\,kWh^{-1}$]
ΔE_{el}	Electricity saved in one year comparing the solar system to the reference system [$kWh\,a^{-1}$]
ΔGHG	Saved greenhouse gas emissions specific to the heating and cooling energies supplied [$kg_{CO2}\,kWh^{-1}$]
Δh	Enthalpy difference between outdoor air conditions and indoor air set point conditions [$kJ\,kg^{-1}$]
Δh_{lat}	Latent heat of PCM [$kJ\,kg^{-1}$]
Δp	Pressure drop in a hydraulic or pneumatic circuit [Pa]
ΔPE	Saved primary energy specific to the energies for heating and cooling supplied
ΔQ_{imb}	Energy imbalance [$kWh\,a^{-1}$]
Δt	Time step in TRNSYS [h]
δ	(1) Declination [°]. (2) Phase change fraction (equation 9.4c). (3) The allowed time to reduce indoor humidity to set point levels (equation 7.25)
$\dot{E}_{bat,max}$	Maximal rate at which the battery can be charged or discharged [kW]

$\dot{E}_{el}$	Rate of electricity consumption (parasitic and/or auxiliary)	[kW]
$\dot{G}_{tot,coll}$	Solar radiation normal to the collector's surface (equation 7.37)	[W m^{-2}]
$\dot{m}$	Mass flow rate	[kg s^{-1}]
$\dot{m}_r$	Solution flow rate in absorption chiller	[kg s^{-1}]
$\dot{m}_{water}$	Instantaneous water consumption of the HVAC system	[kg s^{-1}]
$\dot{Q}$	Heat rate	[kW]
$\dot{Q}_{E,0}$	Rated cooling capacity of absorption chiller in section 7	[kW]
$\dot{V}$	Volumetric flow rate	[m^3 s^{-1}]
ϵ	(1) Emissivity in section 4.3. (2) Heat exchanger effectiveness in section 9.2 and 9.1	
η_{bat}	Efficiency of the battery	
γ	Scaling parameter for the latent cold storage as (equation 9.29)	
ι	Radio between the outer diameter of the tubes within the latent cold storage tank to the tank's diameter (equation 9.15)	
κ	Radio between the cross sectional area of the tank and its height (equation 9.14)	
λ	Valve position (equation 9.60)	
$\lambda_1, \lambda_2, \lambda_3$	Valve positions for the chilled water circuit including a cold storage tank (figure 9.5)	
λ_{chb}	Ratio of chilled water used to feed chilled beams as (equation 8.11)	
μ	Dynamic viscosity	[N s m^{-2}]
ν	Kinematic viscosity	[m^2 s^{-1}]
ω	Humidity ratio	[kg$_{H2O}$ kg$^{-1}_{\text{dry air}}$]
$\overline{GHG}_{ref}$	Population weighted average specific greenhouse gas emissions of the reference system	[kg$_{CO2}$ kWh^{-1}]
ϕ	(1) Solar zenith angle (equation B.2) [°]. (2) Chilled water flow rate increase for discharging the cold storage tank (equation 9.40)	
ψ	Proportion of chilled water flow used to charge the cold storage tank (equation 9.44)	

ρ	Density	$[\mathrm{kg\,m^{-3}}]$
ρ_{wall}	Density of building wall layers	$[\mathrm{kg\,m^{-3}}]$
σ	Standard deviation	
τ	Greenhouse gas emission per kWh of liquified natural gas or per kWh of electricity	$[\mathrm{kg_{CO2\text{-}eq}\,kWh^{-1}}]$
$\tau\alpha$	The product of transmission and absorption of the solar thermal collector's surface (equation 7.37)	
ζ	Flow resistance factor	
a, b	Regression coefficients (equation 7.4)	
a_c, a_{GHG}	Shape factors for the overall performance factor functions in section 4.2.3.	
A_n	Annual cost of operation	$[\$\,\mathrm{a^{-1}}]$
A_{attic}	Opening area in attic through which air can enter (equation 4.33)	$[\mathrm{m^2}]$
A_{house}	Conditioned area (space) of building	$[\mathrm{m^2}]$
A_{HX}	Heat exchanger area	$[\mathrm{m^2}]$
A_{pipe}	Cross sectional pipe area	$[\mathrm{m^2}]$
ACH_{attic}	Air changes in the attic due to natural ventilation	[1/h]
$ACH_{ventilation}$	Air changes due to ventilation	[1/h]
B	Dühring parameter on a Dühring plot	
b	Regression coefficient (equation 9.52)	
C	Cooling or heating capacity in table 4.12	[kW]
c	Coefficient for heat transfer characteristic of wet cooling towers (equation 7.29)	
c_0, c_1, c_2	Coefficients defining the collector efficiency curve	
c_m	Average cost specific to the cooling and heating energies supplied over the life time of the system (levelized cost of energy) (equation 4.19)	$[\$\,\mathrm{kWh^{-1}}]$
$c_{p,wall}$	Specific heat capacity of wall layers	$[\mathrm{kJ\,kg^{-1}\,K^{-1}}]$
c_p	Specific heat capacity	$[\mathrm{kJ\,kg^{-1}\,K^{-1}}]$

C_v	Effectiveness of openings (equation 4.33)	
Cap_{avl}	Storage capacity of a battery which is available	[kWh]
Cap_{nom}	Nominal storage capacity of a battery	[kWh]
$Cap_{PV,design}$	Capacity of photovoltaic array at standard conditions	[kW]
Cap_{rated}	Chiller's rated cooling capacity under design conditions	[kW]
CF, CF^*	Latent cold storage compactness factor and modified compactness factor (*)	
$comf_{RH}$	Humidity discomfort levels (equation 4.18)	[%]
$comf_T$	Temperature discomfort levels (equation 4.17)	[%]
COP	Coefficient of performance as an instantaneous measure. The ratio of heat rate for cooling and heating to the energy rate consumed	
cov, $corr$	Covariance and correlation coefficient	
d	Diameter of pipe/ tube	[m]
DoD	Depth of discharge of battery	
E'_{el}	Annual electricity consumption (parasitic and/or auxiliary) specific to the conditioned floor area	[kWh m_{CS}^{-2} a^{-1}]
E_{el}	Annual electricity consumption (parasitic and/or auxiliary)	[kWh a^{-1}]
$ElecD$	Electricity demand on the NEM	[MW]
ES	Specific electricity consumption for the generation of 1 kWh of cooling and heating (equation 4.7)	
F_R	Heat removal factor	
f_{peak}	The annual fraction of saved electricity during peak hours as (equation 4.13)	
$frac_{PV}$	Ratio of the financial benefit for each kWh of electricity exported into the grid to the price paid for each kWh of electricity purchased from the grid	
g	Shape factor as in table 4.2	
$G_{diff,hor}$	Diffuse radiation falling on the horizontal	[MJ m^{-2}]
$G_{direct,hor}$	Direct radiation falling on the horizontal	[MJ m^{-2}]

G_{direct}	Direct (beam) radiation falling on a plane perpendicular to the sun's rays	[MJ m^{-2}]
$G_{tot,hor}$	Total (global) radiation falling on the horizontal	[MJ m^{-2}]
GHG	Greenhouse gas emissions specific to the heating and cooling energies supplied	[kg$_{CO2}$ kWh^{-1}]
h	Height	[m]
h_f	Heat transfer coefficient of fluid	[W m^{-2} K^{-1}]
h_{surf}	Surface heat gain coefficient of cold storage tank	[W m^{-2} K^{-1}]
hr	Hour angle	[°]
I	Capital cost	[$]
i	Interest rate	
I_{eq}	Capital cost of the main components with "eq" standing for "equipment"	[$]
I_{sys}	Capital cost of system including auxiliary equipment	[$]
$I_{t=0}$	Capital cost including planning and installation (Initial investment)	[$]
j	Shape factor as in table 4.2	
k	Thermal conductivity	[W m^{-1} K^{-1}]
k_c, k_{GHG}	Shape factors for the overall performance factor functions in section 4.2.3.	
k_{bent}	Loss coefficients in bents of pipe through latent cold storage tank	
k_{pipes}	Friction factor in the pipes of the latent cold storage tank	
L	Length of tube per circuit consisting of multiple paths	[m]
l	Latitude	[°]
L_{path}	Length of one path (height of latent cold storage tank)	[m]
l_{shell}	Shell thickness around heat transfer tubes within the latent cold storage tank	[m]
l_{wall}	Wall thickness of tube within latent cold storage tank	[m]
$liqfrac$	Liquid fraction of latent cold storage tank	

m	Regression coefficient (equation 9.52)	
M_{water}	Annual water consumption of the HVAC system	[kg a^{-1}]
$maint$	Annual cost for maintenance	[\$ a^{-1}]
N	(1) Life time of a system [a]. (2) Amount of tubes (paths) in the cold storage tank in section 9	
n	(1) Day of the year (equation B.5). (2) Index for the year in section 4.2.2. (3) Percentage of total Australian population living in a particular climate zone (equation 4.32). (4) Coefficient for heat transfer characteristic of wet cooling towers (equation 7.29). (5) Coefficient for heat transfer characteristic (equation 9.7)	
N_R	Amount of rooms	
N_{circ}	Number of circuits	
N_{path}	Number of coil paths per circuit	
NTU	Number of transfer units	
Nu	Nusselt number	
OPF	Overall performance factor	
OPF_{c_m}	Partial overall performance factor concerning cost	
OPF_{comf}	Partial overall performance factor concerning comfort	
OPF_{GHG}	Partial overall performance factor concerning greenhouse gas emissions	
$p_{el,sol}$	Value of solar generated electricity exported to the grid	[\$ kWh^{-1}]
p_{el}	Electricity price	[\$ kWh^{-1}]
p_{gas}	Price for gas	[\$ kWh^{-1}]
p_v, $p_{v,sat}$	vapor pressure, sat=saturated	[kPa]
p_{water}	Price for water	[\$ m^{-3}]
PLF	Part load factor	
PLR	Part load ratio	
Pr	Prandl number	
Q	Heat	[kWh]

q	(1) Fraction of rated capacity in section 7.2. (2) Fraction of capital cost due to auxiliary equipment or planning/ installation in table 5.3 and table 8.1	
q'	Modified fraction of rated capacity (equation 7.6)	
Q_{CS}	Heat transferred in or out of the cold storage tank	[kJ]
R	Thermal resistance (equation 9.4)	[K W^{-1}]
r	Radius	[m]
r_{CS}	Percentage of the pump electricity consumption due to the cold storage tank (equation 9.52)	
R_{htf}	Resistance to heat transfer of fluid at inner surface of tube in latent cold storage tank	[K W^{-1}]
R_{total}	Total thermal resistance as (equation 9.4)	[K W^{-1}]
R_{wall}	Thermal resistance of wall	[m^2 K W^{-1}]
$ratio_N$	The ratio between the enclosing circle to the radius of each of the N unitary inner circles when determine the maximum number of circles within a circle	
Re	Reynolds number	
RH	Relative humidity	[%]
s, r	Regression coefficients (equation 7.5)	
$scalefactor$	Scale factor to scale the HVAC system according to the load	
T	Temperature	[°C]
t	Temperature in section 7.2 regarding the external circuits of the absorption chiller	[°C]
T_{cs}	Cold storage media temperature	[°C]
T_{dp}	Dew point temperature	[°C]
T_{melt}	Melting temperature of PCM	[°C]
$T_{set,air,CC}$	Set point cooling coil outlet air temperature	[°C]
$T_{set,air,HC}$	Set point heating coil outlet air temperature	[°C]
$T_{set,chw}$	Chilled water outlet set point temperature to be generated by the chiller	[°C]

T_{setC}	Indoor cooling set point temperature	[°C]
T_{setH}	Indoor heating set point temperature	[°C]
T_{sub}	Latent cold storage media subcooling temperature	[°C]
T_{wb}	Wet bulb temperature	[°C]
u_{wind}	Wind speed	[m s^{-1}]
V	Volume	[m^3]
v	Velocity	[m s^{-1}]
V'_t	Cold storage tank volume specific to the installed cooling capacity	[m^3 kW^{-1}]
V_{attic}	Volume of attic	[m^3]
V_{house}	Conditioned volume of building	[m^3]
V_{room}	Volume of one room	[m^3]
vol_{z_i}	Specific volume of zone i	
x, $\bar{x}$	Variable representing either $c_{m(,dhw)}$ and $GHG_{(dhw)}$ or their population weighted averages $\bar{c}_{m(,dhw)}$, $\overline{GHG}_{(dhw)}$	
SF	Solar fraction defined in equation 4.1 to 4.6	

Chapter 1

Introduction

1.1 Significance

Solar air-conditioning is an emerging global industry with international attention now focused on Australia. Solar air-conditioning is desirable to help offset extremes of electricity grid loading during hot summer days and to reduce greenhouse gas emissions from building air-conditioning.

The Australian Solar Cooling Interest Group (AusSCIG) (www.auscig.org.au) was established in 2009 and is now the world largest group with this purpose. The group aims to provide commercial direction and policy advice to government but is struggling to answer fundamental questions. It became important enough to become incorporated in the Australian Institute of Refrigeration, Air-conditioning and Heating (AIRAH) as a special technical group in 2013.

Most of the research takes place in Europe and most solar cooling plants are installed there. However, European research results and conclusions cannot be simply transferred to Australian climates. Australian climates have a much higher insolation on average and water for heat rejection is a scarce commodity. The north of Australia is in the tropics and heat rejection conditions are difficult there.

Research in solar cooling is surprisingly sparse in Australia and there is insufficient research basis to guide the emerging industry. Australian research focuses mainly on small-scale applications. The Australian National University (ANU) is positioning itself to take on a leadership role in aspects of solar cooling research and a cost effective and reliable (small-scale) air-conditioning system based on ejector technology is being developed. An ejector has been integrated with a conventional heat pump to realize electricity savings. The ejector design has been improved using variable geometry, internal heat recovery and smart control. To overcome shifts between solar irradiation and cooling demand, the ANU has also developed a cold storage using gas hydrates to raise the freezing point of water. Another application for this are storage condensers as a mean to reduce the water consumption of solar air-conditioning systems.

The CSIRO is Australia's national science agency. Its division "CSIRO Energy Technology" in Newcastle develops a cost effective space conditioning application for the domestic sector using desiccant cooling. In addition to this CSIRO is able to test air-conditioning equipment in a "Controlled Climate Test Facility" while varying

humidity and temperature. Particularly for the evaluation of solar air-conditioners, a solar air-conditioning prototype test facility has been designed to test different technologies under variable indoor and outdoor conditions [CSIRO, 2013]. The university of South Australia has developed a liquid desiccant air-conditioning system and also conducts research on heat storage via phase change materials.

Solar cooling research is set against a context of rapid and enforced change in the air-conditioning industry. Traditional refrigerant gases are being phased out due to concerns over damage to the planet's ozone layer and over the effects of the very high greenhouse gas intensity of these gases. HCFC refrigerants will be phased out by 2015 and HFC refrigerants will be strongly phased down by 2030. Carbon pricing came into action in July 2012 and even though repealed in 2014 by the prevailing government, the traditional air-conditioning technology will face difficult challenges to adapt to these changes. This provides the opportunity for solar cooling to become an alternative.

Unlike in Europe, environmental concerns about scarcity of resources or pollution due to high population density are not yet an issue driving politics in Australia. Environmentally friendly and greenhouse gas saving technologies are perceived by the wide public as a left-wing threat rather than a chance to improve resource efficiency and consolidate future energy supply to protect Australia's high quality of life. Lobby groups supporting extensive depletion of resources have a large political influence and financial advantages.

In order for solar cooling to be feasible in Australia systems must not only perform environmentally better than the conventional systems, but also offer a cost advantage. Demonstration plants do exist in Europe but there are less than a dozen operating systems in Australia. Furthermore, despite reasonable design practice, technical installation know-how is missing and as a result the systems performed below expectations, leading to bad reputation. Consequently this discourages further investment in solar cooling. Fundamental questions must be answered for industry and research. It is important that the young industry does not waste precious resources repeating established research or attempt to optimize an inappropriate technology.

This work focuses on residential applications and follows a modeling approach to analyze various solar cooling systems in the different climates of Australia. The systems analyzed also include solar space heating and domestic hot water in order to increase annual solar collector utilization. The following questions are addressed:

1. Under what physical and economic circumstances would solar cooling be favored over a conventional air-conditioning installation?

2. Should solar cooling use solar-electric (photovoltaic) or solar-thermal driving energy? Under what physical and economic circumstances would one be favored over the other?

3. What advantage concerning peak electricity demand can solar air-conditioning provide?

4. Can cold storage help to reduce greenhouse gas emissions further and is it physically and economically viable?

5. Are there important differences in the needs of domestic and commercial solar cooling systems?

As energy efficiency of buildings becomes more and more important, and air-conditioning plays naturally a major factor in Australia, the Australian Institute of Refrigeration, Air-conditioning and Heating (AIRAH) became aware of the importance of solar cooling in Australia. The AIRAH HVAC&R research summit organized in 2014 [Institute for sustainable futures and AIRAH, 2014] was attended by at least 4 Australian solar cooling cooling experts and over the last 4 years a handful of scientific articles concerned with the topic have appeared in AIRAH's journal *Ecolibrium* [Kohlenbach and Dennis, 2010; Dillon, 2011]. In 2012 the Australian solar cooling interest group (AusSCIG) became a special technical group of AIRAH, lifting awareness towards solar cooling to a higher level for all industry partners. It organizes workshops on the topic and every two years a solar cooling conference.

1.2 Thesis outline

This thesis provides a simulation based study on thermal and electric solar cooling technologies. The systems provide also heating and domestic hot water to typical Australian residential buildings throughout seven different Australian climate zones. The terminology "solar cooling" and "solar air-conditioning" can be used interchangeably, meaning heating is not included in the term "air-conditioning".

In Chapter 2 an introduction to Australia's air-conditioning and refrigeration demand is given along with the status of solar cooling in Australia in regards to the installed system base. The international research activity takes mostly place in Europe even though the diverse climatic conditions in Australia with its high insolation favor solar air-conditioning.

Chapter 3 focuses on the electricity demand resulting from air-conditioning. Electricity market data from the National Electricity Market (NEM) and recorded weather data from the Bureau of Meteorology (BOM) have been analyzed from 2005 until 2012 to find a correlation between hot weather, hence air-conditioning demand, and peak electricity demand. Furthermore, the impact of the increase in residential photovoltaic systems on the peak electricity demand over the same time period is investigated.

In Chapter 4 an overview on the modeling environment is provided, and on all modeling parameters, which are used to compare electrically and thermally driven cooling, heating and DHW systems. Furthermore, the performance parameters used to compare HVAC (and DHW) systems with each other are introduced. The main

three factors are comfort, cost and greenhouse gas emission. To make the performance comparable, cost and greenhouse gas emissions are specific and refer to the amount of cooling and heating (HVAC) (and domestic hot water (DHW)) provided in order to keep the residential building within a certain comfort range. The three factors are merged into one novel overall performance factor (OPF), which is used to compare various systems. The building, which defines the cooling and heating load is also discussed in this chapter. The building model is a 230 m^2 conditioned space with six rooms, divided in three zones. The building structure is chosen to be the most common in each climate zone, and insulated according to the Building Code of Australia Australian Building Codes Board [2011].

In Chapter 5 one conventional reverse cycle air-conditioner for each comfort zone in the building model and an electric solar water heater are defined as the reference case to compare the solar alternatives against.

In Chapter 6 the contribution of photovoltaic modules on the reference case from an economic and environmental perspective is investigated. To conclude this chapter the use of electricity storage in form of batteries has also been included.

The most extensive simulation work is presented in Chapter 7, which is the development of a thermal cooling, heating and DHW system using an absorption chiller, a hot water storage tank and evacuated tube solar collectors. The system is backed up by gas and maintaining comfort conditions has highest priority. An important and novel aspect of this work is that the HVAC system is scaled depending on the cooling and heating load of the building in each climate. Subsections of this chapter are concerned with the development of the actual absorption chiller model, which is based on a look-up approach and the characteristic equation. Furthermore, the control and the design of the HVAC (and DHW) system are presented.

Chapter 8 deals with the findings of the annual solar thermal simulations in seven different climates of Australia. Collector size and hot water tank size are varied and after deciding on one configuration with at least 60% solar fraction in each climate a sensitivity study is performed. The aim of this exercise is to analyze how the different variations of the heat supply sub-system, the cooling sub-system or of the load itself effect the overall performance. Amongst the variations are different dehumidification strategies, chiller sizes, collector efficiencies, inclusion of night flush ventilation, set point temperatures for air and chilled water, radiant cooling applications in form of chilled beams and varying building structures.

To conclude the simulation work in Chapter 9 a cold storage option on the chilled water side is added to the solar thermal model. Latent PCM material is compared to a chilled water tank and the control strategy is adjusted to the new design. Discharging of the tank occurs via fan coils or chilled beams.

Chapter 10 summarizes the results and wraps up the thesis work into a conclusion comparing solar electric and solar thermal cooling technologies with or without energy storage in regards to the diverse Australian climate and its high solar irradiation levels.

The computer model of the HVAC (and DHW) system has been developed in the transient simulation software environment *TRNSYS 16.1* [Thermal Energy System Specialists (TESS), 2007]. The latent cold storage tank, controls and the absorption chiller are components programmed and compiled by the author, using the compiler *Compaq Visual Fortran* [© Compaq Computer Corporation, 2000]. Furthermore, the simulation output files from TRNSYS have been processed using Visual Basic for Applications scripts in the *MS Excel* programming environment [© Microsoft Corporation, 2007].

1.3 Extracurricular work and publications

This PhD thesis is strongly orientated on applied research using simulation tools to come to a conclusion on the feasibility of certain solar cooling technologies for Australia.

Policy support for a solar cooling industry and solar cooling research is weak in Australia as fossil fuel resources are extensive and there is no pressing need for Australia to moderate its consumption. Nevertheless, the Australian Solar Cooling Interest Group (AusSCIG) has been formed to promote solar air-conditioning and to address Australia's problems of high summer peak electricity demands. AusSCIG has been transferred into a sub-group of AIRAH in 2013 and the author has been a member of both groups since the beginning of her PhD candidature.

In order to convey Australia's efforts to the international community the paper *Solar cooling in Australia - a review* [Doemland and Dennis, 2011] was presented on the 4th international conference on solar air-conditioning in Cyprus. The conference served the author as a platform for knowledge exchange and networking.

The summer peak electricity demand is one of the driving forces in Australia to promote solar air-conditioning, hence, the author presented the paper *The effects of air-conditioning on the summer peak electricity demand and the role of PV* in 2013 on the Australian solar cooling 2013 conference in Sydney [Doemland and Dennis, 2013]. It could be shown that the uptake of PV from 2009 until 2012 had already a positive effect on the peak electricity demand.

As a representative for AIRAH the author worked in 2011 and 2012 intensively on the development of the solar heating and cooling standard AS 5389(Int)-2013 [Australian/ New Zealand Standard, 2013] on the committee CS-028. The standard was the first of its kind and was finally published in 2013 as an interim standard. On the basis of the existing solar water heater standard AS/NZS 4234:2008 [Australian/ New Zealand Standard, 2008] a TRNSYS model was developed for a solar cooling system in order to perform annual simulations and to calculate electricity savings

compared to a reference system. The author transferred the existing model from the mere text based model in TRNSYS 15 into a TRNSYS 16 model, which is easier to modify due to its visual interface.

For the development of her own residential solar thermal cooling, heating and DHW model in TRNSYS, the author had to decide on an absorption chiller component. The existing TRNSYS 16 component type 107 was not sufficient for the purpose of developing a comfort controlled HVAC model and performance data was missing to create an input file. A new TRNSYS component was developed based on the characteristic equation with an internal control algorithm, using the hot water inlet temperature to control the cooling capacity. The paper *A non-linear absorption chiller model for TRNSYS with internal control algorithm* was presented on the 5th international conference on solar air-conditioning [Doemland and Albers, 2013].

From October 2013 until March 2014 the author decided to gain industry experience in the field of solar air-conditioning and worked as a research scientist for six months in Singapore for the company SOLID. Asia Energy Services Pte. Ltd., which is a branch of the Austrian company SOLID [S.O.L.I.D., 2014]. The company operates the two world largest solar cooling plants and the second largest one is located in Singapore, generating chilled and hot water to supply a college with hot water using nearly 4000 m^2 flat plate collector. The conference paper *Monitoring of the solar cooling installation UWC Singapore in 2013 and improvements based on TRNSYS simulation* was written in Singapore and presented at the Austrian conference Gleisdorf Solar 2014 by the CEO of SOLID, Christian Holter. Next to the work on the existing large scale solar cooling installation the author developed the research plan for a joint laboratory between SOLID and the Singaporean university Nanyang Technological University (NTU). A test rig for small-scale absorption chillers was set up to measure the chiller's performance under variable inlet temperatures and mass flow rates and to observe its reaction time towards fluctuating heat inputs. In Chapter 7.2.3 the test results are presented in form of an "excursion".

Chapter 2

Context for solar air-conditioning in Australia

Solar thermal cooling in Australia is in its early demonstration phase. A "solar cooling industry" does not exist and solar air-conditioning solutions are not readily realizable. With respect to climate change, electricity grid stability, increasing electricity prices, high penetration of residential air-conditioning and the available insolation in Australia, the introduction of solar cooling technologies is highly desirable.

The scope of this chapter covers the cooling demand in Australian residences in order to show that most regions in Australia rely strongly on air-conditioning. Only a few dozen solar cooling systems are installed in Australia, but with the motivation of improving energy efficiency, reducing greenhouse gas emissions and peak electricity demand a clear market niche for solar cooling and heating has opened up, which Australia should take to its advantage.

2.1 Australia's cooling, heating and domestic hot water demand

Peak electricity demand is a problem in Australia because it drives peak electricity demand and cost. Residential air-conditioning is often blamed as the main driver for summer peak electricity demand especially in the afternoon from 4pm to 8pm when residential electricity demand and industrial electricity demand coincide [Australian Energy Regulator (AER), 2012].

Cooling demand in Australia can be divided into air-conditioning and food refrigeration. The application is characterized by the required temperature range. For air-conditioning an indoor temperature between 21°C and 25°C is usually aimed at. Food refrigeration requires much lower temperatures.

The air-conditioning (AC) and refrigeration demand can further be split up into stationary AC (domestic and commercial), mobile AC related to vehicles, domestic refrigeration, transport refrigeration and refrigerated cold food chains. Transport refrigeration and refrigerated cold food chain are not considered because they are using liquid fuels.

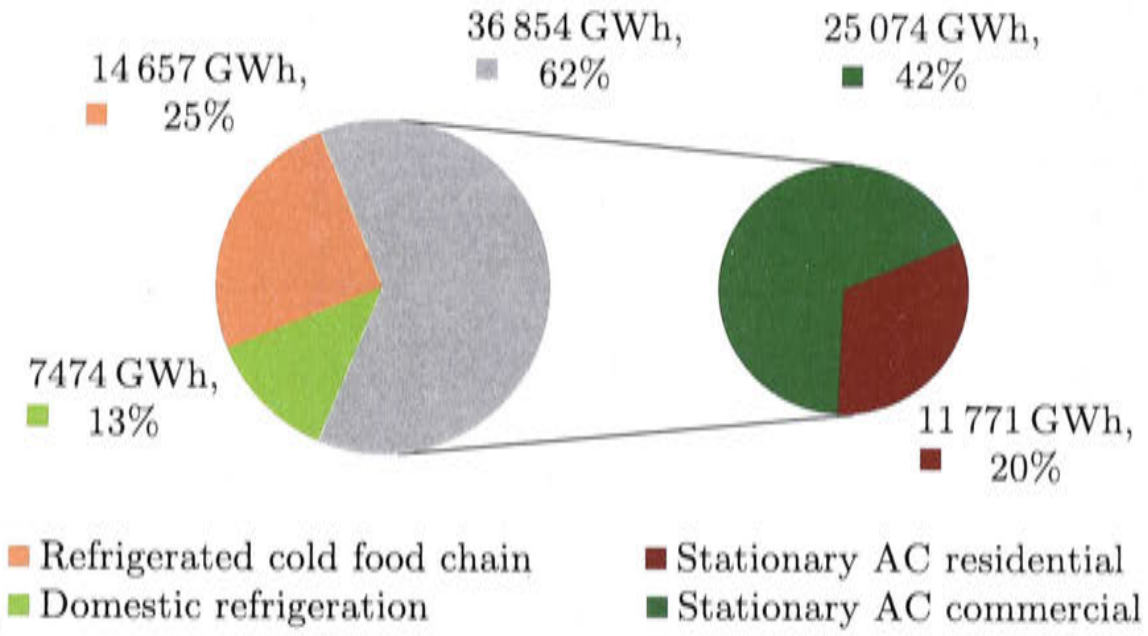

Figure 2.1: Electricity consumption in 2012 for cooling in the different sectors [Expertgroup, 2013]

In 2006 a data base on air-conditioning in Australia was developed and this work has been refined in a recent report published in 2013 [Expertgroup, 2013].

The total electricity consumption for air-conditioning and refrigeration was in 2012 approximately 59 000 kWh of electricity. This means, that in 2012 approximately 23% of the generated electricity (254 700 GWh) were used for cooling Department of Resources, Energy and Tourism [2013][1]. Since the first air-conditioning survey in 2006, this is an increase of electricity consumption for cooling of 31%.

Figure 2.1 shows the share of the electricity consumption of each sector. The electricity consumption does not include the total energy use for cooling due to transport refrigeration and mobile air-conditioning. They add up to another 46.5 PJ (12 900 GWh).

In this thesis the main focus lays on the residential electricity consumption for air-conditioning, which equates to approximately 4.6% (11 771 GWh) of the total electricity consumption in 2011/12. With an air-conditioning penetration of 80% throughout the 8.2 million households in Australia this equates to approximately 1780 kWh of electricity for cooling per household. Expressed in a different way approximately 19% of the 62.1 TWh electricity consumed in the residential sector was used for air-conditioning.

In 2012 there were in total more than 11.5 million stationary air-conditioners installed and the majority are single-split units (73%) and window/wall mounted units with (17%) as published by Expertgroup [2013, p. 25]. The same study investigated the types of air-conditioners installed and estimated for each climate cooling operating hours and for reverse cycle air-conditioners also the heating operating hours. Using a general COP_{el} for each machine, the annual electricity consumption could be estimated.

The study expressed the greenhouse gas emissions of the existing stock of air-conditioners which includes direct (directly caused by leakage of refrigerant into the atmosphere) and indirect emissions (caused when operating the machine). The

[1] In the energy statistics published by Bureau of Resources and Energy Economics (BREE) [2014] the total amount of electricity consumed in Australia in 2011/12 is estimated 253 851 GWh

indirect emissions of the stationary air-conditioning stock, which is derived from the electricity consumption, is in total approximately 33.67 $Mt_{CO2\text{-}eq}$, and 10.76 $Mt_{CO2\text{-}eq}$ for the residential consumption.

The direct emissions are more difficult to estimate due to the fact that they strongly depend on the Australian types of air-conditioners and their charging. The predominant refrigerants used are HCFC-22, HFC-410A, HFC-407C and HFC-134a. HCFCs are phasing out in 2015 under the Montreal Protocol [Department of the Environment, 2014]. Nevertheless they take up about a quarter (26%) of Australia's total refrigerant bank with 43 500 t. The rest is made up of HFCs, which are phasing down by 2030.

The leakage rates for refrigerants can be derived from import statistics when deducting the refrigerants used for air-conditioning manufacturing, as they represent the refrigerants to re-charge the existing equipment. The leakage rates in old HCFC-22 chillers is relatively high with approximately 8% per annum. However, the HFC refrigerants dominating the market, due to the ban on HCFCs, have a lower leakage rates of 4 to 5% per annum[2] [Expertgroup, 2013, p. 122].

Of the 5.4 $Mt_{CO2\text{-}eq}$ direct emissions from the the refrigerant in the bank, stationary air-conditioning participates with a proportion of 42%. This proportion has increased since 2006 due to an increase of the stationary air-conditioning stock from 37% in 2006 to 63% in 2012.

Nevertheless, a trend is observed that the growth rate of air-conditioning equipment over the last 4 years has slowed down. Reasons might be market saturation as widely believed, milder summers or a weaker economy. It is questionable how much consumed electricity and leaking refrigerants can be saved when switching to solar thermal assisted cooling. Solar assisted cooling promises to replace electricity and gas consumption and the chillers, for example absorption technologies, use refrigerant of no global warming or ozone depletion potential.

Results from an extensive simulation based study in 2008 [Energy Efficient Strategies (EES), 2008] showed that the saturation of air-conditioning is being reached and the market penetration seems to plateau at 80% by 2020. Nevertheless, population growth and the increase of conditioned space due to increasing floor area of new residences lead to an increase in total electricity demand for air-conditioning (and for heating in winter in the colder climates). Reverse cycle air-conditioners (mostly split systems) account for about 65% of the total share of air-conditioners (figure 2.2). About one million units are sold each year of which about 2/3 are for residential applications.

Figure 2.2 also shows the estimation of electricity consumption by Energy Efficient Strategies (EES) [2008] due to residential air-conditioning and it is important to mention that the results from this study deviate by the factor of 2 from the electricity consumption proclaimed by Expertgroup [2013].

[2]Before the introduction of an equivalent carbon price on HFCs in July 2012, it is estimated that 2.7 years of average supplies have been imported in the year before the introduction of the scheme. A scaling factor was incorporated by Expertgroup [2013] to cancel out the impact on the annual leakage rate.

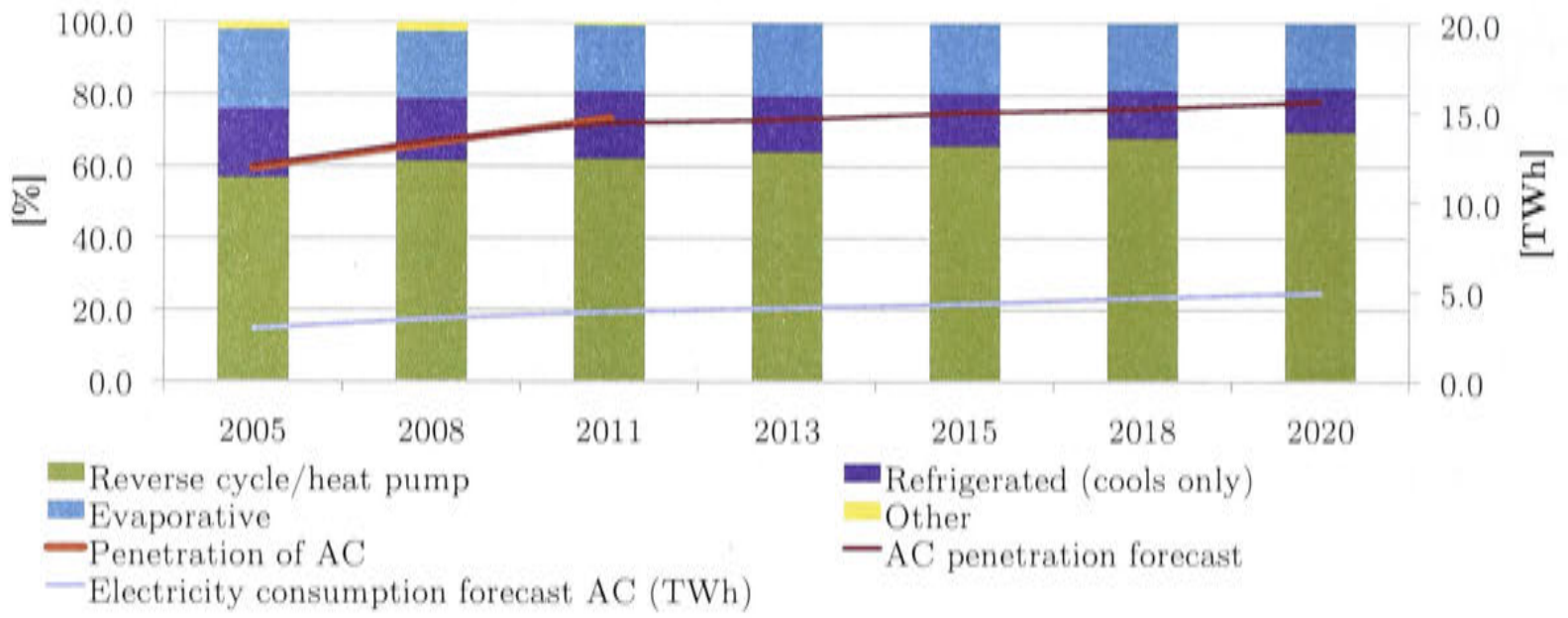

Figure 2.2: Penetration, types and energy consumption of air-conditioning in Australia [Che and Pham 2012; Energy Efficient Strategies (EES) [2008]; Australian Bureau of Statistics (ABS) [2013]]

A third source of information estimating the electricity consumption for cooling is the Bureau of Resources and Energy Economics (BREE) [2014], which states that the residential final energy use has been growing annually by 1.6% since 1990 to 126 TWh in 2011/12 and equates to roughly 11% of the total final energy use in Australia. The residential energy use for cooling has been growing steadily as well and in 2009-10 it reached 3% of Australia's final energy use. This equates to 3.7 TWh [Che and Pham, 2012] which would be electricity as no other energy source is used for cooling in the residential sector. This study mainly agrees with Energy Efficient Strategies (EES) [2008], but it still deviates by the factor of 2 from the estimation by Expertgroup [2013].

The introduction of higher energy performance requirements for new buildings might slow down the increase in total electricity demand and reduce the related greenhouse gas emissions due to cooling.

According to the Bureau of Resources and Energy Economics (BREE) [2014] the final energy consumption in 2009/10 for space heating was 35% and for water heating 26%. The final energy use for space heating and domestic hot water in Australia is comprised of the energy sources electricity, gas or renewables. The information are from the publicly available Yearbook Australia 2012 [Australian Bureau of Statistics (ABS), 2014]. The percentage of households which used electricity for space heating in 2011 was 37%, gas 32% and wood 10%. It can be assumed that 21% of households do not own a heating system.

Regarding domestic water heating (DHW), the Australian Bureau of Statistics states that in 2011 52% of all Australian households supplied hot water via electricity and 36% used gas. The Clean Energy Council [2012] study suggests that almost 10% of households used solar hot water by the end of 2012[3]. The use of solar hot water

[3]The newest report Clean Energy Council [2013] claims that in 2013 there were in total 847 700 solar hot water systems installed.

increased by 6% points since 2005 due to policy initiatives, but since 2010 market growth has contracted due to the removal of rebates.

The insulation levels of the existing housing stock are rather poor. Table 2.1 shows for the year 2005 and 2011 how many houses were insulated. In terms of effectiveness and the extent to which the insulation was installed no information is given.

Table 2.1: Residential building insulation levels in each state derived from Australian Bureau of Statistics (ABS) [2014]

	ACT	NSW	VIC	QLD	SA	NT
2005	47%	54%	60%	58%	85%	90%
2011	70%	65%	76%	73%	93%	92%

2.2 Policy and governance

The Australian government introduced the renewable energy target scheme in January 2011 which ensures that 20% of the generated electricity in 2020 must come from renewable energy sources. This corresponds to an estimated 41 TWh of renewable electricity generation. In 2011/12 approximately 24 TWh were harvested from renewable sources, mainly from hydro power (14.1 TWh).

The scheme is divided into large scale and small scale depending on the size of renewable power installation. The scheme provides an financial incentive in generating marketable certificates for each MWh of electricity saved or generated in a renewable way.

Even though solar thermal installations generate heat rather than electricity, they can help to displace electricity consumption. Therefore, for domestic hot water applications, certificates were issued, mostly upfront based on system performance simulation, to give a start up financial incentive. Certificates value each MWh of electricity for 10 years with a floating market price per certificate.

Solar electric as well as solar thermal systems for solar hot water heating experienced a boom upon the introduction of the scheme in 2009. Approximately 202 000 solar hot water systems were installed in 2009. The rate of new installations dropped steadily since then to merely 60 000 in 2012. In Figure 2.3 the amount of households with a solar hot water system installed are shown. In 2011 there were 8.18 million households in Australia, meaning today roughly one in ten households possesses a solar hot water system.

Solar thermal systems are included in the renewable energy target based on their ability to replace electric water heaters which are the most common water heating technology for residential buildings. This opens up the discussion why heat pumps or even gas heaters should not be eligible for certificates as they replace the common electrical water heaters as well. Furthermore, it opens the possibility for solar thermal cooling systems to be included in the scheme as they replace electricity of conventional heat pump systems. Electrical driven heat pumps for water heating are already eligible for rebate certificates which is an anomaly of the scheme.

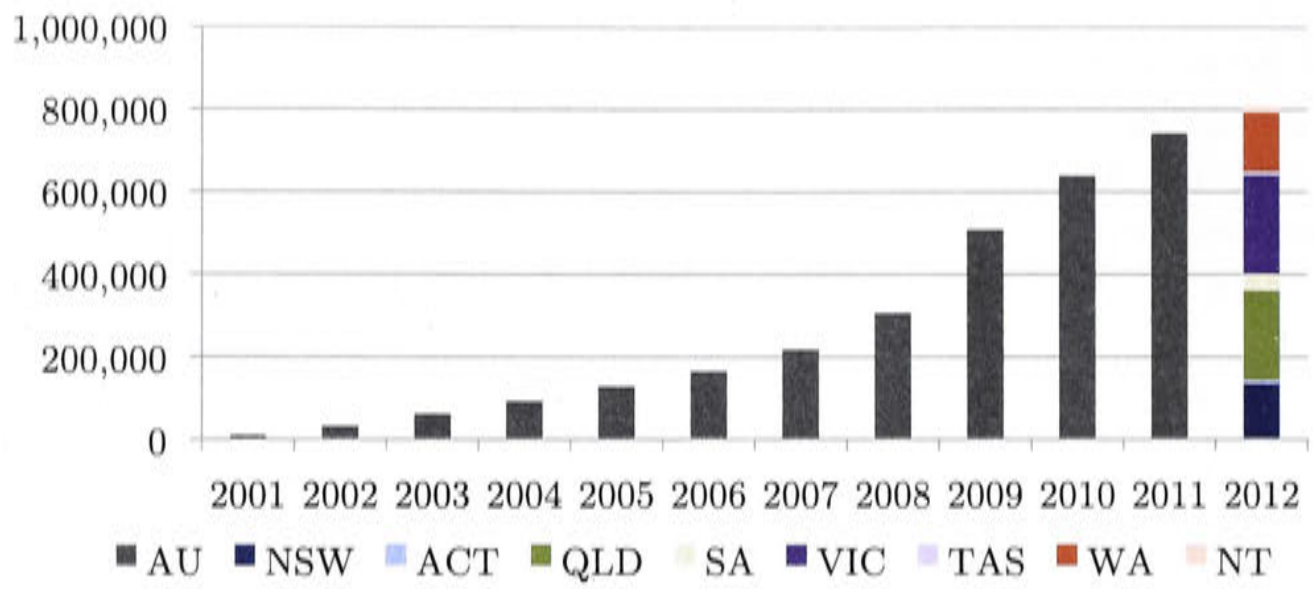

Figure 2.3: Households with installed solar hot water heaters (Information from Clean Energy Council [2012])

Unlike other countries, Australia has published an interim solar cooling and heating performance standard AS 5389 [Australian/ New Zealand Standard, 2013] in 2013, which could provide a base to financially support solar cooling systems and make them applicable for rebates. Similar to the solar hot water heater standard AS/NZS 4234 [Australian/ New Zealand Standard, 2008] the new standard could provide a methodology to calculate displaced fossil energy. However, the standard is only applicable for desiccant systems so far, of which there are only a few installations in Australia. Furthermore, it requires extensive knowledge with the software suite TRNSYS, which is an expense not every building service designer would deem necessary.

The solar hot water standard was based on replacing electric water heaters, which use most valuable energy in form of electricity, by solar thermal water heaters. High electricity savings could be achieved. The replacement of heat pumps with solar thermal sources is less rewarding as such reference systems thermodynamically operate already under a coefficient of performance of 3 and higher.

The current standard should be extended to absorption chiller systems and photovoltaic systems and should also include heating in winter as the population in climate zones with cold winters is rather large. Cooling (,heating and DHW) systems are more complex than solar water heaters and if the energy performance within the standard remains based on TRNSYS simulations, the freedom of system modeling should be extended and handed over to the system designers in order to represent their particular system. Consequently, such models need to be validated and double checked by certified bodies with good modeling knowledge of solar thermal systems. The standard committee is not able to provide pre-fabricated models for all system configurations, however, performance indicators like auxiliary and supplementary energy consumption, cooling, heating and domestic hot water and a representative building model can be provided.

The Australian government should financially stimulate the uptake of displaced electricity due to air-conditioning and maintain and audit capability to monitor solar cooling, heating and DHW proposals based on the defined standard. The standard

should be open to new innovative technologies and be able to distinguish between ambiguous and real efficiency improvements. A possible rebate scheme could also increase the value of saved electricity during peak hours in order to favor technologies reducing peak electricity demand. Another rebate alternative are split rebates with upfront and performance based components.

Instead of reducing the electricity consumption for air-conditioning during peak hours by using renewable energy sources, it is also possible to implement predictive demand response devices which trigger the air-conditioners to pre-cool the building or to generate and store chilled water for later usage. The Australian standard AS/NZS 4755.3.1 [Australian/ New Zealand Standard, 2012] specifies the required reactions for air-conditioners under four different demand side response modes. The standard has three parts covering next to air-conditioners also swimming pool pump units and electric-boosted storage water heaters.

Policy instruments to increase energy efficiency or lower greenhouse gas emissions in respect to solar cooling have been summarized in Rowe et al. [2013]. Next to market-based instruments there are fiscal instruments and incentives (e.g. taxes, capital subsidies) or control regulatory instruments (e.g. standards or building codes). Raising awareness to solar cooling and voluntary action is also a valid measure. By conducting a survey the report found that direct financial funding dominates the field of solar cooling support schemes, including subsidies on capital cost, tax deductions and access to capital. The countries analyzed were Australia, Austria, France, Germany, Italy and the USA.

The renewable energy target is only one part of the overall objective to lower the carbon emissions in Australia and it focuses strongly on electricity. The proclaimed goal is to achieve 95% of the greenhouse gas emission levels in 2000 by 2020 and down to 20% by 2050. This equates to 555 $Mt_{CO2\text{-}eq}$ and 115 $Mt_{CO2\text{-}eq}$ emissions respectively. The EU members in contrast committed to a reduction of 20% by 2020 compared to the levels of 1990. Germany tries to achieve even up to 30% depending on the efforts of the other industry countries; this would equate to 750 $Mt_{CO2\text{-}eq}$ of greenhouse gas emissions in 2020. The German population of 2013 was approximately 3.5 times larger than the Australian and the GDP approximately 2.3 times. The European road map for 2050 aims at least at 80% emission reduction compared to 1990, but this goal is not mandatory yet and strongly depends on economic development, implementation of energy efficiency measures and reorganization of the energy generation and distribution structure towards renewable sources within Europe [Umweltbundesamt, 2014].

A trading scheme for carbon emissions, commonly known in Australia as "carbon tax", was introduced in July 2012, fixing the price for emissions at $23 per tonne of carbon emission for the first three years. In July 2015 the transition towards a real market based trading scheme was planned to start, but in September 2013 the direction of government changed towards being environmentally rather indifferent. The "carbon tax" was repealed in July 2014 and replaced by an "Emissions Reduction Fund". The $1.55 billion dollars of that fund will be allocated directly to projects intending to reduce greenhouse gas emissions. It remains to be seen if this is the

most cost-effective option for the Australian people as free market trading schemes usually provide a more cost effective outcome to reduce greenhouse gas emissions than a governmental grandfathering scheme. Cramton and Kerr [2002] also came to the conclusion that auctioning permissions for carbon emissions is superior.

The Clean Energy Council [2012] provides a summary of 11 federal financial initiatives for a more energy efficient, low-emissions future. Of those projects, three were completed and closed and three, the "carbon price", the "energy efficiency opportunities program" and the "clean technology program" were repealed in 2014. The renewable energy target (RET) is still in operation and provides rebates for small and large scale renewable energy project, but it focuses strongly on solar electricity and solar water heating. The "Clean Energy Finance Corporation" (CEFC) was set out to invest into selected renewable energy, low-emissions and energy efficiency industry projects but the intent of the current government is to abolish the CEFC as well. The Australian Renewable Energy Agency (ARENA) provides the only, hence, highly competitive, fund for research in renewable energies and also funding for renewable energy projects in industry. Its future is also uncertain as bills are put forward to repeal the ARENA act. The "national strategy on energy efficiency" from 2009 does not directly provide funding but instead provides guidance to governments, businesses and households how to improve their energy use towards higher energy efficiency. Next to skills and training it focuses on the development of standards and codes for electrical appliances, transport and the energy performance of buildings (e.g. insulation and water heating) [Council of Australian Governments (COAG), 2009].

2.3 Installed base of solar thermal cooling and water heating in Australia

Worldwide the amount of solar thermal systems was estimated to be approximately 750 in 2011 Mugnier [2013]. This number is very likely to have increased during the last 3 years.

Most of those systems are installed in Europe and are demonstration plants and proved themselves technically feasible. The chiller types are mostly single stage absorption chillers or adsorption chillers, which are the state of the art in Europe. This was investigated amongst other statistics by the International Energy Agency in their reports from the solar heating and cooling program task 38 [International Energy Agency Solar Heating and Cooling Project (IEA-SHC), 2011b] in 2009.

Most of the in 2009 investigated systems use flat plate solar collectors or evacuated tubes collectors. At the low temperature range between 60°C and 95°C, at which absorption and adsorption chillers operate, a careful choice of the appropriate collector type is required. The collector efficiency depends on the mean fluid temperature, ambient temperature and insolation levels.

There are no evacuated tube manufacturers and few flat plate manufacturers in Australia, but those collectors can be imported from China for a lower cost than from

Europe. For Australia the cost-quality balance is strongly influenced by low cost components manufactured in China. Evacuated tube collectors have to be imported but parabolic trough collectors are manufactured in Australia.

Table 2.2: Installed solar thermal cooling systems in Australia known to the author (October 2014). Collector types are PT=parabolic trough, ET=evacuated tubes, FP = flat plate collectors

location	year	capacity [kW]	collector [m^2]	chiller type
Ipswich, QLD (air-cond. - hospital)	2007	290	570 (PT)	2-stage absorption
Padstow, NSW (air-cond.)	2008	175	165 (PT)	2-stage absorption
Wyong, NSW (air-cond.)	2009	7	20 (ET)	adsorption
Charlestown, NSW (air-cond. - cinema)	2011	233	350 (PT)	2-stage absorption
Newcastle, NSW (demo)	2007	18	58 (PT)	absorption (?)
Echuca, VIC (air-cond. - hospital)	2011	500	442 (ET)	2-stage absorption
Araluen, NT (air-cond. - art gallery)	2010	230	450 (PT)	absorption
Blackall, QLD	2011	10	22 (ET)	adsorption
Newcastle, NSW (air-cond. & hot water)	2011	80	400 (FP)	desiccant

In Australia there are only a few small to medium scale solar cooling installations in the commercial sector which are mainly demonstration projects (Table 2.2). They are based on absorption chillers and most of them use parabolic troughs or evacuated tube collectors. This is an indication for a climate with a high percentage of direct radiation and little cloud cover. The global horizontal irradiation (GHI) and the direct normal irradiation (DNI) are shown in Figure 2.4. The high GHI $> 1600\,\mathrm{kWh\,m^{-2}}$ and DNI $> 1700\,\mathrm{kWh\,m^{-2}}$ in Australia compared to Europe is one positive factor making Australia well suited for solar air-conditioning [Kohlenbach and Jakob, 2014, p. 155].

Parabolic trough collectors are usually installed when high amounts of direct radiation are available, which is true for many parts of Australia. Their hot water supply temperatures, up to 250°C, allow for double stage absorption chillers with higher thermal COPs in the range of 1.2-1.4. The Australian manufacturer NEP-solar provided collectors for the installation in Charlestown (Table 2.2). Double stage chillers combined with parabolic trough collectors require higher capital cost than flat plate collectors with single stage machines, but with a careful design to maximize collector utilization and in a climate with high solar radiation, they promise a higher cooling yield for a given collector size.

Small scale absorption chiller developers are mainly located in Europe. The large scale absorption chillers (>300 kW) are mainly manufactured in Asia (e.g. China, India) and must be imported. The Asian market can provide absorption chillers at high quality. The use of waste heat in tri-generation plants is relatively common in Australia and it is a matter of experience and know-how to also integrate solar thermal collectors.

When comparing thermal chilled water production directly to electrical chilled water production, a solar thermal system must be optimized for lowest auxiliary heat and electricity consumption, using variable speed drives and a good control strategy to achieve savings compared to today's high efficient chillers with electrical COPs be-

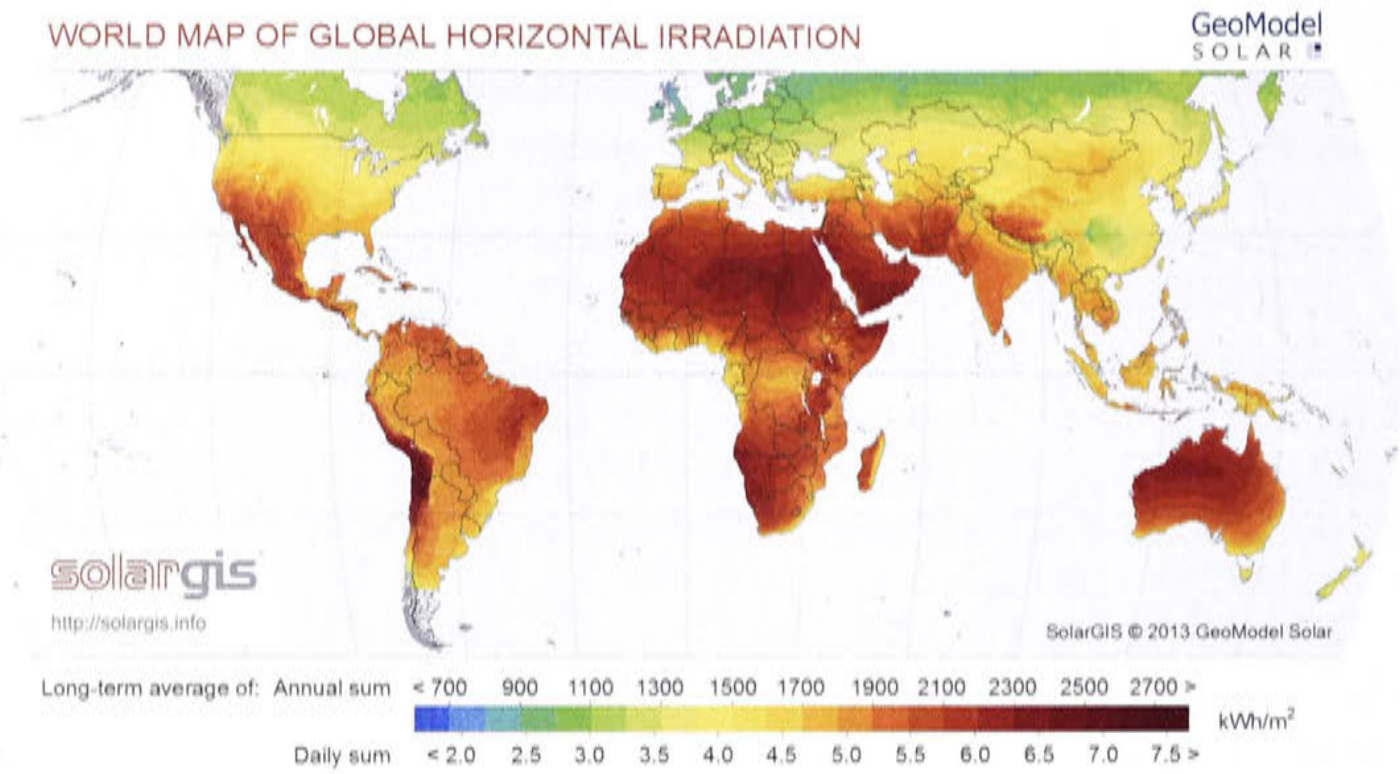

(a) GHI

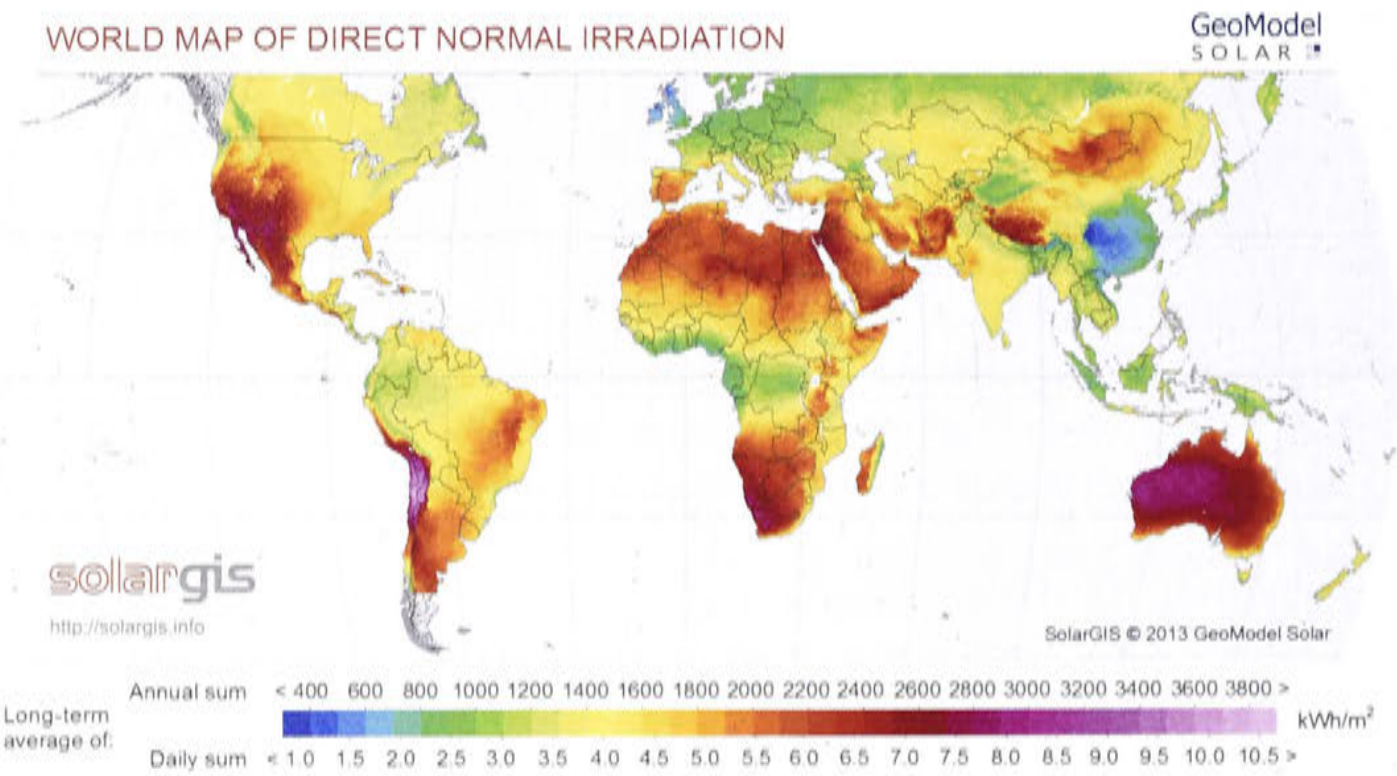

(b) DNI

Figure 2.4: World map of global horizontal irradiation (GHI) and direct normal irradiation (DNI) [solargis, 2014]

tween 5 and 7 at full capacity and an excellent part load performance. Unfortunately, most Australian solar cooling systems did not work as expected upon commissioning or became overly expensive due to technical faults and a lack of know-how. As a result solar thermal cooling gained a poor reputation. The solar cooling industry in Australia is very small and most of the expertise lays in the hands of a handful people with strong links to Europe. However, high solar irradiation level, low cloud cover and large cooling loads are good pre-conditions for the development of Australian expertise in the field.

The Australian focus in regards to low temperature solar thermal applications has been strongly on hot water heaters but the interest in solar cooling is there, which

became obvious through the development of an interim solar cooling and heating performance standard AS 5389 [Australian/ New Zealand Standard, 2013]. The standard requires additional development to be become applicable to absorption chiller systems and to provide a future base to estimate primary energy or greenhouse gas savings of all solar cooling designs.

The International Energy Agency (IEA) stated that in 2011 4.8 GW of thermal collector peak capacity were installed in Australia of which 57% were unglazed pool collectors. Worldwide there were 234.6 GW thermal peak capacity installed in 2011. The IEA further estimates that solar heat will contribute 17% to the energy use for cooling worldwide. For the OECD Asia and Oceania region 12 GW of installed solar cooling capacity are predicted by 2050 [International Energy Agency (IEA), 2012]. Nevertheless, a pathway on how to achieve this goal is not provided.

2.4 Australia's position in the international context

Large scale commercial installations have shown that solar cooling is financial viable when assisting conventional chilled water systems in well suited climatic conditions and when solar heat below 60°C can be utilized as well. For example the "desert mountain high school" project of the company SOLID with a 1.75 MW absorption chiller[4]. Furthermore, it depends strongly on the quality and the price of the energy source replaced.

For residential applications in European countries with a large domestic hot water demand solar thermal cooling can be viable because hot water is needed all year round. Still, it has not established itself as a common technology as capital costs are high and space for the bulky absorption chiller and re-cooling unit is sparse.

In commercial applications financial feasibility comes with a reasonable hot water demand and hotels, schools, shopping malls with food courts, hospitals and apartment buildings are large consumers of low and high temperature heat. Other industrial applications well suited due to their heating and cooling demand are listed in Kohlenbach and Jakob [2014] and include food processing plants for dairy, meat, bread, seafood and wineries. Compared to small scale systems the cost related to the unique design of a large scale solar thermal system is comparable to the design of a conventional large scale cooling plant.

Internationally the International Energy Agency is the largest coordinator of solar cooling activities. After Task 25 a guidance book was published Henning [2007] which was completely revised after Task 38 Henning [2013a]. Most institutions participating were located in Europe. Even though Australia took part in Task 38 already, the Australian position becomes more visible in the new IEA Task 48, where sub task C will be lead by Australia. Task 48 covers the quality assurance and support measures for solar cooling. Table 2.3 covers the IEA tasks relevant to solar cooling.

[4]That system operates under a financing scheme different to conventional chiller plants. The absorption chiller assists the conventional system and is not a stand-alone system. That makes it difficult to judge the financial viability. Nevertheless, on a cost and energy efficiency base the operation of the entire cooling system is improved [Christian Holter (CEO SOLID), 2014].

Table 2.3: A summary of the IEA tasks concerning solar cooling since 1999 [International Energy Agency, 2014]

Task	Title	Duration
25	Solar Assisted Air Conditioning of Buildings	June 1999 - May 2004
A	Survey of Solar Assisted Cooling	
B	Design Tools and Simulation Programs	
C	Technology, Market Aspects and Environmental Benefits	
D	Solar Assisted Cooling Demonstration Projects	
38	Solar Air-Conditioning and Refrigeration	Sept 2006 - Dec 2010
A	Pre-engineered systems for residential and small commercial applications	
B	Custom-made systems for large non-residential buildings and industrial applications	
C	Modelling and fundamental analysis	
D	Market transfer activities	
45	Large Scale Solar Heating and Cooling Systems	Jan 2011 - Dec 2014
A	Collectors and collector loop	
B	Storages	
C	Systems	
48	Large Scale Solar Heating and Cooling Systems	Oct 2011 - Mar 2015
A	Quality procedure on component level	
B	Quality procedure on system level	
C	Market support measures	
D	Dissemination and policy advice	

Technical knowledge is readily available on the internet, mainly due to the IEA tasks. Literature on solar cooling apart from IEA outputs are for example the recently published specialist textbooks by Kohlenbach and Jakob [2014] and Eicker [2014].

There are two key conferences to disseminate solar cooling experience. Firstly, the "International Conference of Solar Air-Conditioning" organized by the Ostbayrisches Technologie-Transfer-Institut e.V. (OTTI) is held every two years and brings together research and industry. Secondly, the "International Conference on Solar Heating and Cooling - SHC conference" is a conference by the IEA and is held annually.

2.5 The national electricity market (NEM) and Australian electricity prices

The National Electricity Market (NEM) in Australia started operating as a wholesale spot market in 1998 to facilitates interation between electricity generators and retailers. The NEM consists of 5 jurisdictions ACT, NSW, QLD, VIC and since 2005 TAS. WA and NT are not included, mainly due to their distance to the east coast.

Generators and retailers express their offers and bids on the NEM and The Australian Electricity Market Operator (AEMO) aggregates and dispatches the supply every 30 min to meet the demand in the most cost effective way for the retailers. Figure 2.5 shows the principle of this operation.

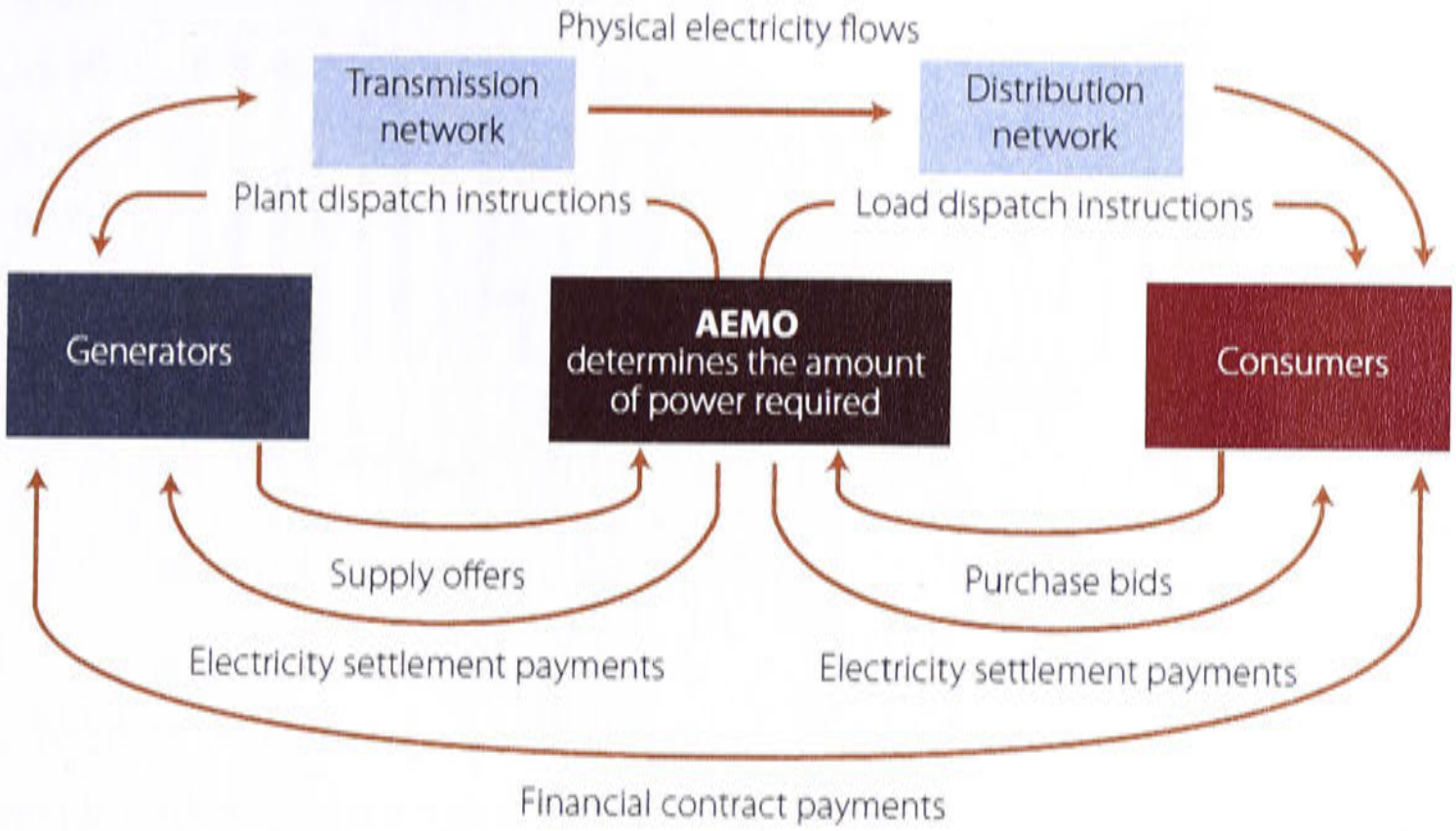

Figure 2.5: The role of AEMO within the NEM [Department of Resources, Energy and Tourism, 2013]

A set of rules (National Electricity Rules - NER) governs the operations on the national electricity market and they are reviewed and modified by the Australian Energy Market Commission (AEMC). To guarantee that the rules are observed by all participants, the Australian Energy Regulator (AER) monitors this procedure and in addition regulates the energy networks (distribution and transmission). Regulating the networks includes price setting for network utilization and decisions on infrastructure upgrades.

The total electricity supplied on the Australian National Electricity market (NEM) has declined since 2007/08 reaching 192 TWh in 2012 [Australian Energy Market Operator (AEMO), 2012]. Reasons for the drop in total electricity consumption could be explained by an uptake of PV and of energy efficiency measures such as solar hot water in response to rising electricity prices and policy initiatives. Further, the global financial crises has led to a more moderate economic growth, hence less electricity demand in the manufacturing industry sectors. However, it is expected to rise again at a moderate rate due to population and industry growth (mainly due to LNG projects in Queensland). Figure 2.6 shows this trend and also the maximum electricity demand since 2005 and the maximum electricity demand forecast for the next 20 years in each state. The Australian Energy Market Operator (AEMO) [2012] provides detailed scenario analyzes and the presented data reflects a medium growth scenario. To put it in perspective, in Germany an estimated 607 TWh of electricity were used in 2012 [AGEB AG Energiebilanzen e.V., 2014].

Peak electricity demand is expected to rise with air-conditioning being a main driver, depending strongly on industry and population growth. It is acknowledged though that the update of PV shifted peak electricity demand later in the afternoon [Australian Energy Market Operator (AEMO), 2012].

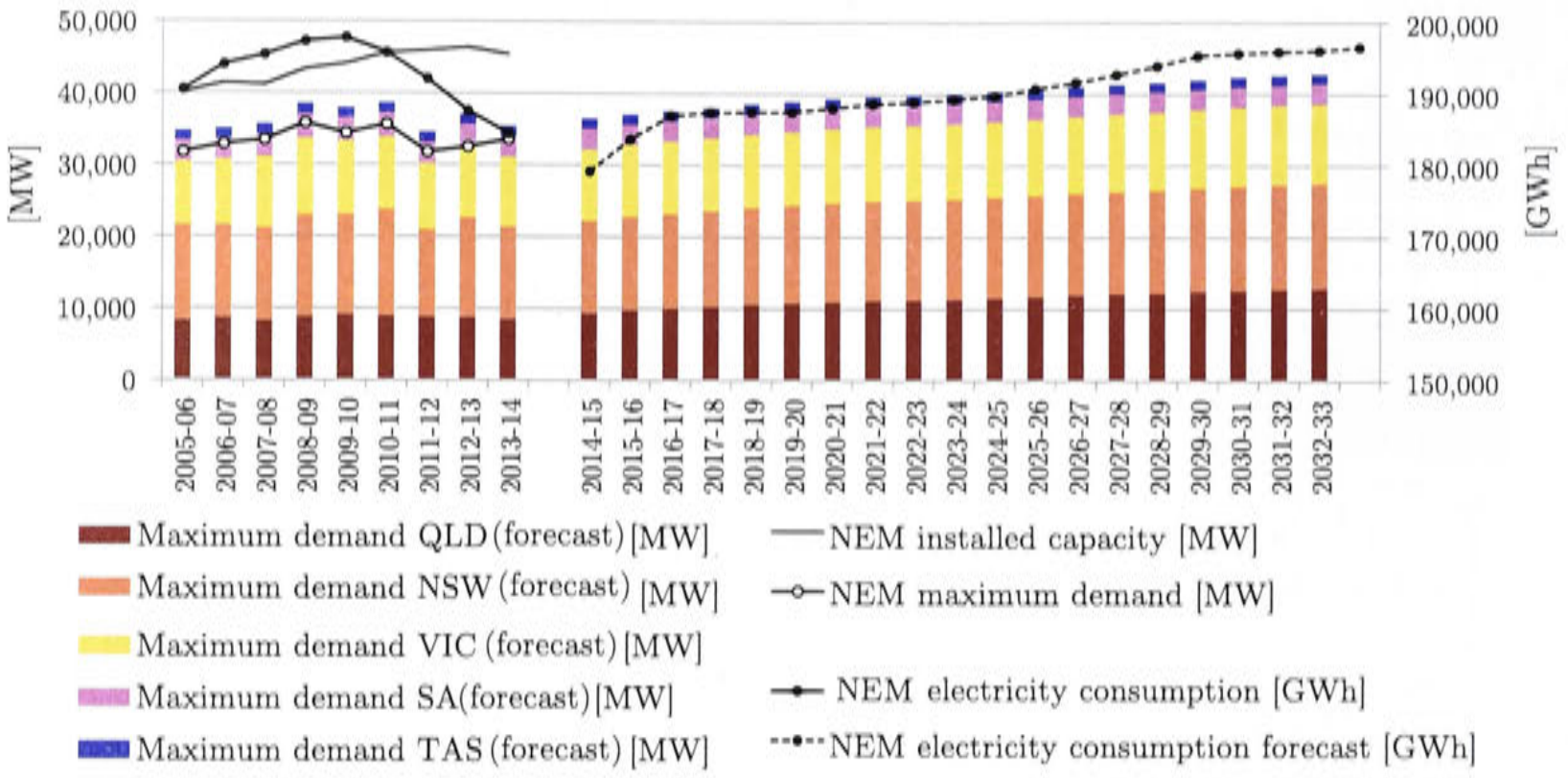

Figure 2.6: Maximum electricity demand [MW], installed capacity [MW], maximum demand forecast [MW] and electricity consumption and forecast [GWh] on the NEM (2014) [Australian Energy Regulator (AER), 2014; Australian Energy Market Operator (AEMO), 2012]

The threat of rising peak electricity demand lead to costly electricity infrastructure upgrades. The AER forecast the investment for electricity network infrastructure upgrades, operation and maintenance to be $61 billion over the current 5 year regulatory period, mainly for distribution networks. This imposes a cost on each of the 9.7 million electricity costumers in the NEM of $6300 The make up of the cost can be seen in Table 2.4. The regulatory periods differ between the individual network operators in each jurisdictions and most of them end 2014 and 2015.

Table 2.4: Cost for electricity infrastructure upgrades in the current 5 year regulatory period [Australian Energy Regulator (AER), 2012]

	operation & maintenance	network upgrade
distribution	$35 billion	$36 billion
transmission	$15 billion	$7 billion

Retail electricity prices have risen from 2007 to 2012 by around 70%[5] [Productivity Commission, 2013, p. 104], strongest in VIC and NSW. The retail electricity prices are expected to increase further from 2011/12 until 2014/15 on average in Australia by 21% [Productivity Commission, 2013, p. 104]. Network services have a share of the total retail electricity prices between 45 and 55% [Productivity Commission, 2013, p. 108]. Figure 2.7 shows the cost distribution of the retail price published by Bureau of Resources and Energy Economics (BREE) [2014, p. 40] in 2012/13.

In the energy management plan for Queensland the governmental owned network operator Energex stated that each MW_{el} of additional capacity to be made available at peak times for the consumers would impose costs of in total $3.5 bil-

[5] 50% in real terms.

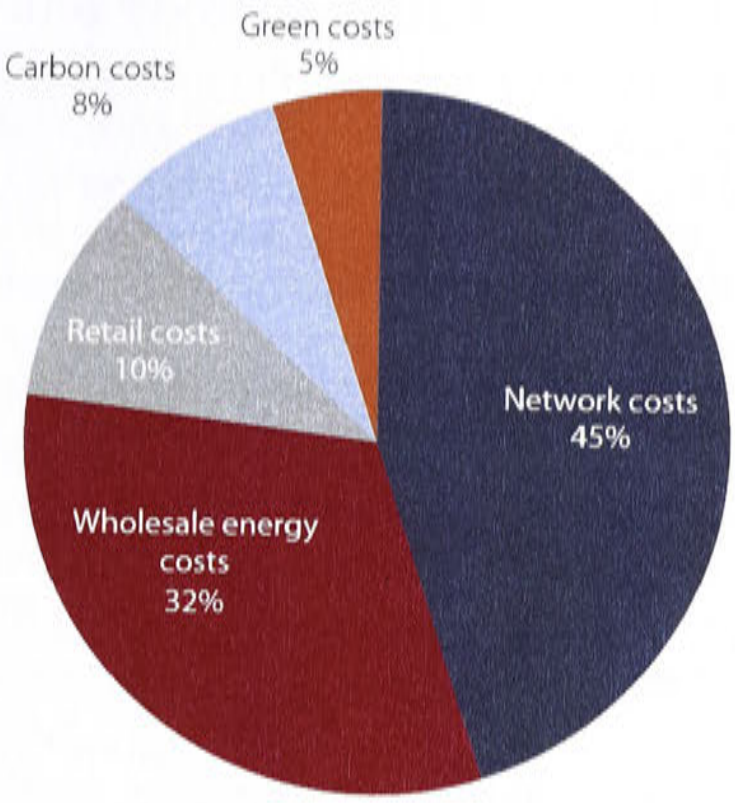

Figure 2.7: Cost allocation of electricity retail price in 2012 [Bureau of Resources and Energy Economics (BREE), 2014, p. 40]

lion dollars on the electricity grid. That number is comprised of $2.7 million for distribution and transmission network assets and $0.8 million for the electricity generation [Department of Employment, Economic Development and Innovation, 2011]. This has been interpreted as if each newly installed residential air-conditioner with a rated electricity consumption of $2\,kW_{el}$, costing $1500 would impose additional network costs on all electricity consumers of $7000. However, such a calculation might be too simple, because not every air-conditioner is switched on during peak demand or operates at full load. Furthermore, not every air-conditioner leads necessarily to new electricity generation or network infrastructure upgrades since those capital intensive decisions happen over time and take multiple developments into account. Nevertheless, the Productivity Commission revised the financial impact of each newly installed air-conditioner within the NEM electricity grid and suggests that an additional air-conditioner costing $2400 would represent an implicit subsidy of $33 from everybody not owning an air-conditioner [Productivity Commission, 2013], because everyone has to pay for the costly network upgrades.

Nevertheless, the Australian Energy Market Commission (AEMC) [2014] predicts a moderation of the retail electricity increase for the three years from 2012/13 to 2015/16. At a national level an average annual retail price increase of around 1.2% can be expected. The reason for this slow down is that the costly network infrastructure upgrades of the last regulatory period have now been completed. The average electricity prices in 2012/13 and the annual average price increase until 2015/16 in each NEM jurisdiction are listed in Table 2.5. Most states offer market driven retail prices and compared to "standing offers" set by jurisdictional regulators, they are 5% to 16% cheaper, but not available to everyone depending on their location. NSW, south-east QLD, SA, VIC and the ACT offer a market driven retail price structure. Tasmania has standing offers only. For the ACT the standing offer is presented in the

table as 80% of the population pay the standing offer rates.

The retail prices differ strongly between the states depending on population growth, industry, environmental schemes and other governmental regulations. The study has been published before the carbon tax repeal in July 2014 and the carbon price is still included.

Table 2.5: Average retail electricity price in each jurisdictions of the NEM. The assumed annual electricity consumption of the medium household size, which is presented here, varies between the states [Australian Energy Market Commission (AEMC), 2014] (MO: market offer, SO: standing offer)

	QLD (MO)	NSW (MO)	ACT (SO)	SA (MO)	VIC (MO)	TAS (SO)
transmission & distribution	53%	59%	40%	48%	39%	48%
wholesale & retail	28%	24%	38%	32%	42%	49%
environmental regulation	20%	17%	22%	20%	19%	3%
p_{el} 2012/13 [ct kWh^{-1}]	23.71	27.86	20.78	31.27	27.66	28.98
annual price increase until 2015/16	8.6%	-0.7%	-0.7%	-0.9%	1.3%	0.0%

There are varying trends of the electricity price development in each jurisdiction. For NSW, ACT and the SA the average prices are expected to decrease over the three years from 2012/13 to 2015/16. In TAS and VIC prices are expected to remain constant or increase by less than inflation. In Queensland prices are expected to increase and a significant part of this increase has already occurred in 2013/14. The main driver for the price increase in QLD is an end to a standing offer price freeze, which allows that cost from network infrastructure upgrades and cost from a closed "premium Queensland Solar Bonus scheme" can now be priced in.

Peak pricing is referred to as "flexible pricing options" in the report Australian Energy Market Commission (AEMC) [2014]. It is excluded from the calculation of average electricity pricing, because it was not available on a "broad scale" in the base year of 2012/13. Peak pricing is usually a pricing scheme dividing the times of usage in three blocks. The hours from Monday to Friday between 15:00 and 21:00 are commonly referred to as "peak", from Monday to Sunday between 22:00 and 7:00 as "off-peak" and consumption during the remaining hours of the week falls under the "shoulder" tariff. The report acknowledges the existence of peak-pricing and if the offers amongst retailers increase it will be considered in future reports. The Australian energy retailer and generator Origin offers three block peak electricity pricing for residences through their electricity distributors in the ACT, NSW, QLD and VIC [origin, 2014]. Origin is responsible for 13% of the Australian electricity generation, as stated on their website. The prices vary drastically from the highest peak electricity price in NSW with 0.51 \$ kWh^{-1} through the distributor AusGrid to the lowest offer in the ACT with 0.22 \$ kWh^{-1} through ActewAGL. On the contrary the solar feed-in tariff can be as low as 0.06 \$ kWh^{-1} in the ACT and NSW, depending on the year the system was installed.

2.6 Conclusion and recommendation

It can be said for Australia that the pre-conditions are met in favor for solar cooling. A high cooling load is paired with high insolation levels, increasing electricity prices and low population density, where space is not an issue. Cost on the other hand is an issue. The rebate scheme existing for solar hot water heaters may be extended to solar cooling and heating systems as outlined in section 2.2, taking into consideration the unique characteristics of each design.

Greenhouse gas reduction efforts require research to improve the energy efficiency of conventional residential air-conditioning systems or to develop other alternatives. This becomes especially important in regards to the HCFS phase out in 2015 and the HFC phase down in 2030. Conventional air-conditioning may become more challenging from a safety, financial and thermodynamically point of view, as alternative refrigerants will be necessary.

In regards to developing know-how in order to design and install solar cooling and heating systems in Australia, universities should include solar thermal technologies in their curriculum and training facilities should focus on teaching the handling of high pressure and temperature equipment as those skills are necessary when installing concentrating collectors with double (or triple) effect absorption chillers.

A peak electricity problem has been identified which is closely related to Australia's air-conditioning demand. In the following chapter this problem is investigated in detail and the effects of the already installed residential photovoltaic base is analyzed.

Chapter 3

The impact of air-conditioning and the uptake of photovoltaic on the NEM

Peak electricity demand is a recognized problem in Australia and residential air-conditioning is often proclaimed to be the main driver [Australian Energy Regulator (AER), 2012]. In this chapter the electricity consumption on the National Electricity Market (NEM) will be analyzed in detail in regards to the demand peaks in the afternoon in summer.

To investigate the relation between air-conditioning demand and electricity demand on the NEM in each state, a correlation coefficient between weather conditions and electricity demand will be calculated. To perform the calculations half hourly wholesale electricity demand data has been downloaded from the Australian Energy Market Operator (AEMO) website from the years 2005 to 2012 for each state [Australian Energy Market Operator (AEMO), 2013a]. The influence of the installed residential photovoltaic (PV) capacity since 2005 on this correlation coefficient will be investigated by modeling the solar electricity generation in each state using the software tool TRNSYS.

The weather data used to determine the correlation between electricity demand and air-conditioning demand has been obtained from the Bureau of Meteorology (BOM). The data included hourly ambient conditions (temperature, humidities etc.) and half-hourly solar exposure levels, where available.

The results of this chapter have been published in Doemland and Dennis [2013] at the Australian Solar Cooling 2013 Conference and it could be shown that the generated solar electricity had a positive effect on the peak electricity demand. The correlation between peak demand and air-conditioning intensive weather conditions was weakened.

3.1 Summer peak electricity demand on the NEM

The magnitude of peak electricity demand can be expressed in financial terms or physical terms. For example $11 billion in system (network & generation) capacity

assets is used for only 100 hours per year [Productivity Commission, 2013]. In physical terms it can be expressed as the "load factor" which is the average power demand in a certain time period (e.g. summer) relative to the maximum power drawn from the grid in that period. If the power demand is expressed in load duration curves, as in Figure 3.1, the gradient of the first 50-100 hours indicate the severity of the peak electricity problem.

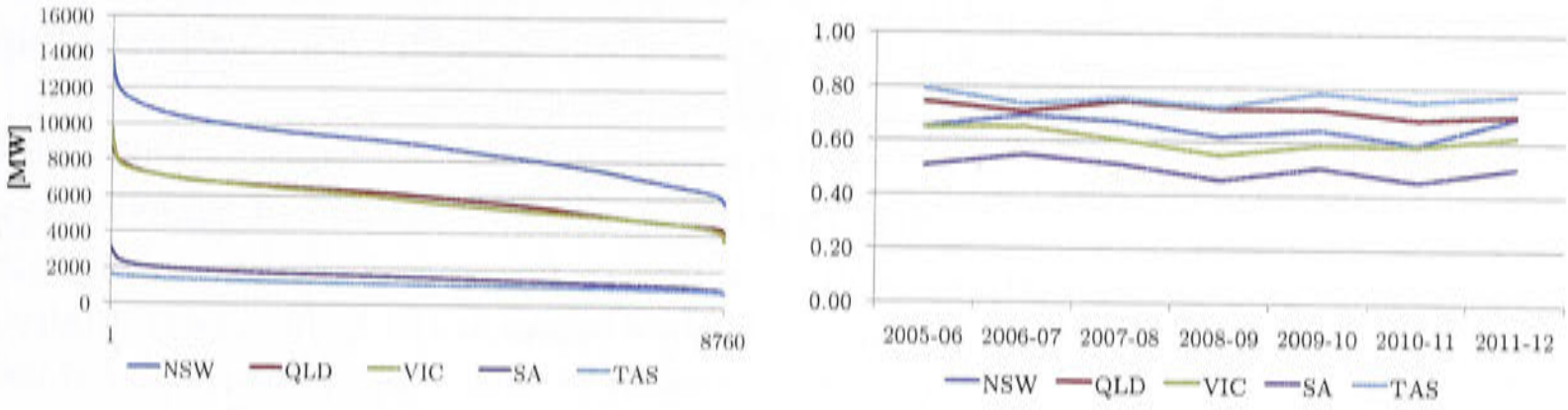

(a) Load duration curves 2010

(b) Summer load factor

Figure 3.1: Peak electricity demand on the NEM

Local system electricity peaks occur mainly in the distribution network and are often caused by high residential electricity demands around 18:00 - 20:00. They do not necessarily coincide with wholesale market peaks of demand and spot price. Those peaks occur around 13:00 and include industrial loads as well as residential loads.

Nevertheless, during peak times the residential load can take up more than 2/3 of the peak demand [Productivity Commission, 2013]. In this chapter the impact of air-conditioning on the peak electricity demand and will be shown and it will be distinguished between the jurisdictions on the NEM.

The Australian Electricity Market Operator (AEMO) provides half hourly aggregated price and demand data for each jurisdiction (NSW [1], QLD, VIC, SA and TAS[2]) and year back to 1998 [Australian Energy Market Operator (AEMO), 2013a]. Data processing macros were written to calculate the maximum electricity demand each day, the maximum electricity demand each summer and the annual maximum electricity demand. The macro also recorded corresponding dates and times. Subsequently load factors and load duration curves were derived from this data (Figure 3.1b). In Appendix A a relative and absolute load duration curve is shown for all jurisdictions in 2012. Furthermore, the electricity demand of the one day when the peak demand occurs is shown for each months in summer and winter in 2012. The time of the day of high demand is visible for each jurisdiction.

[1] includes the ACT

[2] Tasmania joined the NEM in 2005

3.2 The correlation between air-conditioning demand and weather conditions

In this section the air-conditioning demand is compared to the electricity demand which is represented by the half-hourly data supplied by AEMO. The air-conditioning demand is derived through the analysis of the temperature and humidity outdoor conditions in each region and for each year. This made the purchase of historical weather data necessary. It is assumed that most electricity demand in each jurisdiction is generated in the highly populated capital cities. Therefore, the weather profile of those cities was correlated to the air-conditioning demand.

Data sets for hourly ambient conditions (temperatures, humidities etc.) and half-hourly solar exposure levels were purchased from the Bureau of Meteorology (BOM). Unfortunately, the weather station in Brisbane only recorded weather data until February 2000. Therefore, Rockhampton has been chosen to be representative for Queensland. All other states were represented by their capital's weather data. More details about the processing of the weather data will follow in section 3.3.

Figure 3.2 shows the summer's peak electricity demand compared to severity of the weather which is expressed in days above 38°C and Figure 3.3 shows the change of the maximum electricity demand since 2005/06, which was set as the base year. The dip in 2009/10 in all states, besides QLD, could be an indicator for the global financial crisis (GFC) in 2008. It is followed by a jump in peak demand in NSW and SA in summer 2010/11 which might be due to recovery. QLD didn't seem to suffer much from the crisis since the summer maximum demand was even increasing until 2009/10. However, a second strong reason for the change in peak electricity demand seems to be the severity of weather. The summer of 2011/12 was rather mild (no days with maximum temperatures above 38°C) and the peak electricity demand dropped in all states. The peak electricity demand in QLD is rather steady and rather constant latent air-conditioning loads may be the main driver.

In the first approach the summer peak electricity demand has been compared to the air-conditioning demand in each state by calculating the correlation coefficient between the ambient temperature (T_{air}) and the electricity demand ($ElecD$) (equation 3.1). The variable $cov(T_{air}, ElecD)$ is the covariance of T_{air} and $ElecD$ and σ is the standard deviation. The electricity demand is assumed to show a strong variation with energy drawn for the supply of air-conditioning equipment. Other high electricity consumers (manufacturing plants, mining etc.) are not taken into account or are assumed to be rather independent of weather conditions[3].

$$corr(T_{air}, ElecD) = \frac{cov(T_{air}, ElecD)}{\sigma_{T_{air}} \cdot \sigma_{ElecD}} \tag{3.1}$$

In a second approach the air-conditioning demand has been represented by Δh,

[3]In a more detailed approach known electricity demand profiles from other electricity intensive industries could be derived and removed from the demand curve.

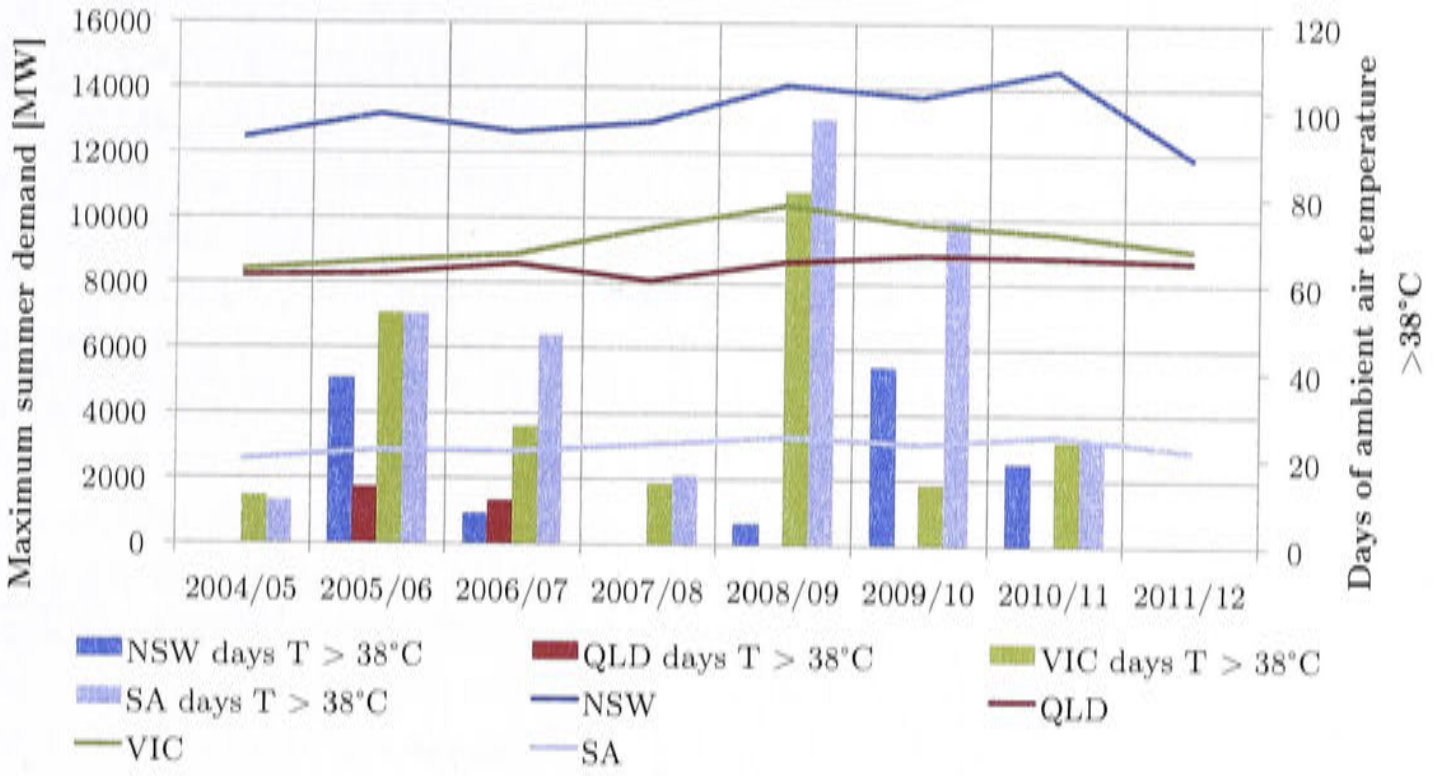

Figure 3.2: Summer maximum electricity demand and days above 38°C

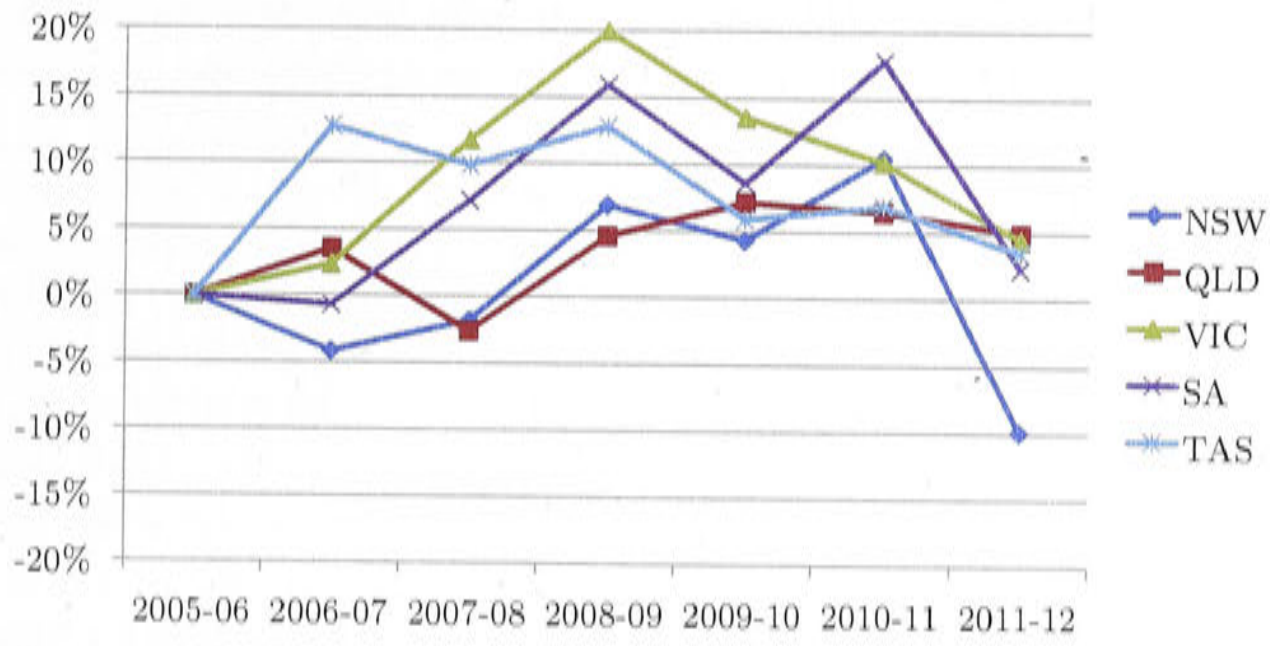

Figure 3.3: Change of summer peak demand since 2005/06

the difference between the enthalpy of the outdoor air and the set point indoor air enthalpy, determined by the set point temperature of 20°C and set point relative humidity of 50%. In equation 3.1 the air temperature T_{air} is replaced by Δh.

Both correlations have been performed with data points covering every half hour time interval for 24 hours of each summer's day and covering only the time period between 16:00 to 20:00 of each summer's day. The time frame was chosen, because higher correlation coefficients in that critical time period were expected.

The 24 hour correlation coefficients for T_{air} and $ElecD$ showed a very good correlation between 0.6 and 0.8 for all states, indicating a positive correlation. The 16:00 to 20:00 correlation coefficient for T_{air} and $ElecD$ is even larger (in the magnitude of 10%) in NSW, SA and VIC. Surprisingly, in QLD the correlation coefficient 4-8pm is unexpectedly low compared to the 24 hour coefficient. This may be due to

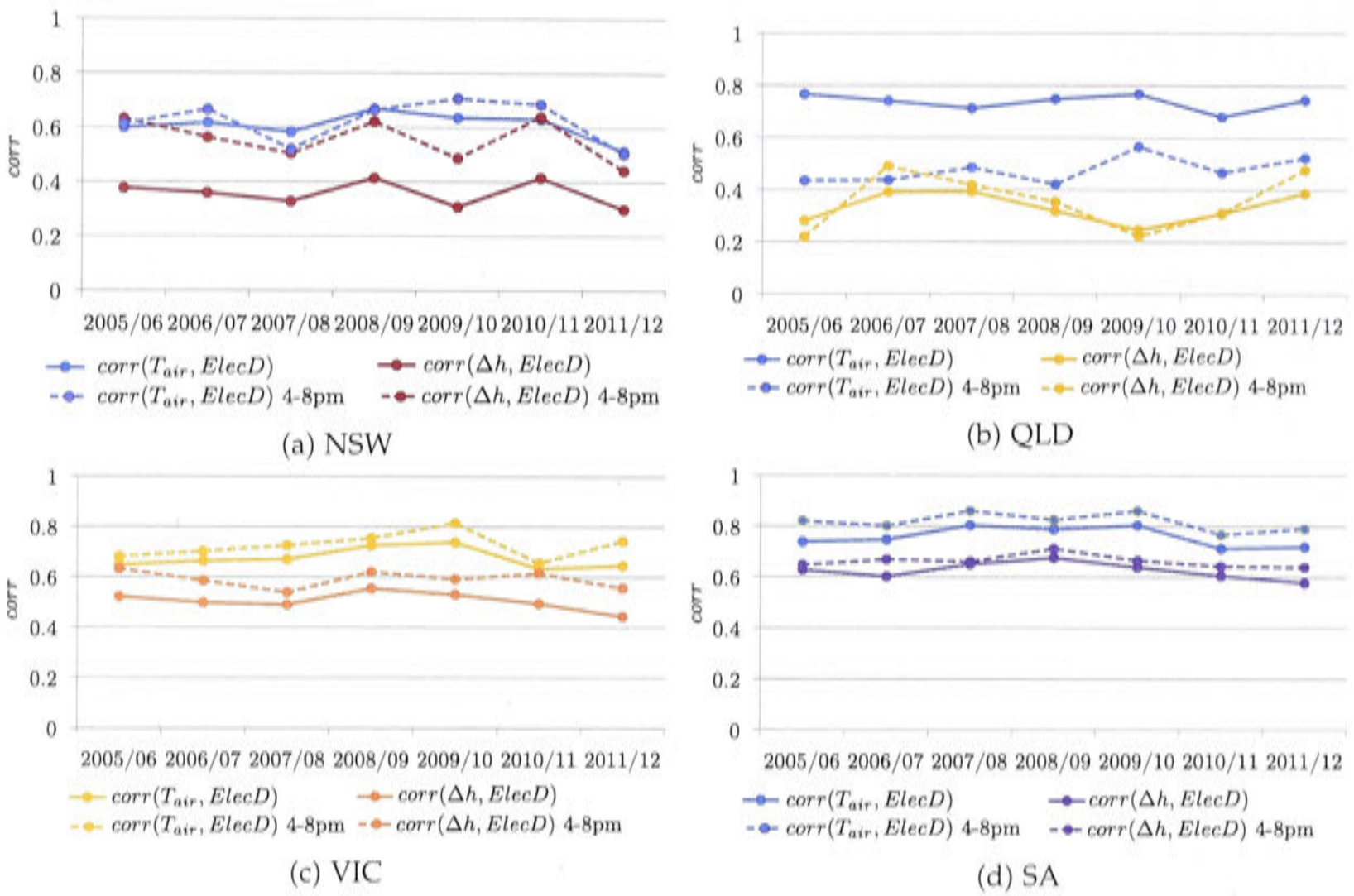

(a) NSW (b) QLD

(c) VIC (d) SA

Figure 3.4: Correlation coefficients between weather conditions and peak electricity demand

Queensland (Rockhampton) being a very humid climate and the air-conditioners are in operation all day. The air-conditioning demand is also determined by the latent cooling load. On some days the outdoor temperature can be relatively low, but air-conditioning is still needed due to high humidity. On other days if the humidity is not high, air-conditioning at the same temperature is not required and the correlation is weakened.

The correlation coefficient $corr(\Delta h, ElecD)$ for 24 hours is in general much lower in each state than the 24 hour coefficient for T_{air} and $ElecD$. Presumably this would have been different if the penetration of evaporative cooling would be higher, because high temperatures and low humidities result in a relatively small Δh. Cooling with evaporation would in theory be sufficient, but in reality the cooling effect is mainly generated by heat pumps. Therefore, at a small Δh there can be still a large electricity demand. Or in other words if the combination of humidity and temperature vary a lot in the climate zone the air-conditioner might switch on at low and high Δh and the correlation coefficient becomes weaker. Since SA is a rather steadily dry climate, this correlation coefficient is also relative high compared to the other states. It must be noted here, that in humid climates the humidity enters the building via infiltration, which should be as low as possible, and fresh outdoor air requirements. Therefore, the effect on the air-conditioning demand might be smaller than that of the air temperature which is directly linked to solar radiation and an increase of indoor temperature.

In QLD the Δh approach shows a good agreement between the 24 hour and the

16:00 to 20:00 correlation coefficients. Nevertheless, both are relatively low on the correlation scale. In NSW the Δh approach shows a much better correlation for the 16:00 to 20:00 coefficient than for the 24 hour coefficient, indicating a rather stable humidity and temperature conditions in this time interval.

For Tasmania the correlation coefficients were only between 10 and 20% which can be explained by the little need for cooling due to the cooler climate and the relatively long period over which summer is defined. A higher positive correlation might have been calculated for Tasmania if the summer months would have been reduced by 2 months (1st December - 28th February).

This section showed without modeling an actual air-conditioning system that a relatively strong correlation exists between air-conditioning demand and electricity demand. The following chapter will investigate if this correlation has been weakened over the past 3 years by the increase of PV in the electricity generation mix. The section will also investigate whether PV played a role in the reduction of summer peak demand and whether it influenced the correlation between air-conditioning demand and electricity supplied by the NEM.

3.3 The effects of PV on the peak electricity demand

The uptake of PV and solar hot water usage was driven by the renewable energy target and the energy efficiency schemes in Victoria and NSW. It was estimated to account for 53% of the reduction of total electricity demand in 2011 [Green Energy Market, 2012]. To determine the effect, the electricity generation from PV has been modeled in the NEM region from 2005 to 2012 using historical weather data from the same time period.

Marked on the map in Figure 3.5 are the locations where weather data was available and which are in the desired jurisdictions of the NEM. The locations are marked where half hourly solar exposure data from 2005 to 2012 was available. The other locations only provide hourly ambient weather conditions for the desired time period. All the weather stations available are listed in Appendix B, including the last year of solar exposure recordings.

The hourly weather data included the ambient temperature, relative humidity, wet bulb temperature, dew point temperature, vapour pressure and saturated vapor pressure, wind speed, wind direction and speed of maximum wind gust in the last 10 minutes prior to record, cloud amount and height of four cloud groups in eighths, the horizontal visibility in km, station level pressure and sea level pressure.

Recorded solar exposure data was available in four different measurements. The total (global) radiation on the horizontal surface ($G_{tot,hor}$), the direct (or beam) radiation on the horizontal ($G_{direct,hor}$), the diffuse radiation on the horizontal ($G_{diff,hor}$) and the direct (or beam) radiation (G_{direct}) on a plane perpendicular to the sun's rays. The diffuse radiation on the horizontal is the total radiation apart from the direct radiation falling on this surface. Values were expressed in MJ m^{-2} and were recorded every 30 min.

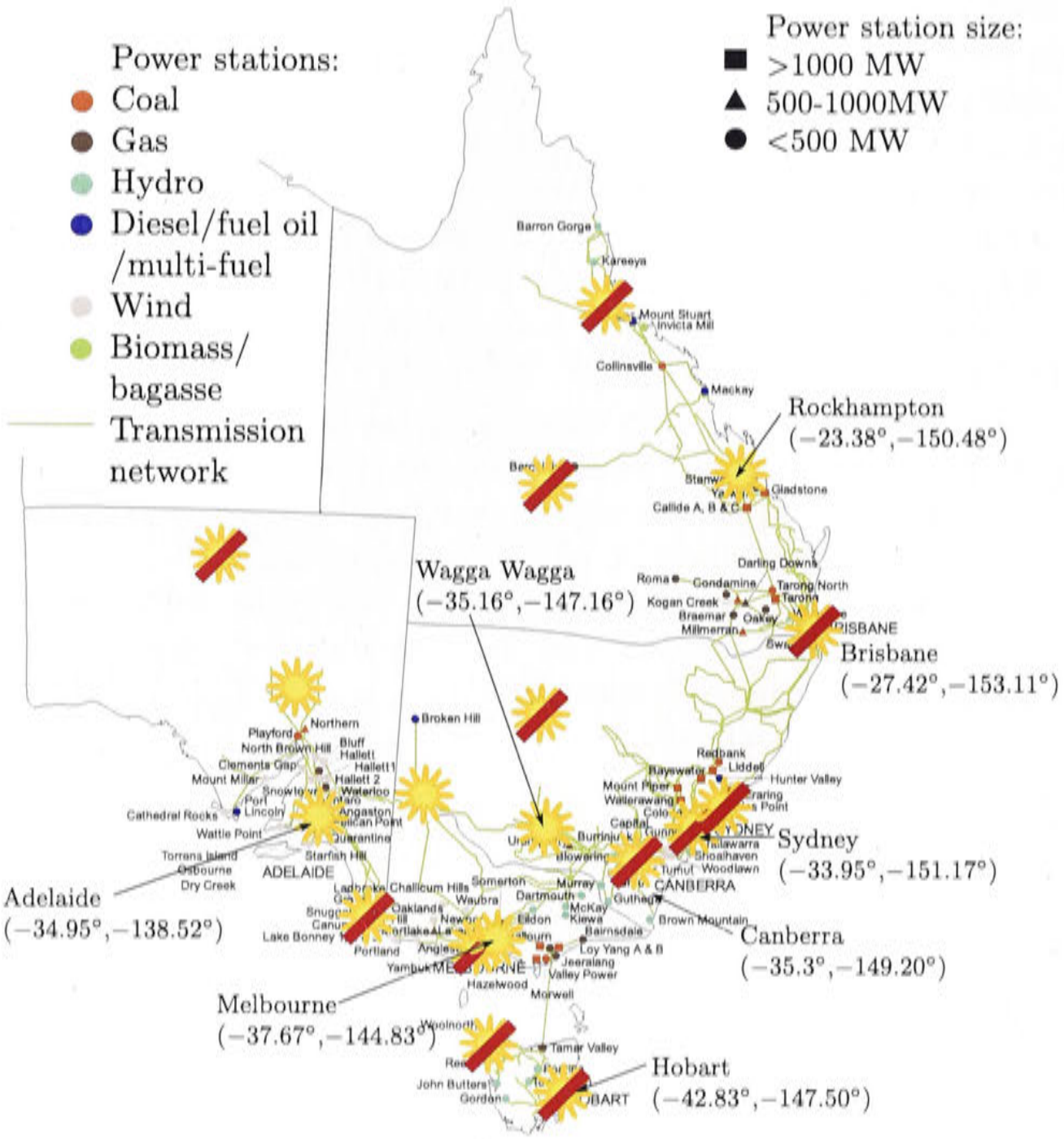

Figure 3.5: Power generators on the NEM [Australian Energy Regulator (AER), 2012, p. 31] and weather stations with and without solar exposure recording between 2005 and 2012

Data processing macros were written to calculate the correlation between electricity supplied on the NEM and air-conditioning demand for the previous section 3.2. Furthermore, to model the PV generation, weather files needed to be created from the BOM data which served as input files for the TRNSYS weather data reader type 109. The final format covered half-hourly time steps and an excerpt is presented in Figure 3.6.

Appendix B lists the locations of which weather data could be obtained. For some locations and time periods the weather data was incomplete and needed further processing. Each location was flagged from 1 to 3 to distinguish between the types of solar radiation measurements.

Flag=1 indicates that only the global radiation on the horizontal was recorded ($G_{tot,hor}$).

Flag=2 indicates that all four types of solar radiation have been recorded: global radiation on the horizontal ($G_{tot,hor}$), direct radiation on the horizontal ($G_{direct,hor}$),

the direct/beam radiation (G_{direct}) and the diffuse radiation on the horizontal ($G_{diff,hor}$).

Flag=3 indicates that only the diffuse radiation on the horizontal $G_{diff,hor}$ and the global radiation on the horizontal ($G_{tot,hor}$) have been recorded.

For the six locations in Table B.1, which are marked with flag=1, no weather files could be created. Locations with flag=2 could be used to fill in all solar radiation requirements for type 109 (Figure 3.6)[4]. For locations marked with flag=3, the direct radiation on the horizontal $G_{direct,hor}$ and the direct beam radiation G_{direct} had to be calculated and the methodology is explained in Appendix B. The data processing scripts generated weather data files for each year from 2005 to 2012 where this was possible.

For Melbourne (VIC) and Adelaide (SA) there was appropriate weather data with recorded solar exposure available from 2005 to 2012. For QLD the city of Rockhampton was chosen. Due to the poor availability of solar radiation data in NSW between 2005 and 2012, the solar exposure of Wagga Wagga had to be chosen for Canberra and Sydney. To account for the difference in location solar radiation factors (Table 3.1) have been calculated on the basis of the difference in average daily solar exposure for each month [Bureau of Meteorology (BOM), 2013a]. Those factors have been multiplied with every half our radiation value and the weather file for Wagga Wagga was manipulated accordingly. In the same way an adjusted weather file of Melbourne was generated to represent Hobart (TAS) since no solar exposure data for TAS was available

Modeling the electricity generation from PV throughout the NEM from 2005 to 2012 is not simple since no data is available on the exact locations of the systems, single system size, orientations, shading, quality and deterioration. Nevertheless, a

[4]IBEAM_H is $G_{direct,hor}$, IBEAM_N is G_{direct}, IGLOB_H is $G_{tot,hor}$ and IDIFF_H is $G_{diff,hor}$

Adelaide_2005.109 - Notepad

File Edit Format View Help

```
<userdefined>
<longitude>     -138.52         ! east of greenwich negative
<latitude>      -34.95
<gmt>     solar
<interval>      0.5             ! Data file time interval between consecutive lines
<firsttime>     0          ! Time corresponding to first data line (hours)
<var>   IBEAM_H <col>   1  <interp> 0  <add>  0  <mult>  1       <samp>  -1     !...to get radiation in w/m*
<var>   IBEAM_N <col>   2  <interp> 0  <add>  0  <mult>  1       <samp>  -1     !...to get radiation in w/m*
<var>   IDIFF_H <col>   3  <interp> 0  <add>  0  <mult>  1       <samp>  -1     !...to get radiation in w/m*
<var>   IGLOB_H <col>   4  <interp> 0  <add>  0  <mult>  1       <samp>  -1     !...to get radiation in w/m*
<var>   TAMB    <col>   5  <interp> 1  <add>  0  <mult>  1       <samp>  -1     !...to get 'C
<var>   RHUM    <col>   6  <interp> 1  <add>  0  <mult>  1       <samp>  -1     !...to get relative humidity in %
<var>   WSPEED  <col>   7  <interp> 1  <add>  0  <mult>  1       <samp>  -1     !...to get wind speed in m/s
<var>   WDIR    <col>   8  <interp> 1  <add>  0  <mult>  1       <samp>  -1     !...to get wind direction in degree
<var>   udef1   <col>   0  <interp> 0  <add>  0  <mult>  1       <samp>   0     !...to get ... in ...
<var>   udef2   <col>   0  <interp> 0  <add>  0  <mult>  1       <samp>   0     !...to get ... in ...
<var>   udef3   <col>   0  <interp> 0  <add>  0  <mult>  1       <samp>   0     !...to get ... in ...
<var>   udef4   <col>   0  <interp> 0  <add>  0  <mult>  1       <samp>   0     !...to get ... in ...
<data>
0000.0  0000.0  0000.0  0000.0  23.8    036.0   004.1   200
0000.0  0000.0  0000.0  0000.0  23.4    035.5   004.4   200
0000.0  0000.0  0000.0  0000.0  23.0    035.0   004.6   200
0000.0  0000.0  0000.0  0000.0  22.8    037.5   004.6   195
0000.0  0000.0  0000.0  0000.0  22.6    040.0   004.6   190
0000.0  0000.0  0000.0  0000.0  22.2    044.0   003.4   170
0000.0  0000.0  0000.0  0000.0  21.8    048.0   002.1   150
0000.0  0000.0  0000.0  0000.0  22.2    044.0   002.4   095
0000.0  0000.0  0000.0  0000.0  22.6    040.0   002.6   040
0000.0  0000.2  0004.5  0004.5  21.9    054.0   003.4   130
0002.1  0025.7  0030.5  0032.4  21.1    068.0   004.1   220
```

Figure 3.6: Example input file for TRNSYS weatherfile reader type 109

Table 3.1: Solar radiation factors (H=Hobart, M=Melbourne, S=Sydney, C=Canberra, W=Wagga Wagga)

	Jan	Feb	Mar	Apr	May	Jun	Jul	Aug	Sep	Oct	Nov	Dec
H:M	0.84	0.86	0.81	1.09	0.75	0.50	0.38	0.67	0.89	0.92	0.95	1.00
C:W	0.94	0.92	0.93	0.88	0.92	1.00	1.00	1.00	0.94	0.95	0.96	0.94
S:W	0.89	0.88	0.81	0.93	1.00	1.13	1.22	1.08	1.00	0.89	0.84	0.89

rough estimation can be performed from knowing the installed capacities in each state. The Clean Energy Council published data on installed PV systems in 2011 until September 2011. The installed capacity has been extrapolated to 2012 using the average monthly growth rate in the first 9 month of 2011 [Clean Energy Council, 2011], resulting in a total capacity of 1200 MW being installed in 2011 and 1800 MW in 2012 (Table 3.2)[5].

Table 3.2: Installed photovoltaic capacity in MW in each state

	2005	2006	2007	2008	2009	2010	2011	forecast 2012
ACT	0.04	0.05	0.02	0.72	1.94	6.92	25.68	44.44
NSW	0.67	0.91	2.01	6.10	24.46	173.65	403.01	632.37
QLD	0.39	0.49	1.06	5.10	29.11	119.17	322.23	525.29
SA	1.87	2.54	3.71	8.52	20.65	53.01	166.54	280.08
VIC	0.83	1.13	2.10	4.89	15.90	74.67	189.57	304.47
TAS	0.03	0.03	0.07	0.30	1.98	4.84	10.00	15.15
Total	3.81	5.16	8.96	25.63	94.04	432.26	1117.03	1801.80

A single residential system has been modeled using the modeling software suite TRNSYS with a rated solar system capacity of 2.5 kW_{el}. The parameters for the panels and the inverter were taken from catalog data[6]. Knowing the installed capacity in each jurisdiction the multiplier for the single PV array power output could be determined. A shading factor was also introduced reducing the array output by 5% until 8am and starting to drop to 0.5% at 1pm and rising again until it reaches 5% at 6pm.

3.4 Results from the PV modeling

Using the results from the simulations, the PV power generated in each half-hour time step was added to the wholesale electricity demand. In this manner it became apparent how much electricity the grid would have had to provide if no photovoltaic systems were installed. The correlation coefficients from the previous chapter were calculated again and they showed an interesting result. The correlation became weaker since 2009/10 when the PV industry started growing due to governmental subsidies (Figure 3.7). Or in other words, it became stronger if the electricity grid had had to provide the electricity generated by the PV systems as well.

[5]Today the most recent report from the clean energy council states that by the end of 2013 2900 MW of PV were installed in the seven states, excluding NT and WA [Clean Energy Council, 2013]

[6]PV panel E19 318W from the American manufacturer Sunpower and the inverter SunnyBoy 3000 from the German manufacturer SMA

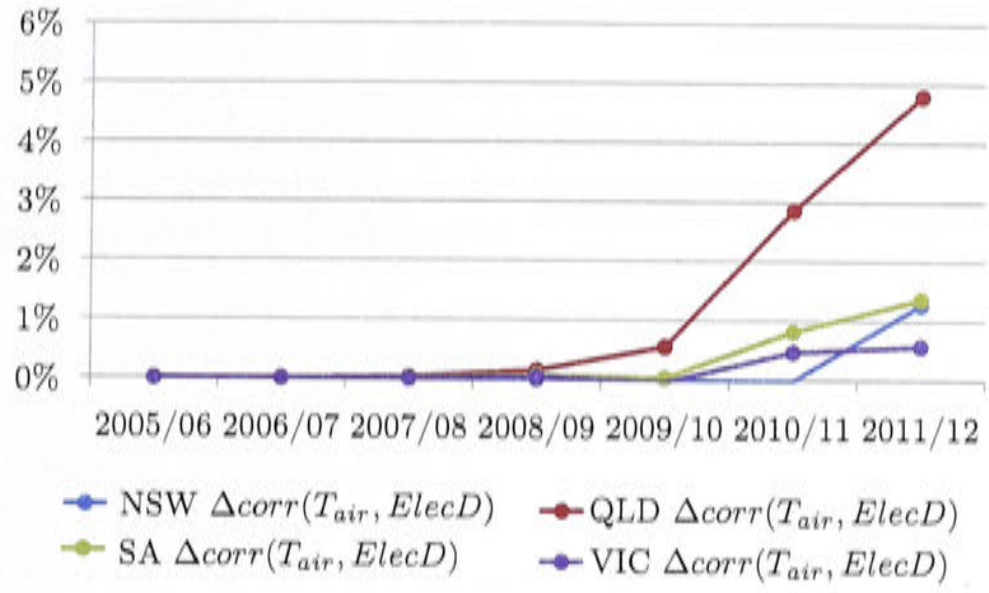

Figure 3.7: Percentage in increase of correlation coefficients between the air temperature (T_{air}) and the maximum electricity demand ($ElecD$) if no PV was installed

Even though the model was relatively simplistic, the increase in photovoltaic generation lead to a marginal reduction of summer electricity peak demand in each state (less than 5%) until 2012 (Figure 3.8). The summer peak demand in 2012 has also been shifted later in the afternoon in NSW, QLD and SA, but only by half an hour. A shift of the peaks towards the late afternoon has been stated also by the Australian Energy Market Operator (AEMO) [2012] in their national forecast report 2014. The report includes an historical model of past solar electricity contributions and future estimations on PV development. The AEMO and their partners developing the model had access to more detailed information and conducted this study published in 2013. The simulation base of installed solar electric systems is the same as for this study, coming from the Clean Energy Regulator, but additional systems from 2012 and 2013 are included. The PV generation is directly incorporated in the AEMO's electricity demand forecasting model. More information can be found in Chapter 4 of the forecasting information paper by the Australian Energy Market Operator (AEMO) [2013b].

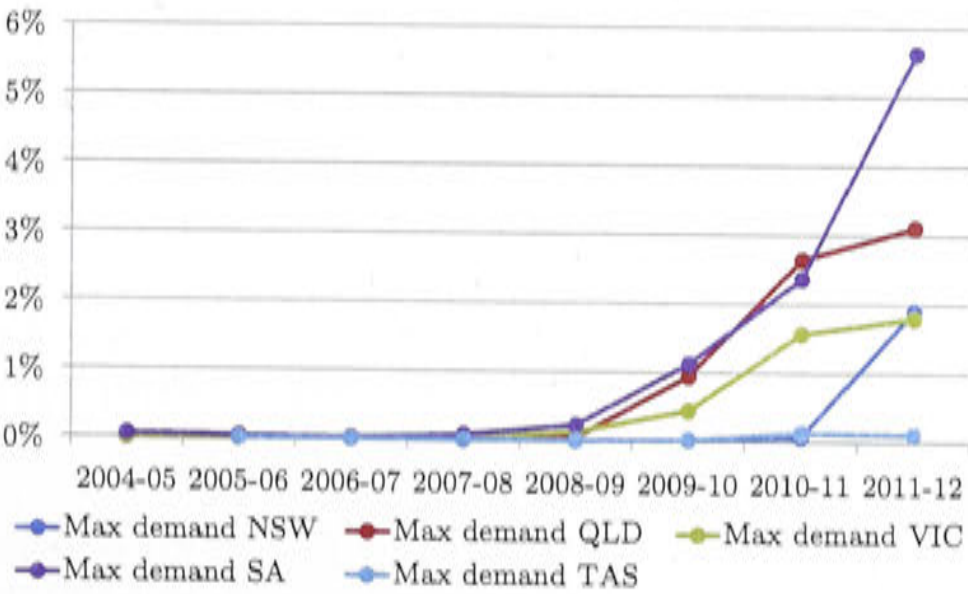

Figure 3.8: Percentage increase of maximum summer electricity demand if no PV was installed

3.5 Conclusion

From the results of this chapter it can be seen that there is a correlation between air-conditioning requirements and the wholesale peak electricity demand on the NEM. The installation of PV systems on Australian homes since 2009 has already weakened that correlation.

The results were obtained from a macro analysis. On the contrary, the next chapters will zoom in on a single building in seven different Australian climate zones. A typical residential building model with cooling, heating and domestic hot water demand will be developed and solar electric as well as solar thermal alternatives are compared to each other in detail on an annual base. Additional performance measures will be introduced apart from the potential for peak electricity demand reduction.

Chapter 4

Modeling residential solar cooling, heating and DHW systems in Australia - overview

This chapter describes the common features of all models covered in this feasibility study and introduces the performance parameter the systems are evaluated with.

The performance parameters which are going to be used in this work to rate solar assisted HVAC (and DHW) systems are explained in detail to emphasize their significance. The performance of a system is evaluated considering economic, financial and comfort related aspects. Furthermore, a novel overall performance factor (OPF) for Australia is introduced, which merges the three performance indicators. A building model serves as the load and is modified to represent a typical building structure in the different climate zones and to compare the HVAC (and DHW) systems against each other. The model consists of three zone and six room with a conditioned space of 230 m^2.

In Europe the systems which are simulated here are called "Combi+" systems, indicating that heating, cooling and DHW are supplied for an overall energy analysis of the building. The performance analysis in this work distinguishes between a mere HVAC system (heating and cooling) and the HVAC and DHW system, which includes the generation of DHW.

4.1 Simulation software tools

During the IEA-SHC task 38 in 2009 different available simulation tools for solar thermal cooling systems were analyzed, including TRNSYS [Bourdoukan, 2009]. Other software packages presented in this report are INSEL, EES, EnergyPlus and Easycool, but of those TRNSYS is the most popular tool. INSEL has been developed in Germany and is used for the modeling work in Eicker [2014]. EnergyPlus is a building modeling tool from the US and EES is an engineering equation solver software.

The objective to develop other simulation tools apart from TRNSYS are simplicity and user friendliness. The company vela solaris [2014] offers the software package Polysun, which includes models and performance information of mainly on the Eu-

ropean market available components for solar thermal, solar electric and geothermal systems. There is no option to program own components but updates can be purchased annually. Another commercially available modeling environment is Dymola [Dassault Systems, 2014], which uses the open source language modelica for object-orientated programming of physical systems and claims a large degree of freedom for its users. Libraries are included as well, but it is not as widely spread in the solar cooling community as TRNSYS. If it proofs to be more user friendly it is likely to become a strong competitor to TRNSYS.

The ANU has acquired much experience and a strong knowledge base with the use of TRNSYS over the last 10 years. Furthermore, the solar thermal performance standard for solar hot water heaters in Australia was developed based on energy calculations around a building load in TRNSYS 15 [Australian/ New Zealand Standard, 2008]. The TRNSYS package comes with an extensive library of components for modeling solar thermal systems and the individual components don't have to be re-invented.

TRNSYS provides a high degree of freedom for the user to develop customized components, for example in this work an absorption chiller and a latent cold storage tank. To do so, a compiler is necessary (here © Compaq Computer Corporation [2000]) which has to be purchased in addition to the TRNSYS software. Nevertheless, debugging can be tedious and is not very user friendly.

The software TRNSYS 16.1 [Thermal Energy System Specialists (TESS), 2007] has been chosen as a transient simulation modeling tool for all solar cooling, heating and DHW systems in this work. In order for the hundreds TRNSYS simulations to be performed in a semi automatic way an excel macro was created to modify input files for the TRNSYS simulations. Further data automation macros were written to process the TRNSYS results files. The macros were extended to allow parallel processing of simulations such that the time could be reduced to $\approx$30 min to 45 min on the Dell precision T3400 (2.83 GHz and 7.93 GB of Ram). For all HVAC (and DHW) simulations modeled in TRNSYS a time step of 0.05 hours (3 min) is chosen as a compromise between data file size, run time and accuracy. The convergence tolerance is ≤ 0.001. Reducing the convergence tolerance leads to higher accuracy but longer run time.

4.2 Performance parameters for domestic cooling, heating and hot water systems

In the first part of this section performance indicators are defined for HVAC (and DHW) systems. An overall performance factor (OPF) is introduced which takes into account the location and the population density in the different Australian climates and is comprised of three parts, the greenhouse gas emissions, the specific cost and the comfort achieved by the system.

The motivation behind the development of this OPF with three parts is different to a mere economic approach which would put a fictive price on comfort and

greenhouse gas emissions in order to include them in the specific cost.

Greenhouse gas emissions (GHG) are part of the environmental impact of the HVAC (and DHW) system and so is the water consumption for re-cooling. The water consumption is included in the specific cost. It is assumed that the system is integrated in a market where supply and demand determine the cost of water. Hence, the price reflects if there's a drought or if water is abundantly available.

For greenhouse gas emissions, there is not such a market in Australia and therefore greenhouse gas emissions are not included in the specific cost. A price on comfort or a penalty on discomfort, would be the way to include comfort in the specific cost in order to compare different systems. Setting this fictive price is very subjective and the cost term would become distorted. To keep the cost as a real term, the OPF was developed to allow for an arbitrary weighting of any of the three impacts comfort, GHG emissions and cost in order to provide freedom of preference to the user.

4.2.1 Technical and environmental parameters

The solar fraction SF can be either defined for solar thermal systems (equations 4.1 and 4.2) or for photovoltaic driven systems (equations 4.3 to 4.6). The terms $\dot{Q}_{c,hw}$, $\dot{Q}_h$ and $\dot{Q}_{dhw}$ denote the instantaneous heat demand from the hot water tank or the auxiliary heater for cooling, heating and domestic hot water. In case the indoor humidity is controlled, the term $\dot{Q}_{reheat}$ accounts for the additional heat to warm up the supply air stream after over-chilling. The terms $\dot{Q}_{aux,HVAC}$ and $\dot{Q}_{aux,dhw}$ are the instantaneous auxiliary heat demands for the HVAC and the DHW system.

$$SF_{th} = 1 - \frac{\int\limits_{year} \dot{Q}_{aux,HVAC}\,\mathrm{d}t}{\int\limits_{year} \left(\dot{Q}_{c,hw} + \dot{Q}_h\left(+\dot{Q}_{reheat}\right)\right)\,\mathrm{d}t} \tag{4.1}$$

$$SF_{th,dhw} = 1 - \frac{\int\limits_{year} \left(\dot{Q}_{aux,HVAC} + \dot{Q}_{aux,dhw}\right)\,\mathrm{d}t}{\int\limits_{year} \left(\dot{Q}_{c,hw} + \dot{Q}_{dhw} + \dot{Q}_h\left(+\dot{Q}_{reheat}\right)\right)\,\mathrm{d}t} \tag{4.2}$$

When looking at photovoltaic driven solar HVAC systems, there are two possible ways to define the solar fraction.

The first one is $SF_{el,LCov}$ where "LCov" stands for "load coverage" and denotes that the solar electricity included in the solar fraction must be generated at the same time of HVAC (and DHW) electricity demand.

When assuming that the house is connected to the electricity grid and there is no storage option available, the electricity which is not consumed for HVAC or DHW is transferred to the grid. If there is a storage option the solar electricity supplies the HVAC system first and the surplus electricity is stored in the battery to be used at a later time. In equation 4.3 and 4.4 $\dot{E}_{el,sol\rightarrow HVAC(\&DHW)}$ is the solar electricity which supplies the HVAC system directly. If there's a surplus of solar

electricity, the electricity which charges the battery is $\dot{E}_{el,sol\rightarrow bat}$. The total electricity consumption $\dot{E}_{el}$ in the denominator corresponds to either cooling, heating or DHW as indicated by the subscripts "c", "h"and "dhw". In this work the electricity consumption for the cooling and heating system may have the subscript "HVAC" or "HVAC&DHW" if DHW is included. In that case the electricity consumption is written as $\dot{E}_{el,HVAC(\&DHW)} = \dot{E}_{el,c} + \dot{E}_{el,h}(+\dot{E}_{el,dhw})$.

$$SF_{el,LCov} = \frac{\int\limits_{year} \dot{E}_{el,sol\rightarrow HVAC} \left(+\dot{E}_{el,sol\rightarrow bat}\right) \mathrm{d}t}{\int\limits_{year} \left(\dot{E}_{el,c} + \dot{E}_{el,h}\right) \mathrm{d}t} \tag{4.3}$$

$$SF_{el,LCov,dhw} = \frac{\int\limits_{year} \dot{E}_{el,sol\rightarrow HVAC\&dhw} \left(+\dot{E}_{el,sol\rightarrow bat}\right) \mathrm{d}t}{\int\limits_{year} \left(\dot{E}_{el,c} + \dot{E}_{el,h} + \dot{E}_{el,dhw}\right) \mathrm{d}t} \tag{4.4}$$

The index "tot" denotes that the solar fraction includes the total solar electricity $E_{el,sol}$ over the specific time interval regardless of the time of generation.

$$SF_{el,tot} = \frac{\int\limits_{year} \dot{E}_{el,sol} \mathrm{d}t}{\int\limits_{year} \left(\dot{E}_{el,c} + \dot{E}_{el,h}\right) \mathrm{d}t} \tag{4.5}$$

$$SF_{el,tot,dhw} = \frac{\int\limits_{year} \dot{E}_{el,sol} \mathrm{d}t}{\int\limits_{year} \left(\dot{E}_{el,c} + \dot{E}_{el,h} + \dot{E}_{el,dhw}\right) \mathrm{d}t} \tag{4.6}$$

In all cases there is a differentiation between the mere energy consumption for the HVAC system or including the domestic hot water demand, which is denoted using the index "dhw". The hot water demand schedule has been taken from the Australian standard AS/NZS 4234 [Australian/ New Zealand Standard, 2008], according to which the daily energy consumption is drawn from the tank in eight 6 min intervals throughout the day. It is questionable how close those intervals resemble reality and how useful the domestic hot water electricity demand profile is when looking at peak electricity demand reduction.

Another important performance indicator is the specific electricity consumption throughout the year ES_{el}[1] (equation 4.7), which is a measure of the total electricity used for the generation of 1 kWh of cooling and heating. $\dot{Q}_c$, $\dot{Q}_h$ and $\dot{Q}_{dhw}$ represent the instantaneous supplied cooling and heating energies to the zones. If domestic hot water is included, the subscript "dhw" is added.

[1]The reciprocal of this number is the commonly used seasonal performance factor.

$$ES_{el} = \frac{\int\limits_{year} \dot{E}_{el,c} + \dot{E}_{el,h} \, \mathrm{d}t}{\int\limits_{year} \left(\dot{Q}_c + \dot{Q}_h\right) \mathrm{d}t} \tag{4.7}$$

$$ES_{el,dhw} = \frac{\int\limits_{year} \dot{E}_{el,c} + \dot{E}_{el,h} + \dot{E}_{el,dhw} \, \mathrm{d}t}{\int\limits_{year} \left(\dot{Q}_c + \dot{Q}_h + \dot{Q}_{dhw}\right) \mathrm{d}t} \tag{4.8}$$

Parasitic energy consumption is defined as energy consumption (here electricity) which supplies equipment like pumps and fans. Auxiliary energy consumption is the energy consumption which supplements the heating and cooling system in form of a backup. This is usually gas boosting the heat supplied to the hot water or an electric additional heat pump. Often the auxiliary energy is called supplementary energy. Both, parasitic and auxiliary energy consumption can be calculated including or excluding DHW.

When looking at thermally driven solar systems, the $SF_{th(,dhw)}$ only deals with quantities of heat and the $ES_{el(,dhw)}$ only accounts for the electricity consumption but not for auxiliary heat supply (e.g. gas for boosting). To find a mutual factor to compare the performance the prime energy consumption can be calculated using the primary efficiency factors of the region the system operates in. The difference between the primary energy consumption specific to the generated cooling, heating (and DHW) of a reference system PE_{ref} compared to specific primary energy consumption of the solar system PE, defines the saved primary energy per kWh of cooling and heating ΔPE (equation 4.9). The reference system is identified by the subscript "ref" whereas the solar alternative has no subscript.

ΔPE can be calculated with and without domestic hot water. In Australia where hot water generation is mainly done by electricity, the primary energy savings are much larger if domestic hot water is included.

$$\begin{aligned} \Delta PE &= PE_{ref} - PE \\ PE_{ref} &= \frac{\int\limits_{year} \dot{E}_{el,HVAC,ref} \xi_{el} \, \mathrm{d}t}{\int\limits_{year} \left(\dot{Q}_{h,ref} + \dot{Q}_{c,ref}\right) \mathrm{d}t} \\ PE &= \frac{\int\limits_{year} \left(\dot{E}_{el,HVAC} \xi_{el} + \dot{Q}_{aux} \xi_{gas}\right) \mathrm{d}t}{\int\limits_{year} \left(\dot{Q}_h + \dot{Q}_c\right) \mathrm{d}t} \end{aligned} \tag{4.9}$$

$$\begin{aligned}
\Delta PE_{dhw} &= PE_{dhw,ref} - PE_{dhw} \qquad (4.10)\\
PE_{dhw,ref} &= \frac{\int\limits_{year} \dot{E}_{el,HVAC\&DHW,ref}\xi_{el}\,\mathrm{d}t}{\int\limits_{year} \left(\dot{Q}_{h,ref} + \dot{Q}_{c,ref} + \dot{Q}_{dhw,ref}\right)\,\mathrm{d}t}\\
PE_{dhw} &= \frac{\int\limits_{year} \left(\dot{E}_{el,HVAC\&DHW}\xi_{el} + \dot{Q}_{aux}\xi_{gas}\right)\,\mathrm{d}t}{\int\limits_{year} \left(\dot{Q}_{h} + \dot{Q}_{c} + \dot{Q}_{dhw}\right)\,\mathrm{d}t}
\end{aligned}$$

The primary energy factors were calculated with data available from the Australian energy statistics data in 2012 [Bureau of Resources and Energy Economics (BREE), 2014]. The primary energy factor in each state was found by the ratio of the total primary (non-renewable) energy used to the total electricity generated in each state[2]. If gas is used as auxiliary energy to back up the HVAC (and DHW) system, a primary energy factor of 1 is assumed. The primary energy factors are displayed in Table 4.1 together with the greenhouse gas factors.

Table 4.1: Primary energy and greenhouse gas factors for the chosen locations, depending on their states

	Primary energy factors		**GHG emission factors**	
	ξ_{el} -	ξ_{gas} -	τ_{el} $\mathrm{kg_{CO2\text{-}eq}\,kWh_{el}^{-1}}$	τ_{gas} $\mathrm{kg_{CO2\text{-}eq}\,kWh_{gas}^{-1}}$
Canberra	2.48	1	0.88	0.18
Brisbane	2.67	1	0.86	0.18
Sydney	2.48	1	0.88	0.18
Griffith	2.48	1	0.88	0.18
Tennant Creek	2.92	1	0.71	0.18
Darwin	2.92	1	0.71	0.18
Melbourne	3.41	1	1.19	0.18

Instead of using primary energies in this work the author decided to express the environmental impact and fossil fuel efficiency in terms of greenhouse gases emitted (GHG) or saved (ΔGHG) by the solar system compared to the reference system. The value is specific to the cooling and heating energies supplied and may or may not include the domestic hot water generation, specified by the subscript "dhw". Greenhouse gas emission factors τ are published by the Australian government Department of Climate Change and Energy Efficiency [2012]. Similar to the primary energy factors they are location dependent.

[2]The updated information can be found on the Australian government website referred to in Bureau of Resources and Energy Economics (BREE) [2014].

$$\begin{aligned} \Delta GHG &= GHG_{ref} - GHG \\ GHG_{ref} &= \frac{\int\limits_{year} \dot{E}_{el,HVAC,ref}\,\tau_{el}\,\mathrm{d}t}{\int\limits_{year} \left(\dot{Q}_{h,ref} + \dot{Q}_{c,ref}\right)\,\mathrm{d}t} \\ GHG &= \frac{\int\limits_{year} \left(\dot{E}_{el,HVAC}\,\tau_{el} + \dot{Q}_{aux}\,\tau_{gas}\right)\,\mathrm{d}t}{\int\limits_{year} \left(\dot{Q}_h + \dot{Q}_c\right)\,\mathrm{d}t} \end{aligned} \tag{4.11}$$

$$\begin{aligned} \Delta GHG_{dhw} &= GHG_{dhw,ref} - GHG_{dhw} \\ GHG_{dhw,ref} &= \frac{\int\limits_{year} \dot{E}_{el,HVAC\&DHW,ref}\,\tau_{el}\,\mathrm{d}t}{\int\limits_{year} \left(\dot{Q}_{h,ref} + \dot{Q}_{c,ref} + \dot{Q}_{dhw,ref}\right)\,\mathrm{d}t} \\ GHG_{dhw} &= \frac{\int\limits_{year} \left(\dot{E}_{el,HVAC\&DHW}\,\tau_{el} + \dot{Q}_{aux}\,\tau_{gas}\right)\,\mathrm{d}t}{\int\limits_{year} \left(\dot{Q}_h + \dot{Q}_c + \dot{Q}_{dhw}\right)\,\mathrm{d}t} \quad . \end{aligned} \tag{4.12}$$

The next measure introduced is the ratio of electricity saved at peak hours to the total electricity saved by the solar system compared to the reference system (equation 4.13). It reflects the potential to reduce peak electricity demand. As a peak time interval the 4 hour period from 16:00 until 20:00 in the afternoon was chosen. In equation 4.14 the specific peak electricity savings are calculated.

$$f_{peak(,dhw)} = \frac{\int\limits_{peak} \Delta\dot{E}_{el,HVAC(\&DHW)}\,\mathrm{d}t}{\int\limits_{year} \Delta\dot{E}_{el,HVAC(\&DHW)}\,\mathrm{d}t} = \frac{\int\limits_{peak} \left(\dot{E}_{el,ref} - \dot{E}_{el}\right)_{HVAC(\&DHW)}\,\mathrm{d}t}{\int\limits_{year} \left(\dot{E}_{el,ref} - \dot{E}_{el}\right)_{HVAC(\&DHW)}\,\mathrm{d}t} \tag{4.13}$$

$$\Delta ES_{el,peak} = \frac{\int\limits_{peak} \dot{E}_{el,HVAC,ref}\,\mathrm{d}t}{\int\limits_{year} \left(Q_{c,ref} + Q_{h,ref}\right)\,\mathrm{d}t} - \frac{\int\limits_{peak} \dot{E}_{el,HVAC}\,\mathrm{d}t}{\int\limits_{year} \left(Q_c + Q_h\right)\,\mathrm{d}t} \tag{4.14}$$

$$\Delta ES_{el,peak,dhw} = \frac{\int\limits_{peak} \dot{E}_{el,HVAC\&DHW,ref}\,\mathrm{d}t}{\int\limits_{year} \left(Q_{c,ref} + Q_{h,ref} + Q_{dhw,ref}\right)\,\mathrm{d}t} - \frac{\int\limits_{peak} \dot{E}_{el,HVAC\&DHW}\,\mathrm{d}t}{\int\limits_{year} \left(Q_c + Q_h + Q_{dhw}\right)\,\mathrm{d}t} \tag{4.15}$$

Water consumption is another important performance indicator as thermal chiller systems have thermodynamically a larger heat rejection demand and Australia is known for frequently suffering droughts. The ratio of the annual water consumption

M_{water} to the supplied amount of cooling is calculated as in equation 4.16.

$$M_{water} = \frac{\int_{year} \dot{m}_{water}\,\mathrm{d}t}{\int_{year} \dot{Q}_c\,\mathrm{d}t} \tag{4.16}$$

Comfort conditions of a conditioned space are reflected in room temperature and relative humidity. The comfort conditions for the N_R rooms in the building are determined by set point temperatures for summer and winter. The first comfort criteria is the temperature related comfort ($comf_T$) defined in equation 4.17. The amount of times the cooling or heating system is required in zone i, with $i \in \{1,2,3\}$, but the temperature range is exceeded is accumulated and divided by the total time the HVAC system is required. It is essentially a calculation of the average discomfort of the N_R rooms. When comparing the simulation results in the coming chapters, it is often distinguished between "summer" and "winter". In case $comf_T$ indicates "summer", the calculation does not relate to the actual summer months but omits the term $T_{air,r} < T_{setH} - 1\,^{\circ}\mathrm{C}$ from equation 4.17. The opposite applies for "winter". The variable $T_{air,r}$ is the temperature of room r and T_{setH} and T_{setC} are heating and cooling indoor set point temperatures. $HVAC_{z_i}$ is the control signal for zone i which indicates that cooling or heating is required.

$$comf_T = \frac{1}{N_R}\sum_{r=1}^{N_R} \frac{\int_{year} \left(\{T_{air,r} > T_{setC} + 1\,^{\circ}\mathrm{C}\} \vee \{T_{air,r} < T_{setH} - 1\,^{\circ}\mathrm{C}\}\right) \cdot HVAC_{z_i}\,\mathrm{d}t}{\int_{year} HVAC_{z_i}\,\mathrm{d}t} \tag{4.17}$$

The maximum relative humidity which defines comfort levels is 60%. Similarly to $comf_T$, equation 4.18 defines how well the humidity comfort conditions ($comf_{RH}$) can be kept. The relative humidity of room r is RH_r.

$$comf_{RH} = \frac{1}{N_R}\sum_{r=1}^{N_R} \frac{\int_{summer} \{RH_r > 60\%\} \cdot HVAC_{z_i}\,\mathrm{d}t}{\int_{summer} HVAC_{z_i}\,\mathrm{d}t} \tag{4.18}$$

It occurs in humid climates that there is no sensible load in the room, but the humidity may exceed 60%. This is the reason why $comf_{RH}$ is often relatively high when the HVAC system is merely triggered by indoor air temperatures. In most of the following simulations humidity control is not part of the control strategy. Alternatively a fan can be switched on during these times to increase personal comfort, however, this scenario has not been included in the modeling.

The percentage of people dissatisfied (PPD), based on the predicted mean vote (PMV), was originally considered as a measure to represent the discomfort depending on ventilation rates, clothing factors, humidity and temperatures [ISO, 2005]. After further research into this methodology it became clear that the clothing factor would have to be adjusted to account for seasonal and even daily weather changes

and varies between the different climates. In order to see how well the cooling and heating system performed and to compare them to each other the indicators $comf_T$ and $comf_{RH}$ were considered sufficient to exclude the distorting factor of clothing and ventilation from the results[3].

4.2.2 The specific average cost of cooling, heating and DHW

Cost aspects need to be included when optimizing solar air-conditioning technologies. The average specific cost c_m is a measure of the cost per cooling and heating energy supplied to the building over the lifetime of a system. It is also known as levelized cost of energy. The cost-effectiveness decreases with incremental capacity increase of collector and tank size which is commonly known as diminishing returns. Capital cost ($I_{t=0}$), annual expenditures (A_n) and the real interest rate i need to be estimated to calculate the specific average cost c_m for cooling and heating. In order to take inflation into account, the real interest rate can be be approximated by adding the nominal interest rate to the inflation rate. The subscript n stands for the year and N is the lifetime of the system.

The amount of generated heat for the domestic hot water supply can be included and the modified levelized cost of energy $c_{m,dhw}$ can be calculated using equation 4.20. Both equations 4.19 and 4.20 are derived from the formula to calculate the levelized cost of electricity in Konstantin [2009, p. 169]. In both equations $Q_{c,n} = \int_{year} \dot{Q}_c \, dt$ is the annual cooling energy, $Q_{h,n} = \int_{year} \dot{Q}_h \, dt$ the annual heating energy and $Q_{dhw,n} = \int_{year} \dot{Q}_{dhw} \, dt$ the annual energy for DHW supplied to the building.

$$c_m = \frac{I_{t=0} + \sum_{n=1}^{N} \frac{A_n}{(1+i)^n}}{\sum_{n=1}^{n=N} \frac{Q_{c,n} + Q_{h,n}}{(1+i)^n}} \tag{4.19}$$

$$c_{m,dhw} = \frac{I_{t=0} + \sum_{n=1}^{N} \frac{A_n}{(1+i)^n}}{\sum_{n=1}^{N} \frac{Q_{c,n} + Q_{h,n} + Q_{dhw,n}}{(1+i)^n}} \tag{4.20}$$

The annual running cost of the system A_n is displayed in equation 4.21 and can be derived with or without the inclusion of DHW. It is comprised of the cost for electricity ($A_{n,el}$), the cost for gas ($A_{n,gas}$) and for water ($A_{n,water}$). The variable $\dot{Q}_{aux} = \dot{Q}_{aux,HVAC}(+\dot{Q}_{aux,DHW})$ is the auxiliary gas consumption and $\dot{E}_{el} = \dot{E}_{el,HVAC}(+\dot{E}_{el,dhw})$ is the electricity consumption. The variable $\dot{m}_{water}$ is the cooling water consumption. The abbreviation for the price is p. Utilities usually impose a fixed annual capacity charge marked by the index "fix" as well as a variable charge dependent on the

[3]The TRNSYS building model type 56 actually outputs the PPD.

consumption. The annual cost for maintenance of the system is not taken as a fraction of the initial investment cost as it is usually done for large scale installations, but will be a fixed annual cost $A_{n,maint}$, specific to each system.

$$\begin{aligned} A_n &= A_{n,el} + A_{n,gas} + A_{n,water} + A_{n,maint} \\ A_{n,el} &= \int_{year} \left(p_{el} \cdot \dot{E}_{el}\right) \mathrm{d}t + p_{el,fix} \\ A_{n,gas} &= \int_{year} \left(p_{gas} \cdot \dot{Q}_{aux}\right) \mathrm{d}t + p_{gas,fix} \\ A_{n,water} &= \int_{year} \left(p_{water} \cdot \dot{m}_{water}\right) \mathrm{d}t + p_{water,fix} \\ A_{n,maint} &= p_{maint,fix} \end{aligned} \tag{4.21}$$

For PV assisted systems the cost for electricity depends on the local financial rebate scheme. If the system is grid connected and a solar feed-in tariff is valid, the annual cost for electricity $A_{n,el(PV)}$ is calculated as in equation 4.22. In this equation $frac_{PV}$ is the ratio between the financial benefit for each kWh of electricity exported into the grid ($p_{el,sol}$) to the price per kWh of purchased electricity (p_{el}). If $frac_{PV}$ is set to 1, the cost to purchase 1 kWh of electricity is equal to the benefit from exporting 1 kWh to the grid. $\dot{E}_{el}$ is the system's electricity demand and $\dot{E}_{el,sol}$ is the solar electricity provided by the PV modules.

$$A_{n,el(PV)} = \int_{year} p_{el} \left(\dot{E}_{el,grid \to HVAC(\&DHW)} - frac_{PV} \int_{year} \dot{E}_{el,sol \to grid} \right) \mathrm{d}t + p_{el,fix} \tag{4.22}$$

with

$$\int_{year} \dot{E}_{el,grid \to HVAC(\&DHW)} \, \mathrm{d}t = \int_{year} \max\left\{0, \dot{E}_{el} - \dot{E}_{el,sol}\right\} \mathrm{d}t \tag{4.23}$$

$$\int_{year} \dot{E}_{el,sol \to grid} \, \mathrm{d}t = \int_{year} \max\left\{0, \dot{E}_{el,sol} - \dot{E}_{el}\right\} \mathrm{d}t \tag{4.24}$$

$$frac_{PV} = p_{el,sol} / p_{el} \tag{4.25}$$

To calculate the electricity price at which the solar thermal technology might become cost effective equation 4.26 can be solved for the break even electricity price $p_{el,BE}$. $I_{t=0}$ and A_n stand for the initial investment and the annual cost of the solar technology. The subscript "ref" refers to the reference system and "non-el" is annual cost not related to electricity consumption. $E_{el,n} = \int_{year} \dot{E}_{el} \, \mathrm{d}t$ is the annual electricity consumption of the system, which may or may not include DHW.

$$\frac{I_{t=0,ref}}{\sum_{n=1}^{N}\frac{1}{(1+i)^n}} + p_{el,BE}\cdot E_{el,n,ref} + A_{n,ref,non-el} \tag{4.26}$$
$$= \frac{I_{t=0}}{\sum_{n=1}^{N}\frac{1}{(1+i)^n}} + p_{el,BE}\cdot E_{el,n} + A_{n,non-el}$$

The solution is of the form

$$p_{el,BE} = \frac{\frac{I_{t=0}-I_{t=0,ref}}{\sum_{n=1}^{N}\frac{1}{(1+i)^n}} + A_{n,non-el} - A_{n,ref,non-el}}{E_{el,n,ref} - E_{el,n}} \tag{4.27}$$

For solar electric systems the equations are slightly different as they have to take into consideration a possible feed-in tariff. Equation 4.28 is transferred to equation 4.29 by solving for the break even price.

$$\frac{I_{t=0,ref}}{\sum_{n=1}^{N}\frac{1}{(1+i)^n}} + p_{el,BE}\; E_{el,n,ref} + A_{n,ref,non-el} \tag{4.28}$$
$$= \frac{I_{t=0}}{\sum_{n=1}^{N}\frac{1}{(1+i)^n}} + p_{el,BE}\; \left(E_{el,grid\rightarrow HVAC(\&DHW),n} - frac_{PV}\; E_{el,sol\rightarrow grid,n}\right) + A_{n,non-el}$$

$$p_{el,BE} = \frac{\frac{I_{t=0}-I_{t=0,ref}}{\sum_{n=1}^{N}\frac{1}{(1+i)^n}} + A_{n,non-el} - A_{n,ref,non-el}}{E_{el,n,ref} - E_{el,grid\rightarrow HVAC(\&DHW),n} + frac_{PV}\; E_{el,sol\rightarrow grid,n}} \tag{4.29}$$

4.2.3 An overall performance factor for Australia

Instead of having to evaluate each of the previous factors individually for HVAC systems it might be advantageous to define an overall performance factor for Australia which takes all Australian climates into account.

The specific costs and comfort will be integrated into an overall performance factor (OPF) together with the specific greenhouse gas emissions (GHG).

The peak electricity demand and the water consumption are indirectly included in the cost term c_m and will therefore not be included in the factor directly. If there was a real price on greenhouse gas emissions, which there was in Australia until July 2014, the cost could be included into c_m and the overall performance factor would simply consist of a cost and comfort term.

An economist might put a price on comfort and on the environmental impact (leakage rate of refrigerants used, greenhouse gas emissions etc.), but that price would not be market driven. The resulting specific cost for heating and cooling would therefore not be real but subjective to the beholder.

The overall performance factor (OPF) presented in equation 4.30 serves as a tool

to compare different HVAC (and DHW) systems in a subjective way, because the weighting factors α, β and γ can be set arbitrarily to put importance either on (real) specific cost, environmental impact or comfort.

$$\begin{aligned} OPF &= OPF_{c_m} + OPF_{GHG} + OPF_{comf} \\ OPF &= \alpha \cdot f_c(c_m) + \beta \cdot f_{GHG}(GHG) + \gamma \cdot \left(1 - \frac{comf_T + comf_{RH}}{2}\right) \\ 1 &= \alpha + \beta + \gamma \end{aligned} \tag{4.30}$$

The function $f(x)$ used in equation 4.30 is defined in equation 4.31. The variable x represents either the specific cost c_m or the specific greenhouse gas emissions GHG as defined in equations 4.19 and 4.11.

$$f(x) = k^{\left(\frac{x}{\bar{x}_{ref}}\right)^a} \tag{4.31}$$

The variable $\bar{x}_{ref}$ represents an average specific cost or greenhouse gas emissions of the reference system. The simulated and calculated results for $c_{m,ref}$ and GHG_{ref} for the reference system in each climate are weighted by the population density $n_{climate}$ as in equation 4.32 to calculate $\bar{c}_{ref}$ and $\overline{GHG}_{ref}$. The population density can found in Table 4.13.

$$\bar{x}_{ref} = \sum_{climate=1}^{C=7} n_{climate} \cdot x_{ref,climate} \tag{4.32}$$

The parameters k ad a are shaping factors and they are different for c_m and GHG. Two points on the curve of the function $f(x)$ have to be fixed in order to calculate them. The approach is outlined in Table 4.2 for two points. The factor g is a multiple of $\bar{x}_{ref}$ defining the x value for the second point. In Figure 4.1 the methodology is shown calculating k and a for the specific cost and greenhouse gas emissions used in this work.

Table 4.2: Calculating the shape parameters for $f(x)$

Point	x	$f(x)$	k,a
1	$\bar{x}_{ref}$	$k = f(\bar{x}_{ref})$	$\Longrightarrow k$
2	$g \cdot \bar{x}_{ref}$	$j = f(g \cdot \bar{x}_{ref})$	$\Longrightarrow a = \frac{\ln\left(\frac{\ln(j)}{\ln(k)}\right)}{\ln(g)}$

The function $f(x)$ has been chosen for its asymptotic characteristic. $f(\bar{c}_{ref}) = k_c$ is set to 0.9 as it can be assumed that today's conventional HVAC systems are on the top end of cost effectiveness and most renewable options are more expensive. If a technology becomes three times as expensive ($g_c = 3$) as the reference technology, $f(3 \cdot \bar{c}_{ref}) = j_c$ is set to 0.1, indicating poor performance. For greenhouse gas

emissions $f(\overline{GHG}_{ref}) = k_{GHG}$ is set to 0.5 leaving space for change in both directions. If a technology is able to half the greenhouse gas emissions ($g_{GHG} = 0.5$), $f(0.5 \cdot \overline{GHG}_{ref}) = j_{GHG}$ is set to 0.9.

The shaping factors are a second degree of freedom which can be set by the user arbitrarily.

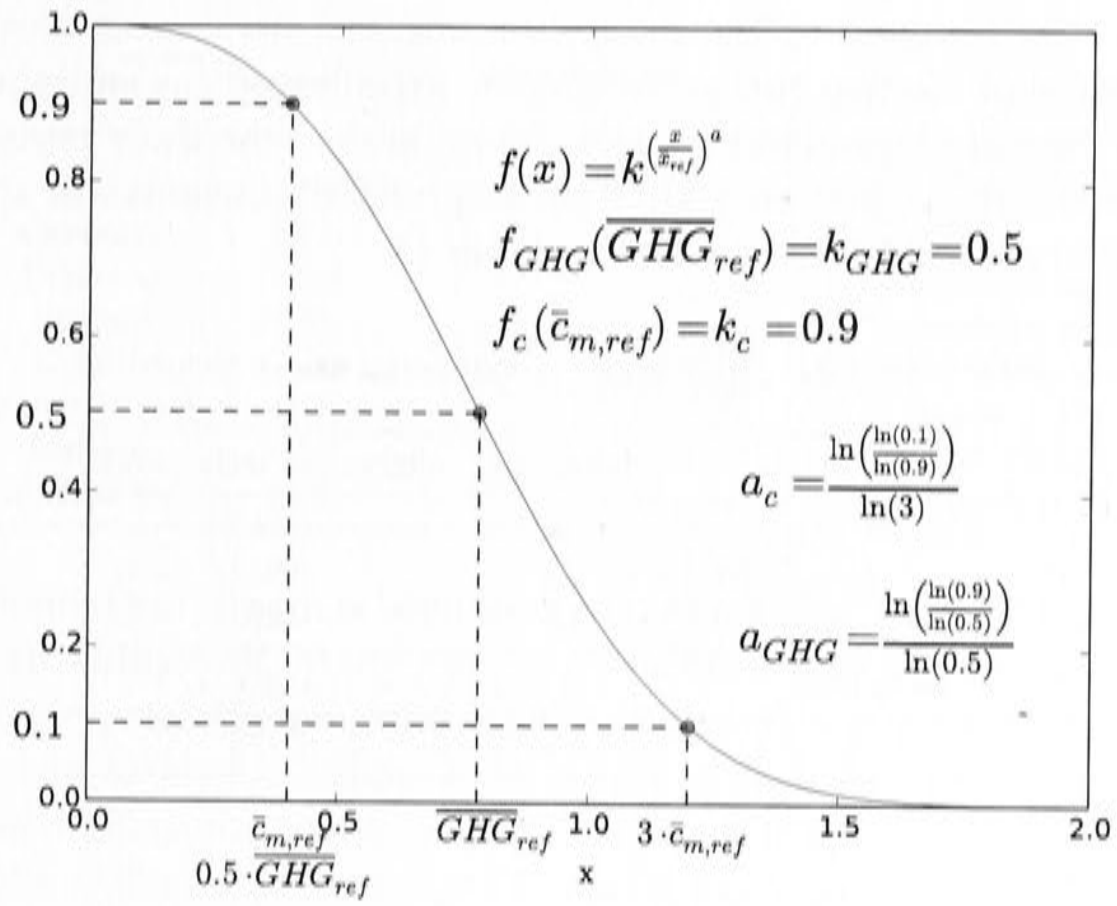

Figure 4.1: Display of the function $f(\bar{x}_{ref})$ to calculate the overall performance factor. The variable $\bar{x}_{ref}$ is either cost c_m or greenhouse gas emissions GHG specific to the generated cooling, heating (and DHW)

Practical example of the OPF

This section shows in a brief example how the OPF is applied. Table 4.3 presents possible simulation results or real measurements of the specific cost, the comfort conditions and the greenhouse gas emissions specific to the amount of cooling and heating generated.

Table 4.3: Cost, greenhouse gas emissions and comfort assumptions for an exemplary reference system and alternative solar assisted system

	reference	alternative technology	unit
c_m	0.16	0.3	$\$\,kWh^{-1}$
GHG	0.32	0.14	$kg_{CO2}\,kWh^{-1}$
$1 - comf$	0.9	0.85	-

In order to generate the OPF the shape factors for the curves are defined according to Figure 4.1. The factors are given in Table 4.4.

Table 4.4: Shape factors

	cost	GHG
shape factor k	$k_c = 0.9$	$k_{GHG} = 0.5$
shape factor g	$g_c = 3$	$g_{GHG} = 0.5$
shape factor j	$j_c = 0.1$	$j_{GHG} = 0.9$
shape factor a	$a_c = 2.81$	$a_{GHG} = 2.72$

After the shape of the two curves for specific greenhouse gas emissions and cost are defined by the four parameters k_{GHG}, k_c, a_{GHG} and a_c, the three parts of the OPF can be calculated using equation 4.31. The weighing coefficients are applied as in equation 4.30 and the total OPF is found in Table 4.5.

Table 4.5: Calculation of the overall performance factor

	reference	alternative technology
$OPF_{c_m} = f_c(c_m)$	0.9	0.540
$OPF_{GHG} = f_{GHG}(GHG)$	0.5	0.929
OPF_{comf}	0.9	0.850
coefficients	$\alpha = 1/3, \beta = 1/3, \gamma = 1/3$	
OPF	0.767	0.773

4.3 Description of the residential building model in each climate zone

In the following chapters the design of the solar cooling, heating and DHW model will be described in detail for electrically driven systems with and without electricity storage, and for thermally driven systems with a hot water tank and with or without cold storage.

As the reference case a conventional reverse cycle split unit for each zone is chosen, which provides heating and cooling by expansion direct circulation of refrigerant. It is compared to a complex solar thermal absorption chiller system, generating chilled water and distributing it to fan coils for summer cooling. The winter heating is provided via fan coil units supplied by the hot water from a storage tank. The solar heat supply is backed up by gas.

The conventional domestic hot water supply is assumed to be electric. In the solar thermal system the domestic hot water is provided by the solar collectors with gas backup. The domestic hot water load profile follows the solar hot water performance standard AS/NZS 4234 [Australian/ New Zealand Standard, 2008] which specifies the heat draw from the tank eight times a day over a 6 min time interval.

The building shell

In order to compare HVAC (and DHW) system performance using simulation tools, a building model must be defined first to represent the load. The building model described here represents the load for a cooling, heating and DHW system varying in each climate. The building construction was deemed to be representative of each climate zone as shown in Table 4.6 [Energy Efficient Strategies (EES), 2008].

Table 4.6: Set point temperatures for heating and cooling, and predominant building construction in each climate

	T_{setC}	T_{setH}	Building structure
Canberra	24°C	20°C from 7:00-24:00, 18°C from 0:00-7:00	Brick veneer (reverse)
Brisbane	25.5°C		Weatherboard
Sydney	25.5°C		Weatherboard
Griffith	25°C		Weatherboard
Tennant Creek	25°C		Double brick
Darwin	26.5°C		Double brick
Melbourne	24°C		Brick veneer (reverse)

The residential building has been designed as a 230 m^2 (A_{house}) conditioned space (CS) with a air volume of 690 m^3 (V_{house}). The floor area of new Australian houses has been growing steadily over the last 10 years and is expect to plateau at 230 m^2 [Energy Efficient Strategies (EES), 2008, p.123] until 2020. The arrangement of the rooms and their allocation to one of the three zones is shown in Figure 4.2 and Table 4.7. The height of the indoor space is 3 m and the roof pitch is 22°.

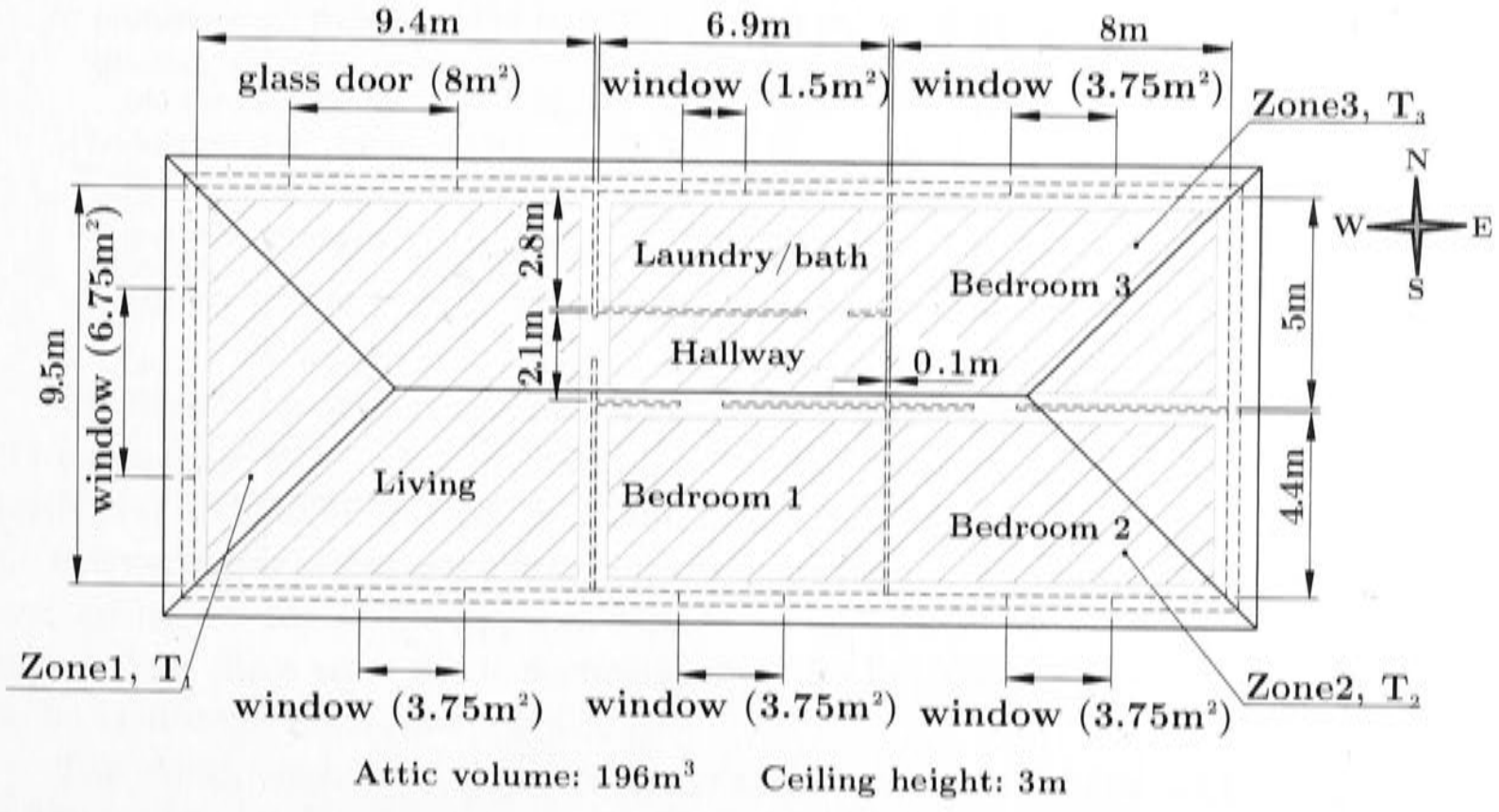

Figure 4.2: Building model dimensions

Table 4.7: Building dimensions

	Zone 1	**Zone 2**			**Zone 3**		**Total**
	Liv	**Bed 1**	**Bed 2**	**Hw**	**Ldry/bath**	**Bed 3**	
Area [m^2]	89.9	30.5	35.6	14.5	19.2	40	230
Volume [m^3]	269.7	91.5	106.7	43.4	57.7	120	689

The external walls are insulated and the structure is either weather board, reverse brick veneer or double brick depending on the most common structure in each climate (Table 4.6). Reverse brick veneer was chosen over brick veneer due to its better energy performance. The thermal mass is located on the inside and the insulation on the outside[4].

The insulation thickness is determined by setting the R-value of the walls to the desired R-value of 2.8 given by the national construction code of Australia [Australian Building Codes Board, 2011]. Reflective foil is also part of the air space in the external walls to achieve the required R-value, which means one surface in the air space has a low emissivity (1 low ϵ). The layers of the three different wall types for the building structures brick veneer (reverse), weatherboard and double brick are outlined in Table 4.8 to 4.10.

Table 4.8: Wall structure of reverse brick veneer

	thickness [m]	conductivity k_{wall} [$W\,m^{-1}\,K^{-1}$]	heat capacity $c_{p,wall}$ [$kJ\,kg^{-1}\,K^{-1}$]	density ρ_{wall} [$kg\,m^{-3}$]	resistance R_{wall} [$m^2\,K\,W^{-1}$]
outdoor air film	0.000	0.00	0.00	0.00	0.030
weatherboards (12mm avg, pine)	0.012	0.10	2.09	506.00	0.120
glasswool batts (med/high density)	0.038	0.03	0.88	56.00	1.165
air space (1 low ϵ)	0.050	0.03	1.01	1.20	0.610
reflective foil	0.000	0.00	0.00	0.00	0.000
air space (1 low ϵ)	0.050	0.03	1.01	1.20	0.610
brickwork	0.110	0.76	0.96	1820.00	0.145
indoor air film	0.000	0.00	0.00	0.00	0.120
total	0.260				2.800
U-value	$0.357\,W\,m^{-2}\,K^{-1}$				

[4]When comparing both in a simulation trial and designing the brick veneer wall backwards in the relevant climate zones, the building used 46% less cooling in summer and 7% less heating energy in winter.

Table 4.9: Wall structure of weatherboard type

	Thickness [m]	conductivity k_{wall} [$W\,m^{-1}\,K^{-1}$]	heat capacity $c_{p,wall}$ [$kJ\,kg^{-1}\,K^{-1}$]	density ρ_{wall} [$kg\,m^{-3}$]	resistance R_{wall} [$m^2\,K\,W^{-1}$]
outdoor air film	0.000	0.00	0.00	0.00	0.030
weatherboards (12 mm avg, pine)	0.012	0.10	2.09	506.00	0.120
air space (1 low ϵ)	0.100	0.03	1.01	1.20	0.610
glasswool batts med/high density	0.061	0.03	0.88	56.00	1.861
10 mm gypsum board (plasterboard)	0.010	0.17	1.05	880.00	0.059
indoor air film	0.000	0.00	0.00	0.00	0.120
Total	0.183				2.800
U-value	$0.357\,W\,m^{-2}\,K^{-1}$				

Table 4.10: Wall structure double brick type

	thickness [m]	conductivity k_{wall} [$W\,m^{-1}\,K^{-1}$]	heat capacity $c_{p,wall}$ [$kJ\,kg^{-1}\,K^{-1}$]	density ρ_{wall} [$kg\,m^{-3}$]	resistance R_{wall} [$m^2\,K\,W^{-1}$]
outdoor air film	0.000	0.00	0.00	0.00	0.030
brickwork	0.110	0.76	0.96	1820.00	0.145
air space (1 low ϵ)	0.020	0.03	1.01	1.20	0.600
polystrene (insulation R1.5)	0.067	0.04	0.34	16.00	1.722
brickwork	0.110	0.76	0.96	1820.00	0.145
pflaster 1:4 (cement:sand)	0.020	0.53	0.84	1570.00	0.038
indoor air film	0.000	0.00	0.00	0.00	0.120
total	0.327				2.800
U-value	$0.357\,W\,m^{-2}\,K^{-1}$				

The floor is modeled as slab on ground with carpet underlay and carpet on top (U-value $1.545\,W\,m^{-2}\,K^{-1}$). The ceiling is made up of gypsum board with ceiling joists and an insulation layer. In a similar manner to the walls, the tiled roof with attic and ceiling was designed for a required R-value of 4.6, and appropriate insulation was added on top of the gypsum board ceiling. The assumptions for thermal resistance of air films were made according to AIRAH [2007] and the attic was assumed to be ventilated as in equation 4.33.

The windows have a wooden frame and are double glazed with an U-value of $3.2\,W\,m^{-2}\,K^{-1}$ and a solar heat gain coefficient (SHGC) of 0.698. The glass thickness is 5.7 mm and the air space between the two glass layers is 6.4 mm. The two north facing windows, the north facing glass door and the west facing window are shaded with a shading projection of 0.6 m, 1 m and 1 m respectively. The height from the

projected area to the window top is 0.2 m for each shaded window. The window-wall ratios are shown in Table 4.11.

Table 4.11: Window-wall ratio of building for each orientation

	North	East	South	West
Wall area [m^2]	74.79	30.14	74.79	30.14
Glazing [m^3]	13.25	0	11.25	6.75
window-wall ratio	18%	0%	15%	22%

Internal loads and ventilation

The **attic is ventilated** and the ventilation air changes are a function of the wind speed as in equation 4.33.

$$ACH_{attic} = \frac{C_v \cdot A_{attic} \cdot u_{wind} \cdot 3600}{V_{attic}} \tag{4.33}$$

$C_v = 0.3$ 0.25 to 0.35 for diagonal winds

$A_{attic} = 0.77\,m^2$ ratio opening area to ceiling area is 1:300

The **infiltration rates** of the building in the base case vary throughout the year with 0.8 ACH from March to December (autumn, winter, spring) and 0.5 from December to February (summer). The **outdoor ventilation rate** is switched on whenever the HVAC system is operating (cooling or heating) and supplies the rooms with fresh air. The ventilation air changes are taken from ASHRAE [2013] according to equation 4.34[5].The occupancy to calculate ventilation air flow is 4 and it is assumed that the whole house is conditioned.

$$ACH_{ventilation} = \frac{0.11\,s^{-1}\,m^{-2} \cdot A_{house} + 8\,l\,s^{-1}\,person^{-1} \cdot occupants}{V_{house}} \cdot 3.6 \tag{4.34}$$

Nevertheless, for the calculation of the heating and cooling load a occupancy profile is assumed for each room. People and any other kinds of thermal heat sources within the building are **internal loads**. The heat gain value emitted by each occupant is taken from the standard ISO 7730:2005 ISO [2005], which assumes that people emit 65 W of sensible heat and 55 W of latent heat when awake and 60 W and 40 W

[5]Another modeling alternative for the ventilation air flow is to keep it ON regardless of the status of the HVAC system. This would guarantee to fulfill fresh air ventilation requirements even when the HVAC system is not operating. The model has high infiltration rates which can make up for the fresh air requirements. Only in section 8.2.8 it might become problematic in summer because infiltration rates are lowered by 80% along with the air-conditioning demand due to very thick walls. However, night flush ventilation is included which can make up for the reduced fresh air supply during the summer days.

respectively when asleep. Further heat gain in the living area is due to cooking and electrical appliances as taken from the Australian AccuRate software for thermal building modeling (CSIRO [2010]). The internal loads in AccuRate are scaled for a 200 m^2 conditioned space. Even though this building is 230 m^2 the area scale factor for the internal loads was kept at 1[6]. Lights are switched on between 8:00 and 9:00 and from 18:00 to 0:00 with a heat gain of 5 $W\,m^{-2}$. The daily internal gains were summarized for a weekday in Figure 4.3. The weekend varies only marginally by 2 more people occupying the living area (zone1).

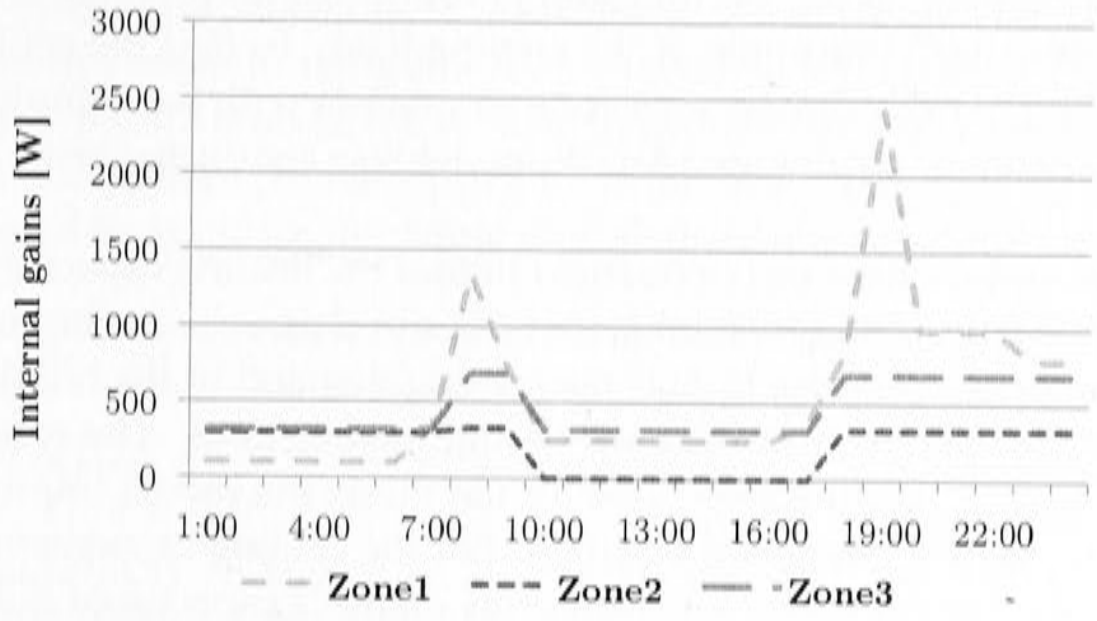

Figure 4.3: Internal gains for each zone

Controls

The cooling and heating system is controlled via set point temperature if not explicitly stated differently. The zones can be controlled individually. The exact control strategy and the dead band of the thermostats is explained later as they differ for the electrically and thermally driven systems.

The (dry bulb) set point temperatures for heating and cooling can be found in Table 4.6. They correspond to the cooling set points from Australian Building Codes Board (ABCB) [2006]. Only the set points of Griffith and Tennant Creek have been modified to 25°C because 27°C seemed too high. The thermostat for zone 1 is located in the living room, the thermostat for zone 2 is located in bedroom 2 and the thermostat for zone 3 is located in bedroom 3. Within every model the same building with the same set points for cooling and heating is implemented, unless otherwise indicated. The control strategies differ slightly between the electrically and thermally driven model. The thermostat control signals for each zone are $HVAC_{therm,c,z_i}$ for cooling and $HVAC_{therm,h,z_i}$ for heating.

In addition to the temperature set points, cooling or heating are enabled only in specific time intervals. They differ for each zone depending on its usage. Zone 1 is

[6]This was mainly to prevent the spike in thermal load in the evening due to cooking from becoming too large.

allowed to be conditioned from 7:00 until midnight, zone 2 from 16:00 until 9:00 and zone 3 during the entire day[7]. These scheduled control signals for each zone i are $HVAC_{sched,z_i}$.

Sizing of the HVAC (and DHW) system

The domestic hot water loads given in the Australian standard AS/NZS 4234 [Australian/ New Zealand Standard, 2008] offers small, medium and large hot water demand profiles. The medium size was chosen for the purpose of the simulations.

The cooling capacity C_c of the building is found from averaging the values between the 95th and 100th percentile of the cooling load. To find the cooling capacity C_c for the building in each climate zone, one simulation with the complex solar thermal absorption cooling, heating and DHW model was conducted with an oversized chiller[8].

The same procedure has been performed to find the heating capacity of the building. The disadvantage of this method is that the simulation has to be run more than once with an excessive capacity to find the cooling demand of the building from the amount of heat transferred over the cooling and heating coils. The results are summarized in Table 4.12. During the course of the thesis the model improved and the results for the capacities changed marginally. For the cooling capacities the numbers in brackets are the results when over-sizing the chiller's capacity of the most recent model. Nevertheless, all simulations of the base case were conducted with the values without brackets[9].

Table 4.12: Heating and cooling capacities in kW for each zone and the entire building

	C_c	$C_{c,z1}$	$C_{c,z2}$	$C_{c,z3}$	C_h	$C_{h,z1}$	$C_{h,z2}$	$C_{h,z3}$
Canberra	3.4 (3.5)	1.9 (2.0)	0.5	1.1	6.8 (5.5)	2.2	2.0	1.8
Brisbane	5.2 (5.3)	3.1 (3.2)	1.0	1.8	1.8	0.5	0.8	0.6
Sydney	3.6 (3.7)	2.2 (2.3)	0.3	1.3	2.4	0.8	1.0	0.9
Griffith	6.6 (6.8)	3.6 (3.8)	1.4	2.2	4.4	1.7	1.6	1.6
Tennant Creek	7.2 (7.3)	3.8 (3.9)	1.9	2.3	0.1	0.1	0.1	0.0
Darwin	7.6 (7.7)	4.2 (4.3)	1.9	2.4	0.0	0.0	0.0	0.0
Melbourne	3.2 (3.5)	1.8 (2.0)	0.4	1.1 (1.2)	4.5 (4.4)	1.8	1.6	1.5

Different solar array sizes and hot water tank sizes in the solar thermal model result into various solar fractions in the different climates. Multiple configurations will be simulated, however, for the purpose of further investigation, one system design configuration with a solar fraction of at least 60% is chosen. This stipulation holds for solar thermal and solar electric assisted systems. For the solar thermal system the solar fraction SF_{th} as in equation 4.1 is used and for solar electric systems

[7]Bedroom 3 is supposed to be a nursery or any other type of room which needs air-conditioning 24 hours a day.

[8]As this model was the first one being completed during the course of this work, it served as the chosen model to determine cooling and heating capacity.

[9]The heating capacity in winter was increased in Melbourne and Canberra to ease the winter's discomfort, which was relatively high.

the total solar fraction $SF_{el,tot}$ as in equation 4.5. The solar fraction of thermally driven systems only accounts for heat and the parasitic electricity consumption is not included.

Climate

The weather data used for all simulations is taken from Meteotest et al. [2004]. For the locations Canberra, Brisbane and Tennant Creek no solar radiations measurements were available and the radiation data was interpolated by Meteonorm. The Bureau of Meteorology divides Australia in six climate zones (Appendix Figure C.1) and one city has been chosen to represent each climate zone[10]. Table 4.13 cites the BOM specific climate zones, however, the winters in Sydney are rather mild and in Tennant Creek almost not existent. In the Appendix in Table C.1 the cities with a population >20 000 are listed to calculate the population density in each climate zone.

Table 4.13: Percentage of Australian population living in each climate zone

City or town	Climate zone	Percentage of total population in climate zone ($n_{climate}$)
Canberra (ACT)	Mild/warm summer, cold winter	2.2%
Brisbane (QLD)	Warm humid summer	17.6%
Sydney (NSW)	Warm summer, cold winter	48.9%
Griffith (NSW)	Hot dry summer, cold winter	2.0%
Tennant Creek (NT)	Hot dry summer, mild winter	0.3%
Darwin (NT)	Hot humid summer	4.3%
Melbourne (VIC)	Mild/warm summer, cold winter	24.8%

To provide an overview on the climate characteristics of the seven different climate zones Figure 4.4 shows the distribution of the total radiation on the horizontal ($G_{tot,hor}$) in percentage of time when $G_{tot,hor} > 100\,\mathrm{W\,m^{-2}}$. The percentage of time when there is no radiation is also included in the graph.

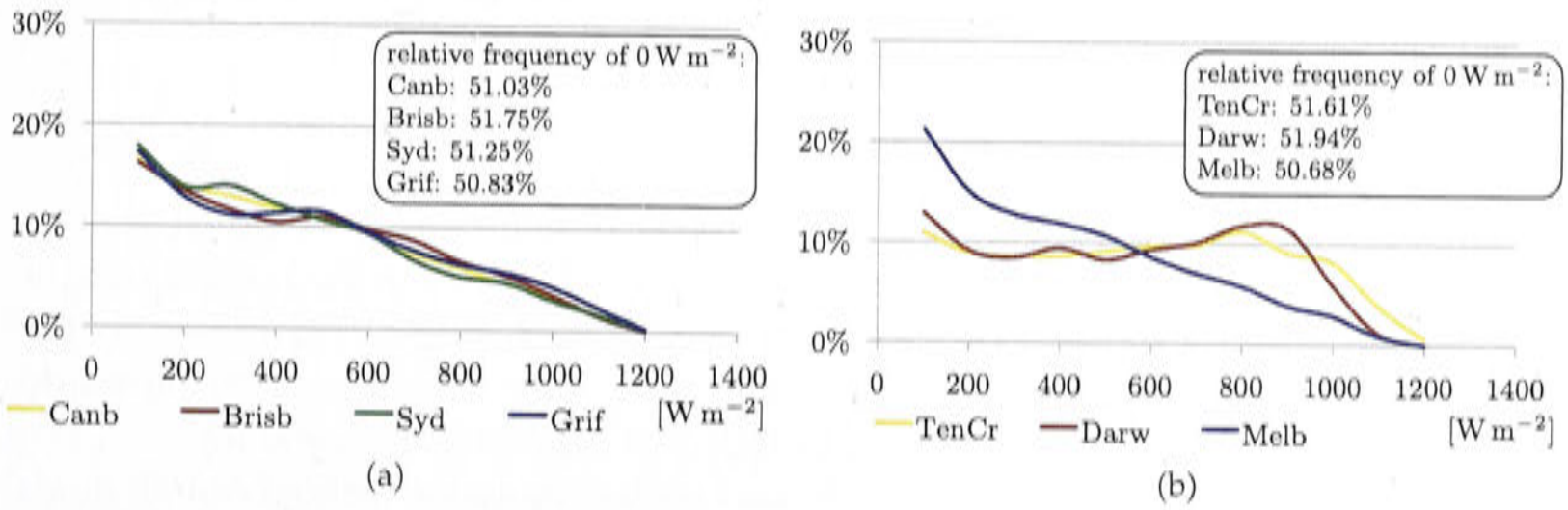

Figure 4.4: Distribution of total solar radiation on the horizontal ($G_{tot,hor}$) in the 7 different climates when $G_{tot,hor} > 0$. The values on the x-axis denote]x-100,x].

[10]Canberra has been chosen in addition to represent the ACT, which is also a jurisdication on the NEM.

Figure 4.6 shows the relative frequency of the outdoor dry bulb temperature and its average. An indication for the humidity levels of the climate is given in Figure 4.5, showing the frequency distribution of the wet bulb temperature and its averages. The dry and wet bulb temperatures are important for cooling systems as they are a measure of the air-conditioning load and the power demand for heat rejection in the particular climate.

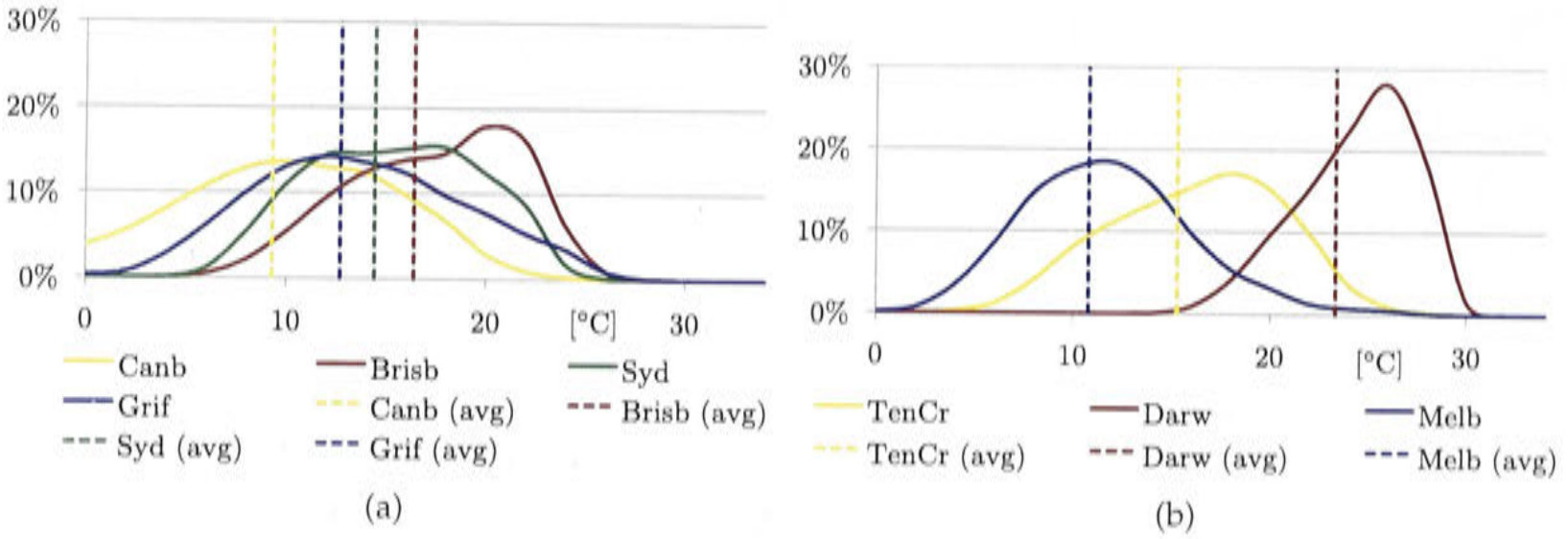

Figure 4.5: Relative frequency and average wet bulb temperature throughout the year using the weather files from Meteotest et al. [2004].

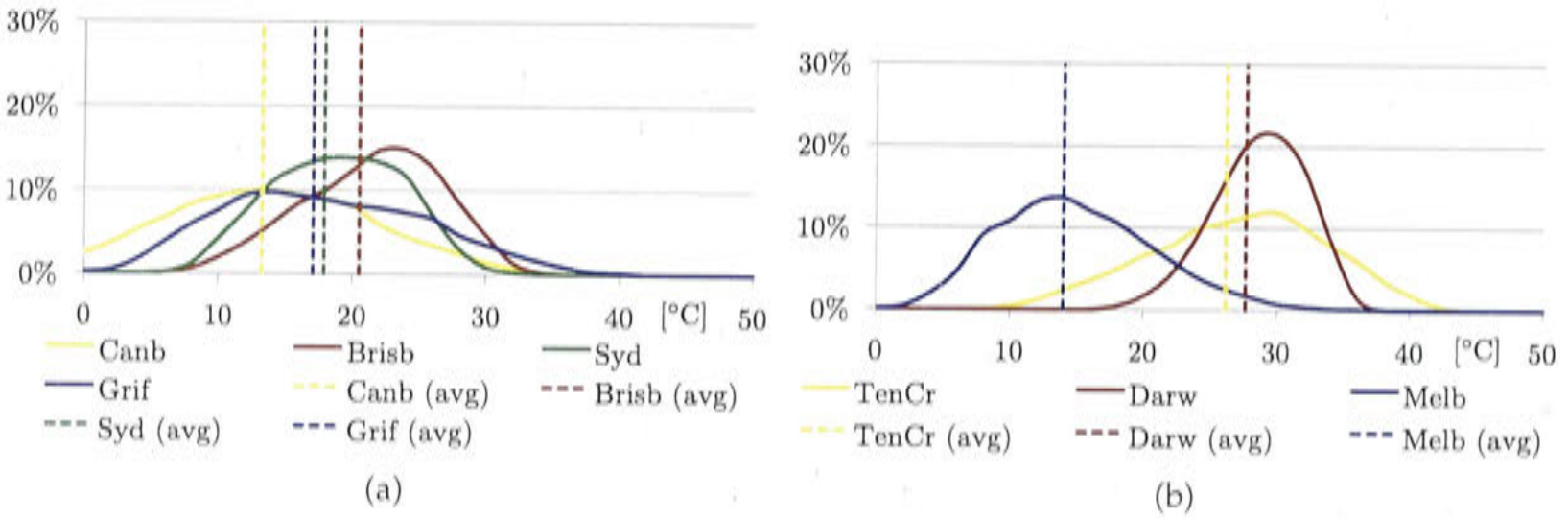

Figure 4.6: Distribution of dry bulb temperatures throughout the seven climates, Meteotest et al. [2004].

Finance

Cost and environmental performance are key indicators for a well designed system. The political favor towards the importance of energy efficiency in the building sector and support for new technologies like solar cooling is strongly determined by the orientation of the political party in power and the conservative forces are currently rather strong. As such, no rebates were included in the financial modeling.

Cost assumptions for water, electricity and gas are the same throughout all models, and so are the interest rate and the system lifetime. Over the lifetime there is no price increase incorporated, but the model is set up to do so if need be. The cost will be expressed specific to the generated amount of cooling and heating (and DHW) as in equation 4.19 and 4.20.

All cost values are in Australian dollars, unless otherwise indicated. On 11 December 2014 the exchange rate was AUD 1 = USD 0.83.

4.4 Conclusion

After having established the necessary performance parameters to rate the technologies against each other and after having defined the building load, the next chapter will introduce the reference case. The reference case represents the status quo or in other words the technology a solar alternative must compete with.

Chapter 5

The conventional cooling, heating and DHW system - reference case

This chapter serves the purpose of defining a reference case as a basis for comparison of solar assisted cooling, heating (and DHW) systems. The reference case represents the conventional, most typical technology for maintaining indoor comfort in Australian homes and production of DHW. The chosen technology is a reverse cycle air-conditioner for cooling in summer and heating in winter. Hot water is provided via electricity with a heating element in the hot water tank.

Two approaches, a simplified reference COP approach and a detailed modeling approach were considered, with the latter being selected to calculate the reference energy consumption.

5.1 Estimating energy consumption of the reference case

Domestic hot water energy consumption is directly taken from the Australian standard AS/NZS 4234 and is provided by electricity in the reference case.

There are two ways which were considered to estimate the electricity demand of the reference cooling and heating system.

The first approach calculates the reference electricity consumption based on the cooling and heating loads from a solar assisted model. A variable electrical COP of a reference reverse cycle air-conditioner as explained in the next section is chosen as conversion factor. The advantage of this approach is its simplicity. Therefore, in the beginning of this work this seemed to be the appropriate way to proceed, because an alternative solar thermal cooling, heating (and DHW) system had been modeled already. Furthermore, this methodology, using a reference COP, has been implemented into the Australian solar cooling performance standard AS 5389 [Australian/ New Zealand Standard, 2013] to calculate energy savings of solar assisted air-conditioning systems compared to reference air-conditioners.

During the course of the work it became increasingly important to generate an actual model of a reference air-conditioning system, because more detail and an extension of scope towards PV assisted reverse cycle air-conditioners were required. Nevertheless, both methods will be discussed next for completion.

1. A reference *COP* of a reverse cycle air-conditioner for heating and cooling can be calculated from the environmental conditions outdoor and indoor temperatures and humidities. Knowing the instantaneous cooling or heating load ($\dot{Q}_c$ or $\dot{Q}_h$) from the alternative solar model, the electricity consumption to satisfy this load can easily be calculated.

2. A detailed model can be established in TRNSYS using reverse cycle air-conditioner components to simulate the electricity consumption of the reference system. The system might not produce exactly the same amount of heating and cooling as the alternative solar system, which can lead to deviations of comfort performance.

5.1.1 A reference COP

A function (equation 5.1 and 5.2) can be used to calculate the electrical COP of the reference inverter reverse cycle air-conditioner for cooling and heating, and to calculate in each time step the exact electricity consumption avoided, depending on the room temperature $T_{air,r}$ and the outdoor temperature T_{amb} [Cleland and White, 2000]. These equations have also been implemented in AS 5389(Int)-2013 [Australian/ New Zealand Standard, 2013].

$$COP_{el,c} = COP_{el,c,rated} \cdot 50.9 \cdot \frac{1 - 0.00667 \cdot (T_{amb} - T_{air,r} + 30)}{T_{amb} - T_{air,r} + 30} \tag{5.1}$$

$$COP_{el,h} = 1 + (COP_{el,h,rated} - 1) \cdot 58.04 \cdot \frac{1 - 0.00603 \cdot (T_{air,r} - T_{amb} + 30)}{T_{air,r} - T_{amb} + 30} \tag{5.2}$$

$$COP_{el,c,rated} = 3.25$$

$$COP_{el,h,rated} = 3.4$$

This approach does not take part load behavior into account. Bettanini et al. [2003] published a methodology to fit a curve for heating and cooling to the relationship between part load factor $PLF_{c/h,z_i}$ and part load ratio $PLR_{c/h,z_i}$.

The part load ratio PLR_{c,z_i} is the ratio of the supplied heating or cooling energy of zone i ($\dot{Q}_{c/h,z_i}$) to the rated heating or cooling capacity of the air-conditioner of zone i ($C_{c/h,z_i}$) presented in Table 4.12. The minimum function catches the incidence when the cooling or heating load exceeds the capacity of the heat pump. The part load factor (PLF) can be estimated in each time step for each zone in heating and cooling mode using equations 5.3 and 5.4.

$$PLF_{c,z_i} = \min\left(1, \frac{PLR_{c,z_i}}{0.83 \cdot PLR_{c,z_i} + 0.17}\right) \tag{5.3}$$

$$PLF_{h,z_i} = \min\left(1, \frac{PLR_{h,z_i}}{0.91 \cdot PLR_{h,z_i} + 0.09}\right) \tag{5.4}$$

Those equations are plotted in Figure 5.1 together with the suggested curves from

literature by Bettanini et al. [2003] to compare. The coefficients a and b were modified so that the curve can achieve a PLF of 1 in heating and cooling mode when $PLR = 1$.

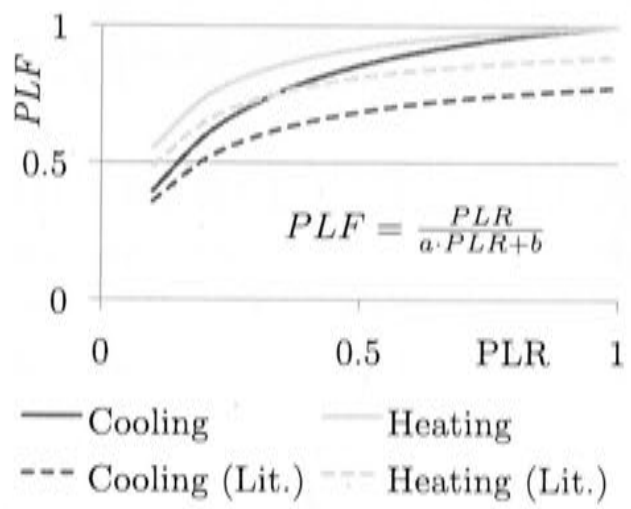

Figure 5.1: Functions between the part load factor (PLF) depending on the part load ratio (PLR) for heating and cooling of heat pumps. The notation "Lit." refers to the figures 4. and 6. in Bettanini et al. [2003]

The electricity consumption of the reference system for each zone is finally calculated using equation 5.5.

$$\dot{E}_{el,c/h,z_i} = \frac{\dot{Q}_{c/h,z_i}}{COP_{c/h} \cdot PLF_{c/h,z_i}} \tag{5.5}$$

5.1.2 A reference model in TRNSYS

The previous methodology presents a rather simple approach of calculating the reference electricity consumption using a reference COP. In this case the cooling and heating output of the alternative solar model can be extracted and the reference COP serves as a conversion factor how much electricity a reference system would use for the same amount of cooling or heating generated. However, for a more detailed approach it is possible to design an entirely separate reference cooling, heating and DHW model in TRNSYS using electrical heat pumps and an electrical element in the hot water tank for hot water generation. Such a model is able to deliver own results from an annual simulation and was chosen for further analysis.

One reverse cycle air-conditioner is allocated to each zone and its capacity is sized according to Table 4.12. The capacity of the zone is the maximum of either heating or cooling.

If the reverse cycle air-conditioner can't provide sufficient heating in winter, it is assisted by an electric supplementary heater. The capacity for the supplementary heating unit is the difference between required heating capacity for each zone C_{h,z_i} and the rated heating capacity of the scaled reverse cycle air-conditioner plus 2 kW extra. If the cooling demand is larger than the heating demand, the system is sized for cooling and the heating is covered automatically due to the higher COP_h. The extra supplementary heater would be smaller than 2 kW or even zero. In climates where heating dominates the full 2 kW are added.

To model a heat pump with two different stages in TRNSYS, hence, two different air flow rates for each zone, two heat pumps of type 665 were used for each zone. Stage two operates at full capacity whereas stage one works at 66%. The performance data from the example TESS file is used and a scale factor sizes the heat pump to the required capacity[1].

The thermostats were set to operate in the same temperature window as the absorption chiller system. The deadband is +/-1°C. Stage one cooling switches on if the room temperature exceeds $T_{setC} - 0.5\,°C + 0.5\,°C$ and switches off if $T_{setC} - 0.5\,°C - 0.5\,°C$ is achieved. In case the room heats up despite of stage one being in operation, stage two switches on (and stage one switches off) at $T_{setC} + 0.5\,°C + 0.5\,°C$ and switches off again at $T_{setC} + 0.5\,°C - 0.5\,°C$. The heating thermostat settings are similar. First stage heating switches on if the room temperature falls below $T_{setH} + 0.5\,°C - 0.5\,°C$ and switches off when $T_{setH} + 0.5\,°C + 0.5\,°C$ is reached. In case the room cools down further and falls below $T_{setH} - 0.5\,°C - 0.5\,°C$, even though stage one was switched on, stage 2 will switch on and stage 1 will switch off. Stage two switches off, when $T_{setH} - 0.5\,°C + 0.5\,°C$ is reached. If it is still not possible to provide sufficient heating and the room temperature falls below $T_{setH} - 1.5\,°C$, stage 3 (electrical supplementary heating) switches on. This switches off at $T_{setH} - 0.5\,°C$.

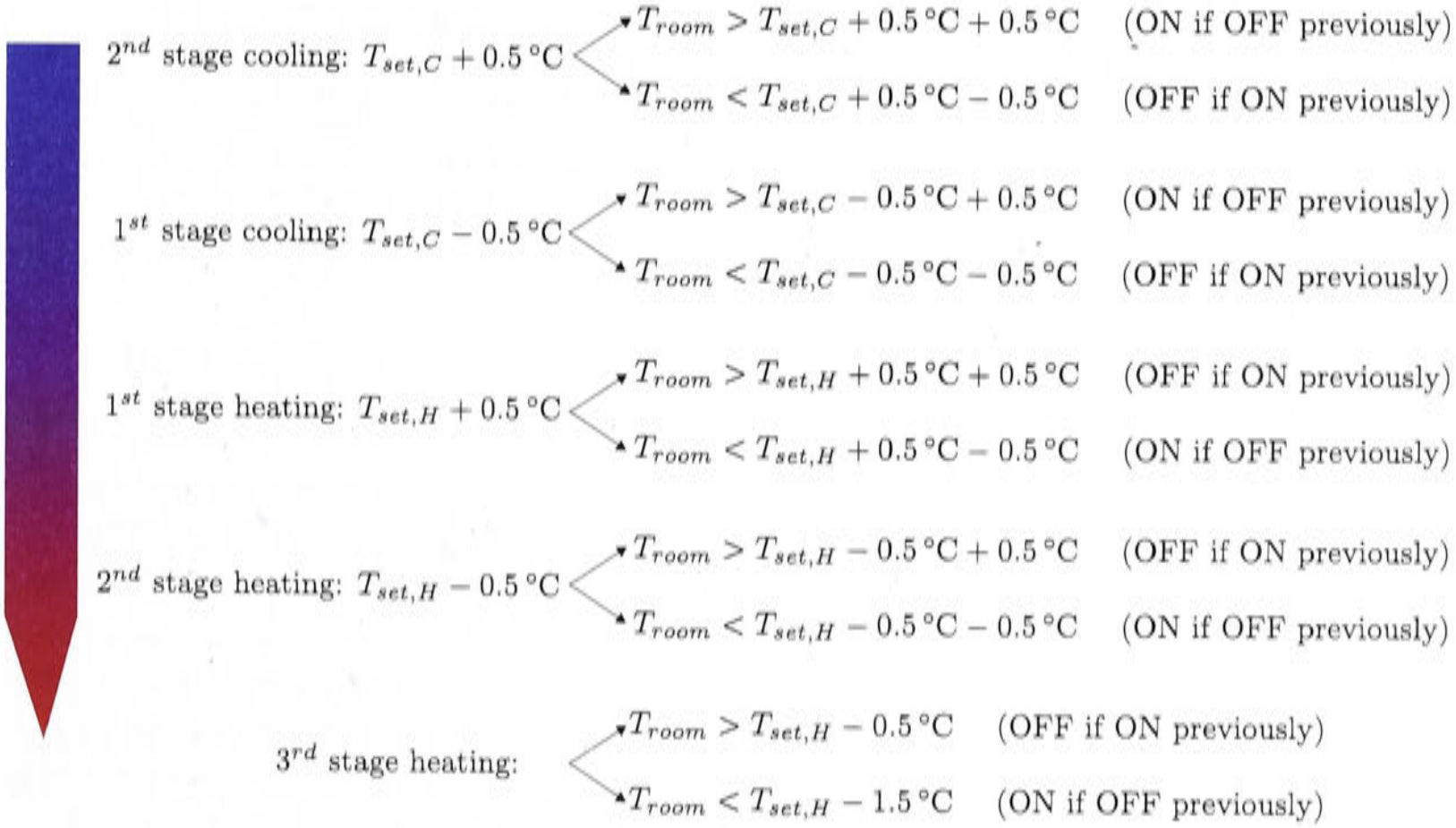

Figure 5.2: Thermostat settings of the reference system

The room set point temperatures and the HVAC schedules are the same as for the thermal HVAC (and DHW) system outlined in Table 4.6.

[1]The rated cooling capacity of the TESS component is 4.98 kW at 294 l s^{-1} air flow, 17°C wet bulb temperature, 24°C return dry bulb temperature and 35°C outdoor air dry bulb temperature. The rated heating capacity is 5.66 kW at 319 l s^{-1} air flow, 21°C return indoor temperature and 5.5°C outdoor dry bulb temperature.

5.2 Simulation results of the reference system

The reference system is used to compare various solar cooling options against. It is a typical installation for residential cooling and heating. The building model is heated and cooled with a reverse cycle air-conditioner for each zone which has been sized for the maximum of the cooling or heating load.

The system is able to provide space heating and space cooling and will be compared to solar systems which also provide both. When utilizing solar thermal systems for heating and cooling, domestic hot water plays a valuable role to make such systems more cost competitive. In Australia most domestic hot water systems are powered by electricity and it is therefore a fair comparison to assume that the service of domestic hot water in the reference case is also provided by electricity.

Occupant comfort in the building is controlled with the control strategy as defined in Figure 5.2. Table 5.1 shows that the air-conditioning system is able to keep the temperature in all climates more than 98% of the time below $T_{setC} + 1\,°C$. However, in Darwin or Brisbane and also in Sydney it is difficult to keep the humidity below 60% by a simple room air temperature control.

Table 5.1: Reference case: comfort conditions, cooling and heating energy supplied to the 230 m² conditioned space and heat demand for DHW generation.

	$comf_T$	$comf_{RH}$	$Q_{c,ref}$ [kWh/a]	latent	$Q_{h,ref}$ [kWh/a]	$Q_{dhw,ref}$ [kWh/a]
Canb	1.9%	12.5%	2445	17.1%	8969	4084
Brisb	0.7%	46.3%	6700	24.2%	1113	4084
Syd	0.6%	40.6%	3132	23.8%	2374	4084
Grif	1.8%	18.0%	6770	17.6%	5623	4084
TenCr	1.4%	1.2%	18165	11.2%	88	3224
Darw	0.2%	77.7%	20368	41.0%	0	3224
Melb	1.4%	18.8%	1962	26.0%	6833	4514

The electricity consumption of the HVAC and DHW system per m² of conditioned space (CS) in each region are depicted in Figure 5.3. The graphic also shows which proportion occurs during peak hours from 16:00 until 20:00. The peak electricity demand including domestic hot water is not very meaningful as the model of the DHW usage pattern is based on the hot water standard with eight fix water draws every day, each 6 min. It is questionable, if real patterns of domestic hot water usage occur exactly at those times in every household every day of the year.

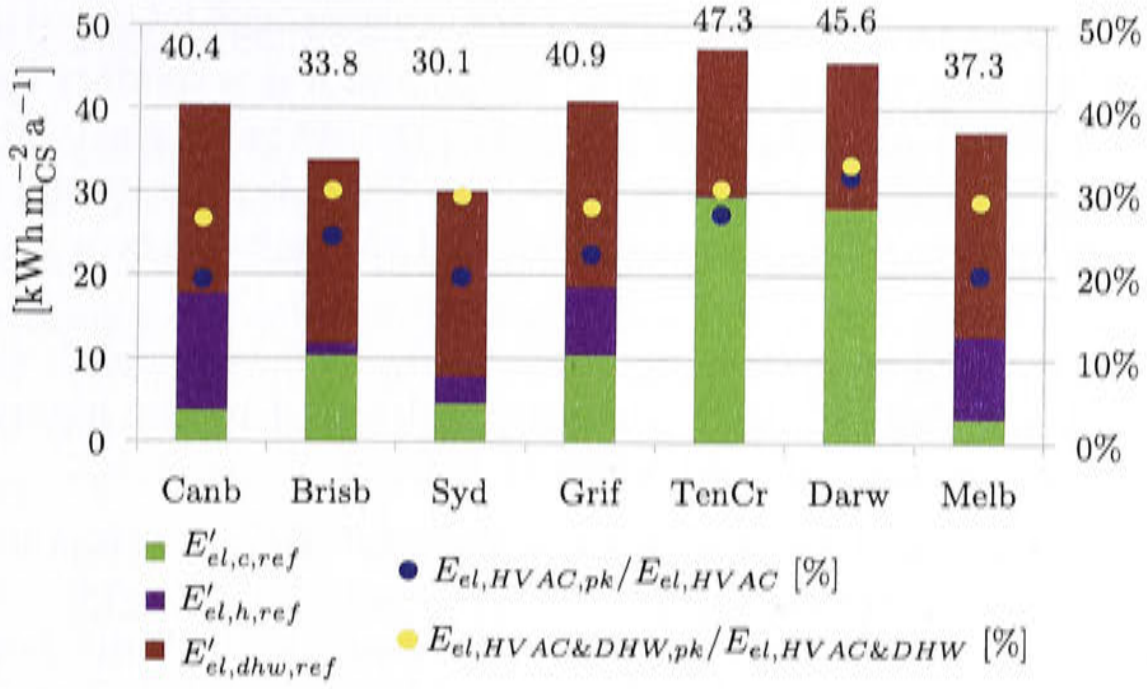

Figure 5.3: Electricity consumption of the HVAC system and the DHW specific to the conditioned space (left), and the proportion of electricity consumed during peak hours (16:00-20:00) (right)

Table 5.2: Electricity consumption specific to the amount of cooling and heating (and DHW) generated (reference case).

	ES	ES_{dhw}
Canberra	0.360	0.600
Brisbane	0.338	0.638
Sydney	0.332	0.722
Griffith	0.347	0.571
Tennant Creek	0.374	0.506
Darwin	0.318	0.445
Melbourne	0.338	0.645

5.3 Economic and environmental performance of the reference system

The work examines solar space conditioning in order to understand if it is possible to achieve the same comfort conditions with lower greenhouse gas emissions and hopefully lower cost. Since reverse cycle air-conditioners are the state of the art in the residential sector their cost represents the reference case. It can be assumed that it also represents the lowest specific cost per kWh of cooling and heating due to technological maturity.

The methodology to calculate the reference specific cost ($c_{m,ref}$) for cooling in Australia is calculated using equation 4.32 and taking the population density of the 7 cities in the 6 climate zones into account (Table 4.13). The population of the cities with more than 20 000 residents can be found in the Appendix in Table C.1 and also their allocation to the seven different climate zones.

To calculate the specific cost per kWh of cooling, heating (and DHW), according to equation 4.19 and 4.20, certain assumptions on the initial investment of all components, the installation and the running cost have to be made. Table 5.3 summarizes these assumptions and includes the cost for solar electric systems in the following

chapter. It is mainly of interest in this work to understand how certain technical or environmental measures effect the specific cost and it is secondary how sensitive these costs are towards market driven changes. The price for electricity is not expected to increase beyond the fixed interest rate i. There is no fraction of the capital cost for auxiliary equipment as no pumps, pipes, heat exchangers or cooling towers are required.

The calculated cost per kWh is depicted in Figure 5.4a for each climate. The reference cost is also shown, which is mostly influenced by the highly populated climate zone 3 ("warm summer, cold winter", Sydney).

Table 5.3: Cost assumptions for the reference system and the PV assisted system in Chapter 6

Reference	Reference + PV	Abbreviation	Cost	Unit
Reverse cycle AC		I_{AC}	600	$\$\,kW^{-1}$
Hot water tank		I_t	3	\$/l
	PV modules	I_{PV}	2	\$/W
	Inverter	I_{inv}	2000	\$
		$I_{eq} = I_{AC} + I_t(+I_{PV} + I_{inv})$		
Planning and installation	$I_{t=0} = \frac{I_{eq}}{1-q_{PInst}}$	q_{PInst}	0.1	-
Maintenance		$p_{maint,fix}$	150	$\$\,a^{-1}$
	Maintenance PV	$p_{maint,fix,PV}$	200	$\$\,a^{-1}$
Fix gas price (capacity charge)		$p_{gas,fix}$	250	$\$\,a^{-1}$
Fix water price (capacity charge)		$p_{water,fix}$	100	$\$\,a^{-1}$
Fix electricity price (capacity charge)		$p_{el,fix}$	300	$\$\,a^{-1}$
Variable gas price (here 2.5ct/MJ)		p_{gas}	0.007	$\$\,kWh^{-1}$
Variable water price		p_{water}	3	$\$\,m^{-3}$
Variable electricity price		p_{el}	0.3	$\$\,kWh^{-1}$
	Feed-in factor $frac_{PV} = \frac{p_{el,sol}}{p_{el}}$	$frac_{PV}$	1, 0.33, 0	-
Life time		N	20	a
Interest		i	0.06	-

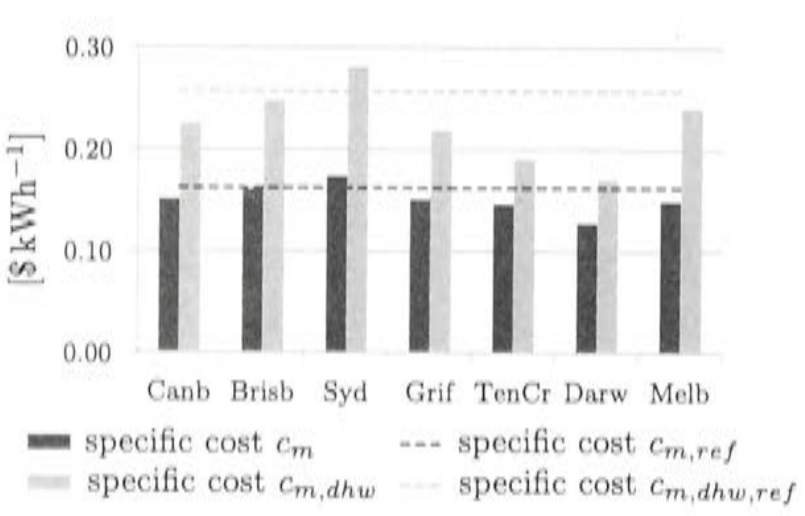

(a) specific cost

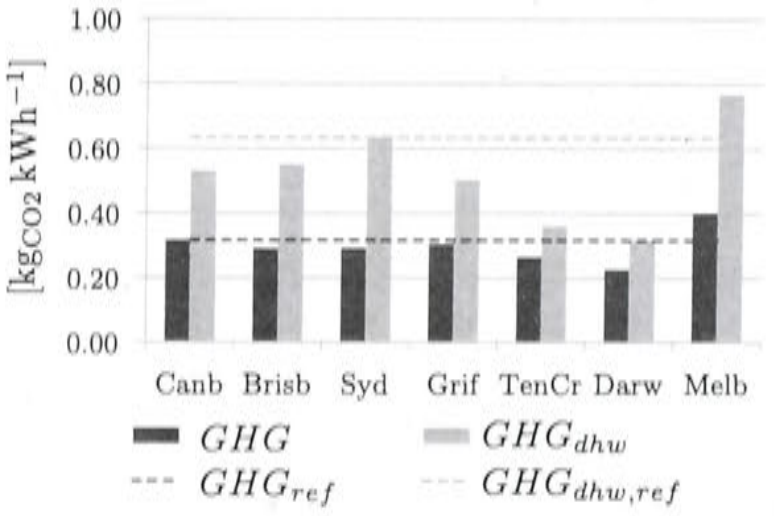

(b) specific GHG emissions

Figure 5.4: The specific cost and GHG emissions of the reference system with and without DHW. The variables $c_{m,ref}$ and GHG_{ref} are the population weighted means including and excluding DHW (equation 4.32)

The specific greenhouse gas emissions are shown in Figure 5.4b and they are

highest in the coldest climate zone "mild/warm summer, cold winter" which occurs in Melbourne.

It is important to note that even though the total electricity consumption for HVAC and DHW demand in Sydney is the lowest of all climates, the specific GHG emissions per kWh of cooling and heating are not, as it is a relative number comprised of the absolute greenhouse gas emissions and the amount of cooling and heating generated. Absolute numbers are presented in Figure 5.3 and Table 5.1 and show that the electricity consumption is proportional to the cooling and heating demand in all climates.

Cost, greenhouse gas emissions and comfort are combined in the overall performance factor (OPF) and granting each part equal importance ($1/3 = \alpha = \beta = \gamma$). Figure 5.5 shows that in Melbourne the greenhouse gas emissions are higher which is related to the higher greenhouse gas emission factors in Victoria. In Darwin the comfort is lowest. This is related to the cooling strategy, since the reverse cycle air-conditioner does not over-chill and reheat to get rid of all the humidity. The OPF is calculated with and without DHW in figures 5.5a and 5.5b respectively. The difference of the OPF with and without DHW are small except for Tennant Creek and Canberra.

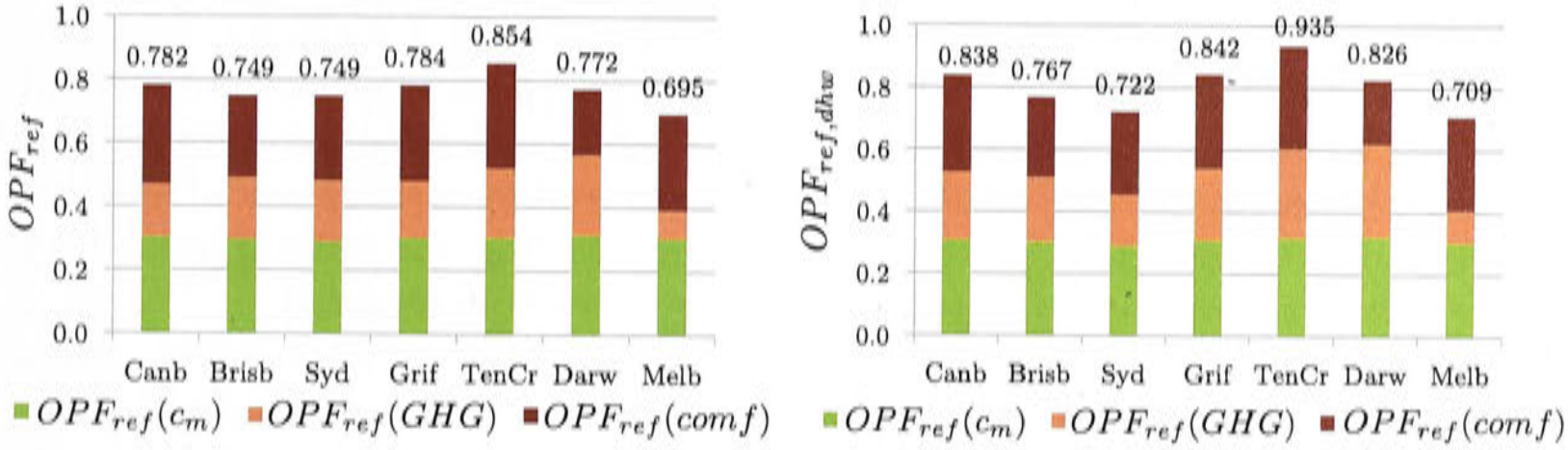

(a) OPF

(b) OPF incl. DHW

Figure 5.5: The overall performance factor OPF of the reference system with and without DHW

5.4 Conclusion

The reference case has been established and all performance parameters are determined which can be used to assess solar cooling, heating and DHW systems. The following chapter will extend this model by including photovoltaic modules, backed up by the grid or a diesel generator. In addition to that the use of electricity storage in form of batteries is included. Two feed-in tariff options will also be investigated to analyze cost effectiveness.

The contribution of photovoltaic to the reference system with and without electricity storage - PV & batteries

As solar air-conditioning today cannot ignore the fact that PV and also battery storage solutions became much more cost effective over the last 3 years, this work analyzes also the performance of PV assisted HVAC (and DHW) systems throughout the different climates of Australia. Rooftop PV systems will assist the reference system and a performance analysis of the results for different system sizes and financial schemes will be conducted. The photovoltaic solar cooling and heating technology proves to be the most viable one for residential systems at this time.

PV modules are able to export surplus electricity to the electricity network. However, not every household is connected to or wants to be connected to the grid. Considering remote and non-grid connected areas, the study has been completed with the inclusion of an electricity storage capacity (battery) which is able to increase the solar fraction. The electricity backup in this case is either the grid or a diesel generator, because having a battery does not necessarily imply being disconnected from the grid.

The following sections outline the modeling approach with and without battery backup and discuss the system performance under varying feed-in tariff assumptions and backup options.

6.1 Modeling assumptions

The nature of photovoltaic systems in homes with electricity grid connection negates the need for storage, if there's a surplus or deficit of electricity to run the HVAC system. The grid serves as the storage and the simulation can be simplified as the HVAC system may operate independently of the solar electricity supply. This is different to the complexity of thermally driven systems which are to come in the following chapters.

The photovoltaic driven system has been modeled using openly available performance data for modules and inverters. The chosen panels are manufactured by the American company SUNPOWER. They generate 195 W m^{-2} at standard conditions[1] [Sunpower, 2013]. The panels produce 318 W module^{-1} and each module measures 1.63 m^2. Efficiency data for the inverter was obtained from the German company SMA [SMA Solar Technology, 2014]. The inverter chosen is the transformer less SunnyBoy 3000TL or 5000TL, depending on the size of the PV array.

As a first design approach the maximum of either cooling or heating capacity for the building in each climate (Table 4.12) provided the base to calculate the required amount of PV modules. The rated thermal COPs for cooling and heating, $COP_{el,c,rated} = 3$ and $COP_{el,h,rated} = 4$, were used together with the rated electricity production of one particular PV module to calculate the amount of PV modules for scenario PV1.

Table 6.1: Scenarios PV1 to PV4 defined by the amount of PV modules and installed electrical capacity [# modules (W m$^{-2}_{CS}$)]. The shaded configurations are the chosen configuration for the purpose of comparison to other HVAC(&DHW) systems.

	1st estimation (PV1)	below 60% $SF_{el,tot}$ (PV2)	above 60% $SF_{el,tot}$ (PV3)	PV1 + 2 modules (PV4)
Canberra	5 (6.9)	4 (5.5)		7 (9.7)
Brisbane	6 (8.3)	3 (4.1)	4 (5.5)	8 (11.1)
Sydney	4 (5.5)	2 (2.8)	3 (4.1)	6 (8.3)
Griffith	7 (9.7)	4 (5.5)	5 (6.9)	9 (12.4)
Tennant Creek	8 (11.1)	6 (8.3)	7 (9.7)	10 (13.8)
Darwin	8 (11.1)	6 (8.3)	7 (9.7)	10 13.8)
Melbourne	4 (5.5)	3 (4.1)		6 (8.3)

From the results of scenario PV1, it was linearly calculated how many modules would be necessary to achieve a solar fraction $SF_{el,tot}$ of 60% for solar cooling and heating only. The result was rounded up (PV3) and down (PV2) to the nearest integer and 2 new scenarios could be simulated with the new PV array size . For Canberra and Melbourne scenario PV3 resulted in the same amount of modules as PV1. For PV4 2 extra modules were installed to the modules of PV1 to analyze the change in performance.

The gray outlined configurations in Table 6.1 are the chosen PV configurations for each climate to provide a solar fraction ($SF_{el,tot}$) of at least 60%.

The cooling, heating and domestic hot water loads are the same as for the reference case as the building and the set points do not change. The only difference is the contribution of the solar electricity in respect to the time of availability and magnitude. The hot water tank capacity is sized to 350 l.

The simulation outputs of the solar PV assisted reference HVAC (and DHW) system have been analyzed in three different ways:

[1] According to their specification, SUNPOWER offers modules producing 200 W m^{-2} today in 2014.

1. System grid connected with varying feed-in tariff (no battery)
2. System grid connected with battery (no feed-in tariff)
3. System off-grid, diesel generator as electricity backup with battery

6.2 On-grid with feed-in tariff (no electricity storage)

Figure 6.1 shows $SF_{el,tot}$ for all 4 PV scenarios. The dashed lines intersect the x-axis, where the installed photovoltaic capacity in $W\,m_{CS}^{-2}$ would achieve a total solar fraction of 60%. The values in Table 6.2 are derived from the same figure.

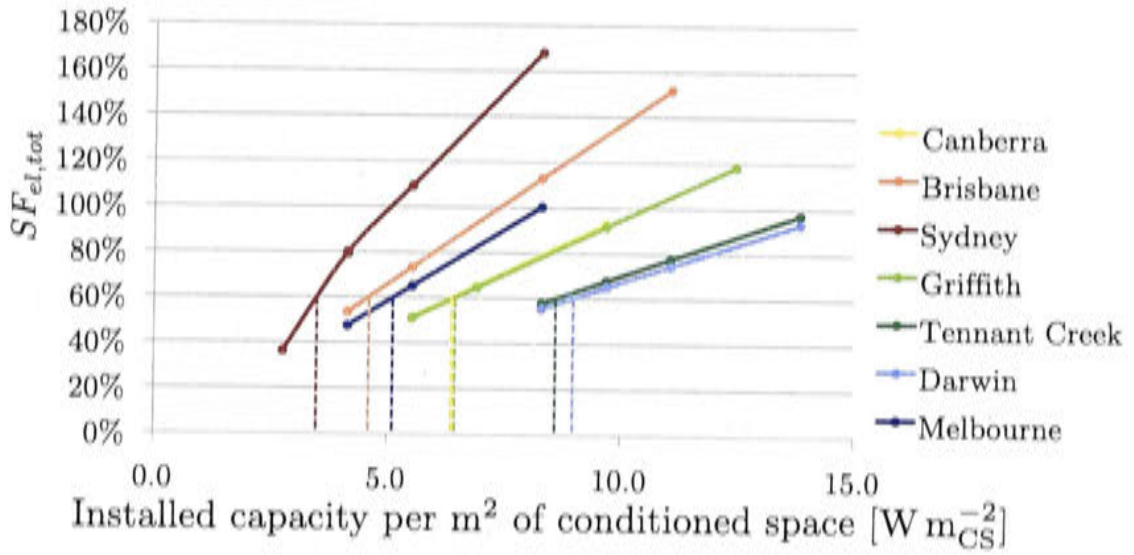

Figure 6.1: The total solar fraction $SF_{el,tot}$ as defined in equation 4.5 (PV)

Table 6.2: Necessary PV capacity per m^2 of conditioned space (CS) to achieve a total solar fraction ($SF_{el,tot}$) of 60%

	$W\,m_{CS}^{-2}$
Canberra	6.40
Brisbane	4.61
Sydney	3.55
Griffith	6.46
Tennant Creek	8.60
Darwin	8.96
Melbourne	5.14

The total solar fraction including the generation of domestic hot water ($SF_{el,tot,dhw}$) can be seen in Figure 6.2. Generating domestic hot water with electricity dramatically reduces $SF_{el,tot,dhw}$ compared to $SF_{el,tot}$.

The solar electricity production in each climate is shown in Figure 6.3. It corresponds to the PV array of the chosen configuration with a solar fraction ($SF_{el,tot}$) of at least 60% as shaded in Table 6.1. The proportion of electricity which is generated during peak hours of 16:00 to 20:00 is relatively small.

The solar fractions represented by figures 6.1 and 6.2 do not consider the time of coverage. The total amount of solar generation was simply divided by the total

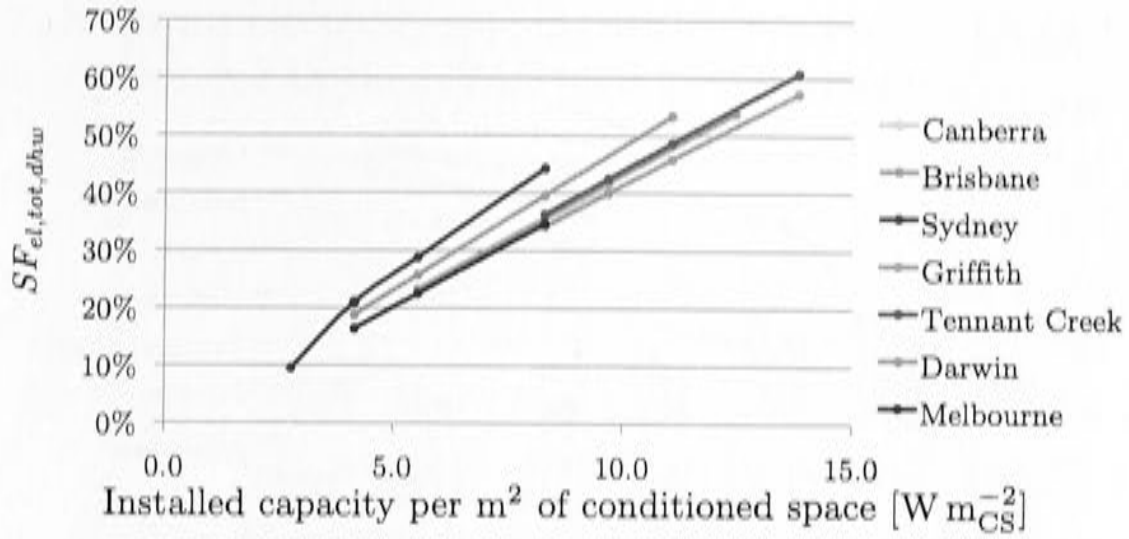

Figure 6.2: The total solar fraction including DHW $SF_{el,tot,dhw}$ as defined in equation 4.6

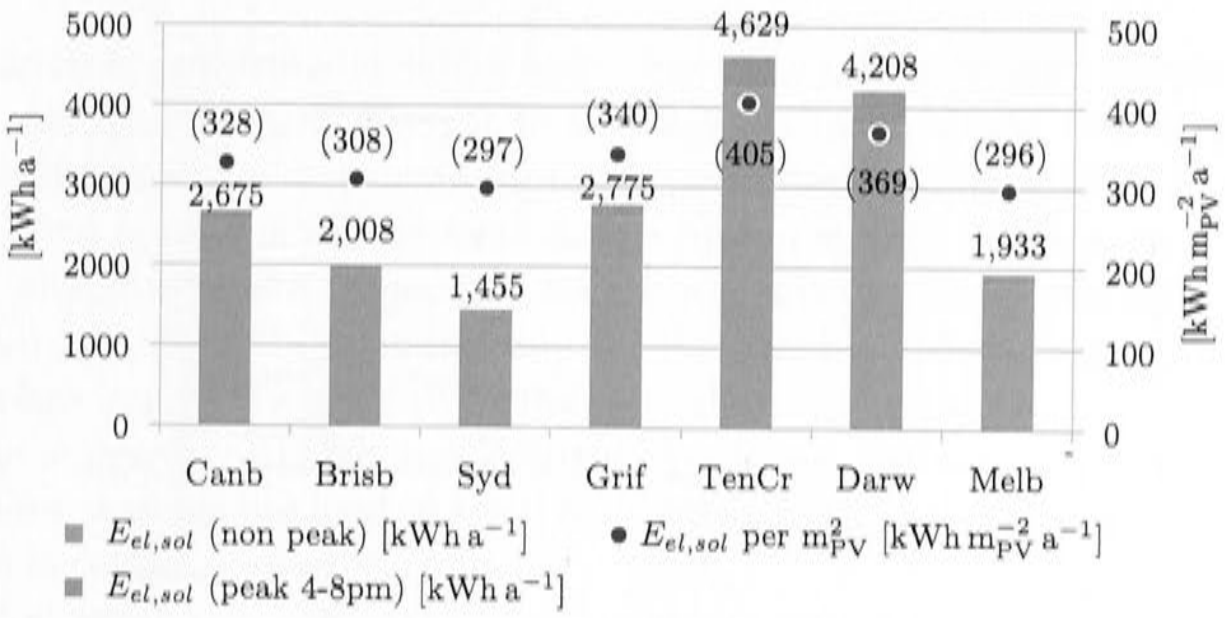

Figure 6.3: Total (left) and collector area specific (right and values in brackets) solar generated electricity in each climate, on and off peak

amount of electricity consumption for HVAC (and DHW). This is different for Figure 6.4 and 6.5. They display the solar fraction $SF_{el,LCov}$ and $SF_{el,LCov,dhw}$ including only that part of the solar electricity which can be used when there is HVAC (and DHW) demand.

For the chosen configuration shaded in Table 6.1, the proportion of solar electricity generation at peak hours (16:00-20:00) to the electricity demand in peak hours with or without DHW is shown in Figure 6.6. The same graphic shows the fractions of solar electricity which can be utilized directly to condition the space (and produce DHW). In the next section a battery is added to the PV system in order to increase the amount of solar electricity utilized.

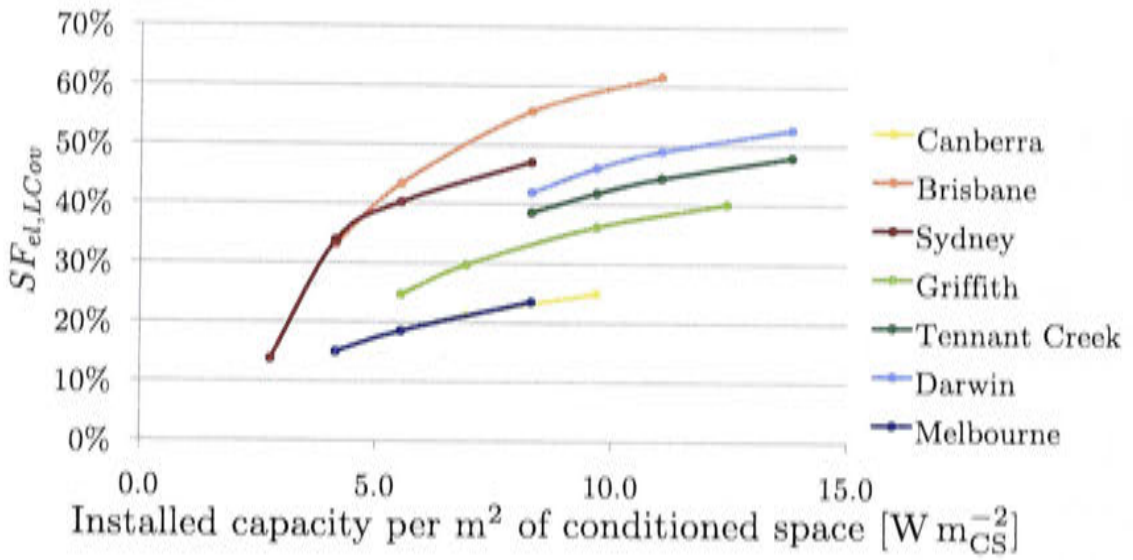

Figure 6.4: The solar fraction considering time of solar electricity generation ($SF_{el,LCov}$) as defined in equation 4.3

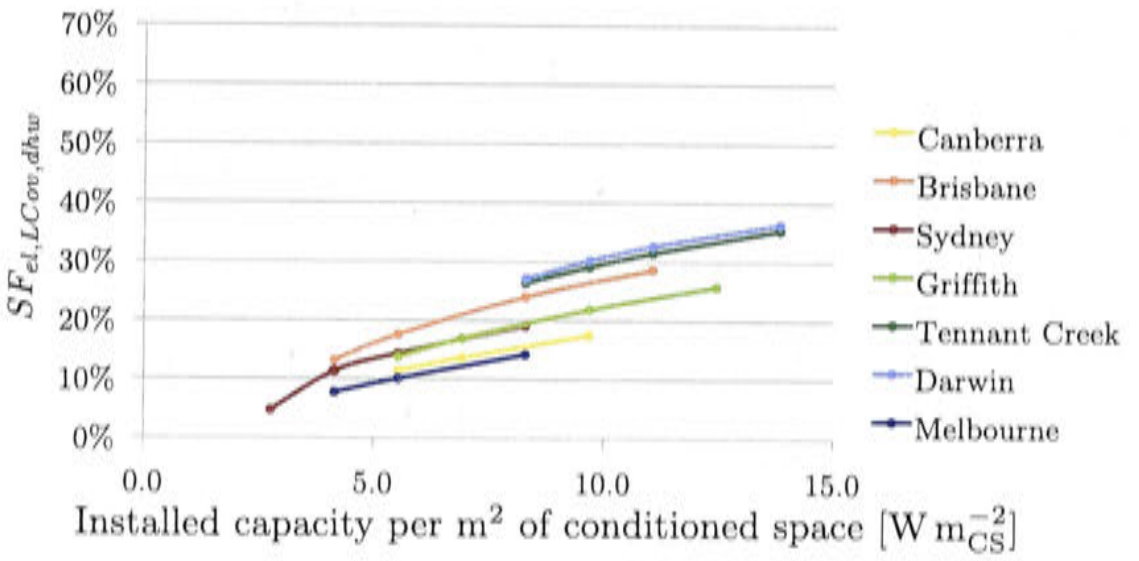

Figure 6.5: The solar fraction considering time of solar electricity generation including DHW ($SF_{el,LCov,dhw}$) as defined in equation 4.4

Figure 6.6: Proportion of HVAC (and DHW) electricity demand that can be covered by PV in peak hours and the proportion of solar electricity production that can be utilized for HVAC (and DHW), for the chosen PV collector array

Figure 6.7 shows the electricity savings during peak hours for each kWh of cooling and heating generated by the HVAC (and DHW) system.

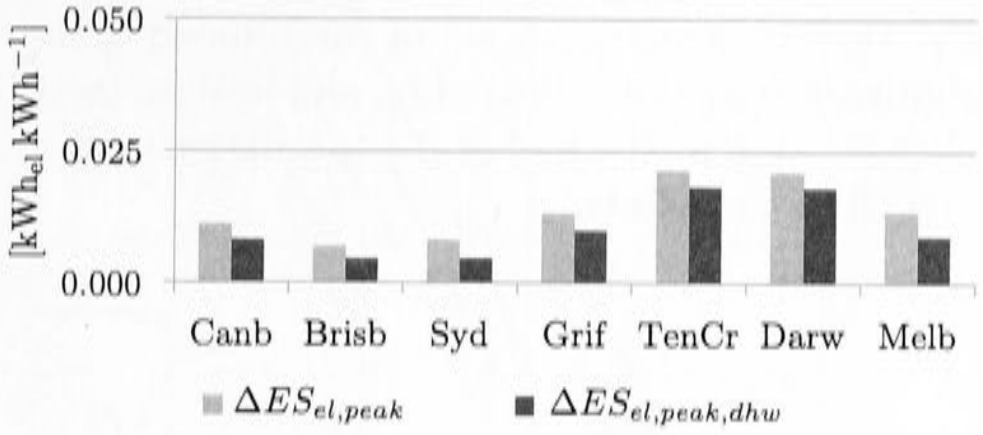

Figure 6.7: Specific electricity saved during peak hours (PV assisted)

The economic performance when including PV modules strongly depends on the subsidies and feed-in tariff present in the state of installation. The feed-in tariffs used in this thesis resemble prevailing tariffs, with the caveat that Australia's climate zones are often spread across several states. State regulations are independent and have been changing quite frequently over the last 3 years. Most states consider a "net" feed-in tariff scheme, paying only for the surplus of solar electricity, after the generation has been subtracted from the total electricity used.

In some states there's also an electricity retailer contribution which is subject to change. In most states the feed-in tariff for the surplus of solar electricity is currently (May 2014) between 7.5 and 16 ct kWh$_{el}^{-1}$.

In the following two subsections the economic performance and the OPF will be calculated with a "net" feed-in tariff and $frac_{PV}$ will be 1 and 1/3. This means, if the cost of electricity is assumed to be 30 ct kWh$_{el}^{-1}$ a $frac_{PV}$ of 1/3 translates to a financial benefit of exported solar electricity ($p_{el,sol}$) of 10 ct kWh$_{el}^{-1}$. Hence, it is much more valuable to use solar electricity than selling it. A reasonable average value is $frac_{PV} = 1/3$ for the feed-in tariff assumption throughout the states.

In remote areas without a strong electricity grid, like for example in climate zone 5 represented by Tennant Creek with "hot dry summers, mild winters", it is reasonable to assume that $frac_{PV}$ is zero instead of 1/3 and no feed-in tariff is paid for exported surplus electricity.

6.2.1 High net feed-in tariff

In this section the system performance is analyzed under a high net feed-in tariff with $frac_{PV} = 1$.

The electricity savings from the photovoltaic array correspond linearly to the saved primary energy and greenhouse gas emissions. For the specific greenhouse gas emissions it is assumed that greenhouse gas emissions are considered to be "offset" when they occur simultaneously with the HVAC (and DHW) demand. Nevertheless, the value of the total amount of electricity purchased from the grid is offset by the value of the solar electricity fed back into the grid regardless of the time. Therefore, the system owner benefits economically from solar electricity fed into the grid at any

time, but since not all specific greenhouse gas emissions are offset at his premisses they are not considered to reduce the emissions for his HVAC (and DHW) system.

In Figure 6.8 the specific cost per kWh of cooling and heating is shown, in relation to the installed solar electric capacity per m^2 of conditioned space. Also shown are the population weighted average cost for cooling and heating (and DHW), $c_{m,ref}$ and $c_{m,dhw,ref}$. The smaller the system, the higher the specific cost. Warmer climates have the lowest cost when DHW is included.

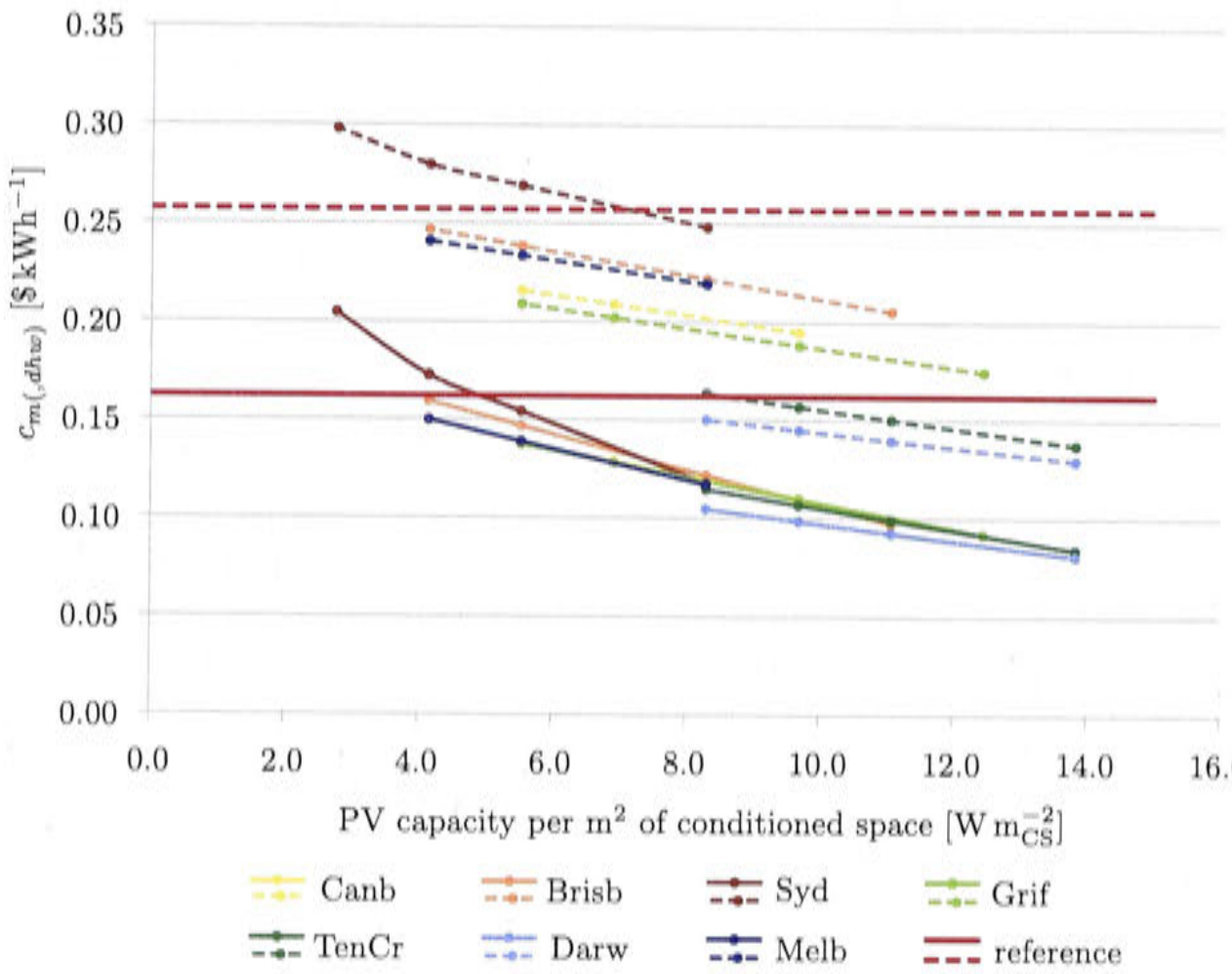

Figure 6.8: The specific cost with and without DHW as a function of the installed PV capacity in each climate (excluding DHW (solid —), including DHW (dashed - -))

Figure 6.9a and Figure 6.9b show the solar fraction $SF_{el,tot}$ and $SF_{el,LCov}$ and the trend shows that the solar fraction increases with dropping specific cost.

In Figure 6.10 the greenhouse gas savings of the PV system per kWh of cooling and heating (and DHW) compared to the reference case are shown. Clearly, the specific greenhouse gas emissions of the reference system are larger than of the PV supported system.

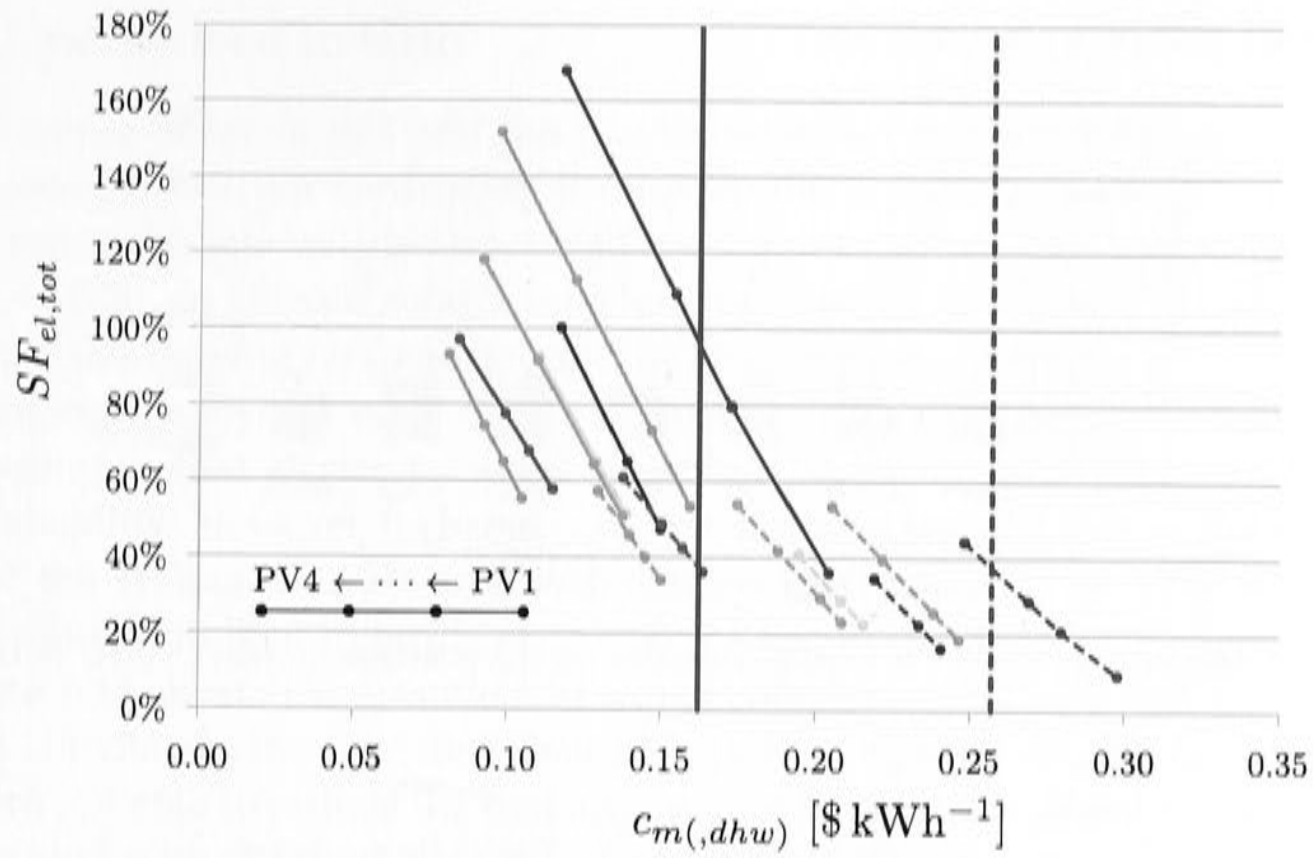

(a) $SF_{el,tot}$

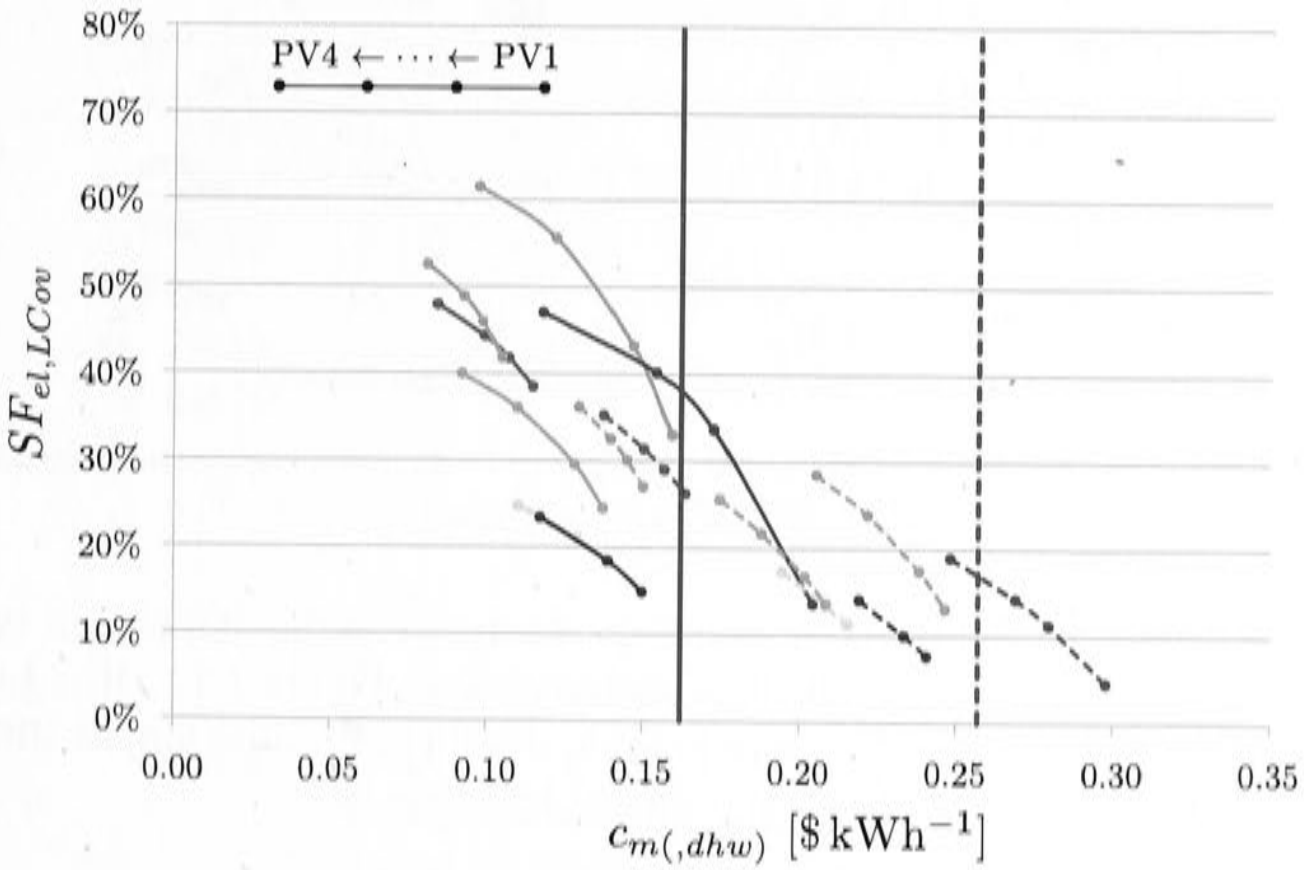

(b) $SF_{el,LCov}$

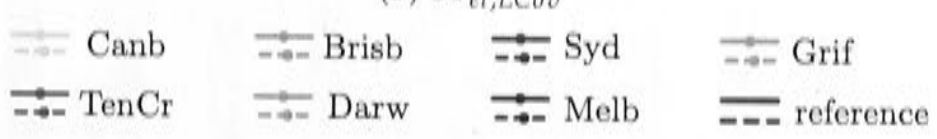

(c) legend

Figure 6.9: $SF_{el,tot}$ and $SF_{el,LCov}$ as a function of the specific cost for all climates (excluding DHW (solid —), including DHW (dashed - -))

The difference in specific cost Δc_m for HVAC (and DHW) is shown in Figure 6.11. The graphic shows that the PV system can generate cooling and heating at a lower cost, provided the feed-in tariff is the same as the retail price. In the next section the

feed-in tariff will be lowered to 1/3.

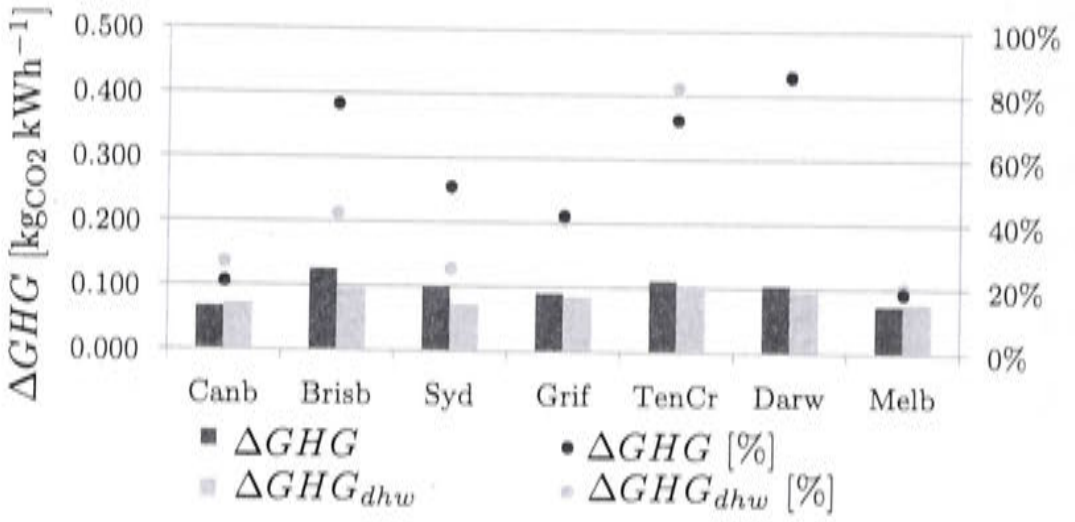

Figure 6.10: GHG savings of the PV system compared to the reference system ($\Delta GHG = GHG_{ref} - GHG$)

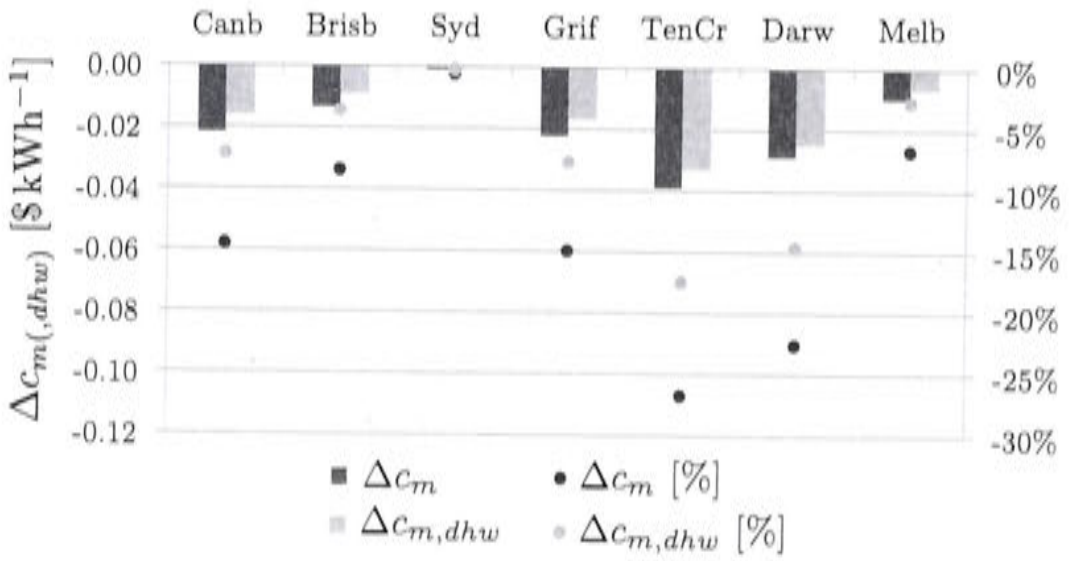

Figure 6.11: Absolute and relative change of the specific cost of the reference system compared to the PV system ($\Delta c_m = c_m - c_{m,ref}$)

As for the reference system, an overall performance factor (OPF) will be calculated with and without DHW and it is represented in Figure 6.12. It is higher in all climates compared to the reference system. Furthermore, the largest difference, when adding DHW occurs in Sydney, followed by Brisbane.

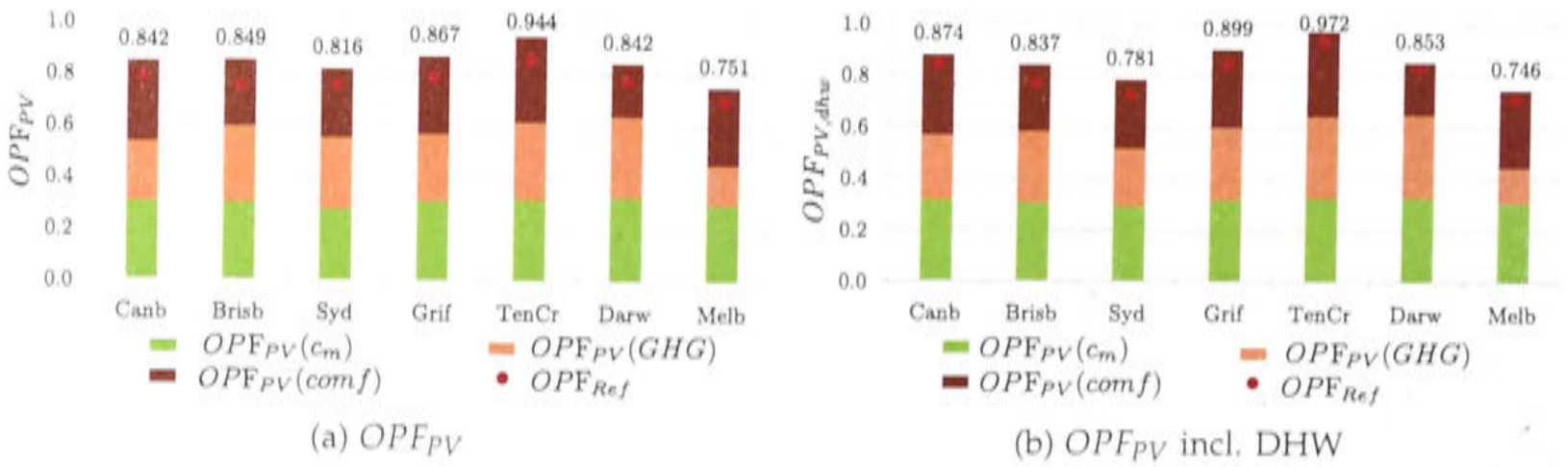

(a) OPF_{PV} (b) OPF_{PV} incl. DHW

Figure 6.12: The overall performance factor OPF_{PV} with and without DHW

6.2.2 Low net feed-in tariff

The difference between this and the previous section is that the surplus solar electricity generated, if not consumed at once by the HVAC (and DHW) system, will be fed into grid but will be rewarded only with 1/3 of the electricity price p_{el} ($frac_{PV} = 1/3$). In climate zone 5, which is represented by Tennant Creek, $frac_{PV}$ is even set to 0, implying no financial reward for exported electricity.

Changing the feed-in tariff does not change the system's performance since the model assumes that electricity will always be generated when it's possible due to solar availability. However, it changes the specific cost, hence the overall performance factor of the system. This section will discuss the sensitivity of a PV driven solar cooling solution to feed-in tariffs and what the implications are.

Figure 6.13 shows the specific cost in dependency of the installed solar capacity for each climate. In the case there is little economy of scale (Figure 6.8). Larger PV arrays are not able to reduce the cost any further because the additional electricity is not rewarded with the same value of purchased electricity.

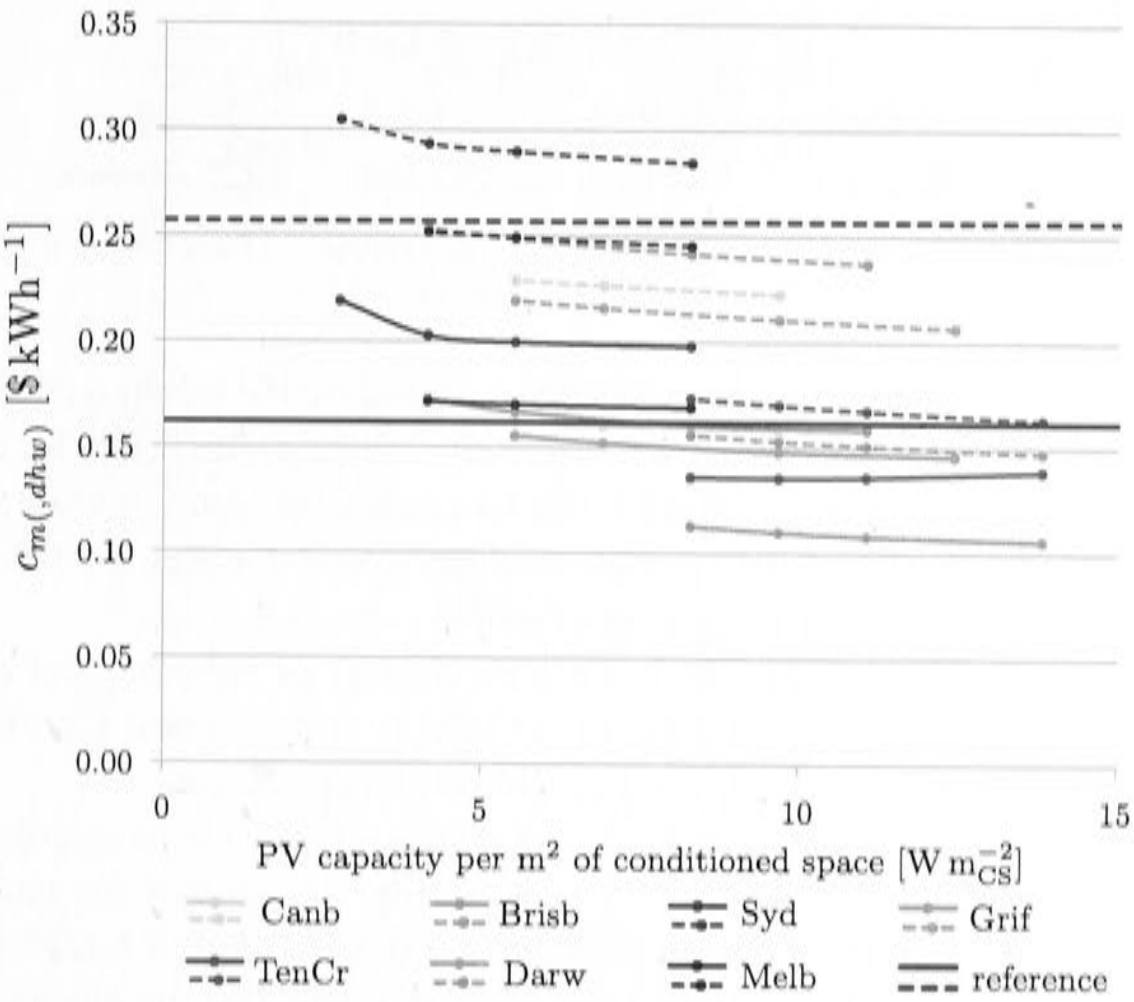

Figure 6.13: The specific cost with and without DHW as a function of the installed PV capacity in each climate for $frac_{PV} = 1/3$ (excluding DHW (solid —), including DHW (dashed - -))

When plotting the solar fraction at time of load coverage ($SF_{el,LCov}$) versus the specific cost with and without DHW (Figure 6.14) it becomes clear that the specific cost for each point of additional solar fraction does not drop nearly as much anymore as in Figure 6.9b with $frac_{PV} = 1$. In Tennant Creek the cost for additional points of $SF_{el,LCov}$ even increases. However, in Tennant Creek $frac_{PV} = 0$ in order to express the remoteness of most towns in that climate zone, which are seldom connected to any electricity network. For those remote areas the use of batteries, which will be

analyzed in the next section, becomes important.

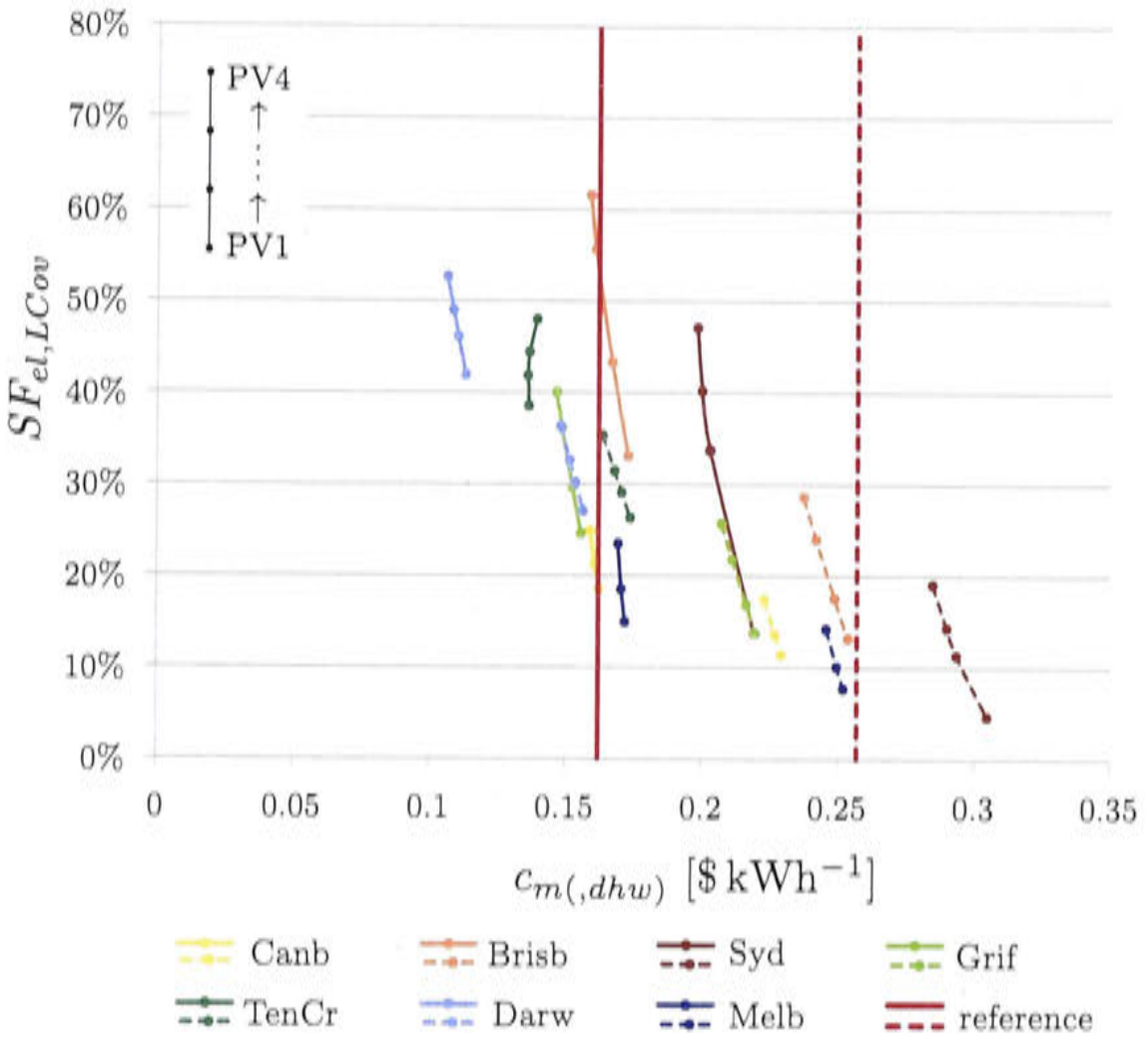

Figure 6.14: $SF_{el,LCov}$ and the specific cost c_m and $c_{m,dhw}$ for $frac_{PV} = 1/3$ (excluding DHW (solid —), including DHW (dashed - -))

Figure 6.15 compares the reference system assisted by PV when a net feed-in tariff with $frac_{PV} = 1$ applies to the surplus of solar electricity to the financial scheme with $frac_{PV} = 1/3$. For the purpose of clarity, the two cases for Sydney were highlighted. The area in between would be the specific cost per solar fraction for $frac_{PV}$ between 1/3 and 1. The same shape occurs for all climates.

Figure 6.16 shows the relative and absolute change of specific cost compared to the reference system. In all climates besides Darwin and Tennant Creek the specific cost for air-conditioning rises compared to the reference system.

The second way to express if a technology is cost effective is to calculate the break even electricity price as in equation 4.29. The results are shown for varying $frac_{PV}$ in Figure 6.17. It seems that for the really hot climates Tennant Creek and Darwin the break even point is reached without any feed-in tariff. For the climates Canberra, Brisbane and Griffith, the break even point lies at a feed-in tariff around 30% to 40% of the electricity price. In Melbourne the fraction must be approximately 70% and for Sydney a tariff as high as the electricity price achieves break even conditions.

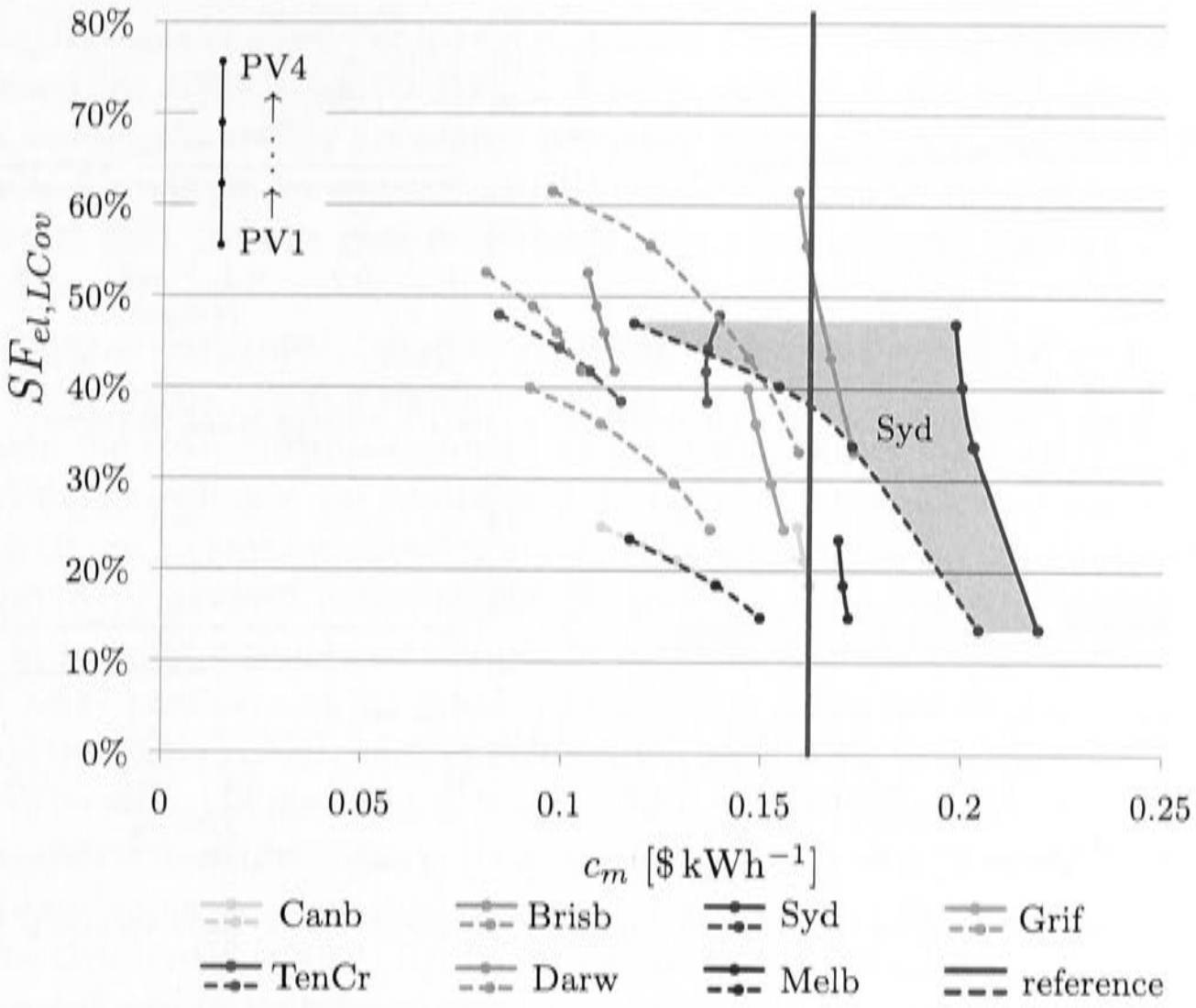

Figure 6.15: $SF_{el,LCov}$ and the specific cost c_m for $frac_{PV} = 1/3$ (solid —), and $frac_{PV} = 1$ (dashed - -) (excluding DHW)

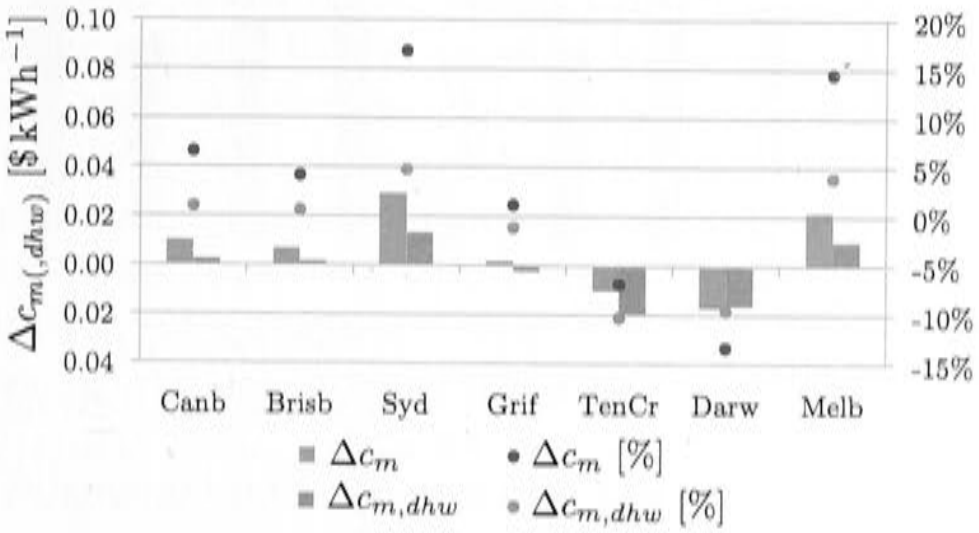

Figure 6.16: Absolute and relative change of the specific cost of the reference system compared to the PV system with $frac_{PV} = 1/3$ ($\Delta c_m = c_m - c_{m,ref}$)

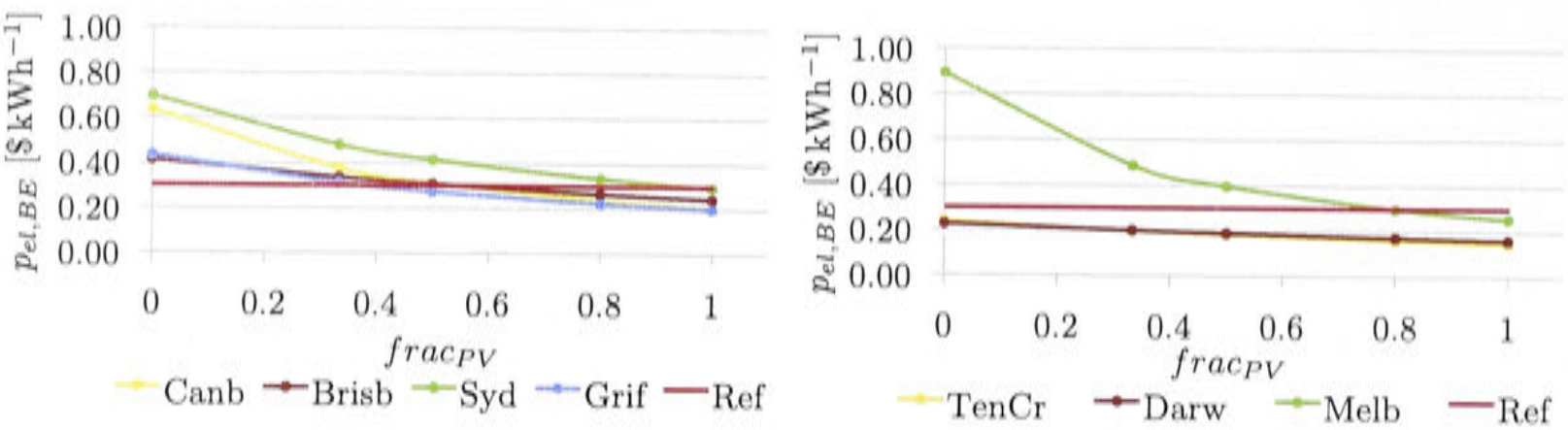

Figure 6.17: Break even price for electricity for the PV assisted HVAC systems

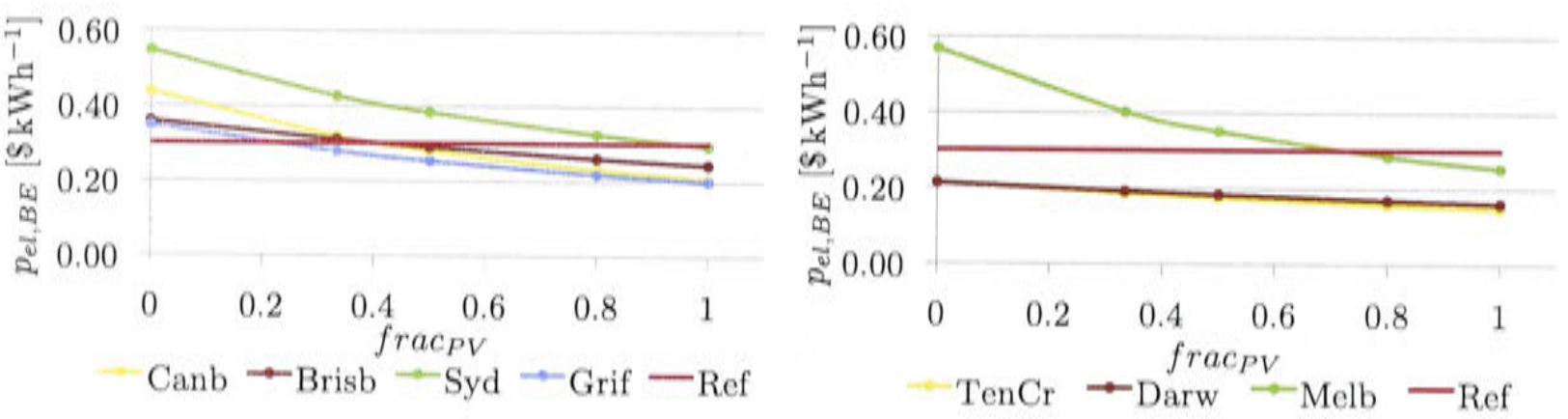

Figure 6.18: Break even price for electricity for the PV assisted HVAC systems including DHW

The overall performance factors have been calculated also for the lower feed-in tariff. Figure 6.19. The total factor slightly decreases due to the higher cost.

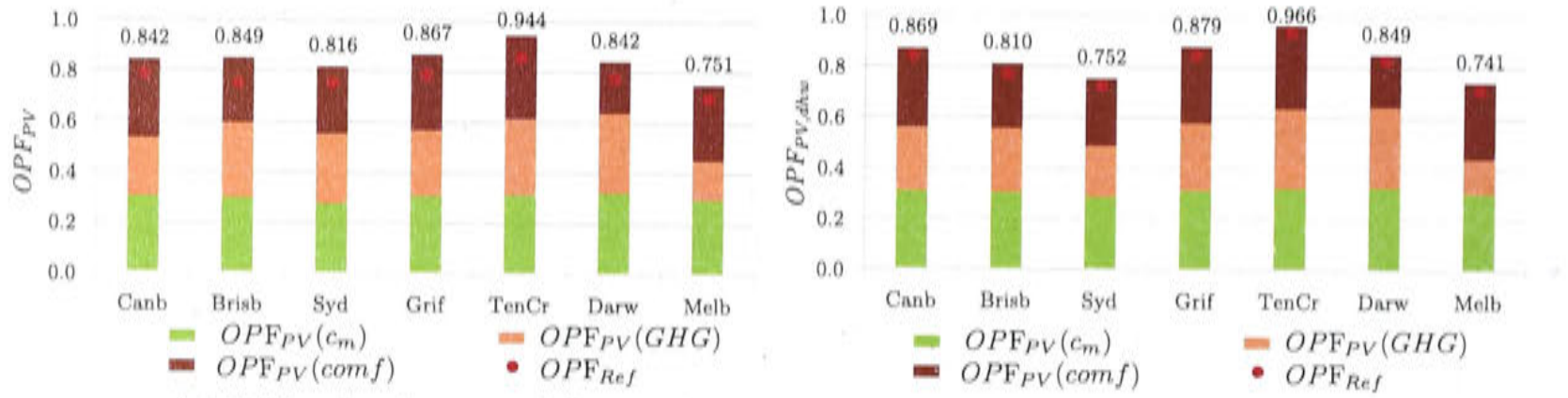

(a) OPF_{PV} for $frac_{PV} = 1/3$

(b) OPF_{PV} incl. DHW for $frac_{PV} = 1/3$

Figure 6.19: The overall performance factor OPF_{PV} of the PV assisted system with and without DHW and $frac_{PV} = 1/3$

6.3 Storage using batteries and no feed-in tariff

The solar PV arrays for each climate as outlined in Table 6.1 are designed to generate in total at least 60% of the air-conditioning's electricity demand ($SF_{el,tot} \geq 60\%$).

Without a battery to store solar electricity, a backup source is necessary if there's a deficit of solar electricity. On the other hand, if the solar electricity production exceeds the HVAC (and DHW) demand, there's a surplus of solar electricity and the grid serves as the sink, unless the electricity is discarded through opening the electric circuits.

In the previous chapter Figure 6.6 displayed the solar electricity which can actually be used for HVAC (and DHW). It was assumed that the grid acts as a source and sink in times of energy imbalance between supply and demand. Furthermore, it was assumed that it bears at least a small financial incentive to export surplus electricity to the grid. In this case now the feed-in tariff is set to zero for all climates ($frac_{PV} = 0$).

As previously assumed, the greenhouse gas savings are calculated only with the amount of electricity saved instantaneously at the HVAC (and DHW) system and do not include the solar surplus exported to the grid. Hence, the surplus export does not affect the greenhouse gas component of the overall performance factor.

In this chapter a storage capacity in form of a lithium-ion accumulator is added to the system to increase the percentage of the solar fraction. The extra storage capacity is sized to provide a number of hours of available storage capacity (Cap_{avl}) if the solar PV array produces at it's rated capacity. It is important to understand at this point, that the "hours of storage" in this context denote the hours the rated PV power output can be stored in the battery. It is not the time the HVAC and/or DHW) system can be supplied from the battery. The sensitivity study was performed from 1 to 6 hours storage capacity. The nominal storage capacity of such a battery would have to take the depth of discharge (DoD) into account and $Cap_{nom} = Cap_{avb}/DoD$ is the nominal battery capacity which must be purchased.

The website Solaranlagen-Portal [2014] provides sample information on installed battery supported solar PV systems mainly with lithium-ion technology. A survey of those systems showed that a typical number for the DoD is 80% and also that a typical ratio between available battery capacity in kWh and charging rate in kW is 0.88 h. This rate was used to determine the maximum rate of solar power which can be stored in one time step or be discharged in one time step ($\dot{E}_{bat,max}$).

The simulations were varied in 4 dimensions: The seven climate zones, the battery storage capacity in hours, including or excluding DHW and two different backup sources, the electricity grid and a diesel generator.

The instantaneous solar electricity generation ($\dot{E}_{el,sol}$) and the HVAC (and DHW) demand ($\dot{E}_{el,HVAC(\&DHW)} = \dot{E}_{el,c} + \dot{E}_{el,h} + (\dot{E}_{el,dhw})$) were used from the TRNSYS simulation output of the chosen PV configurations in Table 6.1 to analyze the performance including a battery storage. An Excel VBA macro was written to calculate the amounts of electricity that could be stored in the battery or be extracted from the battery to supply the HVAC (and DHW) system at each time step. The time step of the simulation was 0.05 hours (3 min).

The first priority of the generated solar electricity is to support the HVAC system if there is a demand, which is represented by $\dot{E}_{el,sol \rightarrow HVAC(\&DHW)}$ in equation 6.1. The surplus electricity is stored in the battery ($\dot{E}_{el,sol \rightarrow bat}$) as described in equation 6.2.

The process of charging the battery is penalized by using an 85% charging efficiency η_{bat} which leads to lost energy to the environment ($\dot{E}_{el,sol \rightarrow lost}$) in equation 6.3. The electricity which can neither be stored, due to a full battery or maximum charging rate, nor directly used for HVAC (and DHW) can either be exported into the electricity grid or if no grid is available, is discarded. In both cases it is denoted

here as $\dot{E}_{el,sol\rightarrow grid}$ (equation 6.4).

$$
\begin{aligned}
&\text{If } \dot{E}_{el,sol} \geq \dot{E}_{el,HVAC(\&DHW)}: \\
&\dot{E}_{el,sol\rightarrow HVAC(\&DHW)} = \dot{E}_{el,HVAC(\&DHW)} && (6.1)\\
&\dot{E}_{el,sol,surplus} = \dot{E}_{el,sol} - \dot{E}_{el,HVAC(\&DHW)} \\
&\text{If battery} \neq \text{full}: \\
&\dot{E}_{el,sol\rightarrow bat} = \min(\dot{E}_{el,sol,surplus}, \dot{E}_{bat,max}) \cdot \eta_{bat} && (6.2)\\
&\dot{E}_{el,sol\rightarrow lost} = (1-\eta_{bat}) \cdot \min(\dot{E}_{el,sol,surplus}, \dot{E}_{bat,max}) && (6.3)\\
&\dot{E}_{el,sol\rightarrow grid} = \dot{E}_{el,sol,surplus} - \dot{E}_{el,sol\rightarrow bat} - \dot{E}_{el,sol\rightarrow lost} && (6.4)
\end{aligned}
$$

Figure 6.20 describes which proportion of the generated solar electricity is allocated directly to the HVAC system, to charge the battery, to be exported to the grid or is lost. It also denotes how much electricity per m^2 of PV modules can be harvested in each climate.

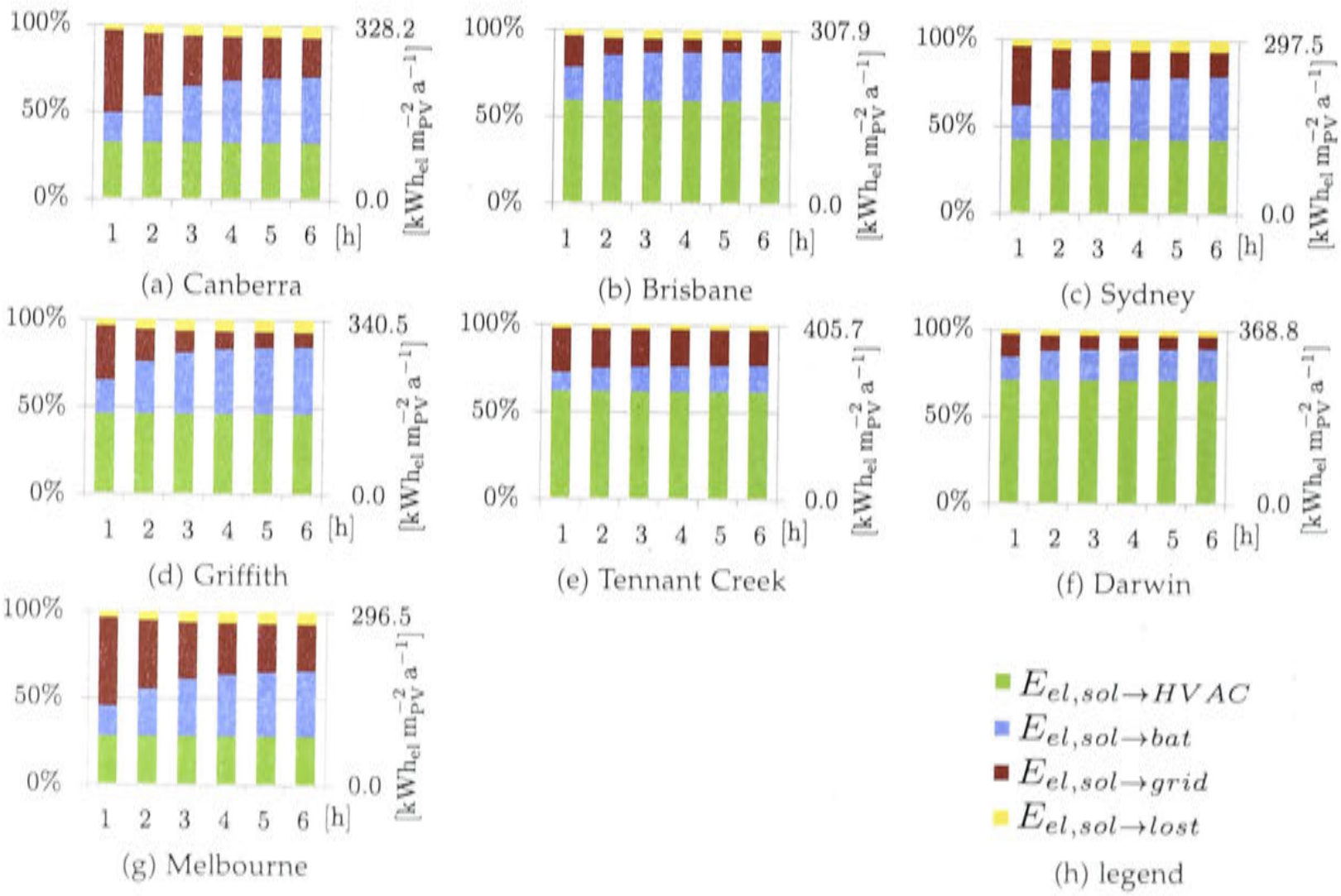

Figure 6.20: Proportional allocation of the generated solar electricity specific to the installed collector area including battery storage

In Figure 6.21 the proportions or shown of which the provided electricity to the HVAC system is comprised of. There are the amount which is directly supplied from the solar generation ($\dot{E}_{el,sol\rightarrow HVAC(\&DHW)}$ in equation 6.5) and the amount which is extracted from the battery ($\dot{E}_{el,bat\rightarrow HVAC(\&DHW)}$ in equation 6.6).

$$
\begin{aligned}
&\text{If } \dot{E}_{el,sol} < \dot{E}_{el,HVAC(\&DHW)}: \\
&\dot{E}_{el,sol\rightarrow HVAC(\&DHW)} = \dot{E}_{el,sol} && (6.5)\\
&\dot{E}_{el,HVAC(\&DHW),deficit} = \dot{E}_{el,HVAC(\&DHW)} - \dot{E}_{el,sol} \\
&\text{If battery} \neq \text{empty}: \\
&\dot{E}_{el,bat\rightarrow HVAC(\&DHW)} = \min(\dot{E}_{el,HVAC(\&DHW),deficit}, \dot{E}_{bat,max}) && (6.6)\\
&\dot{E}_{el,grid\rightarrow HVAC(\&DHW)} = \dot{E}_{el,HVAC(\&DHW),deficit} - \dot{E}_{el,bat\rightarrow HVAC(\&DHW)} && (6.7)
\end{aligned}
$$

The backup electricity is provided either from the grid or, if not connected, from a diesel generator ($\dot{E}_{el,grid\rightarrow HVAC(\&DHW)}$ in equation 6.7). The subscript "diesel" implies therefore, that no grid connection is available. The efficiency of the diesel generator is assumed to be 35% and it's specific greenhouse gas emissions are 69.5 $kg_{CO2}\,GJ^{-1}$ respectively [Department of Climate Change and Energy Efficiency, 2012].

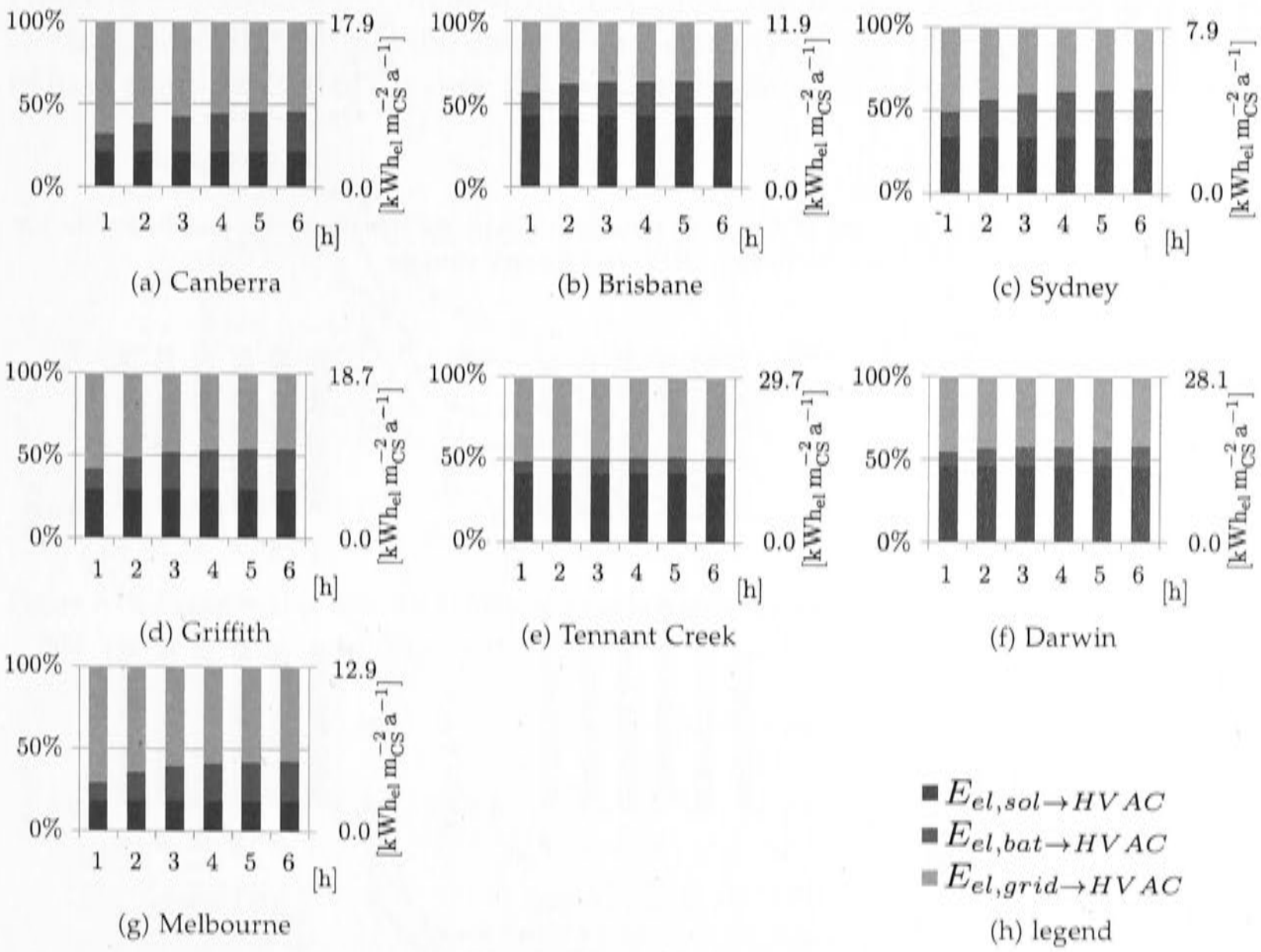

(a) Canberra (b) Brisbane (c) Sydney

(d) Griffith (e) Tennant Creek (f) Darwin

(g) Melbourne (h) legend

Figure 6.21: Proportional allocation of electricity sources to the HVAC system, specific to the conditioned space including battery storage

In contrast to figures 6.22 and 6.23 the graphs of Figure 6.20 and 6.21 did not include the domestic hot water consumption. The higher electricity consumption leads to less surplus electricity which would have to be exported to the grid (or discarded if no grid connection is available).

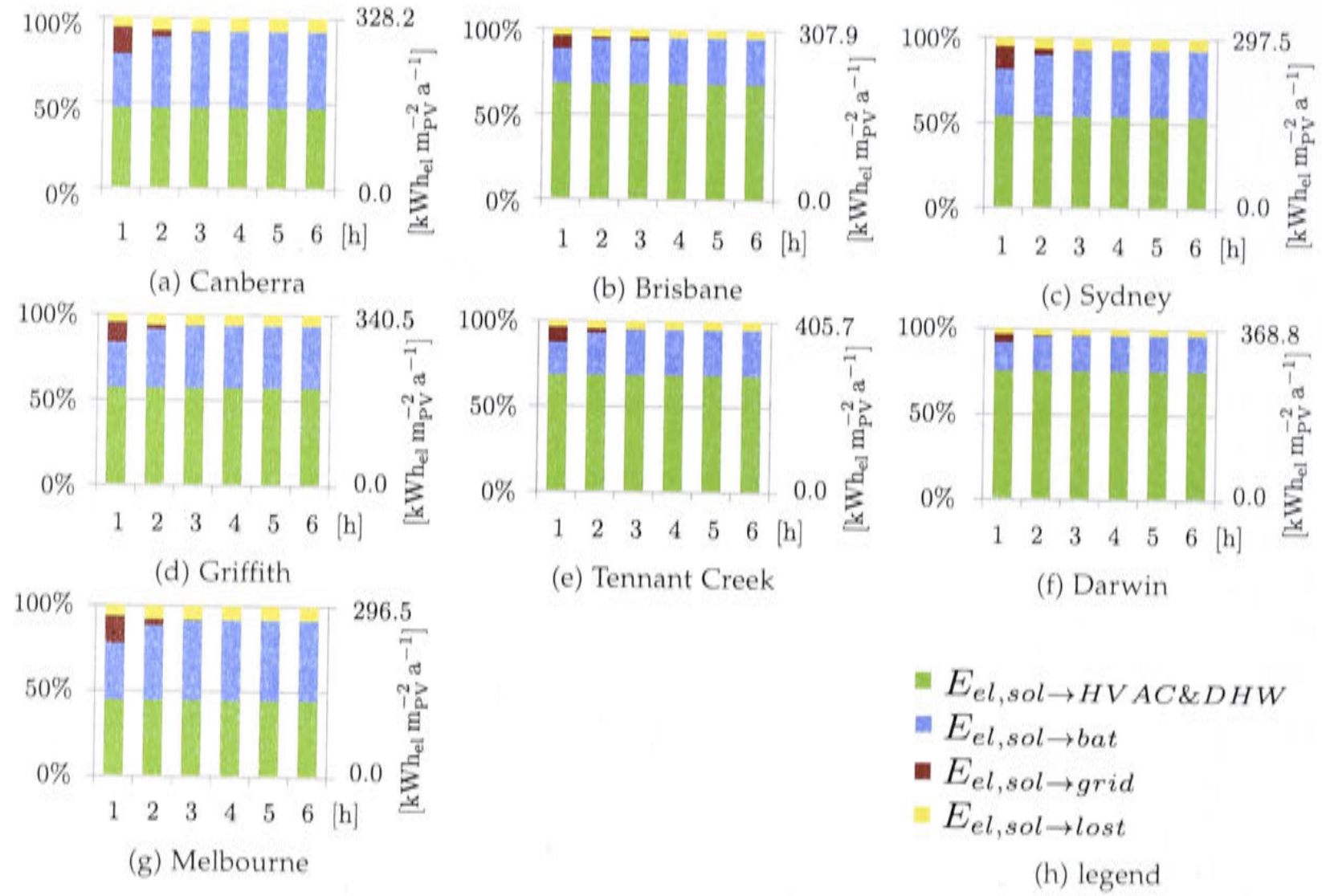

Figure 6.22: Proportional allocation of the generated solar electricity specific to the installed collector area including DHW and battery storage

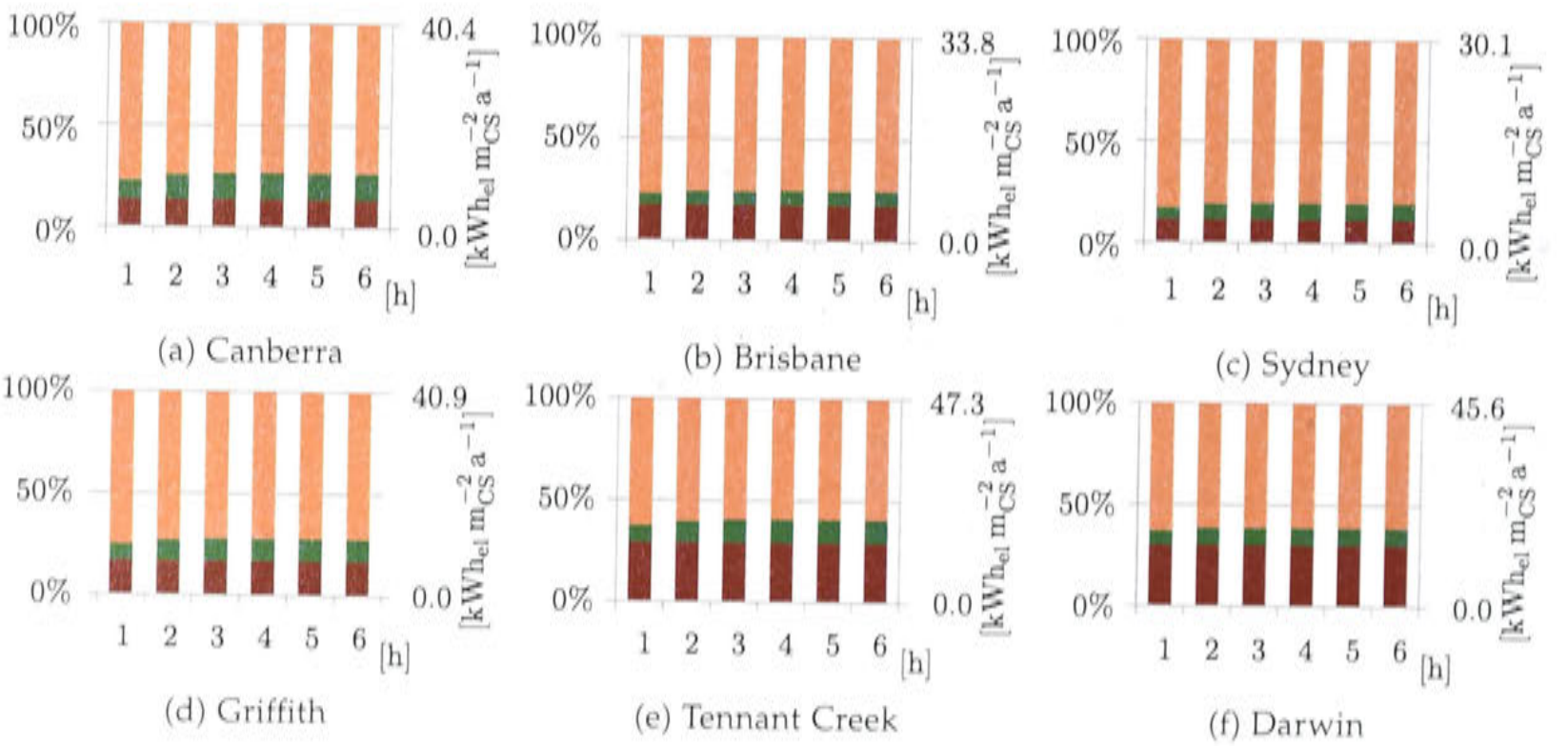

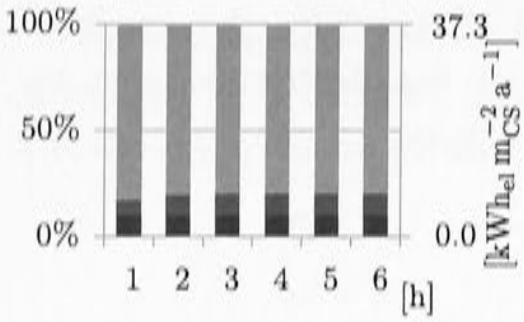

(g) Melbourne

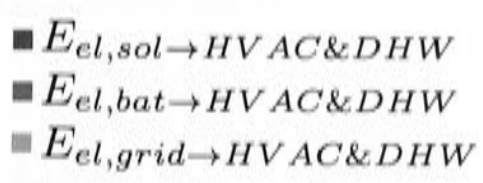

(h) legend

Figure 6.23: Proportional allocation of electricity sources to the HVAC and DHW system, specific to the conditioned space including battery storage

For battery storage systems it is interesting to see how often the battery is fully charged or empty. Figure 6.24 shows how often the battery is fully charged when there is a surplus of solar power available. In that case the surplus can either be exported to the grid or must be discarded if there's no grid connection available. Figure 6.25 provides information on how often the battery is empty if there is a electricity demand beyond the direct solar electricity supply. In other words it shows in how many percent of the time the backup system must supply electricity.

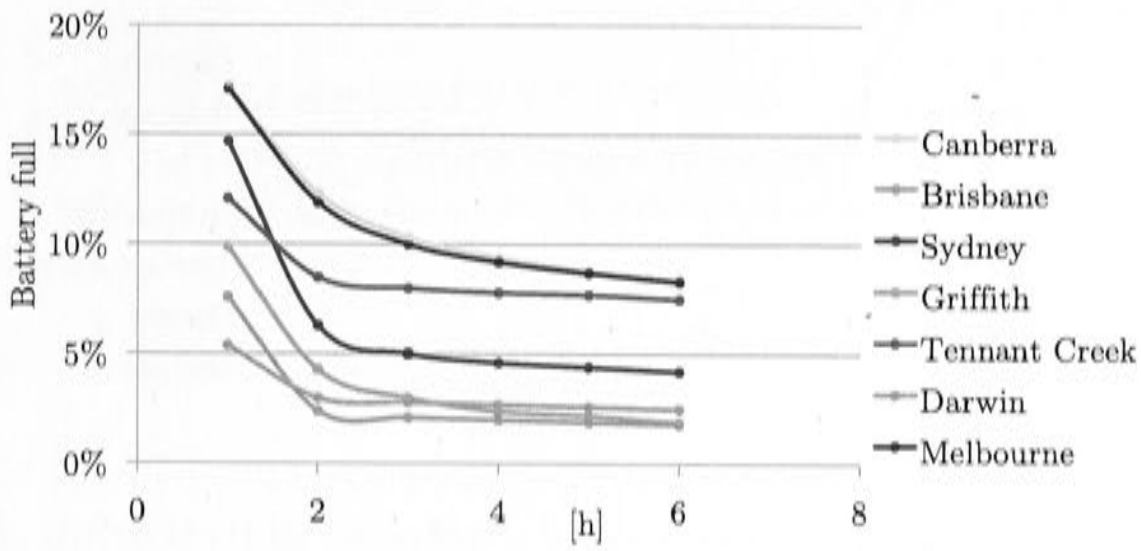

Figure 6.24: Percentage of time the battery is full when there's a surplus of solar electricity available to be stored

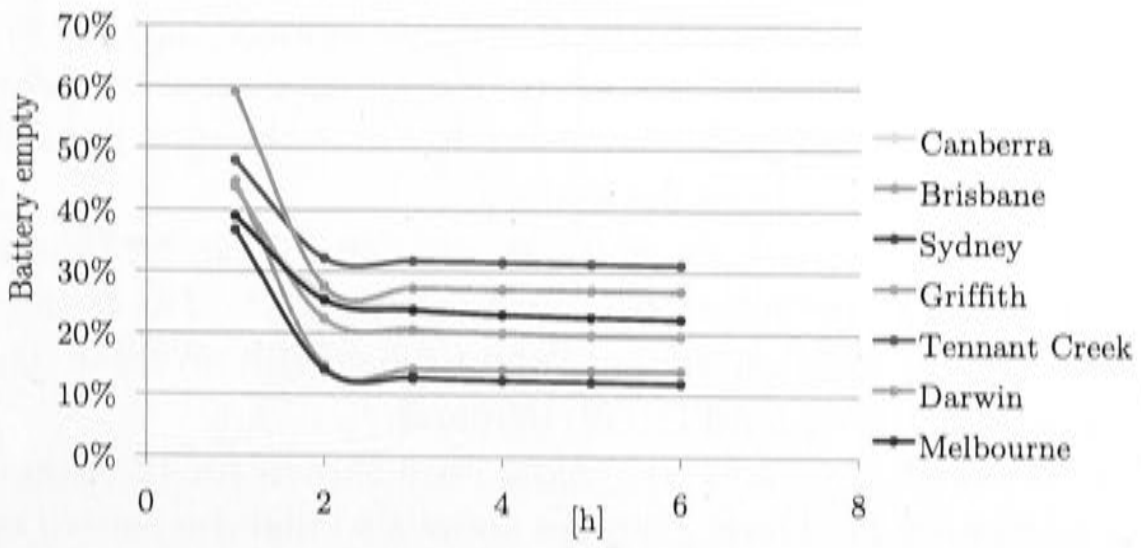

Figure 6.25: Percentage of time the battery is empty when there's an HVAC demand, which cannot be covered by the direct solar electricity generation

If domestic hot water is included in the study (Figure 6.27 and 6.26), the numbers look rather different. The battery is hardly every full because the electricity for water heating depletes it quickly and of course, it is more often empty.

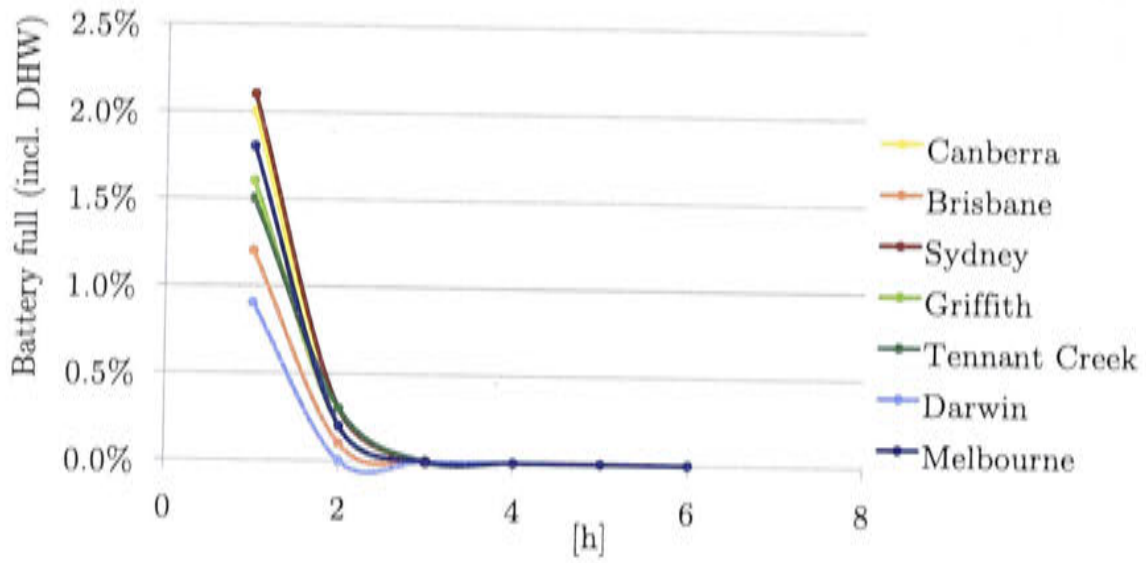

Figure 6.26: Percentage of time the battery is full when there's a surplus of solar electricity available to be stored including DHW

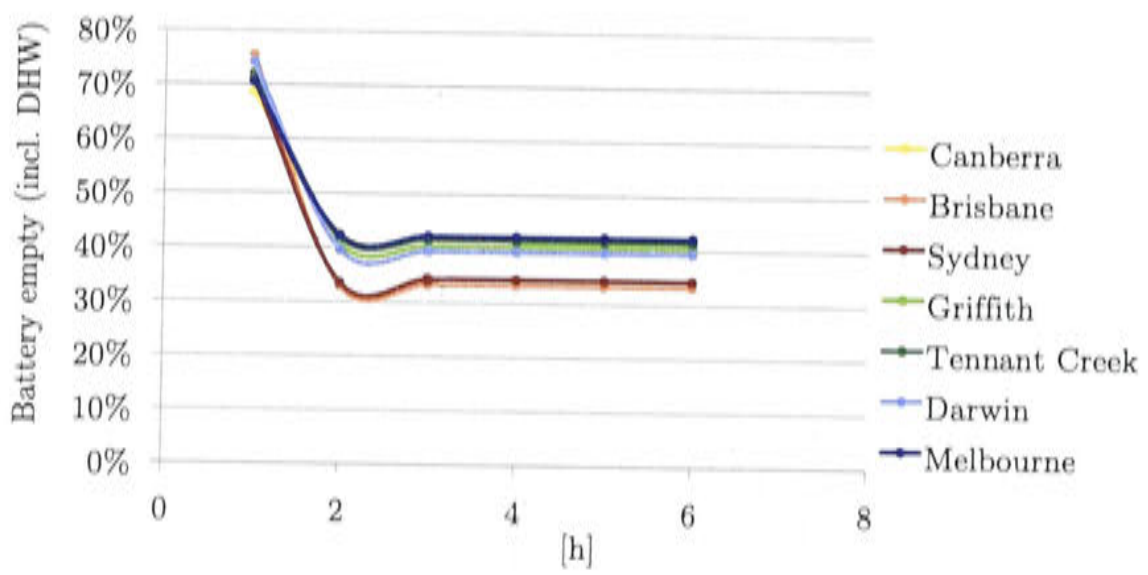

Figure 6.27: Percentage of time the battery is empty when there's an HVAC&DHW demand which cannot be covered by the direct solar electricity generation

It is interesting to see that for the different climates larger storage sizes don't change the percentage for how often the battery is full or empty anymore. Hence, there's a limit of how much extra benefit additional storage capacity will bring. It is important to remember, that the "hours" on the x-axis denote the hours the rated PV power output can be stored in the battery rather than the time the HVAC and/or DHW) system can be supplied from the battery.

Further statistics on the charging status of the battery can be found in the Appendix C.2. In those graphs "full=100%" and empty=0%". The battery states are calculated over the whole year and include night times with no solar electricity generation or times of zero HVAC (and DHW) demand.

The solar fractions $SF_{el,LCov}$ and $SF_{el,LCov,dhw}$ are shown for the different storage sizes in figures 6.28 and 6.29. Those graphics show also that the benefit of additional battery capacity reaches a plateau at 2 to 3 h, and there is no additional gain by installing a larger storage capacity.

As mentioned previously, the backup source of the battery supported system can either be a diesel generator or the electricity grid. The solar fraction versus the specific greenhouse gas emissions are shown in Figure 6.30a and 6.30b.

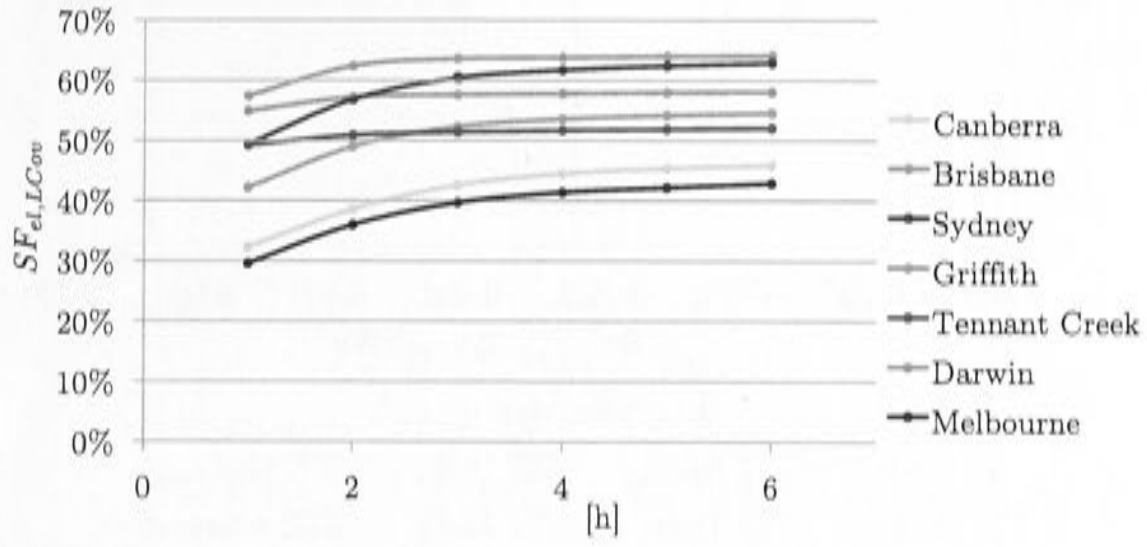

Figure 6.28: Solar fraction for the different battery capacities (storage hours)

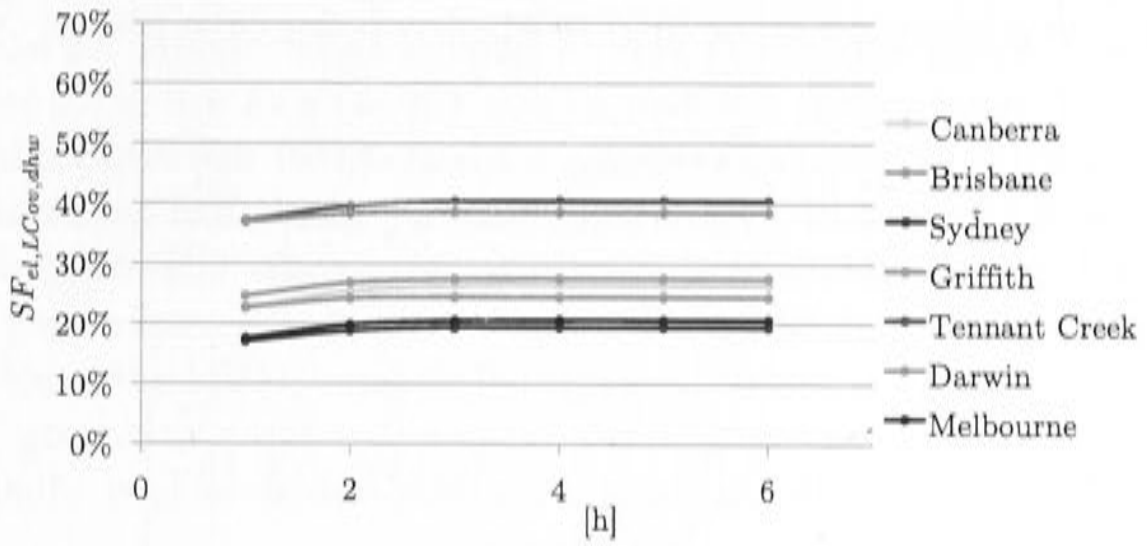

Figure 6.29: Solar fraction for the different battery capacities (storage hours) including DHW

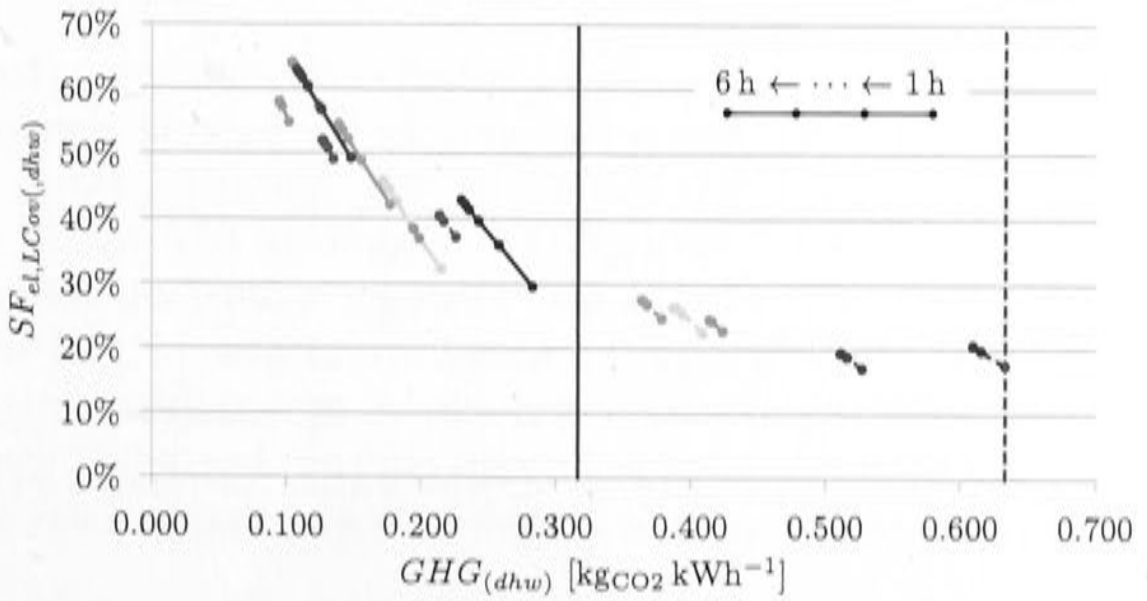

(a) grid backup

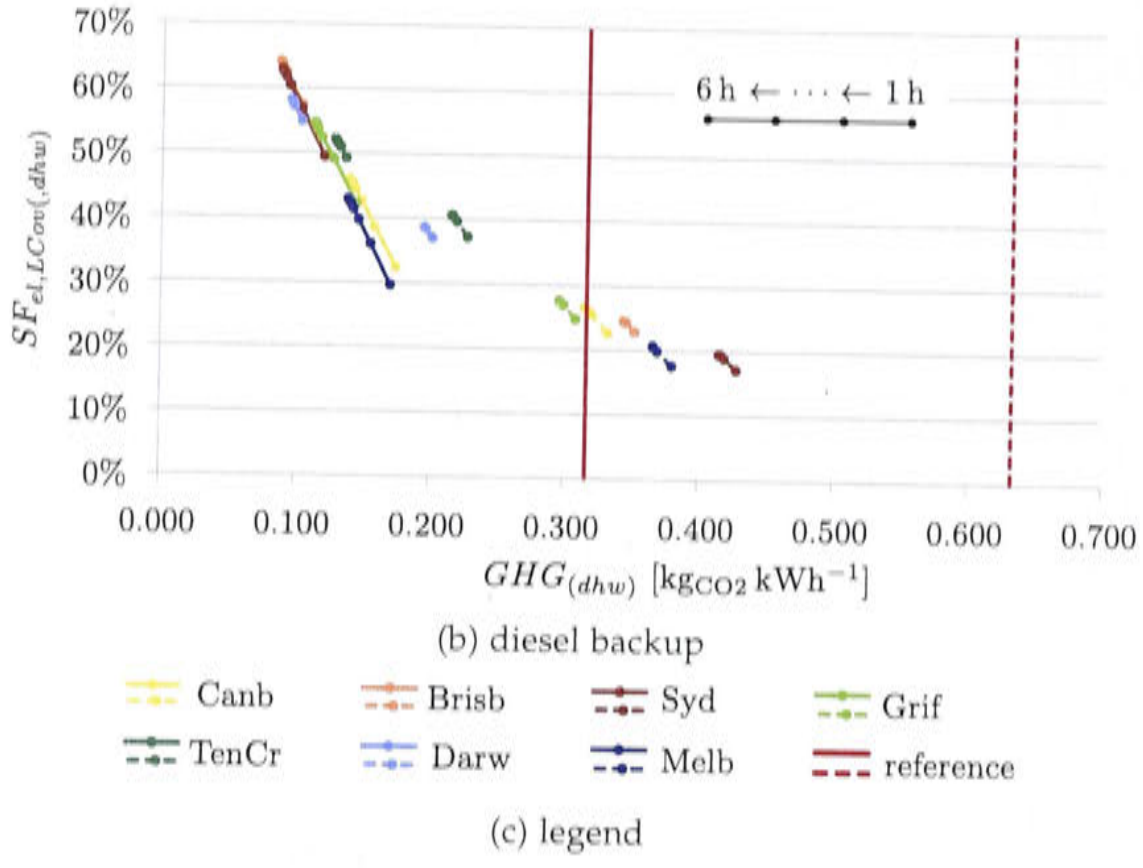

(b) diesel backup

(c) legend

Figure 6.30: The specific greenhouse gas emissions vs. solar fraction with the electricity grid or a diesel generator as backup (excluding DHW (solid —), including DHW (dashed - -))

To emphasize the difference between grid and diesel the direct comparison is shown in Figure 6.31 and 6.32. The saved specific greenhouse gas emissions compared to the reference system are shown in the Appendix C.3 for grid and diesel backup with and without DHW for all storage sizes.

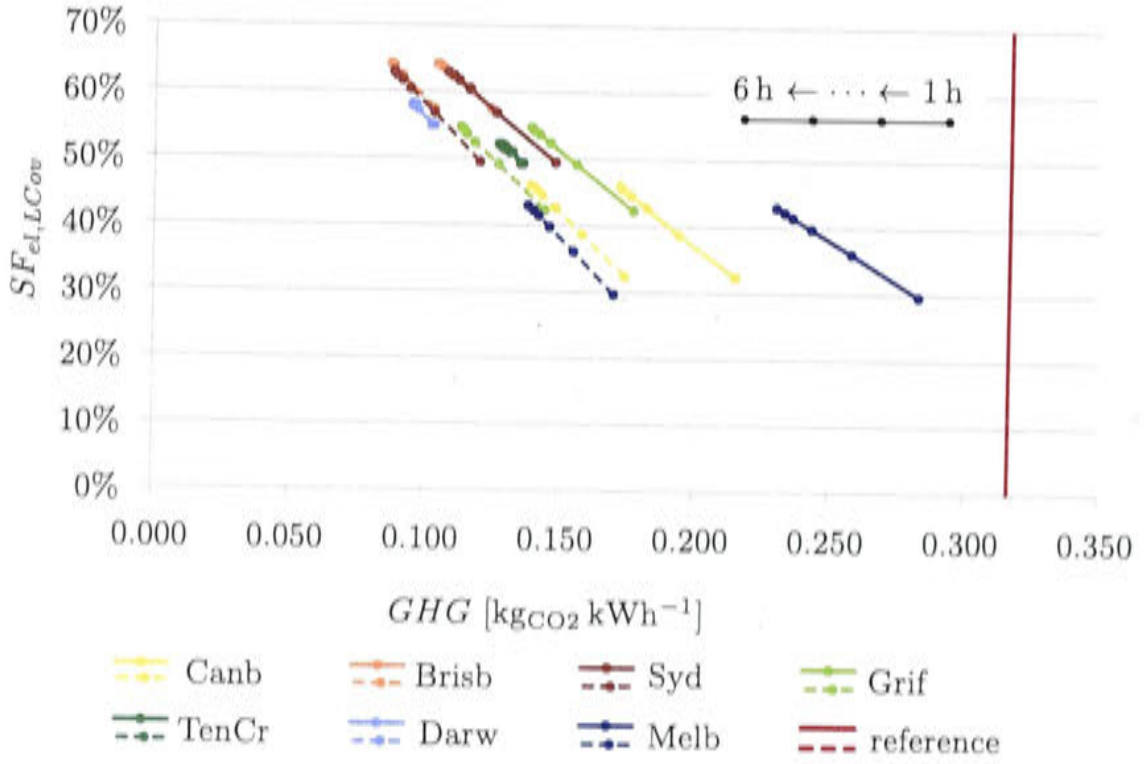

Figure 6.31: The specific greenhouse gas emissions vs. solar fraction comparing the backup sources diesel and electricity grid (grid backup (solid —), diesel backup (dashed - -))

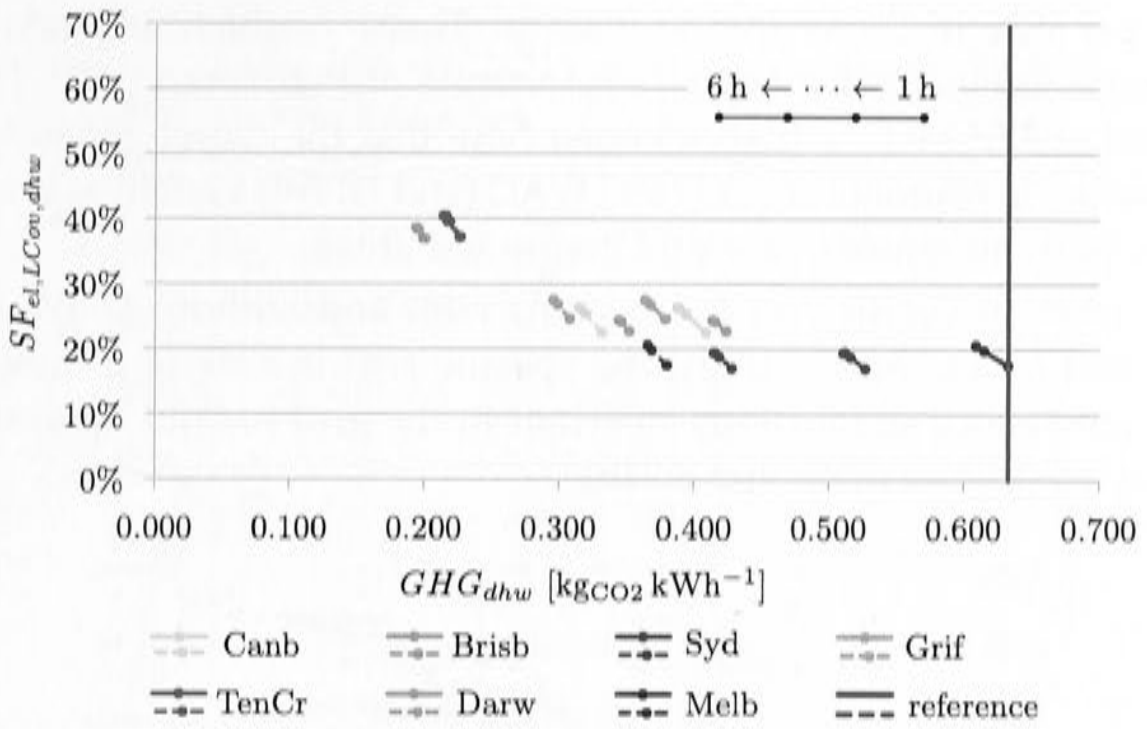

Figure 6.32: The specific greenhouse gas emissions vs. solar fraction comparing the backup sources diesel and the electricity grid, including DHW (grid backup (solid —), diesel backup (dashed - -))

There is an advantage when looking merely at the greenhouse gas emissions of using a diesel generator as a backup source over the electricity grid. It is important to repeat at this point that the greenhouse gas savings shown here do not include the surplus generated when the battery is full or when there is no HVAC (and DHW) demand. Surplus solar electricity, not diverted to the batter, does not lower the greenhouse gas emissions as exported solar electricity reduces emissions not within the boundaries of the HVAC (and DHW) system. If the system is grid connected and the external greenhouse gas reductions would be included, the grid option might perform equally well or better than the diesel option concerning greenhouse gas savings.

The performance parameters in the following sections cover the specific cost and the overall performance factor for the different climates and battery storage capacities.

Additional cost assumptions had to be made to calculate the specific cost when including a battery storage and varying the backup energy source between grid connection and diesel generator. The investment cost I_{bat} for the batteries was taken from Renew [2012a] and assumed to be \$500 kWh^{-1} (of nominal capacity). The investment cost for the battery regulator (I_{BatReg}) was taken from the same literature source Renew [2012b], which provided a market survey on battery regulators. The battery regulators with maximum power point tracking (MPP tracking) are in a similar price range and a cost function depending on the peak capacity of the PV array ($Cap_{PV,design}$) was derived[2] (equation 6.8).

$$I_{BatReg} = 104 \cdot Cap_{PV,design}[\mathrm{kW}] + 335 \qquad [\$] \tag{6.8}$$

[2]The price of a battery regulator for a PV array with 1.25 kW is stated as \$465 and with 2.5 kW as \$595.

The cost per litre of diesel fuel was set to $\$1.60\,l^{-1}$ which was taken from the national average published by Australian Institute of Petroleum (AIP) [2014a]. The energy content is $38.6\,MJ\,l^{-1}$. It is assumed here that the diesel generator does not increase the initial investment cost of the HVAC (and DHW) system as it is a common source of electricity in remote, non-grid connected areas.

The solar fraction versus cost for systems with and without DHW is shown in Figure 6.33a and 6.33b. Surprisingly, the specific cost in case of a diesel generator as backup source is not significantly different to the grid backed up system, only if DHW is included (Figure 6.34a and 6.34b).

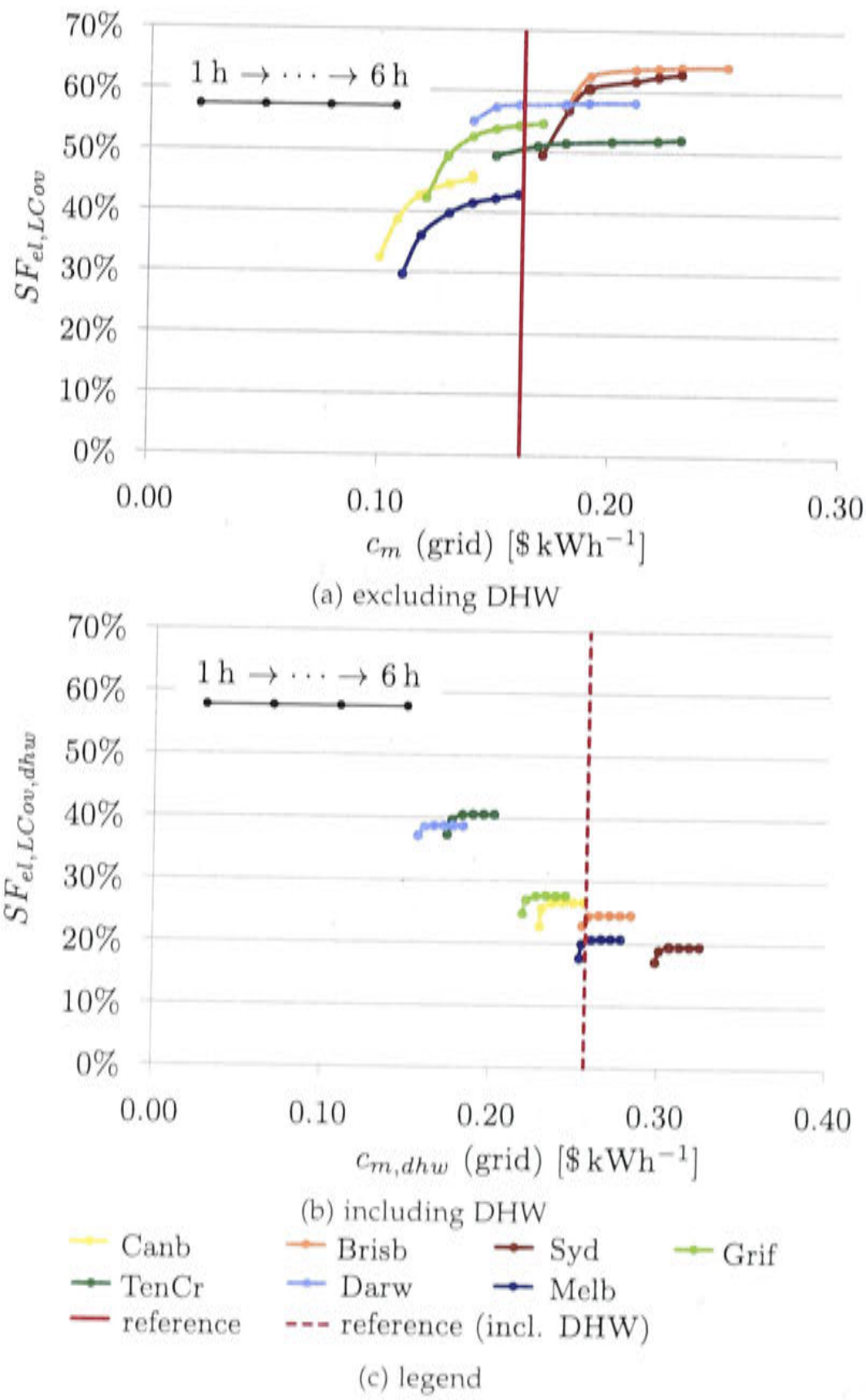

Figure 6.33: The solar fraction vs. the specific cost $c_{m(,dhw)}$ when using the electricity grid as backup.

There are several reasons why diesel in remote areas is more expensive than

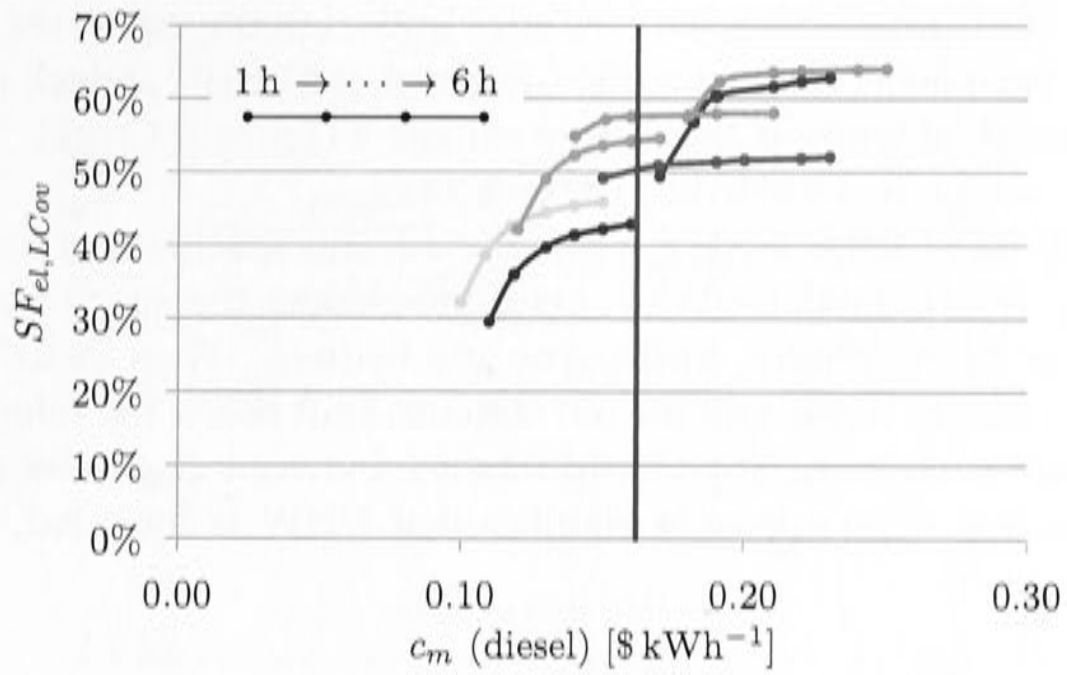

(a) excluding DHW

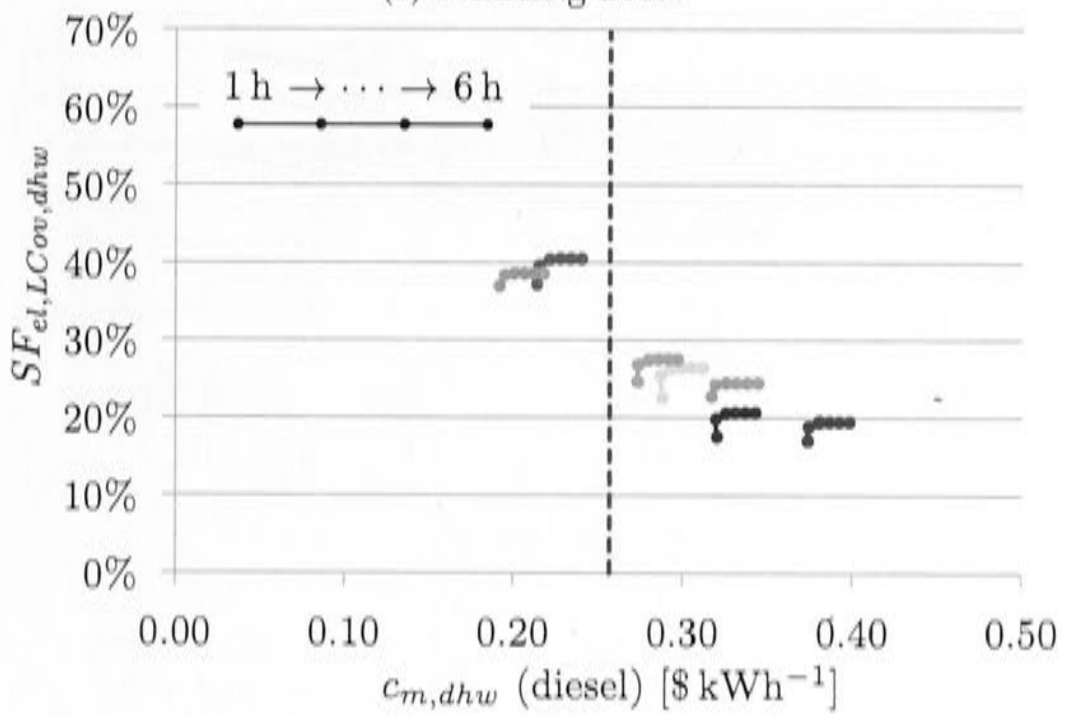

(b) including DHW

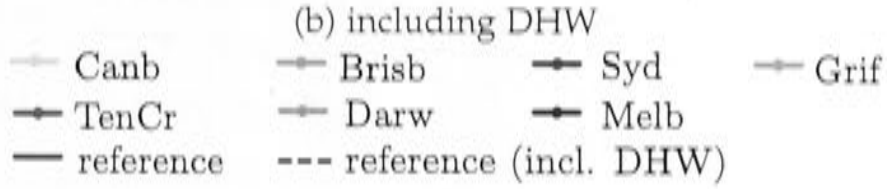

(c) legend

Figure 6.34: The solar fraction vs. the specific cost $c_{m(,dhw)}$ when using the a diesel generator as backup.

in higher populated city areas. The reasons are outlined in Australian Institute of Petroleum (AIP) [2014b] and are mainly due to smaller volumes traded, longer distance traveled, which induces higher freight costs, typically higher storage and handling costs and lower market competition. Cost for diesel in country towns and regional areas of Australia is on average ct5.7 l^{-1} higher than in the five largest capital cities.

However, there's an opposing trend to the higher fuel cost in remote areas. The government offers indirect subsidies in form of "fuel tax credits", which can be claimed by house owners under certain circumstances, for example if they produce their own electricity with a diesel generator [Australian Taxation Office (ATO), 2014].

In this thesis it is assumed that such measures outweigh the extra cost. Figure 6.34a and 6.34b have been generated using the fuel price of $\$1.60\,l^{-1}$, which can be understood as subsidized, at least for the remote climate 5 (Tennant Creek). The Northern Territory State average was $\$1.75\,l^{-1}$ in May 2014.

Even though there is no feed-in tariff offered, the specific cost for the PV and battery assisted HVAC (and DHW) system, lays below the specific reference cost $c_{m,ref}$ for the climates Canberra, Melbourne and Sydney. When including domestic hot water they perform worse and the hot climates shift below the reference cost line ($c_{m,dhw,ref}$) (Figure 6.35a to 6.36b). The difference between electricity grid or diesel generator as backup source is only significant if DHW is included, as the diesel backup is more costly.

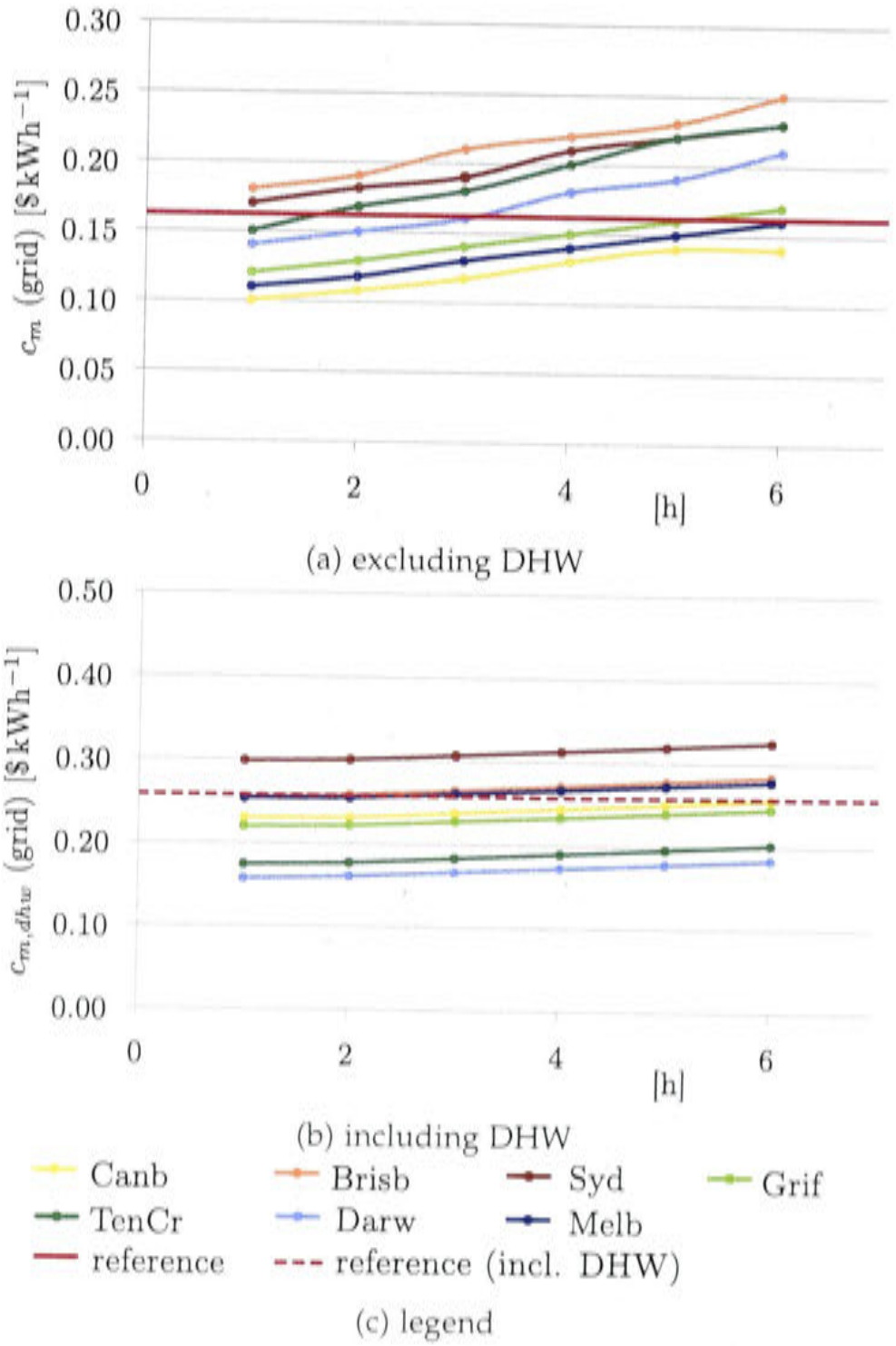

Figure 6.35: Specific cost $c_{m(,dhw)}$ of the battery and PV assisted HVAC (and DHW) system backed up by the electricity grid

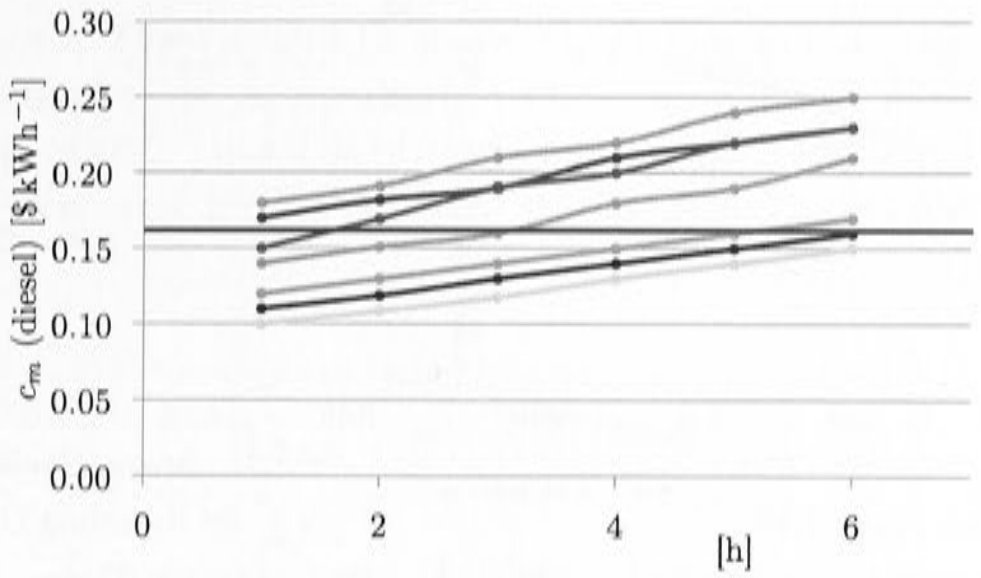

(a) excluding DHW

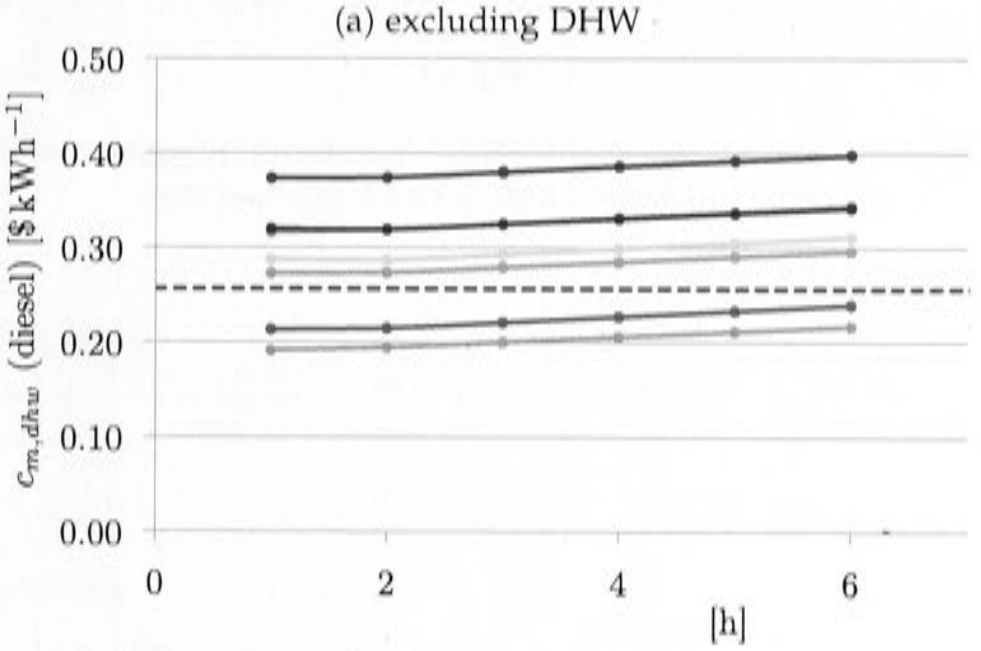

(b) including DHW

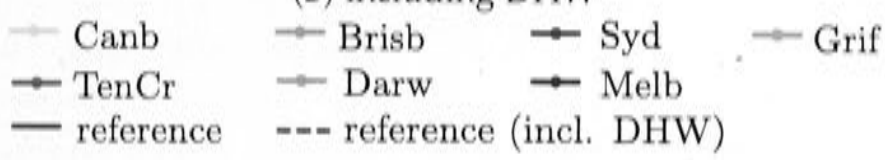

(c) legend

Figure 6.36: Specific cost $c_{m(,dhw)}$ of the battery and PV assisted HVAC (and DHW) system backed up by a diesel generator

The saved greenhouse gases versus additional cost can be seen for grid and diesel backup in Figure 6.37 and 6.38. Diesel as backup seems to emit less greenhouse gases than when backing up with the electricity grid and since the specific cost is relatively similar in both cases, additional greenhouse gases can be saved at lower cost. When including DHW on the other hand, the cost for greenhouse gas abatement increases using a diesel generator compared to the grid as backup. Especially in Melbourne it seems better to use a diesel generator as backup, however, this is related to the high greenhouse gas emission factor for electricity in Victoria (Table 4.1).

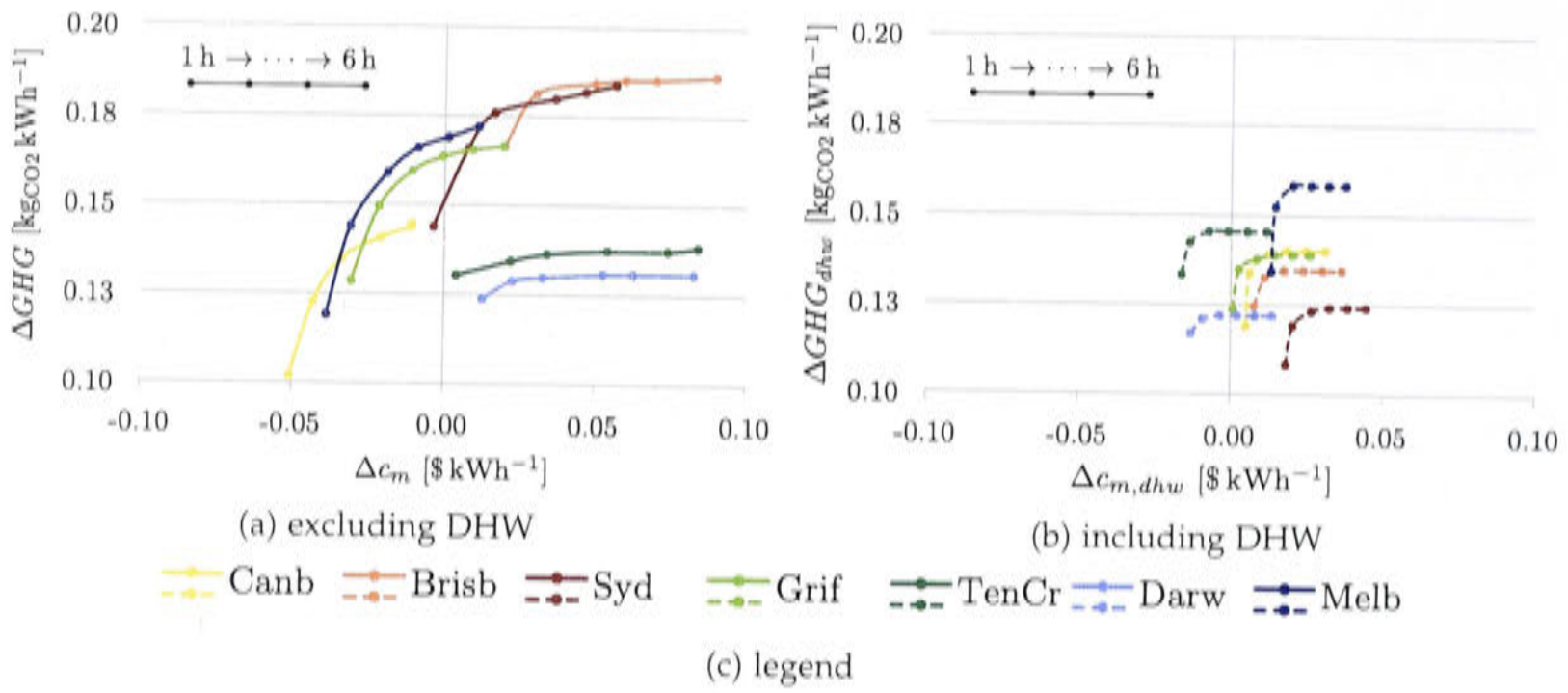

Figure 6.37: The marginal cost for one kg_{CO2} saved using the electricity grid as backup, including DHW (solid —) and excluding DHW (dashed - -)

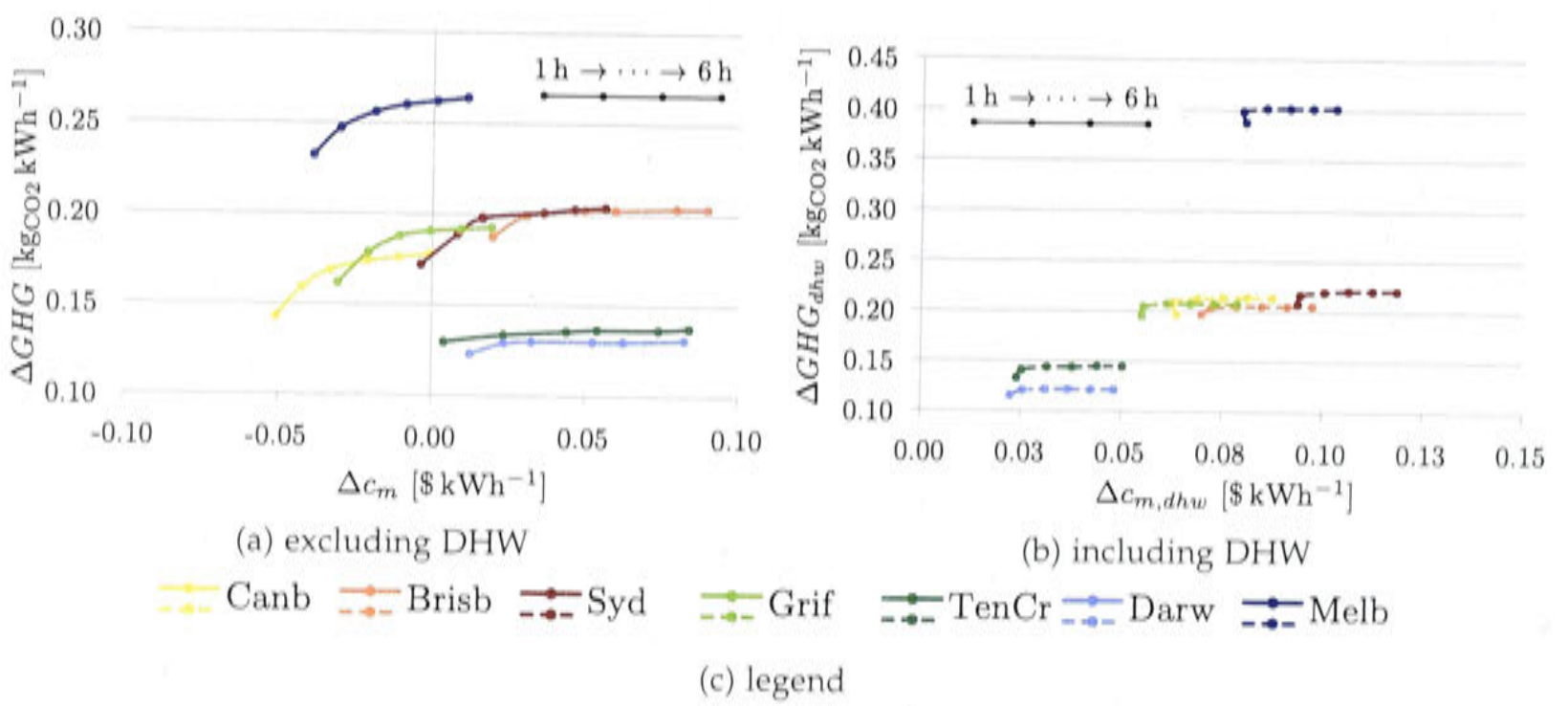

Figure 6.38: The marginal cost for one kg_{CO2} saved using a diesel generator as backup, including DHW (solid —) and excluding DHW (dashed - -)

The overall performance factor (OPF) has been generated for the different storage capacities and different climates. The battery did not influence the comfort conditions as the same TRNSYS output files from the reference case were used. The solar fraction, hence the greenhouse gas emissions as well as the cost have changed though, when adding a battery to the PV system. In Figure 6.39 the OPF is compared to the reference system of section 5.3 and to the gird connected PV system with $frac_{PV} = 1$ from section 6.2.1.

All PV systems with or without storage perform better than the reference system (with and without DHW).

It seems that in climates with colder winters like Canberra, Melbourne and also Griffith the battery storage system with and without DHW has an higher OPF than the hotter climates even though there are no financial incentives included.

In Tennant Creek, Darwin and Brisbane the proportion of OPF_{c_m} drops stronger than OPF_{GHG} increases. In Appendix C.4 the three parts of the OPF for grid and diesel backed up HVAC (and DHW) systems are presented to understand what causes the OPFs to change for the different storage sizes in Figure 6.39.

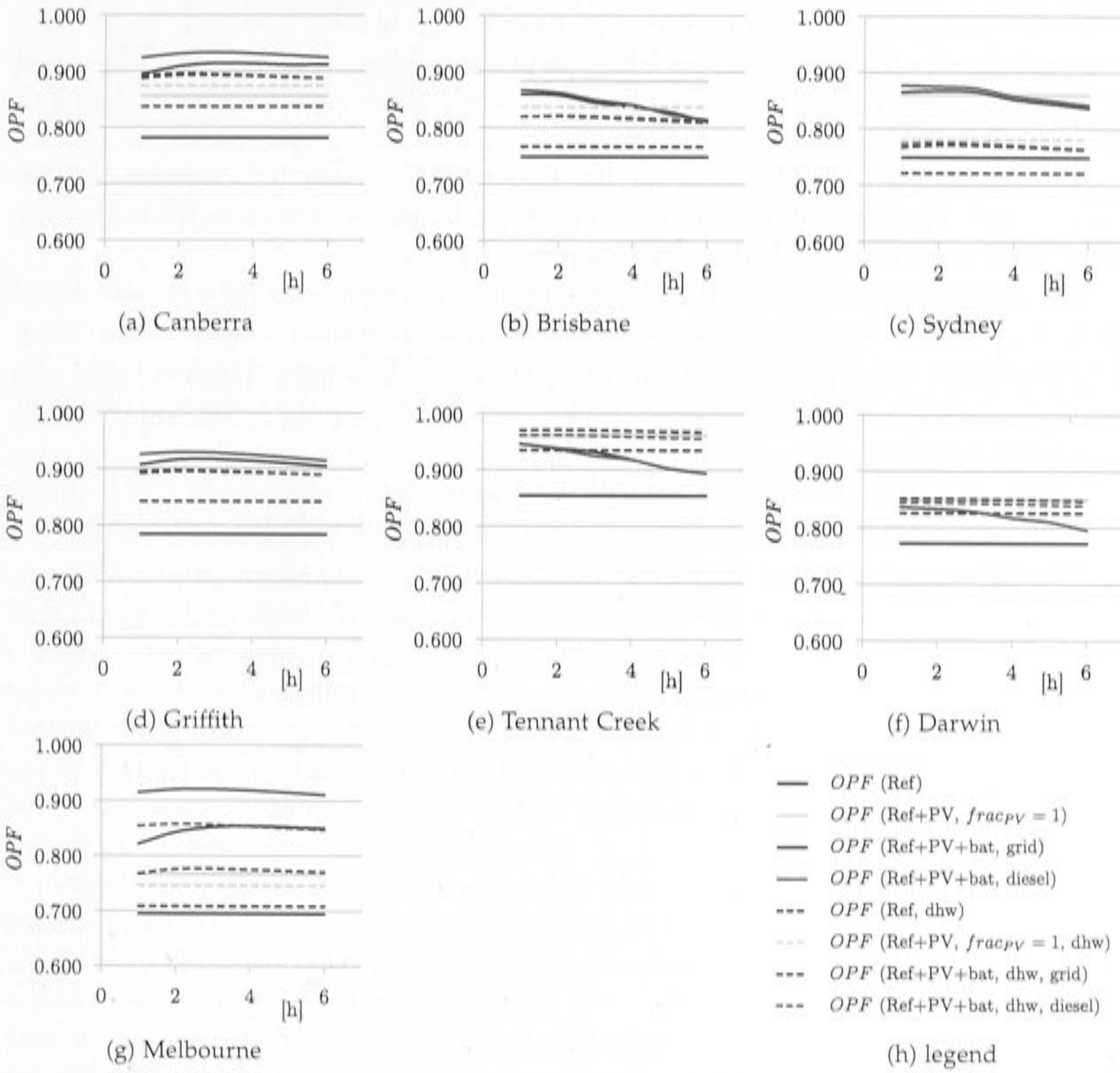

Figure 6.39: Comparing the OPF for the reference system to the PV assisted system with and without battery, backed up by a diesel generator or the electricity grid (excluding DHW (solid —) and excluding DHW (dashed - -))

6.4 Conclusion on PV assisted cooling, heating and DHW systems

Even though in the solar thermal community PV driven systems were ignored for a long time due to high cost and a strong reliance on solar thermal technologies like ab- or adsorption processes, it became clear that PV driven HVAC systems provide

a valuable alternative for solar cooling in a residential context. In the climates of Tennant Creek and Darwin no feed-in tariff is necessary to achieve cost effectiveness. In all other climates it is necessary to a certain degree.

When combined with a battery storage the direct usage of solar electricity could be increased in some climates by nearly 50% (Figure 6.20). The highest additional gain was observed in climates which also have a high heating demand. In climates with cold winters like Canberra, Griffith and Melbourne, the OPF of PV assisted systems with batteries exceed the OPF of grid connected system without battery and the highest feed-in tariff ($frac_{PV} = 1$).

The optimal storage duration for the battery throughout the climates lies between 2 and 3 hours. Additional cost input for a larger storage capacity leads only marginally to an increase of the solar fraction ($SF_{el,LCov}$).

It is also worth mentioning that the greenhouse gas emissions for a remote diesel backed up system are smaller compared to a grid connected system when using the greenhouse gas emission coefficients in Table 4.1. However, this was under the assumption that exported surplus electricity does not add to the reduction of greenhouse gas emissions.

In the next chapter the solar thermal cooling, heating and DHW model is introduced to draw a comparison to this study having used solar electric assistance.

Chapter 7

The residential solar thermal cooling, heating and DHW model

This chapter will introduce the modeling basics to investigate into a solar thermal design approach as an alternative to solar electricity. Comparing solar electric to solar thermal driven cooling, heating and DHW systems, there are a number of technological differences which should be mentioned first.

Rebates and other governmental subsidies for industry and research in and outside of Australia have helped photovoltaic to become competitive in cost today. It is technically relatively simple to combine PV panels and a split unit for heating and cooling. Furthermore, a grid interactive PV solar cooling solution does not necessarily require any additional storage because the electricity grid serves as a buffer. However, in remote areas without grid connection it is possible to add a direct storage option using expensive batteries. When looking at the generation of domestic hot water side with PV modules, it seems that high quality energy in form of electricity can be put to better use than heating water.

With a solar thermal system on the other hand comes the convenience to storage heat in form of hot water. Domestic hot water and space heating can be provided as well and in regards to the high driving temperatures of solar cooling, domestic hot water provides the perfect opportunity in terms of depleting the hot water storage tank in the evening. For the absorption chiller the hot water tank serves as a buffer for control purposes rather than a storage tank of heat for long operating hours in the afternoon/evening. Next to the provision of hot water, the solar thermal option using absorption chillers also has a potential to reduce the use of HFCs in conventional compression cycles as natural refrigerants are used. Rather disadvantageous is their limited temperature operating range compared to conventional chillers, especially for Lithium-Bromide absorption chillers.

In this chapter the performance of solar thermal applications are explored and the same building model as in the previous chapter is conditioned by a small scale absorption chiller delivering chilled water for cooling fan coils. The absorption chiller was chosen because it represents the most commonly used technology for solar cooling applications in Europe. The development of an absorption chiller model for TRNSYS will be outlined and the design of the system explained. The model in-

cludes solar thermal space heating and domestic hot water as well. The adsorption technology is outlined briefly and could replace the thermal chiller component in the TRNSYS cooling, heating and DHW model if appropriate performance data was available.

7.1 System design and control of the solar thermal cooling, heating and DHW system

A schematic diagram of the solar thermal heating, cooling and DHW system modeled in this thesis is shown in Figure 7.1. The building model (17) provides the HVAC load.

The evacuated tube solar collectors TRNSYS type 71 (1) provide the buffer hot water tank (2) with hot water. Attached to the tank is a energy relief valve (3) to prevent the tank from overheating. The hot water tank model TRNSYS type 60 has been modified to separate the heat loss output into "heat relief due to overheating" and "heat loss to the environment".

The same tank also provides domestic hot water (DHW) (18). The mains supply is connected to the tank via coil heat exchanger and a second gas heater as back up is installed in series to the domestic hot water supply to the building. The hot water load profiles for each climate zone are from the Australian standard AS/NZS 4234 [Australian/ New Zealand Standard, 2008].

The main auxiliary gas heater TRNSYS type 659 (4) is switched in parallel and not in series to the tank to prevent from heating up unnecessarily. This is necessary as the chiller's generator usually has a ΔT_{hw} between inlet and outlet of 5 to 15 °C. In cooling mode the absorption chiller (7) dictates the hot water temperature $T_{hw,req}$, which is required to supply the fan coil units TRNSYS type 508 (9) with the chilled water set point $T_{chw,set}$. There is one fan coil for each of the three zones and the air flows are modulated to the rooms according to energy demand. The chilled water flow rate is constant and is distributed proportional to the space. The development of the chiller model is explained in section 7.2.

The hot water supply temperature to the chiller is regulated via bypass heat exchanger TRNSYS type 650 (6). The auxiliary gas booster switches on when cooling is required and the tank outlet temperature falls below $T_{hw,req}$. Once the tank has heated up and the sensor in the middle of the tank indicates $T_{hw,req}$, the auxiliary heater switches off and the tank supplies the heating and cooling system.

A wet cooling tower TRNSYS type 51 is used to reject condensing heat (8).

For the space heating system the required temperature ($T_{hw,req}$) of the heating coil TRNSYS type 670 (5) is set to the minimum of 60°C[1]. In heating mode only one coil is modeled and the air is distributed to the zones, which have a heating demand. Again, the distribution is based on demand and proportional to the space of the room.

[1]It is possible to vary that temperature to whatever is available in the tank since the air temperature to leave the heating coils is only 32°C

The pumps (12) to (14) (TRNSYS type 110) supply the chiller with hot water, chilled water and cooling water. Pump (11) supplies the solar collector circuit with water. Furthermore, a pump for the re-heating circuit (15) was added. The fans (TRNSYS type 111) (16) supply the zones with conditioned air.

The thermostats, which are located in each zone, have a dead band of 2°C. This means cooling switches on at $T_{setC} + 1\,°C$ and switches off at $T_{setC} - 1\,°C$. In heating mode, heating switches on at $T_{setH} - 1\,°C$ and off at $T_{setH} + 1\,°C$. The control algorithm implemented prevents cooling and heating is on at the same time. If cooling is demanded in one of the three zones (signal $HVAC_{therm,z_i,c} = 1$), heating can't switch on in any zone. This prioritizes cooling over heating. The logic for the thermostat control also includes the HVAC schedules (signal $HVAC_{sched,z_i}$) of the zones and the overall cooling and heating HVAC control signals $HVAC_c$ and $HVAC_h$ can be written as in equation 7.1 and 7.2 .

$$HVAC_c = HVAC_{therm,z_1,c} \cdot HVAC_{sched,z_1} \vee HVAC_{therm,z_2,c} \cdot HVAC_{sched,z_2} \vee HVAC_{therm,z_3,c} \cdot HVAC_{sched,z_3} \tag{7.1}$$

$$HVAC_h = \{HVAC_{therm,z_1,h} \cdot HVAC_{sched,z_1} \vee HVAC_{therm,z_2,h} \cdot HVAC_{sched,z_2} \vee HVAC_{therm,z_3,h} \cdot HVAC_{sched,z_3}\} \cdot \neg HVAC_c \tag{7.2}$$

The indoor temperature is the main control parameter in the base case simulation, but two additional indoor humidity control strategies for summer are presented in Chapter 7.3. For those strategies the reheating units (10) are utilized.

Furthermore, the absorption chiller is able to switch off the cooling supply whenever its maximum or minimum ranges of the three external inlet temperatures are exceeded.

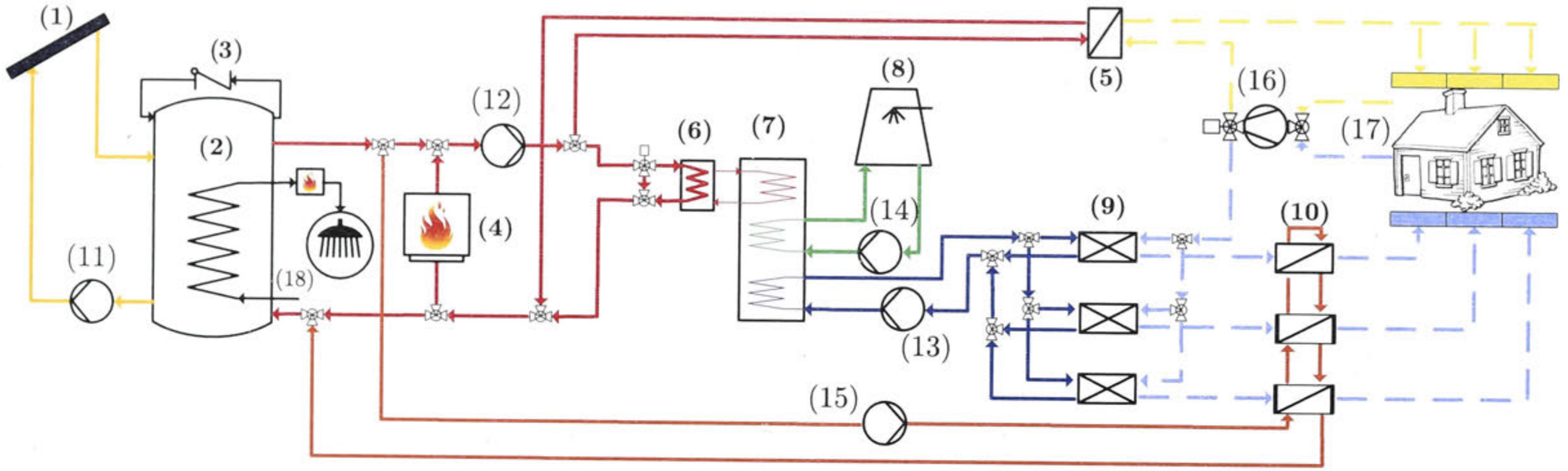

	component	technical parameters	section
(1)	evacuated tubes solar collector array	$9\,m^2$ to $33\,m^2$ collector area	7.5.1
(2)	hot thermal storage tank	400 L to 1500 L water volume	7.5.2
(3)	heat relieve valve	$T_{boil} = 120\,°C$ and $150\,°C$	8.2.3
(4)	auxiliary gas boiler	rated capacity is maximum of heat demand for cooling or heating	
(5)	water - air space heating coil	effectiveness 0.9	
(6)	water - water heat exchanger	effectiveness 0.9	
(7)	absorption chiller	capacity depends on climate zone, building type and control mode	7.2.6
(8)	wet cooling tower	capacity depends on absorption chiller capacity	7.4
(9)	water - air space coolig coils	coil bypass fraction 0.15	
(10)	water - air re-heating coils	effectiveness 0.9	7.3
(11)-(15)	water pumps	flow rates and pressure drops depend on cooling capacity	7.6
(16)	fans	flow rates and pressure drops depend on cooling capacity	7.6
(17)	space cooling and heating load	3 zones, $230\,m^2$, variable building structure	4.3 and 8.2.8
(18)	domestic hot water system	load from AS/NZS 4234:2008, in series auxilary gas boiler	7.5.2

Figure 7.1: Solar heating and cooling scheme

7.2 The absorption chiller component

A model for an absorption chillers has been developed to be implemented in a TRNSYS component, based on an look-up approach carried out only in the initial time step. The same model can also be used for adsorption chillers. The paper describing the development of the absorption chiller model has been presented at the 5th International Conference on Solar Air-conditioning in Germany (2013) [Doemland and Albers, 2013].

The component is based on the method of the characteristic equation and derives the necessary regression coefficients in the initial time step of a TRNSYS simulation, using a user supplied performance file. The file contains the fraction of the cooling capacity and heat demand at different operating points.

The operating points are characterized by the three external inlet temperatures of chilled, cooling and hot water. Furthermore, the component has an algorithm which controls the part load behavior of the machine and calculates the required hot water temperature for the next time step from the load at the previous time step. Therefore, the chiller can react to varying loads but a predictive control is not implemented.

7.2.1 Development of the absorption chiller model

The standard TRNSYS absorption chiller component type 107 is a steady-state model, which interpolates between the external inlet temperatures to look up cooling and heating capacities in an input file. The absorption chiller is seen as a black box.

Kohlenbach and Ziegler [2008] on the other hand presented a very detailed physical model with dynamic transients. The heat transfer in each chamber of the absorption chiller is calculated individually and time lags due to thermal masses are included.

The third approach, which has been chosen for this work due to its simplicity, is the characteristic equation method for absorption chillers derived first by Hellmann et al. [1999]. In their approach the cooling capacity $\dot{Q}_E$ and the driving heat $\dot{Q}_D$ are two linear functions of the characteristic temperature difference $\Delta\Delta t$. The characteristic temperature difference is a function of the mean external temperatures in desorber $\bar{t}_D$, absorber $\bar{t}_A$, condenser $\bar{t}_C$ and evaporator $\bar{t}_E$ in equation 7.3. The mathematical coefficients used to determine the relationship between $\Delta\Delta t$ and $\dot{Q}_E$ have physical relevance (e.g. UA-values of the heat exchangers, saturation enthalpy of the refrigerant, Dühring parameter B).

$$\Delta\Delta t = (\bar{t}_G - \bar{t}_A) - B \cdot (\bar{t}_C - \bar{t}_E) \tag{7.3}$$

Kuehn and Ziegler [2005] showed that an absorption chiller can be modeled more exactly with a modified characteristic temperature difference. In contrast to Hellmann et al. [1999] regression coefficients without physical meaning have been derived showing a high correlation with measured data. The same approach has been

undertaken and compared to the characteristic equation by Puig-Arnavat et al. [2009] with the conclusion that it provides the simplest approach with high accuracy.

Nevertheless, all these evaluations are restricted to absorption chillers with constant solution flow rate. However, for the simulation of high efficiency solar air-conditioning systems also multi stage chillers with or without solution control are of interest.

As mentioned previously the model is based on the method of the characteristic equation by Hellmann et al. [1999]. It is essentially a steady-state description of an absorption chiller. Since the control algorithm described later requires a relatively small time step (3 min are chosen in the simulations) a quasi steady state can be assumed for the transient behavior. The reaction time of real absorption chillers is often longer[2] but this simplification is sufficient for moderate changes in cooling capacity.

For a single stage absorption chiller Kuehn and Ziegler [2005] have shown that cooling capacity $\dot{Q}_E$ and driving heat $\dot{Q}_D$ can also be described as a function of a modified characteristic temperature difference $\Delta\Delta t'$ as in equation 7.4. Here the Dühring parameter B in the established characteristic temperature difference equation 7.3 has been replaced by two regression coefficients, a and b. Instead of mean values $\bar{t}_X$ of the external flows the inlet temperatures are used. The cooling water travels through both, the absorber and the condenser, hence $t_{AC,in}$ is the cooling water inlet temperature.

$$\Delta\Delta t' = t_{D,in} + a \cdot t_{AC,in} + b \cdot t_{E,in} \tag{7.4}$$

If the method's boundary conditions are fulfilled (e.g. constant solution flow rate $\dot{m}_r$, constant UA values and consequently constant external mass flow rates), the fraction q_E of the rated cooling capacity $\dot{Q}_{E,0}$ is a linear function of $\Delta\Delta t'$ (equation 7.5).

$$q_E = \frac{\dot{Q}_E}{\dot{Q}_{E,0}} = s \cdot \Delta\Delta t' + r \tag{7.5}$$

But, when the solution flow rate is controlled under part load conditions, equation 7.5 is not necessarily a linear function of $\Delta\Delta t'$ anymore because the slope parameter s is proportional to $1/\dot{m}_r$ and the loss parameter r is proportional to $\dot{m}_r$ Albers and Ziegler [2011]. This leads to a rational function for q_E in $\Delta\Delta t'$, if the solution flow rate is assumed proportional to the load, i.e. $\dot{m}_r \propto q_E(\Delta\Delta t')$. In the next section it is shown that a second order polynomial is accurate enough for an approximation of the rational function (equation 7.6).

[2]The shift between heat supply and cooling generation of a small scale absorption chiller has been investigated for the author's research work in Singapore and is presented in section 7.2.3

$$q'_E = \alpha \cdot \Delta\Delta t'^2 + \beta \cdot \Delta\Delta t' + \gamma \tag{7.6}$$

The same relationships for the characteristic parameters do not only apply to the generated cooling in the evaporator of the absorption chiller but also to the desorber and its heat demand ($q'_D = \dot{Q}_D / \dot{Q}_{D,0}$).

Inserting equation 7.4 into equation 7.6 leads to equation 7.7.

$$q'_E = \alpha \cdot (t_{D,in} + a \cdot t_{AC,in} + b \cdot t_{E,in})^2 + \beta \cdot (t_{D,in} + a \cdot t_{AC,in} + b \cdot t_{E,in}) + \gamma \tag{7.7}$$

The five characteristic parameters α, β, γ and a, b can be determined through multi-variate regression with the three predictor variables $t_{E,in}$, $t_{D,in}$ and $t_{AC,in}$. Those coefficients must be derived for the desorber and the evaporator. The results lead to the thermal COP of the machine at different part load operating points.

7.2.2 Component configuration and application

To develop a TRNSYS component to simulate an absorption chiller in normal operating mode, regression coefficients needed to be derived to predict the performance based on the three external inlet temperatures.

An external file containing performance data is called by the TRNSYS component. The operating points provide the fraction of rated cooling capacity and fraction of rated heat demand depending on the three external inlet temperatures $t_{E,in}$, $t_{D,in}$ and $t_{AC,in}$. The rated cooling and heating capacity is given as a parameter to later determine the actual capacities in operation using equation 7.8.

$$\dot{Q}_E = q'_E \cdot \dot{Q}_{E,0} \tag{7.8}$$

Three approaches have been analyzed to derive regression coefficients to predict the operating behavior of the absorption chiller.

- **Multi 5:** Non linear Multivariate regression with 5 regression coefficients
- **Split:** Two linear regressions
- **Multi 7:** Non linear Multivariate regression with 7 regression coefficients

The quality of each approach by calculating the mean error and its applicability for TRNSYS were evaluated using published data for the 233 kW double stage chiller from the company Broad [Broad Air Conditioning, 2008]. This chiller has a rated capacity of $\dot{Q}_{E,0} = 233\,\text{kW}$ and a rated thermal COP of 1.41. The heat demand at rated conditions can therefore be calculated to $\dot{Q}_{D,0} = 168\,\text{kW}$.

The standard TRNSYS function set contains the function 'DFIT' which can perform a linear regression on a set of predictor variables. Excel has a similar function called 'LINEST'.

The general form which is used to solve linear regression models for their coefficients $\vec{\beta}$ is given in equation 7.9. This equation contains the error vector $\vec{\epsilon}$ and the response vector $\vec{y}$, which both consist of N data points (the operating points). In order to derive the regression coefficients $\vec{\beta}$ the error vector is minimized by the model. The vector $\vec{x}$ lists the predictor variables. The P different functions $f_p(\vec{x})$ define the regression model. When a constant term is required in the final solution, for example γ in equation 7.7, $f_P(\vec{x})$ is set to 1.

$$\vec{y} = X \cdot \vec{\beta} + \vec{\epsilon} \tag{7.9}$$

$$X = \begin{pmatrix} f_1(\vec{x}_1) & \cdots & f_P(\vec{x}_1)) \\ \vdots & f_p(\vec{x}_n) & \vdots \\ f_1(\vec{x}_N) & \cdots & f_P(\vec{x}_N) \end{pmatrix}$$

Matlab on the other hand is able to perform a multivariate regression on a specified function (curve fit) which does not have to have linear regression coefficients (such as equation 7.7). The Matlab function is called 'nlinfit'.

Non linear multivariate regression with 5 coefficients (Multi 5)

The multivariate regression has been successfully performed for 57 operating points using the function 7.7 as input function to the matlab function 'nlinfit'.

Matlab was able to calculate the five regression coefficients α, β, γ and a, b directly without converting equation 7.7 to the form of equation 7.9. The results for the coefficient and the average error($\bar{\epsilon}$) can be seen in Table 7.1[3].

Table 7.1: Regression coefficients and error for matlab function 'nlinfit'

	α	β	γ	a	b	$\bar{\epsilon}$
$q'_E \cdot \dot{Q}_{E,0}$	-0.023	10.3793	-877.6186	-2.3413	4.5998	1.01%
$q'_D \cdot \dot{Q}_{D,0}$	-0.0147	6.6341	-541.795	-2.5528	4.9703	0.9%

Split linear regression (Split)

This approach to derive the regression coefficients and to predict the operating behavior has been chosen to be implemented in the TRNSYS component.

Instead of a non-linear multivariate regression with high level math algorithms as for "Multi 5", two simple linear regressions are carried out using the quadratic characteristic temperature difference calculated after the first regression as predictor variable in the second one.

[3]These coefficients are not for the fractions of rated power q_E' but for the cooling capacity and heating capacity $\dot{Q}_E$ and $\dot{Q}_D$

Substituting equation 7.4 in 7.5 yields $q'_E = s \cdot (t_{D,in} + a \cdot t_{AC,in} + b \cdot t_{E,in}) + r$. This can be simplified to equation 7.10 which is used in the first linear regression step to determine the coefficients A_0 to A_3.

$$q'_E = A_4 \cdot t_{D,in} + A_3 \cdot t_{AC,in} + A_2 \cdot t_{E,in} + A_1 \tag{7.10}$$

Substituting $a = A_3/A_4$ and $b = A_2/A_4$, the characteristic temperature differences $\Delta\Delta t'$ are calculated from equation 7.4 for each operation point in the input file.

The resulting values for $\Delta\Delta t'$ are used as predictor variables in the second linear regression step to find the coefficients α, β, γ of equation 7.6.

The same two regressions are performed for the fraction of rated driving heat.

The derived regression coefficients characterize the part load behavior of the machine but the split regression procedure is done only once during the initial time step of the simulation. The 10 coefficients are saved in a TRNSYS storage array. Time consuming look-up approaches with linear interpolation in each simulation time step can be avoided.

The result of the split regression approach can be seen in Table 7.2[4].

Table 7.2: Regression coefficients and error for split regression

	α	β	γ	a	b	$\overline{\epsilon}$
$q'_E \cdot \dot{Q}_{E,0}$	-0.0231	10.2985	-856.3997	-2.3916	4.5334	1.05%
$q'_D \cdot \dot{Q}_{D,0}$	-0.0143	6.3885	-508.2089	-2.6556	4.9824	0.94%

It is not as accurate as the Multi 5 approach but can be implemented in TRNSYS easily.

Multivariate regression with 7 coefficients (Multi 7)

It is also possible to perform a linear regression for equation 7.11 which is derived from equation 7.7 as it is expanded. 7 regression coefficients A_1 to A_7 can be calculated by the linear regression functions in TRNSYS, Excel and of course Matlab.

$$q'_E = A_7 \cdot t^2_{D,in} + A_6 \cdot t^2_{AC,in} + A_5 \cdot t^2_{E,in} + A_4 \cdot t_{D,in} + A_3 \cdot t_{AC,in} + A_2 \cdot t_{E,in} + A_1 \tag{7.11}$$

It becomes clear that this approach although easy to implement, returns the least accuracy. Therefore, the split regression was chosen for implementation due to its high accuracy.

[4]The coefficients are not for the fractions of rated power q_E' and q_D' but for the cooling capacity and heating capacity $\dot{Q}_E$ and $\dot{Q}_D$

Table 7.3: Regression coefficients and error for linear regression Multi 7

	A_7	A_6	A_5	A_4	A_3	A_2	A_1	$\bar{\epsilon}$
$q_E{}'$	-0.0486	-0.2824	-0.8708	19.5933	10.0084	35.9611	-2097.7	1.22%
$q_D{}'$	-0.0332	-0.1776	-0.6078	13.2852	5.8003	25.1594	-1395.5	1.37%

7.2.3 Excursion: experimental analysis of a small scale absorption chiller in Singapore

During a six months project in Singapore the author took part in the set up of a testing facility for a small scale (23 kW) absorption chiller in Singapore. The project started in October 2013 until October 2014 and was a joint collaboration between the Singaporean branch SOLID Asia Energy Services Pte. Ltd. of the Austrian company SOLID Gesellschaft für Solarinstallation und Design mbH [S.O.L.I.D., 2014] and the Nanyang Technological University (NTU) in Singapore.

The project was divided into work packages; installation of the laboratory to test absorption chillers, the structuring of the research goals, the execution of the experiments and the analysis of the results

In Singapore the author was mainly occupied with structuring the lab set up and planning the experiments the absorption chiller had to undergo. The experimental research was divided into the following milestones:

1. Milstone A: Variation of inlet temperatures within the recommended temperature range at fixed external (and internal) flow rates
2. Milestone B: Variation of the external inlet temperatures beyond manufacturer's recommendation under fix (rated) external flow rates.
3. Milestone C: Variation of inlet temperatures and external flow rates.
4. Milestone D: Chiller behavior under varying heat input

Milestone A to C are of importance for this chapter as they outline the methodology of the characteristic equation in the previous sections using experimental data. Milestone D gives an indication how long it takes in reality until a variation of heat input results in a change of chilled water output.

The chiller is manufactured by the company Shandong Lucy New Energy Technology Co., Ltd in China and its rated conditions can be found in Table 7.4.

Milestone A

Upon the return in Australia the author worked on the analysis of the results and their representation. The tests were performed with the rated mass flow rates derived in the laboratory and provided in Table 7.4.

Milestone A and B can be presented using the characteristic equation in section 7.2.1. Equation 7.12 to 7.15 show how the eight coefficients for the hot water circuit

Table 7.4: Rated conditions of the chiller from manufacturer and tested in the laboratory.

	manufacturer	experiment	Unit
$\dot{Q}_{chw}$	23	22.2	kW
$T_{chw,in}$	15	16	°C
$T_{chw,out}$	10	11	°C
$\dot{V}_{chw}$	4		$m^3\,h^{-1}$
$\dot{m}_{chw}$	1.11	1.11	$kg\,s^{-1}$
$T_{hw,in}$	90	84	°C
$T_{hw,out}$	85	71	°C
$\dot{V}_{hw}$	5.8		$m^3\,h^{-1}$
$\dot{m}_{hw}$	1.61	0.7	$kg\,s^{-1}$
$\dot{Q}_{hw,calc}$	33.83	36.3	kW
COP_{calc}	0.69	0.61	
$\dot{Q}_{cw,calc}$	57.17	57	kW
$T_{cw,in}$	30	30	°C
$\dot{V}_{cw}$	10		$m^3\,h^{-1}$
$\dot{m}_{cw}$	2.78	2.77	$kg\,s^{-1}$
Solution pump speed		22.2	Hz

(x=hw) and the chilled water circuit (x=chw) have been calculated[5]. Since the solution mass flow rate is kept constant throughout the experiments, the linear approach of equation 7.12 is sufficient.

$$\dot{Q}_x = \alpha_x \cdot \Delta\Delta t + \beta_x \tag{7.12}$$

$$\Delta\Delta t = t_{hw,in} + a_x \cdot t_{cw,in} + b_x \cdot t_{chw,in} \tag{7.13}$$

$$\dot{Q}_x = \alpha_x \cdot t_{hw,in} + \alpha_x \cdot a_x \cdot t_{cw,in} + \alpha_x \cdot b_x \cdot t_{chw,in} + \beta_x \tag{7.14}$$

Substituting equation 7.13 in equation 7.12 yields equation 7.14, which can be expressed as equation 7.15 and solved using multivariate regression.

$$\dot{Q}_x = A_x \cdot t_{hw,in} + B_x \cdot t_{cw,in} + C_x \cdot t_{chw,in} + D_x \tag{7.15}$$

Knowing the coefficients A_x, B_x, C_x and D_x from the regression, $\alpha_x = A_x$, $\beta_x = D_x$, $a_x = B_x/A_x$ and $b_x = C_x/A_x$ it is possible to calculate $\dot{Q}_x$ for each operation point.

Figure 7.2a and 7.2b show the application of the regression on experimental data. The estimated COP can be derived from the calculated $\dot{Q}_{hw}$ and $\dot{Q}_{chw}$ and it is represented in Figure 7.2c vs. the measured COP.

[5]The change in nomenclature originates from the style used in Singapore. D=hw (hot water), E=chw (chilled water), AC=cw (cooling water)

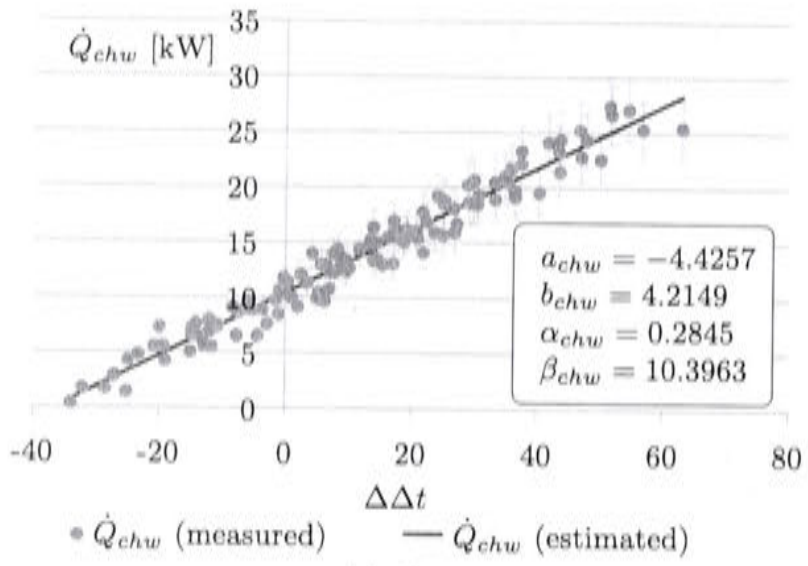

(a) $\dot{Q}_{chw}$

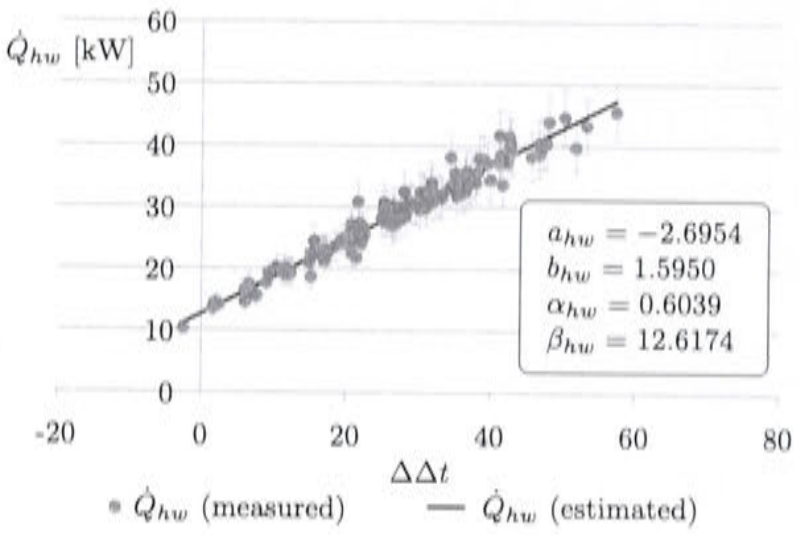

(b) $\dot{Q}_{hw}$

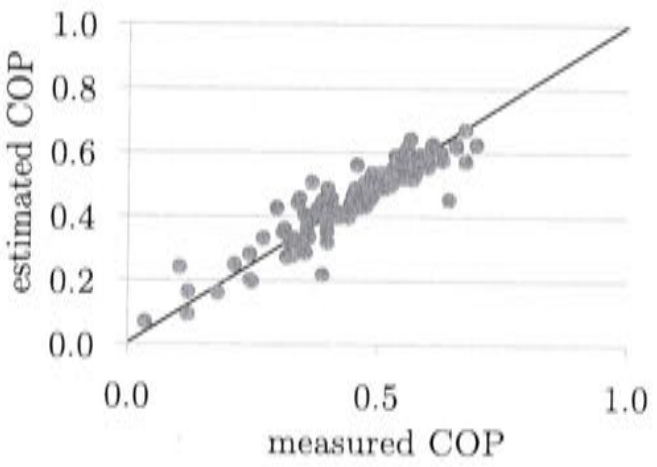

(c) COP estimated vs. measured

Figure 7.2: Application of the characteristic equation to the experimental results for $\dot{Q}_{chw}$ and $\dot{Q}_{hw}$

Milestone C

In this section the mass flow rates have been varied next to the temperatures. A total of 413 set points have been tested and the control to iterate through the test points jumped to the following set point once the defined stability conditions had been reached or 10 min had elapsed. Every 10 seconds the control system recorded a measurement and the values are averaged over the last 3 minutes before a jump to the next set point occurred.

The output data file created had to be processed to combine a set of inlet temperatures for each combination of external mass flow rates ($\dot{m}_{chw}$, $\dot{m}_{cw}$, $\dot{m}_{hw}$). Three cooling water mass flow rates and three chilled water mass flow rates were coupled with up to four different hot water mass flow rates.

The same analysis as in section 7.2.3 has been performed for all combinations of flow rates and for each combination a set of eight regression coefficients has been derived. The results have been included in the Appendix D.2 and each graph in Figure D.1 and D.2 shows a combination of $\dot{m}_{chw}$ and $\dot{m}_{cw}$ and the different $\dot{m}_{hw}$ are categories within each graph. The eight coefficients which were derived via multivariate regression have been printed for each mass flow combination in Figure D.3

Technical limits restricted which of the four hot water mass flow rates were to be tested with each of the chilled and cooling water mass flow rates. These limits

included a minimum achievable chilled water outlet temperature and refrigerant pump noise. In these tests the heat input to the generator and the heat removed from the chilled water circuit had to be kept relatively balanced.

Milestone D

In order to present the time shift between heat input variation and cooling capacity output variation the input file of the small scale absorption chiller was varied according to $\dot{Q}_{hw,set}$ in Figure 7.3.

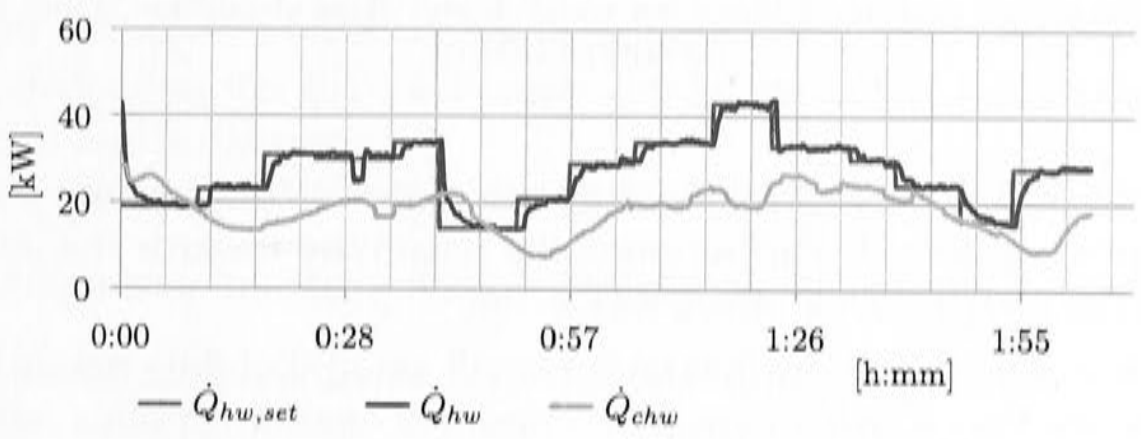

Figure 7.3: Time shift between variation in heat input and generation of cooling of a small scale absorption chiller in the laboratory in Singapore

The set point for the hot water inlet temperature, which is one controlled variable, is calculated in each time step to achieve the desired heat input and the mass flow rates are kept constant. The settings for the three external mass flow rates are the rated flow rates ($\dot{m}_{hw} = 0.7\,\mathrm{kg\,s^{-1}}$, $\dot{m}_{chw} = 1.11\,\mathrm{kg\,s^{-1}}$ and $\dot{m}_{cw} = 2.77\,\mathrm{kg\,s^{-1}}$). The set points for the inlet chilled water temperature was 18°C and for the cooling water temperature 29°C. From the results the time shift can be estimated to be 5 to 10 min. When reducing the inlet chilled water set point temperature the time of the shift seemed similar but less pronounced as the cooling capacity was lower.

7.2.4 Choice of operating points for the model

The motivation for developing a new absorption chiller component for TRNSYS was, next to the requirement for this thesis, to provide a convenient and universally applicable model, which could possible be included in the Australian solar cooling performance standard AS 5389 [Australian/ New Zealand Standard, 2013].

The application of this model for a "solar cooling standard" required an investigation into how many operating points are necessary to achieve a good fit.

The number of necessary data points to perform a good fit was analyzed, varying the sets of data points published on the same Broad absorption chiller as in section 7.2.2. Figure 7.4 shows the cooling capacity vs. $\Delta\Delta t'$ for 57 data points, using the split regression.

Using the split regression and the full set of 57 operating points a correlation coefficient as high as 0.9972 was achieved between the estimated data of the cooling capacity and the published data.

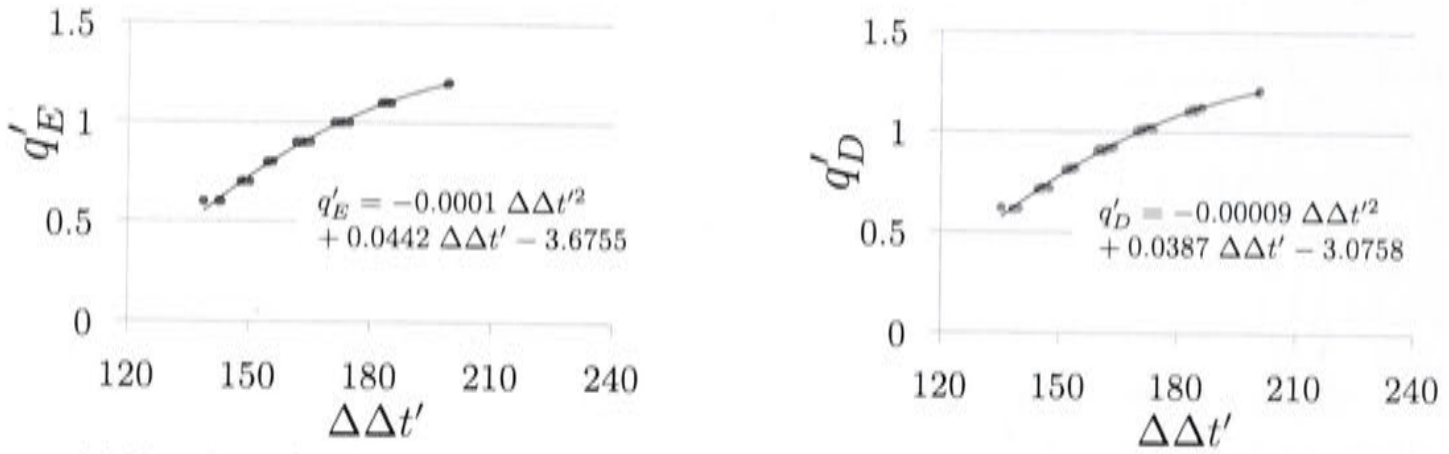

(a) Fraction of cooling capacity

(b) Fraction for heat demand

Figure 7.4: q'_E and q'_D vs. $\Delta\Delta t'$ for a Broad hot water double stage absorption chiller with a cooling capacity of 233 kW

The sensitivity of the quality of the correlation coefficients towards the number of operating points was tested. Furthermore, the sensitivity towards the inlet temperature range of the three external flows was tested.

The results in Table 7.5 show that only a small amount of data points is necessary to achieve a relative good correlation. The amount of operating points can be reduced without a significant loss of accuracy. The inlet temperatures of the three external flows should cover the range of the manufacturer's suggested temperatures. If the points are chosen from a too narrow temperature range like set 2, the accuracy drops from 0.9964 to 0.9884. A relatively small amount of operating points is enough to reach a high correlation coefficient between published data and estimated values.

Table 7.5: Sensitivity of correlation coefficients to amount and range of operating points for q'_E

number of operating points	*temperature ranges & capacity*= $\dot{Q}_E/\dot{Q}_{E,0}$	*correlation coefficient*
57 *(set 1)*	$t_{E,out}$ = (5°C, 6°C, 7°C, 8°C, 10°C) $t_{AC,in}$ = (24°C, 28°C, 30°C, 32°C) capacity = (60%, 70%, 80%, 90%, 100%, 110%, 120%)	0.9972
14 *(set 2)*	$t_{E,out}$ = (6°C, 7°C) $t_{AC,in}$ = (26°C, 28°C) capacity = (60%, 70%, 80%, 90% , 100%)	0.9884
14 *(set 3)*	$t_{E,out}$ = (5°C, 7°C, 10°C) $t_{AC,in}$ = (26°C, 30°C) capacity = (60%, 70%, 80%, 90%, 100%, 110%, 120%)	0.9964
5 *(set 4)*	$t_{E,out}$ = (5°C, 7°C, 10°C) $t_{AC,in}$ = (26°C, 30°C) capacity = (60%, 80%, 100%, 110%)	0.9947

Unfortunately, it is not clear how the published data has been derived; the performance curves published by Broad seem very smooth.

7.2.5 Internal control algorithm of the absorption chiller component

The parameters important for the control of the absorption chiller component are the maximum inlet temperatures, minimum hot water and minimum chilled water inlet temperatures.

There are two important inputs for the algorithm of the chiller's status. The first is the chiller status of the previous time step. The second is the input "cooling required", which is a signal from the room thermostat under the allowed air-conditioning schedule. The chiller status can be used in an HVAC model to switch other components like external pumps and the cooling tower on or off.

The chiller will switch on if cooling is required, but will further determine if it can operate depending on the inlet water conditions of the three external circuits cooling, chilled and hot water.

The chiller must switch off when one of the following conditions occurs:

- the cooling water inlet temperature exceeds the maximum allowed temperature
- the hot water temperature exceeds the maximum temperature
- the hot water temperature falls below the minimum allowed temperature

If the chilled water inlet temperature falls below the minimum allowed temperature, the chiller does not switch off, but does not request any heat input in that time step and does not cool down the chilled water circuit any further.

As previously explained, in the initial time step of the TRNSYS simulation two numerical fits are carried out to calculate the coefficients a, b, α, β and γ. The coefficients are stored to be retrieved in each time step and the cooling capacity and heat demand is calculated depending on the actual inlet temperatures at that time step, using equation 7.7.

For modeling purposes it will be necessary to scale the component to adjust it to the load prior to simulation. A smaller machine will be modeled by scaling $\dot{Q}_{E,0}$ and $\dot{Q}_{D,0}$ while maintaining the operating characteristic which is determined by the correlation coefficients. In this case the external fluid mass flows are scaled proportionally along with the chiller's capacity.

The control strategy implemented to simulate part load operation uses the established relationship between the external inlet temperatures and the cooling capacity. The cooling demand is found from the chilled water return temperature. It is compared to the chilled water set point temperature (e.g. $t_{E,out,set} = 7\,^{\circ}\mathrm{C}$), which is an input to the component, and the required cooling load can be calculated using equation 7.16. The chilled water mass flow rate ($\dot{m}_E$) stays constant.

$$q_{E,req} = \frac{\dot{Q}_{E,req}}{\dot{Q}_{E,0}} = \frac{\dot{m}_E \cdot c_{p,f} \cdot (t_{E,in} - t_{E,out,set})}{\dot{Q}_{E,0}} \tag{7.16}$$

In the next step equation 7.17 and 7.18 determine the required temperature of the hot water flow for the next time step to cover the load.

$$\Delta\Delta t'_{req} = -\frac{\beta}{2\alpha} \pm \sqrt{\frac{\beta^2 - 4\alpha \cdot (\gamma - q_{E,req})}{4\alpha}} \tag{7.17}$$

$$t_{D,in,req} = \Delta\Delta t'_{req} - \alpha \cdot t_{AC,in} - \beta \cdot t_{E,in} \tag{7.18}$$

Equation 7.17 may have two solutions for $\Delta\Delta t'$ or it may have none, depending on the shape of the function in equation 7.6. The component is designed to catch any error which may occur and to choose the correct solution for $\Delta\Delta t'$.

The required hot water inlet temperature can be used to control other components in an input file for TRNSYS. For example it can control a temperature regulating mixing valve to adjust the inlet hot water temperature for the next time step or an auxiliary heater. If the hot water inlet temperature is lower than the required temperature the cooling capacity will be calculated accordingly, but the chilled water set point temperature will not be reached.

7.2.6 The absorption chiller within the solar thermal air-conditioning model

The chiller will switch on if cooling is required, but will then determine if it can operate depending on the inlet water conditions of the three external circuits cooling, chilled and hot water.

Remark *The notation concerning the three external chiller circuits changes from the general absorption chiller model in the previous sections to the integrated cooling, heating and DHW model in the following sections. The subscript for the chilled water circuit will be replaced by "chw" instead of "E", the subscript for the hot water circuit will be replaced by "hw" instead of "D" and the subscript for the cooling water circuit will be replaced by "cw" instead of "AC". Furthermore, the placeholder for the temperature will be a capitalized "T" in all following sections. The rated cooling capacity of the chiller will be no longer $\dot{Q}_{E,0}$ but will be replaced by $\dot{Q}_{E,rated}$.*

The chiller switches off if the hot water inlet temperature ($T_{hw,in}$) falls below the minimum hot water inlet temperature minus 3°C or the chilled water inlet temperature ($T_{chw,in}$) is smaller than the set point temperature ($T_{set,chw}$)[6].

The air flow through the cooling coils warms up the chilled water and depending on the return chilled water temperature to the chiller, the chiller meets the load by calculating a required hot water inlet temperature for the next time step to satisfy the load. The set point chilled water outlet temperature of the absorption chiller is an input to the component and therefore variable. The cooling water, hot water and

[6]This can happen due to the control algorithm of the hot water supply for the chiller. The load might have dropped in the current time step but the reduced required hot water temperature is going to be delivered in the next time step. For the current time step, the current (higher) hot water temperature is used and generates chilled water below $T_{set,chw}$. The occurrence of this event can be minimized by having a minimum air flow rate or by sizing the chiller smaller.

chilled water inlet temperatures determine the capacity the machine operates at and therefore the chilled water outlet temperature of the current time step.

The air set point temperature and chilled water set point temperatures are design parameters for the system.

The operating characteristic of the absorption chiller in the solar thermal HVAC system model is based on the absorption chiller Wegracal SE15 from EAW Energieanlagenbau GmbH Westenfeld [2014]. The operating points used to generate an input file for the TRNSYS component described in the previous sections were derived from the openly available TRNSYS component type 177, published by Jan Albers [Albers, 2011].

The chiller's capacity depends strongly on the external inlet temperatures, and a performance map has been created in Table 7.6 to choose the design condition. The design conditions define the rated chiller capacity $\dot{Q}_{E,rated}$.

Table 7.6: Characteristic of the absorption chiller Wegracal 15 SE from Albers [2011]

	$T_{chw,out,set}$	$T_{chw,in}$	$T_{cw,in}$	$T_{hw,req}$	$\dot{Q}_E$ [kW]
(1)	7°C	12°C	27°C	84.5°C	11.7
(2)	7°C	11°C	27°C	78.2°C	9.3
(3)	6°C	11°C	27°C	86.3°C	11.7
(4)	11°C	15°C	27°C	70.9°C	9.3
(5)	11°C	16°C	27°C	77.1°C	11.7
(6)	10°C	15°C	27°C	78.9°C	11.7
(7)	11°C	17.3°C	30°C	93.1°C	14.7
(8)	11°C	16°C	30°C	85.5°C	11.7

If dehumidification is at least partly desired, it is necessary to decide between configuration (1) or (3). The chilled water inlet temperature ($T_{chw,in}$) is dependent on the supply air set point temperature of the cooling coils.

Configuration (7) are the approximate design conditions published from EAW. Configuration (7) is chosen when a dry fluid cooler is used, which requires a higher cooling water set point temperature. In case of the dry fluid cooler, the lower water consumption is bought with a higher fan electricity consumption (rooms and cooling tower) and with less dehumidification. Even though the chilled water set point is raised, the chiller still needs relatively high hot water inlet temperatures, because the cooling water inlet temperature is increased. There are adsorption chillers which can perform at higher cooling water inlet temperatures but they have lower thermal COPs.

Lowering the chilled water set point temperature increases the auxiliary heat consumption, because lower chilled water outlet temperatures require higher hot water inlet temperatures. Configuration (3) needs most auxiliary power compared to (1) and (6), which require least, but would have the highest dehumidification potential. Increasing the chilled water set point temperature implies increasing the supply air set point temperature and $T_{chw,in}$ to keep the rated chiller's capacity of approximately 11 kW. Higher air set point temperatures lead to a higher indoor air flow

and increase the indoor fan power consumption. Furthermore, the dehumidification potential will be lowered. This is the trade-off between a high auxiliary and parasitic energy consumption and adequate comfort conditions.

Number (1) with 7°C chilled water set point, 12°C chilled water return temperature, 27°C cooling water inlet temperature, 84.5°C hot water inlet temperature and 11.7 kW chilled water generation was chosen as the design condition. In that case the rated capacity is $\dot{Q}_{E,rated} = 11\,\mathrm{kW}$ and the rated thermal COP (COP_{rated}) is 0.7.

A $scalefactor$ as in equation 7.19 has been introduced to size the chiller to the appropriate capacity for each climate. The external mass flow rates are also scaled with this factor. The rated flow rate for the cooling water cirucit is $\dot{m}_{cw,rated} = 4975\,\mathrm{kg\,h^{-1}}$, for the chilled water circuit $\dot{m}_{chw,rated} = 1999\,\mathrm{kg\,h^{-1}}$ and for the hot water circuit $\dot{m}_{hw,rated} = 1940\,\mathrm{kg\,h^{-1}}$. The capacity of each climate can be found in Table 4.12.

$$scalefactor = \frac{C_c}{\dot{Q}_{E,rated}} \tag{7.19}$$

The auxiliary heater's capacity was limited to the maximum of either the rated heat demand of the chiller or the average between the 95th and 100th percentile of the heat demand for space heating (Table 4.12).

7.2.7 Adsorption chillers

In this thesis a solar thermal cooling system with a small scale absorption chiller was modeled. The same modeling strategy using the characteristic equation is also applicable to adsorption systems. Adsorption chillers operate not in a continuous cycle, however, in order to achieve a quasi-continuous cycle, two chambers filled with adsorbent are alternately charged and discharged.

Adsorption systems have advantages and disadvantages to absorption machines.

Since the adsorption technology uses adsorbent instead of a liquid solution to adsorb the refrigerant vapor, there is no danger of crystallization. In general adsorption chillers are able to work at higher heat rejection temperatures which favors dry recooling. The adsorption machine from Invensor GmbH [2014] for example can work with cooling water temperatures up to 47°C. However, in that case the chilled water outlet temperatures are relatively high and the thermal COPs are low. Another advantage over absorption chillers is the internal electricity consumption of the machines. Since the adsorption chiller operates in a so called batch process when charging or discharging the solid adsorbent, no solution pump is necessary.

In general adsorption chillers operate at rated conditions often at higher chilled water outlet temperatures and at lower thermal COPs compared to absorption chillers. For dehumidification purposes the adsorption chiller technology is not well suited since the relatively high heat rejection temperatures and often lower hot water temperatures don't allow for chilled water outlet temperatures below 10°C at a thermal COP comparable to absorption chillers. Adsorption chillers are usually bulkier and heavier than absorption chillers.

The choice of either an adsorption or absorption chiller depends on the desired chilled water temperature, the available heat rejection conditions and the available hot water temperatures. For radiative cooling for example in chilled beams applications with chilled water temperature above 15°C, adsorption chillers are suited as well as absorption chillers.

The design conditions should be chosen at an operating point with the highest thermal COP. Operating a thermal chiller at higher heat rejection temperatures and lower driving temperatures is possible, however, the penalty are lower thermal COPs and higher chilled water temperatures.

7.3 Variable air flow and humidity control strategies

The air flow, which passes through the cooling and heating coils, is variable and depends on the cooling and heating demand in each zone of the building in the current simulation time step. The control adjusts the heat supply to the chiller depending on the chilled water return temperature leaving the coils.

Three air-conditioning strategies for the cooling mode have been modeled and they differ in the calculation of the air flow required to tackle sensible and latent loads.

7.3.1 Sensible load control only (strategy I)

The sensible load can easily be controlled by the room thermostat. The TRNSYS building model type 56 generates the following outputs for each room, which add up to the total sensible heat gain (or loss) in the current time step[7]:

- $\dot{Q}_{surf}$ total convection to air from all surfaces within the room.
- $\dot{Q}_{inf}$ sensible energy gain from room due to infiltration.
- $\dot{Q}_{coup}$ sensible coupling gain of room (coupling refers to the neighboring rooms).
- $\dot{Q}_{gconv}$ internal convection gains of room.

$$\dot{Q}_{sens,gain} = \max(0, \dot{Q}_{surf}) + \max(0, \dot{Q}_{inf}) + \max(0, \dot{Q}_{coup}) + \max(0, \dot{Q}_{gconv}) \tag{7.20}$$

$$\dot{Q}_{sens,loss} = \min(0, \dot{Q}_{surf}) + \min(0, \dot{Q}_{inf}) + \min(0, \dot{Q}_{coup}) + \min(0, \dot{Q}_{gconv}) \tag{7.21}$$

[7]No radiation gain is taken into account for two reasons. Firstly, the air temperature and not the operative temperature is controlled. Secondly, shortwave (solar) radiation gains through the windows are absorbed by the surfaces of the zone and are transferred via convection into the room. Type 56 considers internal radiative gains Q_{grad} in order to calculate a "star temperature" for the zone, which combines radiative and convective gains from the surfaces. It is similar to the operative temperature, which is merely an weighted average of the air and the surface temperatures.

Once the thermostat recognizes the cooling requirement, this sensible heat gain is used together with equation 7.22 to calculate the necessary air flow for cooling $\dot{m}_{air,sens,c}$ to tackle the load in that room. In heating mode the sensible heat loss together with equation 7.23 determines the mass flow of air necessary to supply heating to the room. The heating coils heat the air stream to the chosen set point of 32°C ($T_{set,air,HC}$). There is a minimum air flow to stabilize the chiller's switching. It is set to 200 kg h^{-1} in each zone for cooling and heating.

$$\dot{m}_{air,sens,c} = \frac{\dot{Q}_{sens,gain}}{c_{p,air} \cdot (T_{setC} - T_{set,air,CC})} \tag{7.22}$$

$$\dot{m}_{air,h} = \frac{|\dot{Q}_{sens,loss}|}{c_{p,air} \cdot (T_{setH} - T_{set,air,HC})} \tag{7.23}$$

The cooling coils are designed to cool the air down to the (dry bulb) temperature $T_{set,air,CC}$. The TESS TRNSYS component type 508 is used, which offers a control mode to set the air outlet temperature. In doing this, latent cooling of the air stream can be achieved down to the humidity ratio of saturated air $\omega_{set,air,CC}$ (at $T_{set,air,CC}$)[8], provided the chilled water is cold enough and can remove the necessary latent and sensible heats. The amount of latent heat removed by the cooling coils ($\dot{Q}_{c,lat}$) while sensibly cooling the air down to its dry bulb set point temperature ($T_{set,air,CC}$) is calculated using equation 7.24. The difference in humidity ratio between the room air (ω_r) and the air leaving the coil ($\omega_{T_{air,CC}}$) is multiplied by the air flow rate and yields the moisture removal rate by the cooling coil. If $T_{set,air,CC}$ cannot be achieved, dehumidification effect is reduced.

$$\dot{Q}_{c,lat} = \dot{m}_{air,c} \cdot \Delta h_{vapor} \cdot (\omega_r - \omega_{T_{air,CC}}) \tag{7.24}$$

7.3.2 Sensible load control and latent load control, temperature dominated (strategy II)

The latent heat gains of a room are reflected in the humidity ratio of the room air. Since type 56 assumes uniform mixing of the supply air with the room air, reheating is done for controlling purposes to reach the humidity set point rather than to ease local discomfort.

Latent heat gains humidify the air and increase the humidity ratio of the air within the room ω_r. The humidity is able to accumulate over time when the room is not air-conditioned. In case the air mass flow is merely governed by the sensible load as in strategy I (section 7.3.1) it is likely that the amount of latent heat removed is not able to reduce the humidity in the room sufficiently. The air-condition system might switch off prematurely, because the dry bulb set point temperature is already reached.

[8] e.g 0.010 kg_{H2O} kg^{-1}_{dryair} at $T_{set,air,CC}$ =14°C.

For this reason the air flow, which passes through the cooling coils, is increased following equation 7.25 to remove additional humidity. The meaning behind this equation is the removal of the accumulated humidity in the room with the air flow $\dot{m}_{air,lat,c}$ within δ hours. The variable δ is set to 15 min. The desired humidity ratio $\omega_{set,c}$ is found at the dry bulb set point temperature at 60% relative humidity on the psychrometric chart. The limit in the denominator of 0.001 must be set to prevent frequent switching. The air mass of the room is the product of the room's volume (V_r) and the air density (ρ_{air}). A maximum limit of twice the air flow for sensible load removal is set.

$$\dot{m}_{air,lat,c} = \min\left(2 \cdot \dot{m}_{air,sens,c}, \frac{V_r\, \rho_{air} \cdot (\omega_r - \omega_{set,c}) \cdot \{\omega_r > \omega_{set,c}\}}{\delta \cdot \max(0.001, \omega_r - \omega_{set,air,CC})}\right) \tag{7.25}$$

The total air flow entering the cooling coils is then determined by equation 7.26. In case of high humidity loads, $\dot{m}_{air,lat,c}$ is larger than $\dot{m}_{air,sens,c}$ and the air flow is increased.

$$\dot{m}_{air,c} = \max(\dot{m}_{air,lat,c}, \dot{m}_{air,sens,c}) \tag{7.26}$$

But merely increasing the airflow would only trigger the air-conditioning system to turn off sooner, because T_{setC} is met sooner. The latent loads would not be removed completely. Therefore, the excess sensible cooling, when reaching the desired humidity levels, must be offset and the dehumidified and cooled air stream is reheated again in heating coils using hot water from the tank. The water for reheating in the model is not backed up by the auxiliary gas heater. If it can't provide sufficient reheating, the air-conditioner switches off.

The component uses a hot water bypass to achieve the desired air set point temperature χ in equation 7.27, which is derived from equation 7.22. Obviously no reheating is necessary if the the latent load can be covered by $\dot{m}_{air,sens,c}$.

$$\chi = T_{setC} - \frac{\dot{Q}_{sens,gain}}{c_{p,air} \cdot \dot{m}_{air,c}} \tag{7.27}$$

This strategy works very well during the day when there is a sensible cooling load. Whenever sensible cooling is required, the air is dehumidified to the set point at the same time. However, later in the evening the outdoor temperature might start dropping and the sensible loads might become zero. The thermostat falls below $T_{setC} - 1\,°C$ and the air-conditioner turns off. The indoor dry bulb temperature lies perfectly in the comfort limits (below 20°C and T_{setC}), but the humidity can start to build up, especially in humid climates.

In the living area (zone 1) this is not a problem, because the HVAC schedule does not require air-conditioning during these times. However, the bedrooms can become

uncomfortable due to humidities above 60%.

As a result, it became necessary to define a third strategy to control humidity during the night hours when there is no sensible cooling demand at all.

7.3.3 Sensible load control and latent load control, humidity dominated (strategy III)

Providing latent only cooling is not possible with a chilled water coil without a substantial amount of reheating. There will be an amount of sensible cooling as well, even though there is no sensible cooling required. Strategy III was developed from strategy II to achieve dehumidification during the night but preventing the temperature from dropping below $T_{setH} + 1\,°C$.

The HVAC signal indicating a cooling requirement in each zone was modified as in equation 7.28 in order to include the need for dehumidification.

$$HVAC_{c,z_i} = \{HVAC_{therm,c,z_i} \vee \{\omega_r > \omega_{set,c}\}\} \cdot HVAC_{sched,z_i} \tag{7.28}$$

The set point temperature for the reheating system is 21°C instead of T_{setC} to prevent warming up the room.

It is possible to set the reheating temperature to the room temperature to offset the total amount of sensible cooling generated. However, that seems like a waste of low temperature heat since the heat is required during the day to generate cooling. Furthermore, as long as the set point temperature can be kept above $T_{setH} - 1\,°C$ it can be accepted to over chill the rooms.

The selection of dehumidification strategies depends on how stringent the set points for humidity are to be kept. It is clear that additional dehumidification of strategy II and III uses more energy in form of heat, both for cooling and for reheating. Furthermore, the chiller capacity has to be increased especially in the humid climates. Consequently parasitic electricity demand will increase as well.

7.4 Wet cooling tower for heat rejection

Most European solar cooling absorption chiller systems use wet cooling towers for heat rejection, because they can provide lower cooling water temperatures than dry cooling towers.

In the model a variable speed drive regulates the fan speed (air flow) of the **wet cooling tower** to achieve always a fixed cooling water set point temperature $T_{cw,set}$; here 27°C.

The wet cooling tower model TRNSYS Type 51 determines the heat transfer effectiveness using the net transfer units (NTU) as defined in equation 7.29 from the TRNSYS documentation. This value requires two coefficients n and c, where n is in the range of -0.35 to -1.1 and c is in the range of 0.5 to 5 [Solar Energy Laboratory, Univ. of Wisconsin-Madison et al., 2007; ASHRAE, 2012].

The coefficients were derived with the TRNSYS component type 51 using the 15 data points of the Phoenix cooling tower published by Ciganda [2007] and the results were $n = -0.884$ and $c = 0.71$. This cooling tower provided the heat transfer characteristic for all the simulations.

$$NTU = c \cdot \left(\frac{\dot{m}_{water}}{\dot{m}_{air}}\right)^{n+1} \tag{7.29}$$

The cooling tower rated conditions are cooling water inlet temperature of 32°C, outlet temperature of 27°C and outdoor wet bulb temperature of 21°C. A performance map was created for the cooling tower, varying the wet bulb temperature, but generating always 27°C cooling water outlet temperature. The water flow rate was set to the rated cooling water flow rate of the chiller $\dot{m}_{cw,rated}$.

The main influences on the required air flow are outdoor wet bulb temperature and cooling water return temperature (Figure 7.5). The dry bulb temperature has hardly any effect (Figure 7.6). A correlation curve has been derived between the necessary air flow and wet bulb temperatures for the rated condition $T_{cw,in} = 21\,°C$.

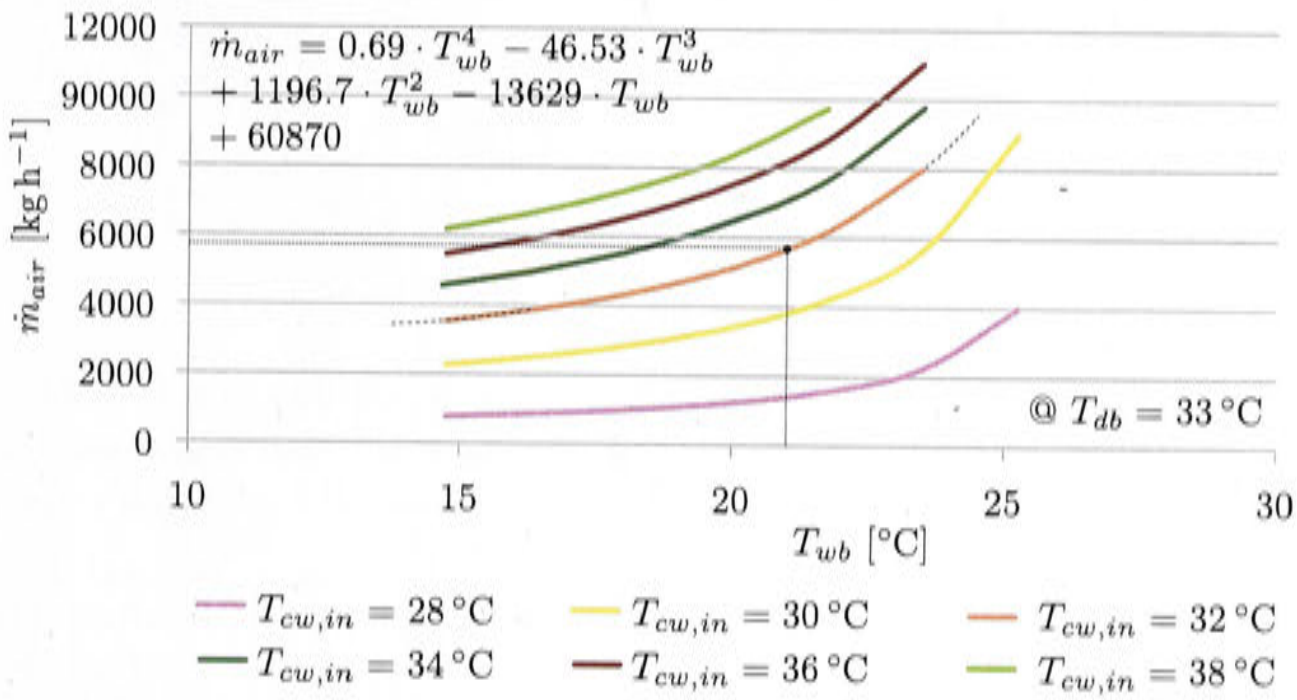

Figure 7.5: Air flow vs. air wet bulb temperature (T_{wb}) of a wet cooling tower at the dry bulb temperature T_{db} =33°C. Rated conditions are marked at $T_{wb} = 21\,°C$.

The rated air mass flow ($\dot{m}_{air,rated}$) at the rated wet bulb temperature $T_{wb,rated} = 21\,°C$ was chosen to correspond to the rated electricity consumption $\dot{E}_{el,rated}$ of the cooling tower. To calculate the scaled rated electricity consumption ($\dot{E}_{el,rated,scaled}$) for each climate the *scalefactor* has been included to account for smaller capacities and the rule of thumb given by Henning [2007] and Rehsler Kuehlsysteme GmbH [2012] has been applied. The rule of thumb assumes a fan electricity consumption at rated conditions of approximately 10 W per kW of rejected heat[9]. It is assumed that the cooling water mass flow rate and the rated air flow are scaled linearly with the *scalefactor* and that the heat transfer characteristic of the cooling tower remains unaffected.

[9]The rejected heat has been calculated for the rated conditions of the chiller at 7°C chilled water outlet temperature, and cooling down the cooling water from 32°C to 27°C.

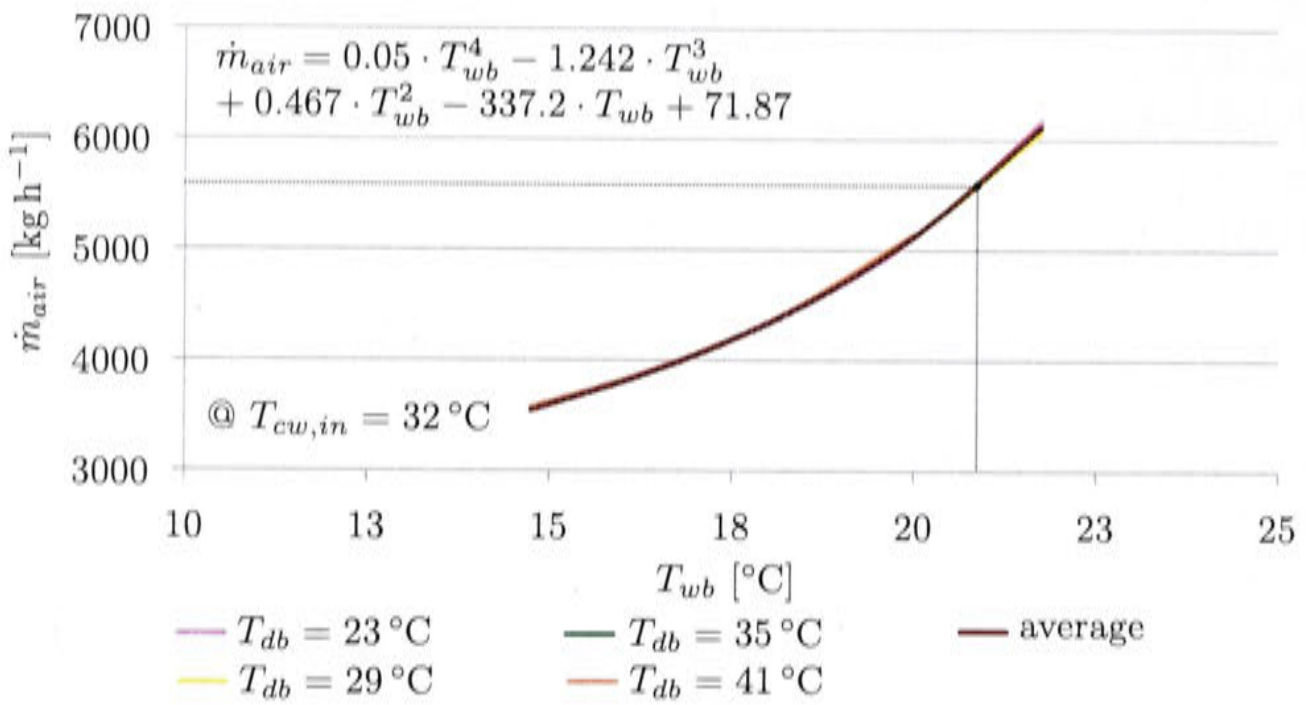

Figure 7.6: Air flow vs. air wet bulb temperature T_{wb} of a wet cooling tower at the cooling water inlet temperature $T_{cw,in}$ =32°C. Rated conditions are marked at T_{wb} = 21 °C.

$$\dot{E}_{el,rated,scaled} = \left(\dot{Q}_{E,rated} \cdot scalefactor + \frac{\dot{Q}_{E,rated} \cdot scalefactor}{COP_{rated}}\right) \cdot 10\,\mathrm{W_{el}\,kW_{th}^{-1}} \qquad (7.30)$$

$$\dot{m}_{air,rated,scaled} = \dot{m}_{air,rated} \cdot scalefactor \qquad (7.31)$$

However, the rated wet bulb temperature for the cooling tower of 21°C is not always the design wet bulb temperature of the climate. For different climates a climate specific design air flow has to be defined to achieve the required rated cooling water outlet temperature of 27°C.

To estimate the design wet bulb temperature for each climate, the frequency densities $q_{T_{wb}}$ were determined for the 1 degree wet bulb temperature bins between 10 °C and 35 °C. Essentially an average was built over a restricted temperature range using equation 7.32. The temperature points were taken from the TMY weather data files and only data points with a dry bulb temperature above 24°C and between 6:00 and 22:00 were counted. Previously, the design air wet bulb temperatures for each climate were taken from AIRAH [2007], but those design wet bulb temperatures seemed too high. In the handbook they were defined as the "3pm wet bulb temperatures which are individually exceeded on 10 days per year (inclusive of one standard deviation)".

$$T_{wb,design} = \sum_{T_{wb}=10}^{T_{wb}=35} \{q_{T_{wb}}\ T_{wb}\}\ \{T_{db} > 24\,°C\} \cdot \{6{:}00 < time < 22{:}00\} \qquad (7.32)$$

Knowing the design wet bulb temperature for each climate $T_{wb,design}$, the flow rate $\dot{m}_{air,design}$ for which 27°C can be generated was calculated using the regression equation presented in Figure 7.6. This flow rate was set the maximum cell air flow

rate of TRNSYS type 51. This means that for every climate the ratio between water mass flow and air flow (L-G-ratio) was set differently. The L-G-ratio is defined in equation 7.33, where $\dot{m}_{water,rated}$ is the cooling water flow determined by the rated chiller capacity.

Table 7.7 shows the design L-G ratios and the calculated design wet bulb temperatures for each climate. Typical L-G ratios are between 0.7 and 1.5 [Wang, 2000, p. 10.41]. Furthermore, it shows the design outdoor wet bulb temperatures from AIRAH [2007].

$$\text{L-G ratio} = \frac{\dot{m}_{cw,rated} \cdot scalefactor}{\dot{m}_{air,design} \cdot scalefactor} \tag{7.33}$$

Equation 7.34 is used to calculate the cooling tower fan power consumption at climate specific design conditions for the scaled chiller, which is a parameter of the cooling tower TRNSYS component type 51.

$$\dot{E}_{el,design,scaled} = \dot{E}_{el,rated,scaled} \cdot \left(\frac{\dot{m}_{air,design} \cdot scalefactor}{\dot{m}_{air,rated} \cdot scalefactor} \right)^3 \tag{7.34}$$

Table 7.7: Design wet bulb temperature and L-G ratio for the wet cooling tower

	$T_{cw,design}$ (eq. 7.32) [°C]	L-G-ratio	$T_{cw,design}$ [AIRAH, 2007, p.163 et seq.] [°C]
Canberra	18.03	1.19	19.6
Brisbane	21.04	0.91	24.9
Sydney	20.87	0.93	22.6
Griffith	20.16	0.99	22.2
Tennant Creek	18.28	1.16	24.4
Darwin	24.80	0.58	27.7
Melbourne	20.22	0.99	20.4

Within the simulation the iterative feed back controller determines the actual air mass flow $\dot{m}_{air}$ necessary to achieve the set point cooling water outlet temperatures at the given operating point. The actual electricity consumption of the cooling tower fan in each time step is calculated using equation 7.35, but $\dot{m}_{air}$ is limited by $\dot{m}_{air,design}$.

$$\begin{aligned} \dot{E}_{el,CT} &= \dot{E}_{el,design,scaled} \cdot \left(\frac{\dot{m}_{air}}{\dot{m}_{air,design} \cdot scalefactor} \right)^3 \\ &= \dot{E}_{el,rated,scaled} \cdot \left(\frac{\dot{m}_{air}}{\dot{m}_{air,rated} \cdot scalefactor} \right)^3 \end{aligned} \tag{7.35}$$

The fan power consumption of such a cooling water control strategy is rather low but a variable frequency drive and a PID controller are necessary to adjust the fan speed to the desired cooling water outlet temperature.

To express the presented approach to calculate the cooling tower fan power con-

sumption in different words, the rule of thumb in Henning [2013b] is modified and made dependent on the wet bulb temperature of the climate the system is installed in (equation 7.36).

$$\mathrm{kW_{el}\,kW_{th}^{-1}} = 10\,\mathrm{kW_{el}\,kW_{th}^{-1}} \cdot \left(\frac{\dot{m}_{air}}{\dot{m}_{air,rated}}\right)^3 \tag{7.36}$$

The return water temperature also plays an important role in the calculation of the air flow rate. The lower the return water temperature, the less air flow is needed to achieve the set point. If the chiller runs at low capacities, its cooling water outlet temperature is relatively low and the fan speed is adjusted.

It is possible to vary the cooling water set point temperature and to adjust it to the prevailing ambient conditions. This strategy will be analyzed in detail in section 8.2.7. A higher cooling water temperature results in higher hot water supply temperatures to the chiller and the auxiliary heat demand might increase.

7.5 The collector and tank loop

7.5.1 Collector type and hydraulic collector arrangement

For residential solar cooling applications using absorption chillers the main collector types are flat plate and evacuated tube collectors.

The collector efficiency follows equation 7.37 and is a function of the optical efficiency ($\tau\alpha$), the insolation normal to the collector's surface ($\dot{G}_{tot,coll}$), the ambient temperature (T_{amb}) and the collector's fluid average temperature ($T_{avg} = (T_{f,out} + T_{f,in})/2$). The average temperature of the collector fluid between inlet and outlet is an approximation for the absorber plate temperature. The $\tau\alpha$ product in equation 7.37 would be multiplied by a heat removal factor (F_R) if the fluid inlet temperature was used instead of the average plate temperature [Kalogirou, 2009, p. 225].

$$\eta = \tau\alpha - c_1 \frac{(T_{f,avg} - T_{amb})}{\dot{G}_{tot,coll}} - c_2 \frac{(T_{f,avg} - T_{amb})^2}{\dot{G}_{tot,coll}} \tag{7.37}$$

$$\eta = c_0 - c_1\, x - c_2\, x^2\, \dot{G}_{tot,coll} \tag{7.38}$$

The coefficients c_0, c_1 and c_2 are published by most collector manufacturers. The main advantage of evacuated tube collectors over flat plate collectors is their higher efficiency at high average fluid temperatures (especially at low insolation). The vacuum within the tubes reduces convection losses to the glass surface and therefore radiation and convection losses to the environment. Almost 50% of all absorption chiller solar cooling systems have been installed using evacuated tubes [Henning, 2013a, p. 293].

In Figure 7.7 the flat plate ('Vitosol 300-F') and evacuated tube collector ('Vitosol 200-F') of the company VIESSMANN are compared VIESSMANN [2008]. The evac-

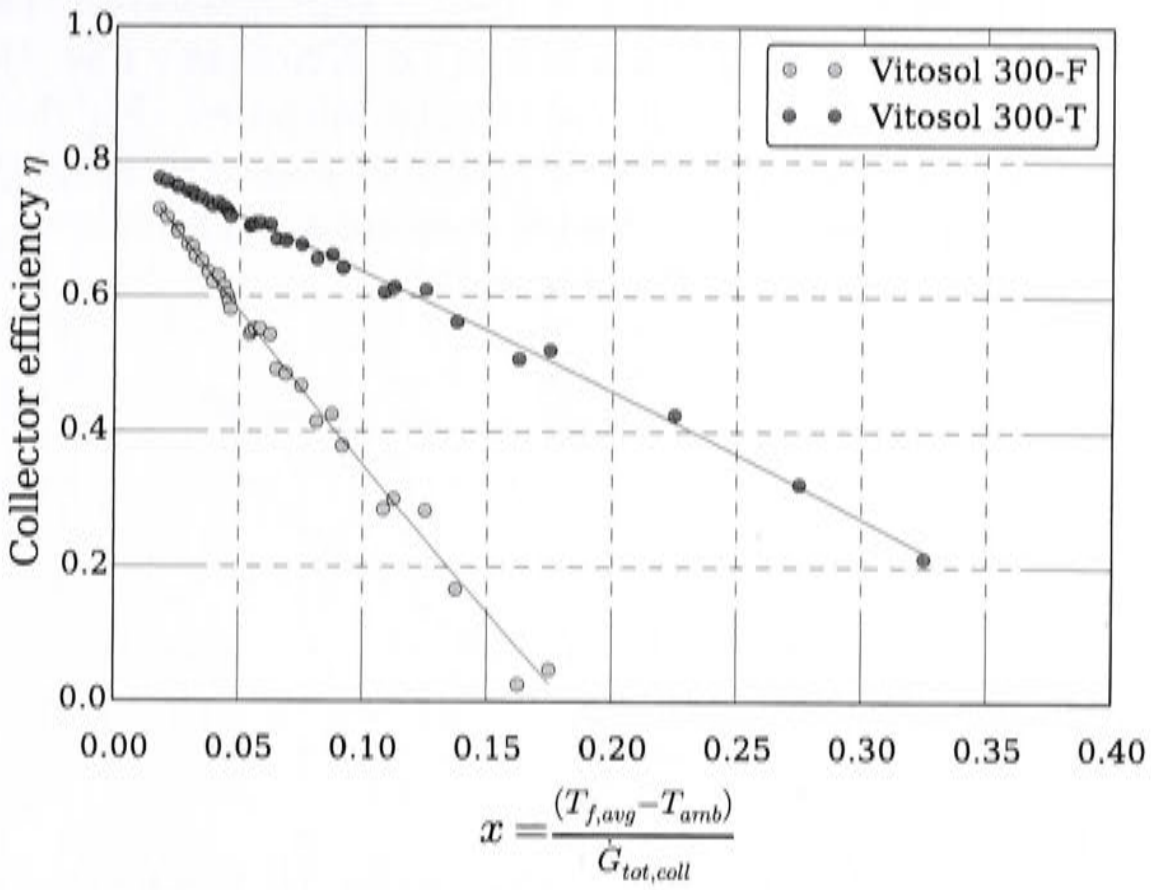

Figure 7.7: Efficiency curve VIESSMANN solar thermal collectors; evacuated tubes $c_0 = 0.802$, $c_1 = 1.37\,\mathrm{W\,m^{-2}\,K^{-1}}$, $c_2 = 0.0068\,\mathrm{W\,m^{-2}\,K^{-2}}$; flat plate collectors $c_0 = 0.803$, $c_1 = 3.77\,\mathrm{W\,m^{-2}\,K^{-1}}$, $c_2 = 0.0156\,\mathrm{W\,m^{-2}\,K^{-2}}$

uated tube collector from VIESSMANN has an absorber area of $3.02\,\mathrm{m^2}$.

The evacuated tube collectors were chosen for the simulations due to their better performance at elevated average collector temperatures, typical of absorption chiller application.

For further consideration in Australia it might be more cost effective to import Chinese evacuated tube collectors although their thermal efficiency might be lower compared to the German/ Austrian collectors.

As the sun is not always normal to the collector surface, the incidence angle modifier (IAM) has to be included to modify the optical efficiency depending on the incidence angle of the sun to the collector. The factor accounts for reflection losses from the collector. The efficiency curve of the collector is modified to equation 7.39. The incidence angle modifiers used for the simulations can be found in Appendix D.1. Evacuated tube collectors can have IAM values above one, at times of the day when tubes can reflect the solar radiation onto each other.

$$\eta = \tau\alpha\ IAM - c_1 \cdot \frac{(T_{f,avg} - T_{amb})}{\dot{G}_{tot,coll}} - c_2 \frac{(T_{f,avg} - T_{amb})^2}{\dot{G}_{tot,coll}} \tag{7.39}$$

The water flow rate for the collectors is sized using $30\,\mathrm{l\,h^{-1}\,m^{-2}}$ which is on the upper bound of a 'medium-flow' arrangement for solar collector arrays [Henning, 2013a].

The pressure drops for various configurations of collector arrangements (parallel

and series) were estimated to calculate the pump power demand. When changing the collector arrangement the flow rate was always kept between 4.5 l min^{-1} and 7.5 l min^{-1} per row of collectors. This leads to 3 to 5 collectors in a row. The number of collectors in a row are kept constant for balance purposes. For the hydraulic design VIESSMANN recommends to choose the pipe diameter, keeping the flow velocity between 0.4 and 0.7 m/s. The pressure drop for a single collector is derived from published data VIESSMANN [2013] (Figure 7.8).

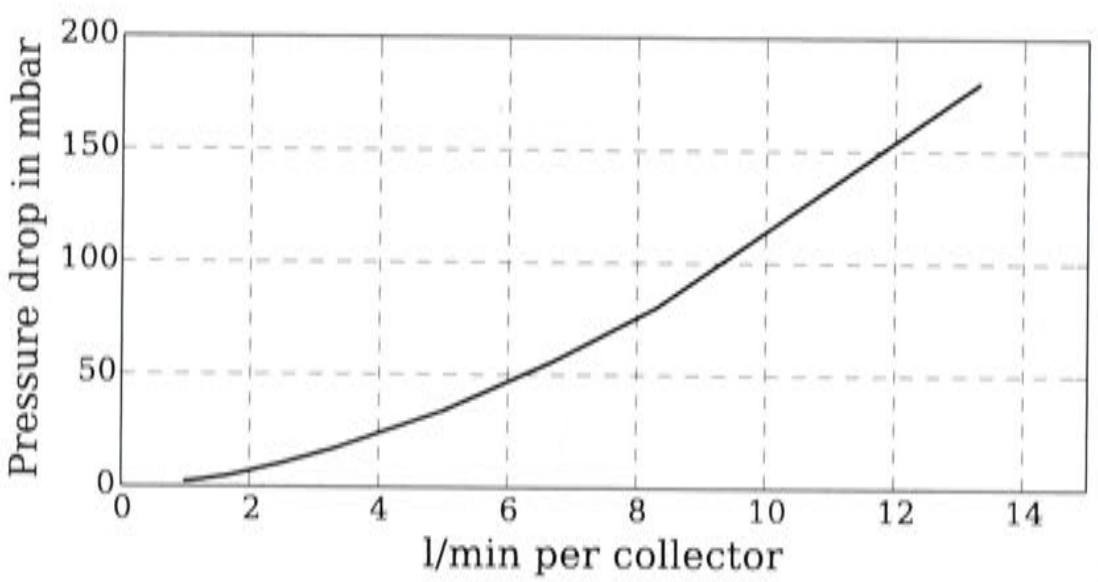

Figure 7.8: Pressure drop of Vitosol 300-T evacuated tube collectors from VIESSMANN

Additional pressure drops had to be estimated for 8 m of pipework and the copper coil heat exchanger within the tank (8 kPa). Using a pump efficiency of 40%[10], the collector pump electricity consumption could be estimated as in equation 7.40. The collector flow rate within one simulation is fixed but the power curve is needed to model different collector sizes (compare Figure 7.9).

$$\dot{E}_{el} = \frac{\Delta p \cdot \dot{V}}{\eta_{pump}} \tag{7.40}$$

In large solar thermal applications the collector mass flow rate is usually not constant, but is controlled to maintain a desired outlet temperature. This is advantageous when using the stratification of a water tank because the top part of the tank heats up faster and the chiller can start earlier.

7.5.2 The hot water buffer tank

The tank water can be used to supply solar collectors, chiller and space heating circuits. In Europe it is common that the collector fluid is an antifreeze (e.g. glycol) and water mixture to protect the water from freezing in winter. The solar loop is then a copper coil heat exchanger located in the bottom part of the tank. The solar heat exchanger and the lower heat capacity of water-glycol cause the solar fraction of the system to decrease. Furthermore, the cost for the tank increases slightly.

[10] It's the combined fluid and electrical efficiency

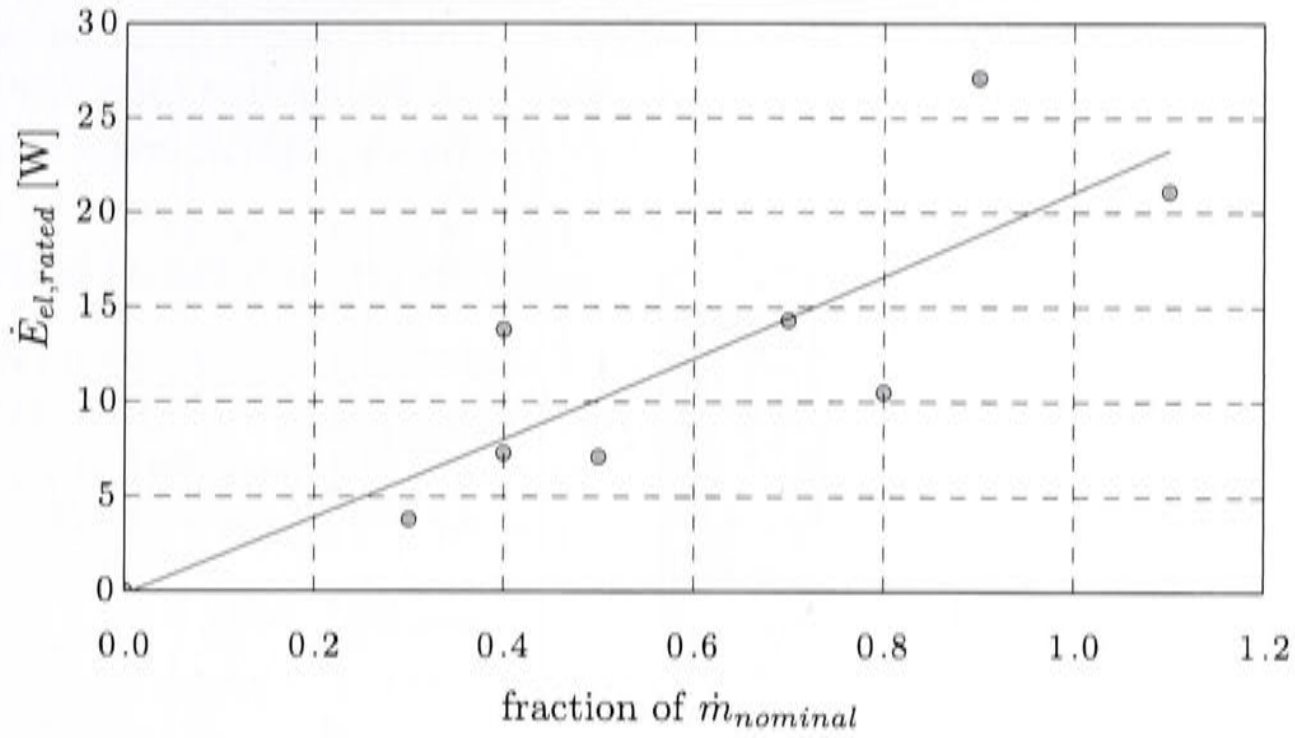

Figure 7.9: Electricity consumption of collector pump with $\dot{m}_{nominal} = 1000\,kg/s$ for various collector configurations

In the beginning of the solar thermal HVAC (and DHW) model development the European style with a solar heat exchanger in the hot water tank was chosen. However, in Australia there is no such a danger of freezing and in very cold climates like Canberra or Melbourne, a drain back system can be used for freezing protection. Hot water storage tanks are usually located outdoors.

The tank design in Figure 7.10 was chosen for the simulations. The water tank has been modeled as a vertical 1.8 m cylindrical tank. The water within the tank is used to supply the space heating and cooling system with hot water, which exits at the top of the tank (hw). The tank volume of the type 60 model is divided into 10 (custom defined) nodes. One of two modes can be chosen to connect the inlet flows. The inlet flows can either enter the tank at fixed inlet positions or they enter the tank at that node closest in temperature. The latter mode has been chosen to favor stratification in the tank. Domestic hot water is supplied via a copper coil heat exchanger which is located in the middle of the tank.

The tank was modeled in TRNSYS using an adaptation of type 60[11]. Type 60 divides the tank volume into defined node volumes and relieves heat when the nodes exceed a specified boiling temperature. In the original source code for the component, thermal heat losses from the tank and the heat relieved due to overheating were combined. In the adapted model they are separated into two independent outputs.

When the average collector temperature becomes too hot, the collectors would stagnate without transferring the excess heat to the tank or cooling devices would be installed to reject excess heat to the environment. In large scale applications it

[11]The TESS component type 534 was used in the first place due to its advantage of multiple ports and heat exchanger options. This tank model cannot solve overheating internally and a relief valve was attached to one port to cool down overheated water from the tank to a specified boiling temperature. However, this, most likely, resulted in a severe energy imbalance around the tank (up to 4000 kWh). During the process of finding the reason for the energy imbalance, tank type 60 replaced type 534 and proofed to be more stable.

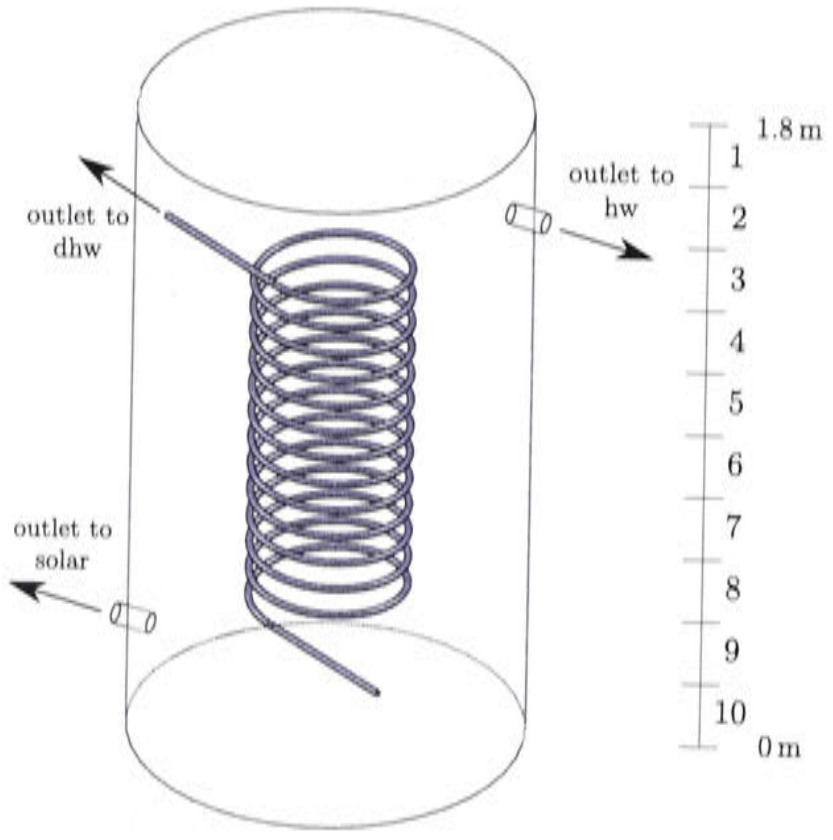

Figure 7.10: Hot storage buffer tank TRNSYS type 60, divided into 10 nodes

is common practice to prevent stagnation by reducing the collector array size in the design phase so that stagnation hardly every occurs.

In this work a sensitivity study will be carried out to compare the the solar fraction to different tank sizes and collector areas.

The coil length and surface area of the domestic hot water heat exchanger are adjusted when increasing the tank size. The tank itself has been designed in SolidWorks® to measure all necessary properties for the internal heat exchanger of the TRNSYS component type 534, which was originally used in the model. However, after switching to the TRNSYS type 60, the tank parameters were easier to calculate and did not require a geometrical model.

The heat loss from the tank has been estimated using equation 7.41 which is published by the German Institute for Standardization (DIN) [2007]. Although the surface area changes for different tank sizes, the U-value of the tank was calculated only for a $0.75\,\mathrm{m}^3$ tank[12].

$$U_{loss}\left[\frac{W}{K \cdot m^2}\right] = \frac{0.16 \cdot V_{tank}^{0.5}[\mathrm{L}]}{A_{surface}} \tag{7.41}$$

During the IEA-SHC task 25 in 2009 many existing solar thermal cooling systems (in Europe) were compared and characterized [Sparber et al., 2009]. Approximately 30% of the analyzed systems utilized evacuated tube collectors and the average tank size for those systems was $30\,\mathrm{l\,m}^{-2}$.

[12] In the Australian standard AS/NZS 4692.1 [Australian/ New Zealand Standard, 2005] performance test procedures for electric water heaters are defined, including the calculation of the standing heat loss of storage tanks using test data. However, the standard does not suggest a similar u-value for hot water tanks as in equation 7.41 for Australia.

In this work no rule of thumb has been applied to size the tank and the collector area, instead both parameters have been varied in order to investigate how the solar fractions SF_{th} and $SF_{th,dhw}$ are affected.

7.5.3 Heat losses due to piping

The collector circuit has been refined by including heat losses due to piping due to a pipelength of 8 m in the supply and return line. The heat loss value of the pipework is assumed to be $4\,W\,m^{-2}\,K$, which is rather high as the u-value of well insulated pipes is around $0.5\,W\,m^{-2}\,K$. This results in a reduced solar fraction.

Table 7.8: Diameter of pipes for various collector sizes

			$0.70\,m\,s^{-1}$	$0.40\,m\,s^{-1}$	
collectors #	A_{coll} m^2	$\dot{V}_{coll}$ $l\,h^{-1}$	diameter mm	diameter mm	DN
3	**9**	270	11.7	15.5	**13**
4	**12**	360	13.5	17.8	**16**
5	15	450	15.1	19.9	**16**
6	**18**	540	16.5	21.9	**20**
7	21	630	17.8	23.6	**20**
8	**24**	720	19.1	25.2	**25**
9	27	810	20.2	26.8	**25**
10	30	900	21.3	28.2	**25**
11	**33**	990	22.4	29.6	**32**

The pipe diameters in Table 7.8 were calculated with a flow rate of $30\,l\,m^{-2}$ of collector area and a velocity between $0.4\,m\,s^{-1}$ and $0.7\,m\,s^{-1}$ as recommended by VIESSMANN [2008].

7.6 Auxiliary equipment: pumps and fans

The **indoor fan** power consumption for each zone was determined from online data for fan coil units SYSDUCT 21 and 22 [Systemair, 2013]. In a water system, 7°C (or 11°C) chilled water is pumped to each zone to supply the fan coils. To find the appropriate fan coil capacity, a statistical distribution revealed that between 200 and $600\,kg\,h^{-1}$ of air flow can be expected for each climate and zone for heating and cooling. The data has been previously modeled using the variable flow equations in section 7.3. Using the affinity laws the power consumption of different air flows can be estimated. Figure 7.11 shows the electricity consumption of two possible fan choices for each zone.

The pressure drop for the pump power calculation of the chilled water pump includes the pressure drop over those fan coils as in Table 7.9.

There are **three external pumps** connected to the chiller and their electricity consumption depends on the pressure drop of the pipework, the heat exchanger within the chiller and the cooling and heating coil. For pressure drop calculation of the

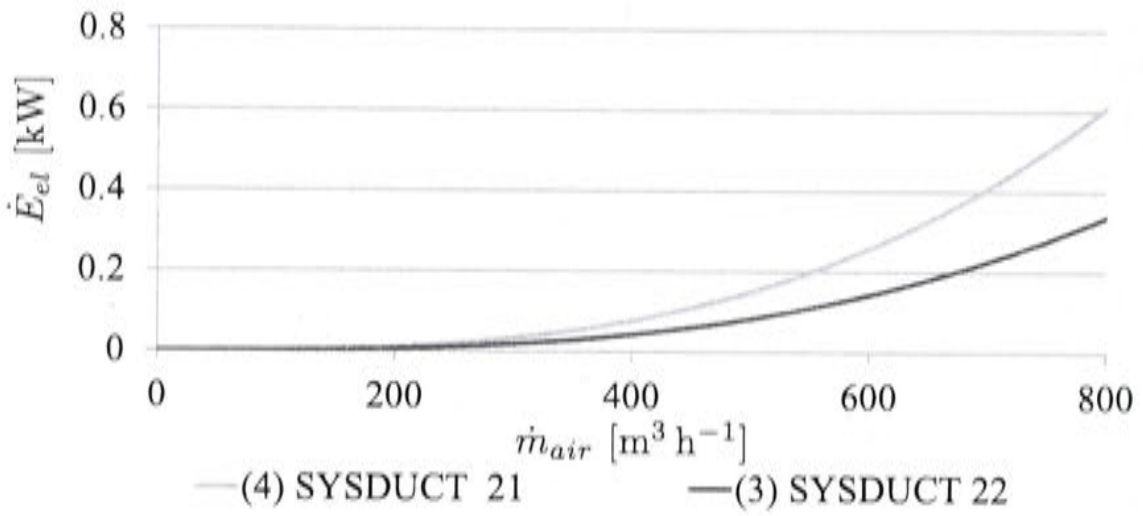

Figure 7.11: Electricity consumption of room fans

pipework of the cooling water loop, the collector loop and the heat supply loop for cooling, 8 m have been estimated. For the chilled water supply loop to the coil fan units and for the heat supply loop for heating, 20 m have been estimated.

Since the chiller is scaled to accommodate different cooling load sizes, the volumetric flow rates of the three external circuits and pressure drops have to be scaled as well. Since $\dot{Q} \propto \dot{m}$ the external flow rates are scaled with the *scalefactor*. It is important to understand that the flow rates stay constant during one simulation for a certain chiller sizes.

On the system (demand) curve of a hydraulic system the pressure drop is proportional to the flow velocity squared ($\Delta p \propto v^2$) when changing the flow rates and keeping the diameters of the pipes constant. The flow velocity can be calculated with $v = \dot{V}/A_{pipe}$ using the cross sectional pipe area A_{pipe}.

However, when scaling the chiller and its external mass flow rates, the pipe diameters (flange diameter given by manufacturer) should be scaled as well to keep the velocity within the pipe constant, here at approximately $1\,\mathrm{m\,s^{-1}}$. This would also keep the pressure drop constant. Equation 7.42 calculates the appropriate pipe diameter.

$$d_2 = d_1 \cdot \sqrt{scalefactor} \tag{7.42}$$

Standard DN pipe diameters (12, 15, 25 etc.) were used and therefore, the velocity deviates from $1\,\mathrm{m\,s^{-1}}$ by up to 10%. The pressure drops vary accordingly with equation 7.43.

$$\frac{\Delta p_1}{\Delta p_2} = \left(\frac{\frac{\dot{V}_1}{d_1^2}}{\frac{\dot{V}_2}{d_2^2}} \right)^2 \tag{7.43}$$

The pressure drops and pipe diameters were calculated for the *scalefactors* 0%, 20%, 30% and 100% of $\dot{Q}_{E,rated}$ and a curve has been fitted for the electricity consumption of each external pump. Table 7.9 shows the pressure drops at full capacity

with $scalefactor = 1$. Using a pump efficiency of 50%[13] the electricity demand can be calculated using equation 7.40 as in Figure 7.12. If exact pipe diameters were used as suggested by equation 7.42 the electricity demand would change linearly with the $scalefactor$.

Table 7.9: Pressure drops of the chiller's external pump circuits at rated flow rates (rounded). cw: cooling water, chw: chilled water, hw: hot water

	cw	chw	hw (cooling)	hw (heating)
Water volumetric flow rate [$m^3\,h^{-1}$]	5	1.9	2	2
Flange (and pipe) diameter [DN]	40	25	25	25
Pressure drop in chiller [kPa]	90	40	40	-
Pressure drop cooling coils [kPa]	-	15	-	-
Pressure drop heating coils [kPa]	-	-	-	15
Pressure drop pipe work [kPa]	3 (8 m)	14 (20 m)	4 (8 m)	13 (20 m)
Total pressure drop [kPa]	**93**	**69**	**44**	**28**

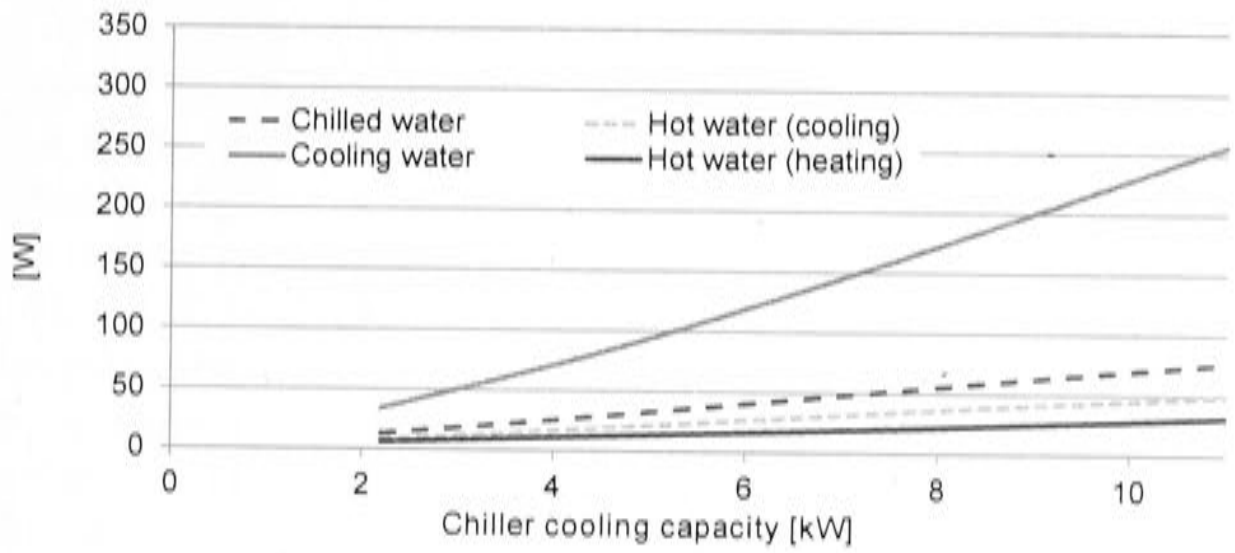

Figure 7.12: Pump power estimation of external pumps for different chiller capacities

7.7 Conclusion

This chapter revealed that the development of an absorption chiller solar thermal cooling, heating and DHW model presented a major body of this work. This is comparable to a real installation. There are no quick design solutions available using absorption chillers in Australia.

The requirement for a larger heat rejection unit, a heavy absorption chiller and a chilled water distribution system increase the complexity of the system dramatically compared to the installation of reverse cycle air-conditioners. Nevertheless, a large collector area is available which can provide heating in winter and domestic hot water.

[13] It's the combined fluid and electrical efficiency

For large scale commercial installations a high degree of complexity for the design is common also for the conventional technology using electric compression chillers. However, for residential applications this is not required. The following chapter will show the economic, environmental and human comfort aspects of the thermal solar system performance and a sensitivity study will be carried out for evaluation and further investigation of system parameters.

Chapter 8

Discussion of the solar thermal cooling, heating and DHW simulation results and sensitivity study

In this chapter the simulation results of the residential absorption chiller system are discussed. As the model claims to be representative for a typical residential solar thermal cooling and heating system, various system parameters are changed to analyze the effects on the results.

Since the HVAC (and DHW) system modeled in this work is not based on a real installation many parameters could undergo a sensitivity study. It became important to reduce the scope of this work to identify the most critical parameters and vary them in order to analyze its effect on either greenhouse gas emissions, cost, comfort or a combination of those factors.

After a comprehensive analyzes of the output covering all different tank sizes, collector sizes and climates, a sensitivity study will follow with only one collector area and tank size. The collector-tank configuration will be chosen so that the SF_{th} is at least 60%.

The outcome of the study is rather disheartening for solar thermal cooling, using absorption chillers. The specific cost is very high for all cases and only the inclusion of domestic hot water reduces it sufficiently to approach the specific cost of the reference system.

8.1 Discussion of the base case results

The simulation of the base case was performed for five different hot water tank volumes and collector areas to gain a performance map for each of the seven climates. This means that merely from the base case a data volume of 175 data sets were generated.

The energy supplied to the building in the form of cooling, heating and DHW is

not expected to vary much for the different collector and tank sizes, since the system necessarily has a gas back up if solar energy is not sufficient. This leads to the fact that the comfort throughout the different tank and collector sizes is also rather constant.

8.1.1 Solar fraction for various collector and tank sizes

Figure 8.1 shows the different solar fractions SF_{th} for cooling and heating for various collector and tank sizes and each climate. When plotting the solar fraction $SF_{th,dhw}$ (Figure 8.2), which includes the generation of domestic hot water, the difference between the tank sizes becomes less relevant and the solar fractions are higher.

The desired water temperature for the chiller lays between 59°C and 96°C. The tank relieves heat if the tank temperature is above 120°C. The tank needs to be relatively large to provide the desired temperature for a long period of time. It can be seen from the results that a large tank doesn't necessarily lead to a large solar fraction even though less heat is discarded through the valve. Once the auxiliary heater has switched on, due to the top of the tank being unable to supply the desired hot water temperature for the chiller, it will only switch off again when the middle of the tank has reached the desired hot water temperature. This control strategy is based on the assumption of a well stratified tank.

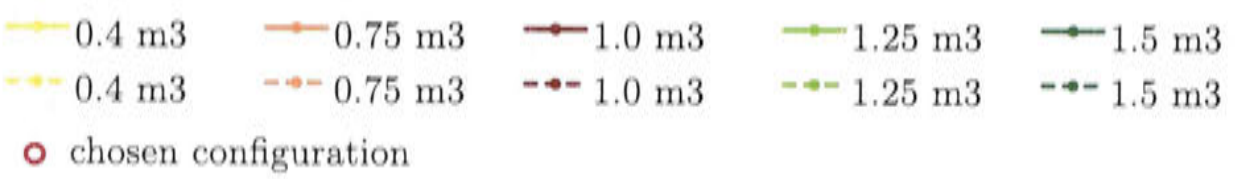

(a) legend

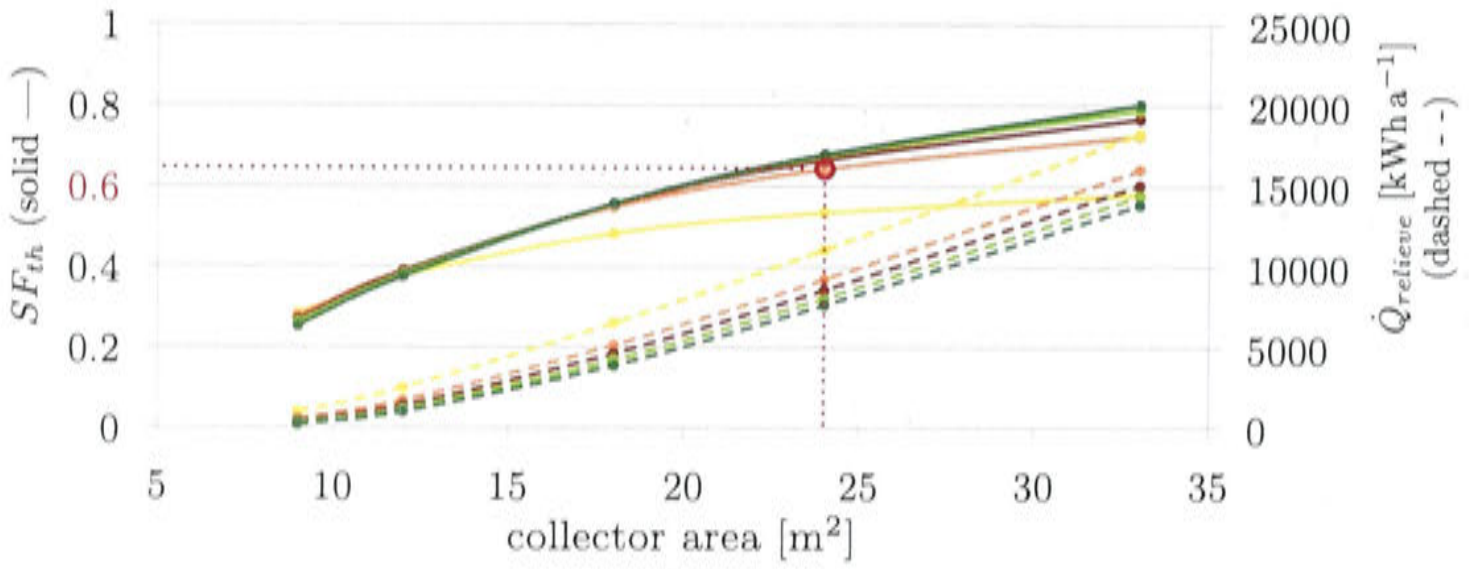

(b) Canberra

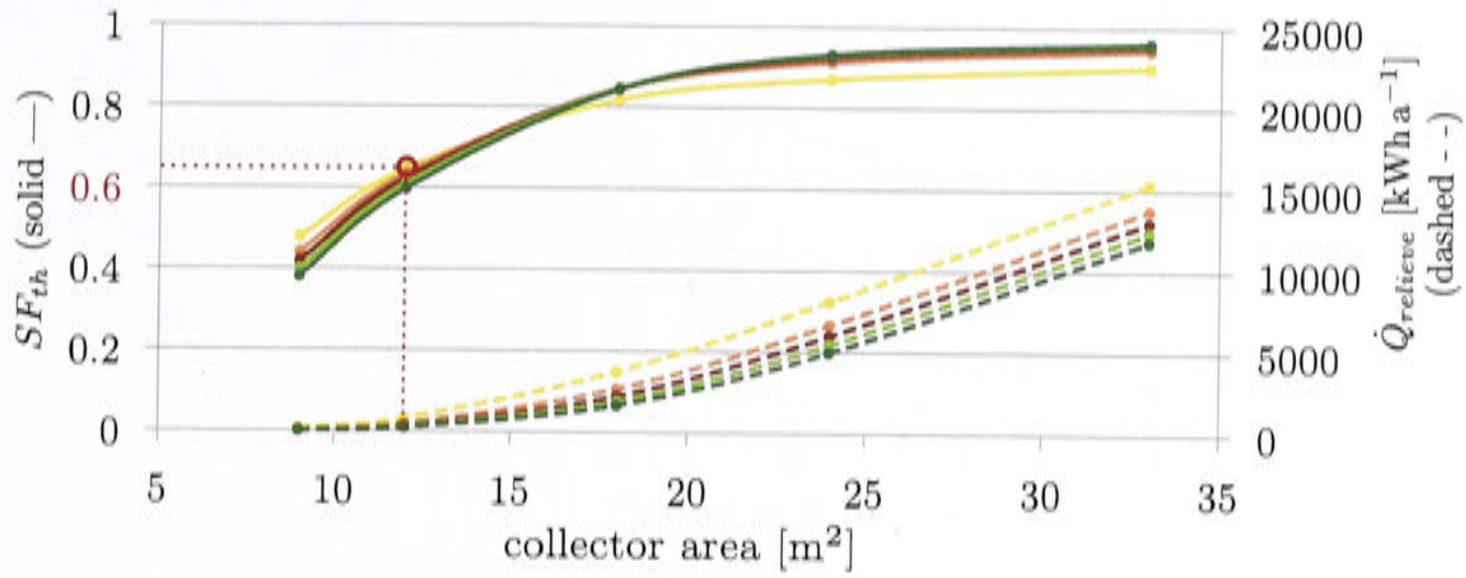

(c) Brisbane

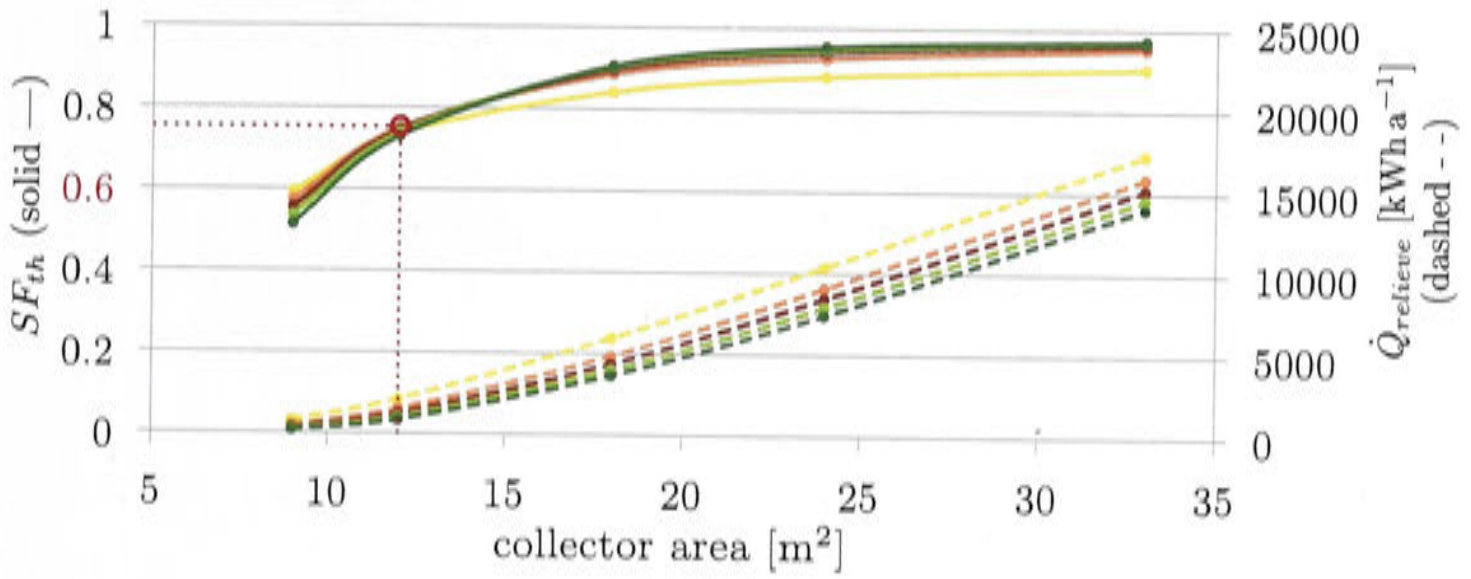

(d) Sydney

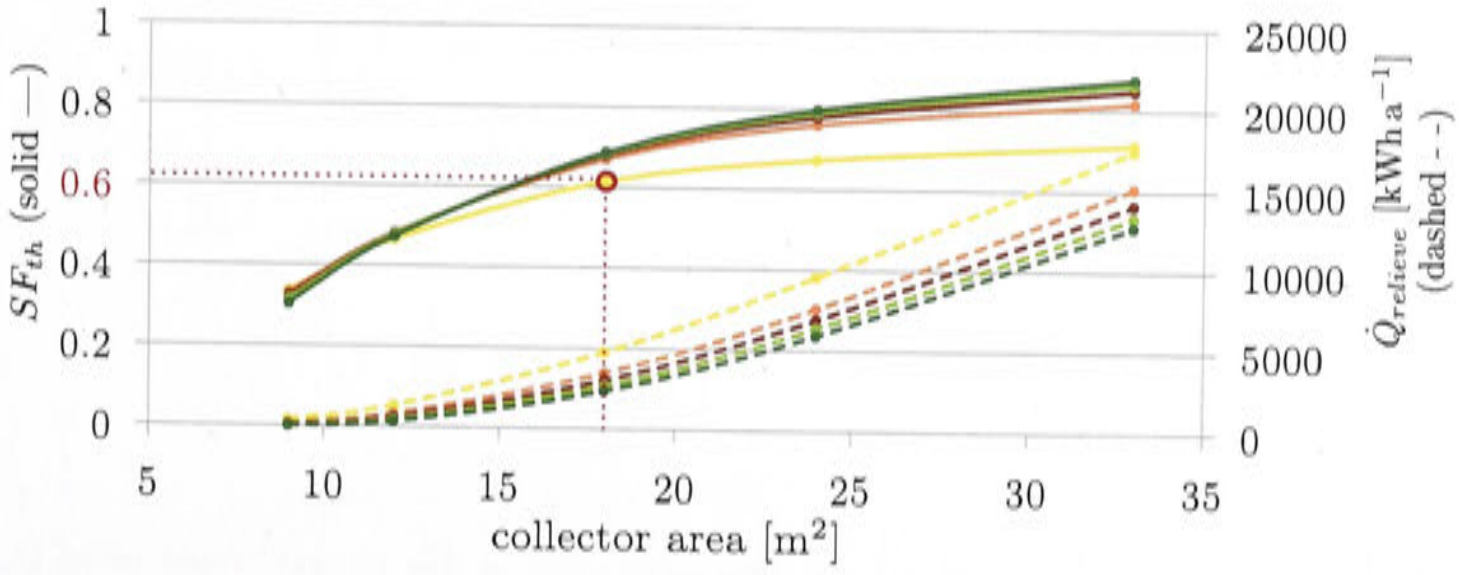

(e) Griffith

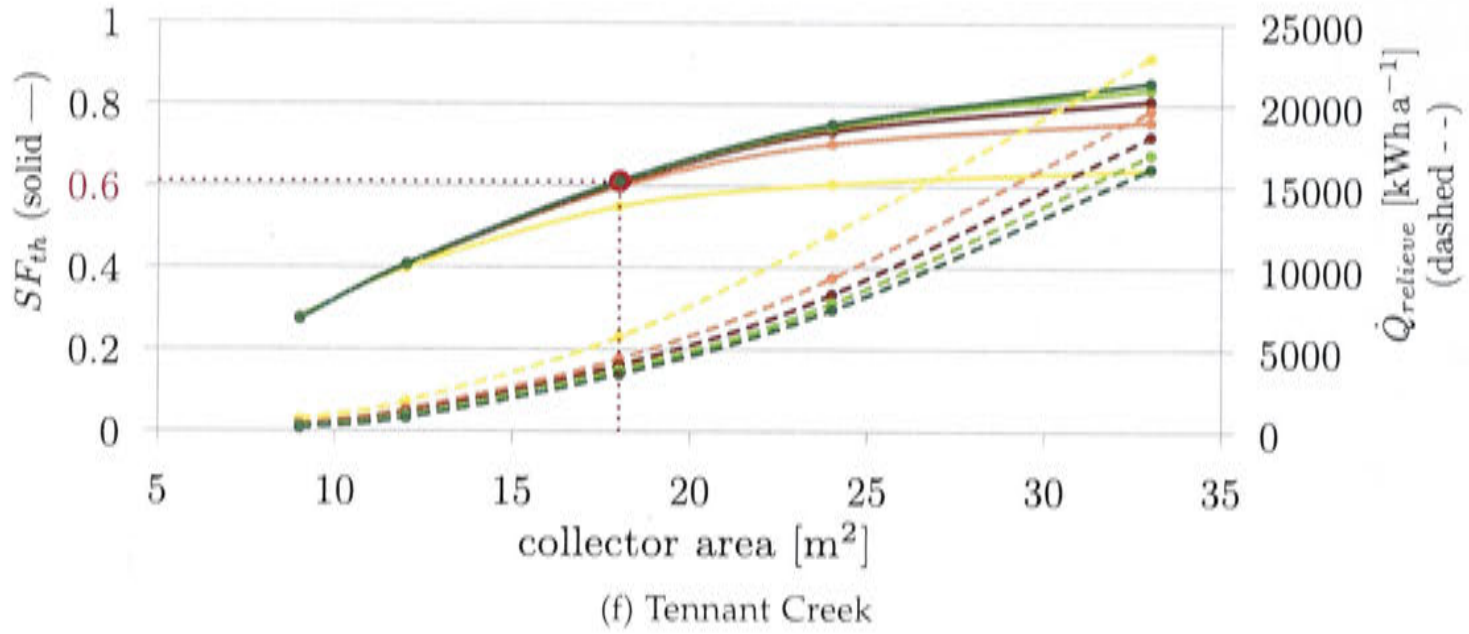

(f) Tennant Creek

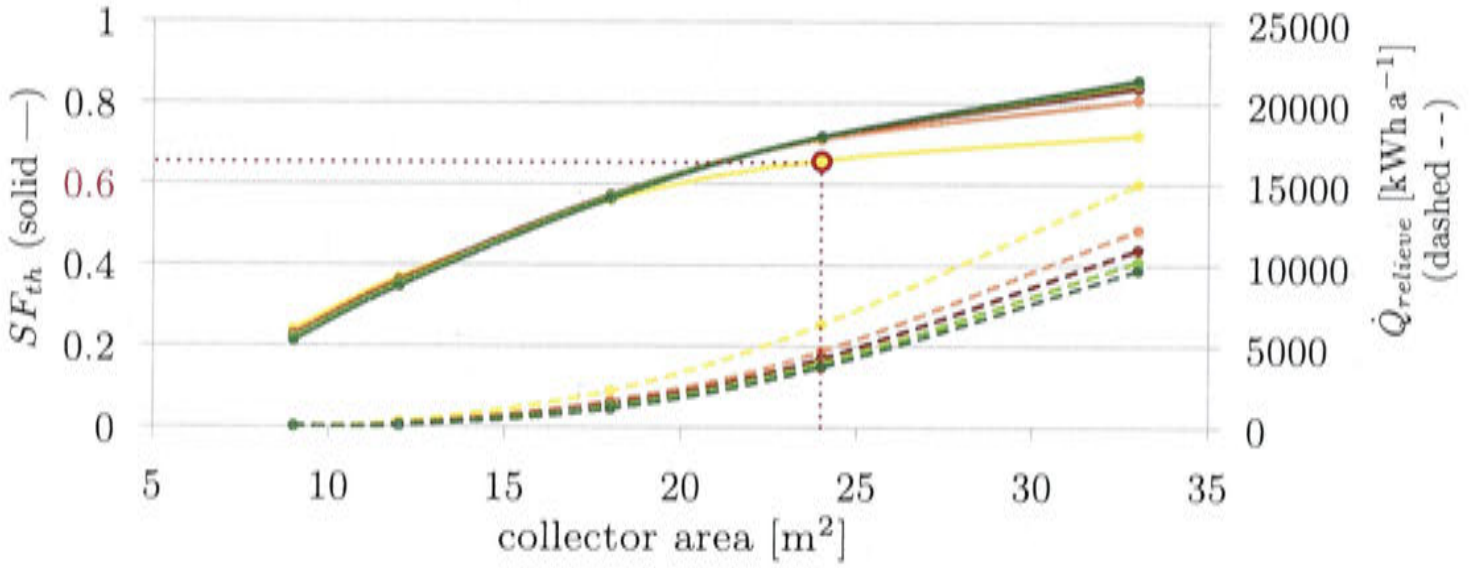

(g) Darwin

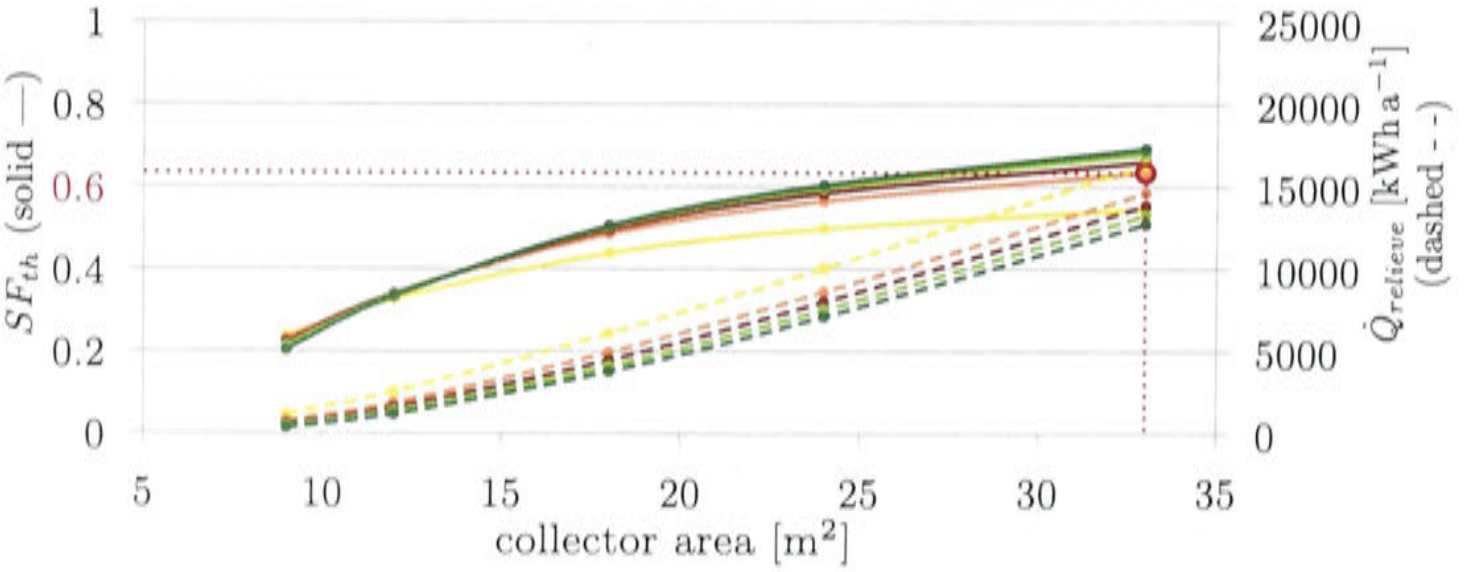

(h) Melbourne

Figure 8.1: Solar fraction SF_{th} (solid —) and heat discharged by the pressure relief valve $\dot{Q}_{relieve}$ (dashed - -).

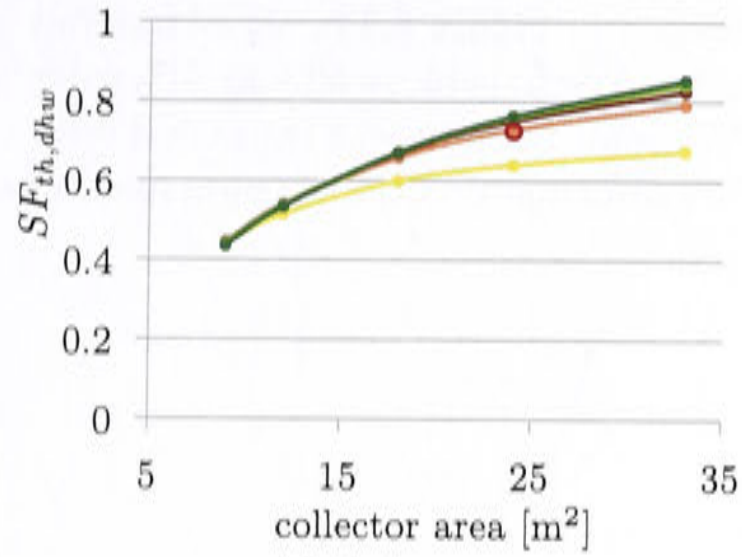

(a) Canberra

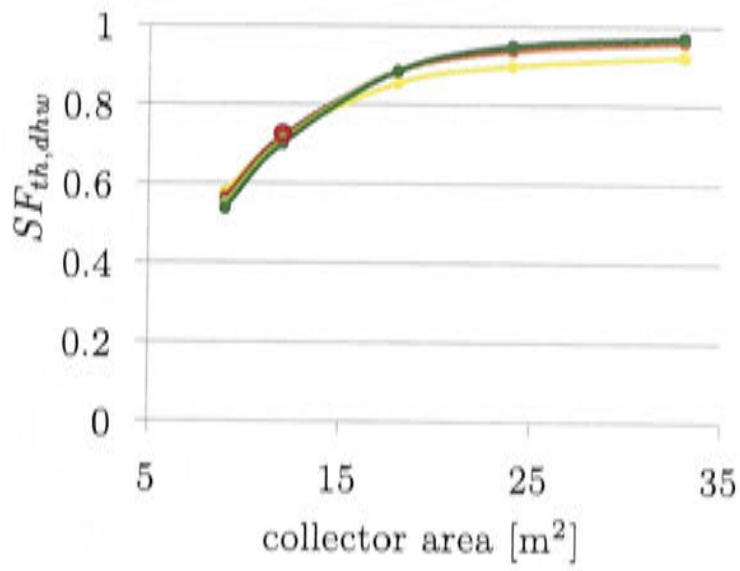

(b) Brisbane

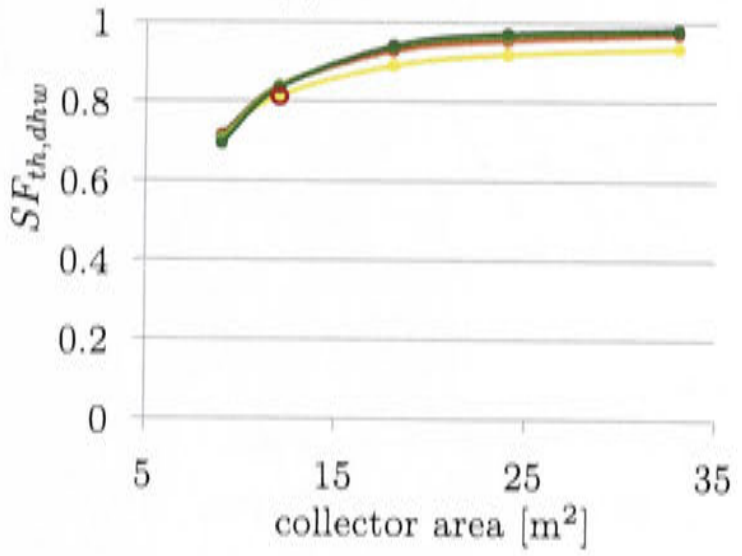

(c) Sydney

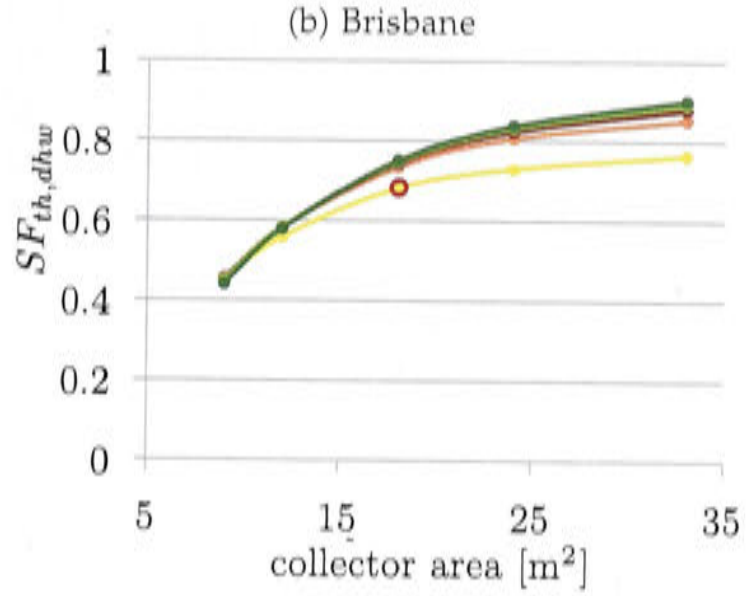

(d) Griffith

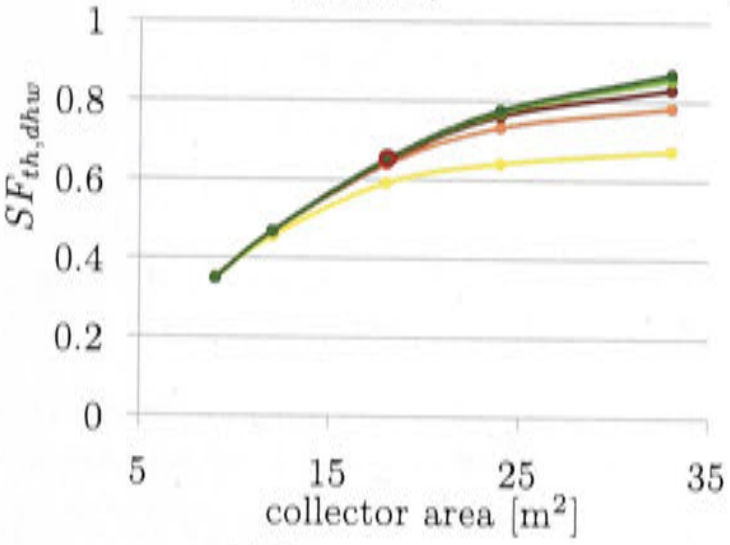

(e) Tennant Creek

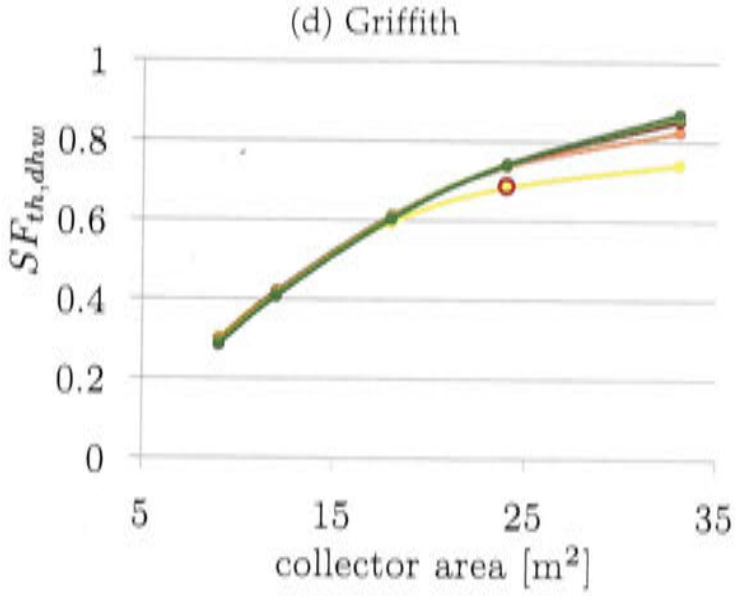

(f) Darwin

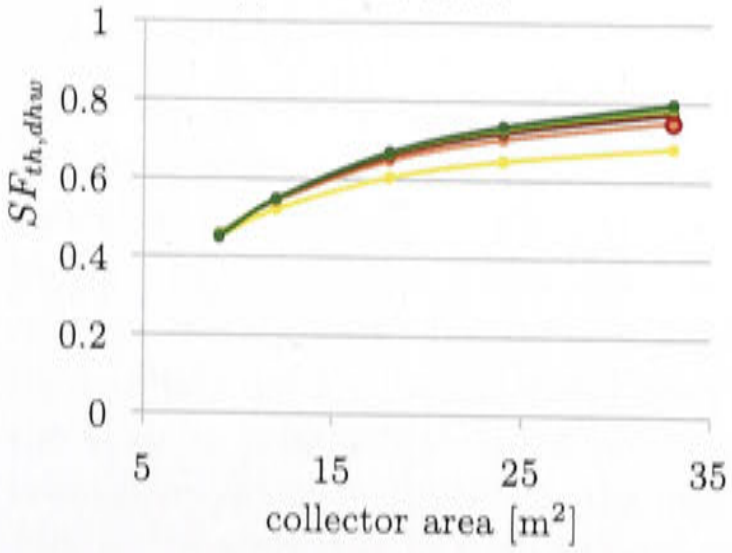

(g) Melbourne

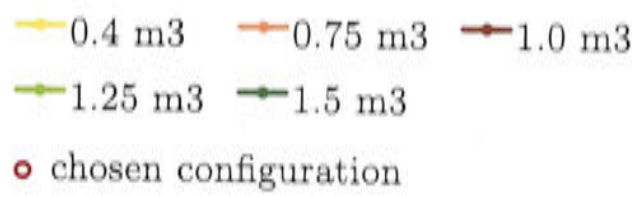

(h) legend

Figure 8.2: Total solar fraction $SF_{th,dhw}$ including DHW.

The curves from Figure 8.1 have been rearranged in Figure 8.3 to show in what range the required collector size in each climate has to be to achieve 60% to 70% solar fraction. The collector area for exact 60% and 70% solar fraction was estimated with a third degree polynomial. In Appendix D.4 more information on the 7 climates can be found.

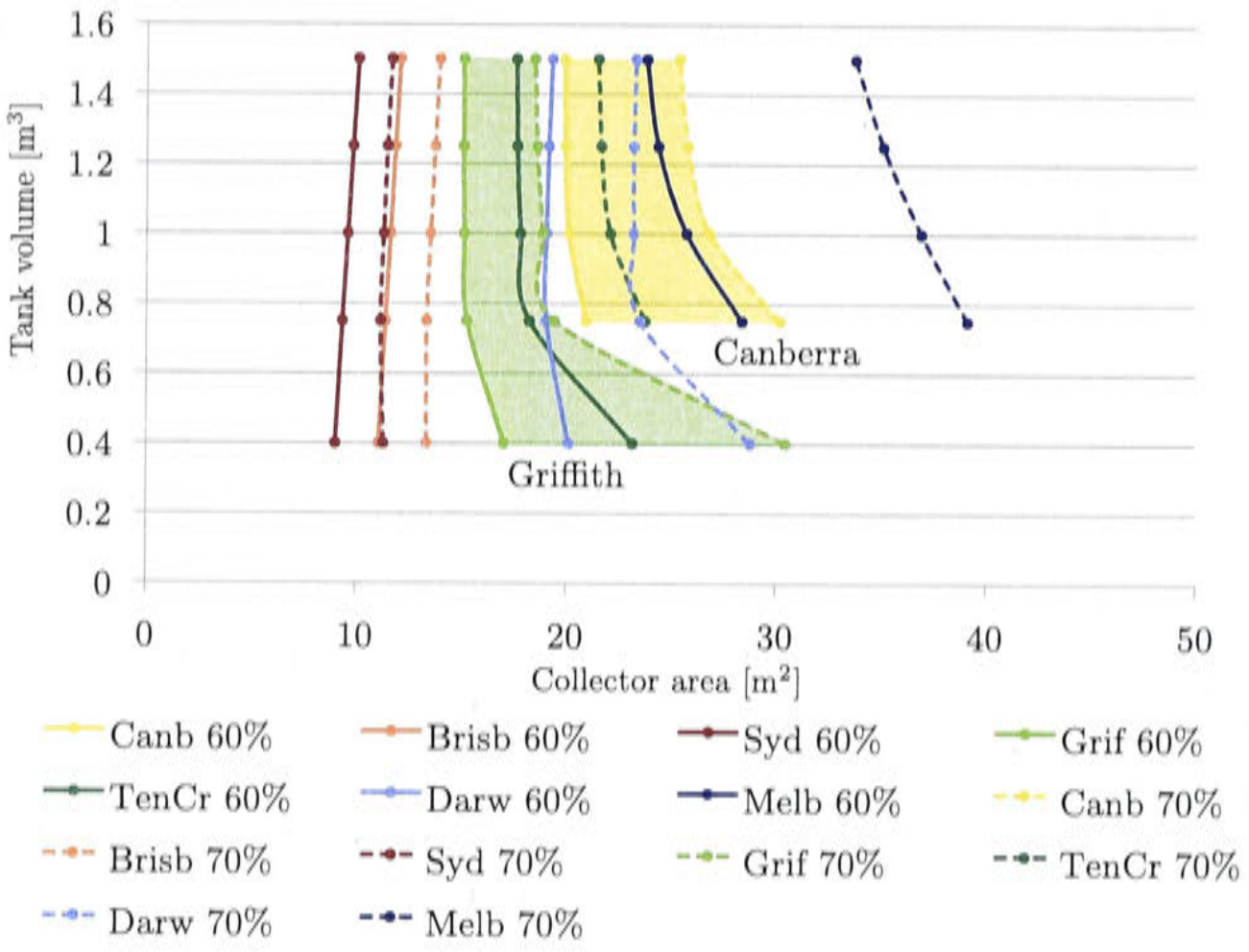

Figure 8.3: Collector area vs. hot water storage size to achieve SF_{th} of 60% and 70%. Two climates have been shaded to simplify the understanding of the chart.

8.1.2 Solar fraction vs. specific greenhouse gas emissions

The following graphs show the solar fraction compared to the greenhouse gas emissions. Only the tank size of the chosen configuration for each climate is presented here, with varying collector area. In Appendix D.5 are three tanks compared for each climate, but the tank size does not influence the greenhouse gas emissions significantly. The greenhouse gas emissions of the reference system represent the average of each climate zone weighted by the population density as explained in previous sections.

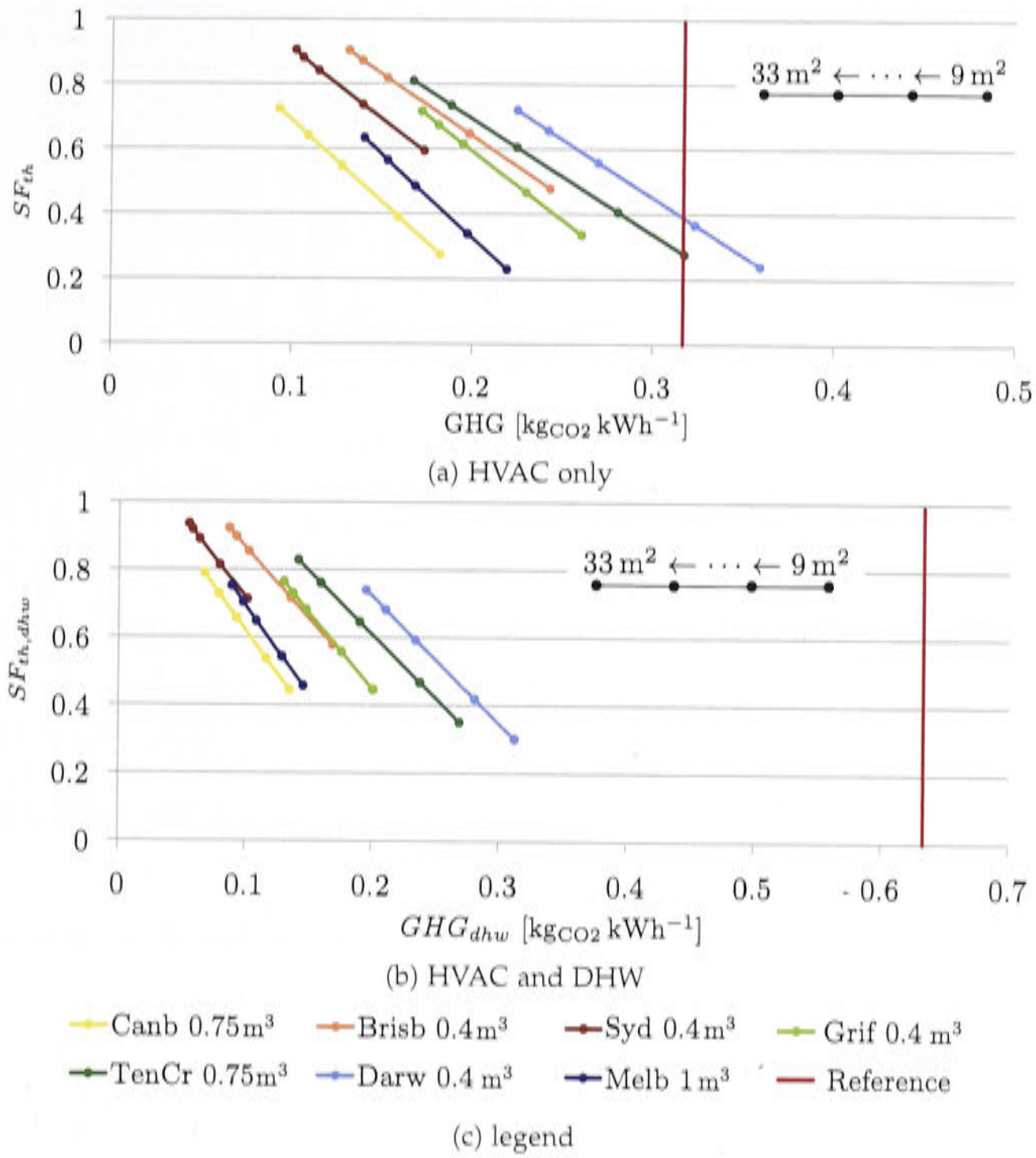

(a) HVAC only

(b) HVAC and DHW

(c) legend

Figure 8.4: Solar fraction ($SF_{th(,dhw)}$) versus greenhouse gas emissions for all climates, all collector sizes, but only one tank size.

8.1.3 Solar fraction vs. specific cost

The cost assumptions for the solar thermal HVAC (and DHW) system are summarized in Table 8.1.

The cost for the small scale chiller is more than 3 times the cost of a reverse cycle air-conditioner and it includes freight charges as small scale chillers have to be imported from either Europe or Asia. The cost for the structure of the solar thermal collectors is included in its specific cost. The proportion for auxiliary equipment (e.g. pumps, pipes, cooling tower, back up etc.) has been set to 35% of the total capital cost for the equipment. The cost for installation and design has been set to 20% of the capital cost for the system, because more plumbing work is necessary to install the system. The initial investment therefore will be noticeably higher than for the reference system in Table 5.3. The annual cost for maintenance has been increased to \$300 a^{-1} mainly due to the wet cooling tower.

In Table 8.2 the electricity break even price has been calculated at which residen-

Table 8.1: Cost assumptions for the solar thermal cooling, heating and DHW system.

Solar thermal	Abbreviation	Cost	Unit
Absorption chiller (small scale)	$I_{chiller}$	2000	$\$\,kW^{-1}$
Hot water tank	I_t	3	\$/l
Evacuated tube collectors	I_{coll}	250	$\$/m^2$
	$I_{eq} = I_{chiller} + I_t + I_{coll}$		
Auxiliary equipment $I_{sys} = \frac{I_{eq}}{1-q_{aux}}$	q_{aux}	0.35	-
Planning and installation $I_0 = \frac{I_{sys}}{1-q_{PInst}}$	q_{PInst}	0.2	-
Maintenance	$maint$	300	$\$\,a^{-1}$
Fix gas price	$p_{gas,fix}$	250	$\$\,a^{-1}$
Fix water price	$p_{water,fix}$	100	$\$\,a^{-1}$
Fix electricity price	$p_{el,fix}$	300	$\$\,a^{-1}$
Variable gas price (here 2.5ct/MJ)	$p_{gas,var}$	0.007	$\$\,kWh^{-1}$
Variable water price	$p_{water,var}$	3	$\$\,m^{-3}$
Variable electricity price	$p_{el,var}$	0.3	$\$\,kWh^{-1}$
Lifetime	N	20	a
Interest	i	0.06	-

tial solar thermal cooling becomes cost effective in each climate. The electricity prices are very high when excluding DHW.

Table 8.2: Break even electricity price $p_{el,BE}$ in $\$\,kWh^{-1}$ at which solar thermal cooling becomes cost effective (equation 4.26).

	Canb	Brisb	Syd	Grif	TenCr	Darw	Melb
$p_{el,BE}$	0.65	1.40	1.41	1.09	0.89	1.72	1.08
$p_{el,BE}$ (incl. DHW)	0.26	0.36	0.29	0.38	0.43	0.60	0.32

In a study by Kohlenbach and Dennis [2010] the break even electricity price for absorption cooling systems was calculated to be $\$0.55\,kWh^{-1}$. That calculation was performed for a large scale 230 kW chiller and no space heating or DHW was considered. The investment cost for the chiller was $\$650\,kW^{-1}$, which is typical for large scale chillers. When replacing the chiller's low investment cost into this estimation, the break even electricity price for solar thermal cooling is approximately 45% lower in all climates besides the cold climates of Melbourne and Canberra, where it is approximately 30% lower. It has to be understood that the break even calculation in equation 4.27 and 4.29 do not reflect the cost of the supplied energies for cooling, heating or DHW. In these equations the reference and the solar thermal system are compared on a cost basis even though the supplied useful energy deviates slightly.

The calculated specific cost ($c_{m(,dhw)}$) on the other hand is related to the amount of useful energy supplied to the building. Figure 8.5 shows the specific cost for the different collector sizes in regards to the solar fraction. The reference cost is calculated in the same manner as the reference greenhouse gas emission using the population density of each climate zone. The figures and Table 8.2 show that the system must include the production of domestic hot water to increase cost competitiveness with

the conventional technology.

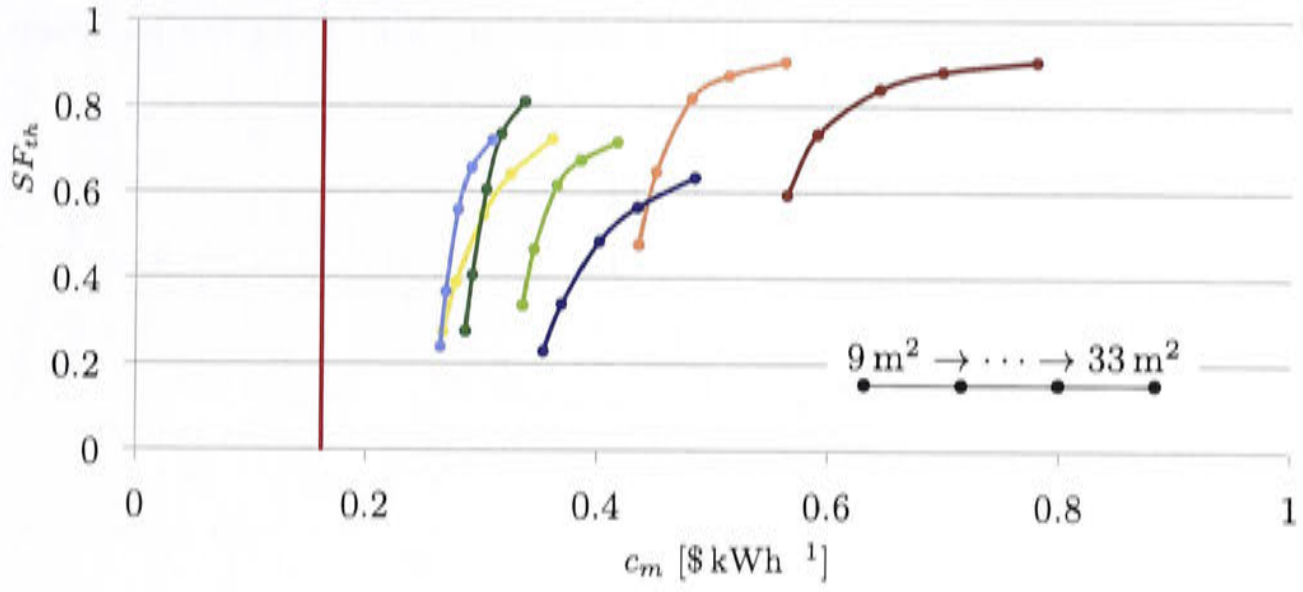

(a) HVAC only

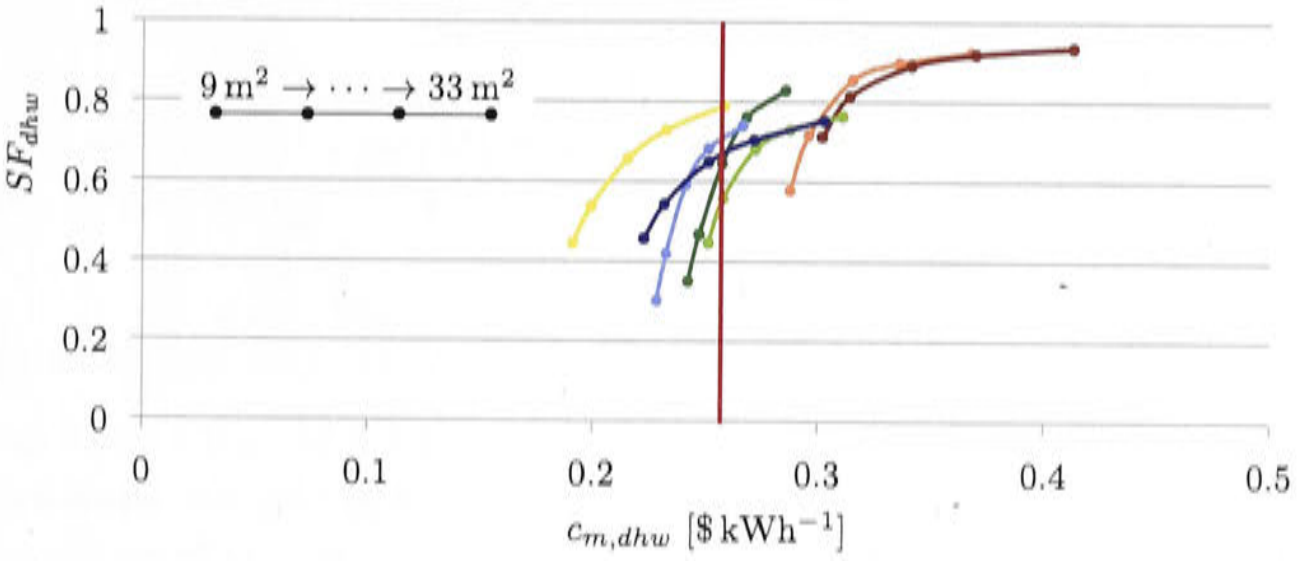

(b) HVAC and DHW

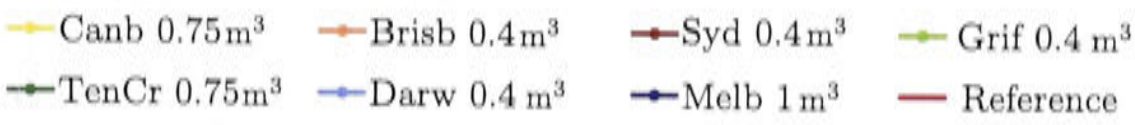

(c) legend

Figure 8.5: Solar fraction ($SF_{th(,dhw)}$) versus specific cost for all climates, all collector sizes, but only one tank size.

8.1.4 Greenhouse gas emissions and specific cost

In Figure 8.6, the greenhouse gas emissions reduction are compared to the difference in specific cost, which represents the marginal cost to save additional greenhouse gas emissions. The shaded area represents the range of cost savings and greenhouse gas emissions reduction of the PV system as in section 6 (without battery). Further on the left of the shaded area are the systems with a full feed-in tariff $frac_{PV} = 1$ and further at the right are system with a small feed-in tariff of $frac_{PV} = 0.3$. With a larger PV array it is possible to increase the greenhouse gas savings at almost constant specific

costs (Figure 6.15). Including domestic hot water increases the cost competitiveness with PV and the reference system, especially in the colder climates. However, no cost savings can be achieved at the current electricity and gas prices chosen for the comparison.

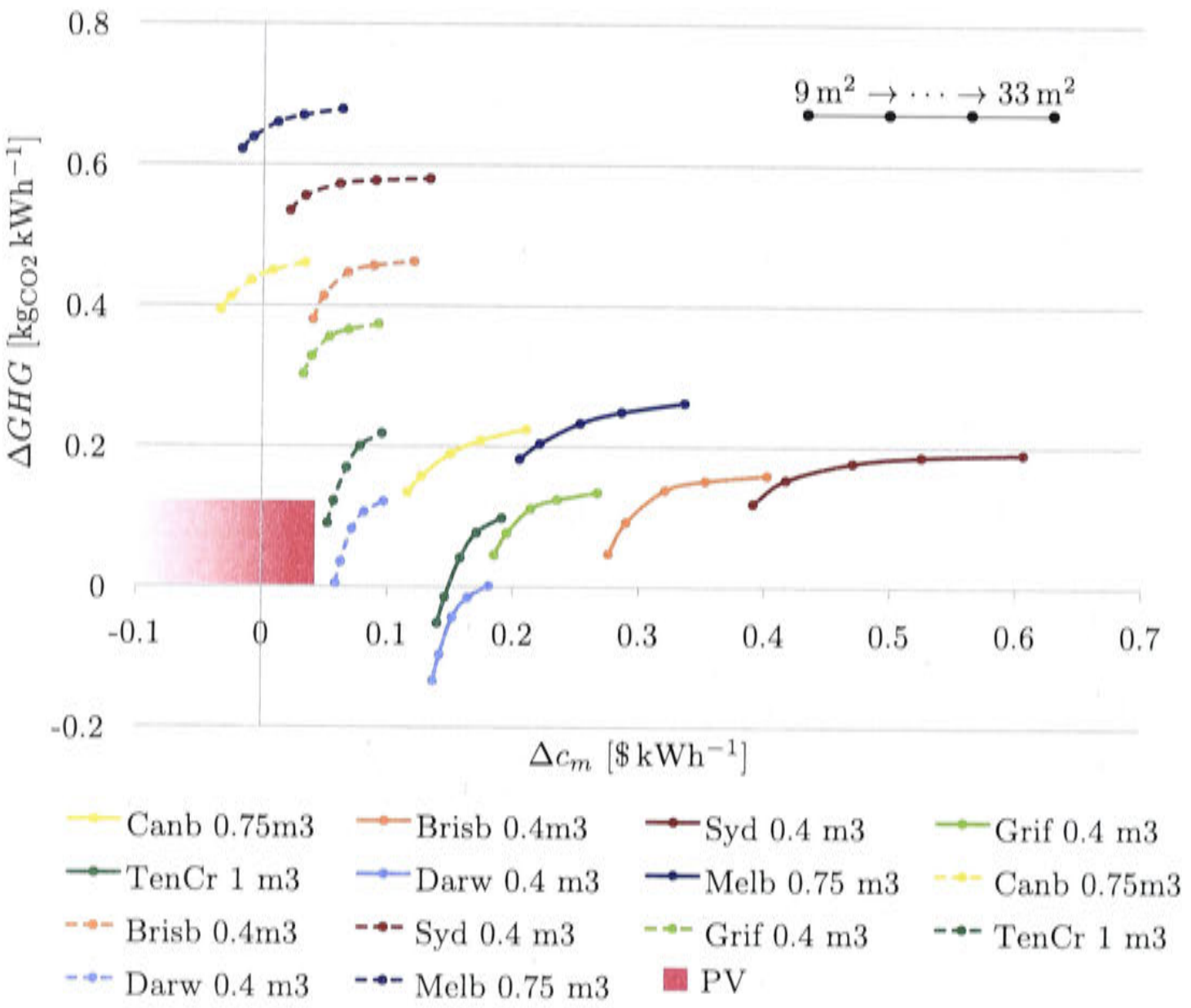

Figure 8.6: The marginal cost to save one extra $kg_{CO2\text{-}eq}$. The shaded area represents the analysis of a PV system in section 6 ($\Delta GHG = GHG_{ref} - GHG$, $\Delta c_m = c_m - c_{m,ref}$).

Figure 8.7 represents the specific cost and the greenhouse gas emissions for the chosen tank size in each climate and for all collector sizes.

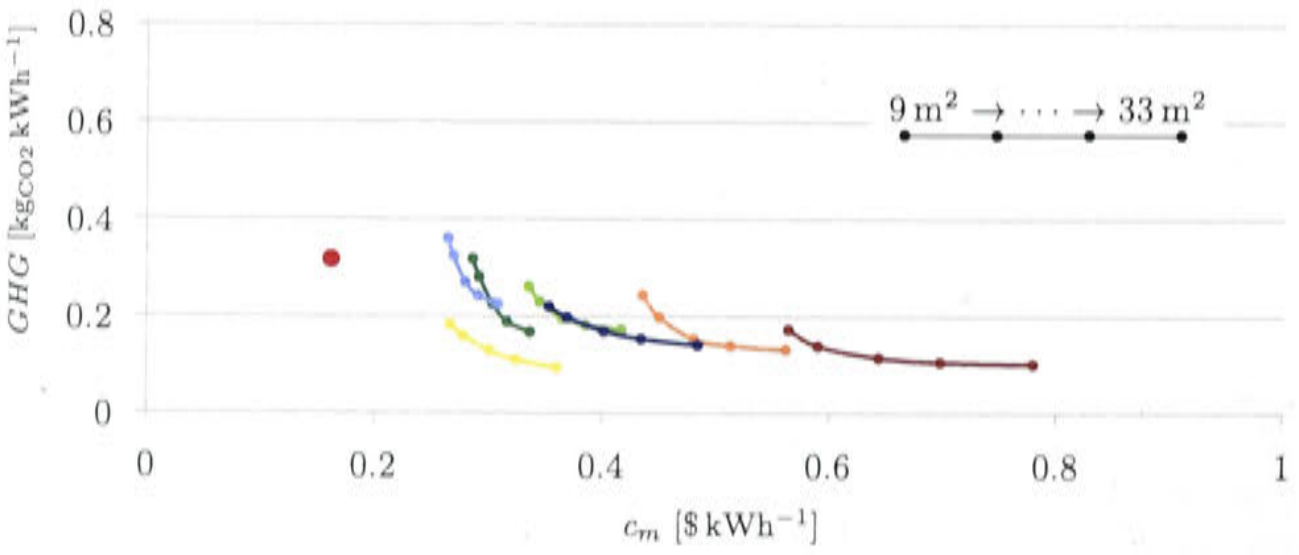

(a) HVAC only

The positive effect on the levelized cost of energy when including DHW is visible.

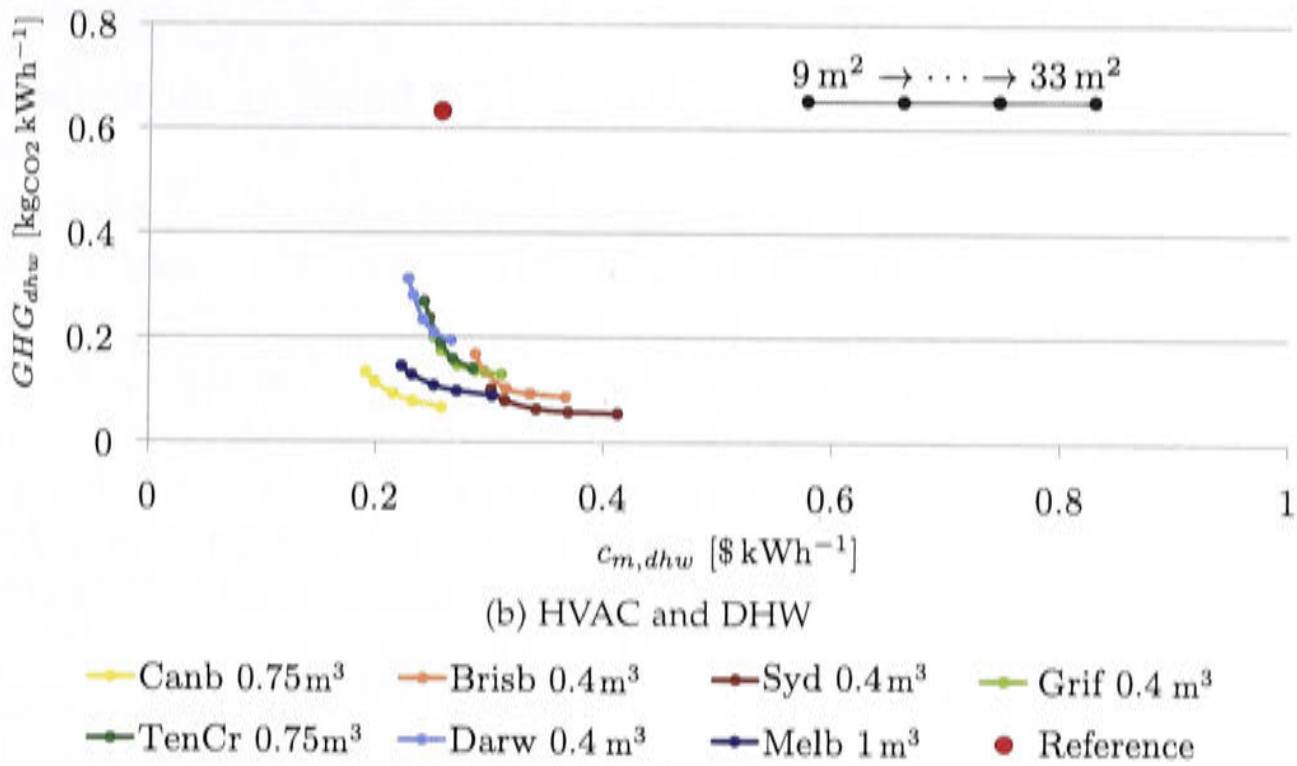

(b) HVAC and DHW

(c) legend

Figure 8.7: Specific greenhouse gas emissions vs. specific cost for all climates, all collector sizes, but only one tank size.

8.1.5 The chosen solar thermal configuration

In order to reduce the scope of work and to provide a base for a sensitivity analysis for each climate one collector and tank configuration was chosen, which provided a solar fraction (SF_{th}) of at least 60%. The configurations have been circled red in Figure 8.1 and are outlined in Table 8.3.

Table 8.3: Chosen configuration for the following sensitivity study.

	coll. area [m^2]	tank vol. [m^3]	spec. coll. area (cooling) [$m^2\,kW^{-1}_{cooling}$]	spec. coll. area (heating) [$m^2\,kW^{-1}_{heating}$]	spec. tank vol. per coll. area [$l\,m^{-2}$]
Canb	24	0.75	7.0	3.7	31.3
Brisb	12	0.4	2.3	6.7	33.3
Syd	12	0.4	3.3	5.0	33.3
Grif	18	0.4	2.7	4.1	22.2
TenCr	18	1	2.5	N/A	55.6
Darw	24	0.4	3.2	N/A	16.7
Melb	33	0.75	10.3	7.3	22.7

The annual cooling and heating load of the building in the base case scenario is defined by the quantity of energy transferred over the cooling and heating coils to the conditioned space or are extracted from the hot water tank by the domestic hot water heat exchanger. Table 8.4 gives an overview of the load in each climate.

The deviation from the reference case in section 5.2 can be found in Table 8.5. The difference in Canberra and Melbourne is rather large. However, the performance pa-

rameters in this work are specific, relating the energy consumption to the amount of cooling or heating generated. In this way the performance parameters are normalized.

Table 8.6 provides the numbers on the comfort conditions for the temperature in summer and winter and for the humidity.

Throughout the different collector and tank configurations the cooling and heating (and DHW) energies provided should not vary much. The standard deviation was calculated and can be found in Appendix D.3.

It is noticeable that there is a rather large discrepancy in the heating supply, which is also visible in the comfort discomfort factor for winter ($comf_T$ (winter)). The auxiliary capacity of the absorption chiller system is set to the maximum of either heating capacity C_h or the absorption chiller's rated heat demand C_c/COP_{rated}. To lower the winter discomfort the heating capacity was already increased by 1 kW in Canberra and Melbourne.

On the contrary, in the reference system the heat pumps are sized for each zone and the reference system has a supplementary heater, which can be sized up to 2 kW extra in the cooler climates. It switches on in the 3rd stage heating together with the 2nd stage, increasing the heating supply compared to the absorption chiller system. This is the reason why more heating is provided in the reference case.

Table 8.4: Cooling, heating and DHW energy supplied to the building (base case).

	Q_c [kWh a^{-1}]	latent [%]	Q_h [kWh a^{-1}]	Q_{dhw} [kWh a^{-1}]	ratio heating to cooling
Canb	2121	17.2%	8228	4116	3.88
Brisb	6900	31.5%	840	4056	0.12
Syd	2854	30.6%	1764	4070	0.62
Grif	6828	23.5%	5105	4080	0.75
TenCr	17955	12.2%	53	3255	0.00
Darw	20560	46.9%	0	3256	0.00
Melb	1648	29.5%	5881	4533	3.57

Table 8.5: Difference of supplied cooling, heating and DHW energies of the base case compared to the reference system.

	ΔQ_c [kWh a^{-1}]	Δ latent [% points]	ΔQ_h [kWh a^{-1}]	ΔQ_{dhw} [kWh a^{-1}]
Canb	-324	0.1%	-740.8	31.7
Brisb	-99.4	7.3%	-272.9	-28.4
Syd	-278.4	6.8%	-609.7	-14.2
Grif	57.6	5.9%	-518.7	-4.4
TenCr	-210.1	1.1%	-34.8	30.6
Darw	192.5	5.9%	0	32.3
Melb	-313.6	3.5%	-951.5	18.8

The energy imbalance around the hot water tank ($\Delta Q_{imb,hw}$) was calculated for each time step as in equation 8.1. The useful heat from the collectors ($\dot{Q}_{coll,useful}$)

Table 8.6: Achieved comfort conditions of the solar thermal system and difference to the reference system $\Delta comf = comf - comf_{ref}$.

	$comf_T$ **(winter)**	$comf_T$ **(summer)**	$comf_{RH}$	$\Delta comf_T$ [% points]	$\Delta comf_{RH}$ [% points]
Canb	2.2%	0.5%	8.9%	1.0%	-3.6%
Brisb	0.6%	0.5%	46.2%	0.6%	-0.3%
Syd	1.0%	0.3%	39.2%	0.8%	-1.5%
Grif	1.5%	1.0%	14.9%	1.1%	-3.4%
TenCr	0.0%	1.2%	1.3%	0.2%	0.1%
Darw	0.0%	0.5%	82.4%	0.4%	4.6%
Melb	2.1%	1.0%	15.2%	1.9%	-3.7%

and the auxiliary gas input $\dot{Q}_{HVAC,aux}$ and $\dot{Q}_{DHW,aux}$ are energy sources in each time step. Energy sinks are the heat demand for domestic hot water ($\dot{Q}_{dhw}$), the generator of the absorption chiller ($\dot{Q}_{c,hw}$) and the space heating unit ($\dot{Q}_h$). Heat is lost from the tank, the pipes and also from the auxiliary heater units ($\dot{Q}_{loss,tank}$, $\dot{Q}_{loss,pipes}$, $\dot{Q}_{loss,aux,HVAC\&DHW}$). Furthermore there is the internal energy change of the tank and the pipes (dU) and the relieved heat from the tank in case of overheating ($\dot{Q}_{relieve}$). The heat sink ($\dot{Q}_{reheat}$) only applies to HVAC systems which are humidity controlled. The energy imbalance was integrated over one year to calculate the annual energy imbalance $\Delta Q_{imb,hw} = \int_{year} \Delta\dot{Q}_{imb,hw}$.

$$\begin{aligned}\Delta\dot{Q}_{imb,hw} = {} & \dot{Q}_{coll,useful} + \dot{Q}_{aux,HVAC} + \dot{Q}_{aux,DHW} \\ & - \dot{Q}_{loss,tank} - \dot{Q}_{loss,pipes} - \dot{Q}_{loss,aux,HVAC\&DHW} \\ & - \dot{Q}_{dhw} - \dot{Q}_{c,hw} - \dot{Q}_h \\ & - dU_{tank}/dt - dU_{pipes}/dt \\ & - \dot{Q}_{relieve}(-\dot{Q}_{reheat})\end{aligned} \tag{8.1}$$

In the course of the model development, the tank model type 534 seemed to lead to a large energy imbalance and the tank type 60 was chosen. This lead to a strong reduction in the energy imbalance, which was always positive. For mathematical consistency the energy imbalance was added to the simulation output of relieved energy from the tank. The energy relief prevents the tank from overheating. Figure 8.8 shows the total heat losses of the simulation as well as relieved heat. Furthermore, it shows the fraction of energy imbalance to the total relieved heat. In Appendix D.8 Figure D.8 shows a histogram of the tank top temperature. It also shows the distribution for the collector outlet temperature, when the collector pump is switched on.

The percentage of energy imbalance of the total amount of relieved heat has been plotted against the actual relieved heat. One trend is visible for all climates. When increasing the collector area, the energy imbalance is a rather constant fraction of the relieved heat regardless of the tank size. This means that for larger collector sizes the energy imbalance increases proportionally with the relieved heat. For small

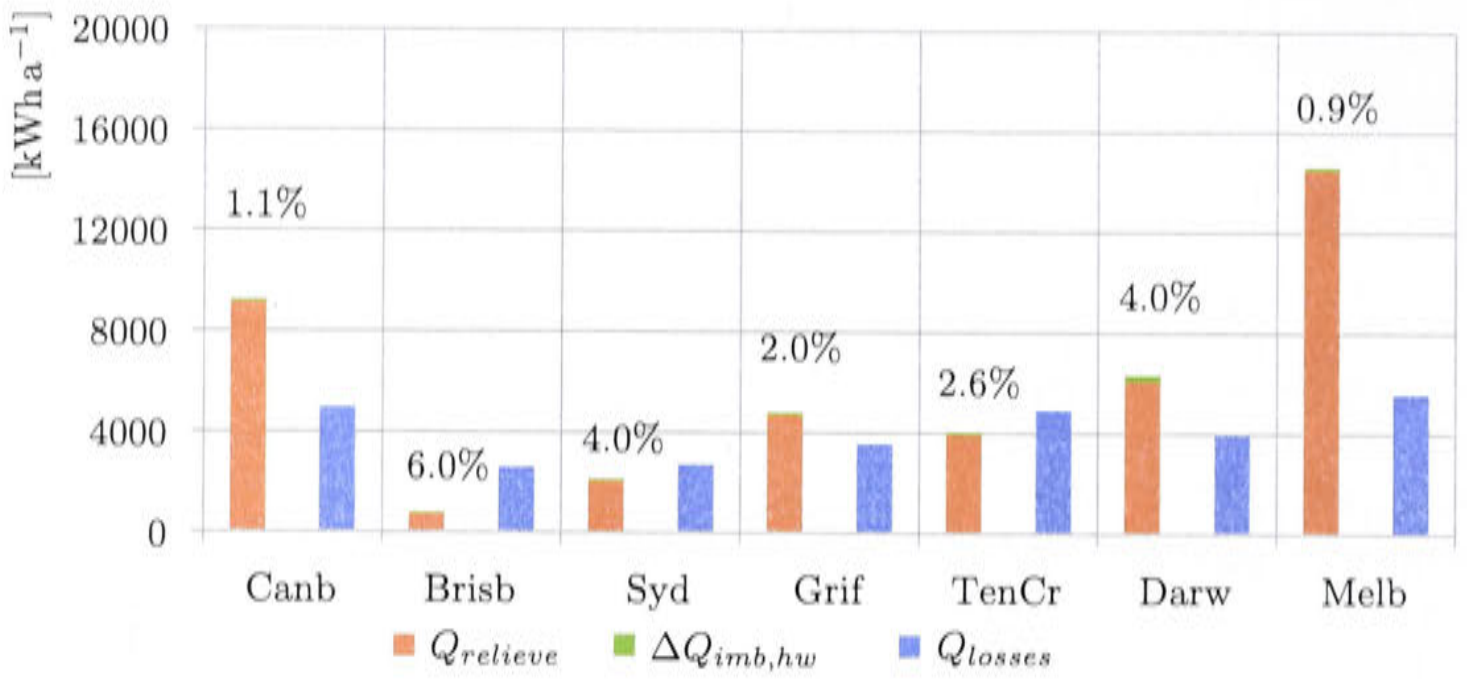

Figure 8.8: Total heat loss and relieved heat from the tank with percentage of energy imbalance.

collector areas there is a strong difference in the percentage of imbalance for different tank sizes, but the relieved heat is very small. As an example Figure 8.9 shows the fraction of energy imbalance for Brisbane and the relieved heat. All other climates are presented in Appendix D.10, Figure D.10.

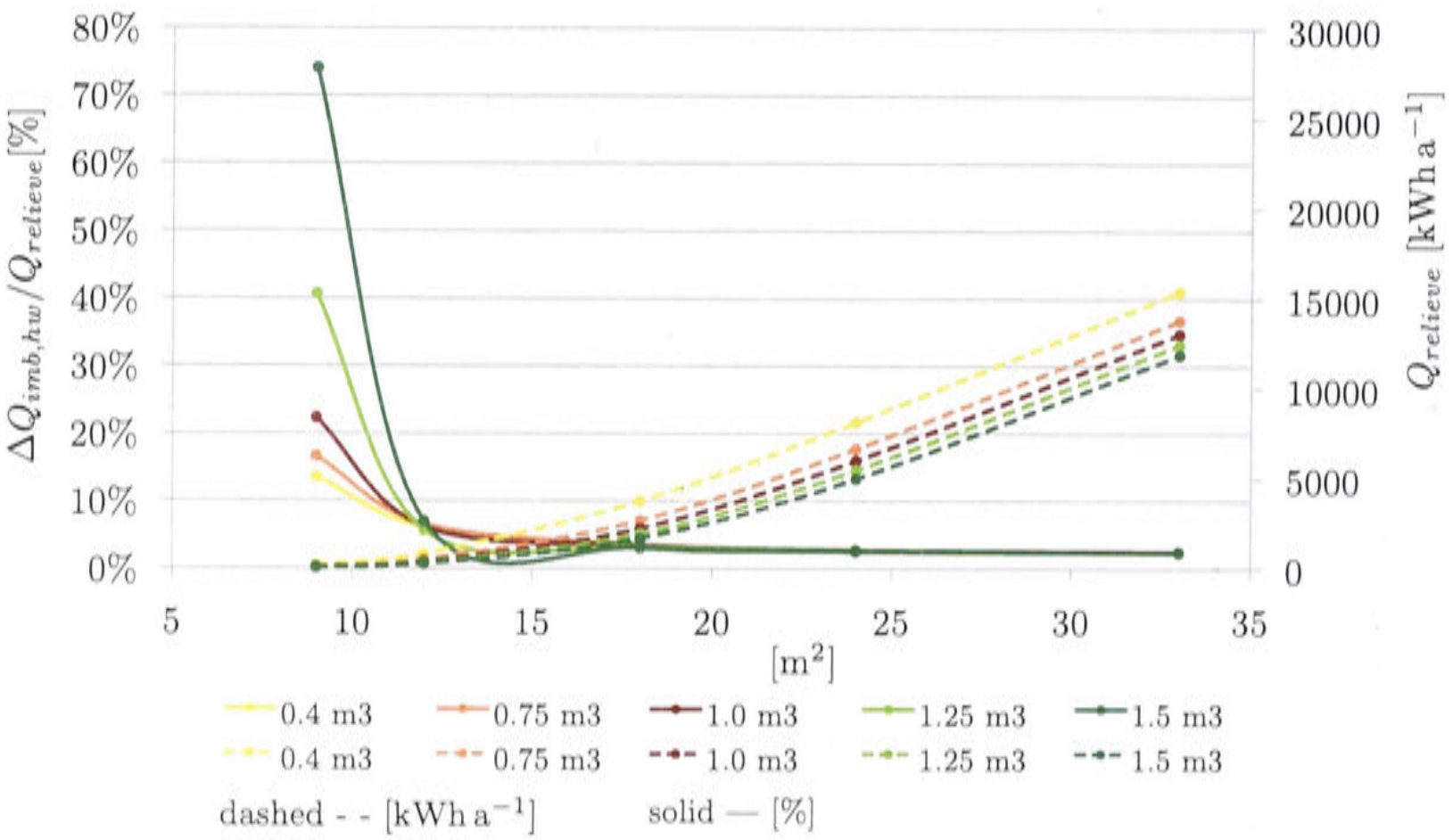

Figure 8.9: Percentage of energy imbalance and relieved heat for Brisbane. The other climates are presented in Appendix D.10.

The hours of room fan operation are summarized in Table 8.7, along with the hours the collector pump circulates water. In Appendix D.9 histograms of the air flow during operation are shown.

Table 8.7: Fan and collector pump operating hours in heating and cooling mode throughout the year dependent on zones 1 to 3.

	Cooling hours			Heating hours			Coll pump
	Z1	Z2	Z3	Z1	Z2	Z3	on
Canb	1045	238	585	1976	2433	2390	3179
Brisb	2393	349	1498	306	426	329	3509
Syd	1417	125	566	587	922	628	3356
Grif	2069	548	1459	1219	1732	1673	3380
TenCr	4527	2634	4660	35	30	10	3669
Darw	4788	1250	3693	0	0	0	3742
Melb	831	146	385	1779	1998	1854	3021

8.1.6 Heat rejection

For heat rejection a wet cooling tower was chosen with a cooling water set point ($T_{cw,set}$) of 27°C in all climates. In Figure 8.10 the percentage of operating time is shown when the cooling water outlet temperature of the wet cooling tower exceeds $T_{cw,set} + 0.5\,°C$. Exceeding the set point temperature may be due to high outdoor wet bulb temperatures, or a high cooling load combined with low hot water supply temperatures. If the cooling water set point temperature is exceeded it causes the chiller to demand higher hot water inlet temperatures. If the hot water inlet temperature is already at the maximum possible temperature, the chilled water outlet temperature deviates from its set point temperature.

The graphic also shows that only in Darwin, a cooling water temperature of 27°C is not achievable approximately 40% of the time due to the high outdoor humidity. In Darwin the wet bulb temperature plus an approach of 3°C is higher than the set point temperature approximately 60% of the time.

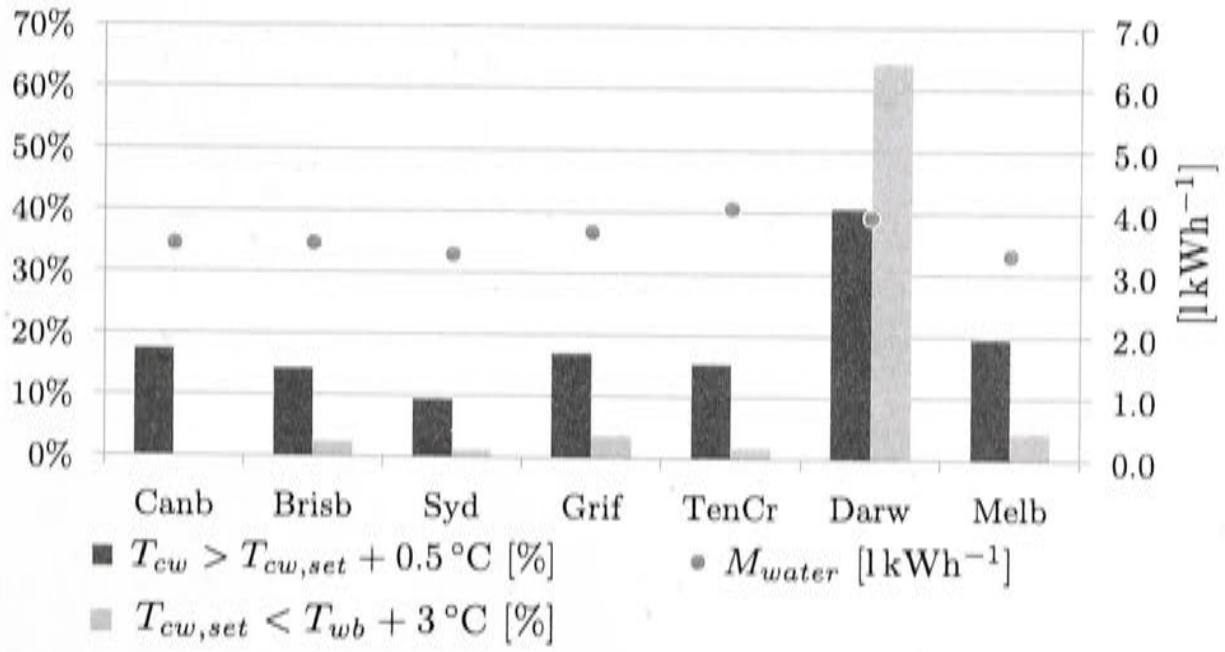

Figure 8.10: Percentage of operating time the cooling tower set point temperature is exceeded, and the climate conditions do not allow for the appropriate set point temperature to be achieved. Furthermore, specific water consumption of the cooling tower in liters per kWh of produced cooling.

The set point temperature for Darwin might be increased to accommodate for it's high humidities. This in return requires less fan power from the cooling tower

at constant performance, but more heat input to the chiller since higher driving temperatures are required. Since the chiller is limited by its maximum hot water inlet temperature, it is possible that the chilled water temperature set point is exceeded in return and the comfort drops.

In section 8.2.7 the cooling water set point temperature will be varied depending on the outdoor wet bulb temperature, by adding an approach of 3°C. The "approach" is defined in Wang [2000, p. 10.36] as the temperature difference between the wet bulb temperature of the air and the cooling water temperature leaving the cooling tower. If the cooling water temperature becomes too high, the chiller will switch off automatically.

Furthermore, a dry cooling tower will be compared to the wet cooling tower, but only for an increased chilled water set point temperature.

8.1.7 Energy demand of the cooling, heating and DHW system

For the chosen configuration, the gas and electricity consumption specific to the conditioned space can be found in Figure 8.11. The solar heat consumption is pictures ad well.

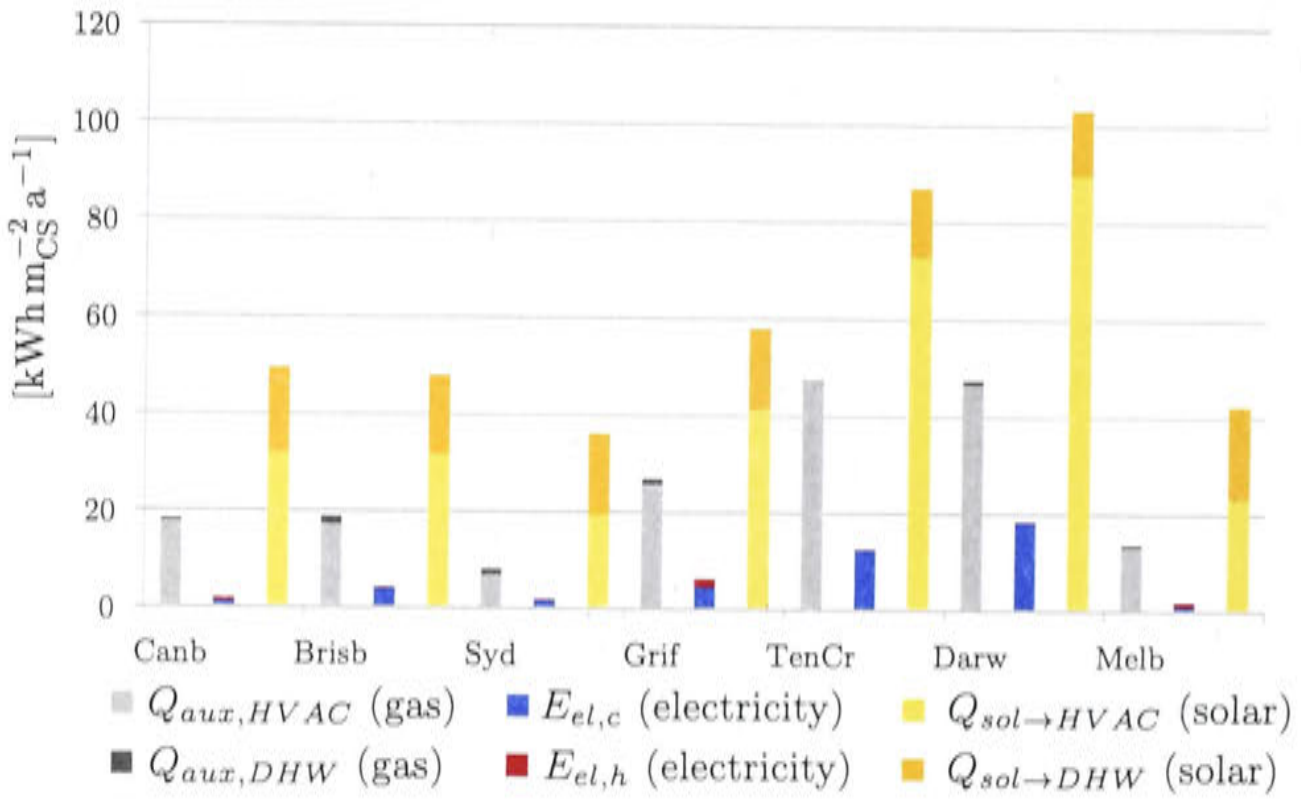

Figure 8.11: Gas, electricity and solar energy consumption specific to the conditioned space.

The following Figure 8.12 shows the amount of specific energy used in all climates for each kWh of cooling and heating (and DHW) generated.

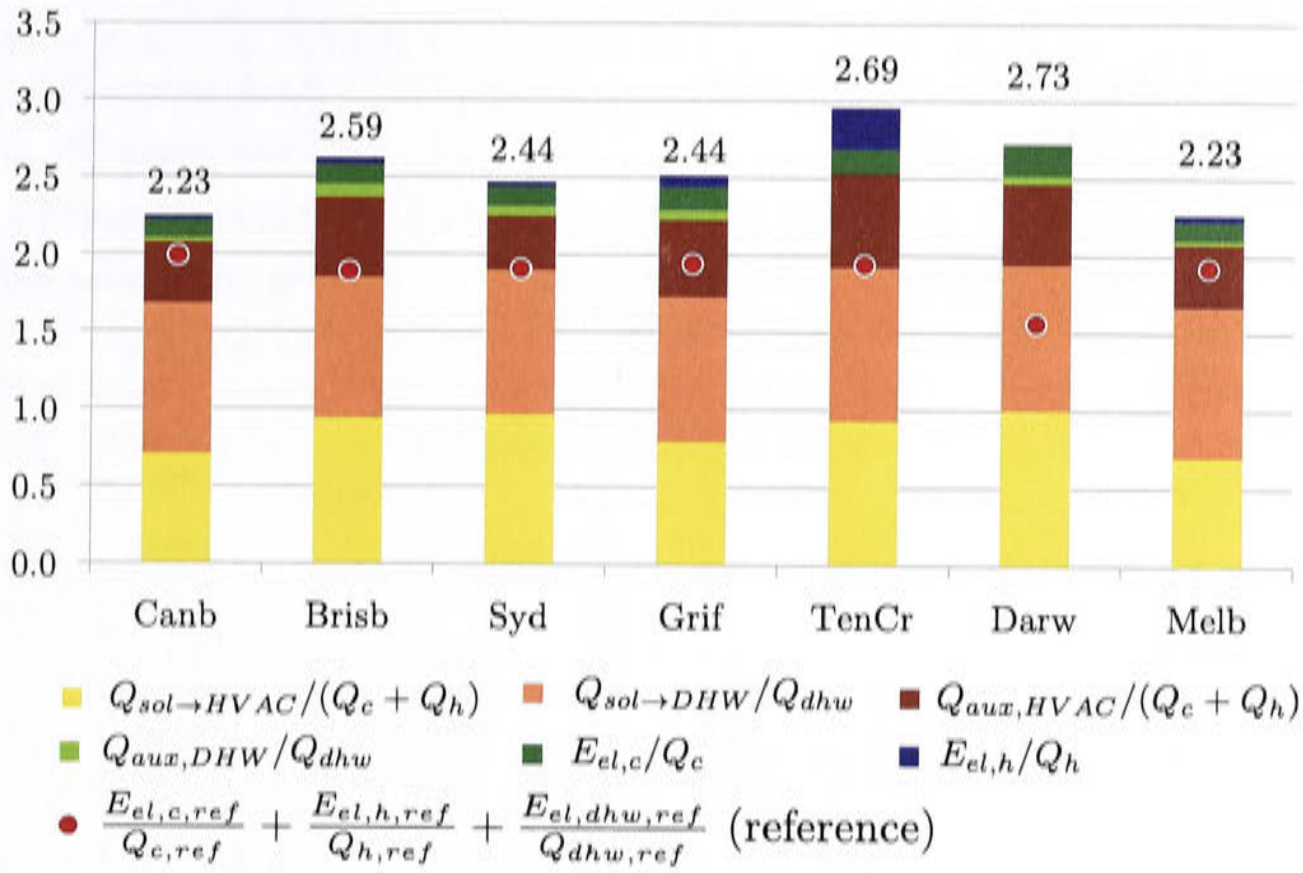

Figure 8.12: Specific energy consumption referred to the generated amount of cooling, heating and DHW.

The electricity consumption can be split up between the different components of the absorption chiller system as in Figure 8.13. The chiller itself and the three external pumps are the largest electricity consumers. The collector pump circulates the water from the collectors to the tank and the indoor fans supply the room with conditioned air. The cooling tower fans use most electricity in Darwin which is the most humid climate.

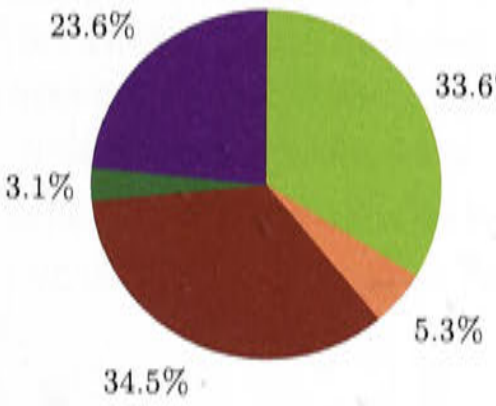

(a) Canberra

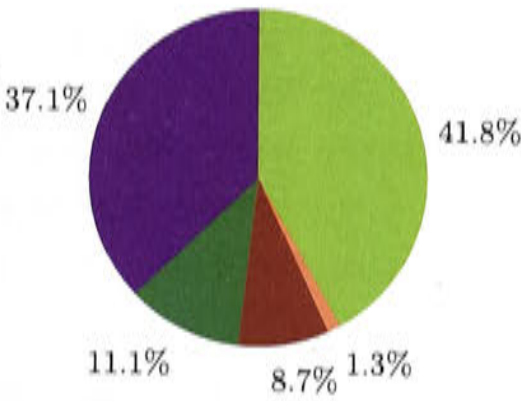

(b) Brisbane

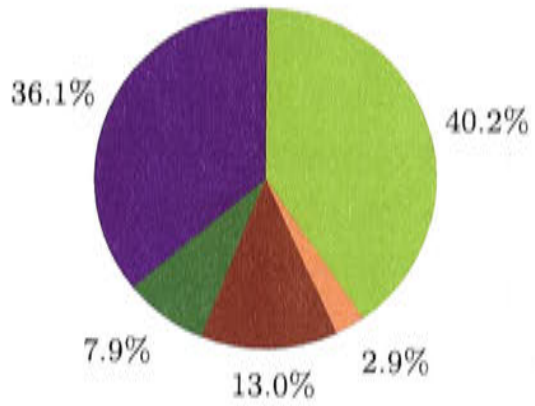

(c) Sydney

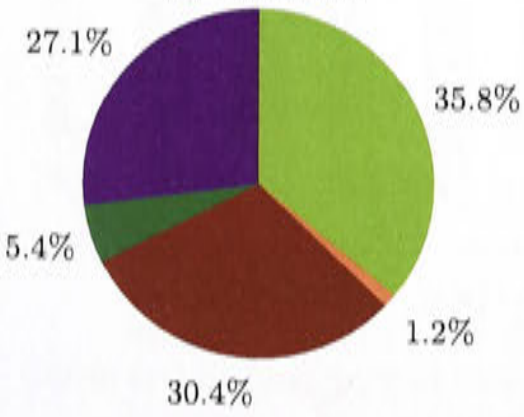

(d) Griffith

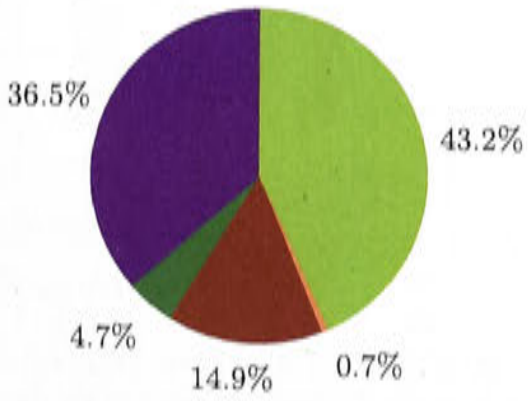

(e) Tennant Creek

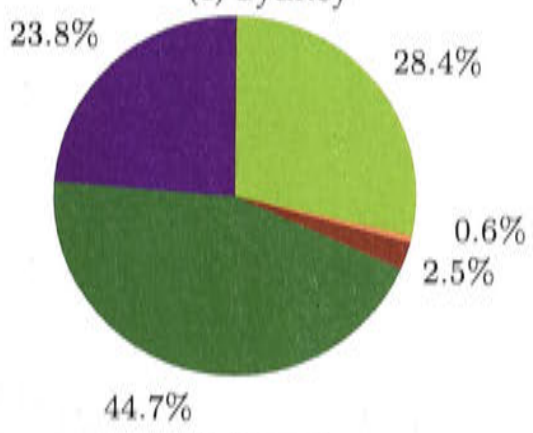

(f) Darwin

(g) Melbourne (h) legend

Figure 8.13: Break down of electricity consumers for the solar thermal system in the 7 climates.

Compared to most European demonstration systems [Henning, 2013a, p. 219], the highest electricity consumer is not the cooling tower, but the chiller and the external pumps. The chiller has a constant electricity demand whenever it is switched on and so do the external pumps, because they provide a constant mass flow rate. The cooling tower on the other hand is fan speed controlled to always generate 27°C cooling water temperature. Hence, under low loads it operates at lower power. When the chiller operates in part load, for example in the morning or evening, the chiller and the pumps have the same power consumption as under full load. This is a clear disadvantage of the model. However, the issue is representative for reality where no conventional chiller can take over part load operation. Therefore, most effective systems are large scale systems, where the back up can be done by additional electrically driven chillers with a good part load performance. The absorption chiller can run full load, depending on the solar supply only.

The cooling tower fan is controlled towards a lower air flow whenever possible, whereas the chiller constantly operates at its fixed power consumption. This is the reason why the chiller's power consumption is relatively high compared to the fan power consumption of the cooling tower. In colder climates the power consumption of the fan coil units has a relatively large proportion as heating is provided via fan coil units as well.

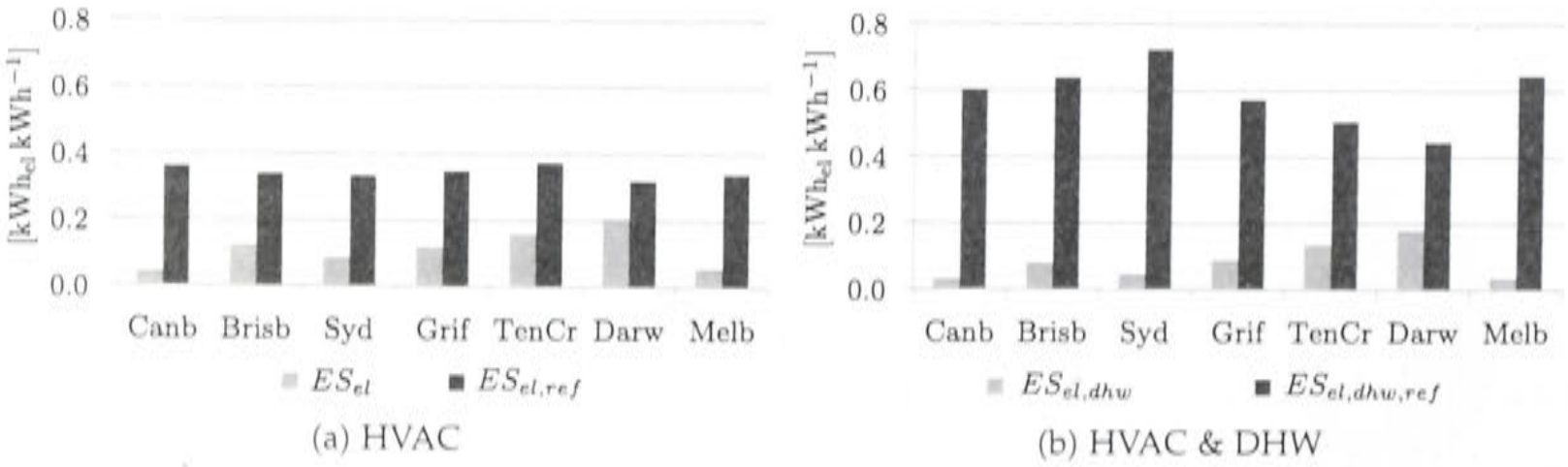

(a) HVAC (b) HVAC & DHW

Figure 8.14: Electricity consumption specific to the amount of cooling and heating (and DHW) generated, comparing the solar thermal base case to the reference case.

The specific electricity consumption can be seen in Figure 8.14 and it is compared

to the reference case, which was previously presented in Table 5.2. It is obvious that the specific electricity consumption can be reduced drastically especially when including DHW.

One of the main drivers for solar cooling is to reduce peak electricity demand. For 16:00 to 20:00 the specific saved electricity is calculated in Figure 8.15. The result for the peak electricity reduction including domestic hot water is questionable again as the Australian demand profile might not reflect reality very well. However, no alternative domestic hot water demand profile has been published to date.

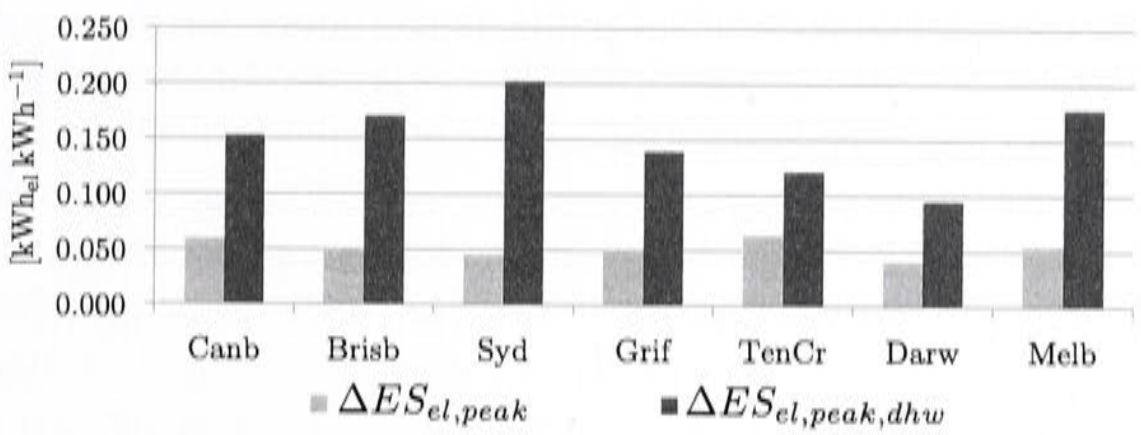

Figure 8.15: Specific saved electricity during peak hours (equation 4.14).

8.1.8 Overall performance factor

The overall performance factor has been calculated for the base case and has been compared to the reference case in Figure 8.16. It becomes obvious that the proportion determined by cost is very poor, but can be improved strongly when including the generation of DHW.

The overall performance factor will not be applied in the following section 8.2 on solar thermal system variations as the main objective will be to analyze the system's performance compared to the solar thermal base case.

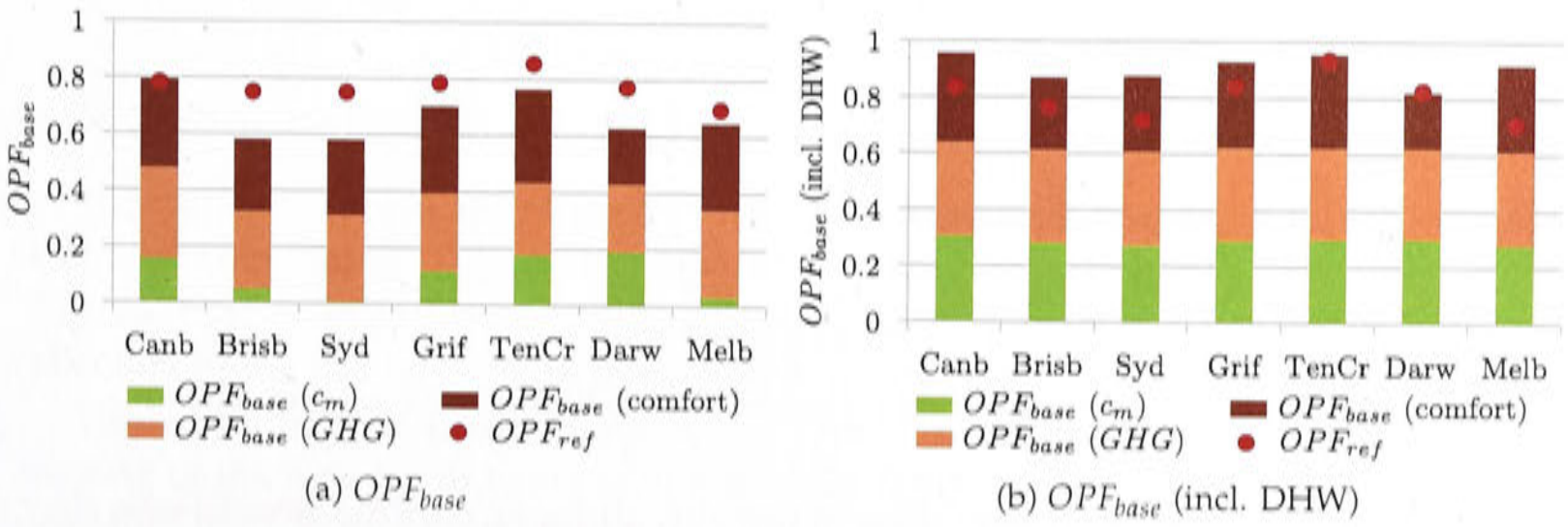

(a) OPF_{base} (b) OPF_{base} (incl. DHW)

Figure 8.16: Overall performance factor base case compared to reference case.

8.2 Sensitivity study of the solar thermal cooling, heating and DHW model

Some parameters in the model are concerned with the design of the cooling and heating supply side and other parameters are concerned with the building load.

Firstly, various parameters of the solar and chilled water system will be varied to investigate the sensitivity of the supply side parameters. This includes changes to the collector array, the hot water tank, the chiller and to the heat rejection strategy.

Secondly, the cooling load will be varied. This includes two additional strategies for dehumidification, a variation of set point temperatures for the supplied chilled water and air as well as the reduction of infiltration rates. Furthermore, the thermal mass of the building model will be varied and night flush ventilation will be included as an option.

The distribution system for cooling will also be varied and radiative cooling via chilled beams replaces the use of fan coil units. The heating will remain as it is with fan coils.

8.2.1 Panel orientation

In this case the panels will be orientated in different directions deviating from north, namely north-east (NE), north-west (NW) and west (W). The building orientation is fixed in order to keep the cooling and heating load constant.

The comfort provided and total electricity consumption do not change compared to the base case. The strongest changes are visible in the solar fraction and the amount of heat relieved.

Figure 8.17 shows the relieved heat and figure 8.18 shows the solar fraction for all four orientations. Orientation due north seems most beneficial.

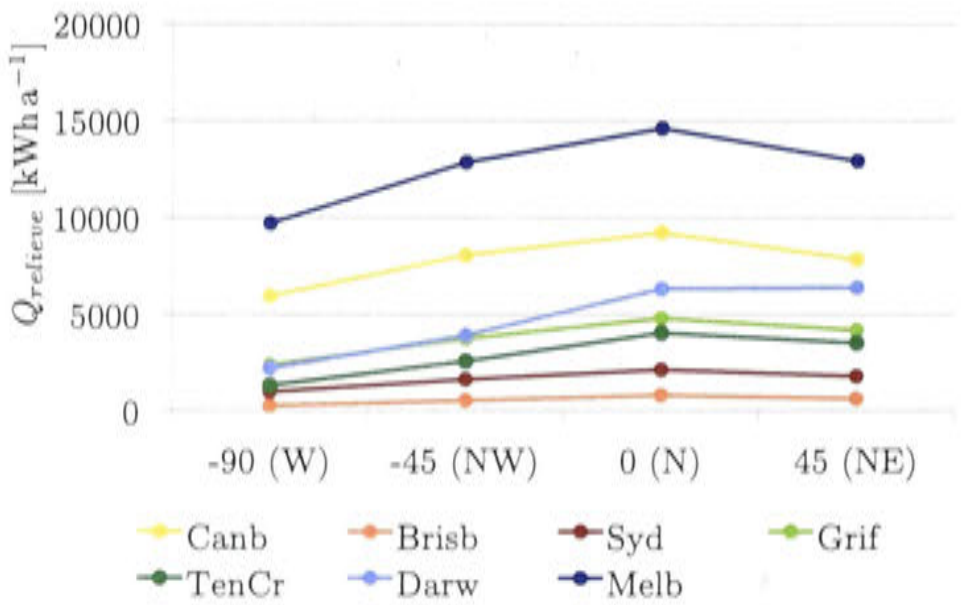

Figure 8.17: Heat relief from the hot water tank for the different collector orientations.

The collector orientation would not show any difference in the saved peak electricity demand as it only affects the gas consumption, hence, the solar fraction. Therefore, the effect on the relieved heat is dominant.

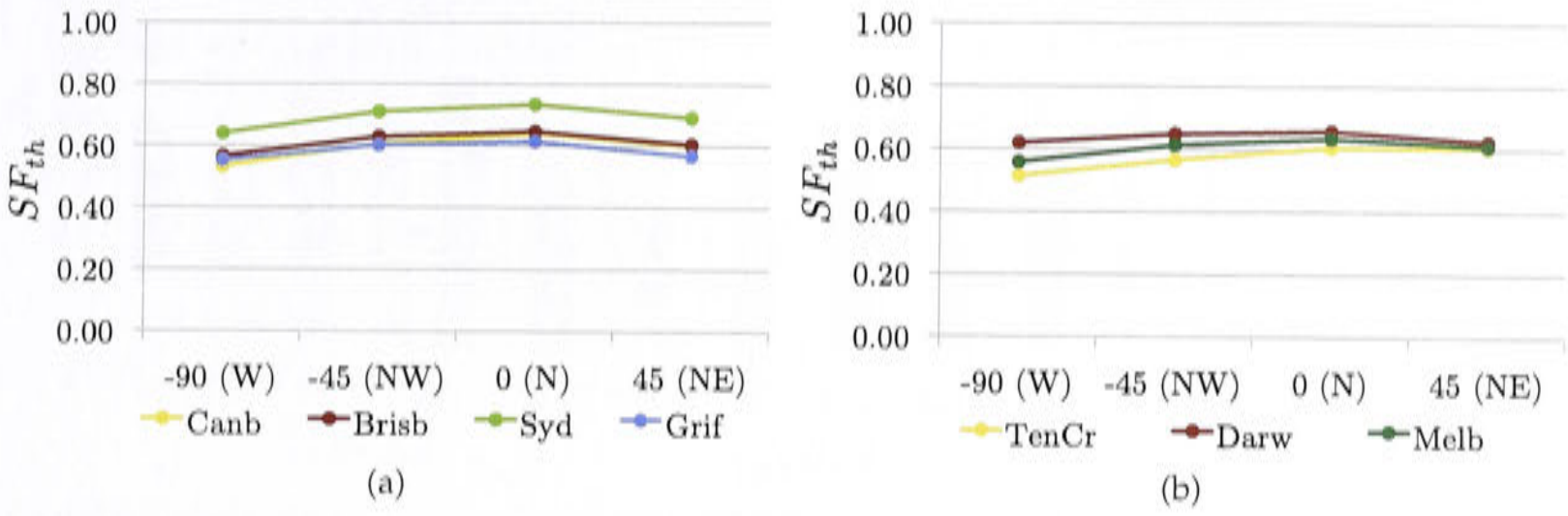

Figure 8.18: Solar fraction throughout the different climates with varying collector orientations.

Usually in large scale solar thermal cooling plants, the absorption chiller system is designed for a smaller solar fraction to operate in a base load arrangement. The solar array is undersized to prevent stagnation, and no heat would have to be relieved. Hence, the effect of changed collector orientation would be much more visible on the times of the day solar cooling can be provided. For example an early start in the morning is favored by orienting the collectors eastward and providing hot water as fast as possible. A simulation based system analysis of the 4000 m^2 flat plate collector absorption system in Singapore revealed that starting the system earlier is of advantage and possible with eastward oriented collectors [Doemland, 2014]. Another advantage of such large scale systems with collectors orientated westward is meeting peak electricity demand while operating the plant longer in the afternoon.

8.2.2 Collector efficiency

The collector efficiency is changed in order to represent two effects. In the first case "coll loss 0.9" the two loss coefficients are reduced by 10% to simulate an improved collector technology. In the second case "coll opt 0.9" the product of IAM and optical efficiency of the collector is reduced by 10% to represent dust and other debris accumulated on the collector surface over time. In that case less solar radiation is able to transmit the glass cover to warm up the abosrber.

Collector loss coefficients reduced by 10%

For the outcome of this case it is important to mention that neither cooling load nor electricity consumption or comfort conditions changed notably.

The effect of improved collector efficiency is an increased heat supply from the collectors to the hot water tank as is shown in Figure 8.19.

The additional heat supply leads to an increase in solar fraction but also to an increase of the amount of heat being relieved from the tank (Figure 8.20). It becomes clear that the solar fraction only marginally increases, but the increased heat supply mainly is relieved from the tank. However, the solar fraction with and without DHW can be improved by 1% to 1.5% points when reducing the thermal loss factors by

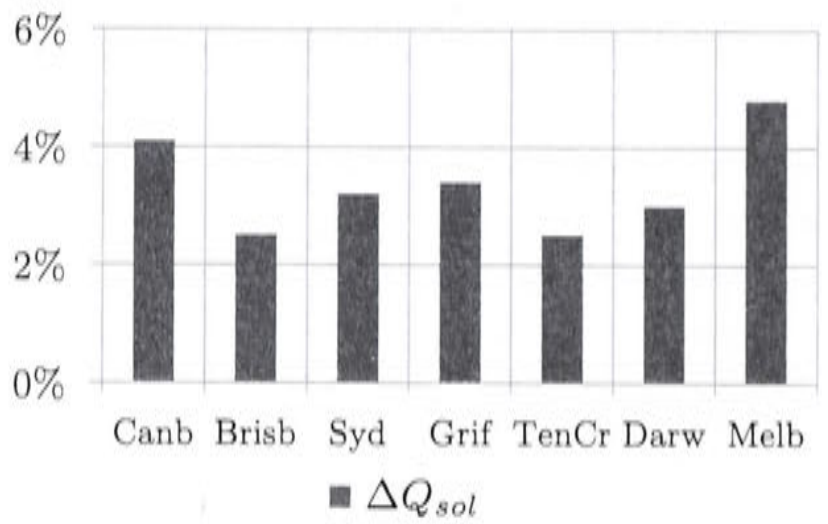

Figure 8.19: Increase in solar energy harvested from the collectors.

10%.

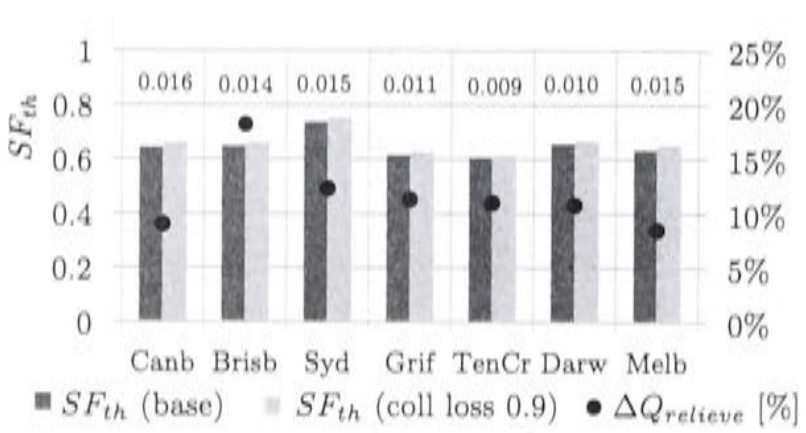

(a) SF_{th}

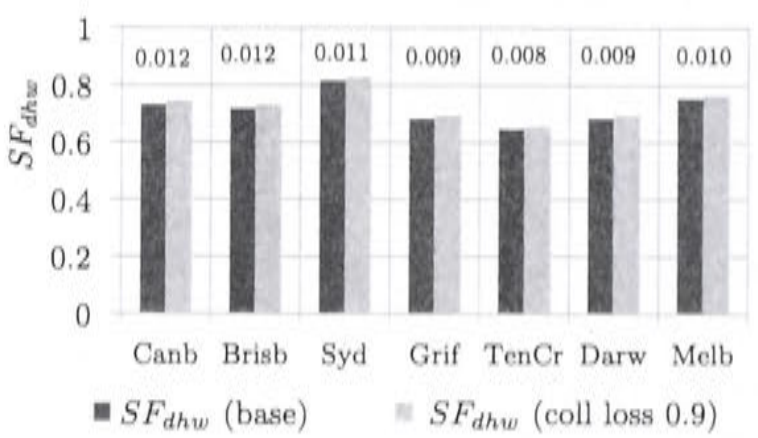

(b) $SF_{th,dhw}$

Figure 8.20: Solar fraction of the system with collectors of increased performance compared to the base case, and heat relieved from the hot water tank.

Collector optical efficiency reduced by 10%

The reduction of the optical efficiency and the IAM product by 10% has a larger effect than reducing the loss coefficients. Figure 8.21 shows that the harvested energy is reduced in most climates by more than 10%.

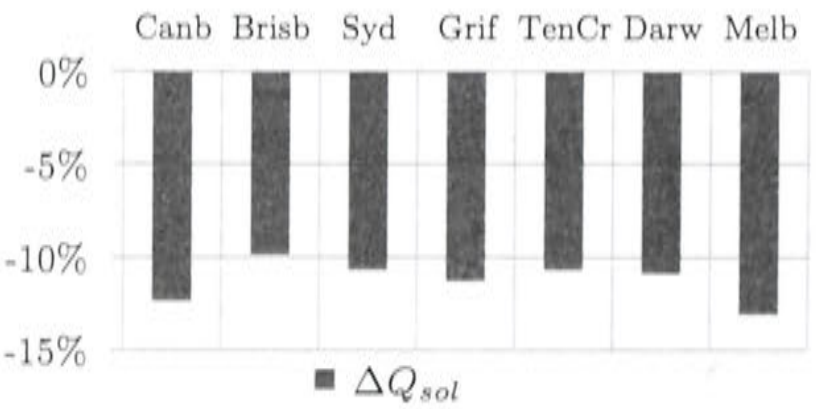

Figure 8.21: Decrease in solar energy harvested from the collectors.

The solar fraction drops by 4% to 7.5% points throughout the different climates, with or without the inclusion of domestic hot water (Figure 8.22). Also, as expected, the amount of relieved heat drops as less solar heat is harvested.

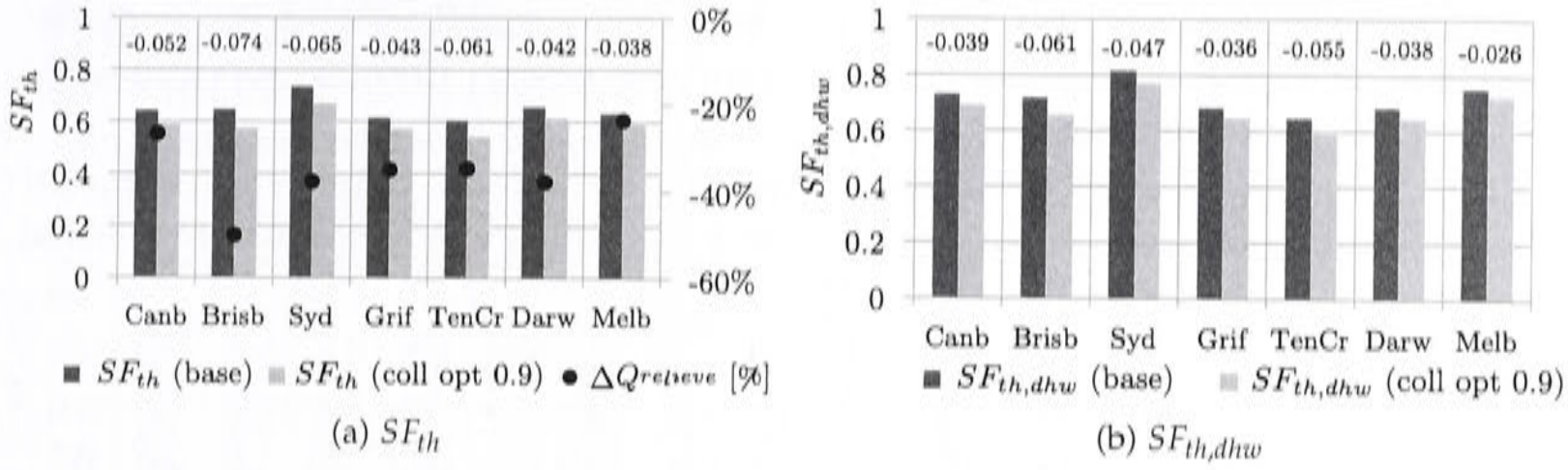

(a) SF_{th} (b) $SF_{th,dhw}$

Figure 8.22: Solar fraction of the system with collectors with reduced optical performance compared to the base case. Heat relieved from the hot water tank.

The specific cost between the two cases does not change significantly. However, the effect on the specific greenhouse gas emissions does and it can be seen in Figure 8.23. With better collectors higher specific greenhouse gas savings can be achieved.

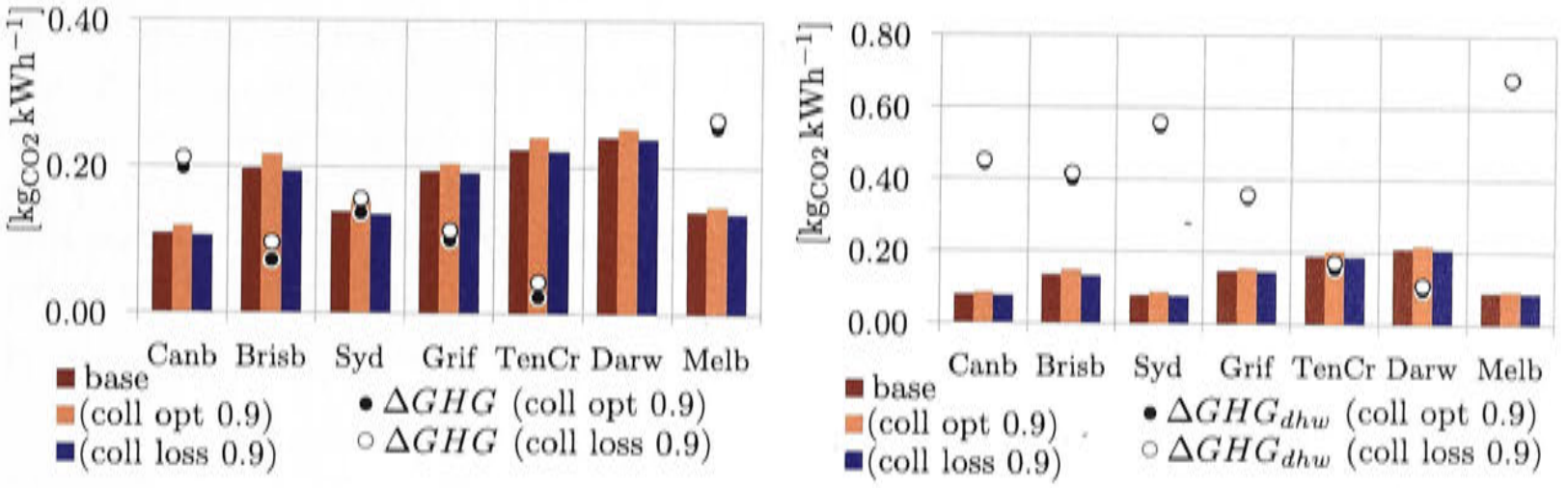

(a) GHG (b) GHG_{dhw}

Figure 8.23: Specific greenhouse gas emission and specific greenhouse gas savings compared to the reference case $\Delta GHG = GHG_{ref} - GHG$.

8.2.3 Hot water tank

Variations around the hot water tank include pressurization and alteration of the auxiliary sensor position.

Pressurized tank

Pressurizing of the hot water storage implies that the boiling temperature is being increased in the model, hence, water can be stored at higher temperatures. The chosen boiling temperature is 150°C, which is an increase of 30°C and has a corresponding saturation pressure of 364 kPa.

If heat can be stored in the water tank at higher temperatures, the losses to the environment will increase but the chiller can be supplied longer with hot water. The solar fraction increases.

Cooling, heating and DHW supplied to the building, and the electricity consumption don't change as only the heat supply source is varied. Comfort conditions are consequently also unchanged.

The change in solar fraction varies between 1.5% and 3% points and is smaller when domestic hot water is included (Figure 8.24). Much less heat must be relieved from the tank.

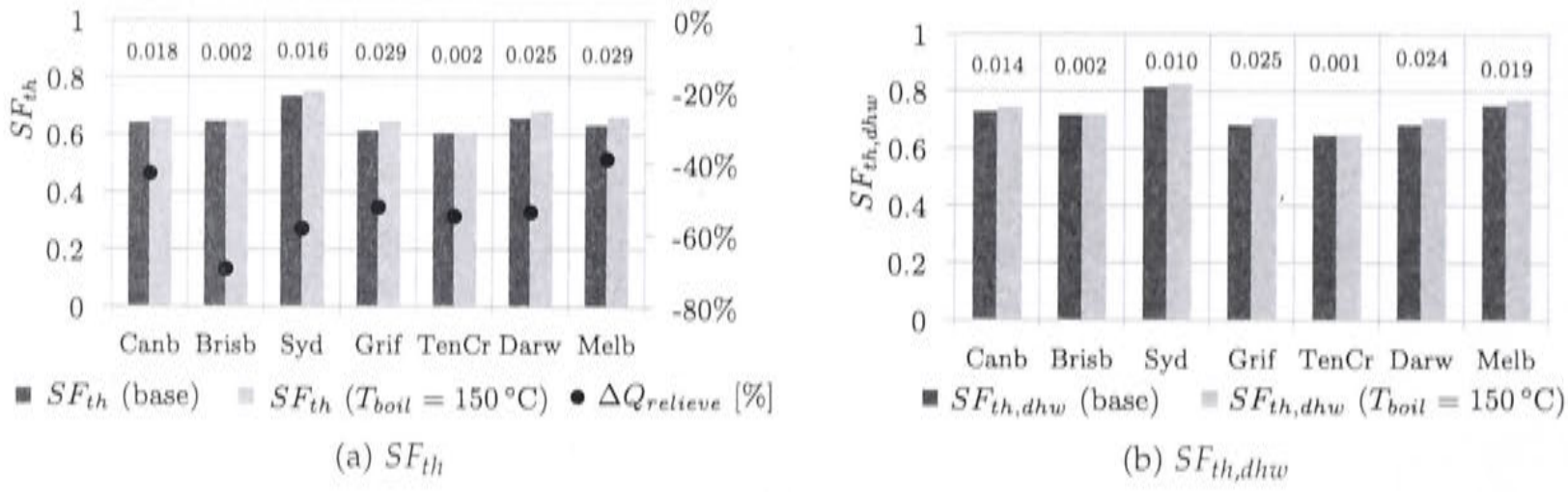

(a) SF_{th} (b) $SF_{th,dhw}$

Figure 8.24: Solar fraction of the system and change of relieved heat when increasing the boiling temperature of the hot water storage tank to 150°C.

Figure 8.25 shows that the collector pump operating hours are reduced and less heat is harvested from the collectors. Furthermore, due to higher temperatures, the heat losses have increased. Nevertheless, overall the higher boiling temperature leads to an increased solar fraction, hence less greenhouse gas emissions.

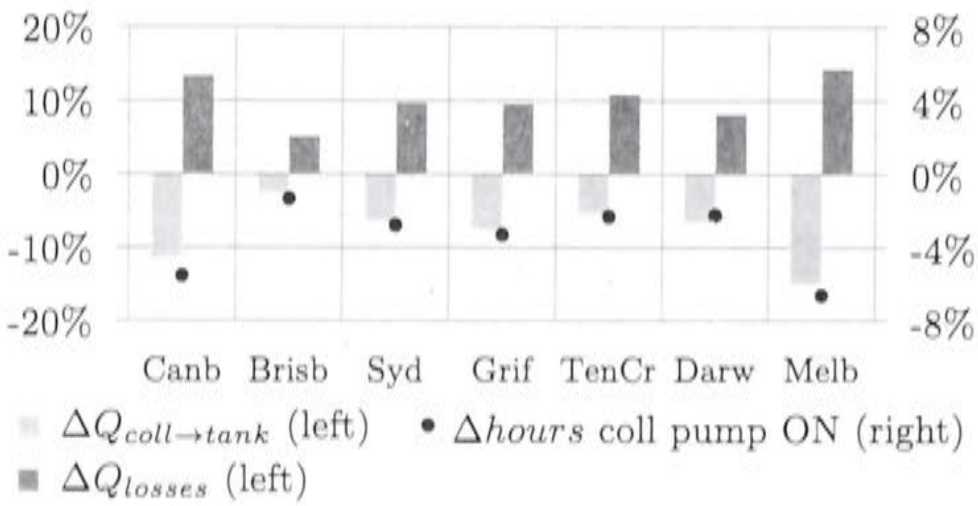

Figure 8.25: Relative change of harvested solar heat, total heat losses and operating hours of collector pump (T_{boil} = 150 °C).

Level of thermostat for auxiliary heater

The auxiliary heater is requested if the solar hot water tank can't provide the hot water temperature required by the chiller.

Once the auxiliary heater receives has been switched on, the signal to switch off again is determined by the tank temperature sensor located near the middle of the tank. This method provides a natural hysteresis.

The thermostat is now moved from the middle to the top of the tank, to the same node as the outlet to the heat supply system.

Figure 8.26 shows that the solar fraction increases only by 0.6% to 1.2% points.

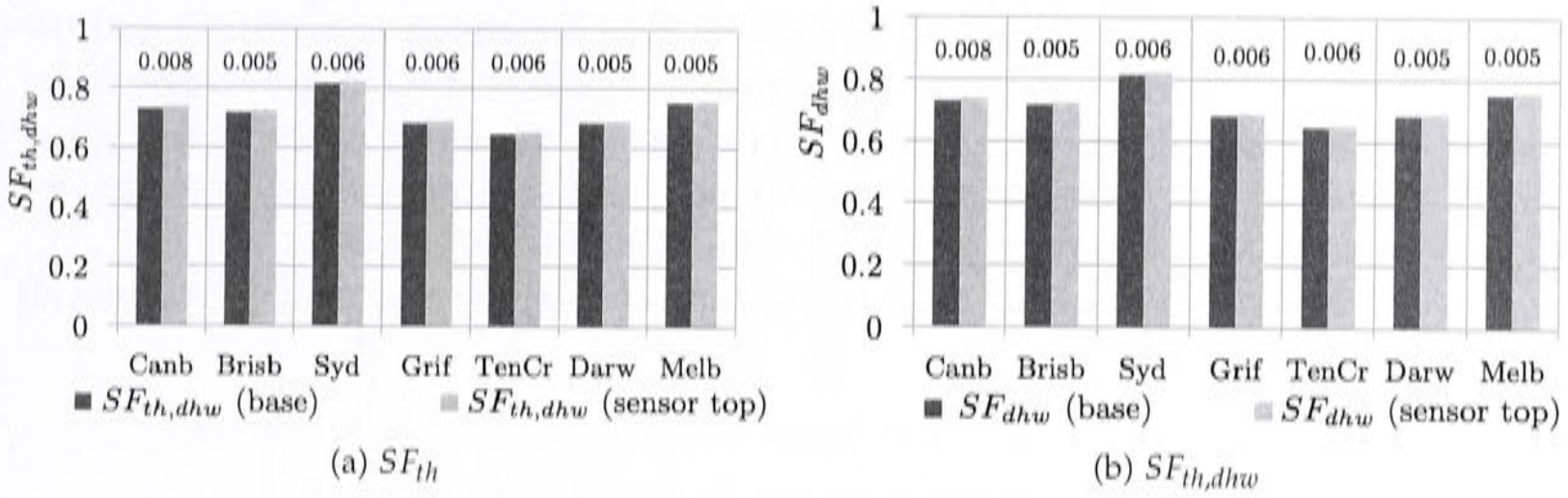

(a) SF_{th} (b) $SF_{th,dhw}$

Figure 8.26: Solar fraction of the system when moving the sensor to the top of the tank.

The increase of the solar fraction including domestic hot water is even smaller. When comparing the gas consumption of the domestic hot water auxiliary heater and the HVAC auxiliary system (Figure 8.27) it is obvious that their energy consumption shows opposing trends. The heat exchanger for DHW is located in the middle of the tank and receives less heat with this control strategy. Nevertheless, the gas consumption of the DHW system is very small compared to the gas consumption of the HVAC system (Figure 8.11, pg. 144). The comfort conditions, which are not shown here, changed negligibly.

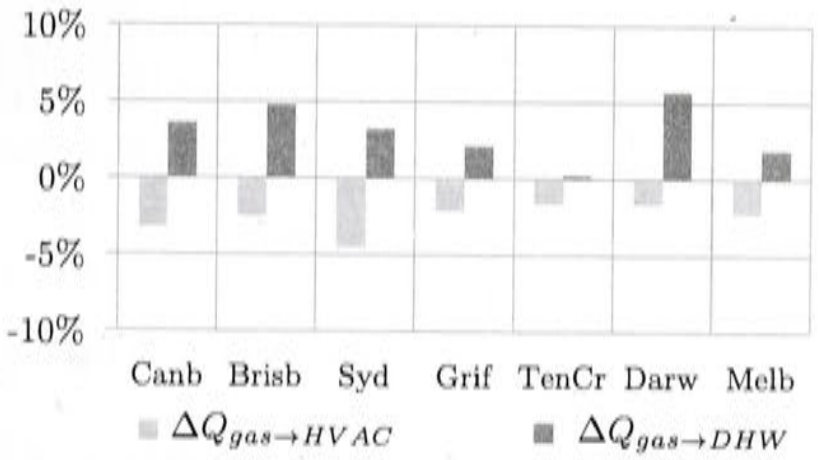

Figure 8.27: Relative change in gas consumption compared to the base case (sensor top)

8.2.4 Chiller capacity

Increasing chiller's capacity by 20%

The base case control strategy tries to switch the chiller on whenever cooling is in demand. If the hot water tank cannot provide enough heat, the auxiliary heater switches on instead. In this section the capacity of the chiller will be increased by 20% as indicated in Table 8.8.

The chiller's external mass flow rates and its power consumption are directly proportional to the *scalefactor* and are also increased by 20%.

Since the chilled water mass flow rate is constant during operation, the modeled cooling power output fluctuates occasionally at the start and end of a daily cycle. This happens especially then when the load is relatively small, for example when only one zone requires cooling, and the low sensible load is satisfied by the minimum air flow. As a result, the chilled water returning to the chiller is very low and the chiller's internal control algorithm would prevent the chiller from generating more cooling. Before actually switching off, it requires the minimum possible hot water inlet temperature to reduce its cooling output. With too large chillers this behavior occurs more frequently in the simulation as the flow rates are larger[1].

On very hot days though, a larger chiller can provide more cooling even when all three zones are in demand.

Table 8.8: Cooling capacity for case "chiller 1.2" in kW compared to the base case.

	Canb	Brisb	Syd	Grif	TenCr	Darw	Melb
ΔC_C	0.7	1.1	0.7	1.4	1.5	1.5	0.7
C_C chiller 1.2	4.2	6.3	4.4	8.2	8.8	9.2	4.2

As expected the temperature comfort conditions increased in each zone and the humidity levels were kept the same as compared to the base case (Figure 8.28).

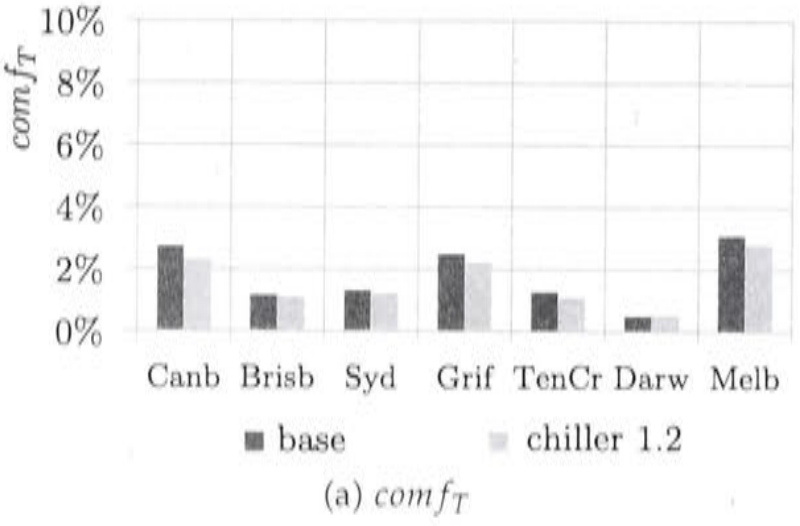

(a) $comf_T$

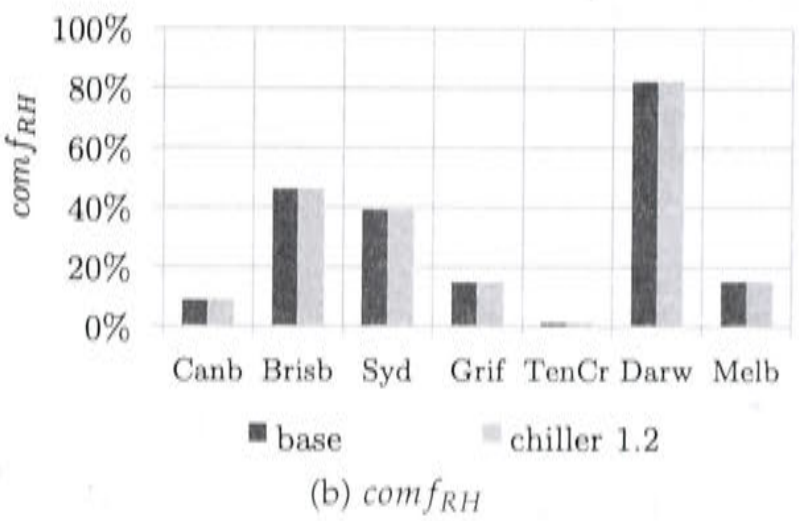

(b) $comf_{RH}$

Figure 8.28: Change of indoor comfort when increasing chiller capacity by 20%.

In Figure 8.29 it can be seen that some of the additional cooling provided helps to remove more latent loads.

[1]In a large scale system one would try to have a relatively constant load when the chiller is in operation, to prevent low chilled water inlet temperatures

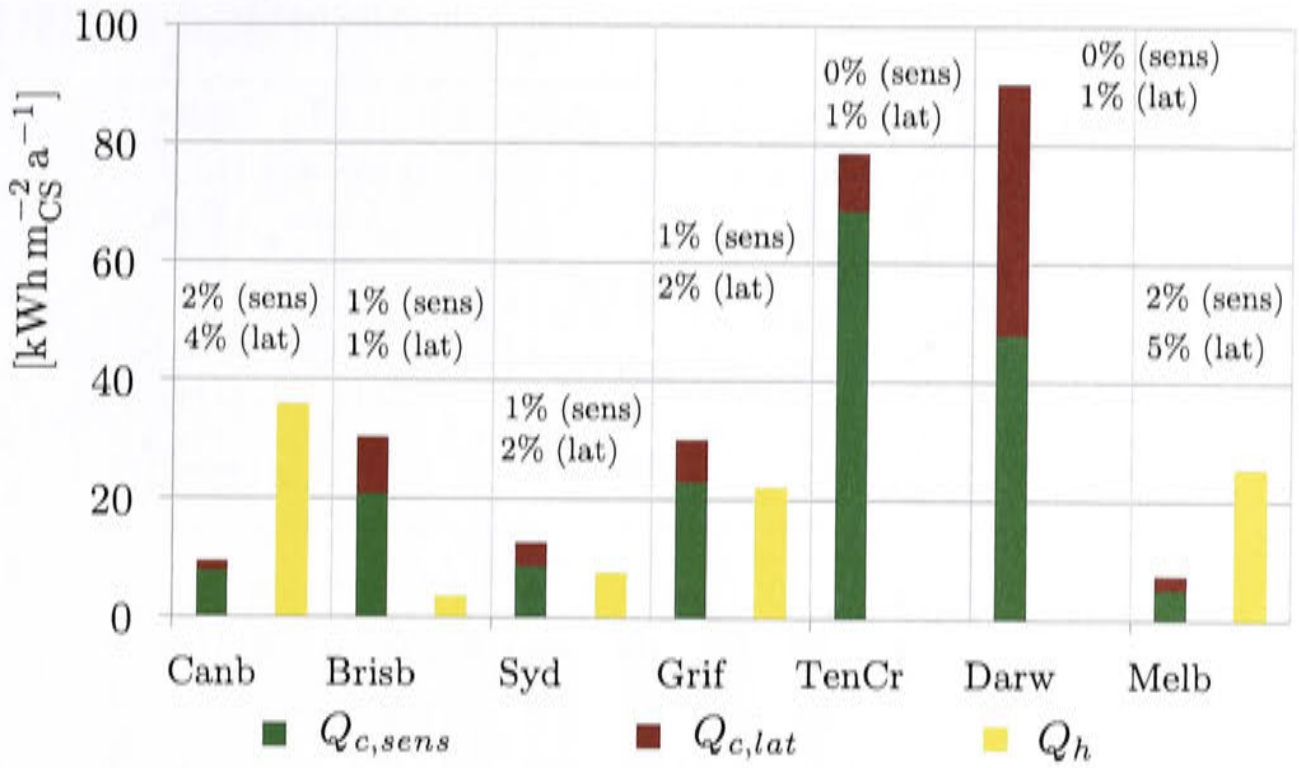

Figure 8.29: Specific cooling and heating energy supplied to the building specific to the conditioned space, and relative change in latent and sensible cooling compared to the base case (chiller 1.2).

The capacity increase happens at the cost of proportionally increased parasitic electricity consumption by the equipment which can be seen in Table 8.9.

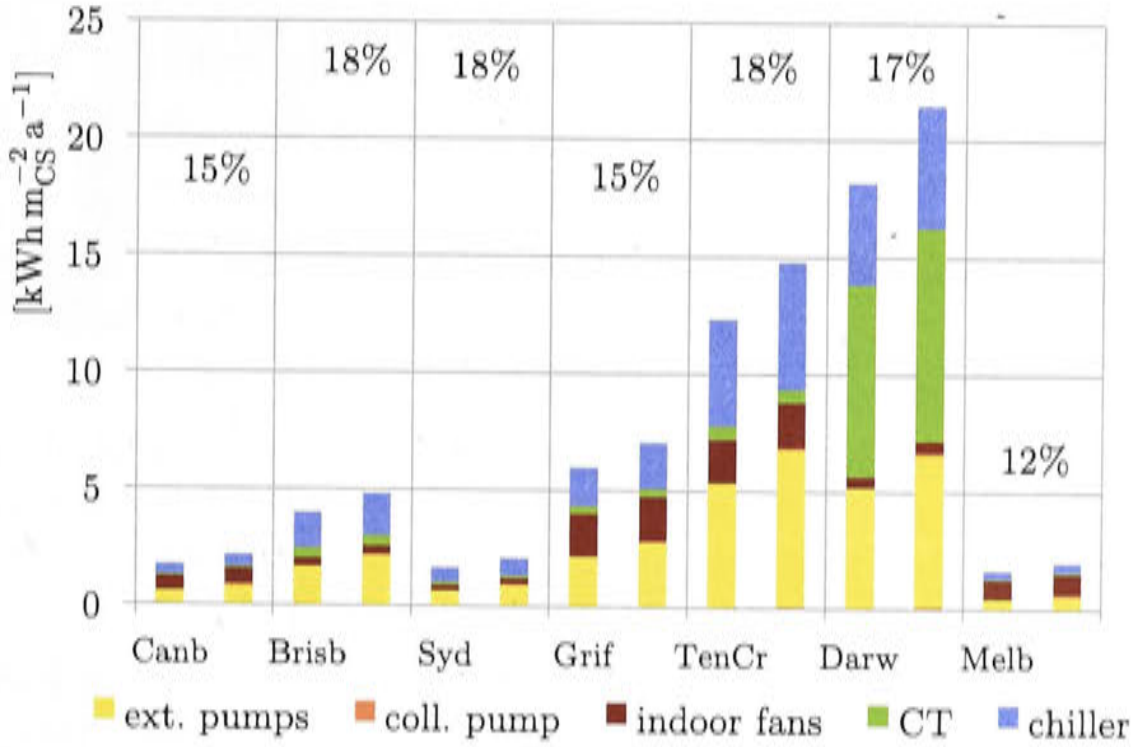

Figure 8.30: Electricity consumption of each individual consumer specific to the conditioned space, and relative change of the total electricity consumption compared to the base case (chiller 1.2).

Figure 8.30 shows the split between the different components and the overall electricity increase.

The solar fraction hardly changed (Figure 8.31) in spite of the slightly increased amount of cooling supplied (Figure 8.32), but the relieved heat dropped because more solar heat could be utilized by the chiller.

Table 8.9: Relative change in electricity consumption compared to the base case (chiller 1.2).

	ext. pumps	coll. pump	indoor fans	CT	chiller
Canb	24.1%	0.1%	8.1%	-0.9%	19.3%
Brisb	24.9%	1.0%	7.5%	-1.8%	19.6%
Syd	24.6%	0.5%	6.9%	-3.5%	19.5%
Grif	24.6%	-0.3%	2.9%	1.4%	19.9%
TenCr	24.7%	0.2%	3.7%	-3.0%	20.1%
Darw	24.1%	-0.1%	6.9%	11.2%	19.7%
Melb	24.5%	0.0%	4.3%	4.9%	19.6%

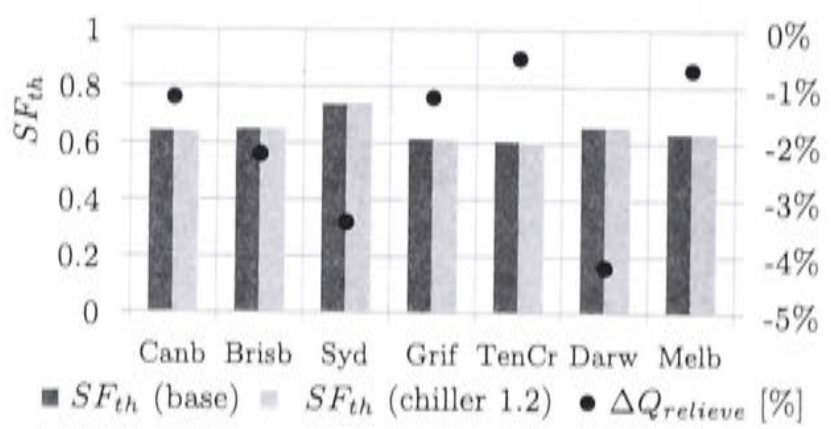

Figure 8.31: Solar fraction (left) and relative change in relieved heat from the hot water tank (right).

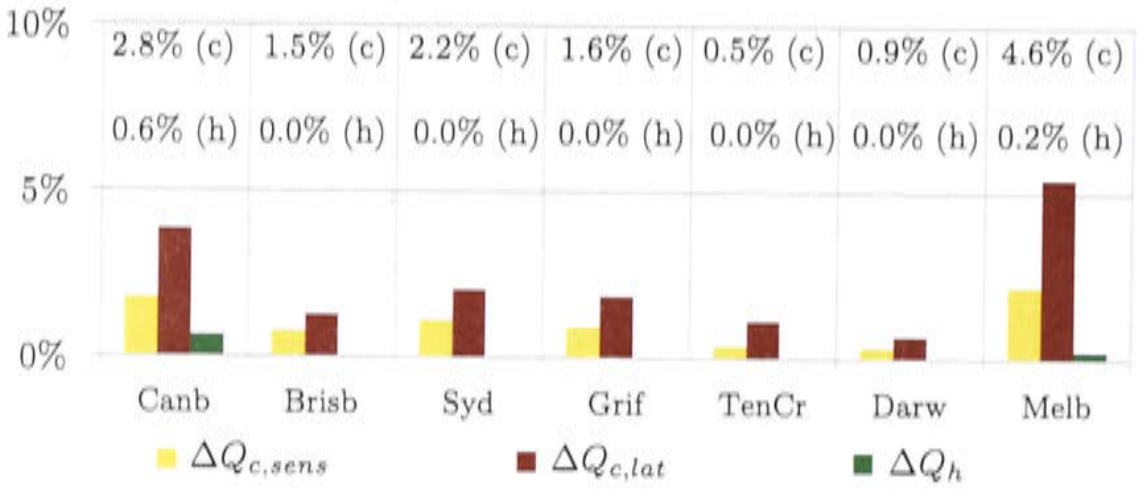

Figure 8.32: Relative change in cooling and heating energy supplied to the building.

Under sizing the chiller by 20%

Reducing the cooling capacity of the chiller by 20% results in a capacity reduction (ΔC_C) for each climate as in Table 8.10. Furthermore, it also decreases the chiller's electricity consumption and external pump electricity consumption by roughly the same proportion as shown in Table 8.11. The change in total electricity consumption specific to the conditioned space, when compared to the base case, is shown in Figure 8.33.

Table 8.10: Installed cooling capacity in the case "chiller 0.8" in kW.

	Canb	Brisb	Syd	Grif	TenCr	Darw	Melb
ΔC_C	-0.7	-1.1	-0.7	-1.4	-1.5	-1.5	-0.7
C_C chiller 0.8	2.8	4.2	2.9	5.4	5.9	6.1	2.8

Table 8.11: Relative change in non specific electricity consumption compared to the base case (chiller 0.8).

	ext. pumps	coll. pump	indoor fans	CT	chiller
Canb	-22.7%	0.1%	-4.6%	-1.3%	-19.0%
Brisb	-23.7%	-0.5%	-13.0%	-2.7%	-19.6%
Syd	-23.0%	-0.1%	-9.3%	0.3%	-19.3%
Grif	-23.7%	-0.4%	-4.7%	-3.8%	-19.7%
TenCr	-24.1%	0.3%	-9.5%	0.3%	-20.0%
Darw	-23.4%	-1.1%	-13.8%	-12.6%	-19.3%
Melb	-22.7%	-0.1%	-8.7%	-6.5%	-19.2%

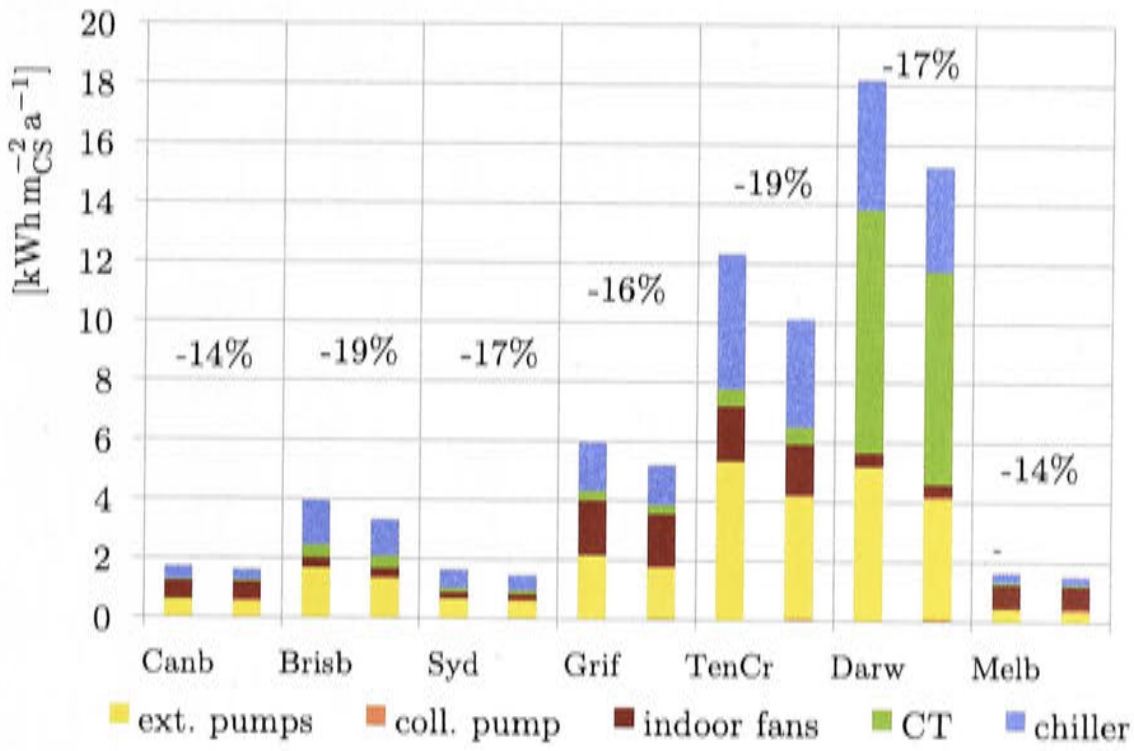

Figure 8.33: Electricity consumption of each individual consumer specific to the conditioned space, and relative change of the total electricity consumption compared to the base case (chiller 0.8).

Since the chiller capacity is reduced the cooling demand cannot always be met which is visible in the comfort levels in Figure 8.34 and the reduced cooling capacity in Figure 8.35. The change in cooling and heating supplied is much larger than when over sizing the chiller, indicating that less heat could be supplied, which was actually requested by the cooling system.

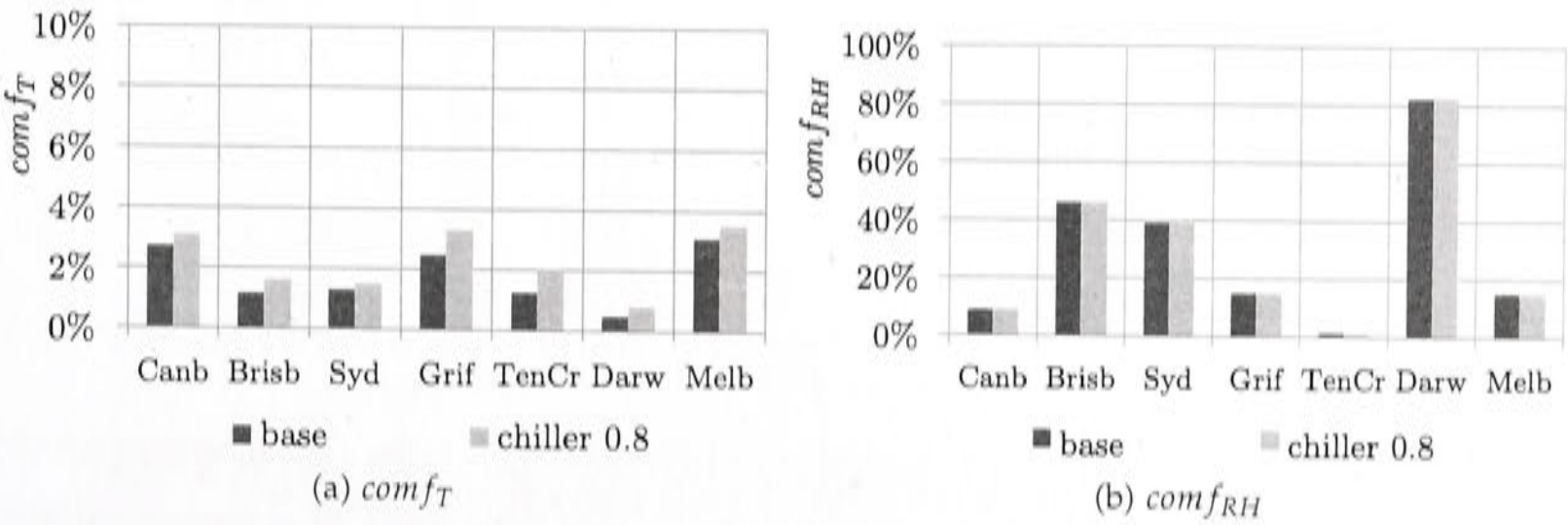

(a) $comf_T$ (b) $comf_{RH}$

Figure 8.34: Change of indoor comfort when under sizing the chiller by 20%.

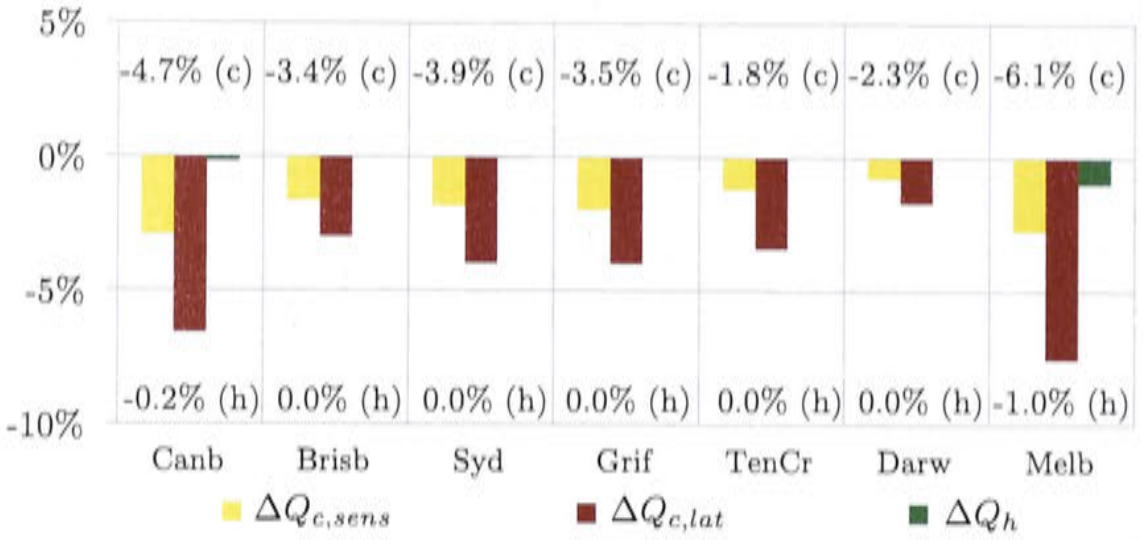

Figure 8.35: Relative change in cooling and heating energy supplied to the building.

The solar fraction hardly changed (Figure 8.36) and the relieved heat increased because less heat is used by the smaller chiller.

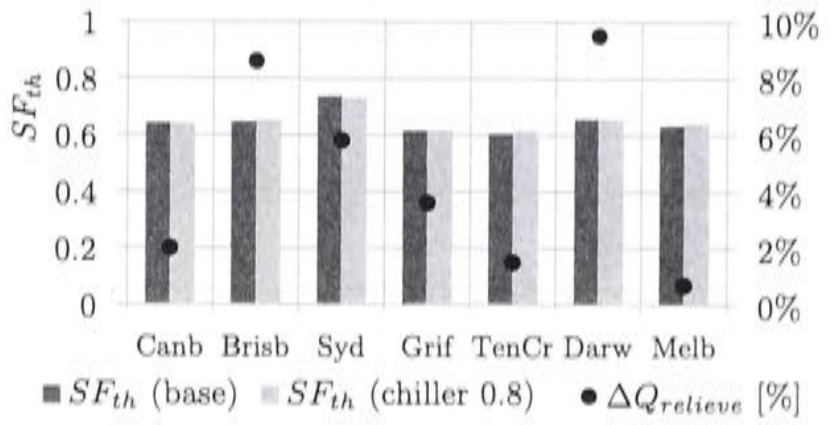

Figure 8.36: Solar fraction (left) and relative change in relieved heat from the hot water tank (right).

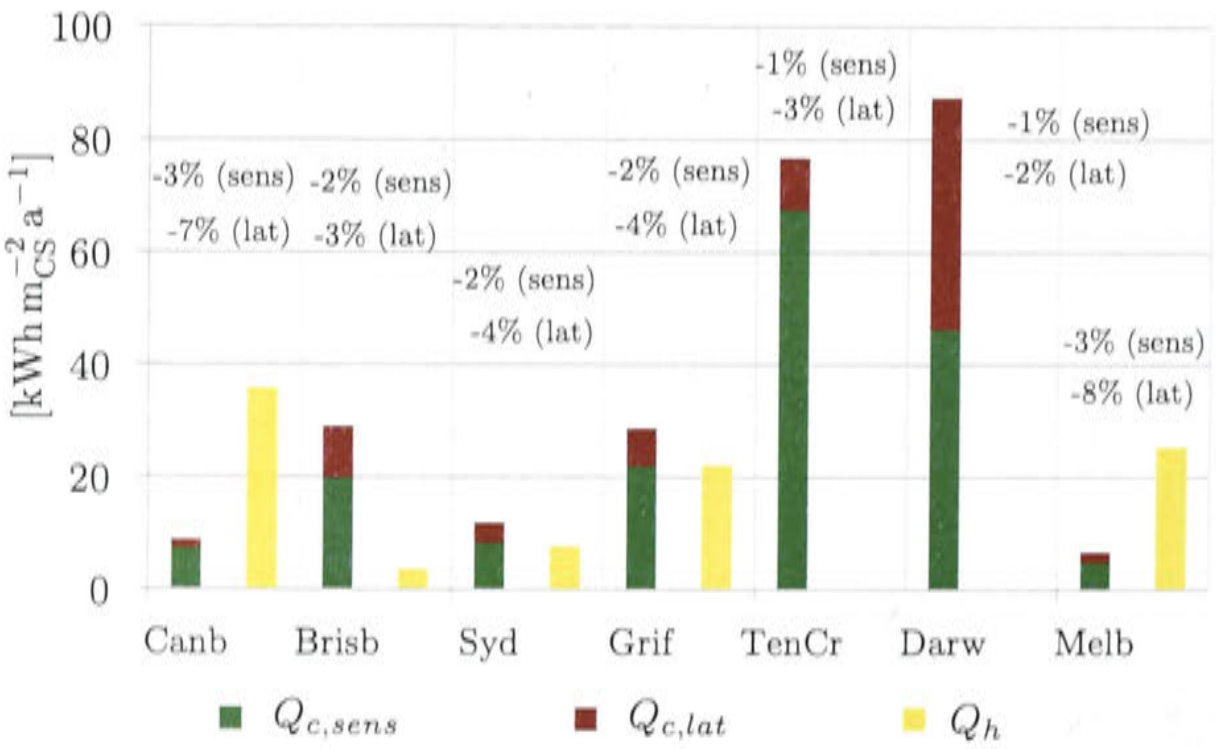

Figure 8.37: Cooling and heating energy supplied to the building specific to the conditioned space, and relative change in latent and sensible cooling compared to the base case.

Comparison of chiller size

This section aims to show how chiller size directly affects greenhouse gas emissions, comfort and cost.

Figure 8.38 shows the specific cost and comfort conditions for the three sizes and Table 8.12 reflects the marginal cost in each climate to reduce the discomfort levels by one percentage point. Increasing the chiller size in Darwin actually increases the discomfort by 0.01 points which is too small to be significant and therefore, indicating that over sizing does not achieve any increase in temperature comfort.

Table 8.12: Marginal cost increase per percentage point reduction of discomfort [$/%].

	Canb	Brisb	Syd	Grif	TenCr	Darw	Melb
$(\Delta c_m / \Delta com f_T)_{0.8\to1.0}$	0.055	0.093	0.228	0.044	0.043	0.096	0.051
$(\Delta c_m / \Delta com f_T)_{1.0\to1.2}$	0.049	0.685	0.459	0.143	0.209	(-2.361)	0.086

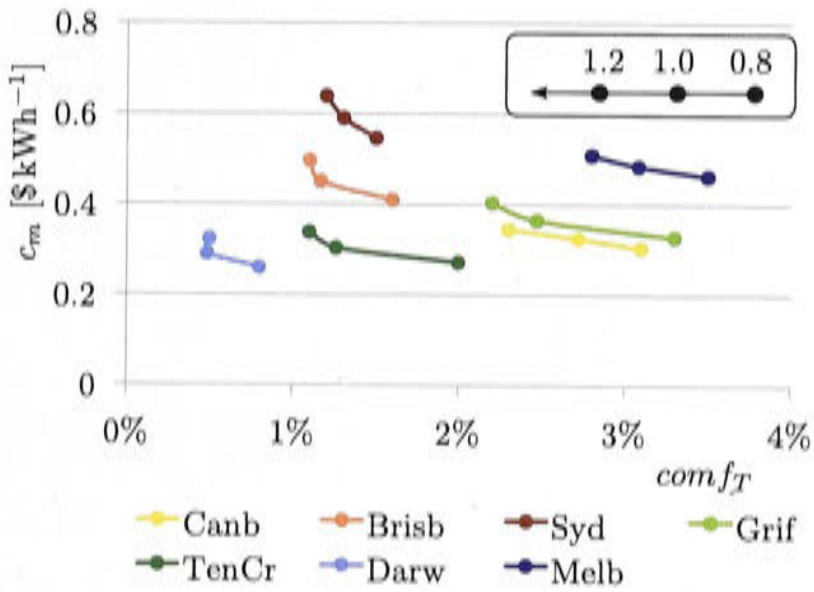

Figure 8.38: Comparison comfort conditions due to temperature to the specific cost for heating and cooling.

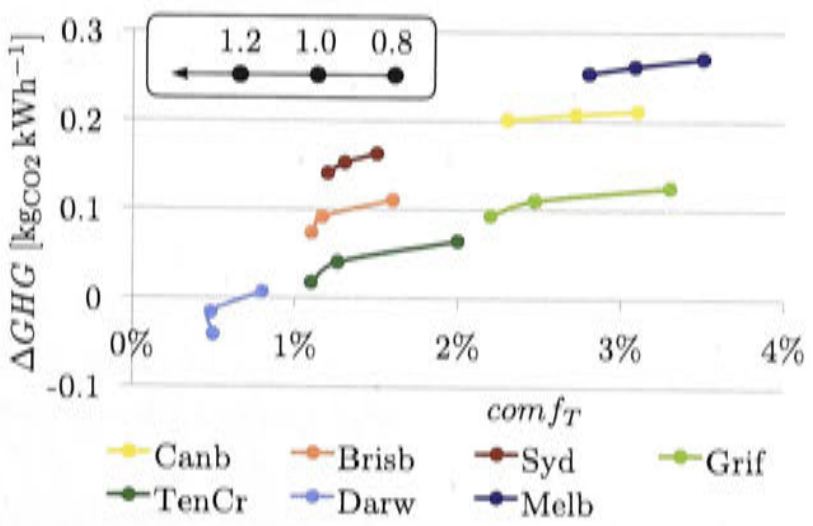

Figure 8.39: Comparison comfort conditions due to temperature to saved specific greenhouse gas emissions (for each of the three chiller sizes).

Figure 8.39 provides a measure on how much more greenhouse gases are emitted for the increase in comfort levels when assuming that the chiller is scaled up and down in the manner described in the previous sections.

Overall the cost of the oversized chiller is higher because of the 20% increased investment and the additional electricity consumption (Figure 8.40). The specific greenhouse gas emissions are slightly higher, too, due to the increased electricity consumption (Figure 8.41) but proportionally smaller cooling increase. For the reduced size chiller the results show the opposite trend.

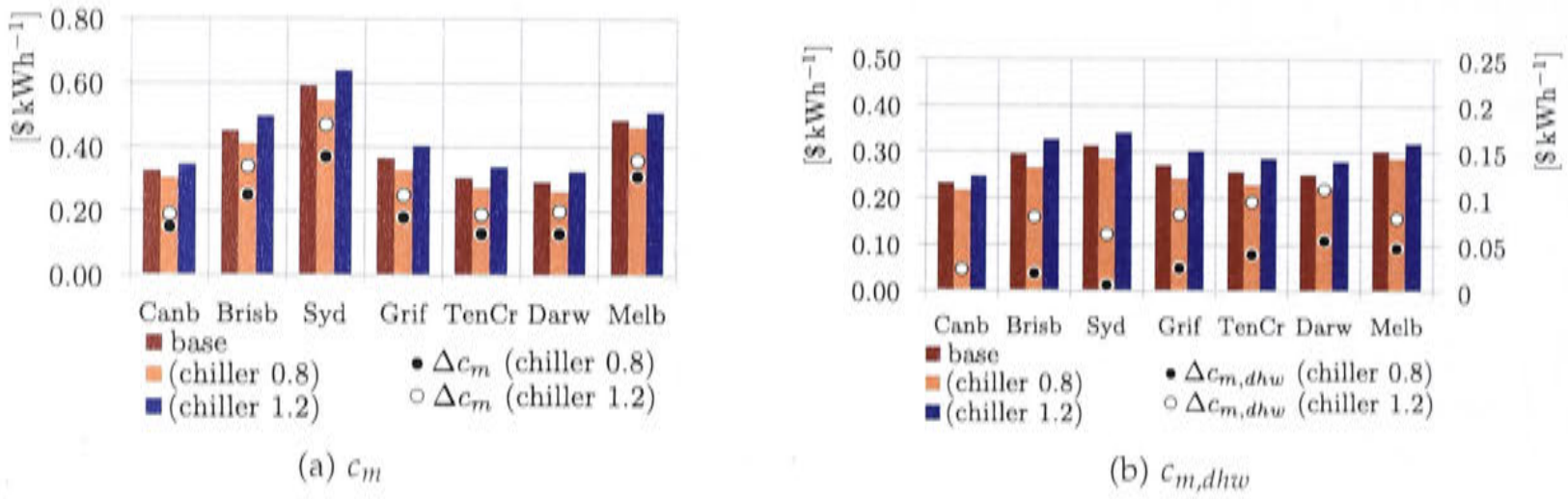

(a) c_m (b) $c_{m,dhw}$

Figure 8.40: Specific cost comparing the two different chiller sizes to the base case. Specific cost difference compared to the reference case $\Delta c_m = c_m - c_{m,ref}$ (on right axis if included).

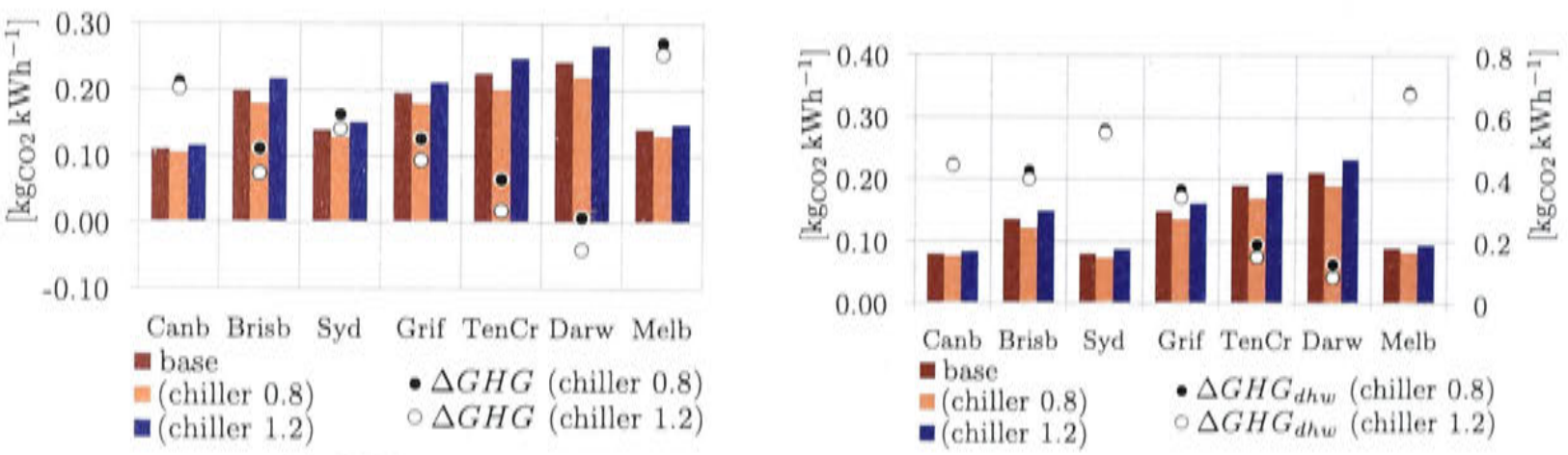

(a) GHG_m (b) GHG_{dhw}

Figure 8.41: Specific greenhouse gas emissions comparing the two different chiller sizes to the base case. Specific greenhouse gas savings compared to the reference case $\Delta GHG = GHG_{ref} - GHG$ (on right axis if included).

8.2.5 Dehumidification strategies II and III

Implementing solar cooling systems brings large electricity savings in areas which are clear, dry and hot. This is because a large proportion direct solar radiation is available and a moderate wet bulb temperature helps to keep fan power consumption at the wet cooling tower low.

In tropical and humid climates, the inconsistency of solar radiation leads to fluctuations in heat input to the hot water system and to difficult heat rejection conditions. Furthermore, the cooling loads are rather latent than sensible.

The base case control strategy switches the chiller on and off depending on the dry bulb temperature within the three zones. Once the desired temperature is reached, it is switched off again, even though the relative humidity levels might

be above the comfort set point for relative humidity of 60% in summer. Dehumidification occurs as well, but only to a certain degree depending on the air outlet temperature and chilled water inlet temperature to the coils.

In section 7.3.2 and 7.3.3 the simulation results of two different control strategies are presented. The strategies switch the chiller on not only when the temperature in the room is exceeded but also when the humidity levels are above 60% relative humidity. Since the air is dehumidified with cooling coils, it is over chilled to achieve the desired humidity conditions. Reheating units are simulated, through which water from the hot water storage is circulated. In this model water from the tank outlet for the heating and cooling supply circuit is tapped off, even though in real systems the temperatures used for re-heating are usually between 30°C and 35°C. However, the return flow rates enter the hot water at the level closest in temperature and stratification can be maintained.

The simulation has been performed with an oversized chiller first to find the required cooling capacity of the building. A larger cooling load is expected, especially in humid climates. The collector and tank size of this simulation were set to the largest collector size 33 m^2 and second smallest tank size 0.75 m^3. The comparison with the base case will be performed for this particular tank and collector size configuration.

Strategy II

When changing the control strategy according to section 7.3.2 the cooling load will increase in the humid climates, and the air needs to be reheated due to over chilling. After running the simulation oversized, the chiller's capacity was determined by averaging the values between the 95^{th} and the 100^{th} percentile of the cooling load. The results are shown in Figure 8.42. It is an indication how much larger the chiller has to be to account for additional dehumidification.

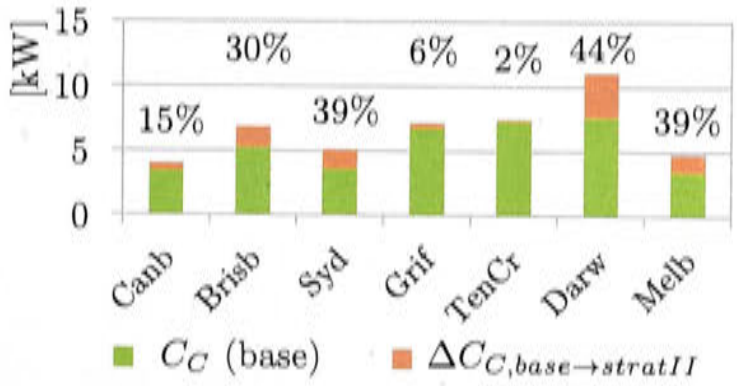

Figure 8.42: Increase in chiller capacity in each climate. Absolute and relative.

The changed control strategy increases the cooling demand especially in the humid climates Brisbane and Darwin. Figure 8.43 shows the increase in sensible and latent cooling compared to the base case (chosen configuration[2]). It also shows the amount of required reheating energy in absolute values and at the percentage of the

[2]The "chosen" collector tank configuration is not used here and instead the largest collector area of 33 m^2

sensible cooling load.

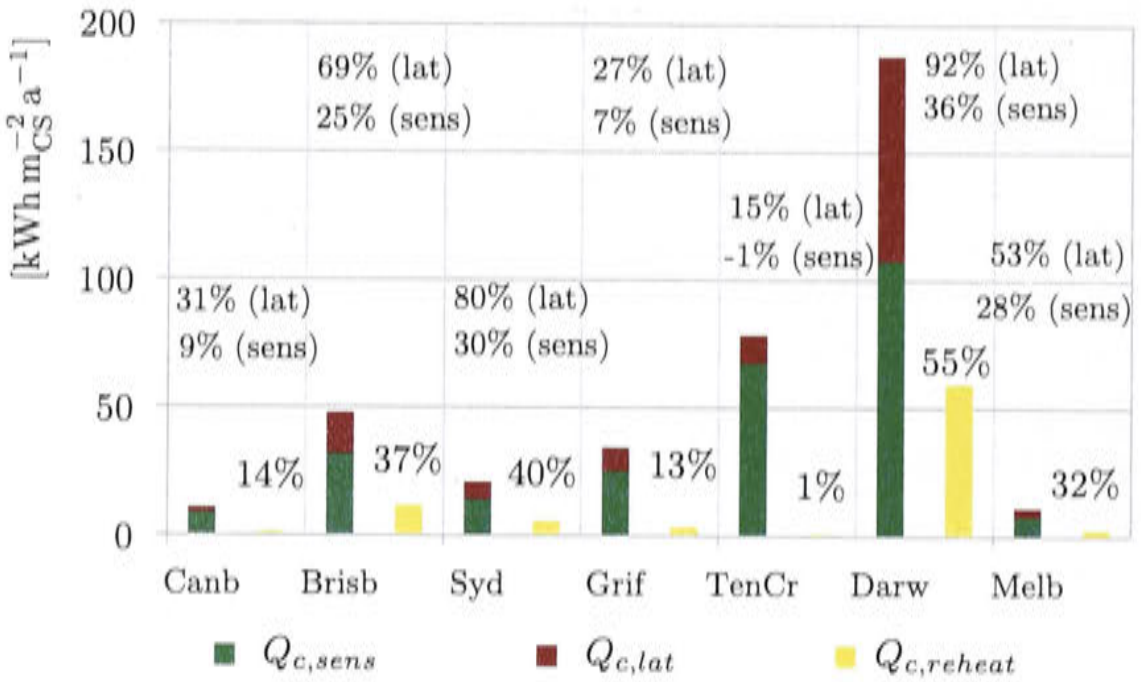

Figure 8.43: Sensible and latent cooling load in absolute and relative terms compared to the base case. Relative changes are in brackets. Energy for reheat absolute and as percentage of sensible cooling load. Energy amounts are specific to the conditioned space (CS).

The control strategies have been varied to achieve higher comfort conditions regarding humidity levels. Figure 8.44 shows by how much this discomfort could be reduced. It also shows in a similar way how often the comfort temperature has been exceeded. This indicator didn't change much, as expected.

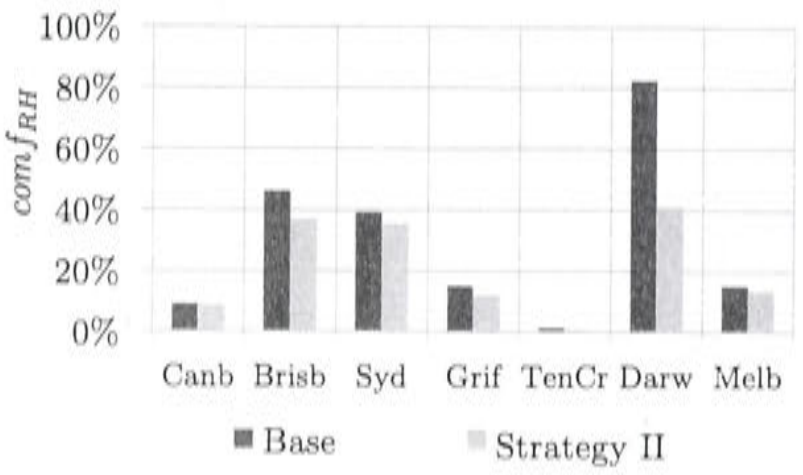

(a) $comf_{RH}$

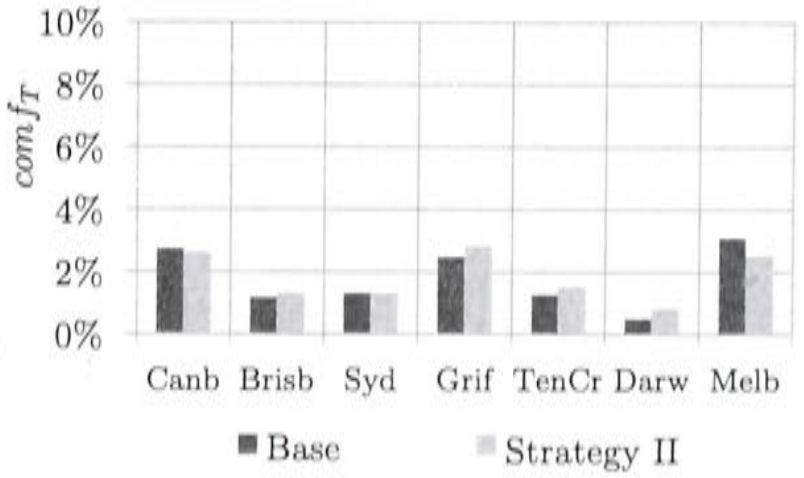

(b) $comf_T$

Figure 8.44: Reduction of humidity discomfort due to strategy II, and discomfort due to indoor temperature

The increase in cooling load can be seen in the fan's operational hours for cooling and heating. The relative change compared to Table 8.7 on page 143 is shown in Table 8.13. The average mass flow rate for cooling can be found in Appendix E.1.

Additional operating hours and increased chiller size lead to an increase in electricity consumption. Figure 8.45 shows the absolute electricity consumption, comparing the base case with strategy II. Furthermore, the figure shows the relative increase and it splits up the total consumption into the individual consumers. The three largest consumers are the cooling towers, the external pumps and the chiller itself.

Table 8.13: Relative change of indoor fan operating hours (strategy II)

	Cooling hours			Heating hours		
	Z1	Z2	Z3	Z1	Z2	Z3
Canb	4.0%	12.2%	-5.3%	0.0%	0.2%	0.0%
Brisb	19.3%	117.4%	36.7%	0.1%	0.0%	0.2%
Syd	22.4%	99.3%	43.9%	0.0%	0.1%	0.3%
Grif	1.8%	28.5%	5.6%	0.1%	0.1%	0.1%
TenCr	-0.8%	-3.3%	-2.9%	1.3%	0.0%	0.0%
Darw	8.5%	223.8%	66.8%	N/A	N/A	N/A
Melb	6.4%	46.4%	16.3%	0.5%	0.3%	0.2%

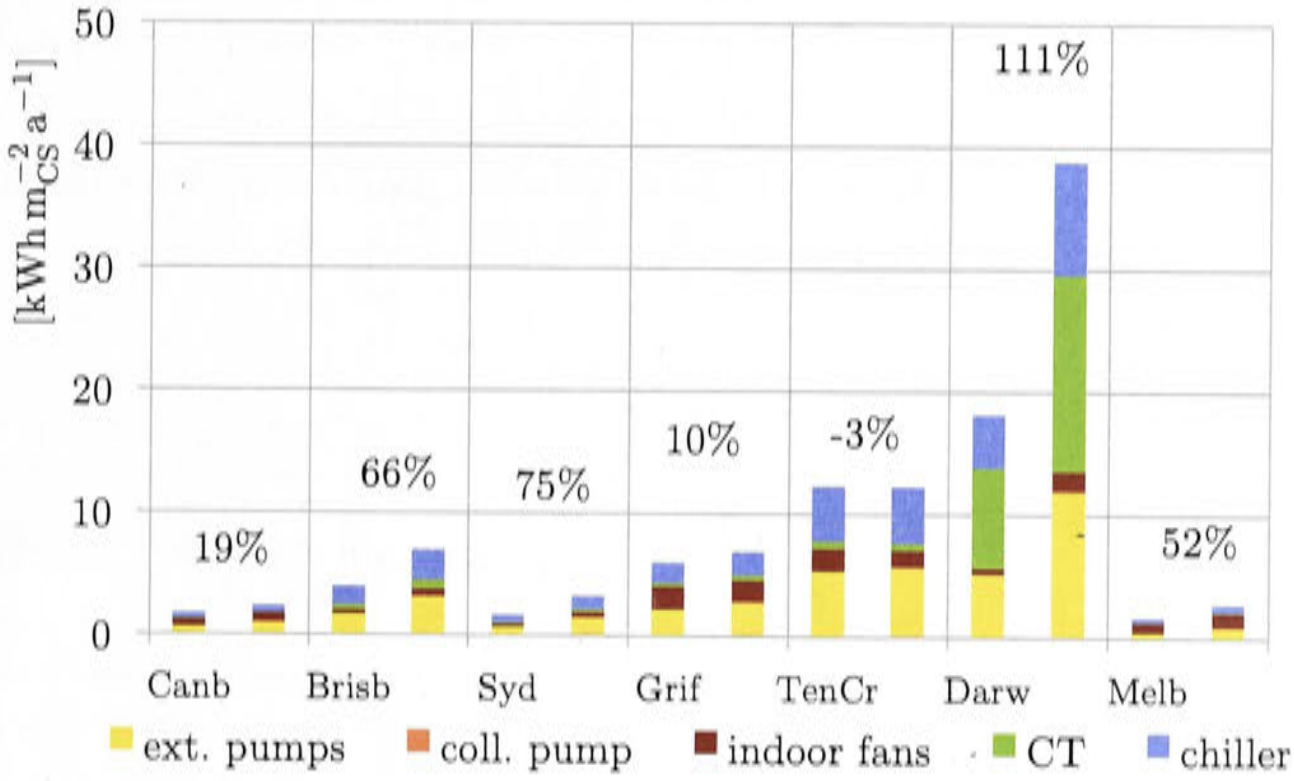

Figure 8.45: Electricity consumption of each individual consumer specific to the conditioned space, and relative change of the total electricity consumption compared to the base case (strategy II)

Finally, the solar fraction is compared to the base case solar fraction with the same tank and collector configuration of 0.75 m^3 and 33 m^2 (Figure 8.46). The heat used for reheating $Q_{c,reheat}$ is included in the solar fraction. The same graphic also includes the relative change in heat relieved from the tank to prevent overheating.

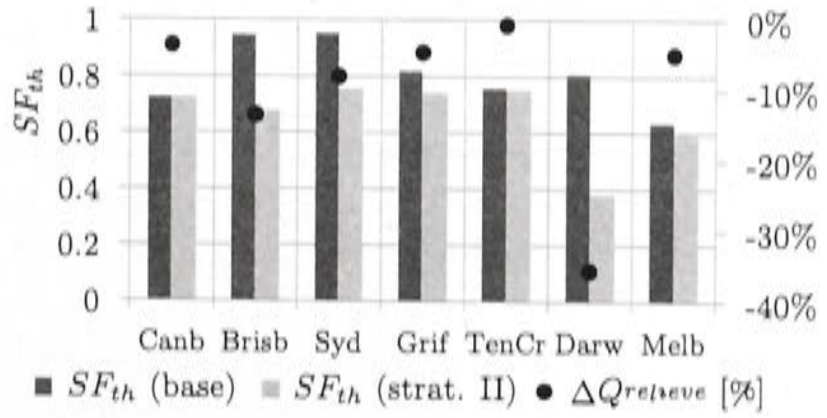

Figure 8.46: Solar fractions comparing base case (and strategy II and the relative reduction in heat relieved by the tank to prevent high pressure

When comparing the cost and greenhouse gas emissions of the increased dehumidification strategy, there is a cost advantage per kWh of cooling and heating, but it

is mainly due to the increased amount of cooling. Since the solar fraction drops, the specific greenhouse gas emissions are larger. Cost and greenhouse gases are compared to the base case with the matching collector and tank configuration (Figure 8.47 and 8.55).

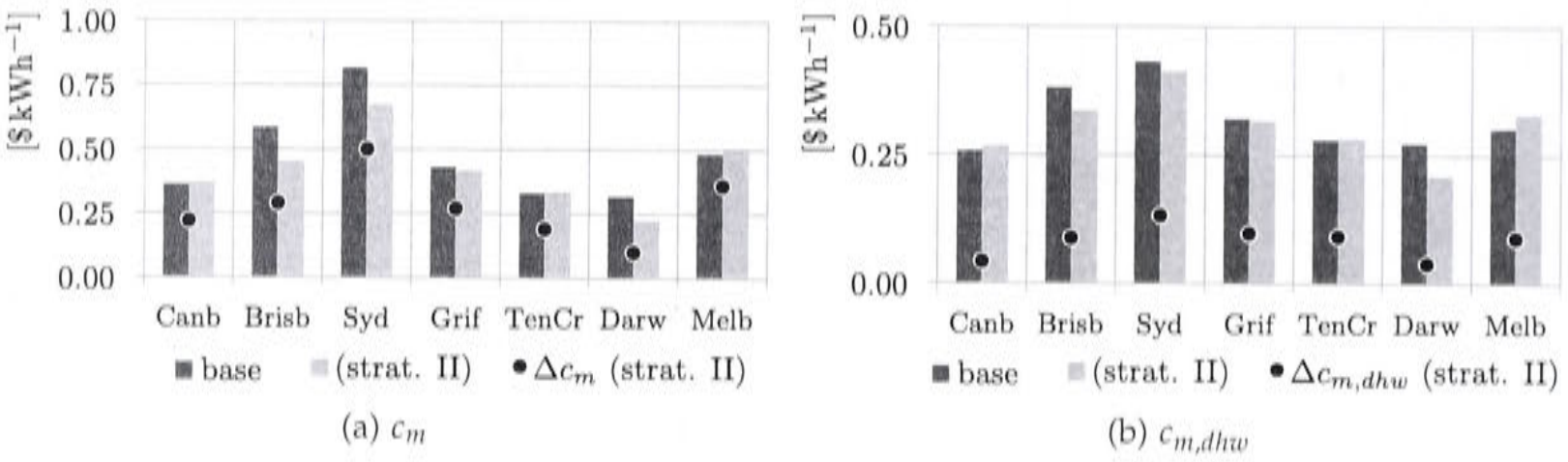

Figure 8.47: Specific cost comparing the base case to dehumidification strategy II. Specific cost difference compared to the reference case $\Delta c_m = c_m - c_{m,ref}$.

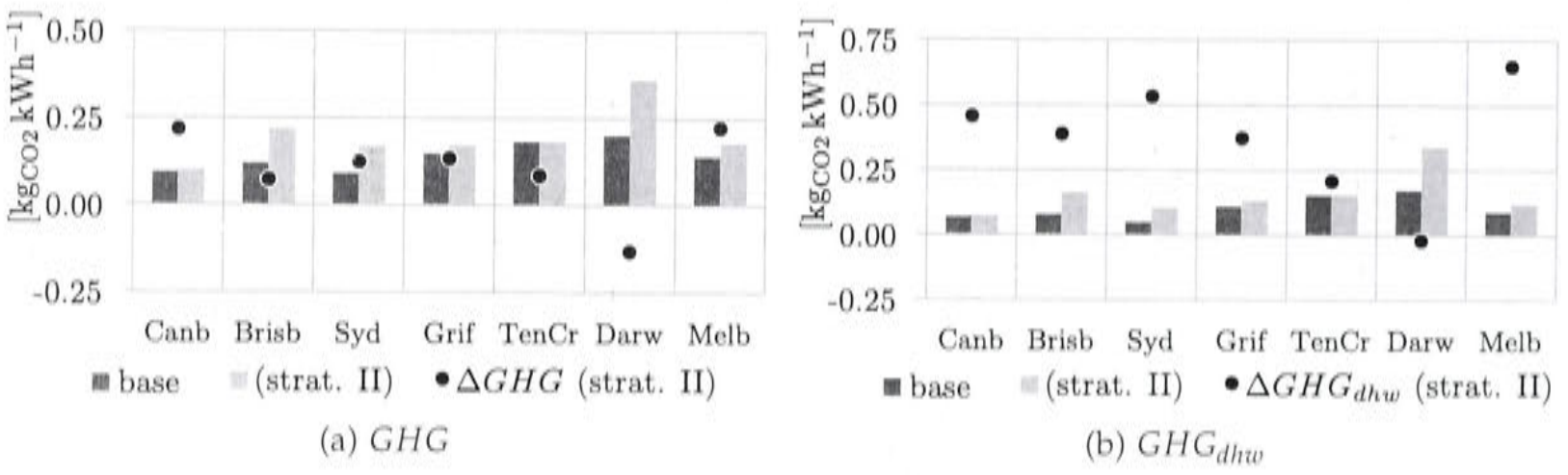

Figure 8.48: Specific greenhouse gas emissions comparing the base case to the dehumidification strategy II. Specific greenhouse gas savings compared to the reference case $\Delta GHG = GHG_{ref} - GHG$.

Strategy III

Dehumidification strategy III goes even further than strategy II. It demands the air-conditioning system also when latent cooling is required exclusively.

When changing the control strategy according to section 7.3.3 the cooling load will increase even more than in the previous section for dehumidification strategy II. The air needs to be reheated due to over chilling but in times when only dehumidification is required the reheating temperature is fixed at 21°C.

Building the average of the values between the 95th and the 100th percentile of the cooling load lead to the cooling capacities represented in Figure 8.49. It is an indication how much larger the chiller has to be to account for the additional dehumidification. The largest capacity increase occurs in Sydney and Melbourne.

The changed control strategy changes the cooling demand especially in the humid climates Brisbane and Darwin. Figure 8.50 shows the increase in sensible and latent cooling compared to the base case. It also shows the amount of reheat in absolute

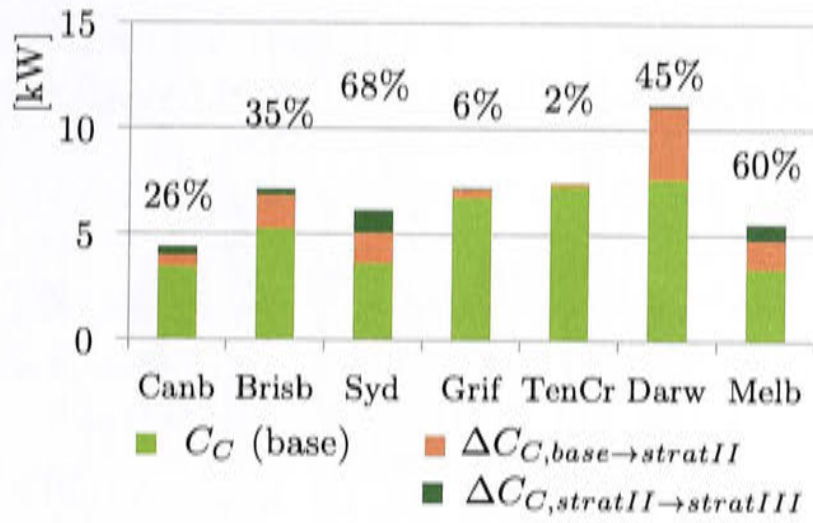

Figure 8.49: Increase in chiller capacity in each climate. Absolute and relative.

values and as a percentage of the sensible cooling load. It is obvious that much more cooling is required to reach the high humidity control criteria.

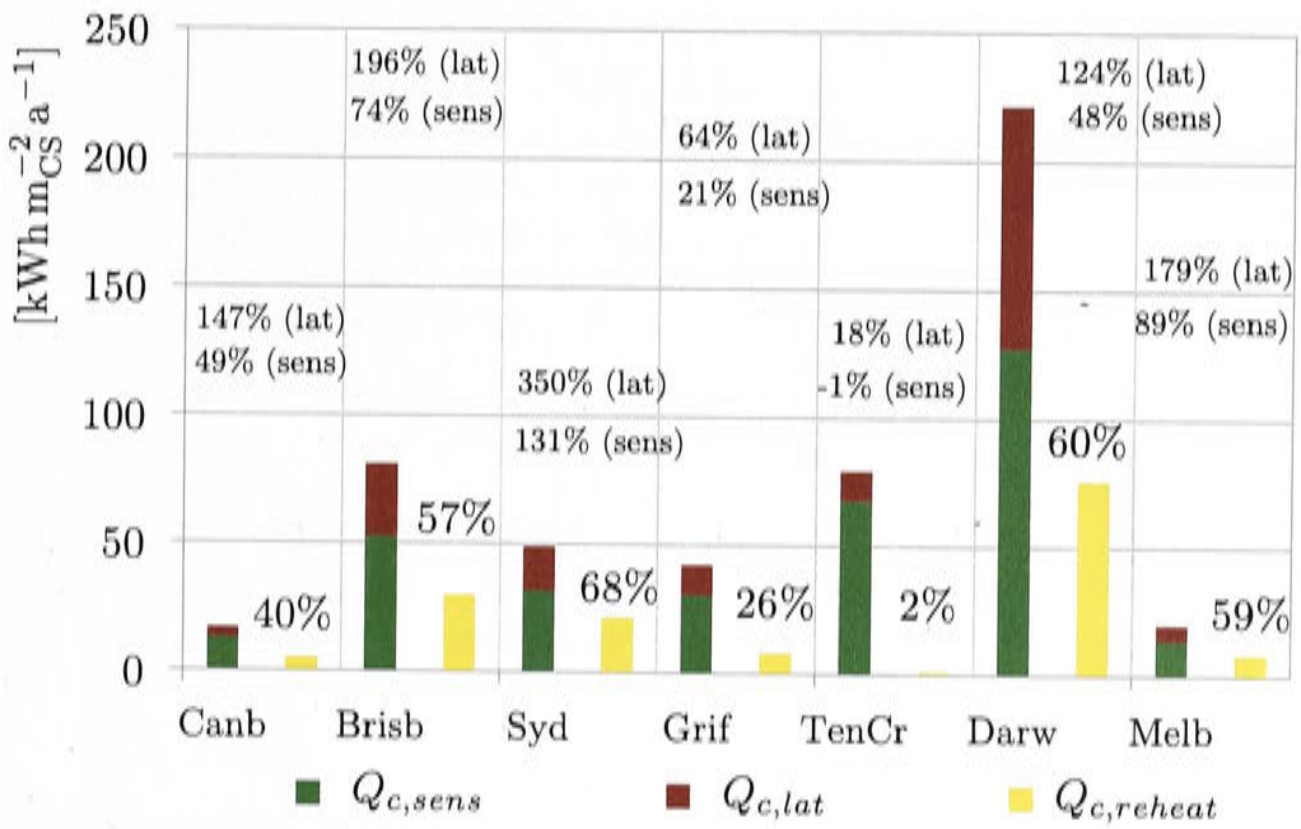

Figure 8.50: Sensible and latent cooling load absolute and relative compared to base case. Energy for reheat absolute and as percentage of sensible cooling load. Energy amounts relative to the conditioned space (CS).

Figure 8.51 shows how much the discomfort due to humidity could be reduced. It also shows in a similar way how often the comfort temperature has been exceeded. The temperature indicator did not change much as expected.

The increase in cooling load also increases the indoor fan operating hours for cooling and heating. The relative change compared to the base case is shown in Table 8.14. The average air mass flow rate for cooling can be found in the Appendix E.2.

Additional operating hours and increased capacity size leads to an increase in electricity consumption. Figure 8.52 shows the absolute electricity consumption, comparing the base case to strategy III. Furthermore, it shows the relative increase and the total consumption of each individual consumers. The three largest con-

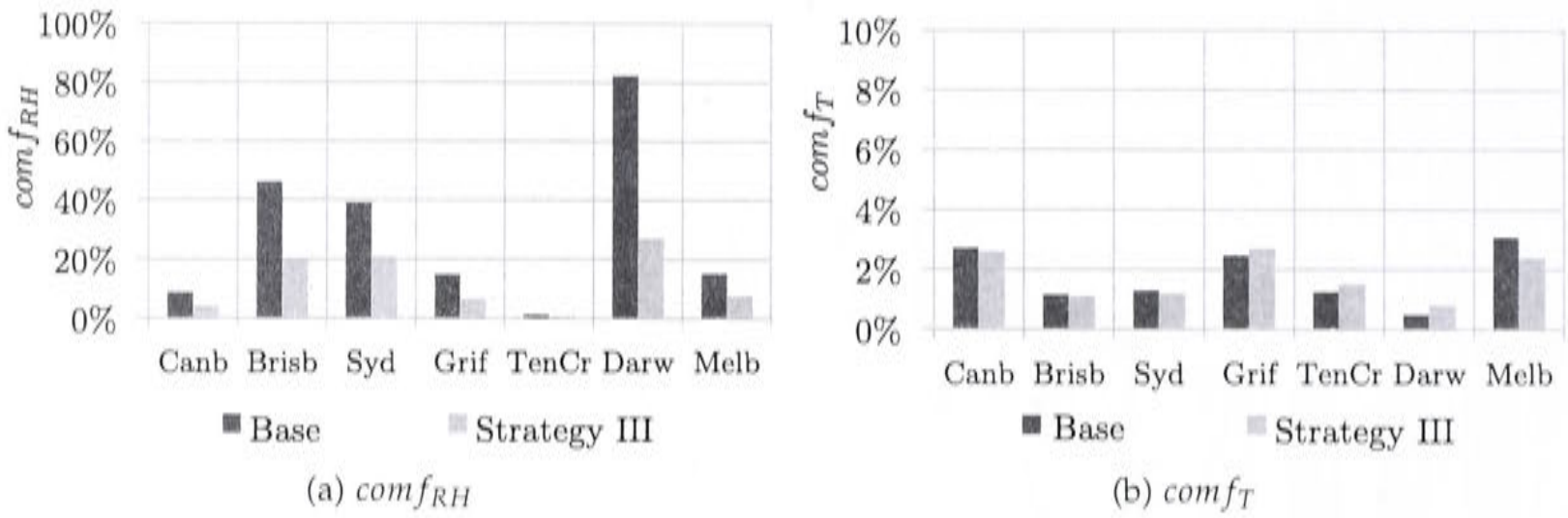

(a) $comf_{RH}$ (b) $comf_T$

Figure 8.51: Reduction of humidity discomfort due to strategy III and discomfort due to indoor temperature.

sumers are the cooling towers, the external pumps and the chiller itself.

Table 8.14: Relative change of indoor fan operating hours (strategy III)

	Cooling hours			Heating hours		
	Z1	Z2	Z3	Z1	Z2	Z3
Canb	35.6%	191.0%	94.8%	-0.3%	-0.6%	0.1%
Brisb	61.9%	788.0%	213.1%	0.0%	-0.2%	0.2%
Syd	89.4%	1591.4%	430.9%	0.1%	0.0%	0.4%
Grif	14.7%	143.6%	54.7%	0.2%	0.1%	0.1%
TenCr	-0.7%	-0.2%	-0.7%	1.3%	0.0%	0.0%
Darw	25.3%	363.8%	125.7%	N/A	N/A	N/A
Melb	55.6%	471.9%	216.1%	0.7%	-0.3%	-0.1%

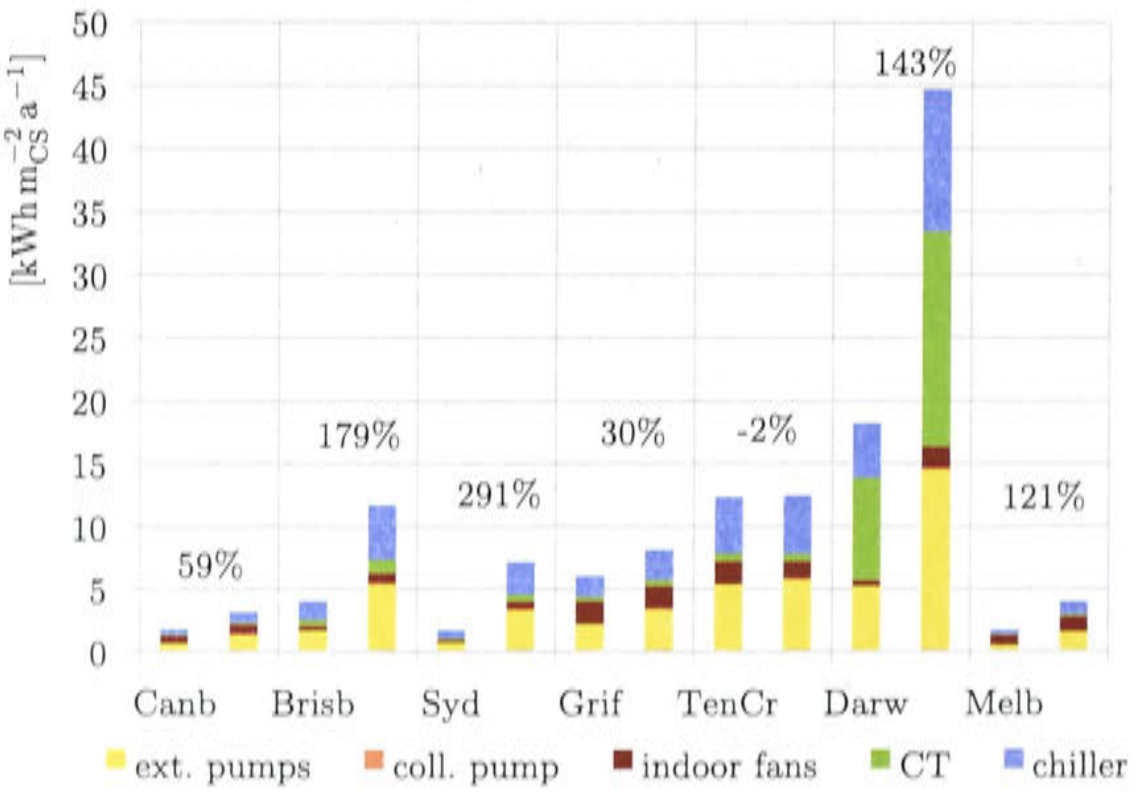

Figure 8.52: Electricity consumption of each individual consumer specific to the conditioned space, and relative change of the total electricity consumption compared to the base case (strategy III).

At last the solar fraction is compared to the base case solar fraction with the same

tank and collector configuration (Figure 8.53). The same graphic also includes the relative change in heat relieved from the tank to prevent overheating.

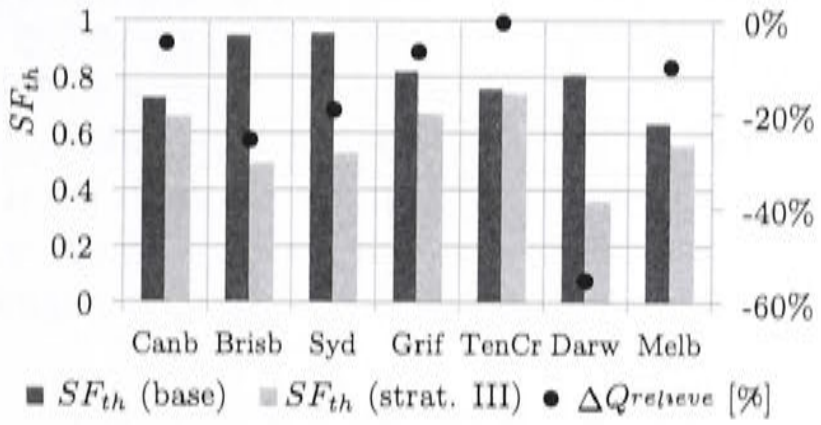

Figure 8.53: Solar fractions comparing base case and strategy III and the relative reduction in heat relieved by the tank to prevent high pressure

Using strategy III the cost advantage per kWh for cooling and heating is increased but the specific greenhouse gas emissions become larger. More cooling is required but the same collectors can't provide more heat (compare Figure 8.54 and 8.55). When comparing the relative greenhouse gas savings compared to the reference case it is important to keep in mind that in the reference case the dehumidification strategy I has been used, without extra humidity removal.

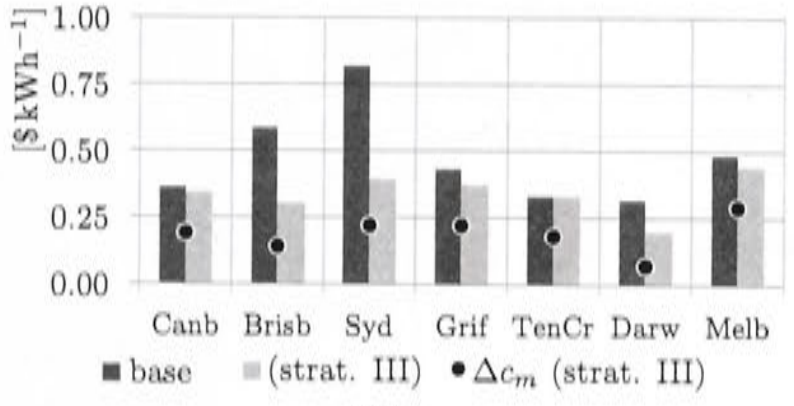

(a) c_m

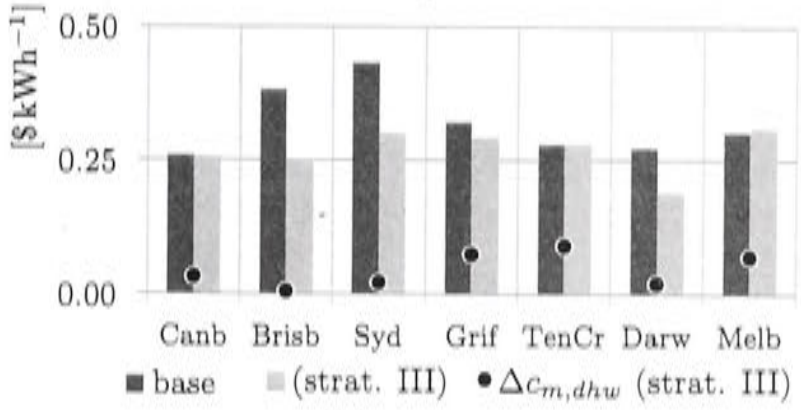

(b) $c_{m,dhw}$

Figure 8.54: Specific cost comparing the base case to dehumidification strategy III. Specific cost difference compared to the reference case $\Delta c_m = c_m - c_{m,ref}$.

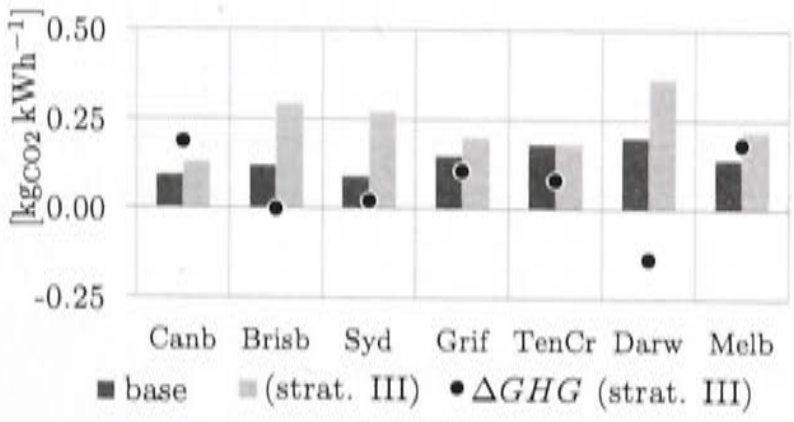

(a) GHG

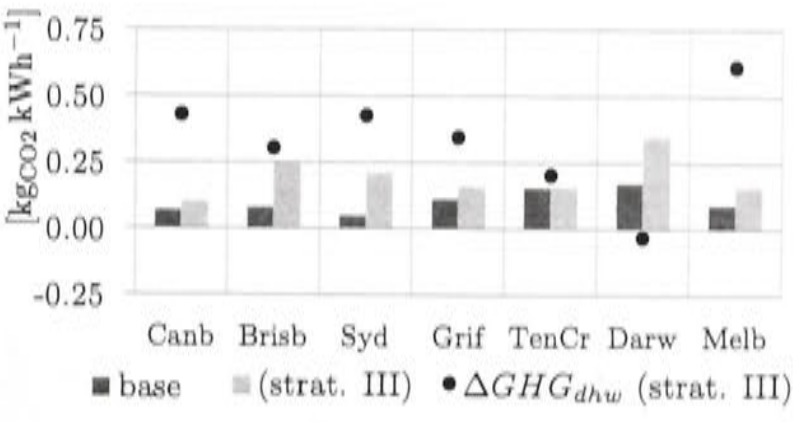

(b) GHG_{dhw}

Figure 8.55: Specific greenhouse gas emissions comparing the base case to the dehumidification strategy III. Specific greenhouse gas savings compared to the reference case $\Delta GHG = GHG_{ref} - GHG$.

Remark *When up sizing the chiller there is a noticeable effect on how often the cooling tower is able to satisfy the set point cooling water inlet temperature to the chiller. The percentage of operating time when the chiller is on and the cooling water temperature exceeds the cooling water set point temperature decreases as the cooling capacity increases (Figure 8.56).*

The minimal indoor fan coil air flow of $200\,\mathrm{kg\,h^{-1}}$ *for heating and cooling is responsible for this. A minimal air flow is required to maintain stability during low load hours, e.g. in the mornings and evenings. Instability is due to the constant chilled water mass flow rate and the minimum hot water inlet temperature of* $59°\mathrm{C}$*. Throughout all simulations it is kept unchanged and as the chiller's capacity increases, the ratio of minimal air flow to chiller capacity becomes smaller.*

The relationship between minimal fan air flow and the percentage of operating time the cooling tower is unable to achieve the required set point temperature became apparent when analyzing the simulation results of the subsequent section 8.2.8. In this section the chiller will be downsized strongly to match a reduced load, however, the minimal air flow remains unchanged. Consequently, the cooling operating hours decreased and the cooling tower is more often unable to provide the desired cooling water temperature.

An explanation may be that the too large minimal air flow cools the building down very fast in low load periods. The slower reaction of the cooling tower leads to an increase in percentage of time the cooling tower can't achieve the set points as the operating hours decrease.

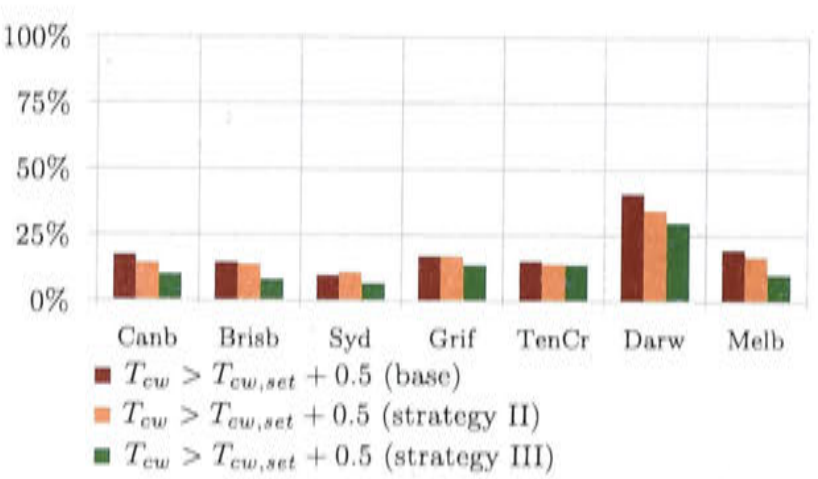

Figure 8.56: Percentage of operating time the cooling water exceeds the set point temperature.

8.2.6 Changing infiltration rates and chilled water and supply air set point temperatures

The infiltration rates of the building will be reduced to 50% of the base case scenario. Furthermore, the chilled water outlet temperature will be set to 11°C and the air flow set point temperature to 16°C.

Scenario (7/12/50): $T_{chw,set} = 7\,°\mathrm{C}$, $T_{set,air,CC} = 12\,°\mathrm{C}$, **Infiltration=50%**

In this scenario neither the set point temperatures for the air exiting the cooling coils nor the chilled water temperature exiting the chiller have been changed compared to the base case. Only the infiltration levels have been halved, which represents 0.4 ACH from March until December and 0.25 ACH from December until February.

Reducing the infiltration levels had a large effect on the heating load of the building as can be seen in Figure 8.57. The heating load nearly halved in every climate[3]. The total cooling was reduced in the very hot climates and in the humid climates of Griffith, Tennant Creek, Darwin and Brisbane. The rather mild climates like Canberra, Melbourne and Sydney actually increased their (rather low) cooling load, which is a sign of the infiltration actually serving partially as ventilation, reducing the cooling load.

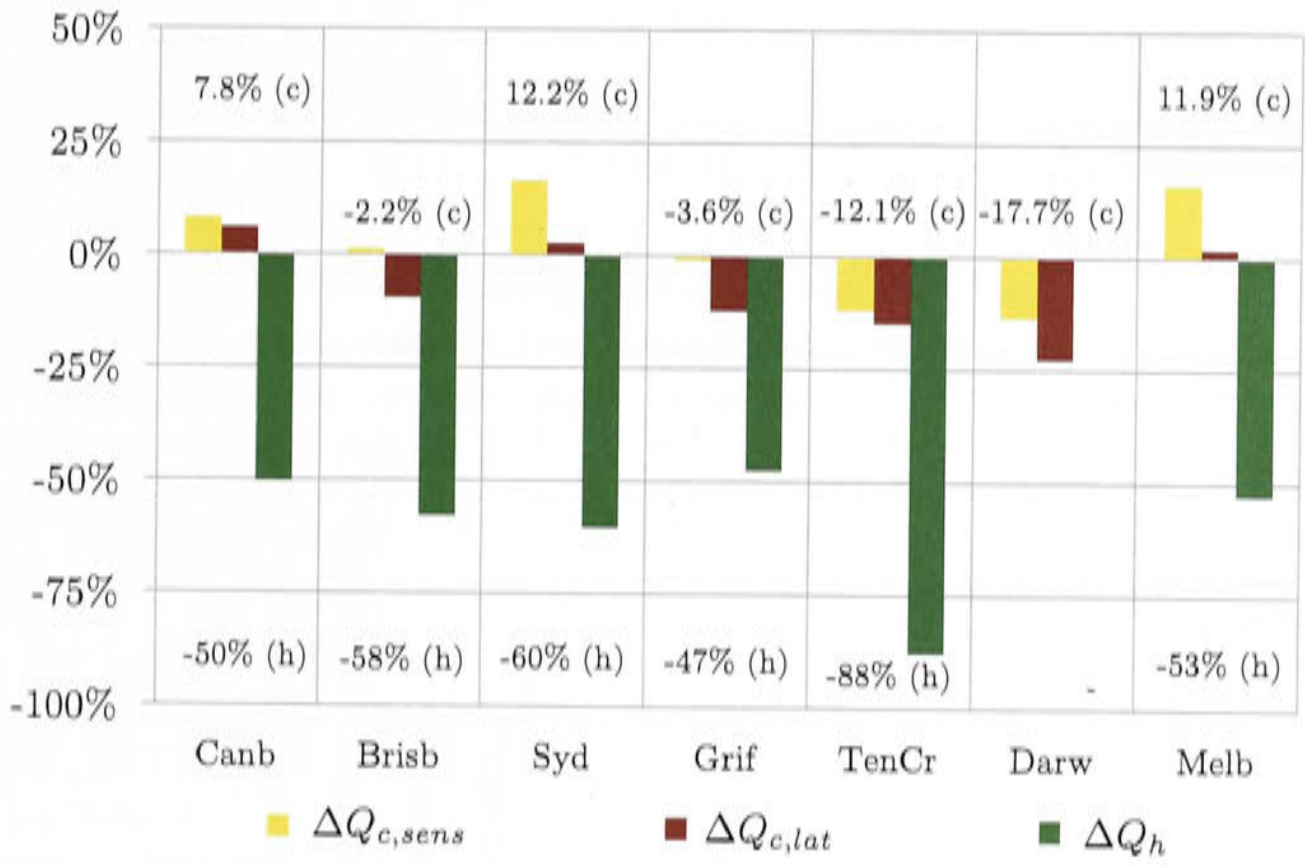

Figure 8.57: Relative change of total cooling (c) and heating (h) supply compared to the base case.

Figure 8.58 shows the total cooling and heating loads normalized by the conditioned space.

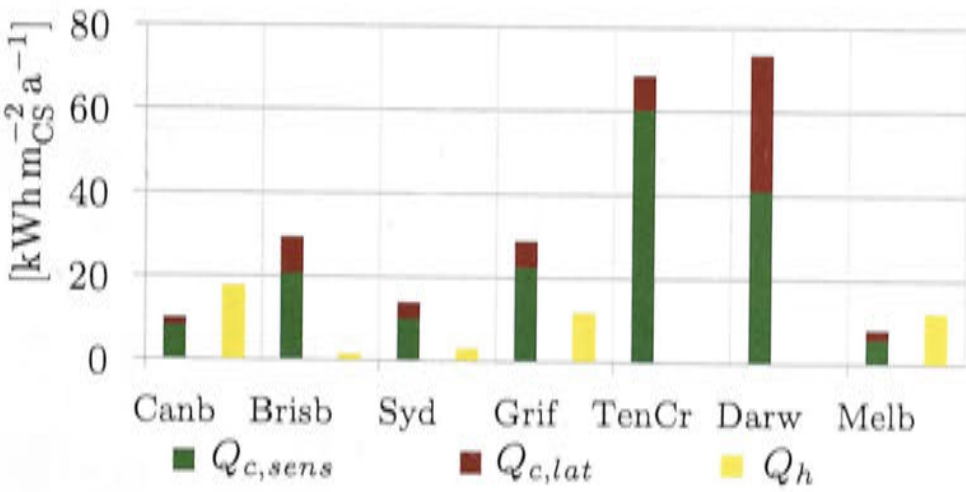

Figure 8.58: Cooling and heating load specific to the conditioned space (CS)

[3]In Darwin there is no heating load and in Tennant Creek the heating load is very small.

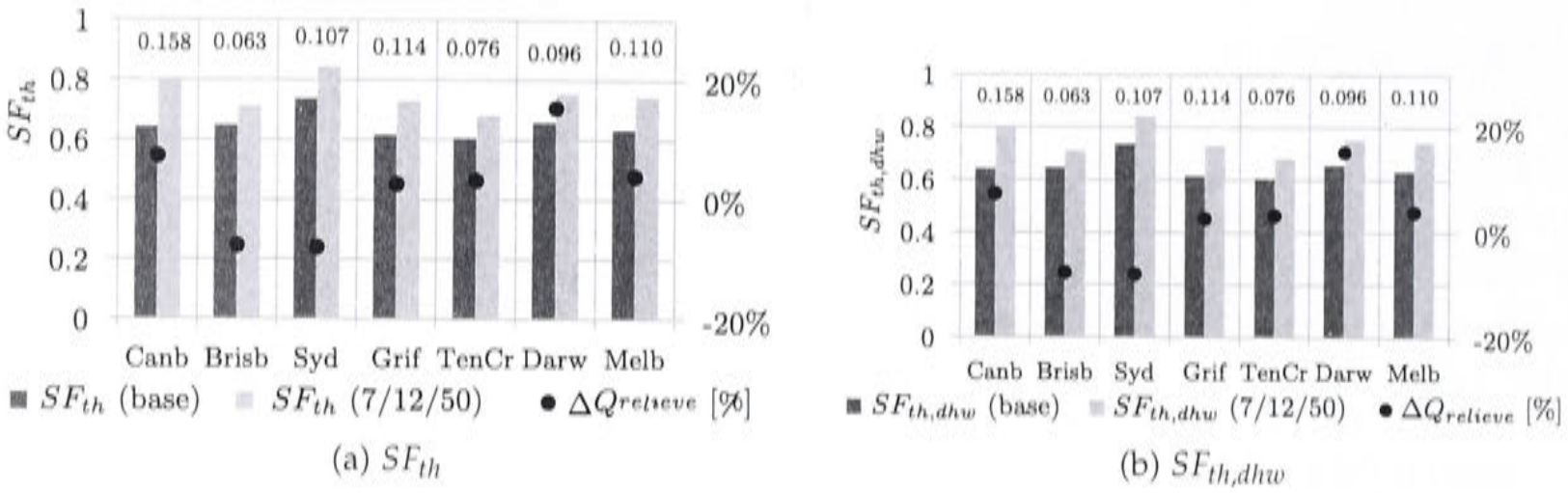

(a) SF_{th} (b) $SF_{th,dhw}$

Figure 8.59: Solar fraction with reduced infiltration levels compared to the base case. Relative amount of heat relieved.

Due to the strongly reduced heating load, the solar fraction increases (Figure 8.59) by 6% to 16% points throughout the climates and the electricity consumption drops due to reduced fan operating hours (Figure 8.60).

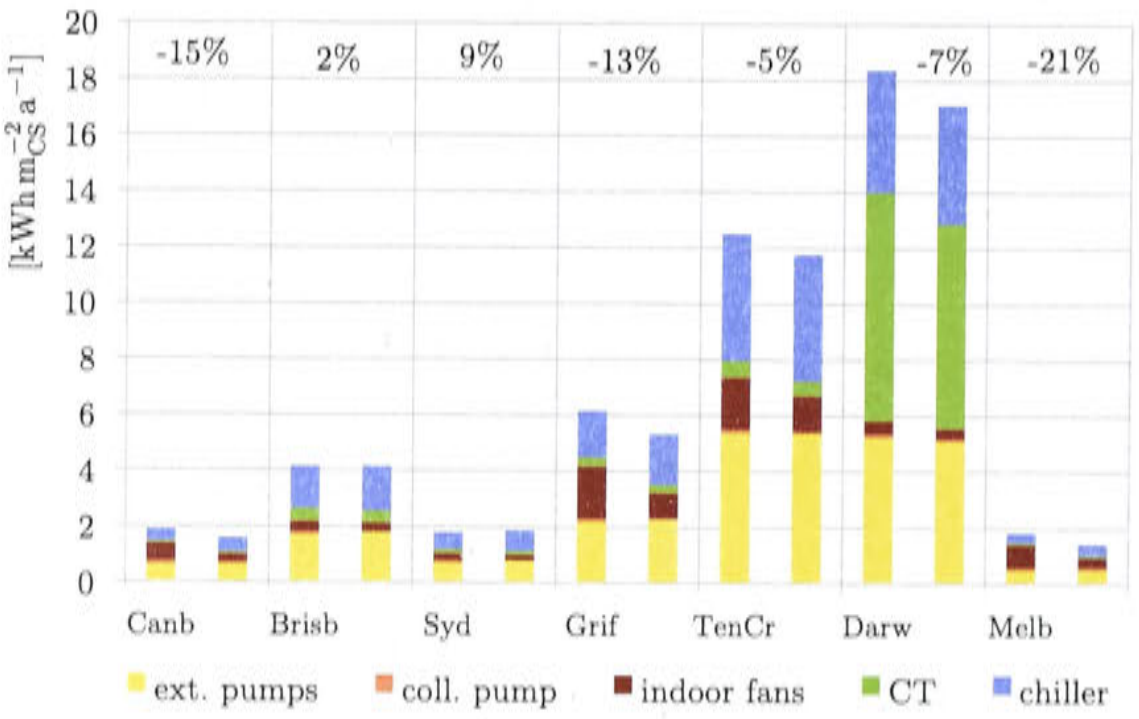

Figure 8.60: Electricity consumption of each individual consumer specific to the conditioned space, and relative change of the total electricity consumption compared to the base case (7/12/50)

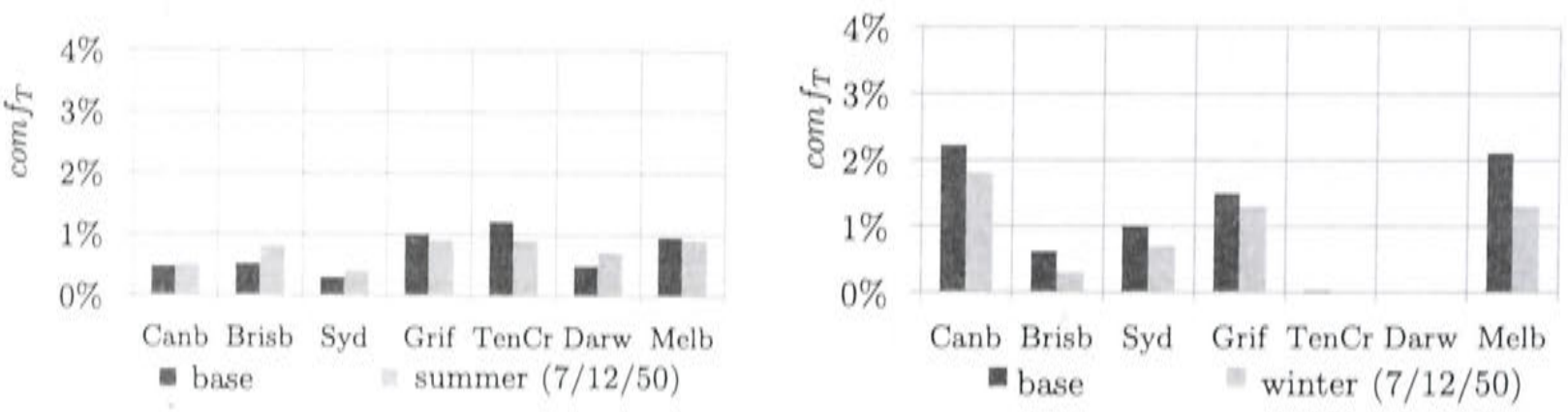

(a) $comf_T$ summer (b) $comf_T$ winter

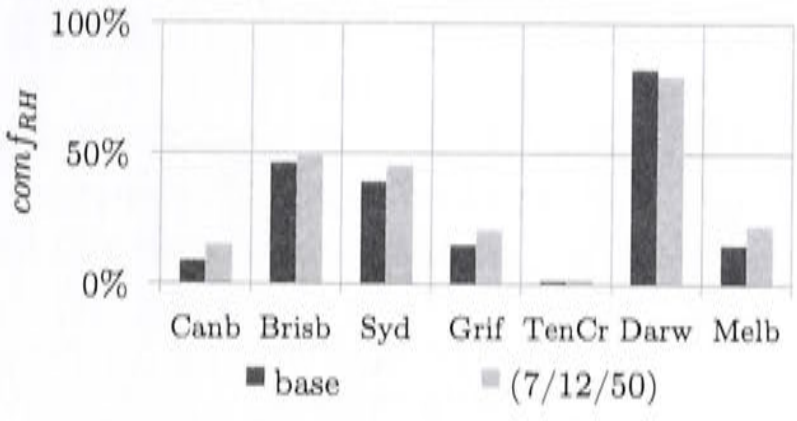

(c) $com f_{RH}$

Figure 8.61: Change of comfort condition in summer and winter.

The temperature comfort conditions in winter correlate to the heating energy supplied to the building. The winter temperature comfort is more often met compared to the base case. The humidity comfort worsens in all climates besides Darwin, indicating that in Darwin the outdoor humidity is the main driver entering the building to increase humidity discomfort and not internal loads.

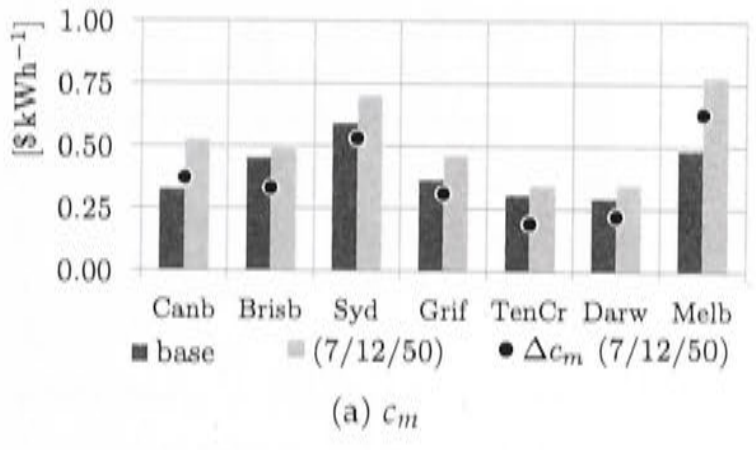

(a) c_m

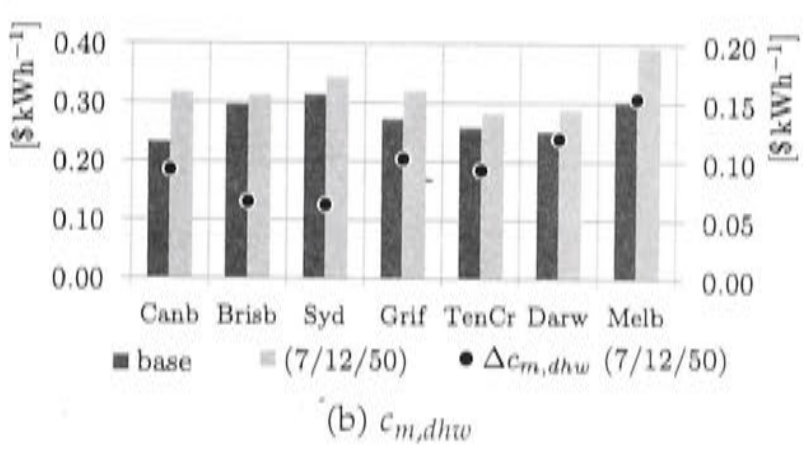

(b) $c_{m,dhw}$

Figure 8.62: Specific cost comparing the base case to (7/12/50). Specific cost difference compared to the reference case $\Delta c_m = c_m - c_{m,ref}$ (on right axis if included).

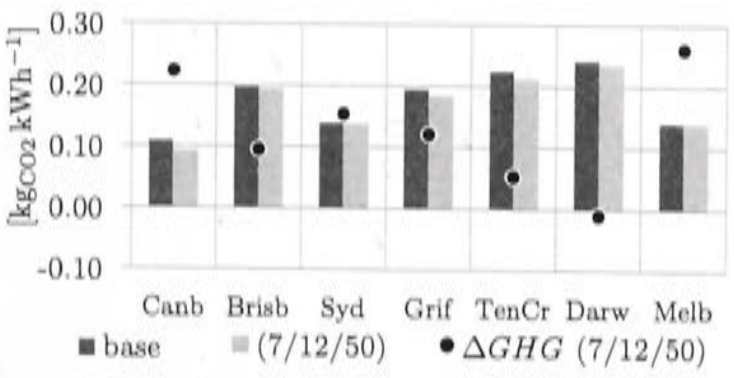

(a) GHG

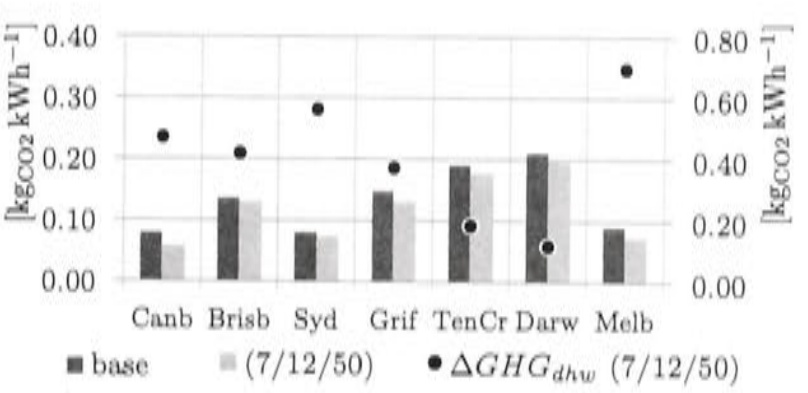

(b) GHG_{dhw}

Figure 8.63: Specific greenhouse gas emission comparing the base case to (7/12/50). Specific greenhouse gas savings compared to the reference case $\Delta GHG = GHG_{ref} - GHG$ (on right axis if included).

Scenario (11/16/100): $T_{chw,set} = 11\,^{\circ}\text{C}$, $T_{set,air,CC} = 16\,^{\circ}\text{C}$, **Infiltration=100%**

In this scenario the set point temperature for the air exiting the cooling coil has been raised from 12°C to 16°C and the chilled water exiting the chiller has been raised

from 7°C to 11°C, compared to the base case. The infiltration rates have been kept at 100% of the base case settings.

Increasing the chilled water outlet set point temperature lowers the potential for latent cooling and the latent heat removal drops. Percentage wise it drops most in climates with low humidity loads. The absolute terms are shown in Table 8.15.

Table 8.15: Absolute change in removed latent heat specific to the conditioned space in kWh m_{CS}^{-2} a^{-1}, comparing (11/16/100) to the base case ($Q_{c,lat}(base) - Q_{c,lat}$).

	Canb	Brisb	Syd	Grif	TenCr	Darw	Melb
$\Delta Q_{c,lat}$	1.07	2.64	1.33	3.08	6.18	1.53	0.82

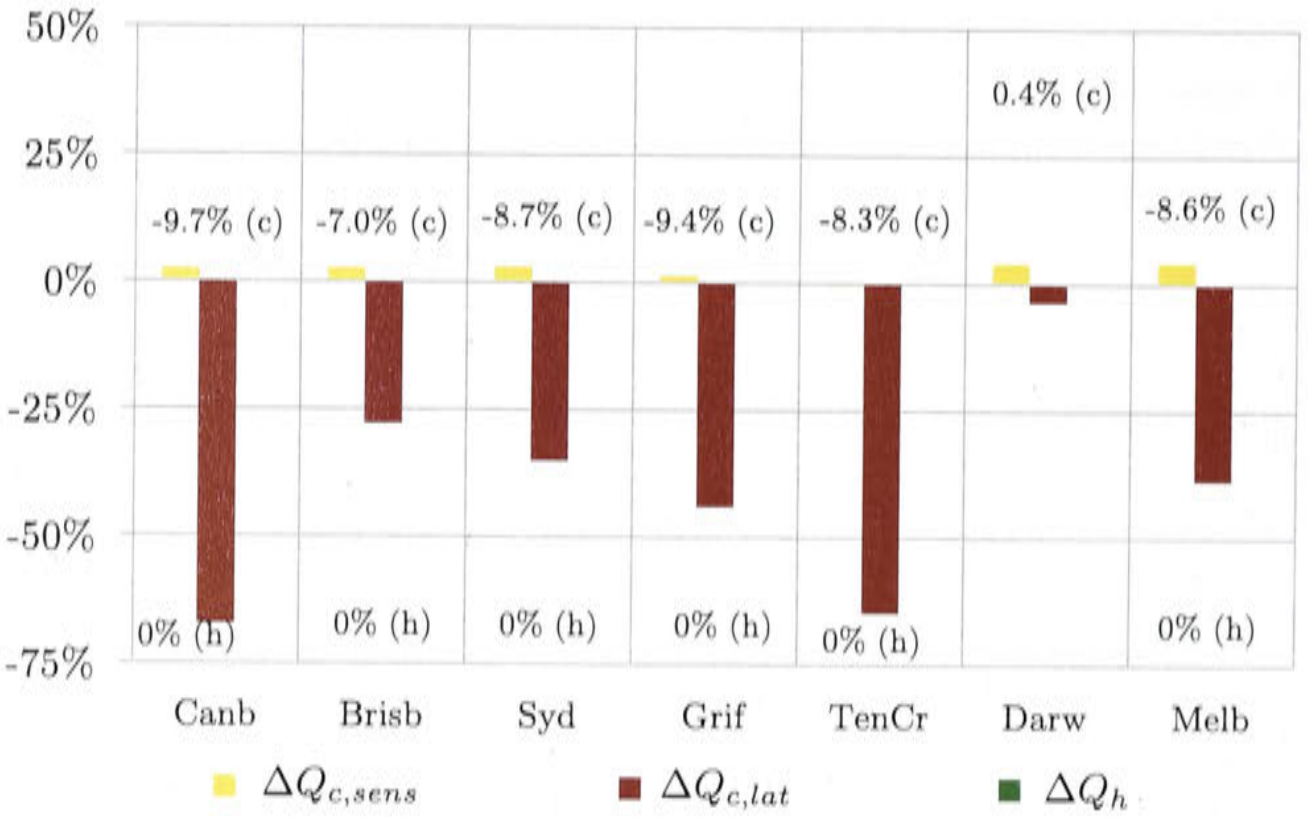

Figure 8.64: Relative change of total cooling (c) and heating (h), comparing case (11/16/100) to the base case.

Figure 8.65 shows the total cooling and heating loads normalized by the conditioned space.

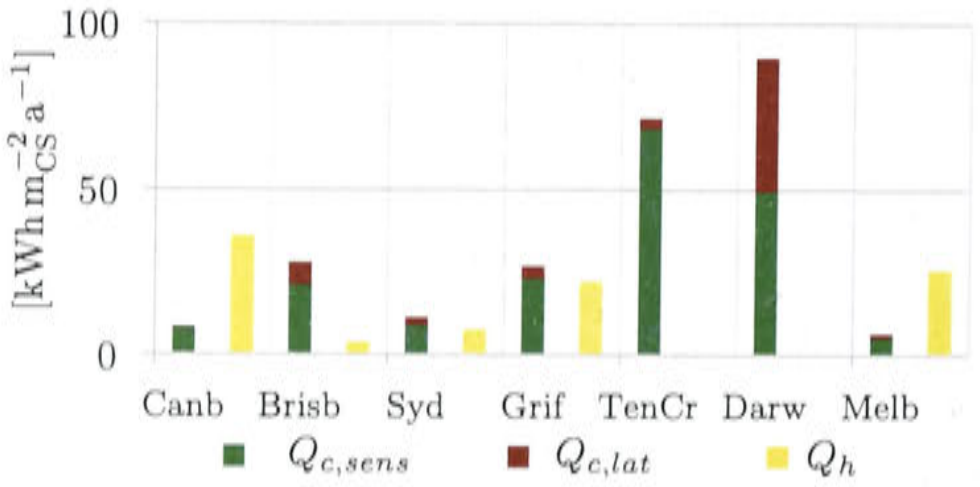

Figure 8.65: Cooling and heating load specific to the conditioned space (CS)

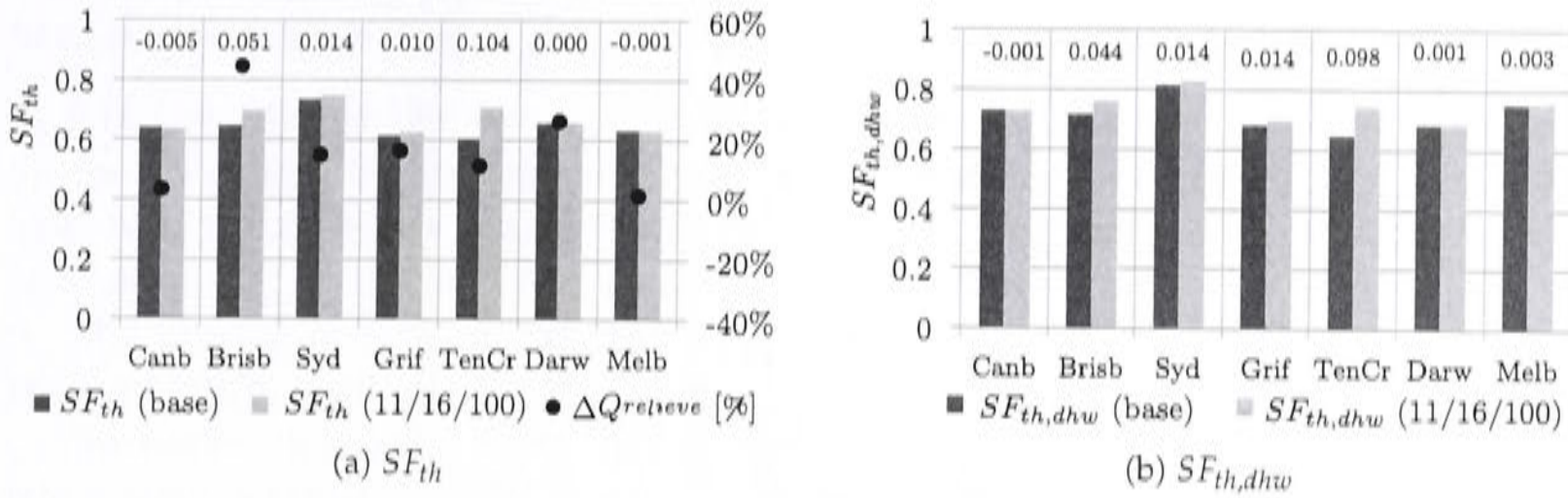

Figure 8.66: Solar fraction with reduced infiltration levels compared to the base case. Relative amount of heat relieved.

Increasing the chilled water set point temperature at the chiller leads to a lower hot water temperature required by the chiller. In all climates besides Darwin less cooling is generated, hence more heat is being relieved from the hot water tank. The heating energy supply does not change, as expected.

Increasing the air set point temperature requires a larger air flow following equation 7.22 as can be seen in Figure 8.67, hence, the fan electricity consumption increases. Even though less cooling is generated, the power consumption increases, which is due to the indoor fans (except in Darwin where the cooling energy provided increases slightly). The average air flow seems to increase strongest in the living area zone 1 and least strong in the bedrooms (zone 2) (Melbourne is an exception). Zone 2 on the other hand has the strongest increase in fan operational hours. The reason is related to the minimal air flow rate, which does not change throughout the simulations. The minimum air flow rate is most often in operation in zone 2 and 3 at night times. In the base simulation with lower air outlet set point temperatures, the minimum flow rate was more often in operation, because the calculation for the required air flow in equation 7.22 would have yielded more often a smaller value and therefore the desired cooling was provided much quicker.

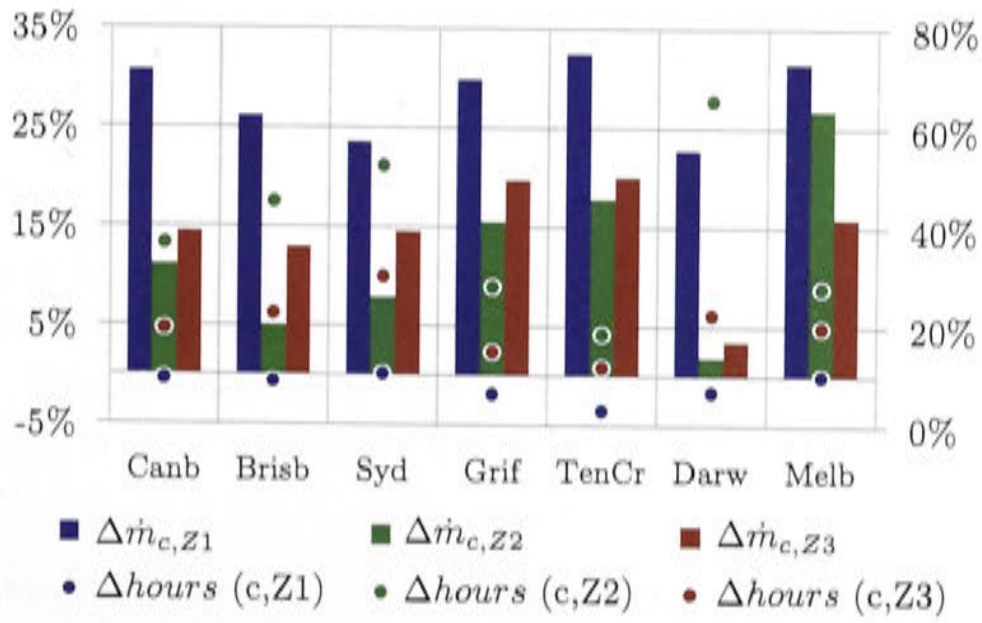

Figure 8.67: Relative change of the average air flow in each zone in cooling mode (left). Relative change of fan operating hours in cooling mode (right).

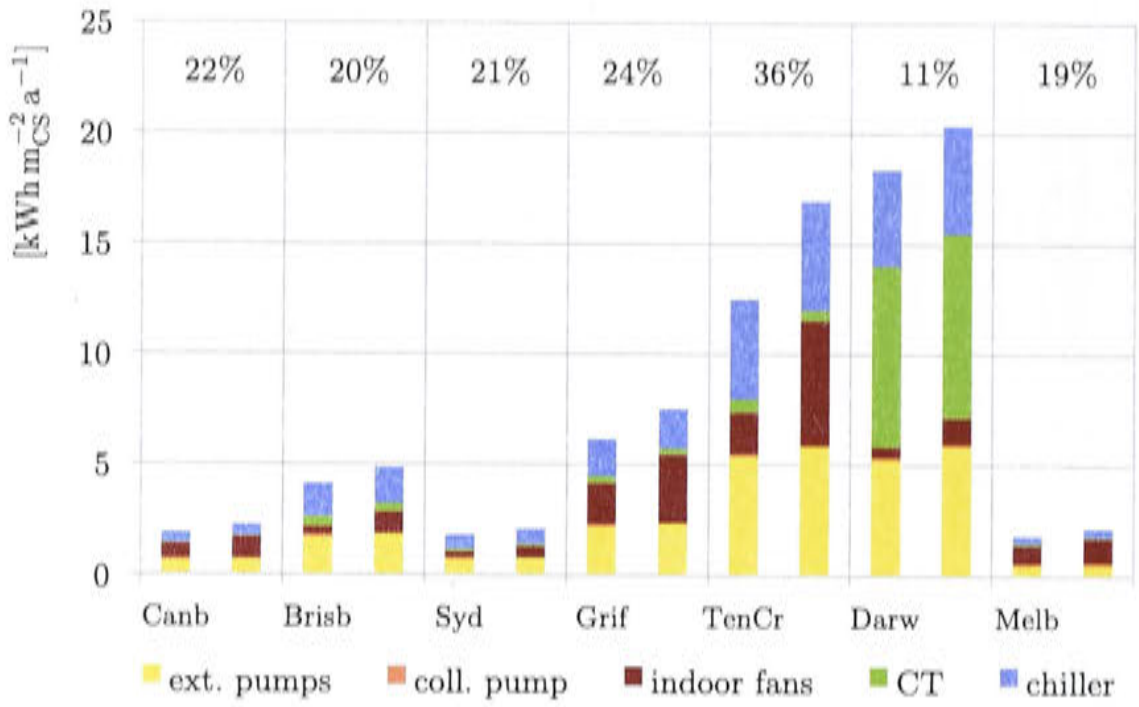

Figure 8.68: Electricity consumption of each individual consumer specific to the conditioned space, and relative change of the total electricity consumption compared to the base case (11/16/100).

The change of the comfort conditions are shown in Figure 8.69. Since the heating energy supply doesn't change at all, the comfort in winter stays constant. The humidity discomfort increases in every climate zone, since less humidity is being removed from the air. The temperature discomfort drops in every climate besides Darwin. This might be related to the in general larger air flows and the smoother on/off behavior[4].

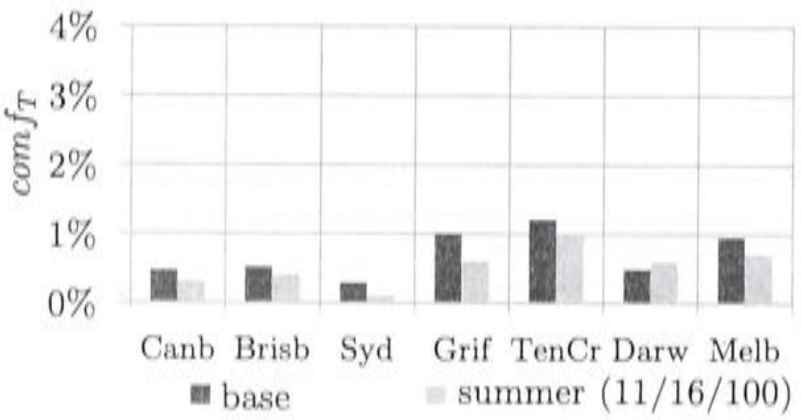

(a) $comf_T$ summer

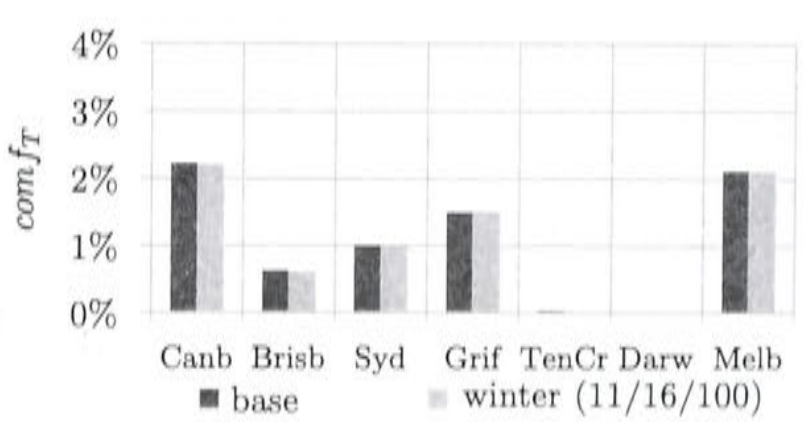

(b) $comf_T$ winter

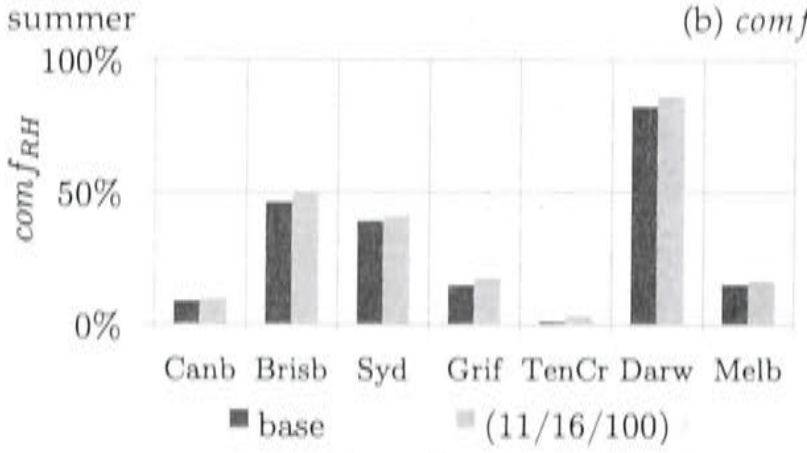

(c) $comf_{RH}$

Figure 8.69: Change of comfort condition in summer and winter.

[4]It occurs less frequently, that the calculated air flow is smaller than the minimum air flow

Scenario (11/16/50): $T_{chw,set} = 11\,°C$, $T_{set,air,CC} = 16\,°C$, **Infiltration=50%**

In this scenario the last two variations are combined. The set point temperatures for the air exiting the cooling coils and the chilled water set point exiting the chiller have been increased to 16°C and 11°C respectively. The infiltration rates have been lowered to 50% of the base case levels.

The change in heating demand in winter drops strongly, which is due to the reduced infiltration.

Increasing the chilled water outlet set point temperature lowers the potential for latent cooling and the latent heat removal drops. This mechanism is the reason for the drop in latent cooling supplied to the building in climates with low humidity loads. In climates with high humidity loads on the other hand (e.g. Darwin and Brisbane), the lowered infiltration levels are the main reason for the reduction of latent cooling supplied. In Table 8.16 the absolute values for the change of sensible heat and latent heat removal compared to the base case are shown.

The difference in latent and sensible heat removal of the two cases (11/16/100) with 100% infiltration and (11/16/50) with 50% infiltration is presented in the two graphs of Figure 8.70. The values in the graphic represent a "double" difference, because they are the difference of the deviations from the base case and each of the two scenarios. The difference between latent and sensible heat removal compared to the base case is outlined in Table 8.16. Figure 8.72 shows the total cooling and heating loads normalized by the conditioned space.

Table 8.16: Absolute change in removed latent and sensible heat specific to the conditioned space in $kWh\,m_{CS}^{-2}\,a^{-1}$, comparing (11/16/50) to the base case ($\Delta Q_{c,lat/sens} = Q_{c,lat/sens}(base) - Q_{c,lat/sens}$).

	Canb	Brisb	Syd	Grif	TenCr	Darw	Melb
$\Delta Q_{c,lat}$	1.03	3.29	1.27	3.57	6.63	10.22	0.85
$\Delta Q_{c,sens}$	-0.73	-0.70	-1.67	0.03	8.22	4.30	-0.96

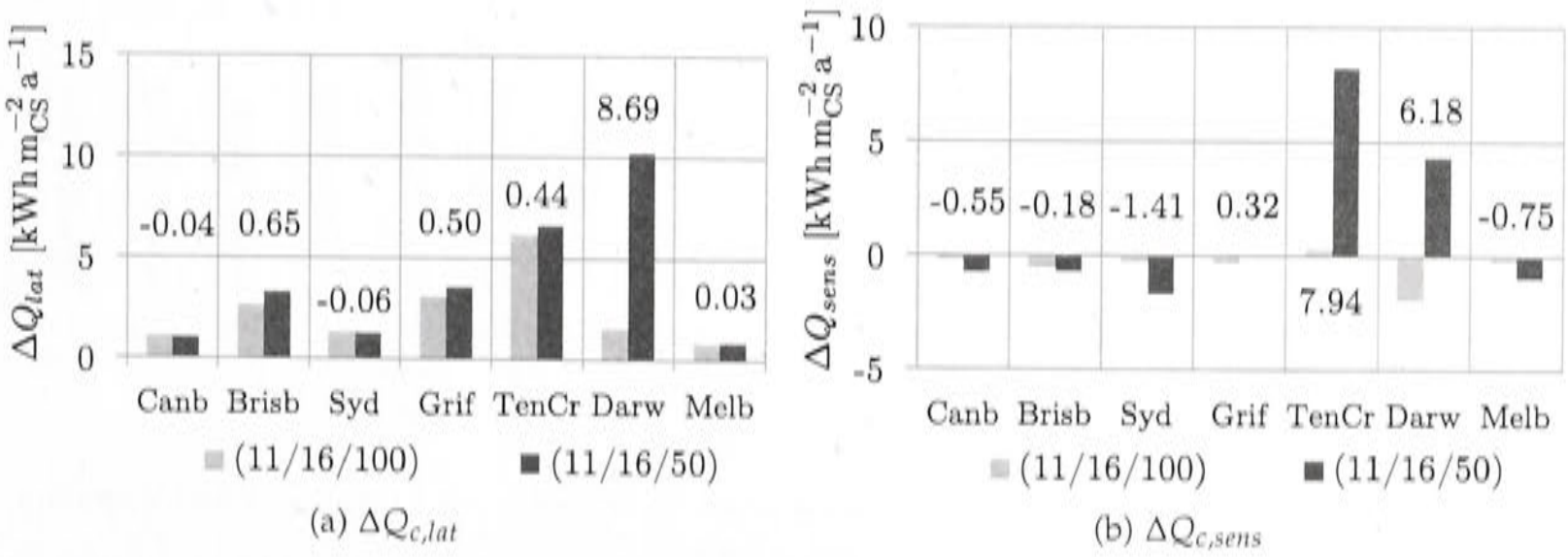

(a) $\Delta Q_{c,lat}$ (b) $\Delta Q_{c,sens}$

Figure 8.70: Change of latent and sensible heat removal relative to the base case, comparing (11/16/100) to (11/16/50). The values on chart represent the differences.

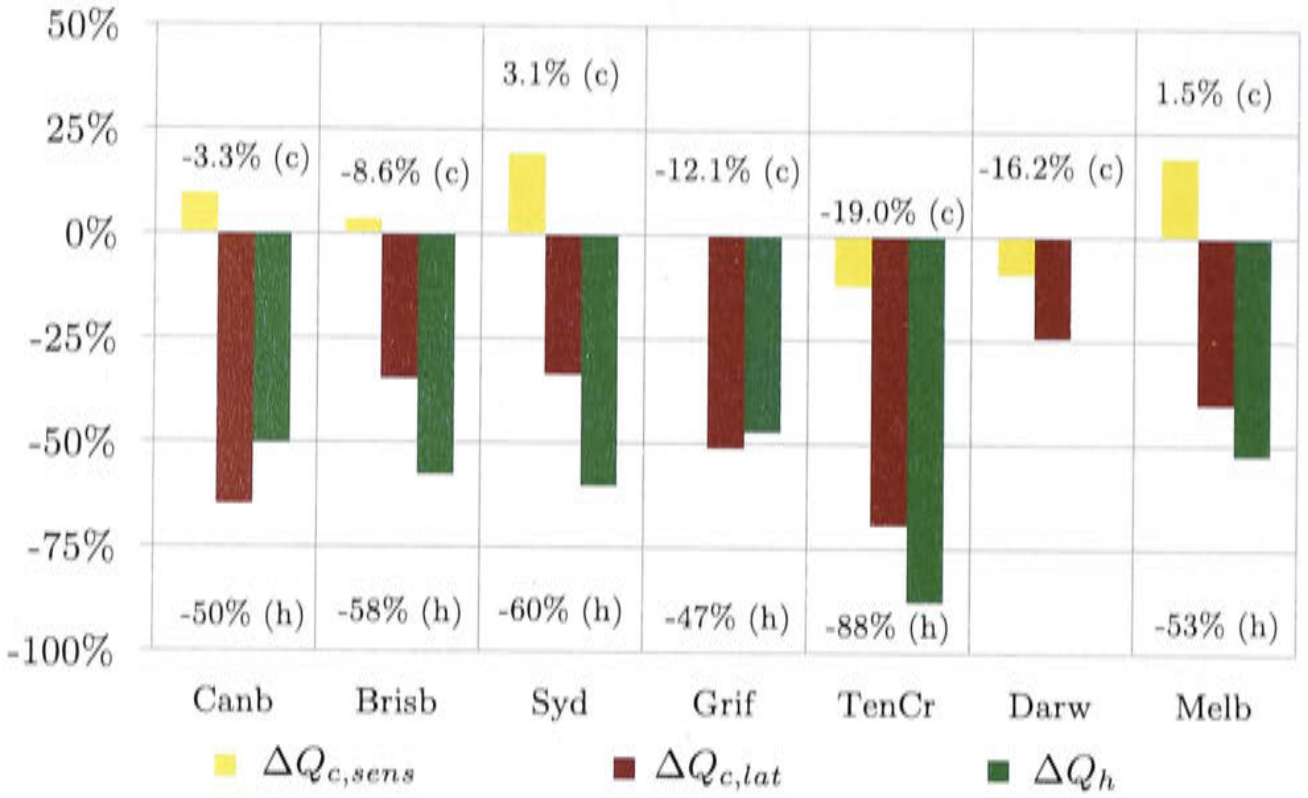

Figure 8.71: Relative change of total cooling (c) and heating (h) demand, comparing case (11/16/50) to the base case.

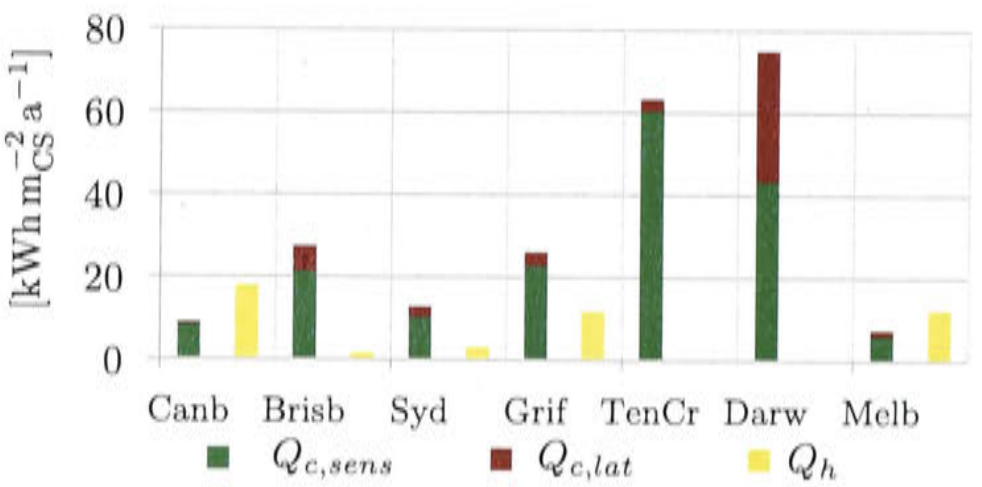

Figure 8.72: Cooling and heating load normalized by the area of the conditioned space (CS)

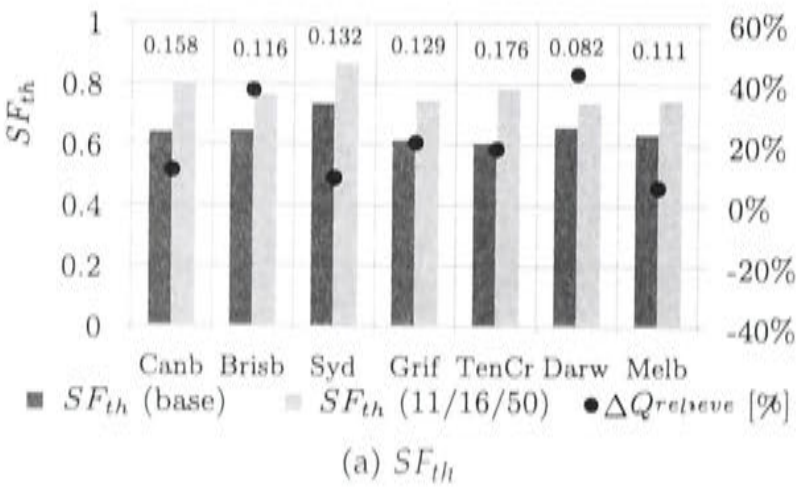

(a) SF_{th}

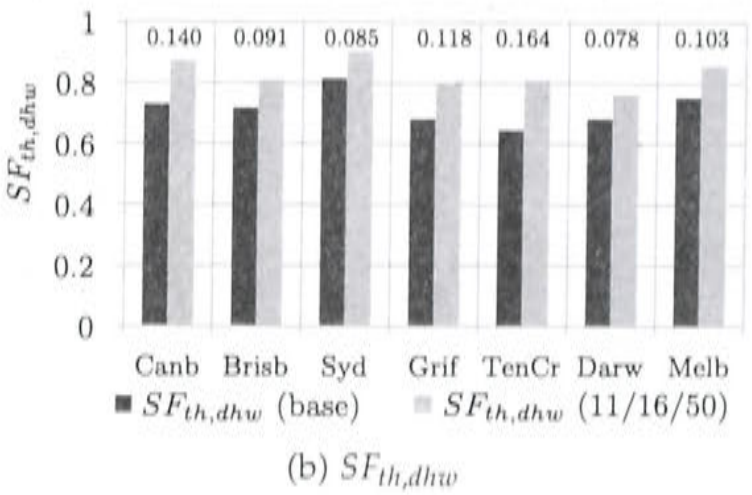

(b) $SF_{th,dhw}$

Figure 8.73: Solar fraction with reduced infiltration levels compared to the base case. Relative amount of heat relieved.

Increasing the chilled water set point temperature at the chiller leads to a lower hot water temperature required by the chiller. The solar fraction increases. It also increases, because less heating in winter is required due to the lower infiltration levels.

Melbourne and Sydney are the only climates where the cooling demand increases. It dropped in all other climates, hence more heat is being relieved from the hot water tank. Therefore, decreasing cooling and heating leads to an increase in relieved energy.

As in the previous section, increasing the air set point temperature requires a larger air flow as can be seen in Figure 8.74, hence the fan electricity consumption increases. However, since the fan electricity consumption in winter is reduced strongly, the overall increase in electricity consumption is smaller than in case (11/16/100).

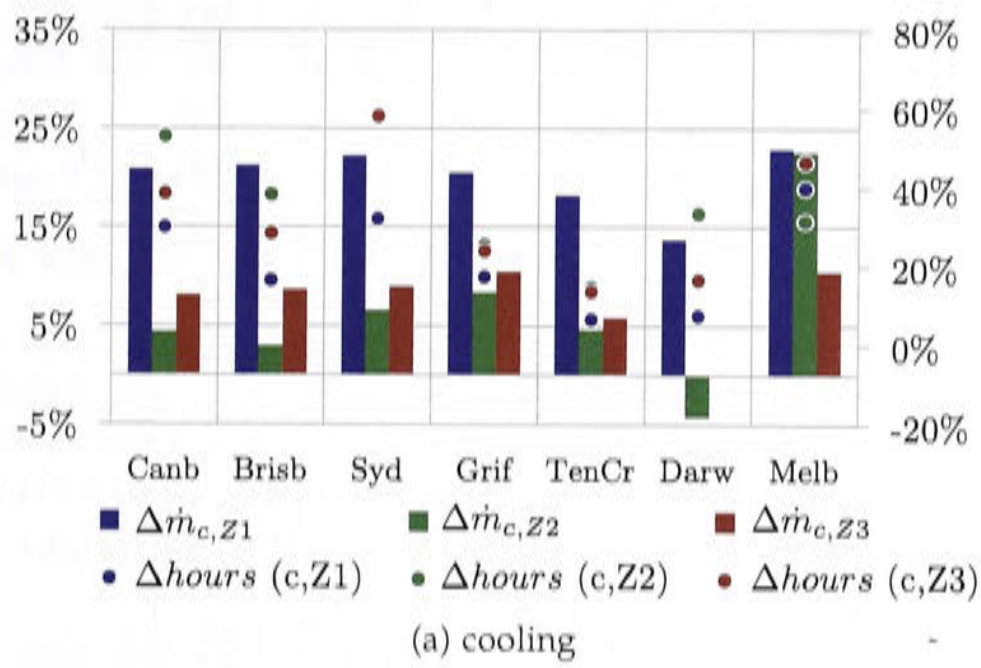

(a) cooling

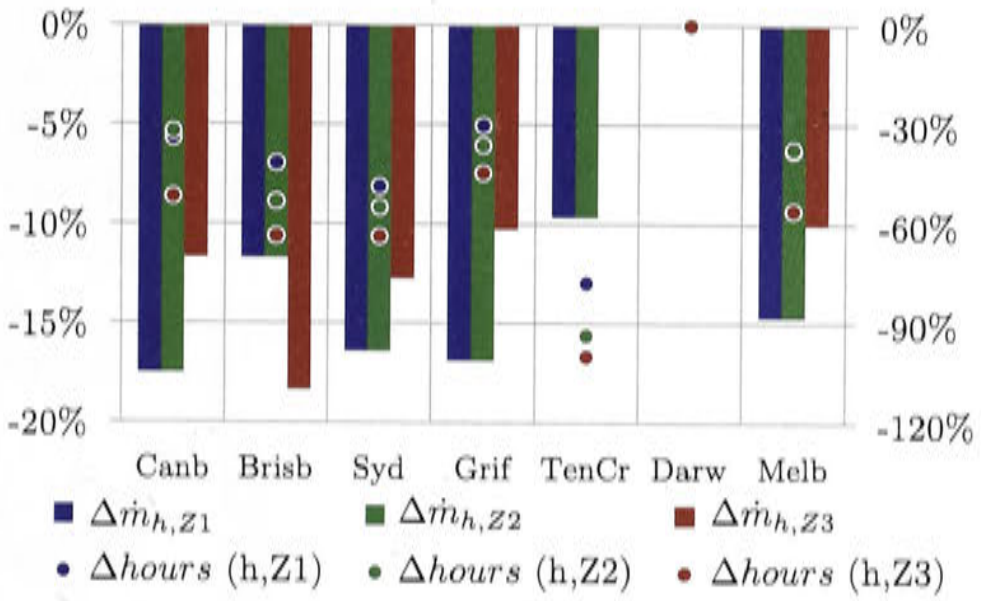

(b) heating

Figure 8.74: Relative change of the average air flow in each zone (left axis). Relative change of fan operating hours in each zone (right axis).

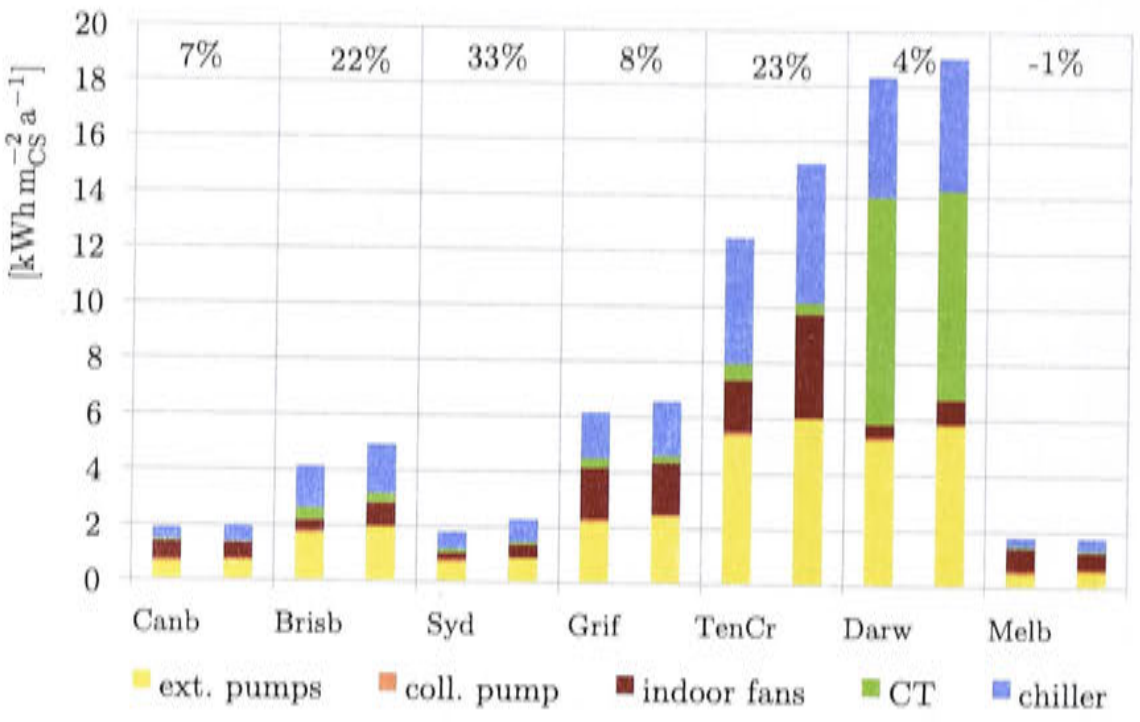

Figure 8.75: Change in electricity consumption in respect to the conditioned space (CS). Left: base case, right: (11/16/50).

The change of the comfort conditions are shown in Figure 8.76. The temperature comfort improves, but the humidity discomfort increases in every climate zone, since less humidity can be removed from the air and the infiltration does not supply sufficient ventilation in all climates besides Darwin.

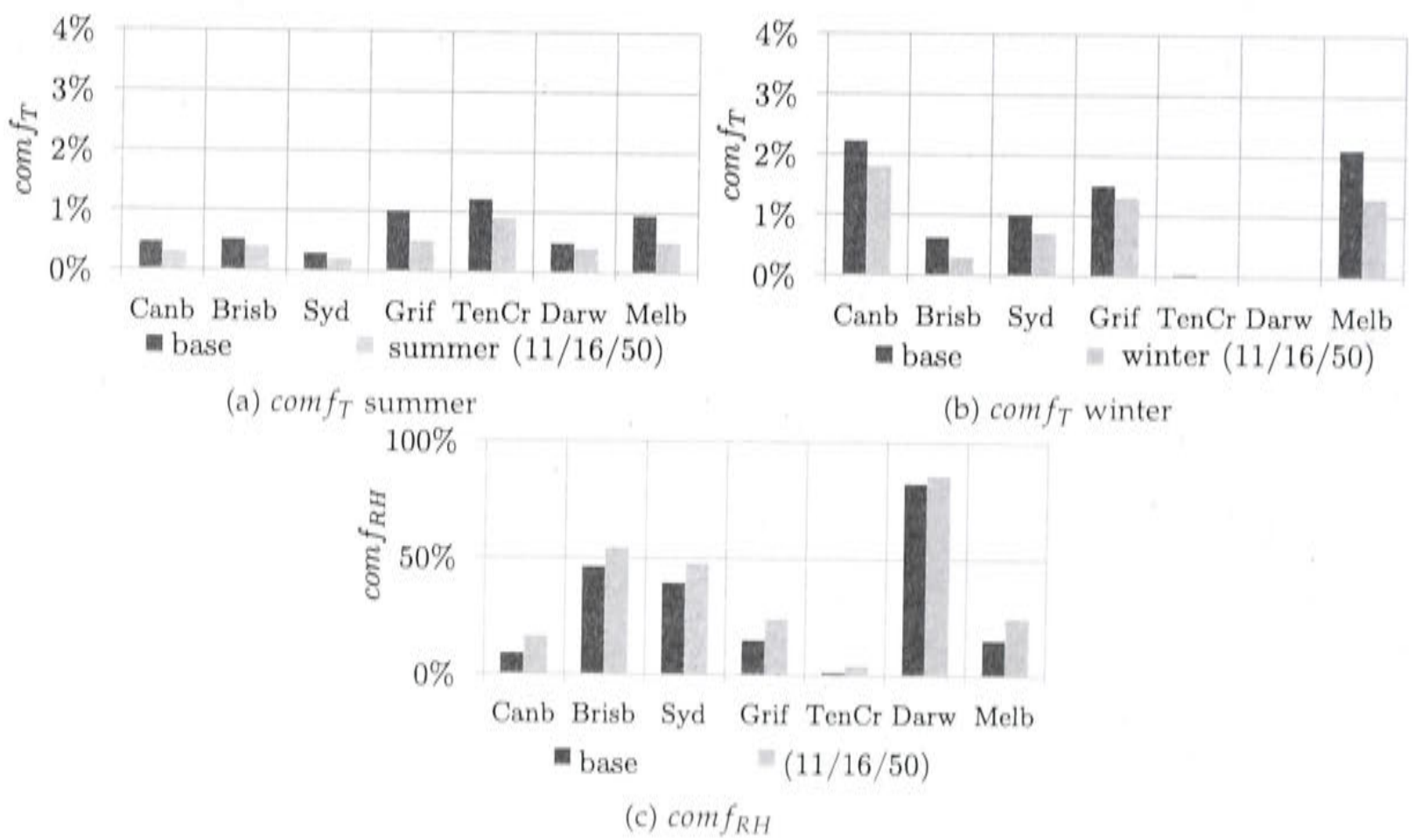

Figure 8.76: Change of comfort condition in summer and winter.

The specific cost and greenhouse gas emissions will be summarized for the cases (11/16/100) and (11/16/50) in one graph (Figure 8.77 and 8.78). The specific cost increases when increasing the set point temperatures. The reason may be due to the increased fan electricity consumption. Surprisingly, when reducing the cooling

and heating load by reducing the infiltration levels, the specific cost increases even further. This is due to the annual cost of the cooling and heating system changing less than the strong drop in useful energy demand for heating. The specific greenhouse gas emissions stay rather stable.

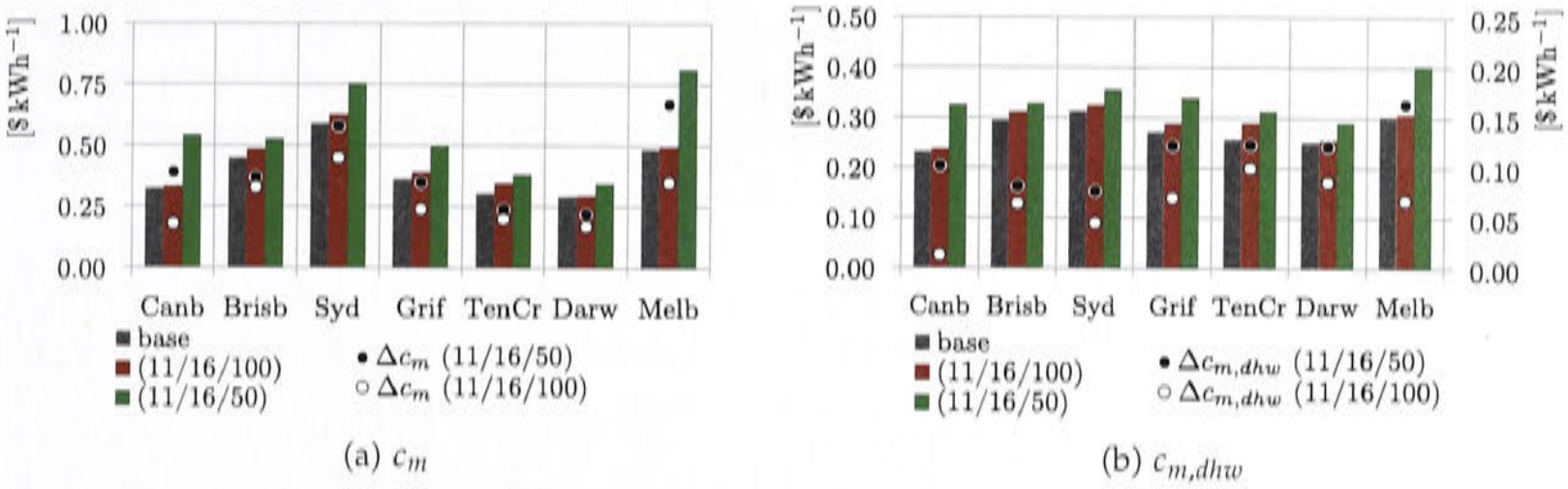

(a) c_m (b) $c_{m,dhw}$

Figure 8.77: Specific cost comparing the base case to cases (11/16/100) and (11/16/50). Specific cost difference compared to the reference case $\Delta c_m = c_m - c_{m,ref}$ (on right axis if included).

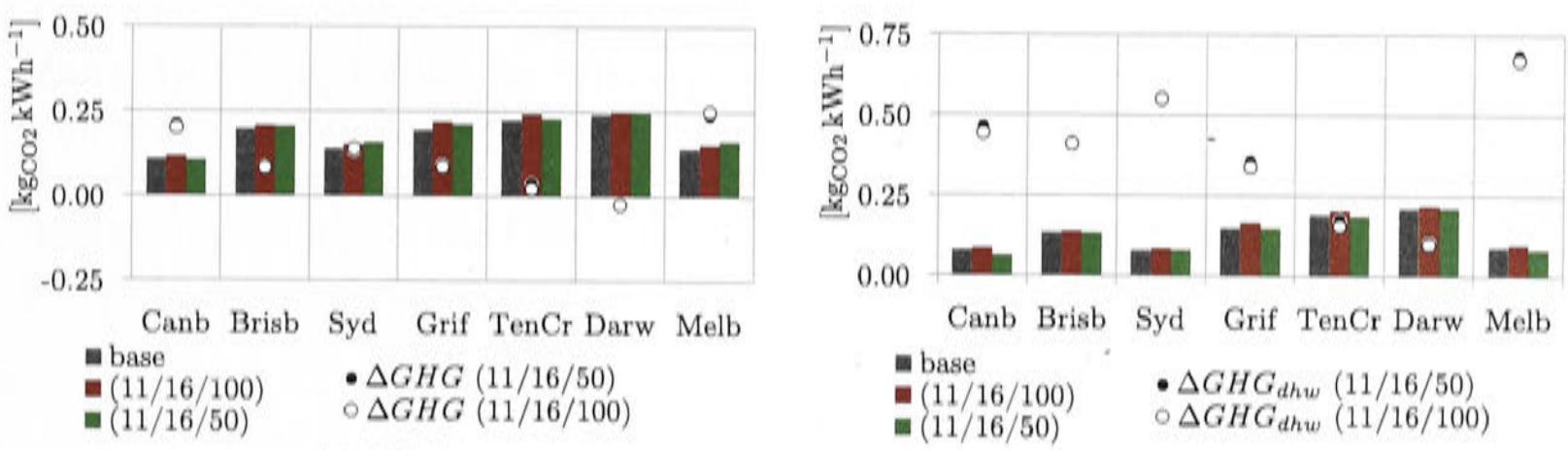

(a) GHG (b) GHG_{dhw}

Figure 8.78: Specific greenhouse gas emission comparing the base case to cases (11/16/100) and (11/16/50). Specific greenhouse gas savings compared to the reference case $\Delta GHG = GHG_{ref} - GHG$.

8.2.7 Heat rejection

Two modifications will be analyzed on the heat rejection side of the system. The first one is a variable set point temperature for the wet cooling tower and the second one is the substitution of the wet cooling tower by a dry fluid cooler.

Variable cooling water set point temperature ($T_{cw,set}$)

This control strategy is especially important in humid climates (e.g. Darwin, Brisbane) because it offers an electricity saving potential for the wet cooling tower fan. The outdoor wet bulb temperature (T_{wb}) plus a certain approach ($\approx 3\,°C$), which is dependent on the cooling tower design, constitutes the limit of how far the cooling water temperature can be lowered. The set point temperature is defined in equation

8.2. The maximum function prevents the cooling tower fan from trying to achieve unreasonable low cooling water temperatures far below 27°C in relatively dry climates. Simulations without the limit showed a strong increase in electricity consumption for this reason. An alternative approach would be to extend equation 8.2 by a minimum allowed cooling water set point temperature. This way the fan would operate at a higher speed if the wet bulb temperatures are low, but the chiller would require lower hot water driving temperatures. The cooling water set point temperature could be the solution of an optimization problem solving for the lowest greenhouse gas emissions.

$$T_{cw,set} = \max(27\,^{\circ}\mathrm{C}, T_{wb} + 3\,^{\circ}\mathrm{C}) \tag{8.2}$$

Figure 4.5 shows the relative frequency of the outdoor wet bulb temperatures throughout the year for each climate and the average wet bulb temperature. The wet bulb temperature of the climate gives an indication where it is possible to save electricity with this control strategy. The distributions have been calculated from the weather files used for the simulations in this thesis, published by Meteotest et al. [2004].

Only in Darwin the re-adjustment of cooling water set point temperature could bring an advantage because in all other climates (including Brisbane) 27°C wet bulb temperature is seldom exceeded. For all other climates the set point adjustment according to equation 8.2 resulted most of the time in the base case set point temperature of 27°C. Table 8.17 shows the change of power consumption in percent for the different consumers and Figure 8.79 shows it graphically.

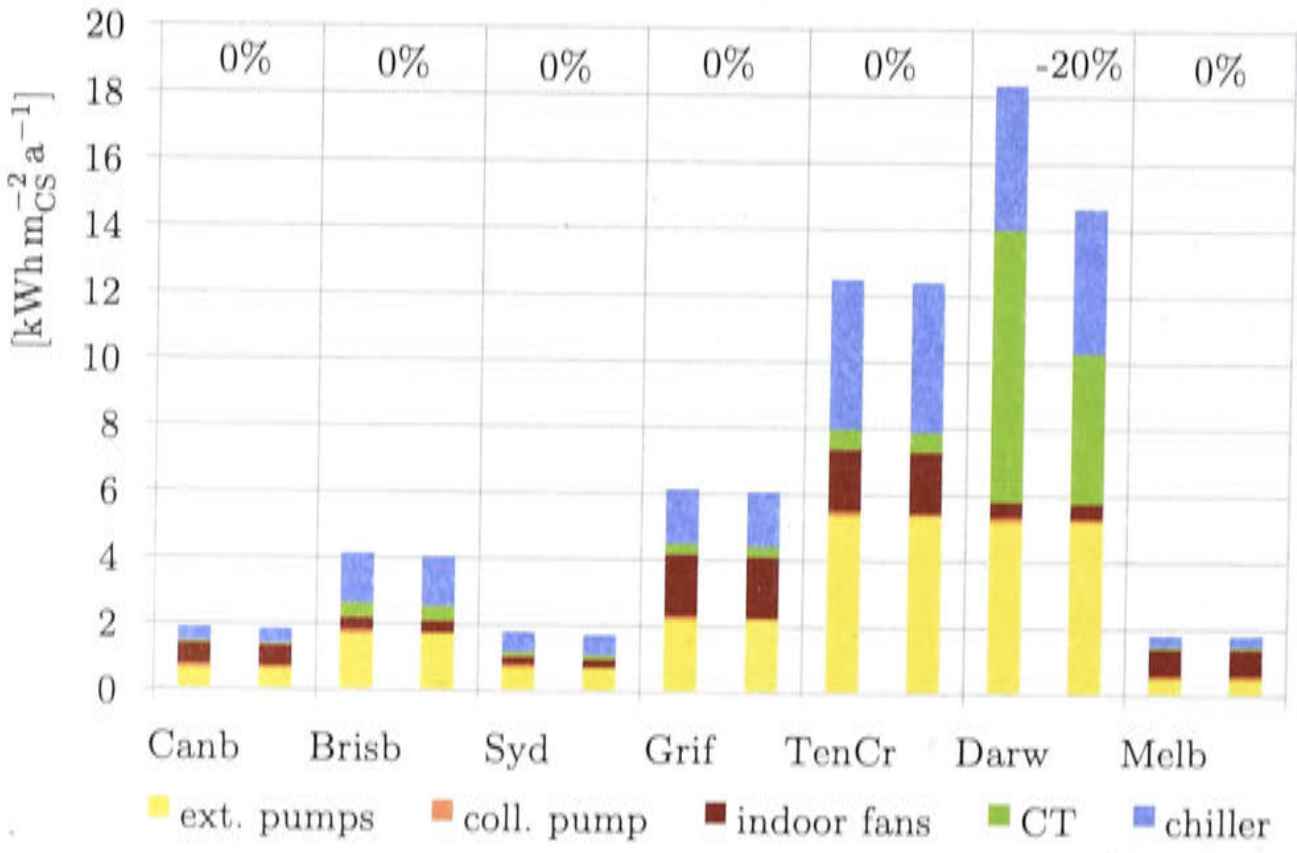

Figure 8.79: Electricity consumption of each individual consumer specific to the conditioned space, and relative change of the total electricity consumption compared to the base case (T_{cw} var)

The simulation results showed that cooling (and heating) supplied changed in-

Table 8.17: Relative change in electricity consumption compared to the base case (T_{cw} var).

	ext. pumps	coll. pump	indoor fans	CT	chiller
Canb	0.0%	0.0%	0.0%	0.1%	0.0%
Brisb	0.0%	0.3%	0.0%	-0.4%	0.0%
Syd	0.0%	0.1%	0.0%	-0.1%	0.0%
Grif	0.0%	0.2%	0.0%	0.0%	0.0%
TenCr	0.0%	-0.2%	0.0%	0.0%	0.0%
Darw	0.0%	-0.5%	0.1%	-44.7%	0.0%
Melb	0.0%	0.0%	0.0%	0.0%	0.0%

significantly compared to the base case (Figure 8.80). The same was true for the comfort conditions. For humid climates it can be concluded that the control strategy using the wet bulb temperature plus 3°C as set point temperature makes a big difference in the electricity consumption, without actually reducing the supplied cooling or the comfort conditions. The same conclusion could be derived for the installation in Singapore [Doemland, 2014].

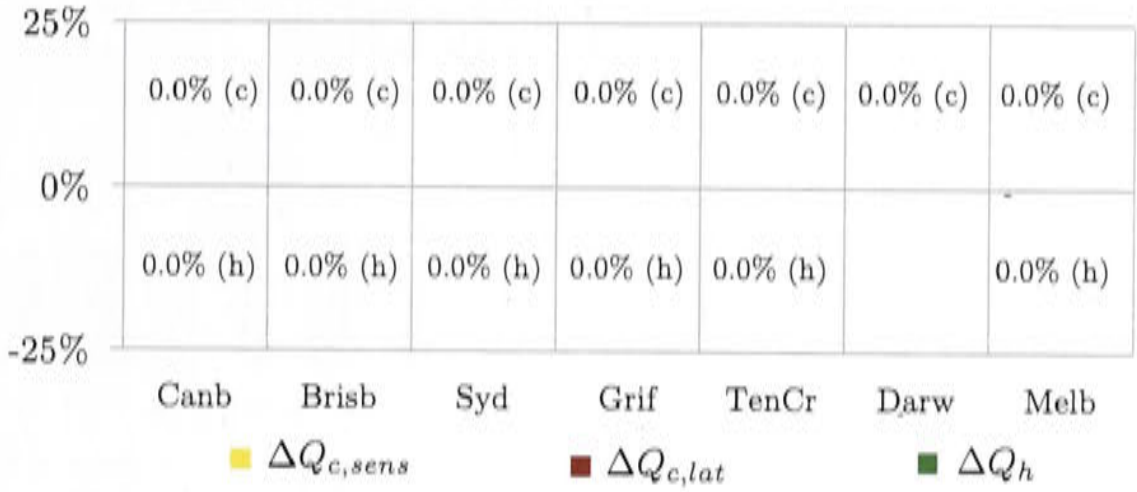

Figure 8.80: Relative change in cooling and heating load

For absorption chiller's low cooling water inlet temperatures and high hot water temperatures favor the generation of cooling effect at low chilled water temperatures. If the cooling water inlet temperature increases, the hot water inlet temperature to the chiller needs to be increased. In Figure 8.81 it can be seen that in Darwin the solar fraction drops for this reason, however, the drop is relatively small.

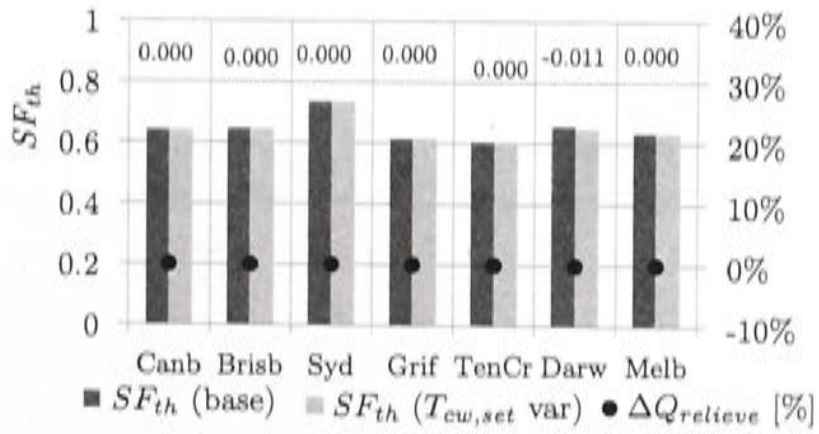

Figure 8.81: Solar fraction (left) and relative change in relieved heat from the hot water tank (right).

It is interesting to compare now with the modified control strategy how often the

cooling water set point temperature is exceeded in each climate. As the cooling water set point temperature became strongly variable for Darwin, the effect is the strongest here.

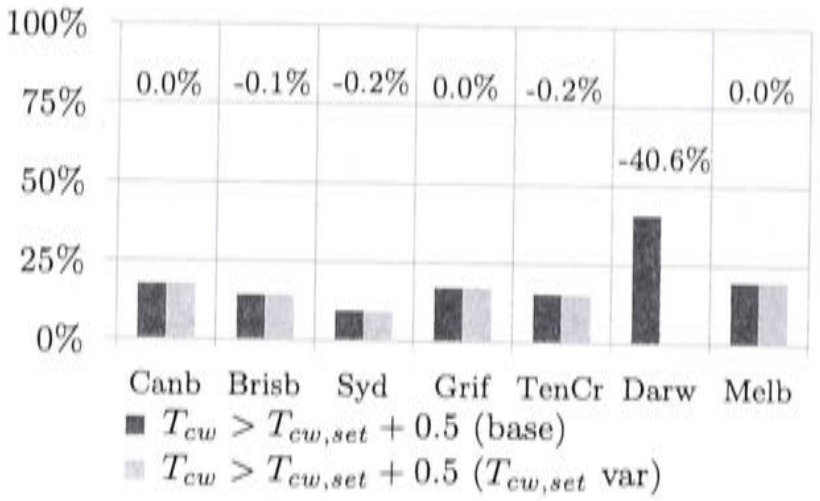

Figure 8.82: Percentage of operating time the cooling water exceeds the set point temperature. Comparison to the base case.

In Figure 8.83 and Figure 8.84 the effect on the greenhouse gas emissions and specific cost are shown. Only in Darwin a change is visible.

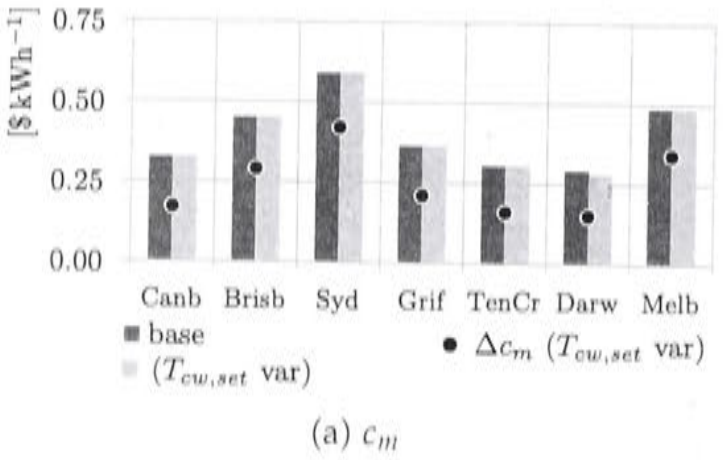

(a) c_m

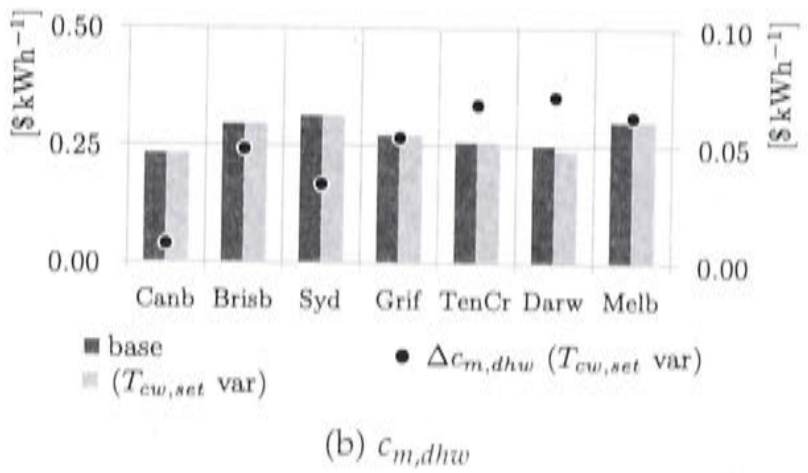

(b) $c_{m,dhw}$

Figure 8.83: Specific cost comparing the base case to the variable cooling water set point temperature. Specific cost difference compared to the reference case $\Delta c_m = c_m - c_{m,ref}$ (on right axis if included).

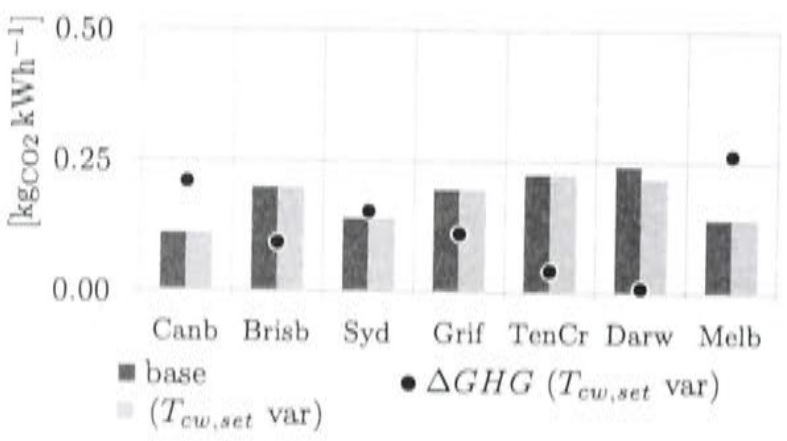

(a) GHG

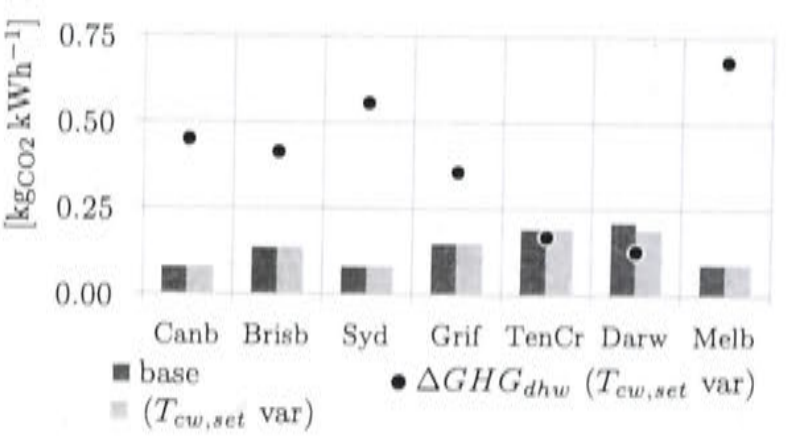

(b) GHG_{dhw}

Figure 8.84: Specific greenhouse gas emission comparing the base case to the variable cooling water set point temperature. Specific greenhouse gas savings compared to the reference case $\Delta GHG = GHG_{ref} - GHG$ (on right axis if included).

Modelling a dry fluid cooler

So far a wet cooling tower was integrated in the model in order to reject the heat from the chiller, which is common practice for absorption chillers. However, high water consumption of wet cooling towers bears difficulties in very arid regions of Australia where water is either scarce or prone to pollution through dust and sand. In this section a dry fluid cooler will be modeled to investigate the trade off between additional fan power electricity consumption and water savings.

The dry fluid cooler type 511 is a component available in TRNSYS 17 only. Based on the mathematical description of the type, it was possible to re-write the component in Fortran for TRNSYS 16.1. The following equations are from the description of the mathematical reference of type 511 [Solar Energy Laboratory, Univ. of Wisconsin-Madison et al., 2012].

In the initial time step, the component calculates the effectiveness ϵ_{design} at design heat transfer conditions as in equation 8.5.

$$\dot{Q}_{design} = \dot{m}_{cw,design}\, c_{p,cw}\, (T_{cw,design,in} - T_{cw,design,out}) \tag{8.3}$$

$$\begin{aligned} \dot{Q}_{design,max} &= C_{min}\, (T_{cw,design,in} - T_{air,design,in}) \\ C_{min} &= \min(\dot{m}_{air}\, c_{p,air}, \dot{m}_{cw}\, c_{p,cw}) \end{aligned} \tag{8.4}$$

$$\epsilon_{design} = \frac{\dot{Q}_{design}}{\dot{Q}_{design,max}} \tag{8.5}$$

The water within the tubes is said to be always "unmixed". The air can be "mixed" (flowing freely around the tubes) or also unmixed if the flow is channeled around the tubes for example through large fins. Each mode has different equations to calculate the heat exchanger effectiveness. The effectiveness is a function of the NTU and the ratio of minimum to maximum capacitance $C_R = (\dot{m}\, c_p)_{min} / (\dot{m}\, c_p)_{max}$.

Both fluids are assumed to be unmixed in this model and equation 8.6 is applied to calculate the heat transfer effectiveness.

$$\epsilon = 1 - \exp\left(\frac{NTU^{0.22}}{C_R}(\exp(-C_R NTU^{0.78}) - 1)\right) \tag{8.6}$$

With ϵ_{design} known, equation 8.6 can be solved for NTU. The equation is solved iteratively using the fixed point iteration as explained in the TRNSYS mathematical description of type 511.

Using equation 8.7 the UA value at design conditions UA_{design} can be determined.

$$NTU = \frac{UA}{C_{min}} \tag{8.7}$$

Furthermore it is possible to calculate the local heat transfer coefficients of the air

and water at design conditions, $h_{air,design}$ and $h_{cw,design}$. The heat transfer coefficients are functions of the fluid conductivity k and Nusselt number as well as the tube diameter.

Knowing UA_{design} equation 8.8 makes it possible to find the UA value and from this the NTU and effectiveness at different mass flow rates (off-design conditions) to calculate the actual heat transfer and fluid outlet temperatures. The terms γ_{air} and γ_{cw} are the mass flow ratios of actual flow rates to the design flow rates.

$$\frac{UA_{design}}{UA} = \frac{\left(\frac{1}{h_{cw,design}} + \frac{1}{h_{air,design}}\right)^{-1}}{\left(\frac{1}{\gamma_{cw}^{0.8} h_{cw,design}} + \frac{1}{\gamma_{air}^{0.6} h_{air,design}}\right)^{-1}} \tag{8.8}$$

Data for a fan with $T_{air,design,in}$ =25°C was available from Thermokey [2013]. Using the relatively high water outlet and inlet design temperatures of 35°C and 40°C respectively, a relatively small airflow is needed[5]. The mass flow of air to the mass flow of water ratio is 1.5. However, when changing the design conditions to water being cooled down from 35°C to 30°C, a much much larger airflow is necessary.

A dry cooling tower which is to generate 27°C water temperature needs a unreasonable large amount of air if the outdoor dry bulb temperature approaches 27°C. The wet cooling tower can generate 27°C with a relatively low air flow previously with a mass flow ratio of 1 between cooling water and air flow rate, because the limit is set by the wet bulb temperature. A share of 80% latent heat removal can be achieved at design conditions.

The absorption chiller can work with a cooling water inlet temperature of $T_{cw,in}$ =30°C and returns 35°C at design conditions, even though it needs relatively high hot water driving temperatures[6].

The dry fluid cooler has been designed for the rated cooling water flow $\dot{m}_{cw,rated}$ with a $scalefactor = 1$ at the air design inlet temperature of 25°C with a moderate air flow of 14 000 $m^3\,h^{-1}$. To derive this design air flow, the air flow has been changed iteratively until a solution for NTU in equation 8.6 was found.

The absorption chiller's chilled water set point temperature was increased from 7°C to 11°C. The design air flow for each climate is scaled with the $scalefactor$, just as the cooling water flow rate is scaled.

The controller of the dry fluid cooler will vary the air flow to achieve the cooling water set point temperature, but an upper limit of 1.5 times the design air flow is set to prevent it from becoming too large.

The power consumption of the fans for the design air flow is derived from manufacturer's data via multivariate regression. Figure 8.85 shows the design air flow and power demand operating points from the WR & WG dry cooler series of the company Thermokey [2013]. The function to calculate the rated power consumption for the specific design air flow is given in equation 8.9.

[5] From the TRNSYS heat transfer model and the provided information from the specification sheets, the air flow at design conditions has been derived iteratively.

[6] Design conditions: $T_{cw,in}$ =30°C, $T_{chw,set}$ =11°C, $T_{hw,in}$ =85.5°C for a design capacity of 11.7 kW

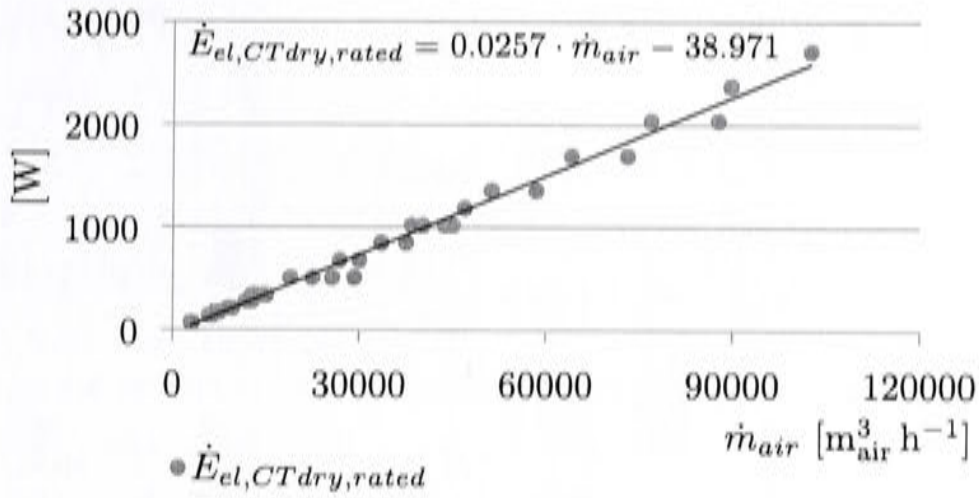

Figure 8.85: Power demand of dry fluid coolers at various air flows (Thermokey, WR & GR series)

$$\dot{E}_{el,CTdry,rated}[\mathrm{W}] = \dot{m}_{air,design}[\mathrm{m^3\,h^{-1}}] \cdot 0.0257 - 38.97 \tag{8.9}$$

The actual power demand at different air flows during the simulation is calculated using the affinity law as in equation 8.10 with $\dot{m}_{air,design}$ being the upper limit for the air flow.

$$\dot{E}_{el,CTdry} = \dot{E}_{el,CTdry,rated} \cdot \left(\frac{\dot{m}_{air}}{\dot{m}_{air,design}}\right)^3 \tag{8.10}$$

To sum it up, the solar air-conditioning model operates at different cooling water temperature ranges compared to the manufacturer's published design conditions. However, the TRNSYS dry fluid cooler model was used to calculate the design air flow at 25°C design air inlet temperature, accommodating for the chiller's design cooling water temperature and mass flow range. The power consumption of the cooling tower at these design conditions was then derived from the regression curve in Figure 8.85, published by Thermokey [2013]. The air inlet design temperature might be too low for some Australian climates, but this will be reflected in the amount of times the dry fluid cooler cannot match the cooling water set point.

Simulation results of the dry fluid cooler

The dry fluid cooler model was implemented and two cooling water set point temperatures were tested, 27°C and 30°C. In contrast to the wet cooling tower, the dry bulb temperature determines the limit of what can be achieved by the dry fluid cooler. Figure 4.6 in section 4.3 shows the distribution of the dry bulb temperatures in each climate throughout the year using the simulation weather file. Figure 8.86 shows for both cooling water set point temperatures how often the set point is exceeded. It is much more difficult to achieve 27°C with a dry fluid cooler than with a wet cooling tower.

Since a higher cooling water temperature can be expected, a chilled water set point temperature of 11°C and cooling coil air outlet set point temperature of 16°C were chosen. The downside will be a reduced amount of removed latent heat. The results will be compared to the case (11/16/100) of section 8.2.6 which uses a wet

cooling tower. The abbreviation for the two cases are "dry 27 11/16/100" and "dry 30 11/16/100".

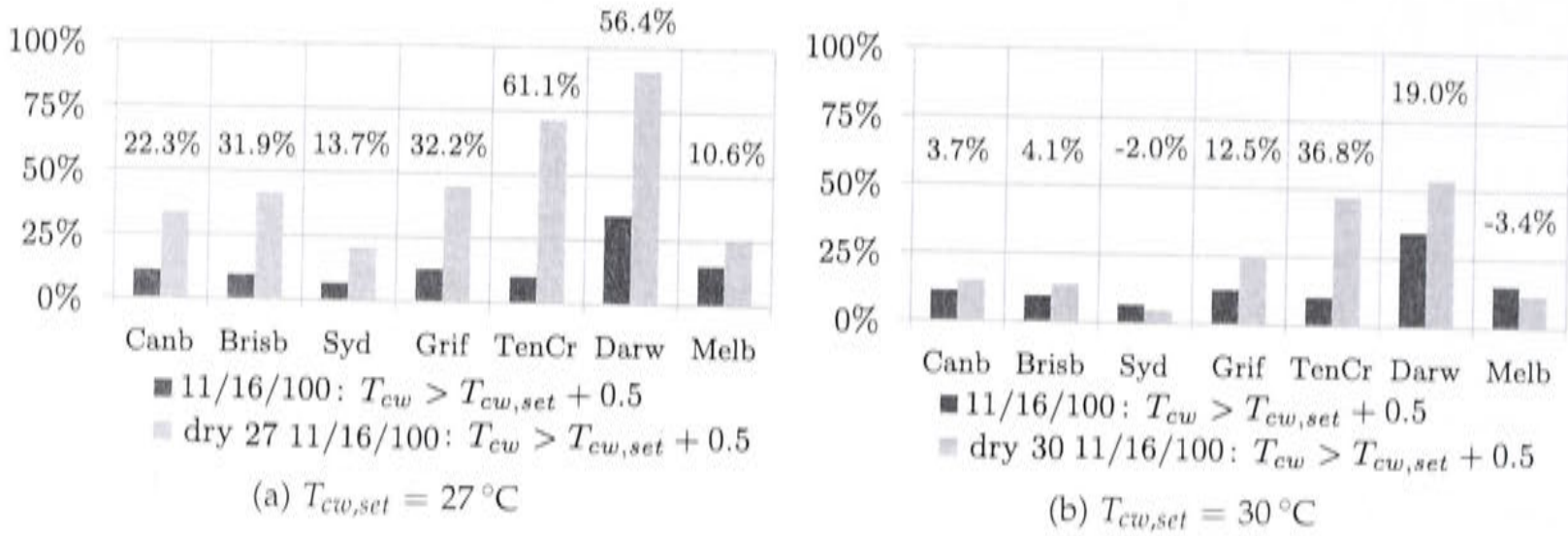

Figure 8.86: Deviation from the cooling water set point temperature in the three scenarios.

With a higher cooling water inlet temperature, the demanded hot water temperature will be higher, too. This has two effects: The relieved heat from the tank drops but also the solar fraction decreases because the auxiliary heater switches on more often at higher required hot water temperatures. Figure 8.87 shows both effects.

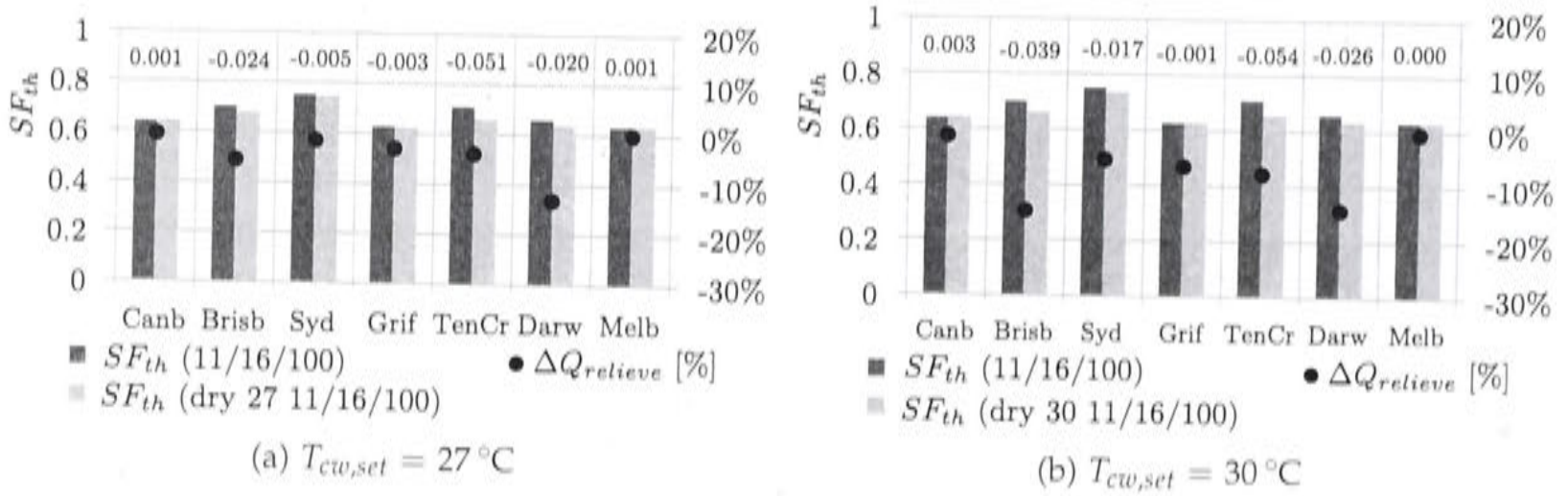

Figure 8.87: Solar fraction (left) and change of relieved heat (right) compared to case (11/16/100).

The next important aspects are the effects on the comfort conditions, on the cooling and heating energies supplied and on the change in air flow to the zones and operational hours of the indoor fans.

The comfort conditions in winter in all climates did not change and neither did the humidity discomfort. The summer temperature and humidity discomfort can be seen in Figure 8.88 and 8.89. The changes of comfort are closely linked to the reduced cooling supplied as in Figure 8.90. Surprisingly, there is no difference between the two cooling water temperature set points. It seems that the tank and solar system and auxiliary heater were equally able to provide the extra amount of heat at higher temperatures, which is visible on the difference in the solar fraction and relieved heat.

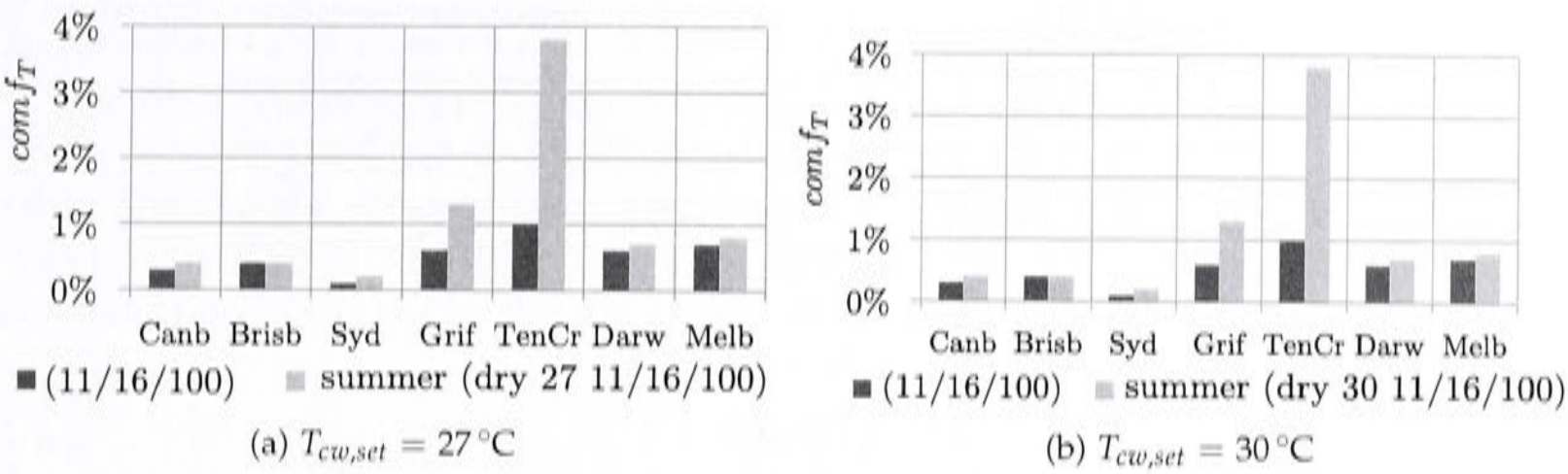

(a) $T_{cw,set} = 27\,^{\circ}\mathrm{C}$ (b) $T_{cw,set} = 30\,^{\circ}\mathrm{C}$

Figure 8.88: Temperature discomfort in summer compared to case (11/16/100).

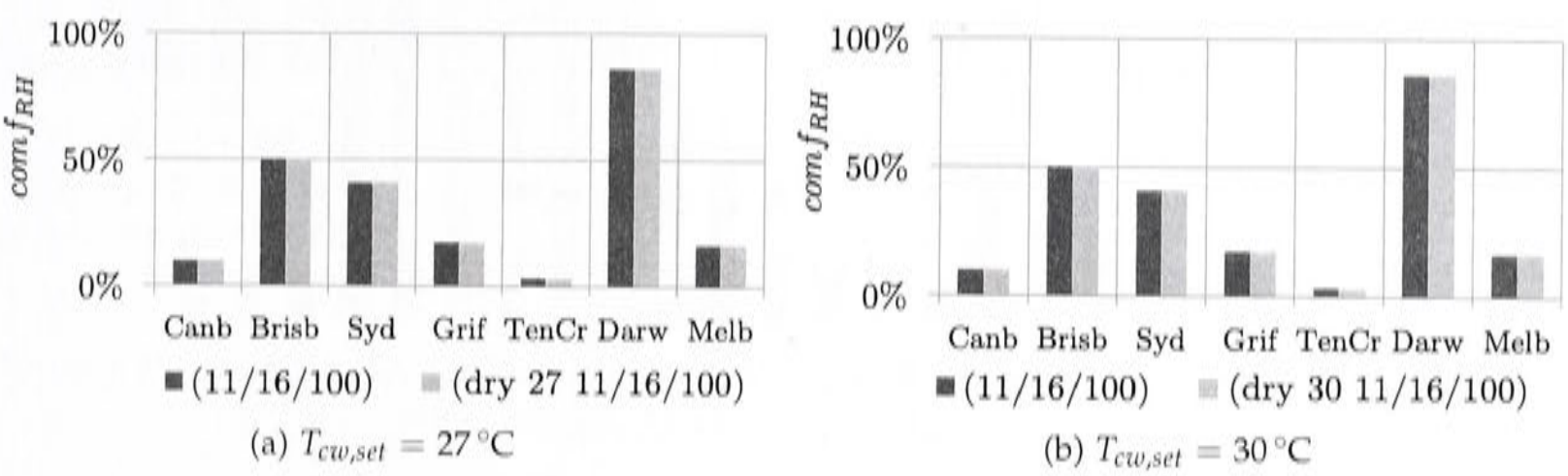

(a) $T_{cw,set} = 27\,^{\circ}\mathrm{C}$ (b) $T_{cw,set} = 30\,^{\circ}\mathrm{C}$

Figure 8.89: Humidity discomfort in summer compared to case (11/16/100).

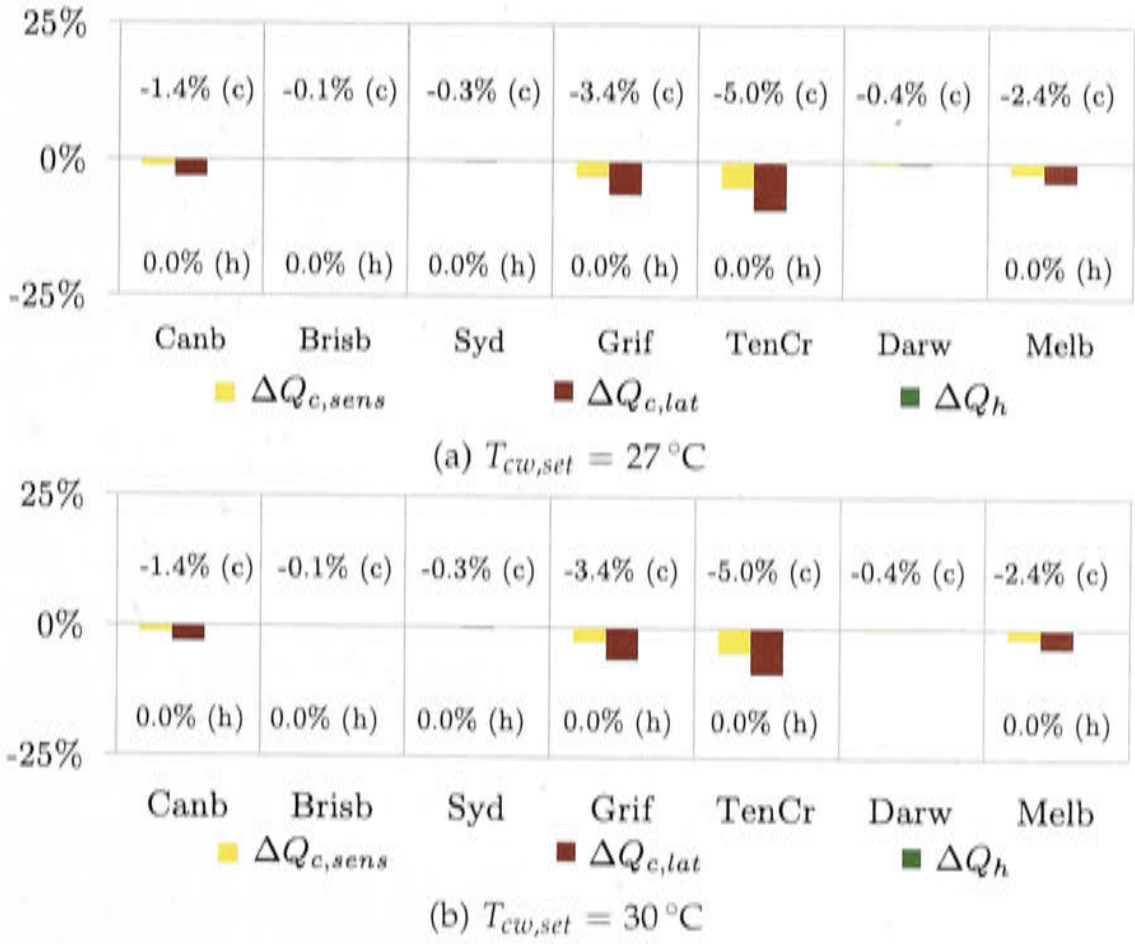

(a) $T_{cw,set} = 27\,^{\circ}\mathrm{C}$

(b) $T_{cw,set} = 30\,^{\circ}\mathrm{C}$

Figure 8.90: Relative change of cooling supplied compared to case (11/16/100).

Figure 8.91 and Table 8.18 show the electricity consumption and it is obvious that it increases strongly due to the higher dry fluid cooler fan electricity consumption, especially when trying to achieve 27°C cooling water set point temperature.

Table 8.18: Relative change of electricity consumption ΔE_{el} compared to the case (11/16/100).

	Canb	Brisb	Syd	Grif	TenCr	Darw	Melb
$T_{cw,set} = 30\,°C$	7%	16%	4%	15%	35%	5%	2%
$T_{cw,set} = 27\,°C$	16%	41%	20%	28%	51%	22%	8%

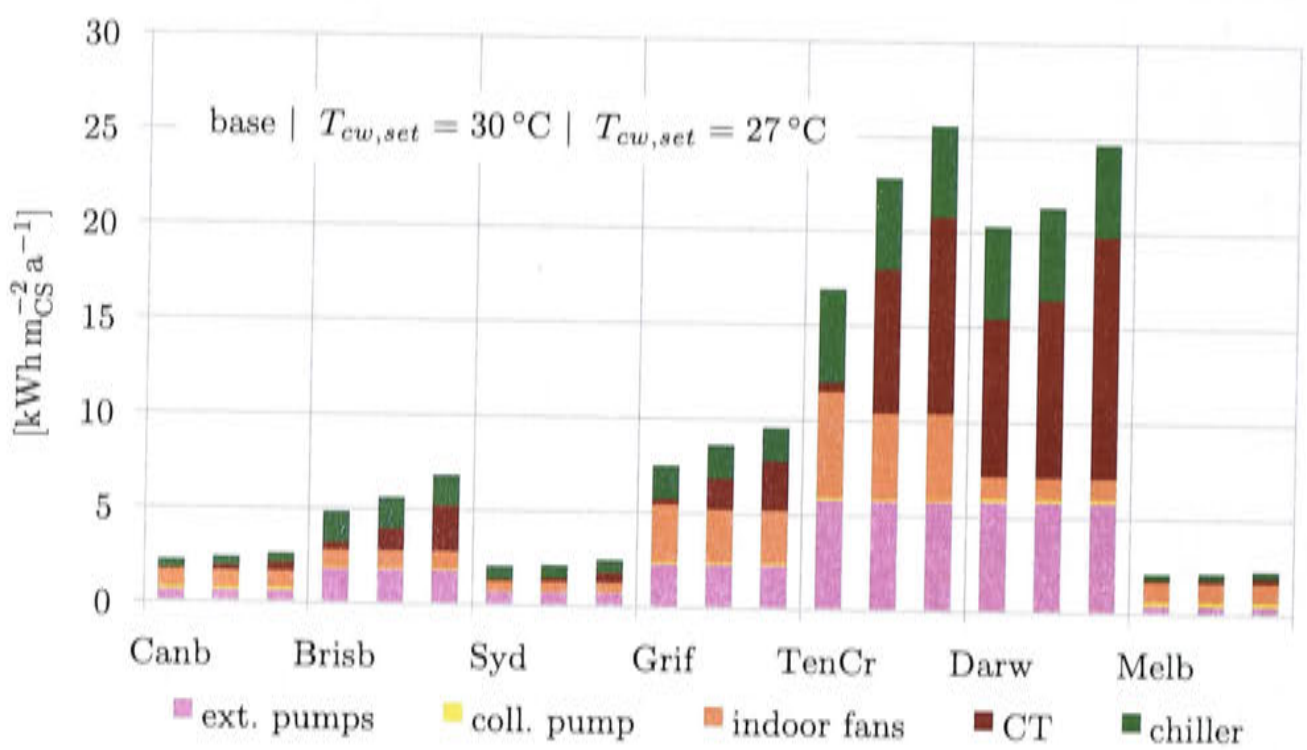

Figure 8.91: Electricity consumption of each individual consumer specific to the conditioned space compared to the case (11/16/100) (dry fluid cooler)

The changes in air flow and hours of operation are minimal (Figure 8.92).

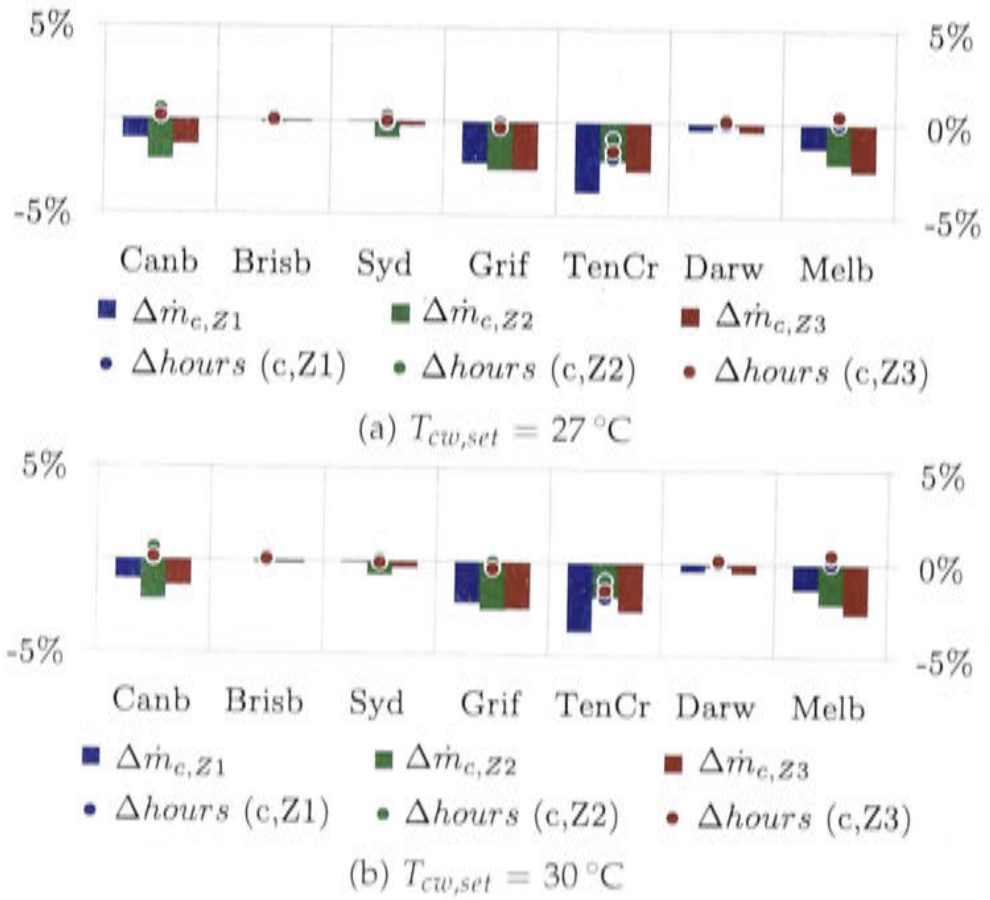

(a) $T_{cw,set} = 27\,°C$

(b) $T_{cw,set} = 30\,°C$

Figure 8.92: Relative change of average air flow in each zone and fan operating hours compared to (11/16/100).

From a comfort and supplied cooling perceptive, the set point temperature can

be increased to 30°C, as long as the tank can provide sufficient heat.

Figure 8.93 shows that the specific cost does not vary much for both set points. Water reduction and increased electricity consumption have an opposing trend on the cost. The specific greenhouse gas emissions increase especially with lower cooling water set point temperatures, due to the increase in electricity consumption and gas consumption as the chiller requires more often higher hot water inlet temperatures.

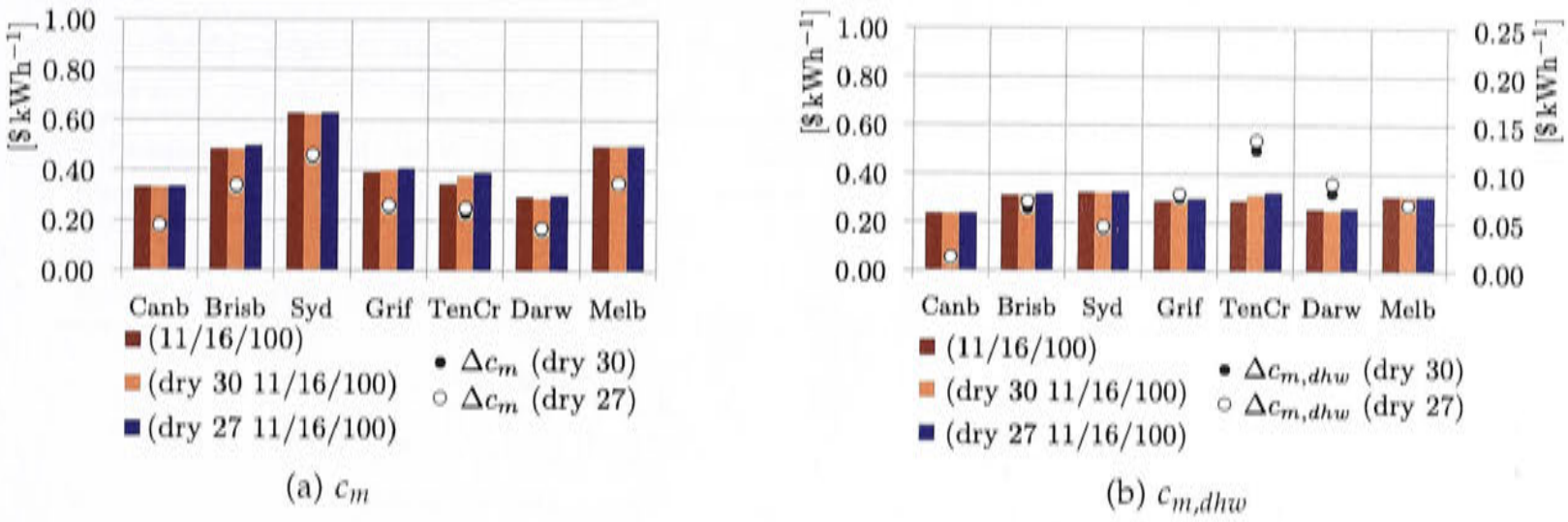

(a) c_m (b) $c_{m,dhw}$

Figure 8.93: Specific cost comparing the three cases. Specific cost difference compared to the reference case $\Delta c_m = c_m - c_{m,ref}$ (on right axis if included).

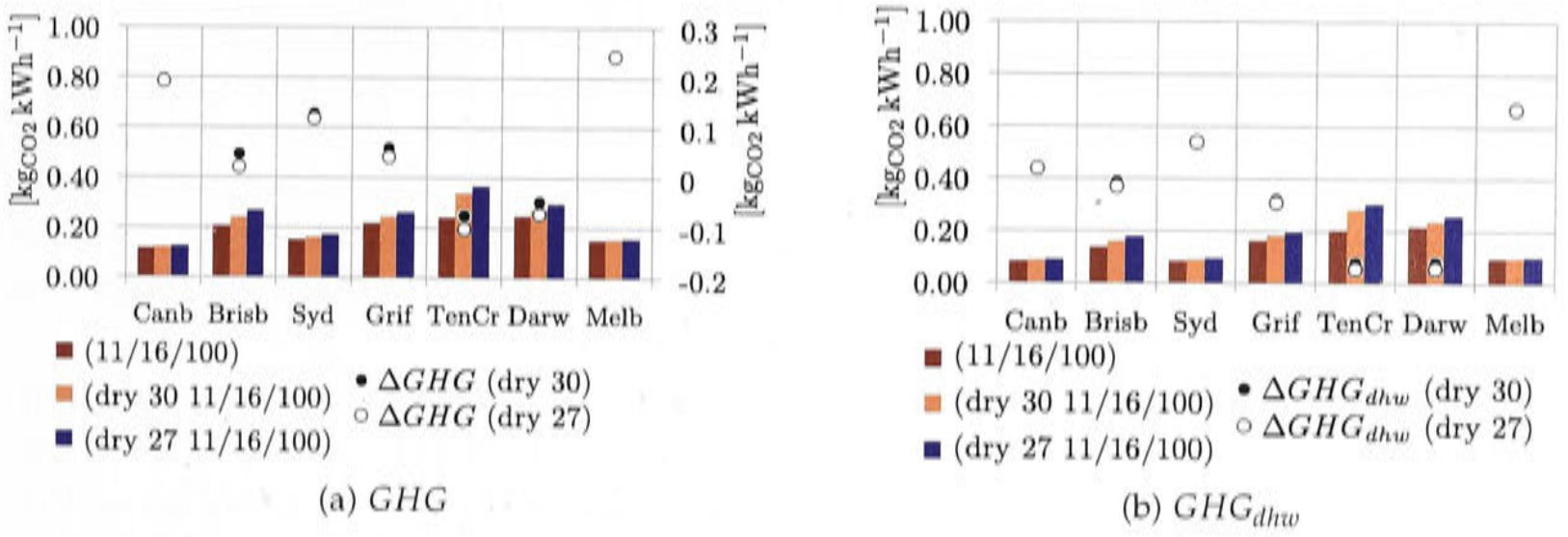

(a) GHG (b) GHG_{dhw}

Figure 8.94: Specific greenhouse gas emissions of the three cases. Specific greenhouse gas savings compared to the reference case $\Delta GHG = GHG_{ref} - GHG$ (on right axis if included).

Nevertheless, even though more electricity is needed, the water consumption of the heat rejection system can be reduced completely. This might be beneficial in arid climates or where water quality is poor.

8.2.8 Including night flush ventilation and changing the building's thermal mass

As a first step the building thermal mass will be changed to a heavier and lighter building construction to examine the effect on the system's performance. A heavier building requires less air-conditioning and heating because the thicker walls have higher thermal inertia. Therefore, the air-conditioning system will be scaled down.

For the lighter buildings, the system will be scaled up. The thermal resistance of the walls will be kept at $2.8\,m^2\,K\,W^{-1}$ as in Tables 4.8 to 4.10, but the thermal mass will be increased and decreased as explained in Table 8.19. The thermal capacitances of the walls and the floor for each scenario are listed in Table 8.20.

Table 8.19: Variation of building thermal mass

climate	base	reduced thermal mass	increased thermal mass
Canb, Melb	reverse brick veneer	weatherboard	inside wall thickness doubled, concrete floor thickness increased
TenCr, Darw	double brick	reverse brick veneer	inside wall thickness doubled, concrete floor thickness increased
Brisb, Syd, Grif	weatherboard	-	reverse brick veneer, concrete floor thickness increased

Table 8.20: Thermal capacitances in $kJ\,K^{-1}\,m^{-2}$ for each wall type and for the floor.

	base	reduced thermal mass	increased thermal mass
brick veneer (reverse)	207	25	398
double brick	411	207	603
weatherboard	25	-	207
floor (slab on ground)	217	217	338

In a second step "night flush ventilation" is included. Night flush ventilation describes the process of pre-cooling the building during the night using cool outdoor air in order to reduce the cooling demand during the day. This is especially effective in climates with a high diurnal temperature difference.

To simulate extra ventilation during the night, the model increases the ventilation rates between 22:00 and 7:00 to 5 ACH if the outdoor temperature is less than the indoor temperature and if the maximum temperature of the previous day exceeded 25°C. During the day the building will have an infiltration rate 80% lower than the base case scenario to simulate a well sealed building.

Heating will be disabled completely when night flush ventilation is switched on anywhere in the building. This might lead to discomfort during the night.

The inside thermal mass of the building will be changed again towards heavy and lighter buildings as in Table 8.19 to see if the effect of night flush ventilation can be increased and to what extend.

Varying the thermal mass of the buildings

In the first step the settings of the base case are going to be compared to lower and higher thermal mass scenarios. A lower thermal mass of the building leads to an increase in cooling load and a higher thermal mass to a reduction (it takes longer for the indoor air temperature to rise).

The first round of simulations in each climate was performed with an oversized chiller to find the actual chiller size desired.

From Figure 8.95 it can be seen that heavier buildings have a very strong potential to decrease the cooling load. In Sydney an air-conditioning system would hardly be required anymore with the increased thermal mass. When reducing thermal mass it seems that the largest effects on the required cooling capacity occurs when changing from brick veneer to weatherboard (Canberra and Melbourne) as opposed to double brick to brick veneer (Tennant Creek and Darwin).

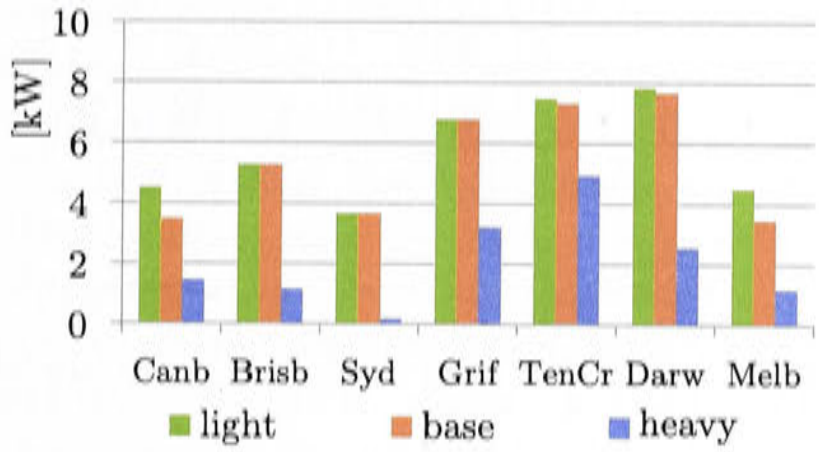

Figure 8.95: Installed cooling capacities for light and heavy weight buildings

The collector area for the light weight building structure has been set according to the chosen configuration in Table 8.21. For the smaller capacities in the heavy weight buildings the collector size has been recalculated according to the specific collector area $m^2\,kW^{-1}_{cooling}$ in Table 8.3. The collectors were rounded to one of the 5 configurations previously used. The smallest configuration was chosen for Brisbane and Sydney with $9\,m^2$, even though the mathematical result only suggested $2.6\,m^2$ and $0.6\,m^2$ collector area respectively[7].

Table 8.21: Collector size in m^2 (heavy & light).

	light	base	heavy
Canb	24	24	12
Brisb	12	12	9
Syd	12	12	9
Grif	18	18	9
TenCr	18	18	18
Darw	24	24	9
Melb	33	33	12

The change of chiller capacity in Sydney implies that hardly any air-conditioning is required at all anymore. When down-sizing the chiller, the minimal air flow has been reduced as well from $200\,kg\,h^{-1}$ to $50\,kg\,h^{-1}$ for each zone. As explained in section 8.2.5 the minimal air flow is related to the performance measure of the cooling tower being able to achieve its cooling water temperature set point. In Sydney, which has the smallest cooling capacity, it seems that an even smaller minimal air flow

[7]The relative increase of relieved heat is larger in Brisbane than in Sydney.

should have been set. Figure 8.96 shows the relationship between the building structures and the cooling tower's capability of achieving the set point temperature. If the cooling tower is unable to achieve the set point temperature, the chiller control compensates with higher hot water inlet temperatures to reach the required chilled water set point temperature. In the following graphs the minimal air flow of $50\,\mathrm{kg\,h^{-1}}$ is presented, unless otherwise indicated.

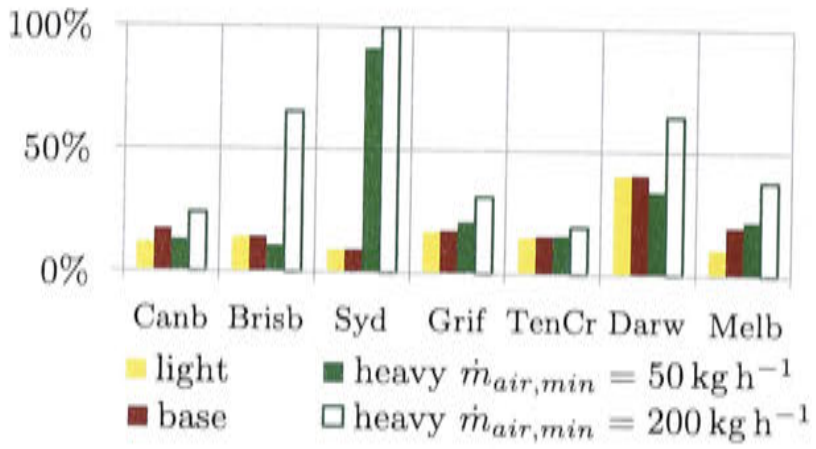

Figure 8.96: Percentage of operating time the cooling water exceeds the set point temperature.

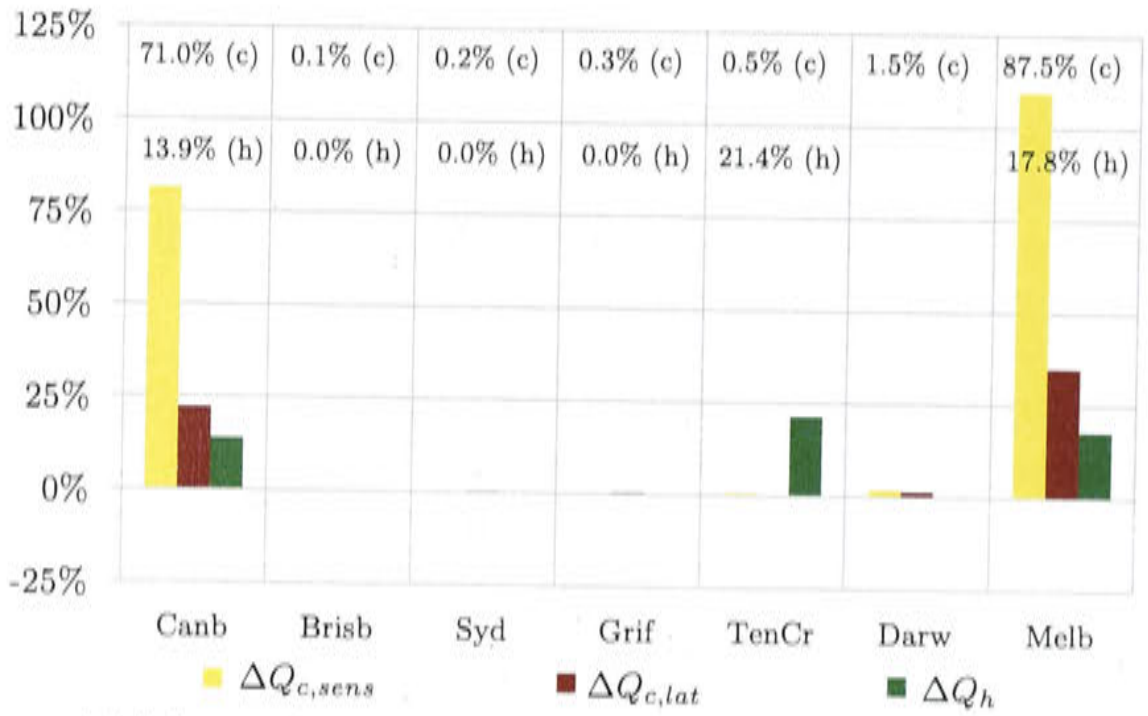

(a) light weight (red: building structure remained unchanged)

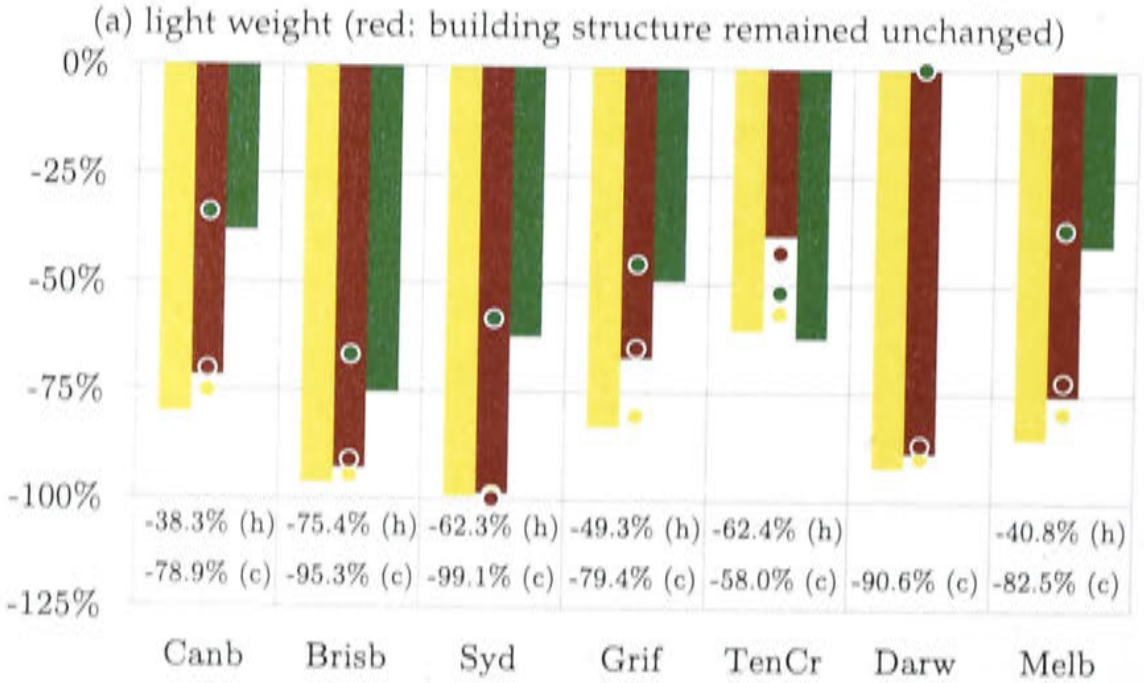

(b) heavy weight (values in brackets at $\dot{m}_{air,min} = 50\,\mathrm{kg\,h^{-1}}$)

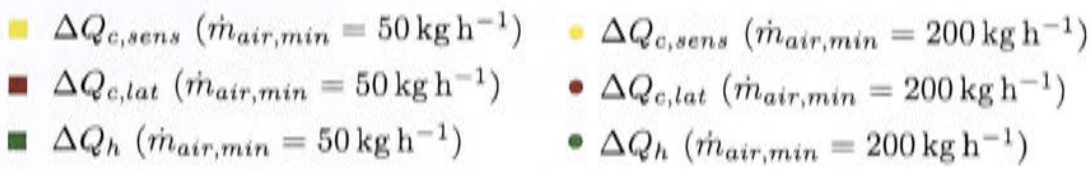

(c) legend

Figure 8.97: Relative change in heating and cooling demand of light and heavy weight structures compared to the base case

The cooling and heating demand in the climates for the two different building structures varied according to Figure 8.97. In Canberra and Melbourne the change towards weatherboard instead of brick veneer results into a strong increase in cooling demand, whereas the change towards brick veneer in Tennant Creek and Darwin does not increase the load noticeably. The reduction in cooling and heating demand towards heavy weight buildings is remarkable for all climates.

Figure 8.98 shows the solar fraction and the relieved heat. The reduction in solar fraction with heavier buildings in Canberra and Melbourne is linked to their heating demand. The collectors were sized to the climate's cooling demand and the ratio of cooling to heating was assumed to stay relatively constant. However, the smaller collector area achieves barely 40% solar fraction in Canberra and 20% in Melbourne. In Brisbane the smallest collector size seems still too large. The solar fraction increases strongly as does the relieved heat. It has to be noted though that the relieved heat in Brisbane was very small in the base case. The increase in Darwin's solar fraction is especially interesting because the collectors have been downsized by 60%, but the absolute cooling load dropped substantially.

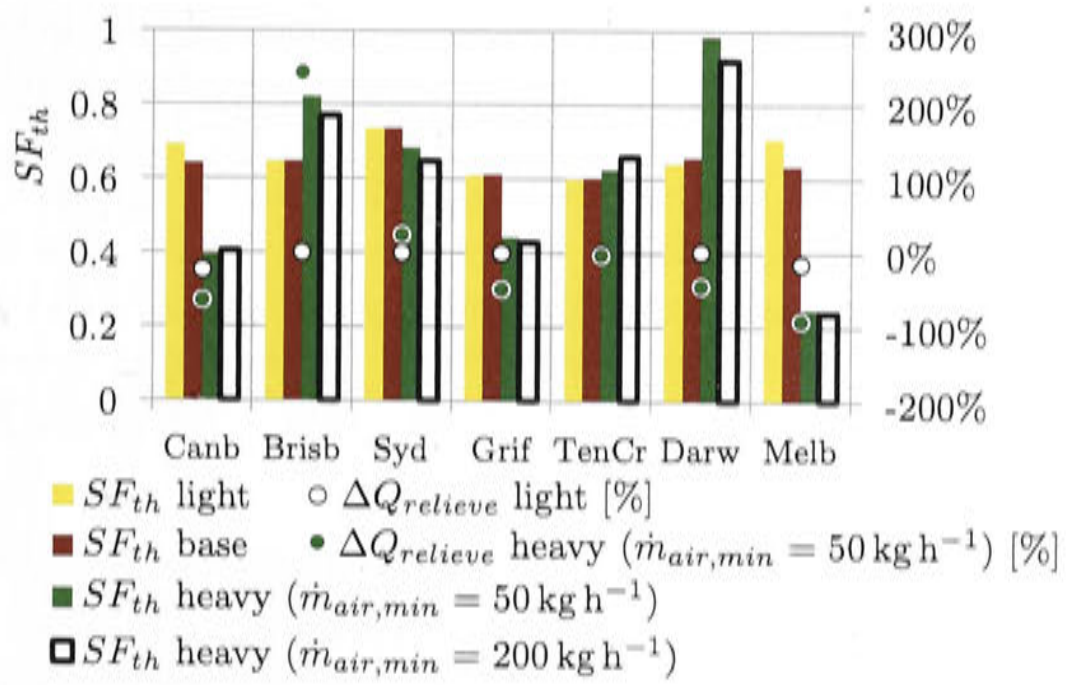

Figure 8.98: Solar fraction (left) and change of relieved heat compared to the base case (right).

The effect on the comfort conditions can be seen in Figure 8.99. The difference between the two minimum air flows is somewhat alarming because it has such a high influence on the comfort conditions. Even though the solar fraction is fairly stable and the amount of cooling and heating supplied to the building does not differ much, the temperature comfort conditions are much more often met with a larger minimum air flow rate. This implies that, especially in the evenings when the cooling demand

declines, a large air flow of conditioned air can meet the cooling load more rapidly[8]. Similarly, for heating the smaller air flow takes longer to reach set point conditions.

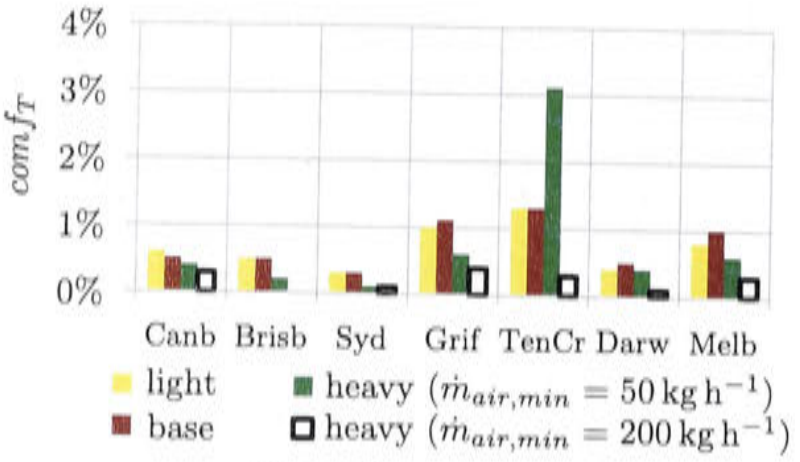

(a) $com f_T$ summer

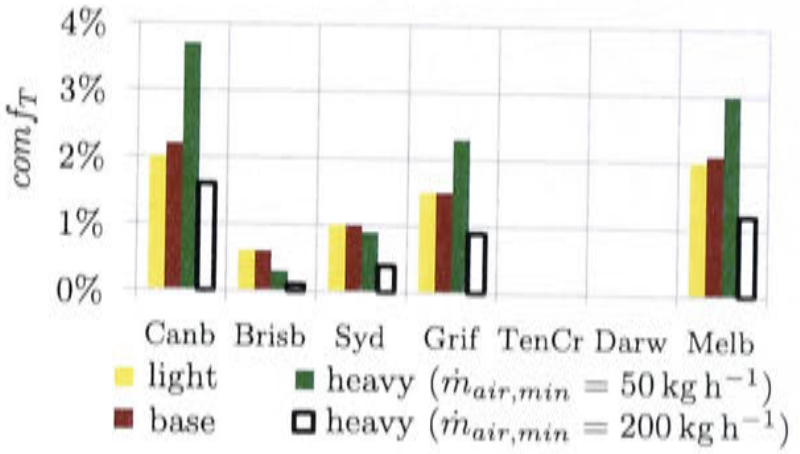

(b) $com f_T$ winter

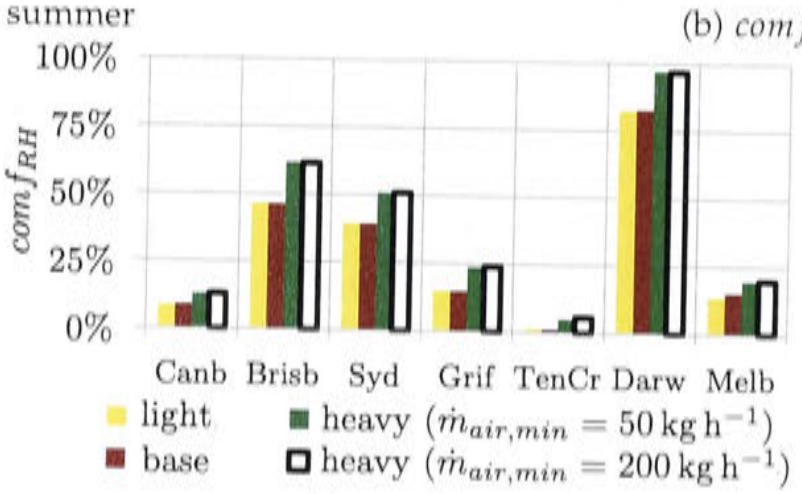

(c) $com f_{RH}$

Figure 8.99: Discomfort levels for temperature and relative humidity comparing the three building structures

The electricity consumption and its change compared to the base case can be seen in Figure 8.100. The electricity consumption shown for heavy weight buildings corresponds to the minimum air flow rate of $50\,\mathrm{kg\,h^{-1}}$. With $\dot{m}_{air,min} = 200\,\mathrm{kg\,h^{-1}}$ it deviates between -1% points and 2% points in all climates besides Tennant Creek and Darwin, where it deviates +6% and -5% points respectively. The electricity consumption corresponding to the light weight buildings in Figure 8.100 should be equal to the base case for Brisbane, Sydney and Griffith. Minimal changes on the system model during the development are responsible for the discrepancy and are small enough to be neglected.

Table 8.22: Relative change of total electricity consumption ΔE_{el} compared to the base case for light and heavy weight buildings ($\dot{m}_{air,min} = 50\,\mathrm{kg\,h^{-1}}$).

	Canb	Brisb	Syd	Grif	TenCr	Darw	Melb
light weight	72%	1%	1%	2%	4%	3%	77%
heavy weight	-67%	-94%	-97%	-75%	-54%	-86%	-73%

[8]The cooling water inlet temperatures becomes very warm in that case, but it seems to be compensated with higher hot water inlet temperatures in order to maintain the chilled water set point temperature.

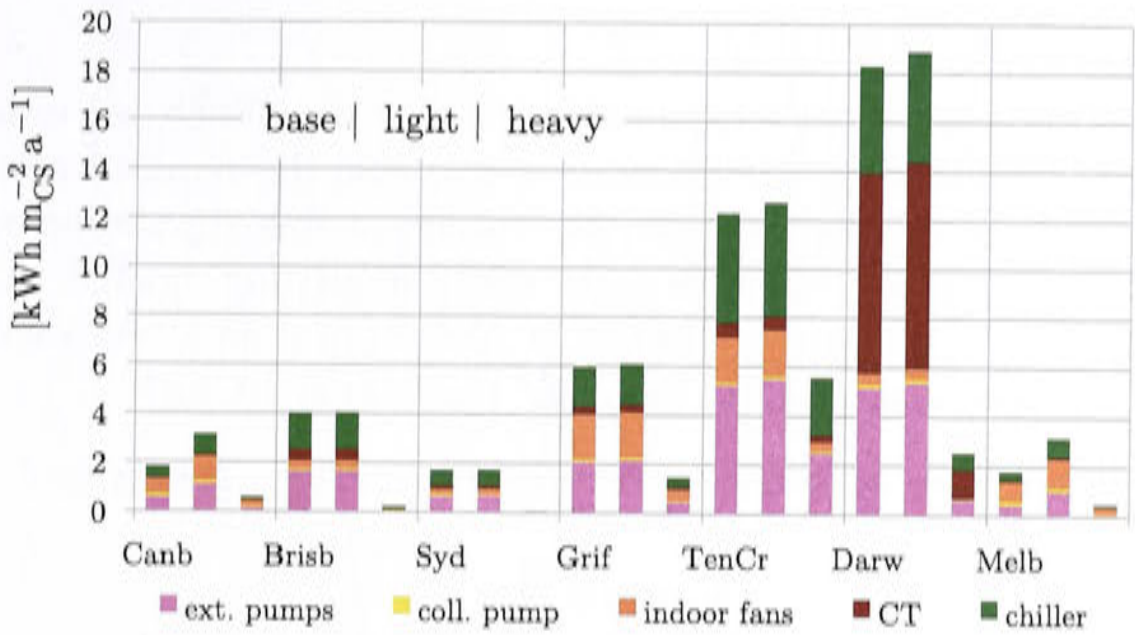

Figure 8.100: Electricity consumption of each individual consumer specific to the conditioned space comparing the light and heavy weight construction to the base case ($\dot{m}_{air,min} = 50\,kg\,h^{-1}$)

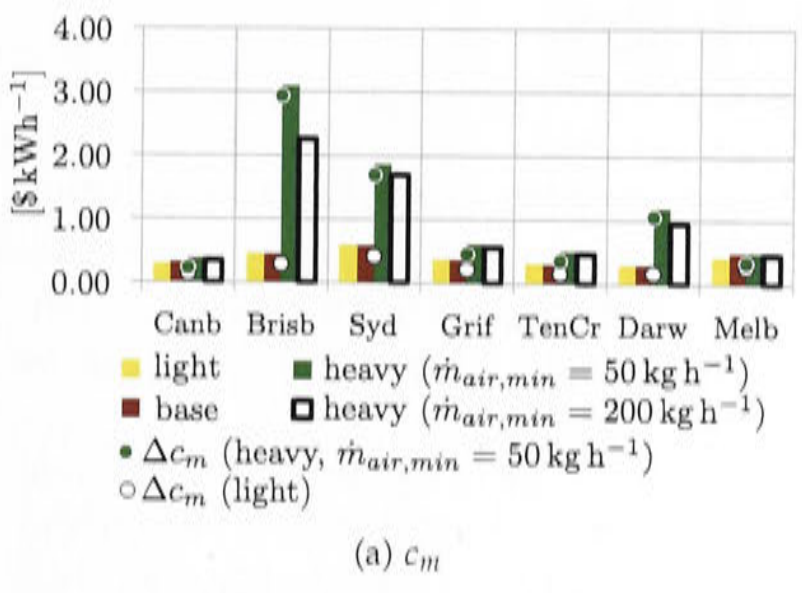

(a) c_m

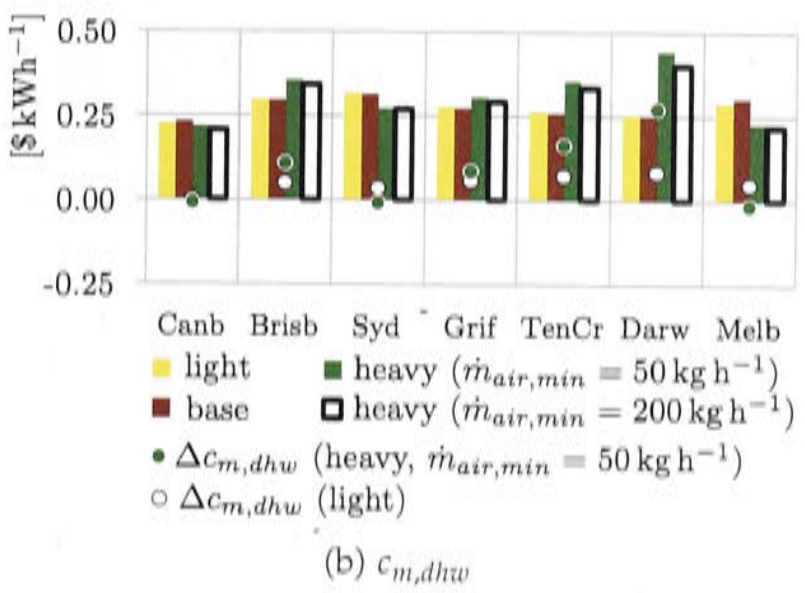

(b) $c_{m,dhw}$

Figure 8.101: Specific cost comparing the base case to heavy and light weight building structure. Specific cost difference compared to the reference case $\Delta c_m = c_m - c_{m,ref}$

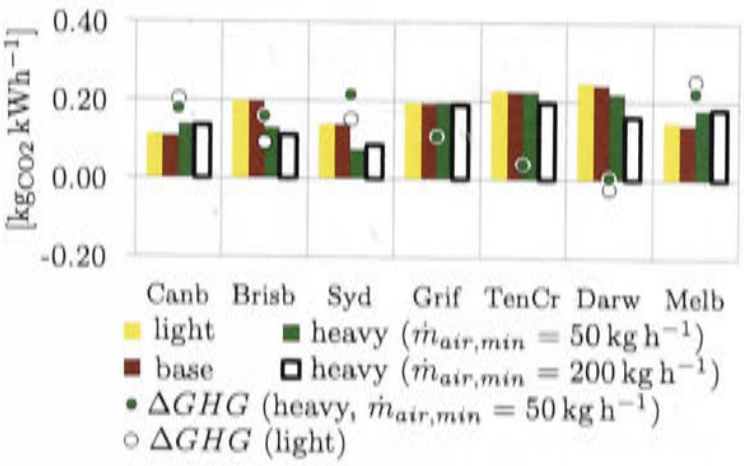

(a) GHG

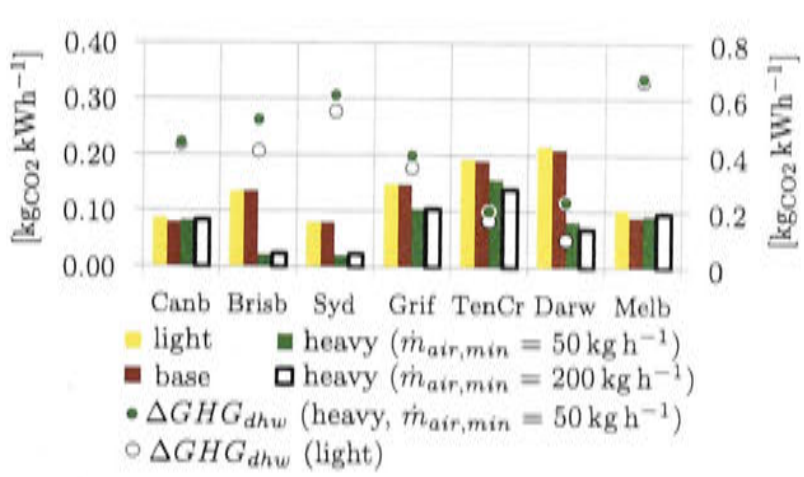

(b) GHG_{dhw}

Figure 8.102: Specific greenhouse gas emission comparing the base case to heavy and light weight structures. Specific greenhouse gas savings compared to the reference case $\Delta GHG = GHG_{ref} - GHG$

The specific cost and greenhouse gas emissions can be seen in Figure 8.101 and 8.102. In Brisbane and Sydney the collectors could have been chosen much smaller, hence, the large cost.

The base case and 20% infiltration levels

After the infiltration rates were lowered by 80%, a simulation set was performed using the base case building and collector size to find the reduced required chiller capacity. The energy demand and supply results of this simulation will be used as the base to compare the effect of night flush ventilation against. The installed capacity for the base case building model at 20% infiltration levels are displayed in Figure 8.103. The minimal air mass flow rate was kept at 200 kg h^{-1}.

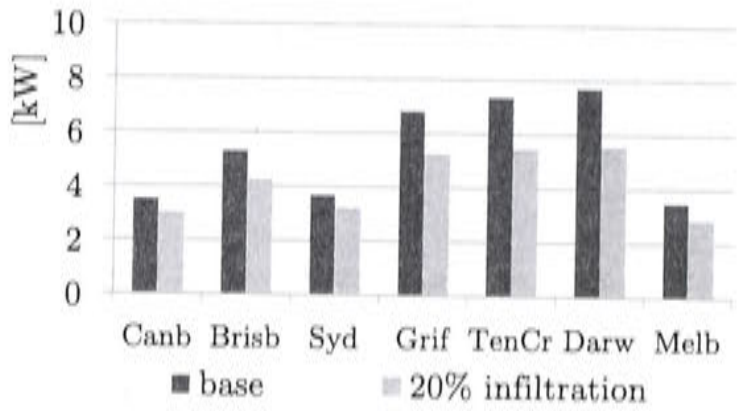

Figure 8.103: Installed cooling capacity for reduced infiltration levels to 20% of base case.

The change in relative heating and cooling demand is comparable to reducing the infiltration by 50% as in section 8.2.6. The heating demand reduces dramatically whereas the cooling demand only reduces in some climates (Brisbane, Griffith, Tennant Creek and Darwin). In Figure 8.105 the absolute demands are shown, specific to the conditioned space.

The solar fraction, not including DHW, shows a high increase which has two reasons. Firstly, the cooling capacity is reduced, but the collector size has been maintained. Secondly, the heating demand dropped drastically and less auxiliary gas was needed in winter.

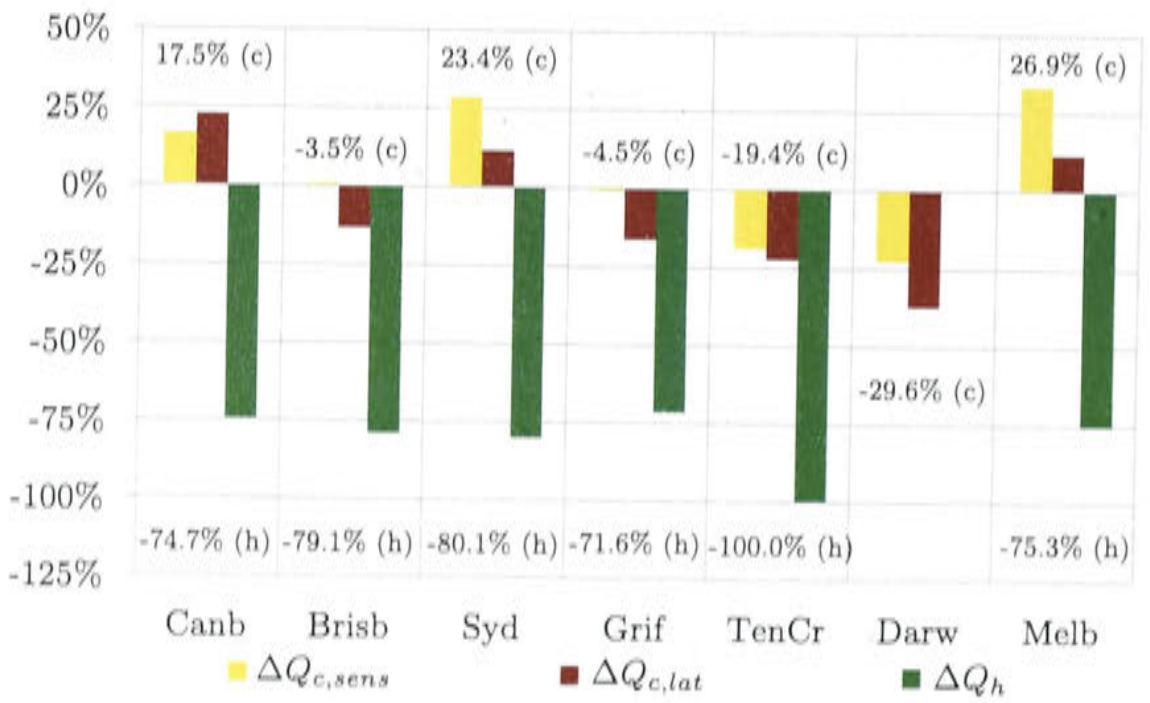

Figure 8.104: Change in heating and cooling supplied to the building. Comparison to base case.

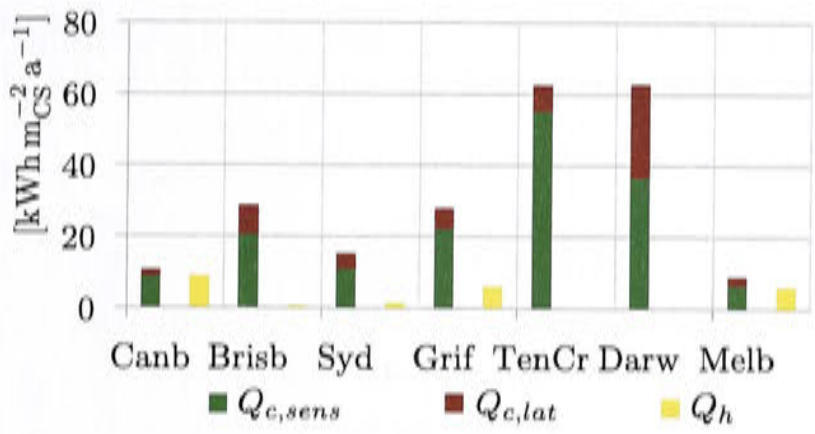

Figure 8.105: Cooling and heating demand with reduced infiltration levels to 20% of the base case.

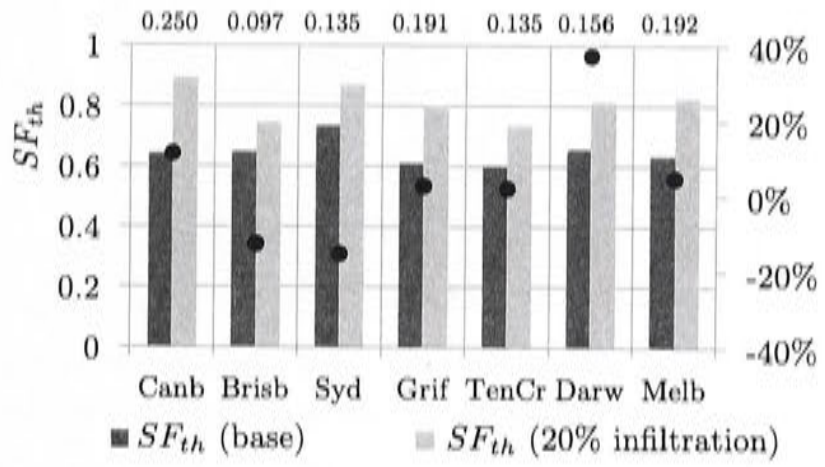

Figure 8.106: Solar fraction (left) and change of relieved heat compared to the base case (right).

The comfort conditions can be seen in Figure 8.107. The improvement in the Canberra and Melbourne winter conditions is due to the reduced heat demand.

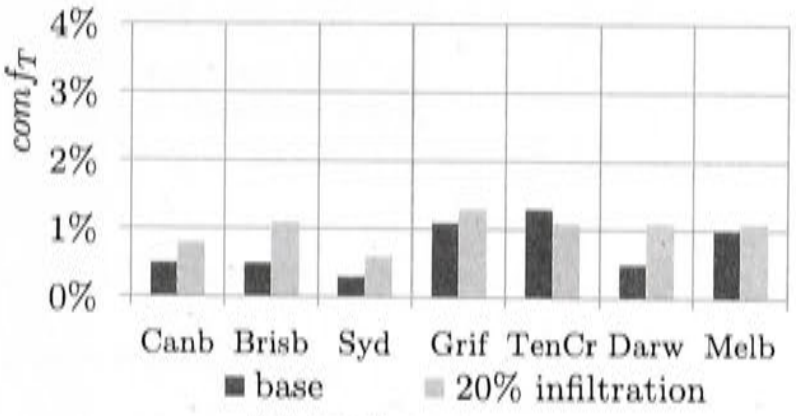

(a) $comf_T$ summer

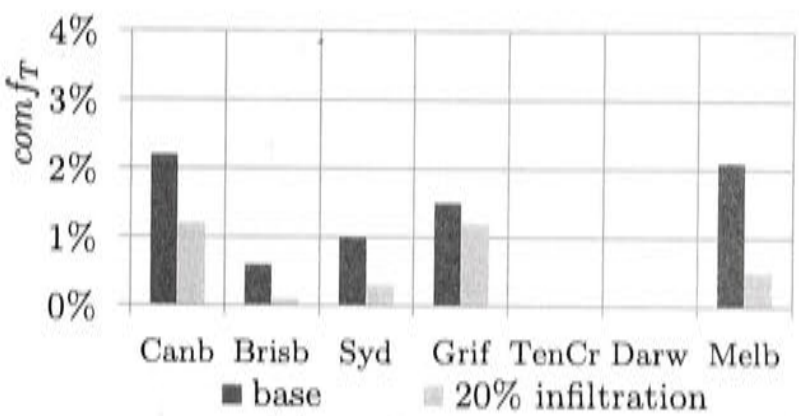

(b) $comf_T$ winter

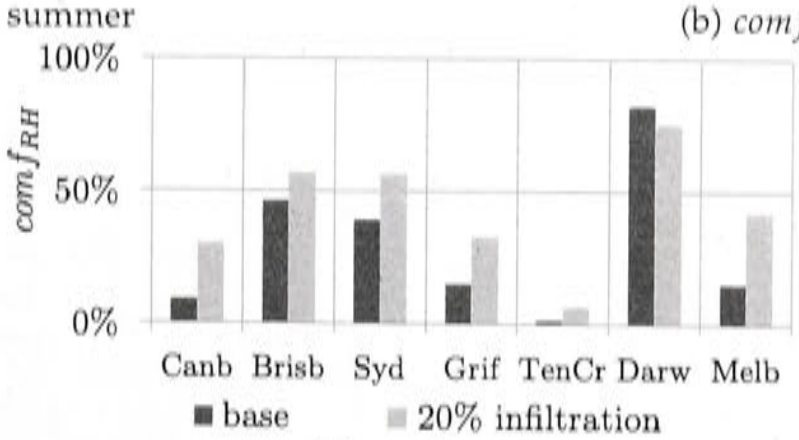

(c) $comf_{RH}$

Figure 8.107: Comfort conditions for temperature and relative humidity compareing 20% infiltration to the base case.

The change of electricity consumption is due to the reduced cooling and heating

demand and due to the down scaled equipment. The effect on specific cost and greenhouse gas emissions are presented in Figure 8.109 and 8.110.

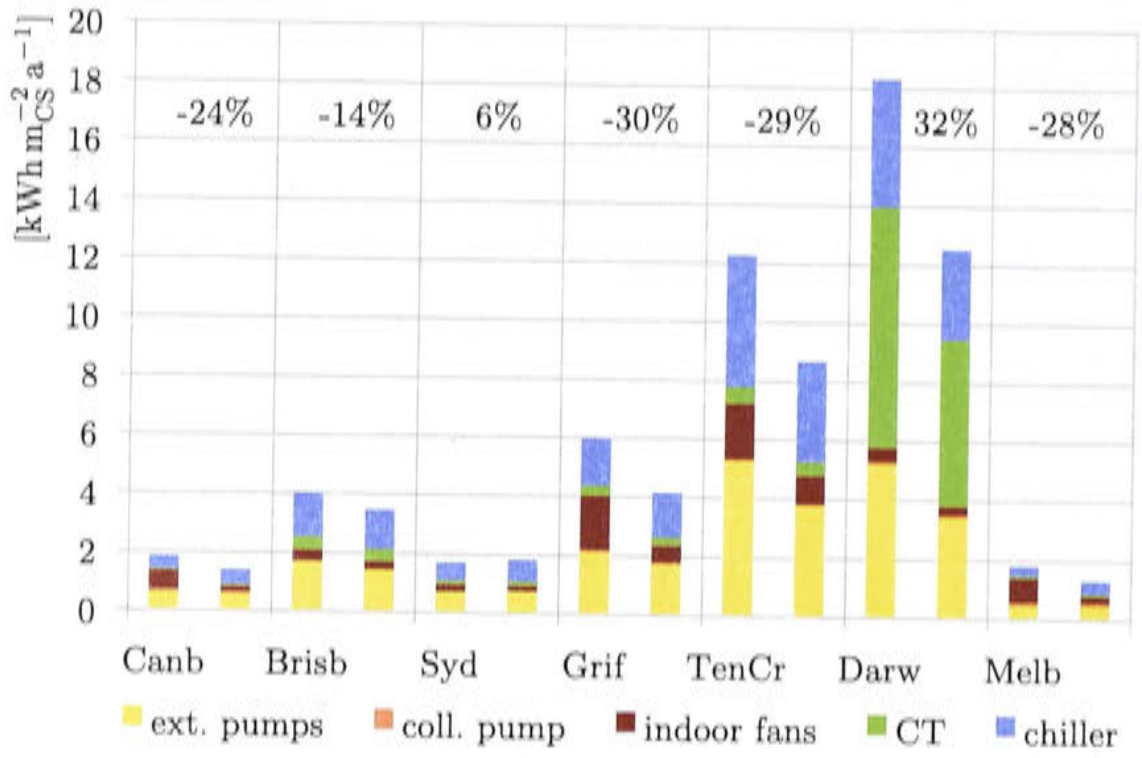

Figure 8.108: Electricity consumption of each individual consumer specific to the conditioned space, and relative change of the total electricity consumption compared to the base case (infiltration 20%)

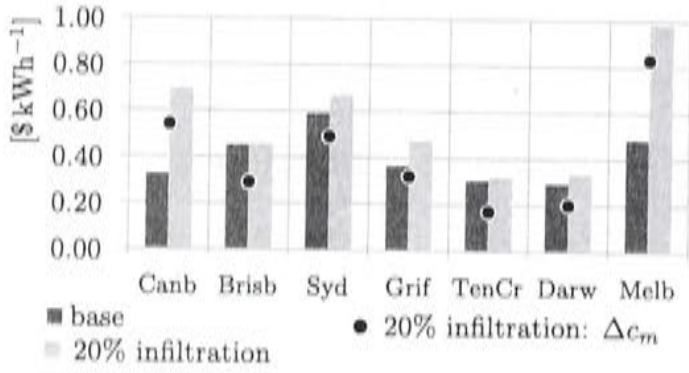

(a) c_m

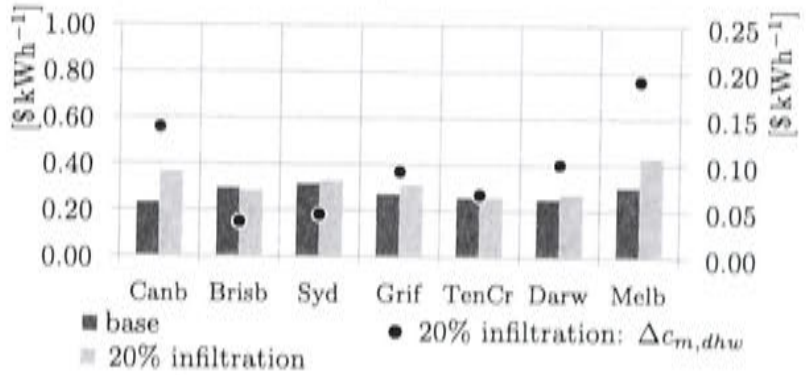

(b) $c_{m,dhw}$

Figure 8.109: Specific cost comparing the base case to the 20% infiltration levels. (Right axis: specific cost difference compared to the reference case $\Delta c_m = c_m - c_{m,ref}$)

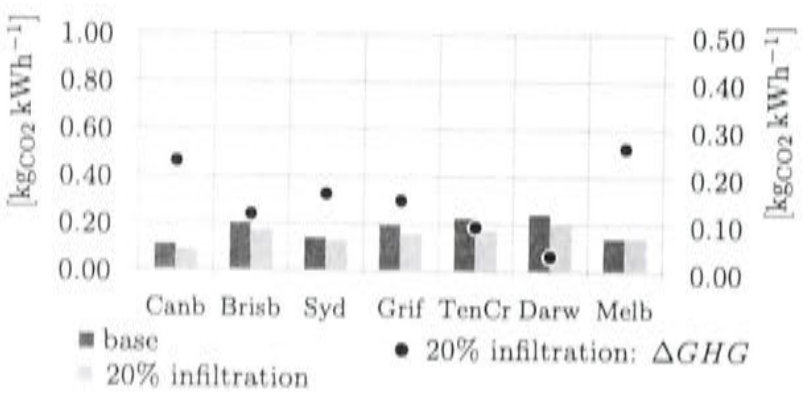

(a) GHG

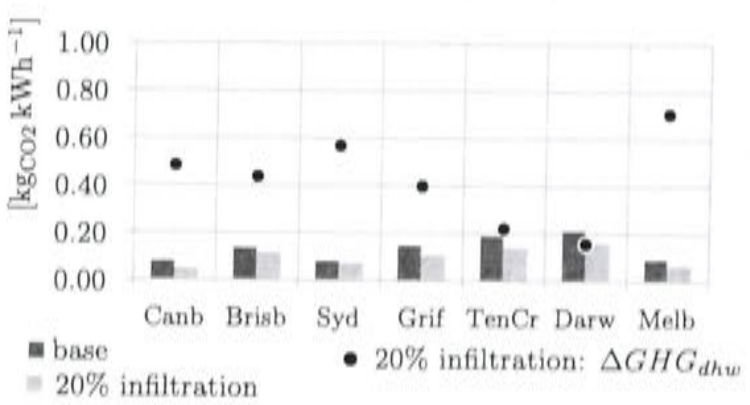

(b) GHG_{dhw}

Figure 8.110: Specific greenhouse gas emission comparing the base case to the 20% infiltration levels. Specific greenhouse gas savings compared to the reference case $\Delta GHG = GHG_{ref} - GHG$ (right axis if included)

Reducing the collector size to a solar fraction of 60% should be the way to reduce

system cost while simultaneously providing greenhouse gas savings.

Including night flush ventilation

In this section night flush ventilation is added to the model and the building is varied between base, light and heavy weight structures. The results are compared to the modeling results of 20% infiltration levels without extra night flush ventilation in section 8.2.8, which has the notation "base" in this section. The heavier and lighter building structures are not modeled with 20% infiltration excluding night flush ventilation. As a result no direct comparison can be drawn. To compare the effect of night flush ventilation for the two alternative structures, the change from the base structure to the alternative building structure at 20% infiltration levels serve as reference without night flush ventilation.

The capacities and rounded collector sizes can be found in Figure 8.111 and Table 8.23. To obtain the capacities the system was initially simulated with an oversized cooling system. In Canberra and Melbourne the effect of night flush ventilation is strongest in reducing system size comparing the two base cases with and without night flush ventilation. For heavy weight buildings the cooling capacity for Sydney is nearly zero. Changing to the light weight weatherboard structure increases the cooling system size in Canberra and Melbourne drastically.

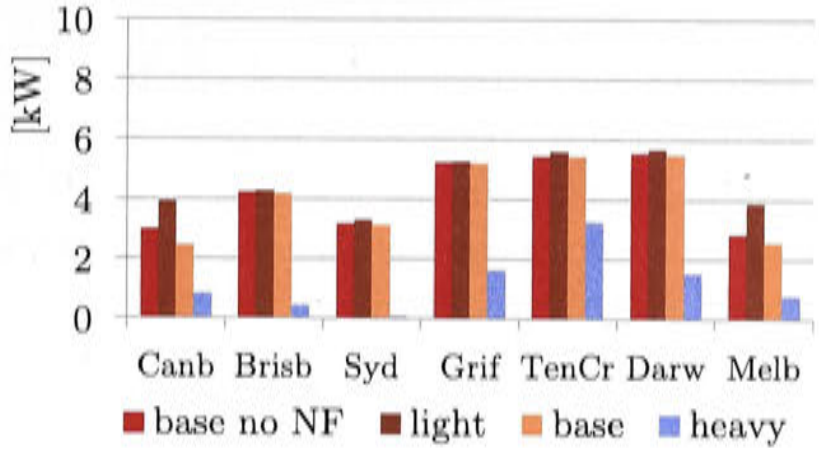

Figure 8.111: Cooling capacities 20% infiltration comparing with and without night flush ventilation for light, base and heavy weight buildings.

Table 8.23: Collector size in m^2 (NF 20%).

	light	base	heavy	base no NF
Canb	24	24	9	24
Brisb	12	12	9	12
Syd	12	12	9	12
Grif	18	18	9	18
TenCr	18	18	9	18
Darw	24	24	9	24
Melb	33	33	9	33

The cooling and heating demand of the buildings can be seen in Figure 8.112. The base case scenario with night flush ventilation reduces the cooling demand in

all climates, mostly in Canberra and Melbourne. The heat demand also increases in those climates due to the introduced outdoor air. However, the heating demand increase is small compared to the drop in cooling demand. The additional heating demand in Brisbane seems high, but the total heat demand is nearly zero (compare Figure 8.105). For Griffith night flush ventilation has the effect of percentage wise larger heating demand than cooling reduction. It seems that the night flush ventilation introduces cooled air which in return is removed during the day again by the heating system. Hence, the set points for heating remained unchanged. In a real systems, the occupants could decide if heating is required or not based on weather forecast and personal preferences. Also, setting the daily maximum higher than 25°C could have reduced the days night flush ventilation is invoked.

When comparing the change of cooling and heating demand of light weight buildings at 100% infiltration levels in Figure 8.97 to the change at 20% infiltration in Figure 8.112, it can be seen that the increase in cooling demand is smaller than without night flush ventilation (at full infiltration levels though). The second effect for all climates is, that the heating demand increases. This effect was most noticeable in the cold climates. Brisbane, Sydney and Griffith do not change their building structure towards light weight and the difference compared to the base case without night flush ventilation is due to the effect of night flush ventilation. It is difficult to distinguish the effect of night flush ventilation directly for heavy and light weight buildings as no simulations were performed with light and heavy weight buildings at 20% infiltration levels without night flush ventilation. For the heavy weight buildings night flush ventilation and 20% infiltration levels reduce cooling demand and heating demand strongly, but again, there is no clear separation on how much reduction is caused by the building thermal mass and how much is due to the night flush ventilation. The heavy weight structure simulations with strongly reduced cooling capacity were performed at a minimal air flow of 50 $\mathrm{kg\,h^{-1}}$.

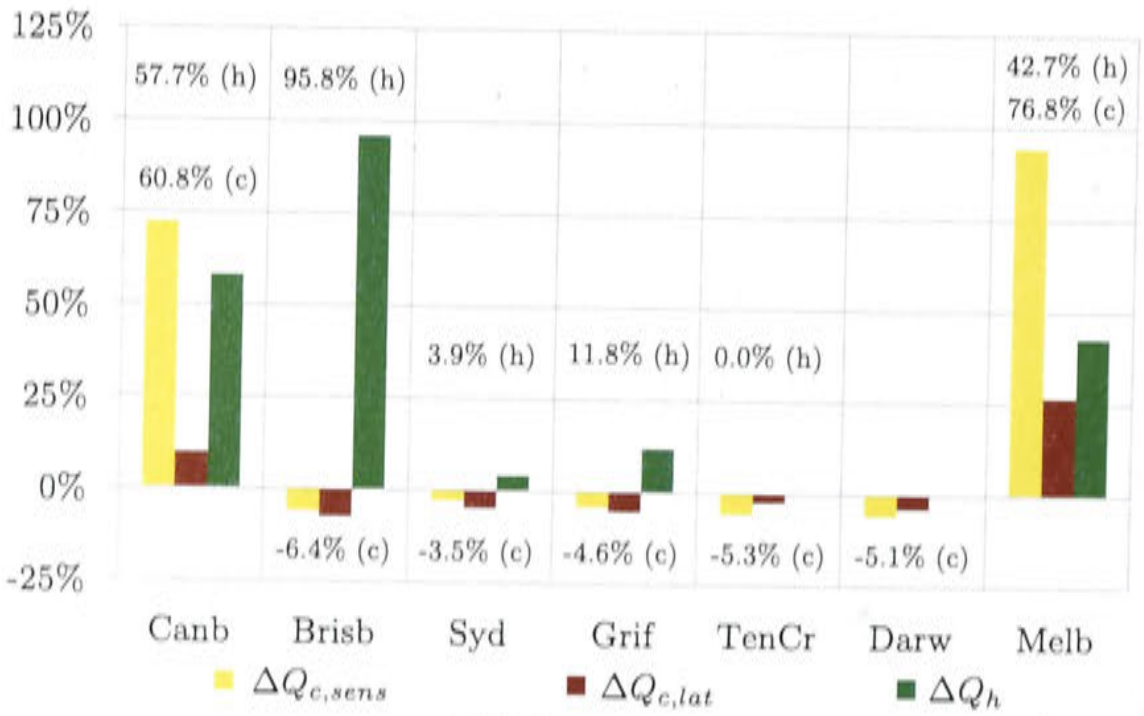

(a) light weight

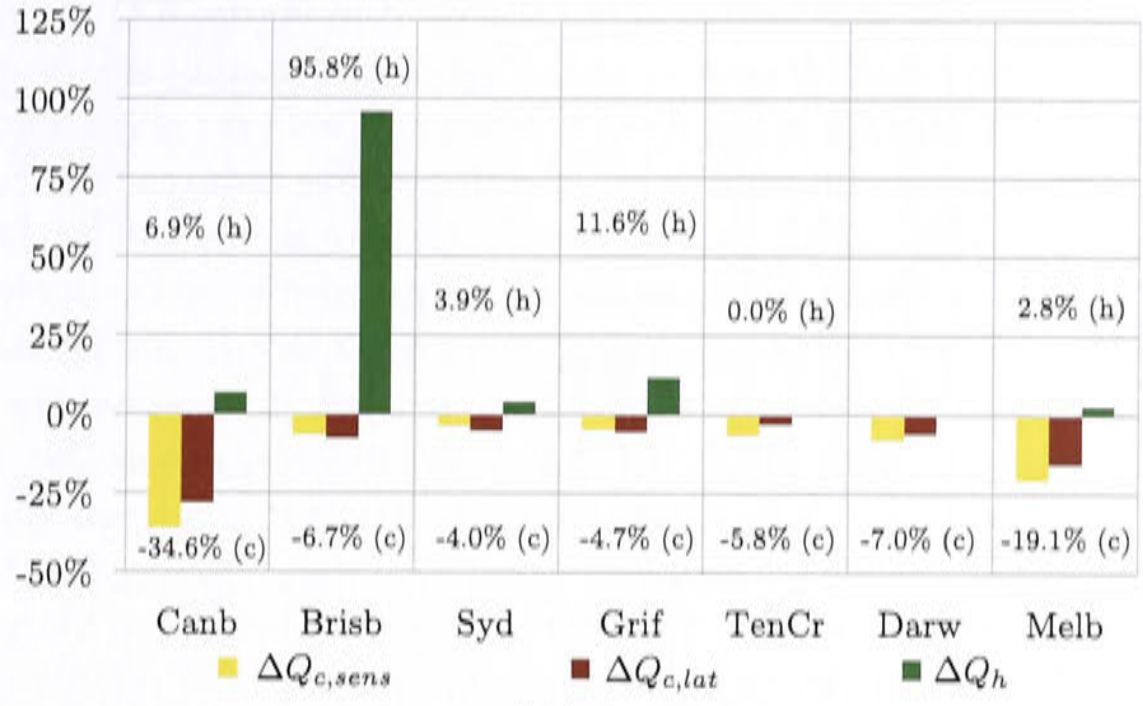

(b) base

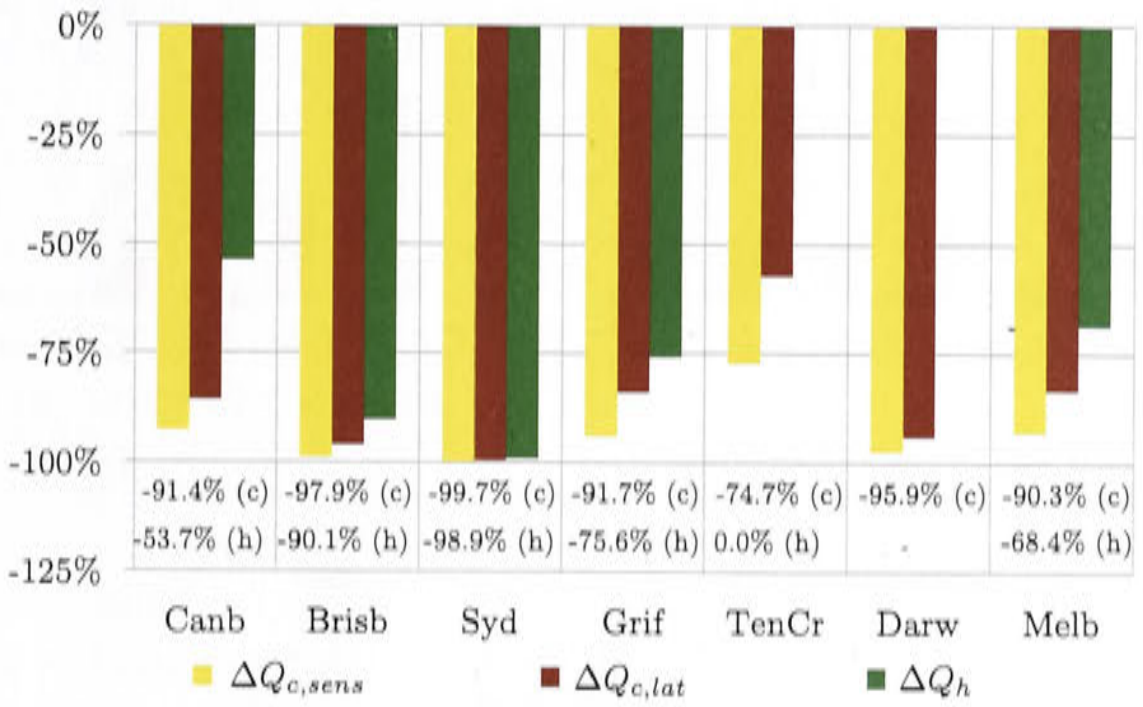

(c) heavy weight

Figure 8.112: Relative change in heating and cooling demand of the different building structures compared to the base case with 20% infiltration levels and no night flush ventilation.

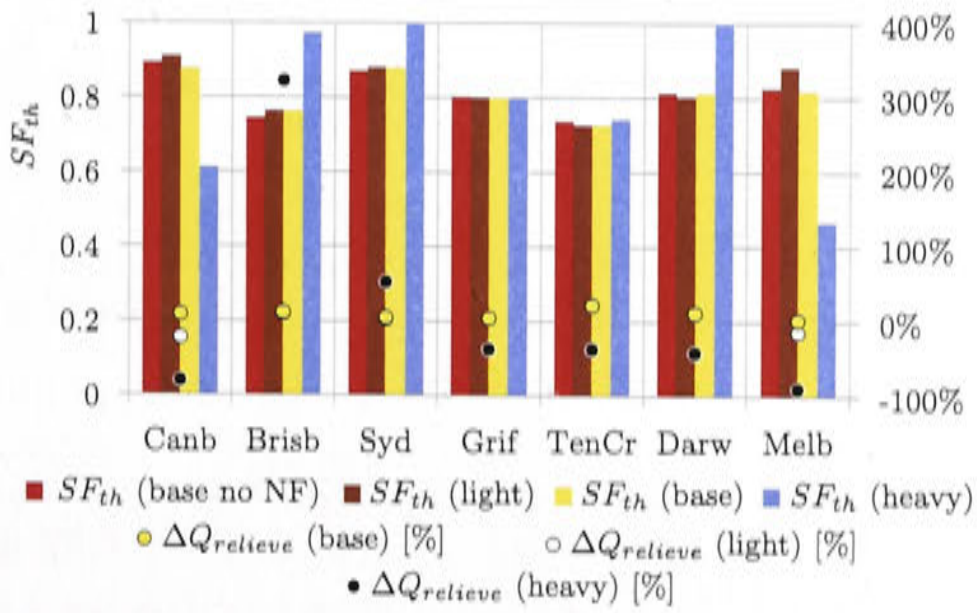

Figure 8.113: Solar fraction (left) and change of relieved heat (right) comparing the different building structures.

The solar fraction for all structures are compared in Figure 8.113. Heavy weight buildings generate by far the largest change, but that is mainly due to the reduced cooling load and the collector being fixed at 9 m^2. In Canberra and Melbourne most of the heat is used in winter and the reduced collector size reduces their contribution. In Darwin, Brisbane and Sydney the small collector size seems still too large. This is especially noticeable in Brisbane which shows the greatest increase in rejected heat.

The temperature comfort conditions in Figure 8.114, which are labeled "winter" and "summer" denote the times when the zone temperature exceeds or falls below the set point for heating and cooling, not necessarily the time of the year. An increase in "winter" discomfort means therefore, that the comfort condition through night flush ventilation might have been slightly too cold at times. The temperature comfort conditions for summer presented in this chart can even be improved for heavy weight buildings with a higher minimum air flow similar as explained previously for 100% infiltration levels.

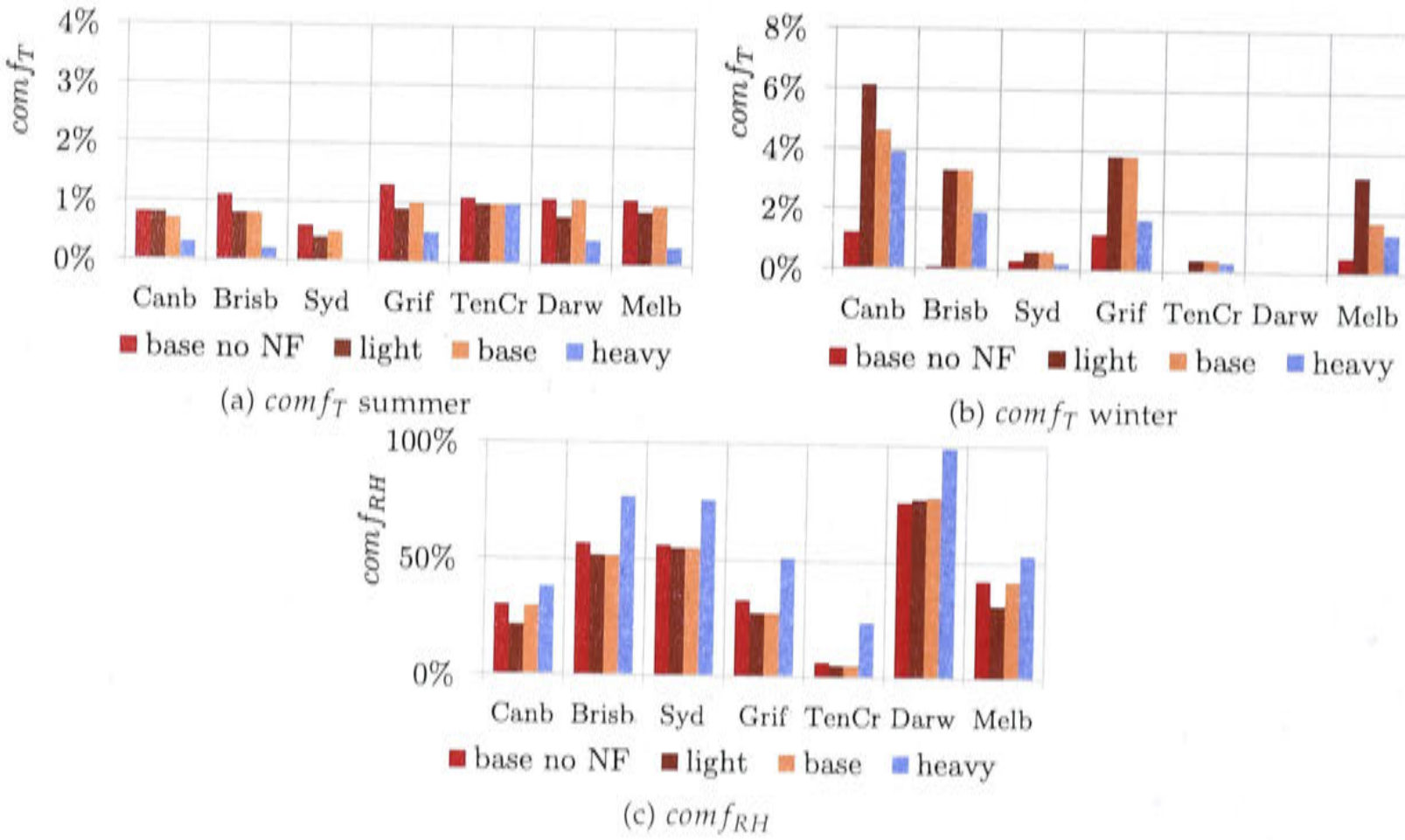

Figure 8.114: Comfort conditions for temperature and relative humidity.

The change in electricity demand for the different structures are shown in Figure 8.115 and correspond strongly to the change in cooling and heating demand. The values of total change compared to the base case without night flush ventilation are presented in Table 8.24.

Remark *Parallel to the development process of the different scenarios for section 8.2.8 and 8.2.8, the absorption chiller component has been slightly modified for the inclusion of a cold storage tank to be developed in Chapter 9.*

In detail, a section has been included in the source code of the absorption chiller component model to make it applicable to operate together with a cold storage tank. The additional control

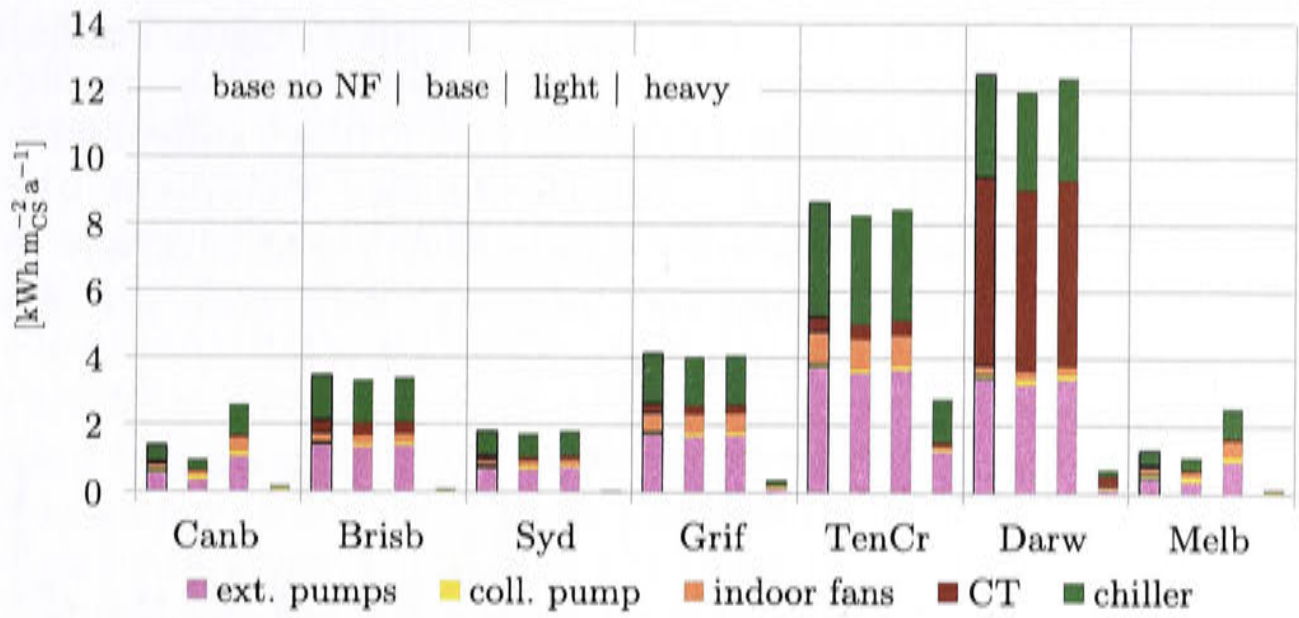

Figure 8.115: Electricity consumption of each individual consumer specific to the conditioned space compared to the base case without night flush ventilation. All at 20% infiltration levels.

Table 8.24: Change in total electricity demand comparing the different structures including night flush ventilation to the base structure without night flush ventilation, all at 20% infiltration levels

	Canb	Brisb	Syd	Grif	TenCr	Darw	Melb
base	-30%	-4%	-3%	-2%	-4%	-4%	-17%
light	88%	-2%	1%	-1%	-2%	-1%	97%
heavy	-88%	-98%	-98%	-91%	-68%	-94%	-89%

switches the chiller completely off when the incoming chilled water temperature ($T_{chw,in}$) is smaller than the minimum allowed inlet temperature. The chiller status is used by downstream components in the simulation. This control algorithm can cause a rapid switching behavior in the morning and evening when the load is small. To smooth this, in the original settings for the base case simulations and most variations the chiller does not change its status to off when the chilled water inlet temperature is too low, but merely the cooling provided in this time step is set to zero. Consequently, even though no cooling is provided, the external pumps, fans and the chiller itself still consume electricity.

A slight deviation from the base case results was detected when re-running the chosen configuration, e.g. the heating and cooling loads deviated between 0 and -1% depending on the climate. Griffith showed the percentage wise strongest deviation. The author decided that this minor issue does not justify re-running all simulations and the affected variations. However, the simulations in this section on building thermal mass and the following section on radiative cooling have been compared to the re-generated base case results using the alternative chiller control algorithm developed for the cold storage tank model.

Very interesting are the specific cost and greenhouse gas emissions in Figure 8.116 and 8.117. The specific cost in Sydney is so high for heavy weight buildings because the collector array is sized too large for the small demand. The cooling tower exceeds the set points too often (Figure 8.118), indicating that the minimal air flow for each zone could have been reduced even further than $\dot{m}_{air,min} = 50\,\mathrm{kg\,h^{-1}}$. For heavy weight structures in Sydney and to some extend in Brisbane the collector area must be downsized, or in other words such a heavy weight building in Sydney does not

need a cooling system. When looking at the base structure, night flush ventilation does not seem to make a large difference, either in specific cost or greenhouse gas savings. In all climates cooling and heating is provided to heavy structured buildings at highest cost, most likely due to the oversized collectors. The specific greenhouse gas emissions for the cooling and heating system alone are all relatively similar to each other. When including DHW on the other hand, the specific greenhouse gas emissions are proportional to the chiller's size in figure 8.111.

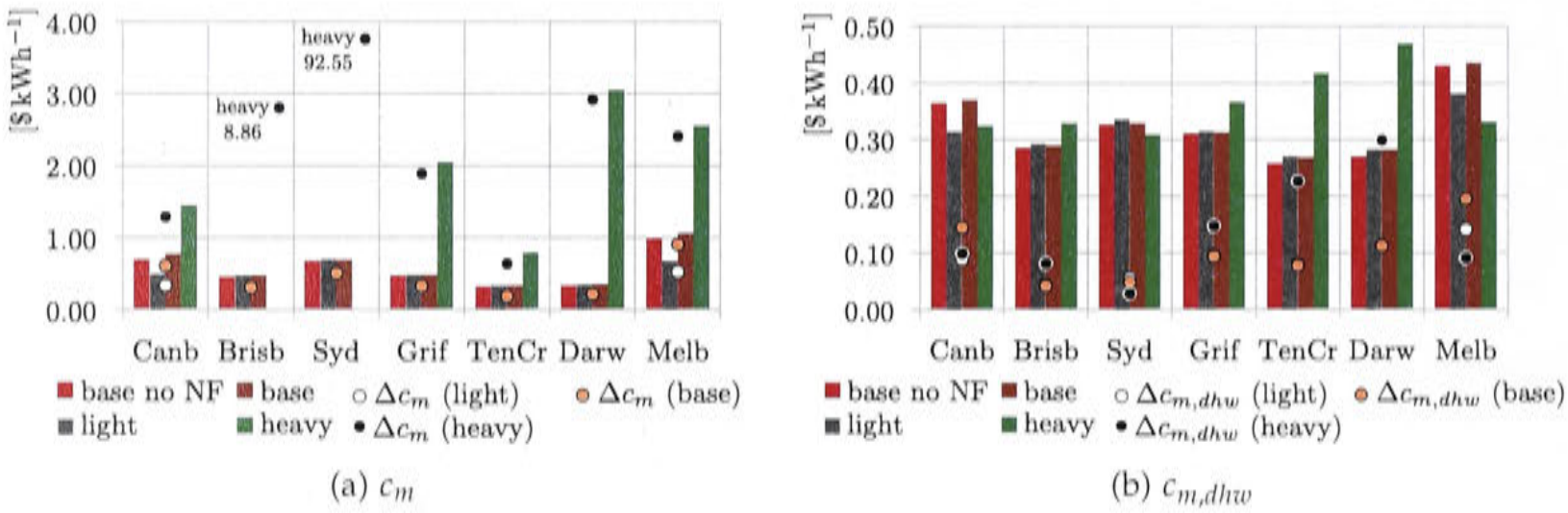

(a) c_m (b) $c_{m,dhw}$

Figure 8.116: Specific cost and cost difference compared to the reference case. $\Delta c_m = c_m - c_{m,ref}$.

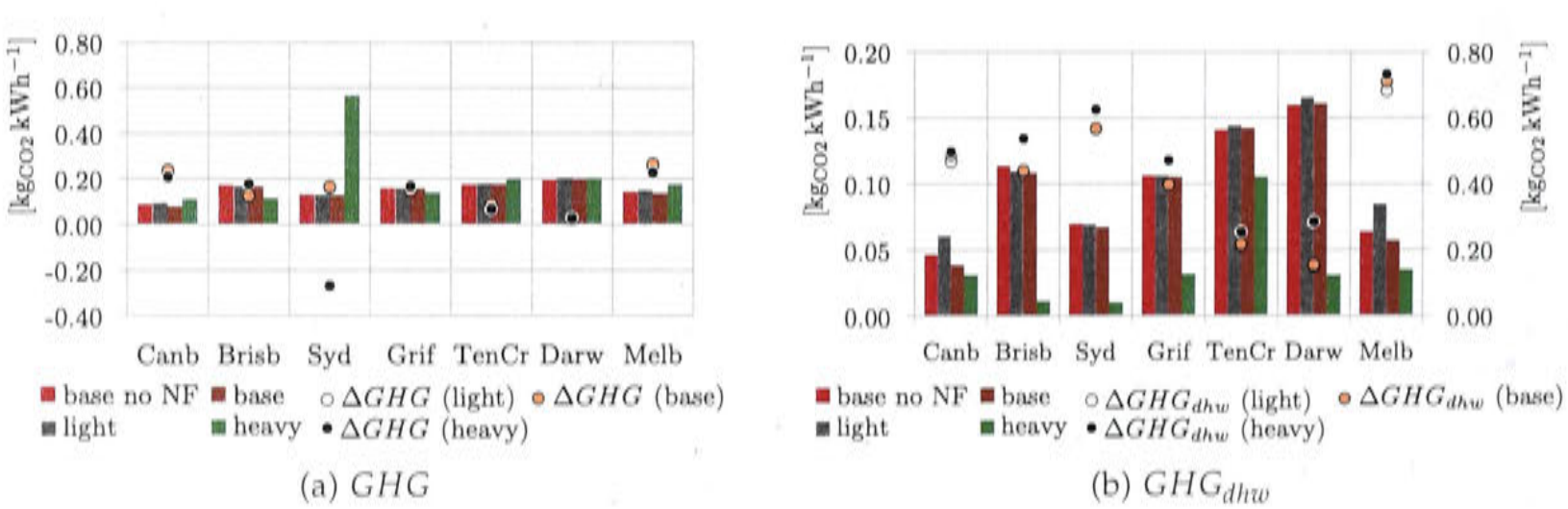

(a) GHG (b) GHG_{dhw}

Figure 8.117: Specific greenhouse gas emission and greenhouse gas savings compared to the reference case $\Delta GHG = GHG_{ref} - GHG$ (on right axis if included).

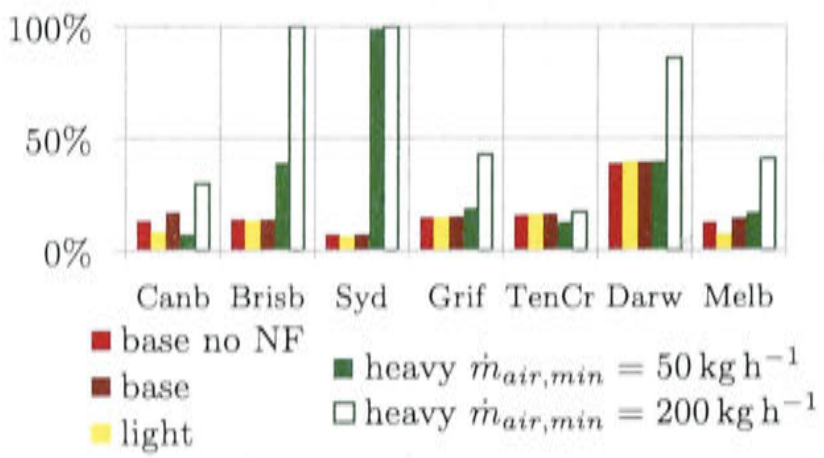

Figure 8.118: Percentage of operating time the cooling tower exceeds the set point temperature.

8.2.9 Radiant comfort applications

For this scenario the model will be amended and passive chilled beams are used to generate the cooling effect via radiative cooling. The electricity consumption for fan power for cooling will be reduced. It has to be noted that this technology exclusively is not suitable for humid climates since no dehumidification can take place. It is not desirable to have condensation on the radiators.

The TRNSYS building model type 56 provides the option to include a layer to any ceiling called "chilled ceiling". The parameters which were necessary to specify this layer for the chilled beams were derived from the chilled beams manufacturer FTF grop climate [2014]. The pipe spacing is set to 0.06 m and the inside pipe diameter to 0.01 m. The specific power of those panels is 170 $\mathrm{W\,m^{-2}}$ and the area of one panel is $0.68\,\mathrm{m} \cdot 5.6\,\mathrm{m} = 3.8\,\mathrm{m^2}$. The number of fluid channels per panel is set to 10 and the amount of panels per room are visible in Figure 8.119; 18 in total. The norm temperature difference to calculate the heat transfer coefficient is set to 5 K[9].

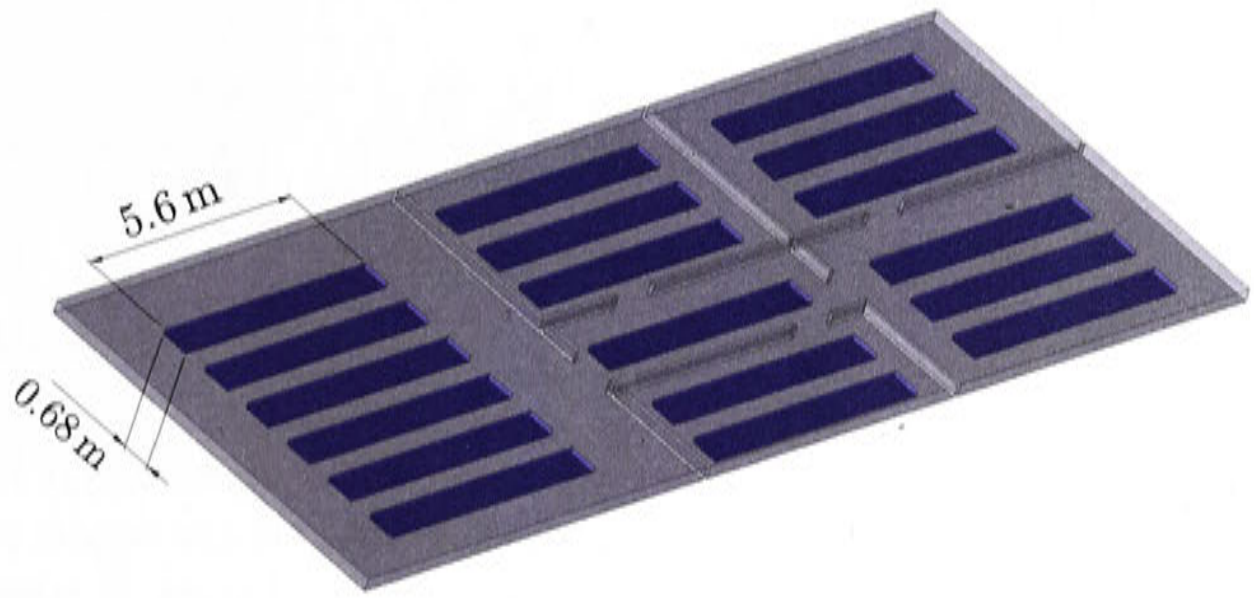

Figure 8.119: Arrangement of the chilled beams in the building, specification from FTF grop climate [2014]

The chilled water set point at the chiller is 15°C which is on the top level of the operating range for absorption and adsorption chillers. At such high chilled water temperatures the cooling water temperatures can be between 30°C and 40°C and the hot water supply temperatures can stay below 90°C.

The chilled beams water set point temperature $T_{chb,set}$ is 18°C to prevent condensation. In the TRNSYS model the chilled water circuit from the chiller was connected to the supply circuit for the chilled beams via heat exchanger. The heat exchanger was modeled without losses. In reality another flow arrangement, for example with two flow diverters, can be used to control the chilled water supply temperature to the beams at 18°C, while the chiller generates 15°C.

The chilled water pump power consumption will be estimated in the model using only one pump supplying the chiller and the beams. To derive the electricity

[9]Setting it to 10 K as per specification causes a "not a number" (NaN) error within type 56.

demand curve in relation to the chiller capacity, hence the chilled water flow rate, the system was scaled to 0%, 30%, 50% and 100% cooling capacity. For those four operating points the pressure drops of for chiller's evaporator and the pipework were estimated as explained in section 7.6, assuming a down scaling of pipes and heat exchanger. The pressure drops of the chilled beams for the different flow rates are derived from the manufacturer's chilled beams specification sheet and it is important to note that when scaling the cooling system, the amount of panels or their geometry (the radiative area) are not changed, merely the chilled water flow rate through the radiators. To calculate the pressure drops over the beams, the panels are assumed to be grouped in series of three to guarantee turbulent flow. The water flow velocity through the tubes of the panels does not exceed $1\,\mathrm{m\,s^{-1}}$. All pressure drops have been added and using equation 7.40 the power demand could be estimated. After fitting a curve to those four operating points the relationship between cooling capacity of the chiller and chilled water pump power demand has been plotted in Figure 8.120.

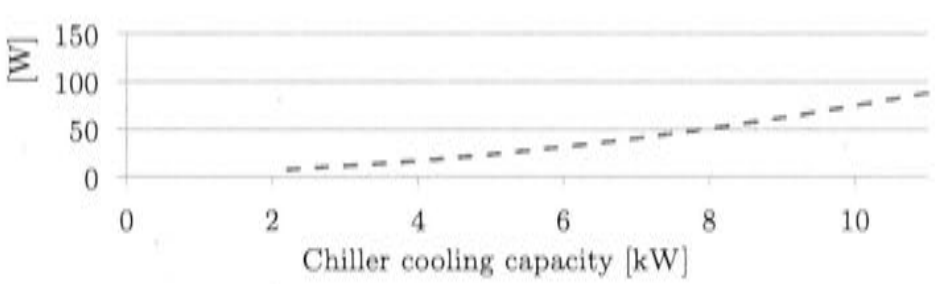

Figure 8.120: Power demand of the chilled water pump supplying evaporator and chilled beams.

In the chilled beams model the chilled water flow to the zones was divided proportionally to the conditioned volume first, as has been done previously to the fan coils. The amount of water actually flowing through the beams of zone i is the proportion λ_{chb,z_i} of that water flow and it is limited to a minimum of 20%. The remaining proportion is bypassed around the beams. The calculation of the chilled water supply to the beams follows equation 8.11. In zone 2 and 3, where there is more than one room, the chilled water is further divided in proportion to the conditioned space. This approach is less accurate than with the fan coil units, where every room was supplied with the exact air flow to cover its cooling demand.

It was necessary to vary the chilled water mass flow rates to the zones depending on the load as explained in the last paragraph, because previous simulations without mass flow control showed a frequent off and on behavior of the chilled water supply and consequently of the supplied cooling to the zone. This distorted the comfort performance factor. The cooling supplied via chilled beams served as a measure of cooling capacity sizing and if it can't be regulated for small loads average between the 95^{th} and the 100^{th} percentile of the cooling load is incorrect.

$$\lambda_{chb,z_i} = \frac{\dot{m}_{chb,z_i}}{\dot{m}_{chb,max,z_i}} \in [0.2, 1] \tag{8.11}$$

$$\dot{m}_{chb,z_i} = \frac{\dot{Q}_{sens,gain,z_i}}{(T_{setC} - T_{chb,set}) \cdot c_{p,water}} \tag{8.12}$$

$$\dot{m}_{chb,max,z_i} = scalefactor \cdot \dot{m}_{chw,rated} \cdot \frac{V_{z_i}}{V_{house}}$$

Two scenarios have been simulated varying the chilled water set point temperature $T_{chw,set}$ and the chilled beam inlet set point temperature $T_{chb,set}$. The first couple is $T_{chw,set}/T_{chb,set} = 13\,°C/16°C$ and the second one with increased set point temperatures is $T_{chw,set}/T_{chb,set} = 15\,°C/18°C$.

The solar fraction increases in most climates because the chilled water set point temperature is increased to 13°C or 15°C. Hence, the chiller needs lower driving temperatures. As a result also the relieved heat from the tank increases. In the two cooler climates Melbourne and Canberra the solar fraction decreases, which could be due to an increased heating demand due to the changed cooling technology.

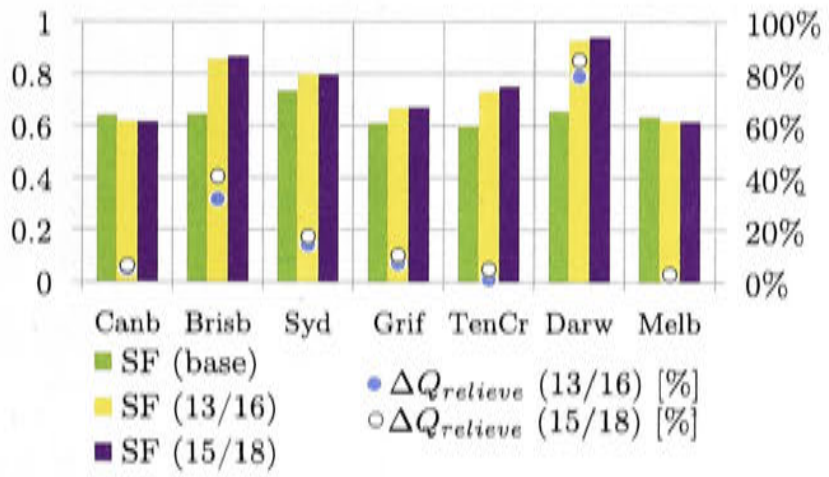

Figure 8.121: Solar fraction (left) and relative change in relieved heat from the hot water tank (right)

In Figure 8.122 and 8.123 the variation in supplied cooling and heating can be seen. The latent load disappears but the sensible load in all climates increases. In contrast to the previous technology of fan coils, which blew cold air into the building, this technology uses convection and radiation to cool the room. It is important at this place to understand that the air temperature is used to control the HVAC system and not the operating temperature. This means that walls cooled down via radiation affect the indoor air temperature once transferred to the room air via convection.

With chilled beams the heat is not merely removed from the air but also from the thermal masses of the room. Hence, it is likely that the heating demand increases to counter act the stored cooling of the day. The sensible cooling demand increases, because not only the air but also the thermal masses of the walls are cooled down through radiation.

The effect can also be seen in Figure 8.124 on the comfort conditions, particularly in Tennant Creek. The building is less comfortable in regards to temperature for longer periods of the day. Also the comfort due to relative humidity decreases as no latent cooling is provided anymore. When having a closer look at each zone, zone 2 and 3 show worse comfort conditions (not shown here). That may be related to the

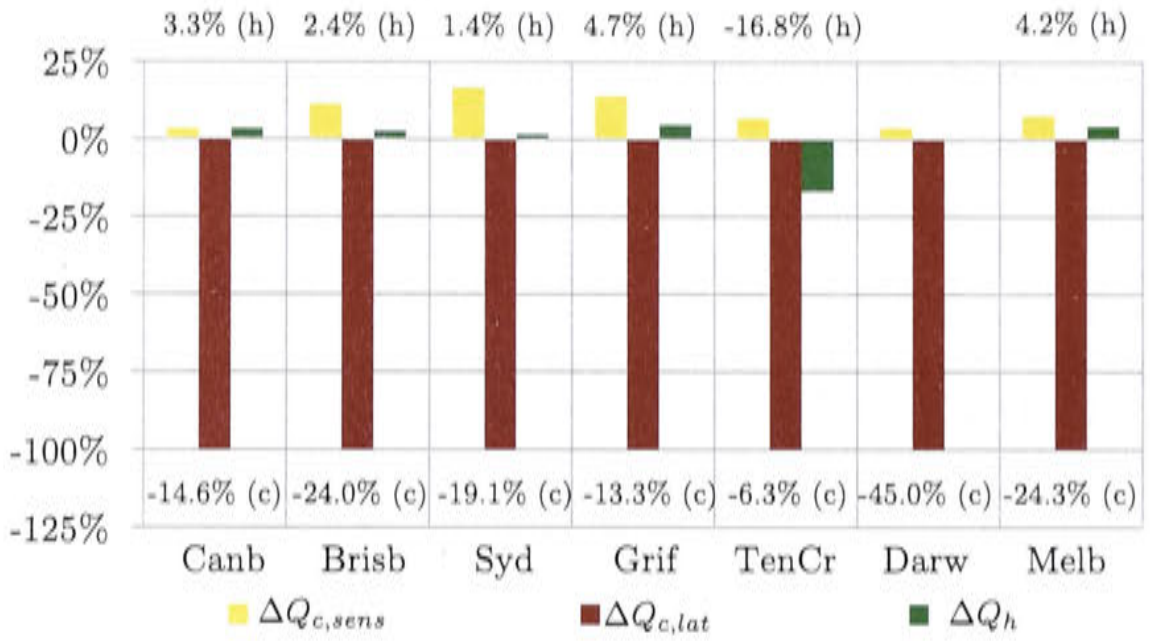

Figure 8.122: Relative change of cooling and heating demand of case (13/16) compared to the base case.

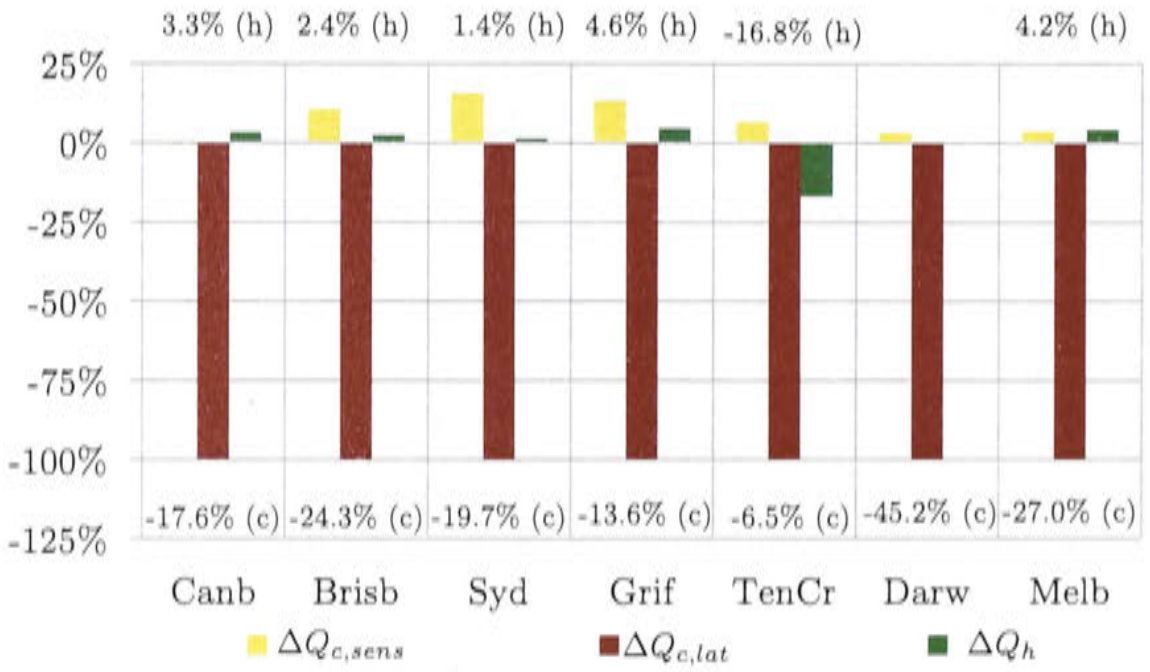

Figure 8.123: Relative change of cooling and heating demand of case (15/18) compared to the base case.

fact that the chilled water distribution between the rooms of one zone is proportional to the conditioned room space and not to the room's load.

The warm walls radiate towards the chilled beams' surfaces and much of the cooling effect is stored in the walls before actually cooling down the room air. In equation 8.12 it is assumed that the warming of the chilled water flow is only due to the sensible load and no radiative warming from the walls is considered. As a result it takes longer to condition the space. This was a valuable assumption for calculating the cooling air flow but it might underestimate the required chilled water flow rate.

The colder chilled beams temperature of 16°C performs slightly better than 18°C and more heat can be removed. The potential to downsize the chiller, and with it the external pump power consumption, is larger in humid climate, but it seems to be reduced very much by the additional radiative heat removal from the walls.

The overall electricity consumption in Figure 8.125 and Table 8.25 is much higher compared to the base case. The chiller operating hours are longer, but the cooling tower works less hard due to the smaller cooling power removed in each time step. The increase of fan power consumption in Melbourne and Canberra is mainly due to

the increase in heating demand; in all other climates it drops.

Table 8.25: Relative change of electricity consumption ΔE_{el} compared to the base case (beams).

	Canb	Brisb	Syd	Grif	TenCr	Darw	Melb
(13/16)	14.7%	13.9%	16.9%	15.2%	2.6%	14.6%	19.1%
(15/18)	15.6%	13.7%	16.8%	15.5%	2.0%	13.5%	20.1%

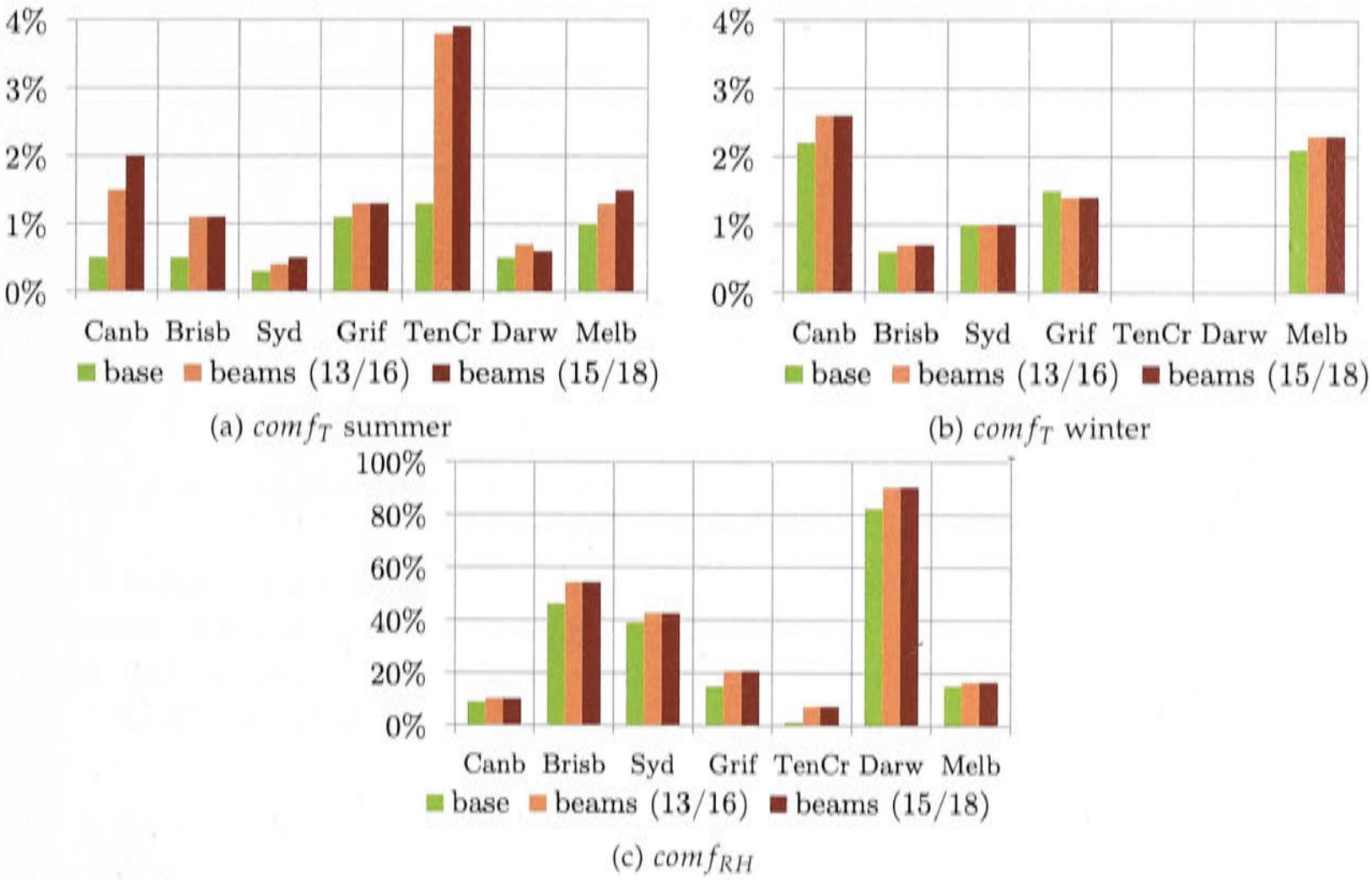

(a) $comf_T$ summer

(b) $comf_T$ winter

(c) $comf_{RH}$

Figure 8.124: Comfort conditions for temperature and relative humidity (beams).

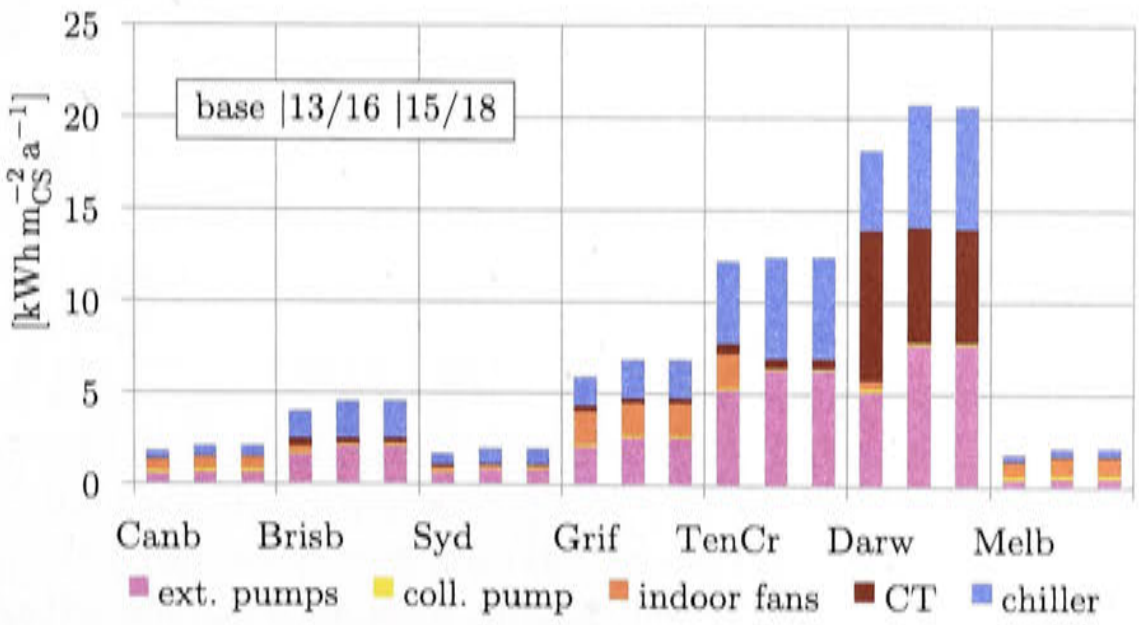

Figure 8.125: Electricity consumption of each individual consumer specific to the conditioned space compared to the base case (beams).

Table 8.26 shows the change in electricity consumption for each consumer when including chilled beams instead of fan coil units and when increasing the chilled water set point temperature.

Table 8.26: Change in electricity consumption of each consumer, comparing chilled beams to the base case.

	ext. pumps	coll. pump	indoor fans	CT	chiller
			(13/16)		
Canb	12.0%	-0.2%	11.8%	-15.1%	29.8%
Brisb	29.1%	-1.2%	-82.5%	-46.4%	38.1%
Syd	27.7%	-1.0%	-45.9%	-46.0%	42.8%
Grif	24.1%	-0.2%	-2.1%	-28.6%	33.4%
TenCr	21.7%	-0.5%	-99.8%	-20.5%	25.5%
Darw	51.4%	-2.1%	-100.0%	-23.9%	55.1%
Melb	13.1%	-0.2%	24.1%	-22.7%	32.1%
			(15/18)		
Canb	13.5%	0.0%	12.4%	-27.2%	32.2%
Brisb	27.5%	-0.5%	-82.4%	-36.6%	36.3%
Syd	26.8%	-0.6%	-45.4%	-38.0%	41.7%
Grif	23.6%	0.0%	-1.8%	-20.0%	32.7%
TenCr	20.3%	0.5%	-99.8%	-10.0%	24.1%
Darw	48.9%	-3.0%	-100.0%	-23.4%	52.6%
Melb	15.2%	-0.2%	24.5%	-29.8%	35.3%

The cost and greenhouse gas performance can be seen in Figure 8.126 and 8.127.

The cooling tower set point temperature in Figure 8.128 is less often exceeded which is due to the chiller being in operation for longer hours, however, the chiller mainly operates in part load.

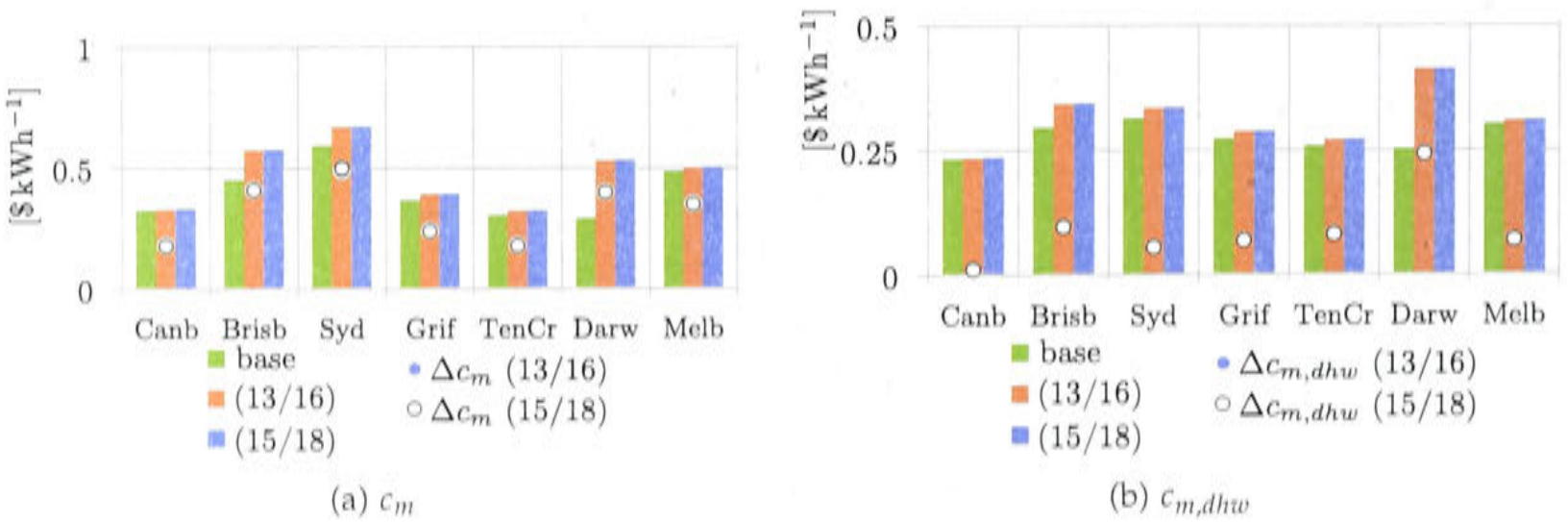

(a) c_m (b) $c_{m,dhw}$

Figure 8.126: Specific cost and cost difference compared to the reference case. $\Delta c_m = c_m - c_{m,ref}$.

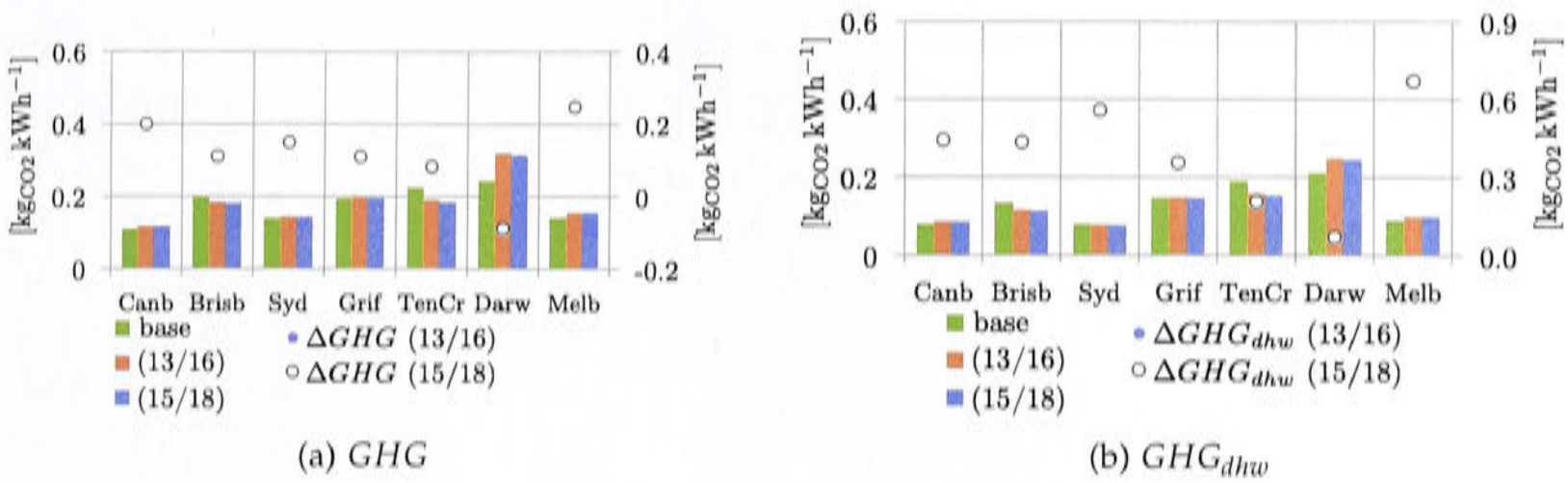

(a) GHG (b) GHG_{dhw}

Figure 8.127: Specific greenhouse gas emission and greenhouse gas savings compared to the reference case $\Delta GHG = GHG_{ref} - GHG$ (on right axis if included).

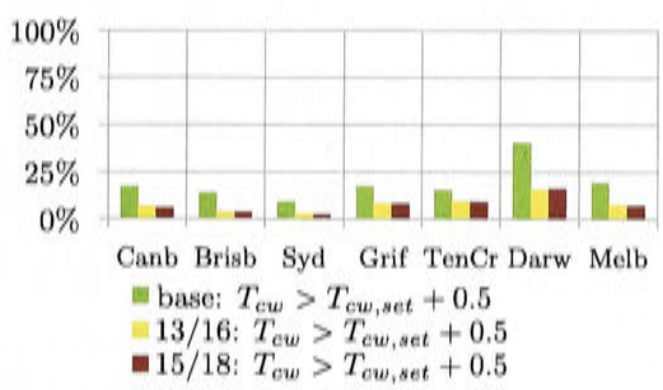

Figure 8.128: Percentage of operating time the cooling tower exceeds the set point temperature.

8.3 Conclusion solar thermal cooling and heating model

Sizing the chillers for the different climates using the *scalefactor* is a rather novel way to perform simulations for a country with such a diverse climate. In reality chillers below 5 kW cooling capacity are not yet available on the market. However, this work attempts to normalize the capacity to the building size and climate. The high electricity consumption of the chiller and its external pumps during part load operation shows the main weakness of the approach to scale the chiller to the average between the 95th and the 100th percentile of the cooling load. Sizing it smaller though, has a negative effect on the comfort conditions as shown in section 8.2.4. The electricity consumption of external pumps and the chiller itself changes proportionally to the chiller up and down-scaling as the flow rates are kept constant.

An overall conclusion for solar thermal cooling is that in order to approach cost effectiveness and being environmentally beneficial at the same time, there must be a demand of domestic hot water which the solar collectors can readily supply. In the following paragraphs the outcomes of the sensitivity study are summarized and recommendations are given for each climate. Furthermore, a comparison is drawn to large scale absorption chiller systems and possible ways of financing the technology are briefly outlined.

8.3.1 The sensitivity study

The amount of relieved heat from the tank is large in order to prevent the tank from overheating. Compared to sizing the **collector array** to a certain solar fraction, as it has been done in this approach, system designers of large scale systems prefer to size them to cope with the maximum solar energy gain of a day to prevent stagnation or not having to relieve excess heat [S.O.L.I.D., 2014]. It is questionable which approach is superior: Either to operate the chiller under full load conditions more often and being prepared to "dump" heat, or to prevent the collectors from stagnation and save the cost of overheating protection.

While varying **tank size** and collector size, it became obvious that the hot water tank served as a buffer to absorb the variations of heat supply of the collector circuit, rather than a storage option to provide the chiller with hot water for long hours in the evening. Increasing tank size above 750 L increases the solar fraction only between 0% and 3%, as the volume has to warm up to a certain degree first before it can provide heat to the chiller. Changing the **sensor height** to trigger auxiliary heating did not change the solar fraction noticeable. **Pressurizing the tank** helped to increase the solar fraction by 0% to 3%, however, the effect of loosing more heat at higher storage temperatures offsets the gains.

Even though **dry cooling towers** for heat rejection increased the electricity consumption and greenhouse gas emissions compared to a wet cooling tower, water for re-cooling could be saved which is a necessary in arid region of Australia.

When using **dehumidification strategy II or III**, the humidity comfort conditions dramatically improved, especially in the humid climates Brisbane and Darwin and in the two coastal cities Sydney and Melbourne. Both dehumidification strategies were simulated using the largest collector size of 33 m^2. Nevertheless, the solar fraction drops, and the operating hours of fans and chiller increase due to increased night and evening demand. Even though the simulations showed a cost advantage, the greenhouse gas savings decreased. Additional collectors would only improve the situation marginally because the heat would be relieved during the day instead of being stored for the evening and night, when strategy III mostly operates.

Increasing the **chilled water and air flow set point temperatures** requires a higher fan electricity input and reduces the dehmuidification potential. Nevertheless, the chiller requires lower driving temperatures and the solar fraction either stagnates or improves.

The effect on **reduced infiltration** levels reduces the heating energy demand in all climates and is most beneficial in the cooler climates. The cooling load increases in the cooler climates indicating that the infiltration might have served as ventilation. In all climates but Darwin, the reduced infiltration leads to an accumulation of indoor humidity. In the very humid climate of Darwin the reduced infiltration rates prevent the humidity to enter the building and lower the cooling load. In the very hot climates the cooling load can be reduced as well but not as strongly.

Regarding the **building structure** it can be concluded that houses with a high thermal mass are best in order to reduce the cooling load and also the heating de-

mand. The entire system has been down scaled to match the reduced load. In Sydney the resulting cooling capacity was too small and the model failed to give reasonable results.

Night flush ventilation and sealed buildings did improve the summer temperature comfort, but did effect the winter's comfort negatively as one of two events could occur: Either, there was a heating demand, but heating was not allowed during times of night flush ventilation, or the introduced flush air was too cold and consequently in the shoulder seasons the heating demand during the day was increased. In the hot climates night flush ventilation could reduce cooling by 4% to 7% and in the colder climates by 20% to 35%, however, the expense in the colder climates was an increase in heating demand. Night flush ventilation did not affect the solar fraction noticeably. In general, night flush ventilation is difficult to model, because human behavior plays an important role in reality. The human comfort range is relatively narrow and in a residential building it might not be desired to cool the zones down below heating set points during the night. In commercial buildings night flush ventilation might be more applicable, as during the night without occupation the comfort range can be extended. As cost are specific to the provided cooling and heating they increase strongly for low infiltrated, heavy buildings with large collector arrays.

Radiant comfort applications modeled as chilled beams decreased the summer's temperature comfort compared to the base case due to the altered heat transfer characteristic. It is not possible to remove any humidity with chilled beams, therefore they are not recommended as the only mean for cooling in humid climates. In the colder climates they lead to an increase in heating demand. In the warmer climates the higher chilled water set point temperature increased the solar fraction. Instead of the room air temperature an operative temperature could be used for control purposes, which considers heat due to radiation. The cooling system cannot be sized smaller, even though the latent loads disappear, because in order to keep the indoor air temperature at its set point, the beams remove radiative heat from the walls in addition to the sensible loads from the room air volume.

8.3.2 Climate specific conclusions

Canberra

Canberra is the Australian capital and is located in the Australian Capital Territory (ACT) (35.3° S, 149.1° E), which is surrounded by the 243 times larger state of New South Wales (NSW). It is approximately 150 km inland from the east coast. The weather is characterized by very clear days all year round with large diurnal temperature swings. Its summers are warm, and its winters cold. The solar radiation data from the meteonorm weather file used shows that the global radiation on the horizontal is above $700\,\mathrm{W\,m^{-2}}$ for 10% of the year, excluding night time hours. The average wet bulb temperature of 9.3°C is lowest of all climates and the **cooling tower** in the model is able to achieve 27°C cooling water supply temperature more than 80% of the time. The water consumption for the cooling tower is $3.51\,\mathrm{kWh^{-1}}$ of cooling supplied.

The building structure implemented in the model for this climate zone is insulated reverse brick veneer. The installed cooling capacity is $15\,W\,m_{CS}^{-2}$ and the average of the heating load between the 95th and 100th percentile is $28\,W\,m_{CS}^{-2}$. The change of the dehumidification strategy towards higher humidity reduction increases the installed cooling capacity by up to 26% (strategy III). The annual **heating demand** of $36\,kWh\,m_{CS}^{-2}\,a^{-1}$ is almost 4 times larger than the total **cooling demand**, and the latent proportion for cooling is below 20%.

Lowering the infiltration levels by 50% reduces the heating demand in Canberra by a remarkable 50%, however, the cooling demand increases by 9%. When reducing infiltration levels further to 20% of the base case levels, the heating demand can be reduced to 75%. In this case, including night flush ventilation provides enough natural cooling to offset and exceed the cooling demand increase of 17% due to the low infiltration rates during the day. Well sealed buildings are highly recommended. However, the temperature discomfort due to exceeding the minimal heating set point temperature for winter, is increased by 2.2% due to including night flush ventilation, compared to the base case. The cooling and heating demand can be reduced strongly using heavier building structures. However, the heating demand does not drop to the same extend as the cooling demand and the collector area cannot be reduced proportionally to the chiller's cooling capacity.

The temperature **comfort** conditions in summer are well met and are exceeded less than 1% of the time. For heating they are exceeded 2% of the time. The model showed a slight increase in temperature comfort when changing the set points of the chilled water temperature to 11°C and for the air outlet temperature to 16°C. The comfort levels due to humidity could be maintained approximately 91% of the time. Sealing the building reduced this value strongly due to accumulation of internal humidity. The dehumidification strategy III improved the comfort due to humidity by almost 5% points, however, the cooling increase was 84%.

To achieve a **solar fraction** (SF_{th}) for heating and cooling of at least 60%, $24\,m^2$ of collector have been chosen. When including the DHW generation in the calculation, the solar fraction improves by approximately 9% points. The large collector area is mainly due to the large demand for heating and leads to a relatively large amount of relieved heat ($\approx 9.2\,MWh\,a^{-1}$) in summer. The relieved heat can be reduced by 1/3 when orienting the collectors westward, but the solar fraction drops by 11% points.

The **electricity consumption** specific to the amount of cooling and heating generated is lowest of all climates ($ES = 0.041\,kWh_{el}$ per kWh of useful energy for cooling and heating). This again is related to the high demand for heating. The largest electricity consumers are the indoor fans. When including DHW in the calculation the specific electricity consumption can be reduced further by 30%.

The **cost** to save $1\,kg_{CO2\text{-}eq}$ using the chosen collector and tank configuration is \$0.82. However, when including DHW in the calculation the cost can be reduced to \$0.02 for each $1\,kg_{CO2\text{-}eq}$ saved. Instead of using cost values specific to the amount of cooling, heating and DHW generated, a break even electricity price can be calculated on the assumption of identical energy output, which is $\$0.65\,kWh^{-1}$ excluding, and $\$0.26\,kWh^{-1}$ including DHW.

Table 8.27: Summary Canberra

Canberra		
Building structure $G_{tot} > 700\,\mathrm{W\,m^{-2}}$	Reverse brick veneer (insulated) 9.6	 %
Chiller capacity	14.9	$\mathrm{W\,m_{CS}^{-2}}$
Heating load	28.3	$\mathrm{W\,m_{CS}^{-2}}$
Collector area (chosen conf.)	24	$\mathrm{m^2}$
Hot water storage volume (chosen conf.)	0.75	$\mathrm{m^3}$
Annual cooling energy demand	9.2	$\mathrm{kWh\,m_{CS}^{-2}\,a^{-1}}$
Latent proportion	17	%
Annual heating energy demand	35.8	$\mathrm{kWh\,m_{CS}^{-2}\,a^{-1}}$
Annual energy demand for DHW	4116	$\mathrm{kWh\,a^{-1}}$
Relieved heat	9.2	$\mathrm{MWh\,a^{-1}}$
Solar fraction increase incl. DHW	9	%
Cost for greenhouse gas abatement	0.82	$\mathrm{\$\,kg_{CO2}^{-1}}$
Cost for greenhouse gas abatement incl. DHW	0.02	$\mathrm{\$\,kg_{CO2}^{-1}}$
Break even electricity price excl. DHW	0.65	$\mathrm{\$\,kWh^{-1}}$
Break even electricity price incl. DHW	0.26	$\mathrm{\$\,kWh^{-1}}$
Add. cooling capacity strategy II	15	%
Add. cooling capacity strategy III	26	%

Brisbane

Brisbane is the capital of the state Queensland (QLD) and located at the coordinates 27.5° S and 153.0° E at the east coast. The summers are warm and humid and the winters very mild. The solar radiation data from the meteonorm weather file used shows that the global radiation on the horizontal is above $700\,\mathrm{W\,m^{-2}}$ for 10% of the year, excluding night time hours. The average wet bulb temperature is second largest of all climates after Darwin with 16.4°C. However, the cooling tower achieves its set point more than 85% of the time using $3.51\,\mathrm{kWh^{-1}}$ of cooling supplied.

The building implemented in the model for Brisbane is a insulated light weight weatherboard structure and the installed chiller capacity is $23\,\mathrm{W\,m_{CS}^{-2}}$ for cooling. The average of the heating load between the 95$^{\mathrm{th}}$ and 100$^{\mathrm{th}}$ percentile is $8\,\mathrm{W\,m_{CS}^{-2}}$. The annual energy **demand for heating** in winter is 12% of the cooling demand in summer. The **cooling demand** is $30\,\mathrm{kWh\,m_{CS}^{-2}\,a^{-1}}$, of which one third is latent cooling. When increasing the reduction of latent heat using strategy II and III, the installed cooling capacity increases by 30% and 35% respectively, compared to the base case. Heavier building structures reduce the cooling demand drastically, however, dehumidification seems insufficient, which is indicated by the strong increase in discomfort due to high indoor humidity levels. Reducing the infiltration levels also reduces the demand for cooling by 3.5% (20% infiltration levels), however, without night flush ventilation the indoor humidity comfort drops by 10% points. In humid climates infiltration seems to act as ventilation.

The temperature **comfort** conditions are well met, exceeding the set points 0.5%

of the time in summer and 0.6% of the time in winter. Comfort conditions with respect to humidity are exceeded 45% of the time, which can be reduced to 18% with dehumidification control strategy III, however, the cooling increase is 170% and the greenhouse gas generation is as high as in the reference case without controlled dehumidification. Increasing the chilled water set point to 11°C reduces the proportion of latent heat removal by 7% points and the comfort due to indoor humidity levels drops by 4% points, nevertheless, the auxiliary gas consumption decreases. Radiant cooling applications without dehumidification support are not recommended for Brisbane.

Table 8.28: Summary Brisbane

Brisbane		
Building structure	Weatherboard (insulated)	
$G_{tot,hor} > 700\,W\,m^{-2}$	10.4	%
Chiller capacity	22.7	$W\,m_{CS}^{-2}$
Heating load	7.8	$W\,m_{CS}^{-2}$
Collector area (chosen conf.)	12	m^2
Hot water storage volume (chosen conf.)	0.40	m^3
Annual cooling energy demand	30.0	$kWh\,m_{CS}^{-2}\,a^{-1}$
Latent proportion	32	%
Annual heating energy demand	3.7	$kWh\,m_{CS}^{-2}\,a^{-1}$
Annual energy demand for DHW	4056	$kWh\,m_{CS}^{-2}\,a^{-1}$
Relieved heat	0.8	$MWh\,a^{-1}$
Solar fraction increase incl. DHW	7	%
Cost for greenhouse gas abatement	3.15	$\$\,kg_{CO2}^{-1}$
Cost for greenhouse gas abatement incl. DHW	0.12	$\$\,kg_{CO2}^{-1}$
Break even electricity price excl. DHW	1.40	$\$\,kWh^{-1}$
Break even electricity price incl. DHW	0.36	$\$\,kWh^{-1}$
Add. cooling capacity strategy II	30	%
Add. cooling capacity strategy III	35	%

To achieve a **solar fraction** (SF_{th}) for cooling and heating of at least 60%, $12\,m^2$ of collector area were chosen with a $0.4\,m^3$ hot water buffer tank. When including DHW in the calculation the solar fraction can be improved by 7% points. For control strategy II and III, $33\,m^2$ of collector area are installed, however, the solar fraction (SF_{th}) drops by 27% and 45% points respectively, compared to a collector configuration with $33\,m^2$ and strategy I. The relative change of relieved heat is very sensitive to variations altering the load because the absolute relieved heat is smallest of all climates with $0.8\,MWh\,a^{-1}$.

The **electricity consumption** specific to the amount of cooling, heating (and DHW) generated (ES) is $0.12\,kWh_{el}$ per kWh of useful energy for cooling and heating. It can be improved by 35% if DHW is included in the calculation. In Brisbane using dry heat rejection at 27°C cooling water set point temperature leads to an increase in electricity consumption 2.6 times larger than the increase in the relatively dry climate of Canberra.

The **costs** to save 1 $kg_{CO2\text{-}eq}$ using the chosen collector and tank configuration is \$3.15. However, when including DHW in the cost can be reduced to \$0.12 for each 1 $kg_{CO2\text{-}eq}$ saved. The cost for strategy II to save 1 $kg_{CO2\text{-}eq}$ is 26% higher and in strategy III no greenhouse gases can be saved compared to the reference technology without additional dehumidification. Instead of using cost values specific to the amount of cooling, heating and DHW generated, a break even electricity price can be calculated on the assumption of identical useful energy outputs, which is \$1.40 kWh^{-1} excluding, and \$0.36 kWh^{-1} including DHW.

Sydney

Sydney is the capital of the state New South Wales (NSW) and is located at the coordinates 33.9° S and 151.2° E at the east coast. The summers are warm and the winters mild, with a low diurnal temperature swing, barely changing throughout the months. The solar radiation data from the meteonorm weather file used shows that the global radiation on the horizontal is above 700 $W\,m^{-2}$ for 9% of the year, excluding night time hours. The average wet bulb temperature is 14.4°C and the cooling tower achieves its set point more than 90% of the time using 3.31 kWh^{-1} of cooling supplied.

The building structure implemented in the TRNSYS model is insulated light weight weatherboard and the installed chiller capacity is 16 $W\,m_{CS}^{-2}$ for cooling. The average of the heating load between the 95th and 100th percentile is 11 $W\,m_{CS}^{-2}$. The annual energy **demand for heating** in winter is 62% of the cooling demand in summer. The **cooling demand** is 12 $kWh\,m_{CS}^{-2}\,a^{-1}$, of which 30% is latent cooling. When increasing the reduction of latent heat using strategy II and III, the installed cooling capacity increases are 39% and 68% respectively, compared to strategy I. Heavier building structures reduce the cooling demand to the point that hardly any cooling is necessary anymore. However, the discomfort related to an increased indoor humidity reveals that a latent cooling demand remains, which is not removed by control strategy I. Reducing the infiltration levels increases the demand for cooling by 23.4% (20% infiltration levels). After including night flush ventilation, the cooling demand can only be reduced by 4%. Nevertheless, as for all other climates, the heating demand can be reduced strongly when reducing infiltration.

The temperature **comfort** conditions are well met, exceeding the set points 0.3% of the time in summer and 1.0% of the time in winter. Comfort conditions with respect to humidity are exceeded 39% of the time, which can be reduced to 35% and 20% with dehumidification control strategy II and III. However, the cooling increase is 68% and 295% respectively. Increasing the chilled water set point to 11°C reduces the proportion of latent heat removal by 9% points, however, the comfort due to indoor humidity levels remains unaffected. Radiant cooling applications without dehumidification only increase the discomfort due to humidity by 3.4% points.

To achieve a **solar fraction** (SF_{th}) for cooling and heating of at least 60%, 12 m^2 of collector area were chosen with a 0.4 m^3 hot water buffer tank. When including DHW in the calculation, the solar fraction can be improved by 8% points. The relieved heat

is second smallest with 2.1 MWh a^{-1}. For control strategy II and III, 33 m^2 of collector area are installed. Nevertheless, the solar fraction (SF_{th}) drops by 20% and 42% points respectively, compared to a collector configuration with 33 m^2 using control strategy I.

The **electricity consumption** specific to the amount of cooling, heating (and DHW) generated (ES) is 0.085 kWh_{el} per kWh of useful energy for cooling and heating. It can be lowered by 47% if DHW is included in the calculation. In Sydney using dry heat rejection at 27°C cooling water set point temperature leads to an increase in electricity consumption by 20%.

The **costs** to save 1 $kg_{CO2\text{-}eq}$ using the chosen collector and tank configuration is \$2.75. However, when including DHW in the calculation the cost can be reduced to \$0.06 for each 1 $kg_{CO2\text{-}eq}$ saved. The cost for strategy II and strategy III to save 1 $kg_{CO2\text{-}eq}$ is 1.5 and 3.8 times larger than in the base case scenario and strategy III becomes unreasonable high. Instead of using cost values specific to the amount of cooling, heating and DHW generated, a break even electricity price can be calculated on the assumption of identical useful energy outputs, which is \$1.41 kWh^{-1} excluding, and \$0.29 kWh^{-1} including the generation of DHW.

Table 8.29: Summary Sydney

	Sydney	
Building structure	Weatherboard (insulated)	
$G_{tot,hor} > 700\,W\,m^{-2}$	9.3	%
Chiller capacity	15.7	$W\,m_{CS}^{-2}$
Heating load	10.5	$W\,m_{CS}^{-2}$
Collector area (chosen conf.)	12	m^2
Hot water storage volume (chosen conf.)	0.40	m^3
Annual cooling energy demand	12.4	$kWh\,m_{CS}^{-2}\,a^{-1}$
Latent proportion	31	%
Annual heating energy demand	7.7	$kWh\,m_{CS}^{-2}\,a^{-1}$
Annual energy demand for DHW	4070	$kWh\,m_{CS}^{-2}\,a^{-1}$
Relieved heat	2.1	$MWh\,a^{-1}$
Solar fraction increase incl. DHW	8	%
Cost for greenhouse gas abatement	2.75	$\$\,kg_{CO2}^{-1}$
Cost for greenhouse gas abatement incl. DHW	0.06	$\$\,kg_{CO2}^{-1}$
Break even electricity price excl. DHW	1.41	$\$\,kWh^{-1}$
Break even electricity price incl. DHW	0.29	$\$\,kWh^{-1}$
Add. cooling capacity strategy II	39	%
Add. cooling capacity strategy III	68	%

Griffith

Griffith is located in the center of New South Wales (NSW) at the coordinates 34.3° S and 146.0° E. Its continental climate is characterized by hot and dry summers and cold winters, with second largest diurnal temperature swings in summer, following

Canberra. The solar radiation data from the meteonorm weather file used shows that the global radiation on the horizontal is above $700\,W\,m^{-2}$ for 12% of the year, excluding night time hours. The average wet bulb temperature is 12.7°C and the cooling tower achieves its set point more than 80% of the time using $3.67\,l\,kWh^{-1}$ of cooling supplied.

The building structure implemented in the TRNSYS model is insulated light weight weatherboard and the installed chiller capacity is $29\,W\,m_{CS}^{-2}$ for cooling. The average of the heating load between the 95th and 100th percentile is $19\,W\,m_{CS}^{-2}$. The annual energy **demand for heating** in winter is three quarter of the cooling demand in summer. The **cooling demand** is $29\,kWh\,m_{CS}^{-2}\,a^{-1}$, of which 24% is latent cooling. When increasing the reduction of latent heat using strategy II and III, the installed cooling capacity increases are 6% and 6% respectively, compared to strategy I. This indicates that no additional cooling capacity is required for strategy III compared to strategy II. Heavier building structures reduce the heating demand by 50% and the cooling demand by 80%, however, the discomfort related to accumulated indoor humidity increases. Reducing the infiltration levels reduces the cooling demand by 4.5% (20% infiltration levels). After including night flush ventilation, the cooling demand can be reduced further by 4.7% and accumulated indoor humidity can be partly removed. The temperature discomfort due to exceeding the minimal heating set point temperature for winter, is increased by 2.3% when including night flush ventilation in Griffith, compared to the base case.

The temperature **comfort** conditions for the base case exceed the set points 1.1% of the time in summer and 1.5% of the time in winter. Comfort conditions with respect to humidity are exceeded 15% of the time, which can be reduced to 12% and 7% with dehumidification control strategy II and III. The cooling increase in these cases is 15.4% and 42.4% respectively, which is very small compared to the other climates. Therefore, additional dehumidification is not necessary in this climate. Increasing the chilled water set point to 11°C reduces the proportion of latent heat removal by 9% points and the comfort due to increased indoor humidity decreases by 2.4% points. Radiant cooling applications without dehumidification increase the discomfort due to humidity by 5.7% points.

To achieve a **solar fraction** (SF_{th}) for cooling and heating of at least 60%, $18\,m^2$ of collector area were chosen with a $0.4\,m^3$ hot water buffer tank. When including DHW in the calculation, the solar fraction can be improved by 7% points. The relieved heat is $4.9\,MWh\,a^{-1}$. For control strategy II and III, $33\,m^2$ of collector area are installed. Nevertheless, the solar fraction (SF_{th}) drops by 8% and 15% points respectively, compared to a collector configuration with $33\,m^2$ using control strategy I.

The **electricity consumption** specific to the amount of cooling, heating (and DHW) generated (ES) is $0.12\,kWh_{el}$ per kWh of useful energy for cooling and heating. It can be lowered by 25.5% if DHW is included in the calculation. In Griffith using dry heat rejection at 27°C cooling water set point temperature leads to an increase in electricity consumption by 27.6%.

The **costs** to save $1\,kg_{CO2\text{-}eq}$ using the chosen collector and tank configuration is

$1.96. However, when including DHW in the calculation the cost can be reduced to $0.15 for each 1 $kg_{CO2\text{-}eq}$ saved. The cost for strategy II to save 1 $kg_{CO2\text{-}eq}$ does not increase noticeably, however, it doubles for strategy III compared to the base case scenario using strategy I. In the rather dry climate of Griffith dehumidification is not as crucial as sensible cooling. Instead of using cost values specific to the amount of cooling, heating and DHW generated, a break even electricity price can be calculated on the assumption of identical useful energy outputs, which is $1.09 kWh^{-1} excluding, and $0.38 kWh^{-1} including the generation of DHW.

Table 8.30: Summary Griffith

Griffith		
Building structure	Weatherboard (insulated)	
$G_{tot,hor} > 700\,W\,m^{-2}$	12.3	%
Chiller capacity	28.7	$W\,m_{CS}^{-2}$
Heating load	19.3	$W\,m_{CS}^{-2}$
Collector area (chosen conf.)	18	m^2
Hot water storage volume (chosen conf.)	0.40	m^3
Annual cooling energy demand	29.4	$kWh\,m_{CS}^{-2}\,a^{-1}$
Latent proportion	24	%
Annual heating energy demand	22.2	$kWh\,m_{CS}^{-2}\,a^{-1}$
Annual energy demand for DHW	4080	$kWh\,m_{CS}^{-2}\,a^{-1}$
Relieved heat	4.9	$MWh\,a^{-1}$
Solar fraction increase incl. DHW	7	%
Cost for greenhouse gas abatement	1.96	$\$\,kg_{CO2}^{-1}$
Cost for greenhouse gas abatement incl. DHW	0.15	$\$\,kg_{CO2}^{-1}$
Break even electricity price excl. DHW	1.09	$\$\,kWh^{-1}$
Break even electricity price incl. DHW	0.38	$\$\,kWh^{-1}$
Add. cooling capacity strategy II	6	%
Add. cooling capacity strategy III	6	%

Tennant Creek

Tennant Creek is located in the center of the Northern Territory (NT) at the coordinates 19.7° S and 134.2° E. Its continental climate is characterized by very hot and dry summers and very mild winters. The solar radiation data from the meteonorm weather file used shows that the global radiation on the horizontal is above 700 $W\,m^{-2}$ for 22% of the year, excluding night time hours. This is the largest cumulative frequency for the given radiation range of all seven climates, closely followed by Darwin. The average wet bulb temperature is 15.3°C and the cooling tower achieves its set point more than 75% of the time using 4.061 kWh^{-1} of cooling supplied.

The building structure implemented in the TRNSYS model is insulated double brick and the installed chiller capacity is 31 $W\,m_{CS}^{-2}$ for cooling. The heating capacity is negligible small (1 $W\,m_{CS}^{-2}$). The **cooling demand** in Tennant Creek is 78 $kWh\,m_{CS}^{-2}\,a^{-1}$, of which as little as 12% is latent cooling. When increasing the re-

duction of latent heat using strategy II and III, the installed cooling capacity increases are merely 2% and 2% respectively, compared to strategy I. Heavier building structures reduce the cooling demand by 60% without a significant increase in indoor humidity discomfort. Reducing the infiltration levels reduces the cooling demand by 20% (20% infiltration levels). After including night flush ventilation, the cooling demand can be reduced further by 5.8% and accumulated indoor humidity can be partly removed. Sealing the building in Tennant Creek is very beneficial for the air-conditioning power consumption.

The temperature **comfort** conditions for the base case exceed the set points 1.3% of the time in summer and 0.0% of the time in winter. Comfort conditions with respect to humidity are exceeded 1% of the time, which can be reduced below 1% with dehumidification control strategy II and III. The cooling increase in these cases is negligible as there is hardly any necessary latent heat removal. Radiant cooling applications decrease the comfort due to indoor temperature by 2.6% points.

Table 8.31: Summary Tennant Creek

Tennant Creek		
Building structure	Double brick (insulated)	
$G_{tot,hor} > 700\,\mathrm{W\,m^{-2}}$	22.0	%
Chiller capacity	31.3	$\mathrm{W\,m_{CS}^{-2}}$
Heating load	0.5	$\mathrm{W\,m_{CS}^{-2}}$
Collector area (chosen conf.)	18	$\mathrm{m^2}$
Hot water storage volume (chosen conf.)	1.00	$\mathrm{m^3}$
Annual cooling energy demand	77.7	$\mathrm{kWh\,m_{CS}^{-2}\,a^{-1}}$
Latent proportion	12	%
Annual heating energy demand	0.2	$\mathrm{kWh\,m_{CS}^{-2}\,a^{-1}}$
Annual energy demand for DHW	3255	$\mathrm{kWh\,m_{CS}^{-2}\,a^{-1}}$
Relieved heat	4.3	$\mathrm{MWh\,a^{-1}}$
Solar fraction increase incl. DHW	4	%
Cost for greenhouse gas abatement	3.90	$\mathrm{\$\,kg_{CO2}^{-1}}$
Cost for greenhouse gas abatement incl. DHW	0.40	$\mathrm{\$\,kg_{CO2}^{-1}}$
Break even electricity price excl. DHW	0.89	$\mathrm{\$\,kWh^{-1}}$
Break even electricity price incl. DHW	0.43	$\mathrm{\$\,kWh^{-1}}$
Add. cooling capacity strategy II	2	%
Add. cooling capacity strategy III	2	%

To achieve a **solar fraction** (SF_{th}) for cooling and heating of at least 60%, $18\,\mathrm{m^2}$ of collector area were chosen with a $1\,\mathrm{m^3}$ hot water buffer tank. When including DHW in the calculation, the solar fraction can be improved by 4% points. The relieved heat is $4.3\,\mathrm{MWh\,a^{-1}}$.

The **electricity consumption** specific to the amount of cooling, heating (and DHW) generated (ES) is $0.16\,\mathrm{kWh_{el}}$ per kWh of useful energy for cooling and heating. It can be lowered by 15% if DHW is included in the calculation. Dry heat rejection at 27°C cooling water set point temperature leads to the largest increase in electricity consumption of all climates by 51%, and the set point is exceeded 71% of

the time. For cooling water set point temperatures at 30°C the increase in electricity consumption is only 35% of the time and the set point is exceeded 47% of the time.

The **costs** to save 1 $kg_{CO2\text{-}eq}$ using the chosen collector and tank configuration is \$3.9. However, when including DHW in the calculation a cost can be reduced to \$0.40 for each 1 $kg_{CO2\text{-}eq}$ saved. The specific cost for strategy II and III to save 1 $kg_{CO2\text{-}eq}$ is reduced by 40%, however, in the dry climate of Tennant Creek hardly any dehumidification is necessary. Instead of using cost values specific to the amount of cooling, heating and DHW generated, a break even electricity price can be calculated on the assumption of identical useful energy outputs, which is \$0.89 kWh^{-1} excluding, and \$0.43 kWh^{-1} including the generation of DHW.

Darwin

Darwin is located at the north coast of the Northern Territory (NT) at the coordinates 12.5° S and 130.8° E. Its tropical climate is hot and humid the whole year round. The diurnal temperature swing is lowest of all climates in the summer months. The solar radiation data from the meteonorm weather file used shows that the global radiation on the horizontal is above 700 $W\,m^{-2}$ for 19% of the year, excluding night time hours. The average wet bulb temperature is 23.3°C, indicating a very humid environment. The cooling tower achieves its set point only 60% of the time using 3.92 kWh^{-1} of cooling supplied.

The building structure implemented in the TRNSYS model is double brick and the installed chiller capacity is 33 $W\,m_{CS}^{-2}$ for cooling. There is no heating demand in winter. The **cooling demand** is 89 $kWh\,m_{CS}^{-2}\,a^{-1}$, of which 47% is latent cooling. When increasing the reduction of latent heat using strategy II and III, the installed cooling capacity increases are 44% and 45% respectively, compared to strategy I, indicating that hardly any additional capacity is necessary when switching from strategy II to strategy III. Heavier building structures reduce the cooling demand drastically by 90%, however, the discomfort related to accumulated indoor humidity increases. Reducing the infiltration levels reduces the cooling demand by 30% (20% infiltration levels). After including night flush ventilation, the cooling demand can be reduced further by 7%. In contrast to other climate zones, sealing the building in Darwin lowers the indoor humidity discomfort by 7% points and night flush ventilation introduces more latent loads in the building, resulting in an increase of discomfort due to indoor humidity again by 2.2%.

The temperature **comfort** conditions for the base case exceed the set points 0.5% of the time in summer and 0.0% of the time in winter[10]. Comfort conditions with respect to humidity are exceeded more than 80% of the time, which can be reduced to 41% and 27% with dehumidification control strategy II and III. The cooling increase in these cases is 110% and 147% respectively. Increasing the chilled water set point to 11°C reduces the proportion of latent heat removal by 2% points and the comfort due to increased indoor humidity decreases by 3.7% points. Radiant cooling applications

[10]The definition of comfort in winter is exceeding the set point temperature for heating towards smaller temperatures. It is not time restrained.

without dehumidification increase the discomfort due to humidity by 8% points and are not suited for Darwin.

To achieve a **solar fraction** (SF_{th}) for cooling and heating of at least 60%, 24 m^2 of collector area were chosen with a 0.4 m^3 hot water buffer tank. The relieved heat is 6.3 $MWh\,a^{-1}$. When including DHW in the calculation, the solar fraction can be improved by 3% points. For control strategy II and III, 33 m^2 of collector area are installed. Nevertheless, the solar fraction (SF_{th}) drops by 43% and 45% points respectively, compared to a collector configuration with 33 m^2 using control strategy I.

The **electricity consumption** specific to the amount of cooling, heating (and DHW) generated (ES) is the largest with 0.2 kWh_{el} per kWh of useful energy for cooling and heating. For dehumidification strategy II and III the value stays rather constant. The largest electricity consumer is the cooling tower with a share of 45%. The ES can be lowered by 13.7% if DHW is included in the calculation. In Darwin using dry heat rejection at 27°C cooling water set point temperature leads to an increase in electricity consumption by 21.5%. However, the set point of 27°C cooling water supply temperature is exceeded 91% of the time in contrast to the wet cooling tower, where it is exceeded only 35% of the time. When introducing a variable set point cooling water temperature, the total electricity consumption can be reduced in Darwin by 20% without any significant loss of cooling supplied. In this case the solar fraction drops by 1.1% points, but the set point for the cooling water temperature is always achieved.

Table 8.32: Summary Darwin (red: no greenhouse gas savings achieved)

Darwin		
Building structure	Double brick (insulated)	
$G_{tot,hor} > 700\,W\,m^{-2}$	18.8	%
Chiller capacity	33.0	$W\,m_{CS}^{-2}$
Heating load	0.0	$W\,m_{CS}^{-2}$
Collector area (chosen conf.)	24	m^2
Hot water storage volume (chosen conf.)	0.40	m^3
Annual cooling energy demand	89.4	$kWh\,m_{CS}^{-2}\,a^{-1}$
Latent proportion	47	%
Annual heating energy demand	0.0	$kWh\,m_{CS}^{-2}\,a^{-1}$
Annual energy demand for DHW	3256	$kWh\,m_{CS}^{-2}\,a^{-1}$
Relieved heat	6.3	$MWh\,a^{-1}$
Solar fraction increase incl. DHW	3	%
Cost for greenhouse gas abatement	-10.00	$\$\,kg_{CO2}^{-1}$
Cost for greenhouse gas abatement incl. DHW	0.77	$\$\,kg_{CO2}^{-1}$
Break even electricity price excl. DHW	1.72	$\$\,kWh^{-1}$
Break even electricity price incl. DHW	0.60	$\$\,kWh^{-1}$
Add. cooling capacity strategy II	44	%
Add. cooling capacity strategy III	45	%

Without the inclusion of domestic hot water there was not a single collector size

in the very hot and humid climate of Darwin that was able to save greenhouse gases let alone reduce the cost compared to the reference case. However, when including DHW in the calculation the cost can be reduced to \$0.77 for each 1 $kg_{CO2\text{-}eq}$ saved. When adjusting the cooling water set point temperature as a function of the outdoor wet bulb temperature, it became possible to operate under equal greenhouse gas emissions as the reference case. Instead of using cost values specific to the amount of cooling, heating and DHW generated, a break even electricity price can be calculated on the assumption of identical useful energy outputs, which is \$1.72 kWh^{-1} excluding, and \$0.60 kWh^{-1} including the generation of DHW.

Melbourne

Melbourne is the capital of the state Victoria (VIC), located at the coordinates 37.8° S and 145.0° E. Its coastal climate is characterized by mild to warm summers and cold winters. The solar radiation data from the meteonorm weather file used shows that the global radiation on the horizontal is above 700 $W\,m^{-2}$ 7.5% of the year, excluding night time hours. The average wet bulb temperature is 11°C and the cooling tower achieves its set point 80% of the time using 3.31 kWh^{-1} of cooling supplied.

The building structure implemented in the TRNSYS model is insulated reverse brick veneer and the installed chiller capacity is 14 $W\,m_{CS}^{-2}$ for cooling. The average of the heating load between the 95th and 100th percentile is 20 $W\,m_{CS}^{-2}$. The annual energy **demand for heating** in winter is 3.6 times larger than the cooling demand in summer, similar to Canberra. The **cooling demand** is 7 $kWh\,m_{CS}^{-2}\,a^{-1}$, of which 30% is latent cooling. When increasing the reduction of latent heat using strategy II and III, the installed cooling capacity increases are 39% and 60% respectively, compared to strategy I. Heavier building structures reduce the heating demand by 40% and the cooling demand by 83%, however, the discomfort related to accumulated indoor humidity increases. Reducing the infiltration levels increases the cooling demand by 27% (20% infiltration levels) and the discomfort due to accumulated indoor humidity rises. After including night flush ventilation, the cooling demand can be reduced again by 19%. Even though a sealed building and night flush ventilation do not show a significant difference to reduce mechanical cooling supplied and even increase the discomfort due to accumulated indoor humidity, the winter heat demand drops strongly. The temperature discomfort due to exceeding the minimal heating set point temperature for winter, is decreased by 0.4% points when including night flush ventilation and sealing the building in Melbourne, compared to the base case.

The temperature **comfort** conditions for the base case exceed the set points 1.0% of the time in summer and 2.1% of the time in winter. Comfort conditions with respect to humidity are exceeded 15% of the time, which can be reduced to 13.5% and 7.5% with dehumidification control strategy II and III. The cooling increase in these cases is 55.3% and 178% respectively. Increasing the chilled water set point to 11°C reduces the proportion of latent heat removal by 10% points, however, the comfort due to increased indoor humidity only increases by 1.3% points. Radiant cooling applications without dehumidification hardly exceed the comfort conditions

of the base case.

To achieve a **solar fraction** (SF_{th}) for cooling and heating of at least 60%, 33 m^2 of collector area were chosen with a 0.75 m^3 hot water buffer tank. The relieved heat is 14.6 $MWh\,a^{-1}$, which is an indication that the collectors are mainly sized to cover the heating demand in winter. When including DHW in the calculation, the solar fraction can be improved by 12% points. For control strategy II and III, 33 m^2 of collector area are installed. In that case the solar fraction (SF_{th}) drops by 3.5% and 8% points respectively, compared to using control strategy I.

The **electricity consumption** specific to the amount of cooling, heating (and DHW) generated (ES) is 0.05 kWh_{el} per kWh of useful energy for cooling and heating. It can be lowered by 38% if DHW is included in the calculation. Using dry heat rejection at 27°C cooling water set point temperature in Melbourne leads to an increase in electricity consumption by only 7.5%.

The **costs** to save 1 $kg_{CO2\text{-}eq}$ using the chosen collector and tank configuration is \$1.30. However, when including DHW in the calculation the cost can be reduced to \$0.09 for each 1 $kg_{CO2\text{-}eq}$ saved. The cost for strategy II and strategy III to save 1 $kg_{CO2\text{-}eq}$ is 24% and 23% times larger than with control strategy I. Instead of using cost values specific to the amount of cooling, heating and DHW generated, a break even electricity price can be calculated on the assumption of identical useful energy outputs, which is \$1.08 kWh^{-1} excluding, and \$0.32 kWh^{-1} including the generation of DHW.

Table 8.33: Summary Melbourne

Melbourne		
Building structure	Reverse brick veneer (insulated)	
$G_{tot,hor} > 700\,W\,m^{-2}$	7.5	%
Chiller capacity	13.9	$W\,m_{CS}^{-2}$
Heating load	19.6	$W\,m_{CS}^{-2}$
Collector area (chosen conf.)	33	m^2
Hot water storage volume (chosen conf.)	0.75	m^3
Annual cooling energy demand	7.2	$kWh\,m_{CS}^{-2}\,a^{-1}$
Latent proportion	30	%
Annual heating energy demand	25.6	$kWh\,m_{CS}^{-2}\,a^{-1}$
Annual energy demand for DHW	4533	$kWh\,m_{CS}^{-2}\,a^{-1}$
Relieved heat	14.6	$MWh\,a^{-1}$
Solar fraction increase incl. DHW	12	%
Cost for greenhouse gas abatement	1.30	$\$\,kg_{CO2}^{-1}$
Cost for greenhouse gas abatement incl. DHW	0.09	$\$\,kg_{CO2}^{-1}$
Break even electricity price excl. DHW	1.08	$\$\,kWh^{-1}$
Break even electricity price incl. DHW	0.32	$\$\,kWh^{-1}$
Add. cooling capacity strategy II	39	%
Add. cooling capacity strategy III	60	%

8.3.3 Small scale versus large scale solar cooling systems

It seems that small scale absorption chiller systems for residences are a rather expensive way to decrease greenhouse gas emissions or to reduce peak electricity demand. Only if heat can be utilized as well in form of space heating or domestic hot water, such systems can become cost effective. The weakness of small scale absorption chillers in residences are that they are usually the only source of cooling installed and have to balance fluctuations in heat supply as well as fluctuations in cooling demand. The models showed that this behavior led to high electricity consumptions for external pumps and the chiller itself as those demands were not proportional to the load, only to the overall *scalefactor*.

Nevertheless, absorption chiller systems are well suited for the support of large scale air-conditioning systems if they can operate under full load most of the time and if they are not meant to follow the cooling demand profile. That way the absorption chiller only has to adapt to fluctuations in the solar heat supply. In large scale systems it is common that absorption chillers only provide a small fraction of the total cooling[11]. For a large commercial system a large collector area is necessary, and the same premise as for small scale system holds, that there should be a hot water demand as well to make the systems cost effective. The absorption chillers can be operated in series to the conventional chillers and pre-cool the chilled water, hence, the chilled water set point temperature can be increased.

Conventional large scale compression chillers alone have no option to provide heating for winter or domestic hot water. A solar absorption chiller system is therefore a total service provider for cooling, heating and domestic hot water. Schools, hotels, but also office buildings combined with facilities with a hot water demand like apartments, gyms etc. are perfect candidates for absorption solar cooling systems. The high proportion of direct solar radiation in Australia favors double and triple effect absorption chillers combined with concentrating solar collectors. A clear advantage to Europe where single stage and flat plate collector systems dominate. Cost disadvantage and complexity of solar thermal cooling compared to PV driven solar cooling systems decrease strongly with larger systems as additional equipment (e.g. frequency regulation) becomes necessary to integrate the large PV array in the electricity grid and to be conform to the rules set by the network operator.

In order to make absorption chillers cost effectively available to residential buildings, the large scale approach can be chosen when multiple houses are combined in a district cooling network. This approach should include a certain amount of conventional chillers to follow the fluctuations in cooling demand. In rural towns there is usually a large availability of land for solar thermal collectors. However, that is subject to further research.

[11]The world second largest solar cooling system in Singapore has an installed cooling capacity of approximately 20% of total system's capacity [S.O.L.I.D., 2014].

8.3.4 Finance

There are multiple option to finance solar cooling systems. The conventional approach especially for small scale systems is to sell the entire system, which might provide difficulties as the initial cost for solar cooling is rather high. A second option for the solar cooling provider of large scale systems is to establish an investment plan, to build the plant and to sell cooling and heating at a arranged variable cost with or without a capacitance charge. When industry R&D project funding for solar cooling systems is provided, it should be bound to a conditional funding scheme, for example proofing via simulation work how effective the system is going to be and comparing this to long term monitoring.

The next chapter will include a cold storage tank into the solar thermal model to evaluate if the performance can be significantly improved and at which extra cost.

Chapter 9

Thermal storage options for solar thermal cooling, heating and DHW systems

This section investigates the inclusion of an additional thermal storage option in the chilled water circuit of the model. This is done in order to analyze if and to what extend a latent phase change material (PCM) storage tank and a chilled water tank are able to increase the performance of the system. The latent storage tank is discharged by supplying either fan coil units or chilled beams with chilled water.

The description of the latent storage tank model and its implementation into the existing absorption chiller TRNSYS model is explained in detail. As in previous chapters, the results of the different scenarios are compared to the base case.

In the last part of this section it is investigated in brief if direct coupling between collectors and the chiller's generator is possible and what the obstacles are.

Cold storage is able to increase the solar fraction, however, the already high solar thermal cost is increases further with sensible storage being the most cost effective option to reduce greenhouse gas emissions. Climates with high cooling and low heating requirements perform best. The low ΔT of the chiller's chilled water circuit requires a careful consideration of control strategy when charging and discharging.

9.1 Including a cold storage tank in the solar thermal cooling, heating and DHW model

In the second part of this chapter the solar thermal absorption chiller TRNSYS model will be extended by incorporating a latent cold storage tank or a chilled water cold storage tank. The control strategies vary and the chiller's status is not only determined by the load alone, but also by the availability of the solar supply and the available cold storage capacity.

Previously, the chiller load was controlled by maintaining a specific chilled water set point temperature. The return temperature of the chilled water was an indicator for the chiller to vary its load by internally calculating the required hot water

temperature ($T_{hw,req}$) to meet the demand. The required hot water inlet temperature ($T_{hw,req}$) was a function of the chilled water return temperature ($T_{chw,in}$), the cooling water inlet temperature ($T_{cw,in}$) and the required load ($\dot{Q}_{E,req}$) as in equation 7.18. Furthermore, the required hot water inlet temperature ($T_{hw,req}$) was calculated to be supplied in the next time step and a mixing valve regulated the hot water temperature entering the generator. The auxiliary gas heater would switch on if the tank could not supply the required temperature. The chiller operated in the hot water inlet temperature range between 59°C and 96°C, depending on the load.

An master control signal primarily controlled the chiller. That signal was a combination of the HVAC schedule ($HVAC_{sched}$) and the thermostat action ($HVAC_{therm}$), which is regulated by the zone's dry bulb temperatures. In addition, the chiller switched off when the external inlet temperatures for cooling water, hot water and chilled water exceeded the minimum or maximum limits. If the cooling load was too high or the required hot water temperature couldn't be supplied, the chilled water exceeded its temperature set point for chilled water.

When combining the absorption chiller with a cold storage tank, the chiller will not only follow the load but also the sun's energy supply and cold storage availability. A complex control strategy at the downstream of the chiller guarantees that comfort conditions are met. Different strategies to control charging and discharging of the cold storage tank, the hot water buffer tank and auxiliary heater demand are described in the following sections.

Two different variations of cold storage tank media are modeled comparing a sensible chilled water tank to a latent cold storage tank using phase change material (PCM). An advantage of latent energy storage over sensible storage is its higher energy density and constant heat exchange temperature difference. In contrast to a latent storage tank, the chilled water tank does not require a heat exchanger, which requires temperatures below the medium's melting temperature for charging and which discharges with fluid temperatures above the medium's melting temperature. The chiller's temperature difference between inlet and outlet of the chilled water at rated flow rates are in the same range, when generating chilled water at 7°C, as the storage latent storage tank's difference between the inlet fluid temperature for charging and its outlet temperature for discharging. Chilled water tanks don't stratify very well compared to hot water tanks.

Literature on ice storage tanks analyzes mainly the peak electricity demand reduction in conventional air-conditioning systems [Kintner-Meyer and Emery, 1995; Henze et al., 2001]. In such studies a refrigerant is the heat transfer medium producing ice during the night in off-peak hours, at times of low electricity prices. The building is then cooled during the day from the cold storage. The goal is to minimize operating cost.

In combining a solar cooling system with cold storage, the main objective is to reduce auxiliary energy demand, hence, greenhouse gas emissions even further by storing heat at a much lower temperature than in a hot water tank. In this manner thermal storage losses to the environment can be reduced. Furthermore, with thermal COPs below 1, and consequently $Q_{chw} < Q_{hw}$, a smaller stored energy to storage

space ratio is advantageous, hence, it is better to store heat at low temperatures then at high temperatures. However with latent storage tanks, another heat exchanger is introduced into the circuit and this lowers the overall thermal efficiency.

The colder the chilled water temperature must be to charge the latent storage tank, the higher are the required hot water driving temperatures for the absorption chiller. Furthermore, the higher the desired hot water temperatures, the shorter the period the hot water buffer tank can supply heat to the chiller to charge the cold storage tank. Chilled water temperature limits of absorption chillers and their poor part load performance are limiting factors to their applicability with cold storage tanks compared to vapor compression chillers.

Control strategies using latent storage are different to those for sensible storage systems. In contrast to a chilled water tank, where the stored water is usually the same heat transfer fluid which exits the chiller, a latent storage tank, filled with phase change material, represents a heat exchanger. A heat exchanger has an effectiveness below 100%, therefore the heat exchanger design of a cold storage tank should stress on a large heat transfer area and facilitate a turbulent flow regime if tubes immersed in the PCM are used.

Commercially available designs of cold storage tanks without immersed tube heat exchangers for solar cooling systems can be found in Kohlenbach and Jakob [2014]. They include ice slurries or encapsulated plastic containers in the cold storage tank filled with the latent storage medium (e.g. a mixture of eutectic salts).

In latent storage designs with tubes immersed within the PCM, a solid PCM shell builds up around the tubes while charging, which drastically reduces the heat transfer. Therefore, in such designs multiple (hundreds) of tubes are used to increase the ability of the PCM to absorb heat from the heat transfer fluid. To increase the heat transfer further, it is possible to use fins or metal meshes.

For modeling purposes in this work immersed tubes are chosen without heat transfer enhancement. Instead of eutectic salts in water or pure water, an organic phase change material based on a mixture of capric or lauric acid is used to increase the freezing point of the mixture to 11°C. In solid state this PCM has a conductivity of approximately 0.4 - 0.7 $\mathrm{W\,m^{-1}\,K^{-1}}$. Compared to water with 2.3 $\mathrm{W\,m^{-1}\,K^{-1}}$ or copper with 385 $\mathrm{W\,m^{-1}\,K^{-1}}$ this is relatively low and reduces the effectiveness of the heat exchanger once the material freezes. Additives in various molecular proportions are able to alter the melting temperature.

The properties of water are compared to caproic acid additives in Table 9.1. Reducing the melting temperature to 11°C requires a mole fraction of the additive caproic acid of 0.17 [Wang et al., 2013]. However, the thermal properties can be assumed to remain constant with sufficient accuracy.

The compactness factor is a measure of the volumetric proportion within the storage tank which is filled with PCM. The remaining proportion is taken up by pipes and, if applicable, by devices to increase the heat transfer.

For the purpose of modeling a latent storage tank the mathematical model of Tay et al. [2011] is used. The model suggests a methodology to calculate the additional resistance around the tubes due to PCM shell-forming.

Table 9.1: Chemical properties of organic PCM on the basis of capric-lauric acid and water

	Mix capric-lauric acid additive caproic acid	water
mole fraction additive caproic acid	0.14	-
Freezing temperature, T_{melt} [°C]	14.68	0
Heat of fusion, Δh_{lat} [kJ kg^{-1}]	100.1	334
Density liquid, ρ_l [kg m^{-3}]	870.8	998.2
Density solid, ρ_s [kg m^{-3}]	870.8	921
Thermal conductivity liquid, k_l [W m^{-1} K^{-1}]	0.372	0.602
Thermal conductivity solid, k_s [W m^{-1} K^{-1}]	0.375	2.24
Specific heat liquid, $c_{p,l}$ [kJ kg^{-1} K^{-1}]	1.891	4.18
Specific heat solid, $c_{p,s}$ [kJ kg^{-1} K^{-1}]	1.853	2.04

Temperatures below T_{melt} are necessary to charge the latent storage tank. A ΔT of 3°C between the cold storage medium temperature and the fluid temperature exiting the tank is generally required. This is a crucial aspect for PCMs combined with absorption chillers. Lithium-bromide absorption chillers generally produce chilled water between 7°C and 15°C. Therefore, a PCM tank with a melting temperature at 11°C can be charged with chilled water produced at the low end of the absorption chiller's chilled water temperature range and is discharged at its high temperature range.

Table 9.2 shows operating points of the absorption chiller used in the previous chapters. The points were derived from the model of Albers [2011], which suggests parameters to model the Wegracal SE15 machine [EAW Energieanlagenbau GmbH Westenfeld, 2014]. It also shows the relationship between chilled water supply and return temperature and the cooling capacity.

Table 9.2: Selected operating points of the Wegracal 15 absorption chiller after using simulation results from Albers [2011])

$T_{chw,out,set}$	$T_{chw,in}$	$T_{cw,in}$	$T_{hw,req}$	$\dot{Q}_E$ [kW]
7°C	12°C	27°C	84.5°C	11.7
7°C	11°C	27°C	78.2°C	9.3
6°C	11°C	27°C	86.3°C	11.7
11°C	15°C	27°C	70.9°C	9.3
11°C	16°C	27°C	77.1°C	11.7
10°C	15°C	27°C	78.9°C	11.7

In contrast to a conventional chiller, the absorption chiller's electricity demand for the external pumps stays constant with a lower chilled water return temperature, hence lower cooling capacity. Therefore, to achieve low electricity consumption per kWh of cooling, it is of advantage to have a rather constant ΔT_{chw} of approximately 5°C. For example, the return chilled water temperature should be approximately 12°C if the chilled water outlet temperature was 7°C. Only if the hot water was generated by auxiliary gas, a reduction of cooling generation could lead to greenhouse gas savings. Hence, in terms of greenhouse gas savings specific to the amount of

cooling generated, it is advantageous to operate the chiller at full capacity whenever possible.

This is a conclusion drawn by many system operators and chiller manufacturers who promote the idea of an absorption chiller solar cooling system assisting a conventional cooling systems on a large commercial scale. In such a configuration the solar cooling absorption chiller system is able to operate at full load if solar heat is available. Part load of such combined systems is achieved by adjusting the conventional chillers, which in general have a better part load performance than absorption chillers.

9.1.1 Heat transfer model of a latent cold storage tank

The cold storage tank is modeled as a vertical cylinder filled with phase change material (PCM). Thin tubes are immersed in the PCM, which carry the heat transfer fluid water.

For the latent cold storage tank a mathematical model was developed and implemented as a TRNSYS component. The model for the cold storage tank is based on the heat exchanger effectiveness or NTU-ϵ method as in Tay et al. [2011]. It was found in this paper that the heat transfer between the heat transfer fluid flowing through multiple tubes within the tank and the PCM can be modeled one dimensional with high accuracy. The tank design parameters are based on Figure 9.1.

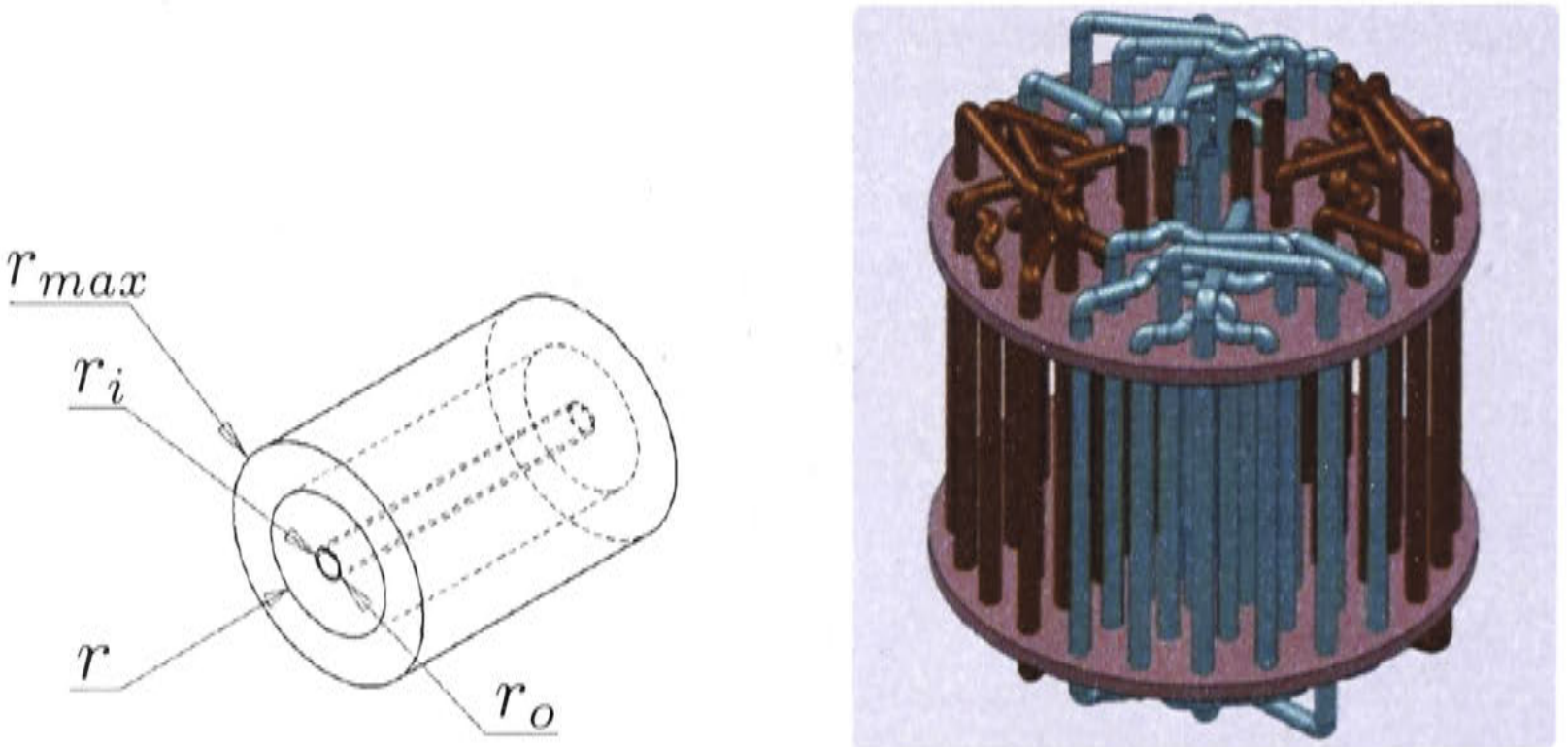

(a) (b)

Figure 9.1: Cold storage tank design. One tube (left). Tank design with four circuits ($N_{circ} = 4$) (right). Pictures from Tay et al. [2011].

The inlet flow rate of chilled water entering the tank $\dot{m}_f$ is divided into N_{circ} circuits to reduce the pressure drop and the pump power consumption. The effectiveness of the heat exchanger in each circuit is found in equation 9.1. The temperatures $T_{f,in}$ and $T_{f,out}$ denote the inlet and outlet temperatures of the fluid and T_{PCM} is the

temperature of the phase change material (PCM).

$$\epsilon = \frac{T_{f,in} - T_{f,out}}{T_{f,in} - T_{PCM}} \tag{9.1}$$

The relationship of effectiveness to the Net Transfer Units (NTU) is given in equation 9.2. In literature (e.g. ASHRAE [2013], Holman [1997]) this equation is used if one medium is undergoing phase change. However, it is usually used for the phase change liquid-gas, rather than solid-liquid. Nevertheless, the correlation has been used by Tay et al. [2011] and proved sufficiently accurate.

$$\epsilon = 1 - \exp(-NTU) \tag{9.2}$$

The number of transfer units (NTU) is calculated using equation 9.3.

$$NTU = \frac{1}{R_{total}\ (\dot{m}_f / N_{circ})\ c_{p,f}} \tag{9.3}$$

The total resistance (R_{total}) is the sum of the thermal resistance due to the heat transfer between wall and fluid (R_{htf}), the resistance due to the conduction of heat through the wall (R_{wall}) and due to the resistance of the growing shell around the tubes (R_{PCM}) (equation 9.4). The latter estimates the resistance dependent on the maximum possible radius (r_{max}) the shell can grow around a tube, before interfering with a neighboring ice shell. The phase change fraction (δ) is determined in the model by one minus the liquid fraction ($liqfrac$) ($\delta = 1 - liqfrac$). The length L is the tube length of one circuit or in other words the product of the amount of paths per circuit and the path length $L = N_{path}\ L_{path}$. The length of one path in this model is set to be the latent storage tank's height.

$$R_{total} = R_{htf} + R_{wall} + R_{PCM} \tag{9.4}$$

$$R_{htf} = \frac{1}{2\,\pi\, r_i\, L\, h_f} \tag{9.4a}$$

$$R_{wall} = \frac{\ln(r_o / r_i)}{2\,\pi\, k_{wall}\, L} \tag{9.4b}$$

$$R_{PCM} = \frac{\ln\left(\frac{\sqrt{\delta(r_{max}^2 - r_0^2) + r_0^2}}{r_0}\right)}{2\,\pi\, L\, k_{PCM}} \tag{9.4c}$$

The conductivity of the wall k_{wall} is determined by the material, and the heat transfer coefficient h_f is determined by the flow regime. For a **laminar flow** within

the tubes equation 9.6 is used [ASHRAE, 2013, p. 4.18].

$$h_f = Nu \frac{k_f}{d_i} \tag{9.5}$$

$$Nu = 4.36 \tag{9.6}$$

For the **turbulent flow** regime equation 9.8 is used and the Nusselt number Nu can be calculated using the Dittus-Bolter equation with $n = 0.3$ for charging and $n = 0.4$ for discharging the cold storage tank (equation 9.7).

$$Nu = 0.023\, Re^{0.8}\, Pr^{n} \tag{9.7}$$

$$h_f = Nu \frac{k_f}{r_i} \tag{9.8}$$

The Reynolds number is a function of the (hydraulic) diameter of the heat transfer tube, the fluid's velocity and its kinematic viscosity [ASHRAE, 2012, p. 3.3] (equation 9.9). The Prandtl number is a function of the fluid's heat capacity, its density, its kinematic viscosity and its thermal conductivity [ASHRAE, 2013, p. 4.17] (equation 9.10).

$$Re = \frac{d\, v_f}{\nu_f} \tag{9.9}$$

$$Pr = c_{p,f}\, \rho_f\, \frac{\nu_f}{k_f} \tag{9.10}$$

The heat exchanger effectiveness determines how much heat can be transferred into and out of the latent storage tank (Q_{CS}) during one time step Δt (equation 9.11). Q_{CS} is not a heat rate but the energy transferred in one time step.

$$Q_{CS} = \epsilon\, \dot{m}_f\, c_{p,f}\, (T_{f,in} - T_{PCM})\, \Delta t\, 3600 \tag{9.11}$$

9.1.2 Design parameters of a latent cold storage model

The parameters determine the design of the cylindrical latent cold storage tank. They cover the dimensions, the heat transfer properties of the medium, the properties of the heat transfer fluid and the flow arrangement of the tubes. The list of parameters used for the TRNSYS component is shown in Table 9.3.

	parameters	*value*	*unit*
V_t	tank volume	*variable*	m^3
h_t	tank height	*variable*	m
h_{surf}	surface heat gain coefficient	3	$W\,m^{-2}\,K^{-1}$
R_t	tank thermal resistance	5	$m^2\,W^{-1}$

	parameters	*value*	*unit*
T_{melt}	PCM melting temperature	11	°C
Δh_{lat}	PCM latent heat	100.1	kJ kg^{-1}
$c_{p,PCM,l}$	PCM liquid heat capacity	1646.7	kJ m^{-3} K^{-1}
$c_{p,PCM,s}$	PCM solid heat capacity	1613.6	kJ m^{-3} K^{-1}
ρ_{PCM}	PCM density	870.8	kg m^{-3}
$T_{PCM,t=0}$	PCM initial temperature	15	°C
CF	storage compactness factor	0.95	-
$c_{p,f}$	heat transfer fluid specific heat	4.18	kJ kg^{-1} K^{-1}
r_i	coil internal radius	*variable*	m
r_o	coil external radius	*variable*	m
L_{path}	coil length per path	$= h_t$	m
N_{path}	number of coil paths per circuit	$= N/N_{circ}$	-
k_{wall}	coil thermal conductivity	384	W m^{-1} K^{-1}
$k_{PCM,s}$	PCM solid thermal conductivity	0.375	W m^{-1} K^{-1}
$k_{PCM,l}$	PCM liquid thermal conductivity	0.372	W m^{-1} K^{-1}
T_{sub}	PCM subcooling	0	°C
$liqfrac_{t=0}$	initial liquid fraction	1	-
r_{max}	maximum freezing radius	*variable*	m
N_{circ}	number of circuits of heat transfer fluid	*variable*	-

Table 9.3: Parameters of the latent TRNSYS cold storage component with N being the total number of paths.

	inputs	*unit*
T_{amb}	ambient temperature	°C
$\dot{m}_f$	heat transfer fluid flow rate	kg s^{-1}
$T_{f,in}$	heat transfer fluid inlet temperature	°C
-	cold inlet bypass	-
k_f	inlet heat transfer fluid thermal conductivity	W m^{-1} K^{-1}
μ_f	inlet heat transfer fluid dynamic viscosity	N s m^{-2}
ρ_f	Inlet heat transfer fluid density	kg m^{-3}

Table 9.4: Inputs of the latent TRNSYS cold storage component

	outputs	*unit*
$liqfrac$	storage liquid fraction	-
T_{PCM}	storage medium temperature	°C
$T_{f,out}$	outlet temperature	°C
$\dot{Q}_{CS}$	heat transferred to PCM medium	kJ h^{-1}
$\dot{Q}_{loss}$	heat loss from surface	kJ h^{-1}
$\dot{Q}_f$	heat transfer to fluid	kJ h^{-1}
l_{shell}	shell thickness	m
Re	Reynolds number	-

Table 9.5: Outputs of the latent TRNSYS cold storage component

Within the component the possible heat transfer rate in each time step is calculated from the fluid inlet conditions. An energy balance around the tubes is estab-

lished to calculate the amount of heat, which is actually transferred in or out of the cold storage medium. As a result the liquid fraction is re-calculated in each time step. It is possible to subcool or superheat the PCM. Table 9.4 and 9.5 show the inputs and outputs of the component.

The parameter r_{max} is an estimation on how far the shell around one tube can grow until it touches the next tube's shell. It has been found from research on optimization of "circle packing in a circle", which aims at finding the minimal radius of an enclosing circle filled with N circles of unit radius. The optimums for different N are published in literature as the ratio ($ratio_N$) of the enclosing circle's radius (r_{encl}) to the inner (unitary) radius of each of the N circles ($r_n = 1$). For example, for 196 circles the ratio is 15.323 [Wenqi Huang, 2010]. Specht [2012] publishes on the website of the university of Marburg in Germany the optimal packaging up to 2604 circles in a circle.

From those results the regression function in Figure 9.2 has been derived to calculate $ratio_N$ for N circles in a larger enclosing circle. The equation is used when designing a vertical and cylindrical latent cold storage tank with N paths, in order to find the maximum possible shell radius (r_{max}). The formula to find r_{max} can be expressed as equation 9.12, where $ratio_N$ is calculated from the regression function in Figure 9.2.

$$ratio_N = -2 \cdot 10^{-5}\, N^2 + 0.0459\, N + 6.9598$$

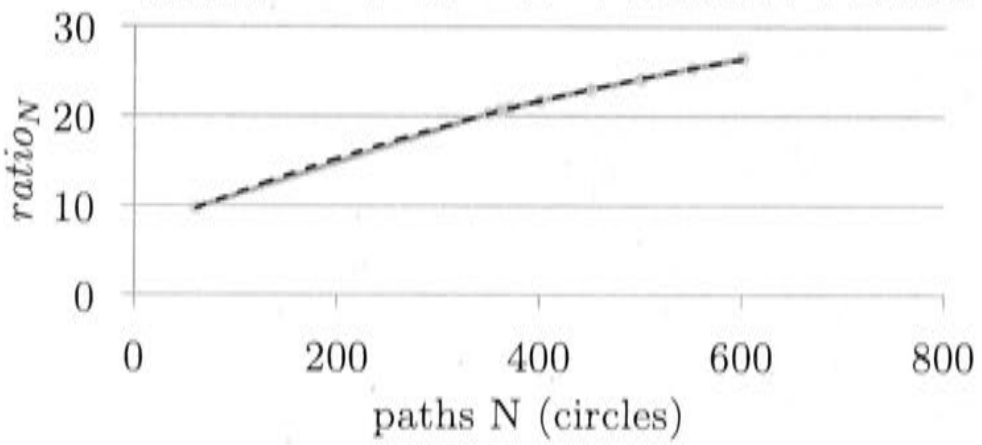

Figure 9.2: Regression function $ratio_N = f(N)$.

$$r_{max} = \frac{\sqrt{\frac{V_L}{h_l \pi}}}{ratio_N} \tag{9.12}$$

The amount of tubes (N) within the cold storage tank is an important design parameter. It influences the mathematical determination of r_{max} and the flow regime, hence, the heat transfer characteristic. Usually more than one bundle of tubes (N_{circ}) are installed in parallel to reduce the pressure drop of the flow. The compactness factor (CF) is the ratio of the volume of the PCM to the total tank volume, or in other words one minus the ratio of tube volume to storage volume (equation 9.13). This compactness factor determines the available heat storage medium for charging.

$$CF = 1 - \frac{\pi r_o^2 h_t N}{V_t} \tag{9.13}$$

The component output T_{PCM} is the temperature of the entire PCM in the latent cold storage tank, assuming a one node model. The fluid outlet temperature depends on the effectiveness of the heat transfer.

9.1.3 Scaling of a latent cold storage tank

In the previous chapters the chiller has been scaled to match the building's cooling demand in each climate. Scaling the latent cold storage tank to obtain comparable results for every climate zone is not easy as it is an arrangement of heat transfer tubes of different diameters, rather than a volume of water.

In a first step a reasonable tank design has been developed which could be scaled and adjusted to the different chiller capacities. The compactness factor (CF in equation 9.13) has been kept constant at 95% and the amount of paths (N) was varied accordingly. The following tank design parameters have been fixed for $scalefactor = 1$:

- V_t: volume of tank [m]
- h_t: height of tank [m]
- d_o: outer tube diameter [m]
- l_{wall}: tube wall thickness [m]
- d_i: inner tube diameter ($d_i = d_o - 2 \cdot l_{wall}$) [m]
- N: total amount of paths using equation 9.13 and $CF = 95\%$
- N_{cric}: amount of circuits

The amount of paths (N) and circuits (N_{circ}) is a trade off between pump electricity consumption due to large pressure drops and heat transfer capability promoted by turbulent flow. The parameters were chosen balancing between pressure drop and Reynolds number. It is desirable to have a high Reynolds number, hence, only a few circuits to facilitate a good heat transfer of the fluid. However, such an arrangement increases the pressure drop over the tubes and the pump electricity consumption increases. In order to reduce the pressure drop more circuits are necessary. Larger tube diameters of only a few circuits also increase the Reynolds number at low pressure drop, however, larger pipes reduce the surface area of the heat exchanger.

When **scaling** the cold storage tank to adjust it to the different chiller capacities, the ratio κ between the tank's cross sectional area (A_t) and the latent storage tank's height (h_t) is kept constant (equations 9.14)[1]. Furthermore, the ratio ι between the

[1] κ is the design area divided by the design height $A_{t,0}/h_{t,0} = V_{t,0}/h_{t,0}^2$

outer tube diameter (d_o) and the latent storage tank's diameter (d_t) were kept constant as well (equation 9.15). With these constraints the four relationships $V_t \propto h_t^2$, $V_t \propto A_t^2$, $V_t \propto d_t^4$ and $V_t \propto d_o^4$ could be derived, keeping the compactness factor at 95%.

$$A_t / h_t = \kappa = const \tag{9.14}$$

$$d_o / d_t = \iota = const \tag{9.15}$$

Using these relationships the tank parameters are scaled depending on the $scalefactor$ and the functions in equation 9.16 to 9.27. When calculating the overall friction resistance ζ in equation 9.24, the friction factor of the pipes k_{pipes} was assumed to be 0.035 and the loss coefficients of the bents k_{bent} 0.391[2]. The volumetric flow rate of the heat transfer fluid is $\dot{V}_{f,rated} = \dot{m}_{chw,rated}\, \rho_f$.

$$\dot{V}_{f,scaled} = scalefactor \cdot \dot{V}_{f,rated} \tag{9.16}$$

$$\dot{V}_{f,circ,scaled} = \dot{V}_{f,scaled} / N_{circ} \tag{9.17}$$

$$V_{t,scaled} = scalefactor \cdot V_t \tag{9.18}$$

$$h_{t,scaled} = \sqrt{scalefactor} \cdot h_t \tag{9.19}$$

$$d_{o,scaled} = d_o \cdot \sqrt[4]{scalefactor} \tag{9.20}$$

$$d_{i,scaled} = d_i \cdot \sqrt[4]{scalefactor} \tag{9.21}$$

$$v_{scaled} = \frac{\dot{V}_{f,circ,scaled} \cdot 4}{d_{i,scaled}^2 \cdot \pi} = v \cdot \sqrt{scalefactor} \tag{9.22}$$

$$\text{with: } v = \frac{(\dot{V}_{f,rated} / N_{circ}) \cdot 4}{d_i^2 \cdot \pi}$$

$$Re_{scaled} = \frac{d_{i,scaled} \cdot v_{scaled}}{\nu_f} = Re \cdot scalefactor^{3/4} \tag{9.23}$$

$$\text{with: } Re = \frac{d_i \cdot v}{\nu_f}$$

$$\zeta = k_{bent} \cdot \left(\frac{N}{N_{circ}} - 1 \right) + k_{pipe} \cdot \frac{d_{i,scaled}}{h_{t,scaled}} \cdot \frac{N}{N_{circ}} \tag{9.24}$$

$$= k_{bent} \cdot \left(\frac{N}{N_{circ}} - 1 \right) + k_{pipe} \cdot \frac{d_i}{h_t \cdot \sqrt[4]{scalefactor}} \cdot \frac{N}{N_{circ}}$$

$$\Delta p_{scaled} = \zeta \cdot \frac{v_{scaled}^2}{2} \cdot \rho_f \tag{9.25}$$

$$\dot{E}_{el,pump} = \frac{\Delta p_{scaled} \cdot \dot{V}_{f,scaled}}{\eta_{pump}} \tag{9.26}$$

$$A_{HX,scaled} = \pi \cdot d_{o,scaled} \cdot h_{t,scaled} \cdot N \tag{9.27}$$

$$= \pi \cdot d_o \cdot h_t \cdot N \cdot scalefactor^{3/4} = A_{HX} \cdot scalefactor^{3/4}$$

[2]Values calculated from Beitz and Grote [1997]

The tank volume specific to the absorption chiller's full load capacity is determined by equation 9.28. Throughout this study the chiller's rated capacity (Cap_{rated}) is 11 kW.

$$V_t' = V_t / Cap_{rated} \tag{9.28}$$

The effect of different specific tank volumes V_t' will be investigated. Therefore, another scaling parameter γ for the latent cold storage tank is introduced. As opposed to the *scalefactor*, γ is independent of the climate and is introduced to compare different latent storage sizes within one climate. The scale factor γ scales the cold storage tank from the design volume $V_{t,0} = 1.5\,\mathrm{m}^3$ and design height $h_{t,0} = 1.5\,\mathrm{m}$, following equation 9.29 and 9.30. The design volume and height of the tank were chosen arbitrarily and define $\gamma = 1$, as well as the ratio κ in equation 9.14. The outer tube diameter d_o is derived from a fixed inner tube diameter (d_i) of 0.01 m and a wall thickness (l_{wall}) of 0.25 mm. This parameters define the design conditions.

When scaling the tank with γ, only the volume of the tank will be modified, but the outer tube diameter (d_o) will be kept constant. In order to keep the compactness factor CF also constant, the amount of paths has to be changed as in equation 9.31.

$$V_t = \gamma \cdot V_{t,0} \tag{9.29}$$

$$h_t = \sqrt{\gamma} \cdot h_{t,0} \tag{9.30}$$

$$N = \sqrt{\gamma} \cdot N_0 \tag{9.31}$$

Figure 9.3 shows at the chosen outer diameter the pressure drop through the cold storage tank for two different tank sizes in dependency of the scalefactor.

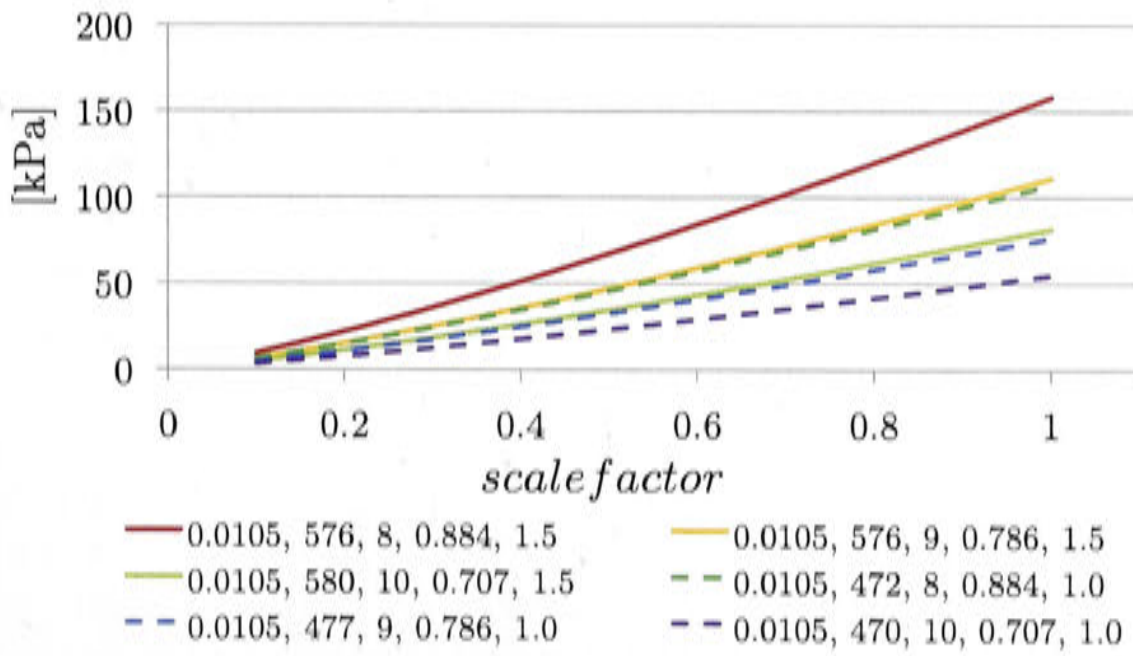

Figure 9.3: Pressure drop in latent storage cold tank depending on chiller capacity (*scalefactor*). Legend: d_o, N, N_{circ}, v, V_t at $scalefactor = 1$.

The Reynolds number is shown in Figure 9.4. Three different numbers of fluid circuits ($N_{circ} \in \{8, 9, 10\}$) and two different tank volumes ($V_t \in \{1.5\,\mathrm{m}^3, 1\,\mathrm{m}^3\}$) are

compared. On the x-axis the *scalefactor* is varied. Even though the total amount of paths N can be accurately calculated to achieve the desired compactness factor, it is rounded in order to be a multiple of N_{circ}.

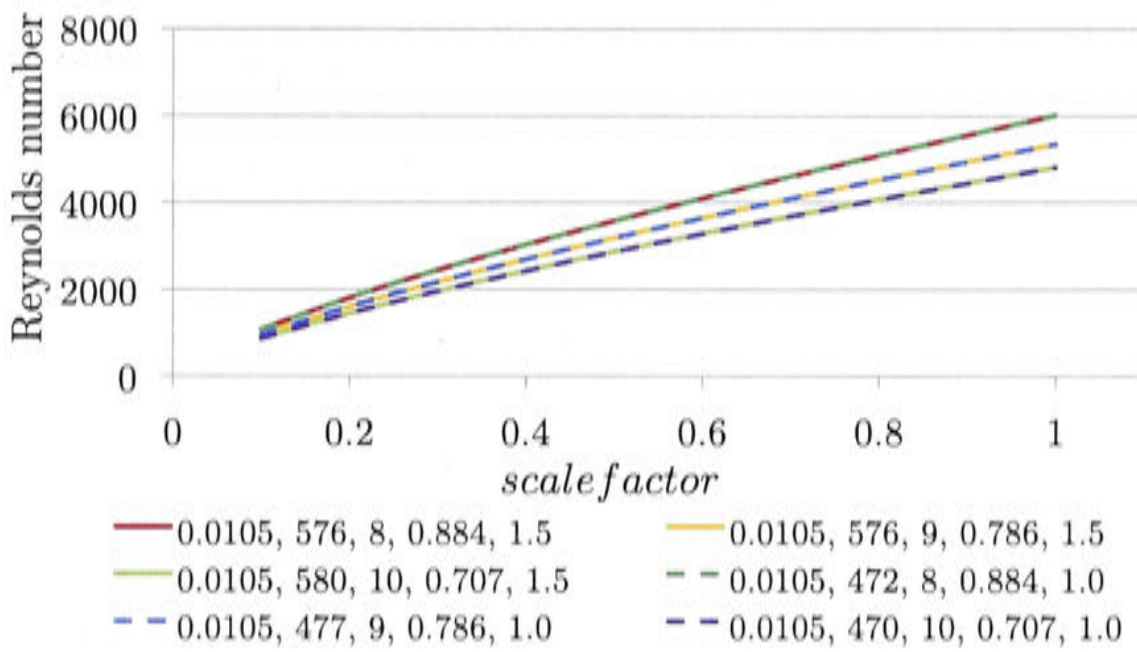

Figure 9.4: Reynolds number depending on chiller capacity (*scalefactor*). Legend: d_o, N, N_{circ}, v, V_t at $scalefactor = 1$.

9.2 Three control strategies to implement a cold storage tank in the solar thermal cooling, heating and DHW model

The aim of this thesis is to derive general conclusions on the feasibility of cold storage tanks for residential solar thermal absorption cooling systems in Australia.

As previously mentioned, the objective compared to incorporating a cold storage tank into a conventional cooling systems changes. The focus lies reducing consumption of fossil fuels, rather than on load shifting to off-peak hours when off-peak prices allow for cheaper electricity consumption.

With respect to the design outlined in the previous sections, three strategies were chosen to implement a cold storage tank in the existing solar cooling model of Chapter 7. The strategies vary depending on the cold storage medium and the type of cold distribution to the zones. The cold storage tank will be installed in the chilled water circuit and according to the three different strategies, three different TRNSYS models were developed. The basic design is shown in Figure 9.5.

The control strategies for the different cold storage scenarios manage charging and discharging of the cold storage tank, the solar and auxiliary heat supply, and the operation of the chiller. The aim is the utilization of solar energy for cooling whenever possible, while maintaining indoor comfort conditions. The following subsections explain the control strategies in detail and differentiate between the following scenarios:

- **Strategy 1**: Chiller and latent cold storage tank supply fan coil units

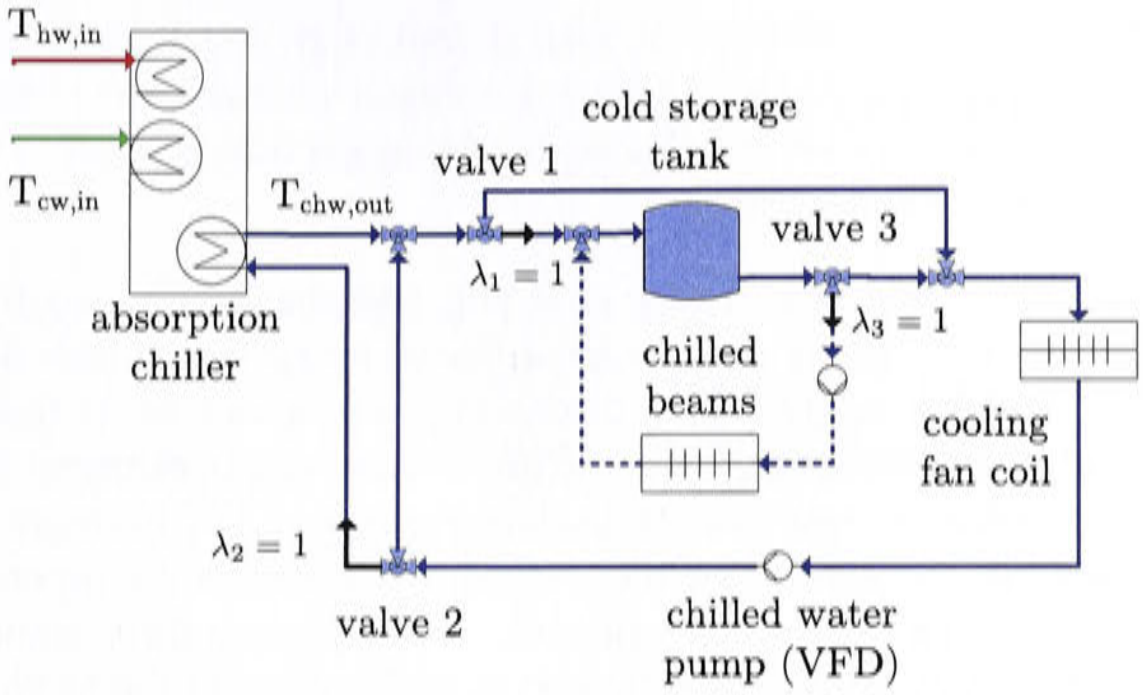

Figure 9.5: Schematic of cold storage tank within solar cooling system

- **Strategy 2**: Chiller supplies fan coil units, latent cold storage tank supplies chilled beams
- **Strategy 3**: Chiller and chilled water cold storage tank supply fan coil units

The control strategies for chiller operation, charging mode, discharging modes and auxiliary demand are explained completely for strategy 1 and any modifications for strategy 2 and 3 are outlined afterward.

9.2.1 Latent storage tank with fan coil units only (strategy 1)

A latent cold storage tank is modeled as a vertical and cylindrical tank, filled with a phase change material with a melting temperature of 11 °C. Water serves as the heat transfer fluid to pass through tubes immersed in the PCM of the cold storage tank. The chilled beams are not in use and discharging takes place when the heat transfer fluid passes through the fan coils. The control can direct the chilled water either through the tank to charge it or directly to the fan coils around the tank (valve 1).

Discharging can happen in one of two modes: Simultaneously when the chiller is operating (mode 1) or when the chiller is switched off (mode 2). When discharging during chiller operation, the water from the chiller is mixed with the cold water discharging from the tank. The higher this mixing temperature at the fan coil entrance, the lower the potential for cooling.

The air flow is calculated using equation 7.22. If the chilled water entering the coils is too warm, it can't achieve the air outlet set point temperature and it is not possible to remove the total load. The result is a drop in comfort.

Firstly, a sensitivity study on the volume of the cold storage tank per installed kW of chiller capacity ($Q_{E,rated}$) will be carried out. Three latent storage volumes (V_t) will be analyzed:

- **1 m^3** per 11 kW chiller capacity
- **1.5 m^3** per 11 kW chiller capacity
- **2 m^3** per 11 kW chiller capacity

The chiller's outlet temperature for charging and the tank's heat transfer fluid outlet temperature in discharging mode are different by approximately 6 °C. Increasing the chiller's outlet temperature in discharging mode decreases this difference. This mechanism prevents that the return chilled water temperature at low loads is as low as to charge the storage tank in discharging mode. Furthermore, the mixing temperature might be too warm to achieve the air flow set point temperature, hence the air flow set point temperature is adjusted. The following three combinations of set points for the chiller's chilled water outlet temperature and the fan coil air outlet temperature will be compared for one specific tank size $V_t = 1.5\,\mathrm{m}^3$ per rated cooling capacity.

- **(7/14):** $T_{chw,set}/T_{air,out,set} = 7°C/14°C$
- **(7/12, 11/16):** $T_{chw,set}/T_{air,out,set} = 7°C/12°C$ and $T_{chw,set}/T_{air,out,set} = 11°C/16°C$ when discharging
- **(7/14, 11/16):** $T_{chw,set}/T_{air,out,set} = 7°C/14°C$ and $T_{chw,set}/T_{air,out,set} = 11°C/16°C$ when discharging

For the purpose of implementing the control strategies in the TRNSYS cold storage tank model, a main controller component has been programmed. The component of the absorption chiller has an output state **ChillerStatus**. The chiller's internal control algorithm evaluates if the three external inlet temperatures are within the allowed temperature range and switches the chiller off if they are outside these parameters. The status output from the chiller serves as an input for the main controller.

A second input to the main controller is **CoolingReq**, which is determined by the HVAC schedules and the room thermostats, and represents the load's requirement for cooling. It was formerly represented by $HVAC_c$ in equation 7.1. A third input is the status of the auxiliary heater of the previous time step, **AuxStatus**.

These three inputs are the base inputs to logically determine the following signals.

AuxReq

In order to switch on the auxiliary heater, equation 9.32 indicates that not only comfort conditions need to be exceeded, but the cold storage tank must be depleted as well. The signal for the auxiliary heater to switch on (*AuxReq*) depends on the requirements of the HVAC system (*CoolingReq* and *HeatingReq*) and on the cold storage tank temperature (T_{cs}), which must be larger than the melting temperature of the PCM to indicate that the tank is depleted.

If auxiliary heating was on in the previous time step and cooling is still required by the building and the cold storage tank is depleted, then the hot water temperature

near the middle of the hot water tank is used to determine when the auxiliary heater can switch off. If the auxiliary heater was previously off, the tank outlet temperature is compared to the required set point temperature to change the control signal.

$$\begin{aligned} AuxReq = \{CoolingReq \cdot \{T_{cs} > T_{melt}\} \vee HeatingReq\} \\ \cdot (\{AuxStatus = 1\} \cdot \{T_{hw,middle} < T_{hw,req}\} \\ + \{AuxStatus = 0\} \cdot \{T_{hw,tank,out} < T_{hw,req}\}) \end{aligned} \tag{9.32}$$

ChillerReq

The request to switch on the chiller is determined by the control logic in equation 9.33.

$$\begin{aligned} ChillerReq = \neg HeatingReq \\ \cdot \Big(AuxStatus + \neg AuxStatus \\ \cdot \Big(\{ChillerStatus = 0\} \cdot \{T_{hw,middle} \geq T_{hw,req}\} \\ + \{ChillerStatus = 1\} \cdot \{T_{hw,tank,out} > T_{hw,min}\} \Big) \\ \cdot \Big(\underbrace{\{liqfrac \geq 0.1\}}_{\text{hysteresis } 0.4} \cdot \{prediction \vee CoolingReq\} \Big) \Big) \end{aligned} \tag{9.33}$$

The chiller is switched on if the auxiliary heater is on. If the auxiliary heater is off, the chiller's own status of the previous time step ("ChillerStatus") determines under which conditions the chiller is requested in the current time step.

In case the chiller was previously off, it changes its status to on, if the the middle of the buffer tank's hot water temperature ($T_{hw,middle}$) reaches an arbitrary required hot water temperature $T_{hw,req}$. This temperature could be the required hot water temperature to generate 7°C chilled water at rated conditions, or a fixed temperature. In this study 75°C has been chosen for $T_{hw,req}$. This is a different required hot water temperature than $T_{hw,req,calc}$, which is the hot water temperature calculated (predicted) by the chiller in each time step, depending on its two external inlet temperatures of cooling water and chilled water.

In case the chiller was previously on, it will only switch off if the buffer tank's hot water outlet temperature ($T_{hw,tank,out}$) falls below the minimum hot water inlet temperature ($T_{hw,min}$) given by the manufacturer (here 59°C).

If the cold storage tank is fully charged and if the hot water tank temperature is still high enough to operate the chiller, but there is no cooling load (for example during the night), the model can become unstable through frequent switching. The chiller would continuously try to switch on but would be stopped again because the

chilled water return temperature is too low. To prevent that behavior, the condition of a minimum liquid fraction was introduced. Once the cold storage drops below a liquid fraction of 0.1, the chiller can't switch on before the cold storage tank has been depleted at least to 0.5 liquid fraction, even though the water in the hot storage tank might exceed the required temperature to start the chiller. This condition stabilized the model.

The parameter **prediction** is used to include a certain degree of weather forecasting in the simulation and to prevent the chiller from switching on in winter instead of using the heat in the tank for space heating. If the dry bulb temperature at the following day at midday (12:00) is greater than the set point indoor temperature, the prediction for the day is set to 1 and the chiller can use up the heat and charge the cold storage tank, even though no cooling might be required at the current time step.

Discharging the tank

Discharging of the tank can be initiated in two mutually exclusive modes, $discharging_1$ or $discharging_2$.

$$discharging = discharging_1 \vee discharging_2 \tag{9.34}$$

In mode 1 the chiller is switched on because cooling is required but its cooling capacity is too small to satisfy the cooling load entirely. The condition $disch_{1,zones}$ states, that in one of the three zones the temperature has exceeded the set point temperature by 2 degrees. This signal is used as an indicator that the chiller needs assistance.

If the cold storage tank is charged and its temperature T_{CS} is less or equal to its melting temperature, it will support the chiller in such a way, that the total chilled water mass flow is increased. Valve 2 separates the flow rate again to keep the chiller's chilled water flow rate constant. Valve 1 will direct the amount of flow, which is led through the chiller, around the cold storage. It is important to mention here, that the chilled water temperature entering the coils will be higher than the chiller's generated 7°C. Therefore, it is likely that less heat will be removed from the building.

$$\begin{aligned} discharging_1 = {} & \neg AuxStatus \cdot ChillerStatus \cdot CoolingReq \\ & \cdot \{T_{cs} \leq T_{melt}\} \\ & \cdot disch_{1,zones} \end{aligned} \tag{9.35}$$

$$\begin{aligned} disch_{1,zones} = {} & disch_{1,z_1} \cdot HVAC_{sched,z_1} \vee disch_{1,z_2} \cdot HVAC_{sched,z_2} \\ & \vee disch_{1,z_3} \cdot HVAC_{sched,z_3} \end{aligned} \tag{9.36}$$

$$disch_{1,z_i} = \underbrace{\{T_{z_i} \geq T_{setC} + 2\,^{\circ}\mathrm{C}\}}_{\text{hysteresis, off: } T_{setC} \text{ -2}} \tag{9.37}$$

In mode 2, discharging occurs when the chiller is not operating simultaneously. In this case cooling may be required or the cold storage tank is emptied in the evening. The cold storage tank temperature is an indicator in what state it is and it is defined as "empty" or depleted when the cold storage temperature is higher than the melting temperature of the PCM. The variable $disch_{2,zones}$ guarantees that no zone is cooled down below the set point temperature for heating.

$$\begin{aligned} discharging_2 = \neg ChillerStatus \cdot \{T_{cs} \leq T_{melt}\} \\ \cdot \{CoolingReq \vee disch_{2,zones}\} \end{aligned} \tag{9.38}$$

$$\begin{aligned} disch_{2,zones} &= disch_{2,z_1} \vee disch_{2,z_2} \vee disch_{2,z_3} \\ disch_{2,z_i} &= \underbrace{\{T_{z_i} \geq T_{setH} + 4\,^{\circ}\mathrm{C}\}}_{\text{hysteresis, off: } T_{setH}} \end{aligned} \tag{9.39}$$

When discharging, the chilled water pump signal ($signal_{chw}$) depends on the mode of discharging. In mode 2 the chiller is switched off and the chilled water flow rate through the tank is equal to the rated chilled water flow rate. In mode 1, the flow rate is increased by a factor ϕ, which is set to an arbitrary amount of 0.5 throughout the simulations.

The indoor fans must be operating in discharging mode 2, which is different to the base case scenario without a cold storage tank, where they were merely dependent on the chiller status.

The air temperature set point determines the air flow as previously explained. A higher set point requires a larger air flow to cover the load. When the chilled water from the cold storage tank and from the chiller's evaporator are mixed in discharging mode 1, the set point air temperature might not be able to be maintained. Therefore, the load might not be covered at all times. This behavior will be analyzed in section 9.4.1.

$$signal_{chw} = ChillerReq + discharging_1 \cdot \phi + discharging_2 \tag{9.40}$$

Valve 2 is controlled by the signal λ_2, which is the fraction of the chilled water mass flow rate that is directed through the chiller. In case of $discharging_2 = 1$, it is zero.

$$\lambda_2 = \frac{ChillerStatus}{(ChillerStatus + \phi \cdot discharging_1)} \tag{9.41}$$

Charging

The charging of the tank can only be initiated once the chiller is in operation, and the temperature of the cold storage tank (T_{cs}) is warmer than the chiller's chilled water outlet temperature. Furthermore, if the auxiliary heater is on, charging can't take place to prevent the auxiliary heater from charging the tank using gas.

If cooling is required ($CoolingReq = 1$), the liquid fraction as well as the cold storage medium temperature determine further if charging shall be triggered.

Charging occurs if the cooling load of the building is lower than the cooling capacity the chiller could potentially produce, utilizing the solar irradiation available. Furthermore, to achieve stability in the model, charging is not allowed when discharging is initiated or when one of the three zones has exceeded the set point by 2 °C.

$$\begin{aligned} charging = {} & ChillerReq \cdot \neg AuxStatus \\ & \cdot \{liqfrac > 0.1\} \cdot \{T_{cs} \geq T_{chw,out,chiller}\} \\ & \cdot \neg discharging \cdot \neg disch_{1,zones} \end{aligned} \tag{9.42}$$

When cooling is required by the building and charging is possible, valve 1 determines the proportion of chilled water which is lead through the cold storage tank and around directly to the cooling coils. The valve position λ_1 represents the proportion which is lead through the cold storage tank (equation 9.43).

$$\lambda_1 = \psi \cdot charging + \neg charging \cdot discharging \cdot (1 - \lambda_2) \tag{9.43}$$

If cooling is required and it is possible to charge the tank, ψ represents the proportion of the potential for charging the tank. The full potential is exploited by warming up the chilled water stream to the rated return water temperature of the chiller $T_{chw,coils,out,set}$ (here 12°C).

$$\psi = 1 - \max\left(0, \min\left(1, \frac{T_{chw,coils,out,set} - T_{chw,coils,in,set}}{T_{chw,coils,out,set} - T_{chw,out,chiller}}\right)\right) \tag{9.44}$$

$$T_{chw,coils,in,set} = T_{chw,coils,out,set} - \frac{\dot{Q}_{load}}{\dot{m}_{chw} \cdot c_{p,f}} \tag{9.45}$$

Remark *The value $1 - \phi$ is a proportion of the cooling potential of the chilled water flow, defined by the cooling demand in the current time step. The total cooling potential is defined by the ΔT between the chiller's chilled water outlet and fixed return temperature. The actual*

mixing temperature $T_{chw,coils,in}$ is not known when ϕ is calculated, however, temperatures in the interval $[T_{melt} - 3\,°C, T_{melt}]$ seldomly occurs. This is due to the cold storage tank heat exchange effectiveness. The cold storage tank's outlet temperature depends on the chilled water flow rate, its inlet temperature and on the resistance due to the thickness of the PCM shell around the heat exchanger tubes, following equation 9.1 and 9.2.

The arrangement of fan coils and cold storage tank could have been installed in parallel instead of in series, which would have enabled the cooling coils to receive water temperatures as low as the chiller's outlet temperatures. However, the flow rates through the coils would have been reduced when charging.

Knowledge of the cooling load $\dot{Q}_{load}$ at the present time step is necessary to calculate $T_{chw,coils,out,set}$. The methodology to calculate the load has been introduced previously in equation 7.22 in order to calculate the indoor fan air flow.

9.2.2 Modification chilled beams (strategy 2)

For this control strategy a latent storage tank with a PCM of 11 °C melting temperature is modeled, but discharging occurs via chilled beams, rather than fan coil units. In the model the chilled water flow through the chiller's evaporator does not mix with the chilled water discharging the tank.

Discharging mode 1 and 2 are still implemented and an extra chilled beams pump is modeled to separate the circuits. In discharging mode 1 the chiller is switched on in parallel to the cold storage tank and provides cooling by distributing the chilled water to the fan coils. Discharging the latent cold storage tank takes place circulating chilled water through the cold storage tank and the chilled beams. In charging mode, the chiller provides the fan coils with cooling first, and, depending on the load, allocates a certain proportion of the chilled water flow to the cold storage tank. The proportion is calculated as in equation 9.43.

The temperature levels of the two water streams for chiller operation and discharging the cold storage tank are kept separate, according to the requirements for chilled beams and fan coil units. The chiller can be operated continuously at 7 °C chilled water set point temperature. The cooling coils outlet set point temperature is 14°C and the set point for the chilled beams is 18°C water supply temperature. As in section 8.2.9 the same climate specific building model (TRNSYS) type 56 with chilled beams is used for the simulations.

The mass flow rate of the chilled water passing through the beams is load regulated as in equation 8.11. The signal for water passing through the beams of one zone or bypassing the zone is determined by equation 9.46.

$$signal_{chb,z_i} = discharging_1 \cdot disch_{1,z_i} \vee discharging_2 \cdot disch_{2,z_i} \tag{9.46}$$

Valve 3 determines the water flow through the cold storage tank and the chilled beams when discharging and it is controlled by the signal λ_3. Whenever discharging

via chilled beams is in operation, valve 1 directs the water from the chiller around the tank ($\lambda_1 = 0$) to the fan coils.

$$\lambda_3 = discharging \tag{9.47}$$

$$\lambda_2 = 1 \tag{9.48}$$

$$\lambda_1 = \psi \cdot charging \tag{9.49}$$

9.2.3 Chilled water tank (strategy 3)

A chilled water tank is used as cold storage device. The signal for chiller request is determined by equation 9.50.

$$\begin{aligned} ChillerReq = \neg HeatingReq & \\ \cdot \Big(& AuxStatus + \neg AuxStatus \\ & \cdot \Big(\{ChillerStatus = 0\} \cdot \{T_{hw,middle} \geq T_{hw,req}\} \\ & \quad + \{ChillerStatus = 1\} \cdot \{T_{hw,tank,out} > T_{hw,min}\} \Big) \\ & \cdot \Big(\neg \underbrace{\{T_{cs,out} \leq 7\,°C\}}_{\substack{\text{hysteresis, off:} \\ T_{cs,out} \geq T_{empty}}} \cdot \{prediction \vee CoolingReq\} \Big) \Big) \end{aligned} \tag{9.50}$$

It is more difficult to determine the state of depletion, as the phase change of pure water at atmospheric pressure occurs at 0°C. Therefore, under the desired conditions, it is not possible to use the melting temperature or liquid fraction of pure water as an indicator for depletion. The tank is deemed to be discharged when the heat transfer fluid outlet temperature rises above 13°C. To initiate discharging the two equations 9.38 and 9.35 are modified and T_{melt} is replaced by T_{empty} and T_{cs} is the temperature of the chilled water exiting at the bottom of the sensible cold storage tank ($T_{cs,out}$).

9.3 Electricity demand of the chilled water pump

The electricity demand of the chilled water pump is caused by the pressure drop through the chiller and the fan coils, but also by the cold storage tank. The resistance to flow is higher for the latent storage tank with its multiple tubes immersed in the PCM, than for the sensible storage tank.

If chilled beams are used for cooling, a second pump supplying the beams and the cold storage tank is introduced for discharging.

When charging, discharging or operating the chiller only, different flow rates pass through the components of the chilled water circuit, resulting in different pressure

drops. In the following section for each cold storage strategy the electricity consumption in the different operation modes in dependency of the *scalefactor* is outlined.

9.3.1 Latent cold storage tank

The PCM cold storage tank has a relatively large pressure drop, due to hundreds of narrow paths through the tank in order to increase heat transfer. The design parameters in section 9.1.1 have been used as a basis to calculate the pressure drops for the modes charging, discharging 1, discharging 2 and chiller operation only.

While **charging**, the pump power consumption depends on the position of valve 1, which is determined by the fraction of the scaled flow rate passing through the cold storage tank (ψ), as defined in equation 9.44. A pressure drop occurs in the evaporator, pipes, fan coils and the cold storage tank. For different *scalefactors* the percentage of the pump electricity consumption due to the cold storage tank (r_{CS}) varies, but can be expressed as a logarithmic function as shown in equation 9.52. For three different cold storage tank sizes ($V_t \in \{1\,\mathrm{m}^3, 1.5\,\mathrm{m}^3, 2\,\mathrm{m}^3\}$) the function is displayed in Figure 9.6. Taking into account the relationship $r_{CS} \propto \Delta p_{CS} \propto \psi^2$ equation 9.51 is derived, in order to calculate the power demand using the fraction of the flow rate lead around the cold storage tank.

$$\dot{E}_{el,pump,\psi} = \dot{E}_{el,pump,\psi=1} \cdot \left(1 - r_{CS}\left(1 - \psi^2\right)\right) \tag{9.51}$$

$$r_{CS} = m \cdot \ln(scalefactor) + b \tag{9.52}$$

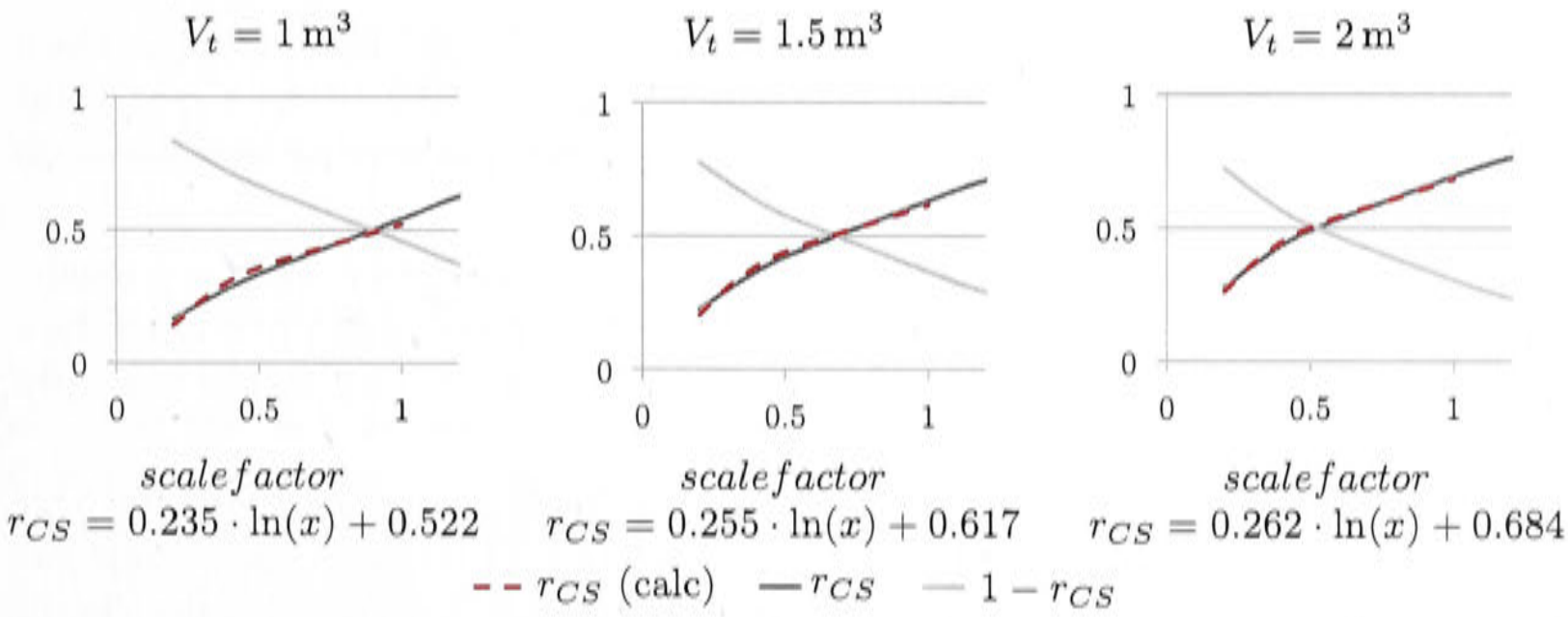

Figure 9.6: Percentage of the electricity consumption due to the pressure drop in the cold storage tank

In **discharging mode 1** the flow rate is increased by 50% and the chiller as well as the cold storage tank are supplied with chilled water. Hence, the pump power consumption is increased. In **discharging mode 2** only the cold storage tank and the fan coils have to be supplied, ergo, the electricity consumption is reduced.

The length of the pipework is always fixed at 20 m and only the diameter is varied as described in equation 7.42. The pump power consumption in dependency of the

$scalefactor^3$ for the different modes for a 1.5 m^3 latent cold storage tank can be seen in Figure 9.7. For the three different tank designs (e.g. size and amount of tubes) the power coefficients of the curves are modified. Within one annual simulation the controller implemented in the TRNSYS model decides, depending on the mode, which curve to choose to calculate the pump power consumption.

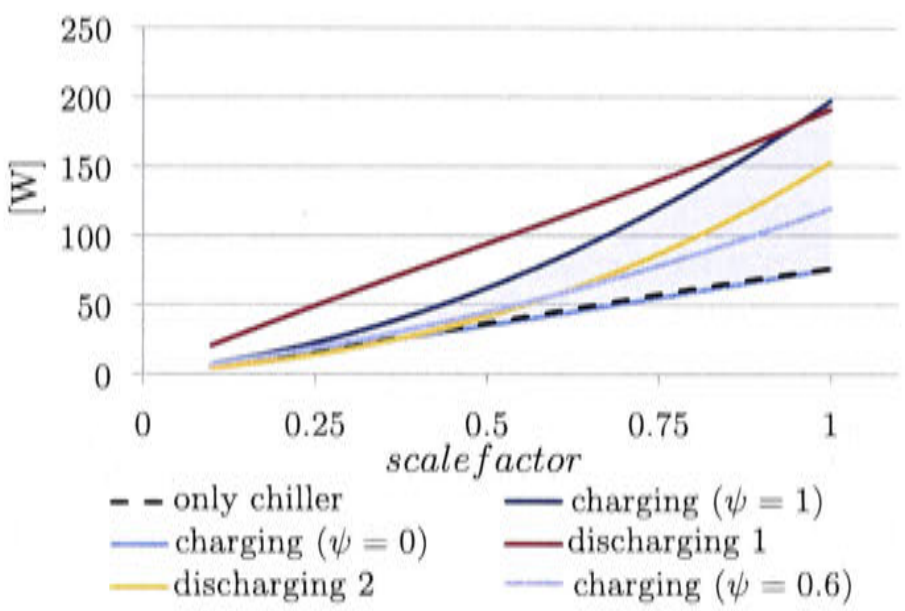

Figure 9.7: Electricity consumption of the chilled water pump for a 1.5 m^3 latent storage tank with $N_{circ} = 9$, $d_o = 0.0105$ m, $N = 576$ at $scalefactor = 1$.

9.3.2 Chilled water tank

A sensible storage tank (TRNSYS type 60) to modeled a chilled water storage. Once the entire tank is at 7°C it is considered charged. Its volume is 2 m^3 per Cap_{rated} and its height is 1.8 m. Similar to strategy one and two, the tank volume is scaled with the climate specific *scalefactor*.

Fan coil units are used as the tank is discharged, and dehumidification is possible. However, the tank is not able to provide a constant chilled water output temperature over a long period of time. The temperature at which the tank is considered empty is set to 13°C.

The large advantage of sensible storage tanks is the absence of an additional heat exchanger to separate the storage medium from the heat transfer fluid. Heat exchangers usually induce a relatively high pressure drop in the chilled water circuit and increase the capital cost of the tank. However, the chilled water outlet temperature does not stay constant over an extended period of time, as it does with a latent storage tank.

The volumetric energy density of the chilled water tank can be calculated as in equation 9.53.

[3] As a reminder, a *scalefactor* of 1 indicates a chiller with a rated capacity of 11 kW.

$$\begin{aligned} Cap_{chw} &= (T_{empty} - T_{charged}) \cdot \rho_f \cdot c_{p,f} \\ &= (13\,°\mathrm{C} - 7\,°\mathrm{C}) \cdot 999\,\mathrm{kg\,m^{-3}} \cdot 4.19\,\mathrm{kJ\,kg^{-1}\,K^{-1}} \\ &\approx 25\,115\,\mathrm{kJ\,m^{-3}} \end{aligned} \tag{9.53}$$

This is 30% of the volumetric energy density of the latent cold storage tank which is calculated in equation 9.54. Calculating the compactness factor CF as in equation 9.13, it is assumed that the entire cold storage medium can potentially be solidified[4].

$$\begin{aligned} Cap_{PCM} &= \rho_{PCM} \cdot CF \cdot \Delta h_{lat} \\ &= 871\,\mathrm{kg\,m^{-3}} \cdot 0.95 \cdot 100.1\,\mathrm{kJ\,kg^{-1}} \\ &\approx 82\,828\,\mathrm{kJ\,m^{-3}} \end{aligned} \tag{9.54}$$

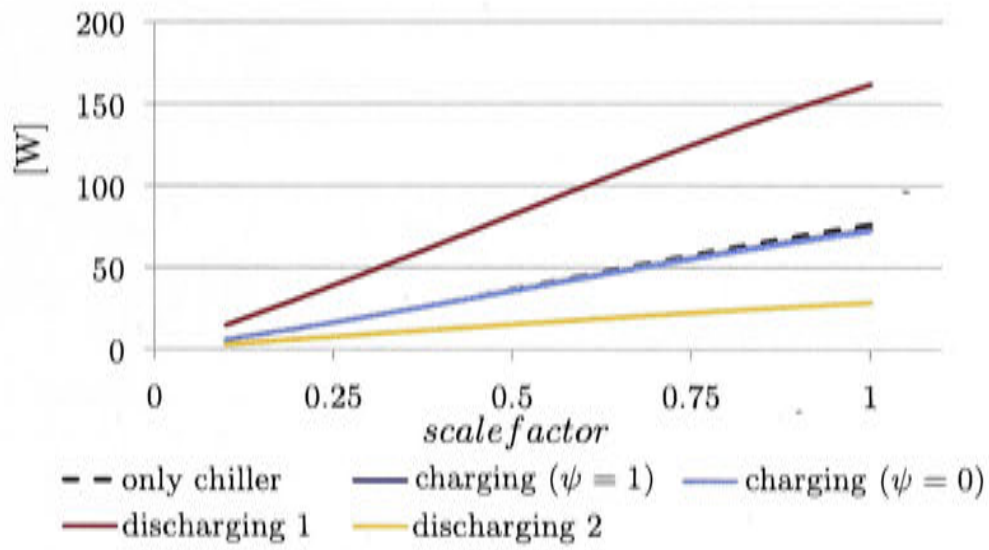

Figure 9.8: Electricity consumption of the chilled water pump when using a chilled water tank instead of PCM material.

The pressure drop of the chilled water tank when charging or discharging is very small compared to the other flow resistances in the circuit as mainly the inlet and outlet of the tank induce a pressure drop. From Beitz and Grote [1997] the inlet flow resistance factor is 1 and the outlet resistance 0.5. These values add up to a total of $\zeta_{CS} = 1.5$ flow resistance factor, which induces a pressure drop of 0.75 kPa, with 100% of the flow lead through the chilled water tank ($\psi = 1$) at $v = 1\,\mathrm{m\,s^{-1}}$. Applying the same methodology as in section 9.3.1, r_{CS} is nearly 0 for all ψ. The power demand curves for charging, discharging mode 1 and discharging mode 2 in dependency of the *scalefactor* are shown in Figure 9.8.

[4]For higher accuracy the maximum radius of each path r_{max} can be used to calculate the cold storage compactness factor CF^* instead of CF. To do so, V_t in equation 9.13 is substituted by $V_{t,max} = N/ratio_N^2 \cdot V_t$, the maximum possible volume that can be solidified. The compactness factor CF^* can be calculated using the relationship $1 - CF^* = (1 - CF) \cdot ratio_N^2/N$. The variation is negligible and mentioned for completeness.

9.3.3 Chilled beams

Including chilled beams in the latent cold storage model only affects the power demand curves for discharging. In charging mode the pump power demand is the same as for the curves labeled charging in Figure 9.7.

A second chilled water pump has been implemented to supply the beams. The chilled water mass flow rate for $scalefactor = 1$ is the same as the chiller's rated chilled water flow rate.

At discharging mode 1, the chilled beams pump and the ordinary chilled water pump are switched on simultaneously and the power consumptions of both pumps in Figure 9.9 add up. The beams pump pressure drop calculation takes into account the pressure drops of the beams and the cold storage tank at the scaled flow rate. The design of the chilled beams agrees with the design in section 8.2.9. In discharging mode 2 only the chilled beams pump is in operation.

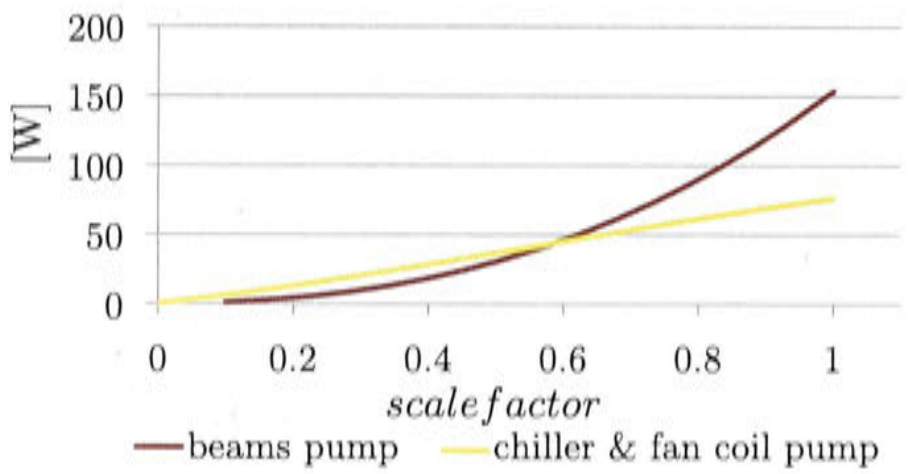

Figure 9.9: Electricity consumption of the chilled water pump and the chilled beams pump in discharging mode.

9.4 Discussion of the results of the cold storage tank strategies

This section presents the simulation results of each of the three system designs using cold storage tanks. The cost parameters are assumed as in Table 8.1 and the cost for the latent storage tank was set to $\$91^{-1}$.

9.4.1 Latent storage tank with fan coil units only (strategy 1)

The latent cold storage absorption chiller model with its various control strategies lead to a tedious debugging process in order to minimize energy imbalances and proper mode switching to prevent fluctuations.

In addition to the energy balance around the hot water tank (equation 8.1), a second energy balance $\Delta Q_{imb,chw}$ was established around the chilled water circuit (equation 9.55). It will be expressed as a percentage of the transferred cooling Q_c via cooling coils (and chilled beams, if beams are included in the model). The term

$\Delta Q_{imb,chw}$ is comprised of the chiller's generated cooling (Q_{chw}), subtracting the energy drawn from the coils and the beams (Q_c), and subtracting the losses from the cold storage tank to the environment ($Q_{CS,loss}$).

$$\Delta Q_{imb,chw} = Q_{chw} - Q_c - Q_{CS,loss} \tag{9.55}$$

In the following two sections, firstly, the latent cold storage volume will be varied. Secondly, the set points for the chiller's chilled water outlet temperature and air outlet temperature leaving the fan coils will be varied at a fixed tank size. The analysis of the results will be presented.

Variation in cold storage tank volume

The size of the cold storage tank, as previously explained, is scaled depending on the *scalefactor* of each climate. The volume V_t denoted on the x-axis of the solar fraction and throughout the labels of the figures denotes the storage size for a *scalefactor* of one. Or in other words, the tank's volume on the x-axis is specific to the chiller's rated capacity ($V_t' = V_t/11\,\text{kW}$) and the scaled tank volume ($V_{t,scaled}$) in each climate is calculated using equation 9.16.

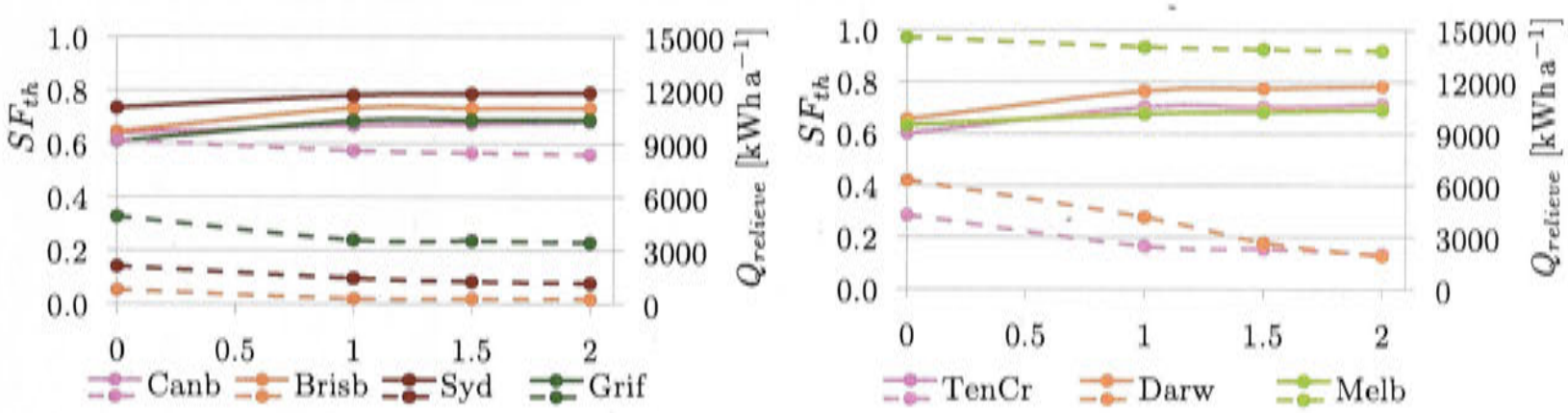

Figure 9.10: Solar fraction excluding DHW (SF_{th}) (left solid —) and relieved heat (right dashed - -) for various cold storage sizes. 0 m^3 denotes base case

Table 9.6 shows the difference of the solar fraction of the three cold storage tank sizes compared to the base case.

Table 9.6: Change of the solar fraction (SF_{th}) for the three different cold storage tank sizes compared to the base case

	Canb	Brisb	Syd	Grif	TenCr	Darw	Melb
1 m^3	2.8%	8.9%	4.6%	7.7%	10.4%	10.9%	4.4%
1.5 m^3	3.3%	8.7%	5.2%	7.9%	10.2%	11.8%	5.1%
2 m^3	4.0%	8.8%	5.5%	8.0%	11.3%	12.6%	5.9%

Figure 9.10 shows the development of the solar fraction with increasing cold storage tank sizes and the drop in relieved heat. The cooling supplied can be seen in Figure 9.11 and the change compared to the base case is visible in Table 9.7 and Figure 9.12. The cold storage tank model seems to transfer more cooling into the

building than in the base case model and the relative change is largest in the climates with the smallest cooling demand (Canberra, Melbourne and Sydney). In Tennant Creek the relative increase in heating demand seems large, however, the absolute heating demand of the base case was negligibly small.

The melting temperature of the tank is 11°C and therefore, the air set point temperature leaving the cooling coils was increased to 14°C to facilitate the fan coil units to achieve the set point more often. However, higher air mass flows are necessary.

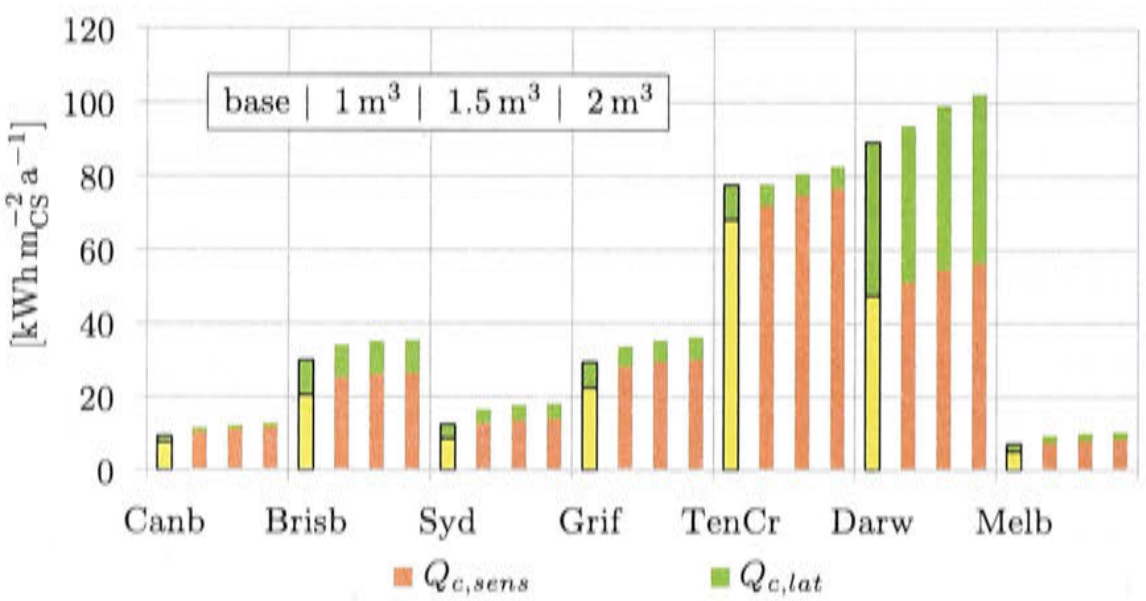

Figure 9.11: Sensible and latent cooling supplied relative to the conditioned space. Columns from left to right represent different latent storage tank sizes: 1 m³, 1.5 m³, 2 m³

Table 9.7: Change of cooling and heating supplied compared to the base case (three latent cold storage sizes).

		Canb	Brisb	Syd	Grif	TenCr	Darw	Melb
ΔQ_c	2 m³	36%	18%	46%	23%	6%	14%	44%
	1 m³	23%	13%	32%	14%	0%	5%	29%
	1.5 m³	30%	16%	41%	20%	4%	11%	38%
ΔQ_h	2 m³	0%	4%	2%	2%	52%	-	1%
	1 m³	0%	3%	2%	2%	22%	-	0%
	1.5 m³	0%	4%	2%	2%	35%	-	0%

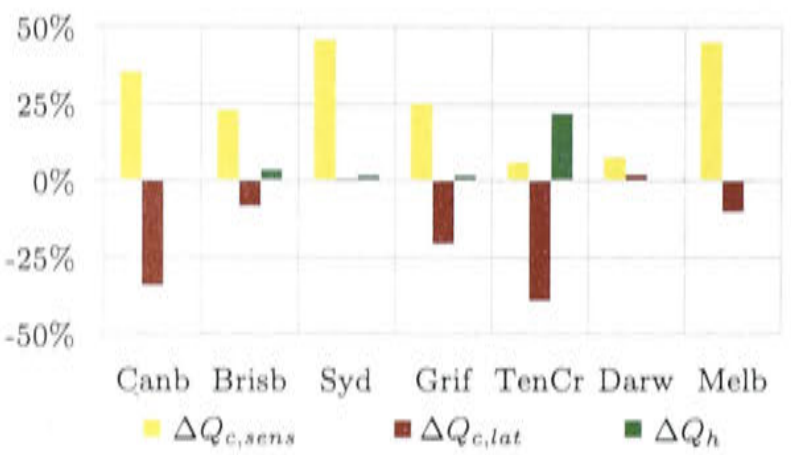

(a) 1 m³

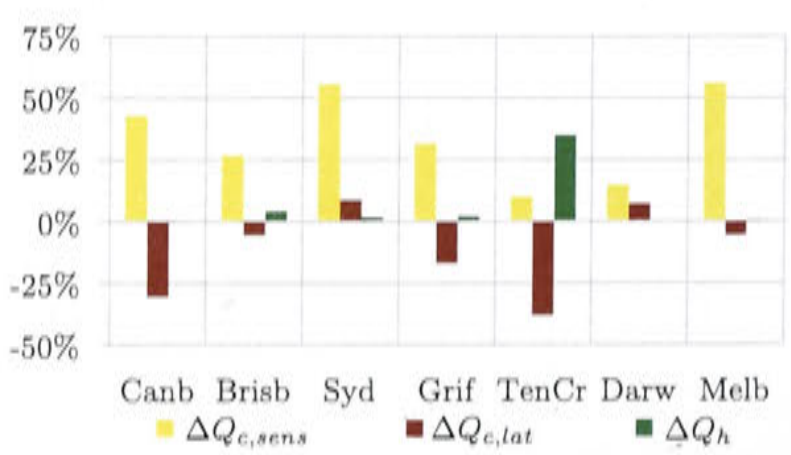

(b) 1.5 m³

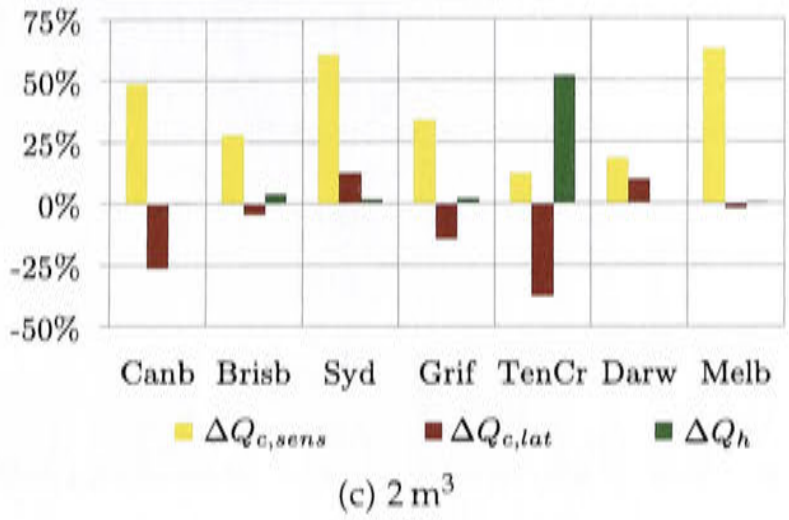

(c) 2 m^3

Figure 9.12: Relative change of supplied sensible and latent cooling and heating, corresponding to Table 9.7

It is important to mention that not only the supplied cooling but also the indoor fan operating hours increase (Figure 9.13). Furthermore, the average air flow drops. The reason being most likely discharging mode 2 and the signal $disch_{2,zones}$ in equation 9.39, which invokes cooling in the evening in order to deplete the tank and to pre-cool the building, occasionally without a direct call for cooling at the current time step. In case of no cooling requested, the minimal air flow provides cooling and reduces the average air flow. Hence, more cooling is provided to the building. However, it occurs at times when no cooling is directly needed.

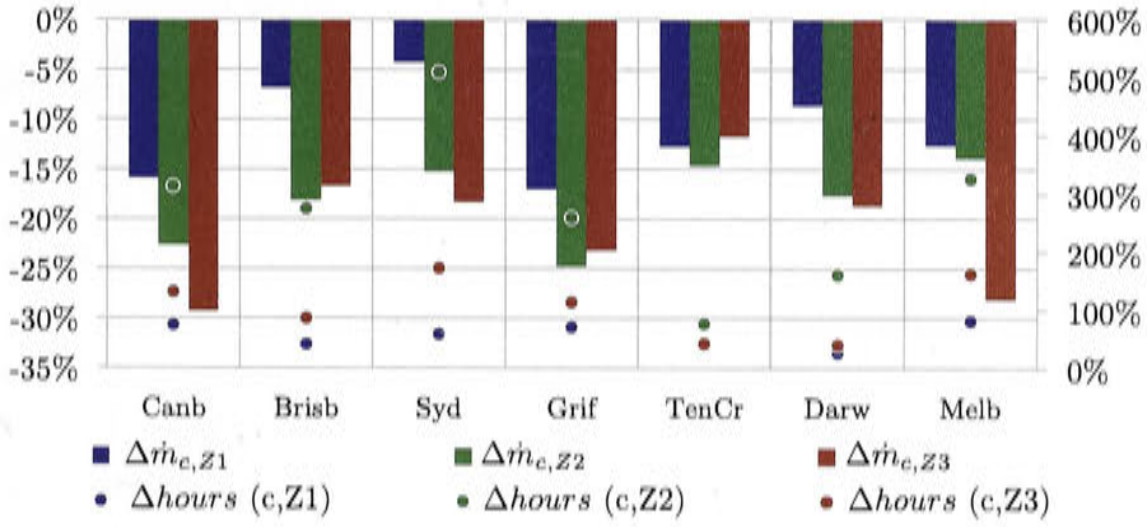

Figure 9.13: Change in average air flow (left) and fan operating hours (right) for the 1.5 m^3 cold storage tank compared to the base case.

The comfort conditions in Figure 9.14 show that the cooling increase in Canberra, Sydney and Melbourne has increased the indoor temperature comfort. Surprisingly, in the hot climates of Tennant Creek, Griffith, Brisbane and Darwin, where the relative cooling increases are moderate, the comfort drops, indicating that the set points are met less often. In the climates Canberra, Griffith and Brisbane a slight increase in discomfort due to too low indoor temperatures is visible ($comf_T$ winter).

During charging mode and discharging mode 1 temperature entering the fan coils is higher than the chiller's chilled water set point temperature. Although This higher amounts of cooling are supplied, the increased air outlet set point temperature of 14°C is less often met. Furthermore, before the auxiliary heater can switch on to

support the air-conditioning system, the cold storage tank must be depleted.

Even though the coils inlet temperature may exceed 7°C during discharging, the relative humidity discomfort only increases slightly.

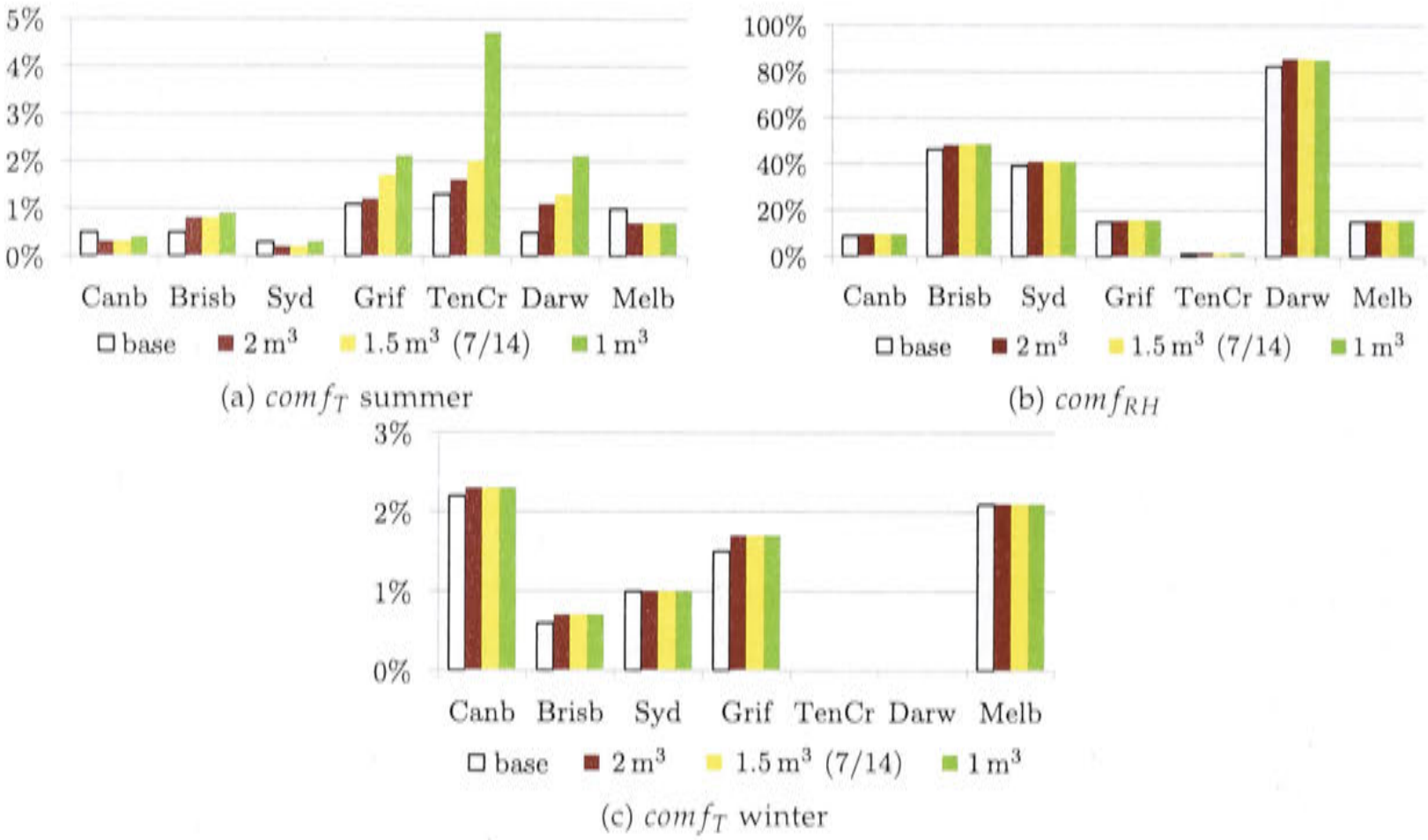

(a) $comf_T$ summer

(b) $comf_{RH}$

(c) $comf_T$ winter

Figure 9.14: Comfort conditions (three latent cold storage sizes)

Figure 9.15 shows how much of the provided cooling was released from the tank $Q_{c,CS \rightarrow coils}$ and how much cooling was provided to the coils directly from the chiller $Q_{c,chiller \rightarrow coils}$. In Table 9.8 the numbers are expressed as percentage. The tank size matters and in all climates a larger tank can provide a larger share of the cooling load. In the colder climates a larger percentage can be supplied from the tank, indicating that more cooling is stored in the tank. This is most likely due to the larger collector area, which is sized for a solar fraction for heating and cooling. In colder climates higher heating loads lead to a larger collector area relative to the cooling load.

Table 9.8: Percentage of cooling supplied by the cold storage tank (three latent cold storage sizes).

	Canb	Brisb	Syd	Grif	TenCr	Darw	Melb
2 m³	44%	27%	38%	36%	26%	27%	42%
1 m³	45%	26%	35%	36%	29%	25%	40%
1.5 m³	48%	28%	37%	37%	30%	29%	44%

The distribution of the cold storage's status from fully charged ($liqfrac = 0$) to empty ($liqfrac = 1$) is interesting to compare for each climate. Figure 9.16 shows the frequency of the cold storage tank's charging states. The elevated region between $liqfrac = 0.1$ and $liqfrac = 0.5$ are due to the control strategy and the hysteresis included to prevent the model from fluctuating between charging and discharging. The elevation is largest for the smaller tanks especially in the colder climates, where

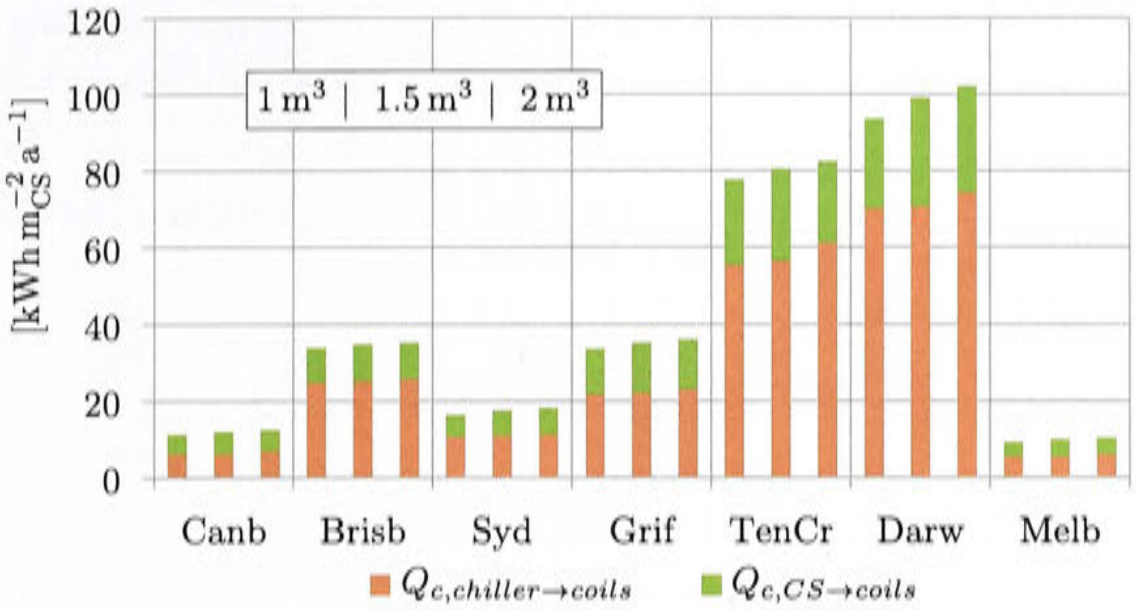

Figure 9.15: Cooling provided via cold storage tank (CS) and directly from the chiller (three latent cold storage sizes)

the collectors are sized primarily for heating in winter.

The percentage of time the tank is completely discharged can be found in Table 9.9. It includes night hours. The discharging strategy tries to deplete the tank in the afternoon. Table 9.10 shows the percentage of time when there is a cooling demand, but the cold storage tank is depleted and heat for cooling is provided by the auxiliary gas heater. The results of varying set point temperatures in the next section are included in these tables. In the three climates Brisbane, Tennant Creek and Darwin the tank is empty between 15% and 20% of the time when there is a cooling demand. This might indicate that a larger cold storage tank is needed.

Table 9.9: Percentage of time the tank is completely empty ($liqfrac = 1$). Only the summer months (September – April) have been taken into account.

	Canb	Brisb	Syd	Grif	TenCr	Darw	Melb
2 m³	50.2%	73.1%	72.2%	41.1%	52.9%	69.6%	65.5%
1 m³	57.9%	69.9%	72.9%	44.0%	47.7%	64.8%	70.4%
1.5 m³ (7/14)	55.4%	71.1%	72.3%	39.5%	50.8%	66.6%	68.4%
1.5 m³ (17/12, 11/16)	51.3%	62.3%	67.5%	34.3%	44.8%	61.3%	64.3%
1.5 m³ (7/14, 11/16)	51.2%	67.1%	68.8%	36.3%	50.3%	67.3%	62.6%

Table 9.10: Percentage of time a cooling demand occurs but the cold storage tank is depleted and the auxiliary heater has to provide the heat demand for the absorption chiller

	Canb	Brisb	Syd	Grif	TenCr	Darw	Melb
2 m³	2.0%	15.3%	6.8%	7.5%	19.8%	17.8%	2.8%
1 m³	2.2%	15.5%	7.2%	7.7%	19.8%	19.3%	3.3%
1.5 m³ (7/14)	2.1%	15.3%	6.9%	7.5%	19.9%	18.0%	3.0%
1.5 m³ (7/12, 11/16)	1.3%	10.8%	4.9%	6.0%	18.4%	14.3%	2.5%
1.5 m³ (7/14, 11/16)	1.6%	13.5%	6.0%	7.1%	19.3%	17.7%	2.6%

The electricity consumption can be seen in Figure 9.17 and Table 9.11. The electricity increase in the hot climates Brisbane, Griffith, Tennant Creek and Darwin is

below 10% and in the cooler climates below 20%. The amount of time the cooling water set point temperature is exceeded stays rather constant throughout the simulations.

Table 9.11: Relative change of electricity consumption ΔE_{el} compared to the base case (three latend cold storages sizes).

	Canb	Brisb	Syd	Grif	TenCr	Darw	Melb
2 m^3	15%	8%	19%	8%	5%	4%	14%
1 m^3	10%	5%	12%	5%	0%	-2%	9%
1.5 m^3	11%	8%	17%	8%	3%	2%	12%

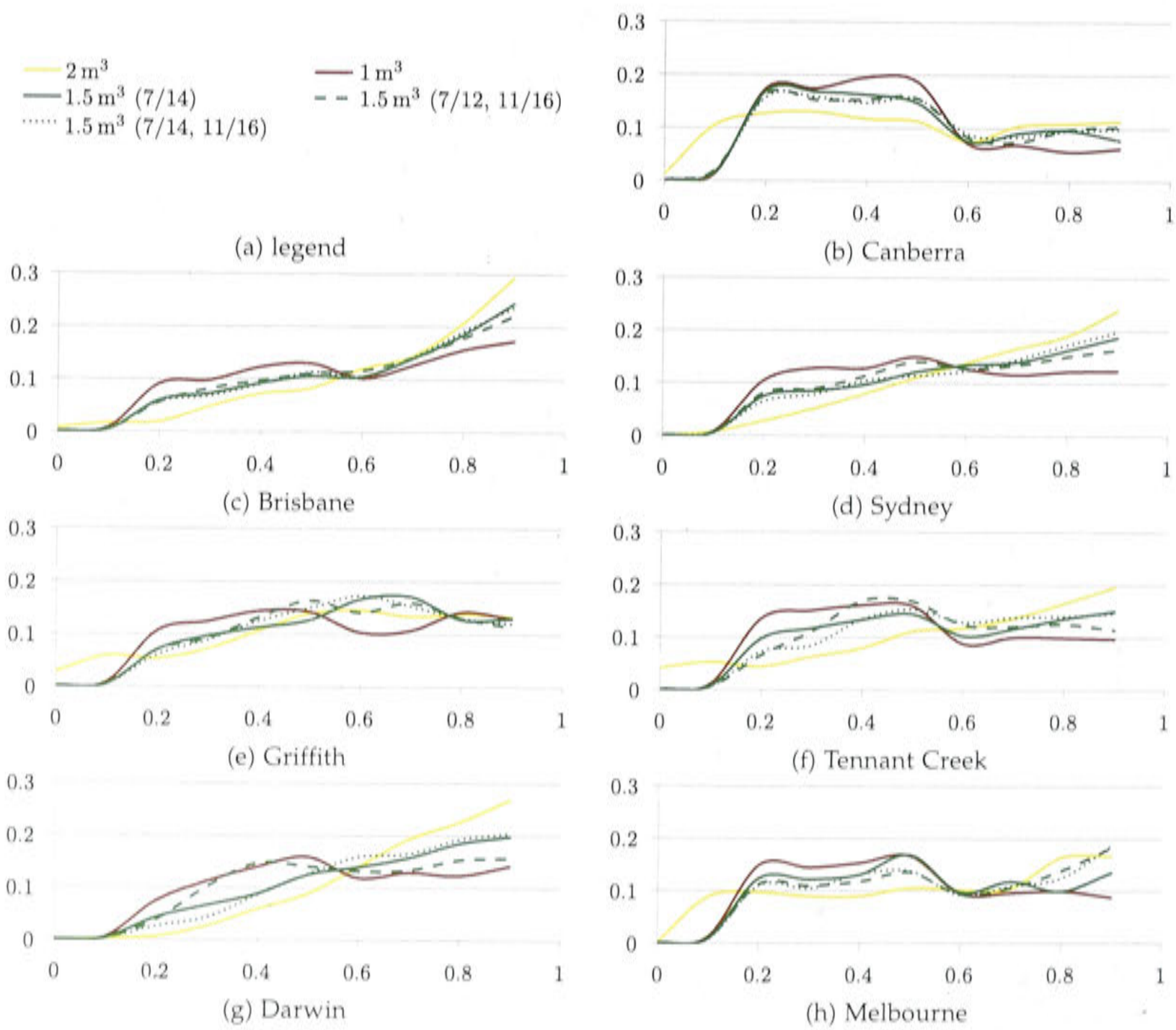

Figure 9.16: Percentage of time the latent cold storage tank is not empty and charged to a certain degree. The liquid fraction *liqfrac* is displayed on the x-axis (The point 0 includes the frequency of the interval [0,0.1[, the point 0.1 includes the frequencies in the interval [0.1,0.2[, etc.)

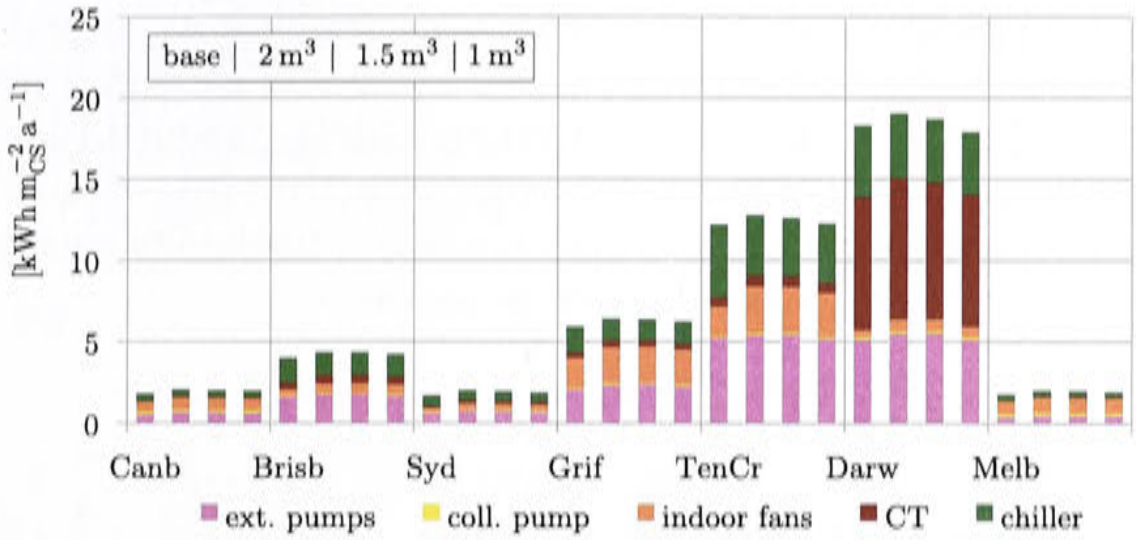

Figure 9.17: Electricity consumption of each individual consumer specific to the conditioned space compared to the base case (latent CS)

Previously, the energy imbalance around the hot water tank ($\Delta Q_{imb,hw}$), as in equation 8.1, has been presented as a fraction of the relieved heat. This value is shown for the cold storage tank simulations in Figure 9.18. The largest imbalance is as previously detected in Brisbane, where the relieved heat is the smallest of all climates.

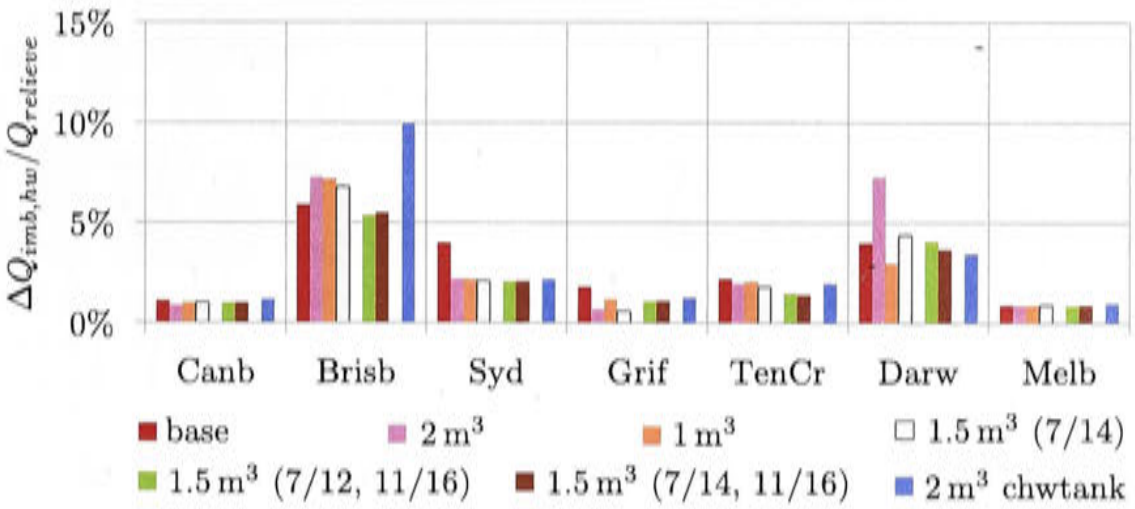

Figure 9.18: Energy imbalance around the hot water tank as a fraction of the relieved heat. The chilled water tank is included.

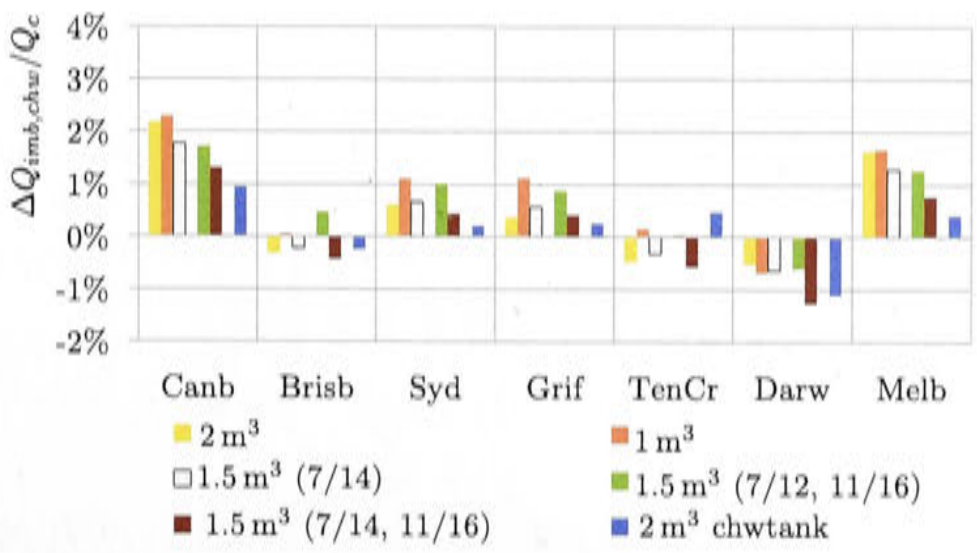

Figure 9.19: Energy imbalance around the chilled water circuit as a fraction of the total amount of cooling supplied. The chilled water tank is included.

The energy imbalance around the chilled water circuit is expressed in equation 9.55. It is presented as a percentage of the total amount of cooling supplied (Figure 9.19), but has not been added to the amount of cooling provided (!). Both graphs include the energy imbalance of the chilled water tank (chwtank) of section 9.4.3. The climates with the smallest cooling load show the largest fraction of energy imbalance. However, in Darwin the absolute imbalance is largest.

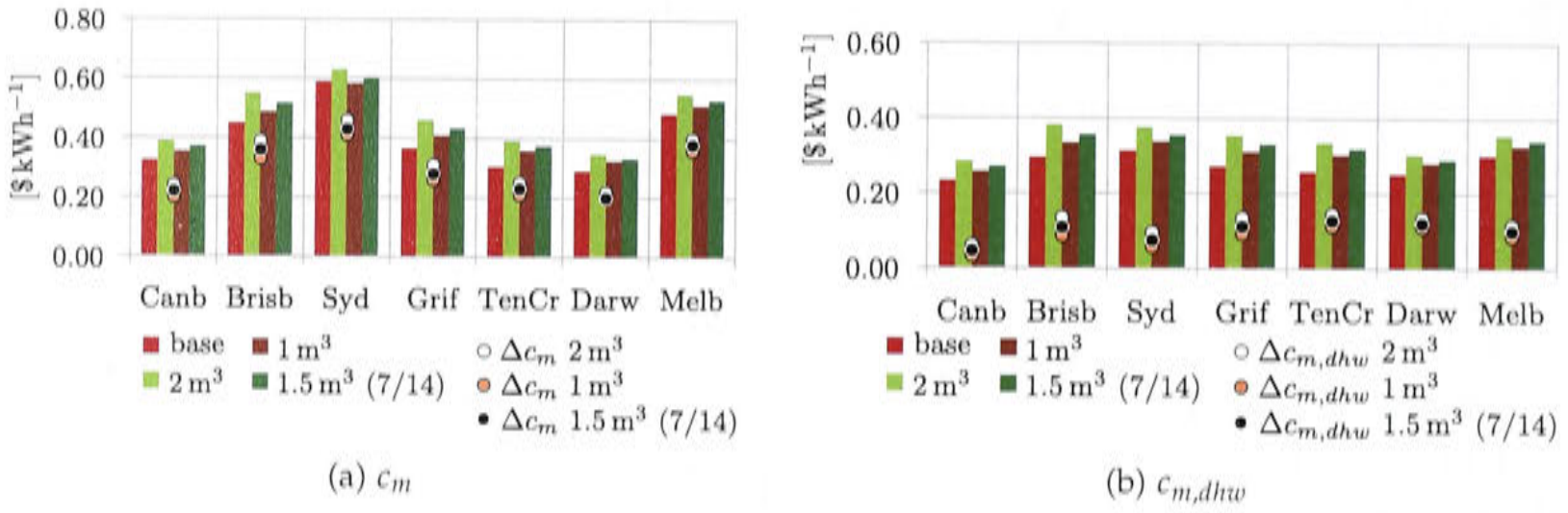

(a) c_m (b) $c_{m,dhw}$

Figure 9.20: Specific cost and cost difference compared to the reference case. $\Delta c_m = c_m - c_{m,ref}$.

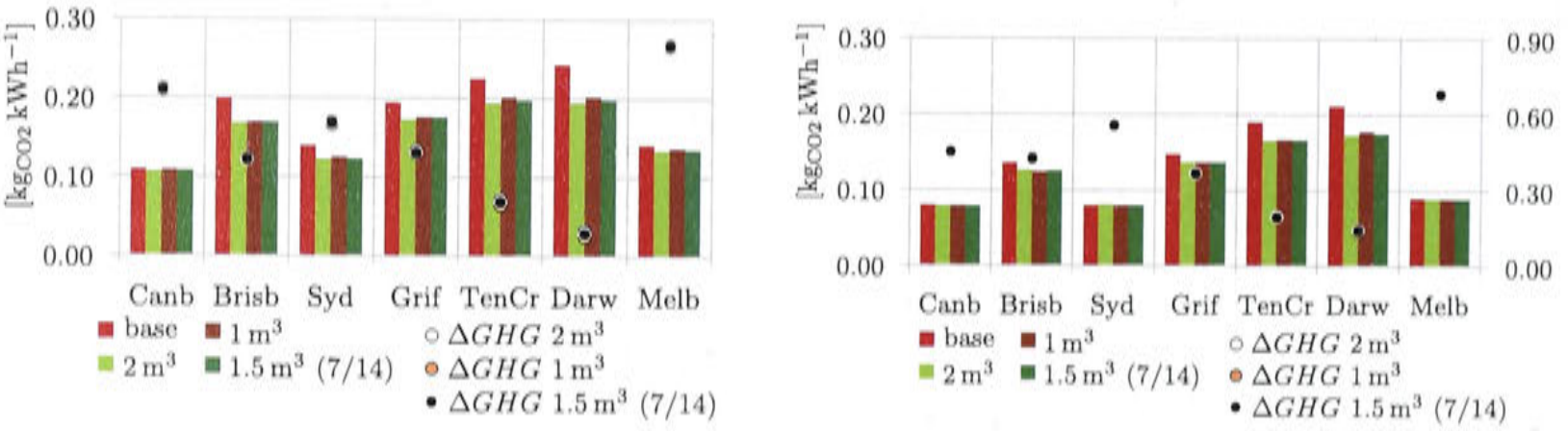

(a) GHG (b) GHG_{dhw}

Figure 9.21: Specific greenhouse gas emission and greenhouse gas savings compared to the reference case $\Delta GHG = GHG_{ref} - GHG$ (on right axis if included).

Cost and greenhouse gas savings are presented in Figure 9.20 and 9.21. Due to the reduced auxiliary gas consumption (and the moderate increase in electricity consumption), the greenhouse gas emissions in the hot climates are smaller than without cold storage tank. Compared to the reference case, greenhouse gas emissions can be saved. The specific cost increase varies between the climates and for the 2 m^3 latent storage the highest cost increase of 28% occurs in Tennant Creek and the lowest in Sydney. In all other climates it is between 20 and 25%.

Variation in $T_{chw,set}$ and $T_{air,out,set}$

The aim of this section is to compare different set point temperatures for the chilled water leaving the chiller and for the air leaving the cooling coils. The set of simulations with varying set point temperatures will only be carried out for the latent

storage tank size of 1.5 m^3 per 11 kW rated chiller capacity. The three different cases are explained in 9.2.1.

The solar fraction between the three different set points does not vary much, with the scenario (7/12, 11/16) performing slightly better in the two humid climates of Brisbane and Darwin. Table 9.12 shows the difference of solar fraction SF_{th} compared to the base case.

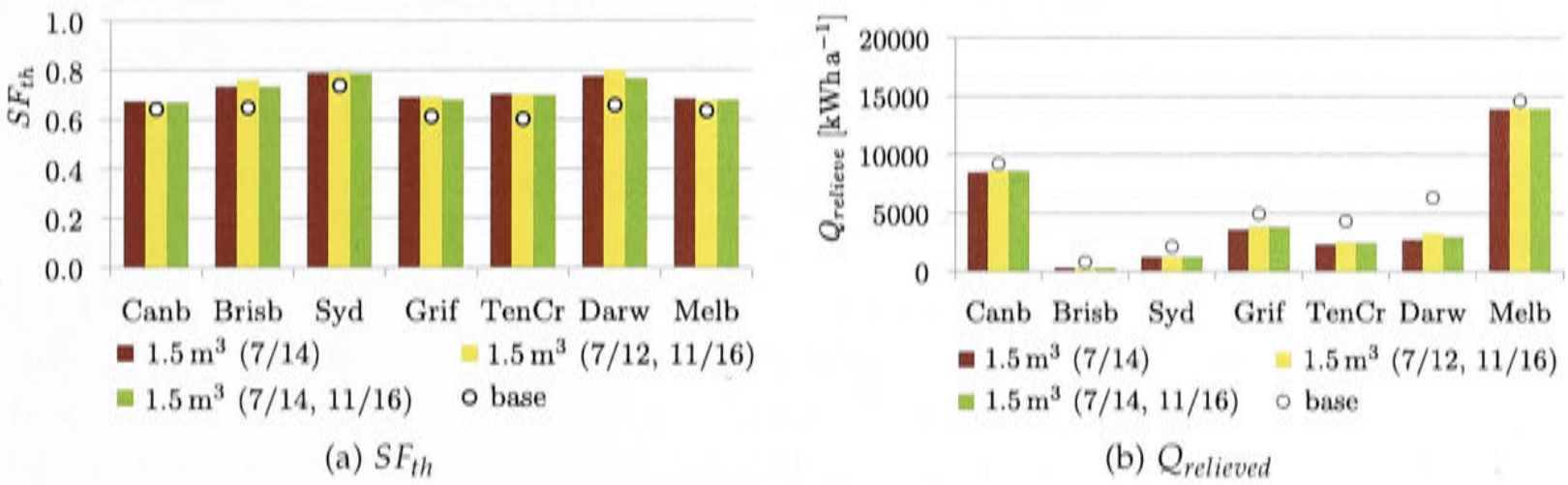

(a) SF_{th} (b) $Q_{relieved}$

Figure 9.22: Solar fraction excluding DHW and relieved heat for different set point temperature combinations.

Table 9.12: Change of solar fraction for the different set point combinations of the latent cold storage model compared to the base case.

	Canb	Brisb	Syd	Grif	TenCr	Darw	Melb
1.5 m^3 (7/14)	3.3%	8.7%	5.2%	7.9%	10.2%	11.8%	5.1%
1.5 m^3 (7/12, 11/16)	3.0%	11.5%	5.9%	8.0%	10.2%	14.4%	4.5%
1.5 m^3 (7/14, 11/16)	3.0%	8.7%	5.1%	7.0%	9.9%	10.9%	4.7%

Figure 9.23 shows that slightly less cooling could be provided in scenario (7/12, 11/16).

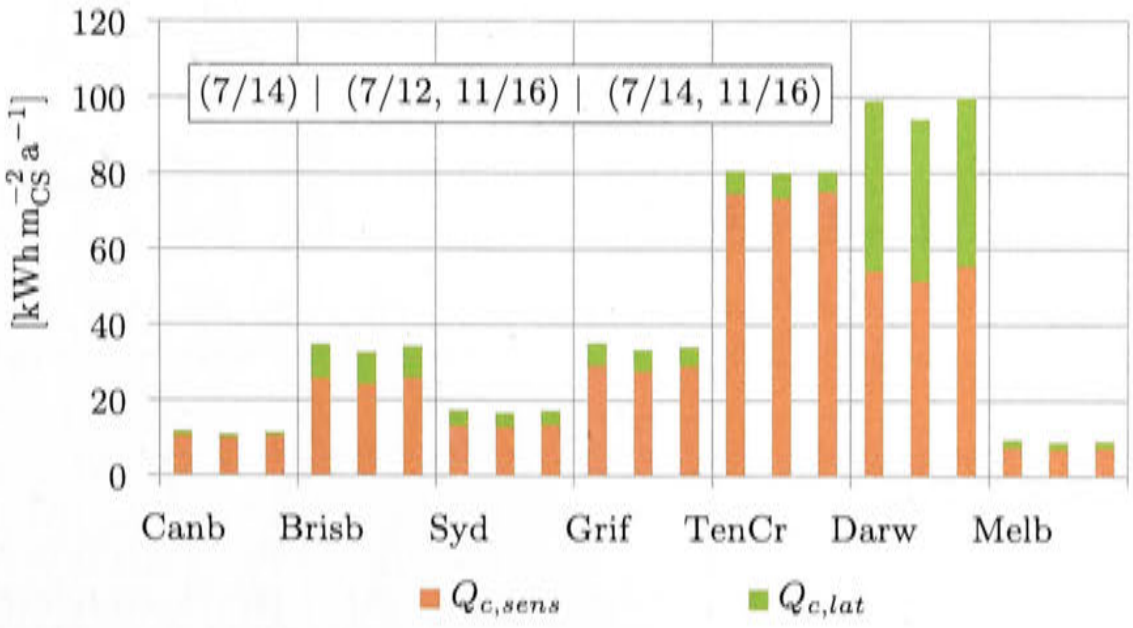

Figure 9.23: Sensible and latent cooling supplied relative to the conditioned space. Columns from left to right represent the set point combinations 1.5 m^3 (7/14), 1.5 m^3 (7/12, 11/16) and 1.5 m^3 (7/14, 11/16).

Table 9.13: Change of cooling and heating supplied compared to the base case (latent CS and variable set points).

		Canb	Brisb	Syd	Grif	TenCr	Darw	Melb
ΔQ_c	1.5 m^3 (7/14)	30%	16%	41%	20%	4%	11%	38%
	1.5 m^3 (7/12, 11/16)	21%	10%	35%	14%	3%	5%	29%
	1.5 m^3 (7/14, 11/16)	25%	15%	40%	17%	4%	12%	33%
ΔQ_h	1.5 m^3 (7/14)	0%	4%	2%	2%	35%	-	0%
	1.5 m^3 (7/12, 11/16)	0%	5%	2%	2%	35%	-	0%
	1.5 m^3 (7/14, 11/16)	0%	5%	2%	2%	42%	-	0%

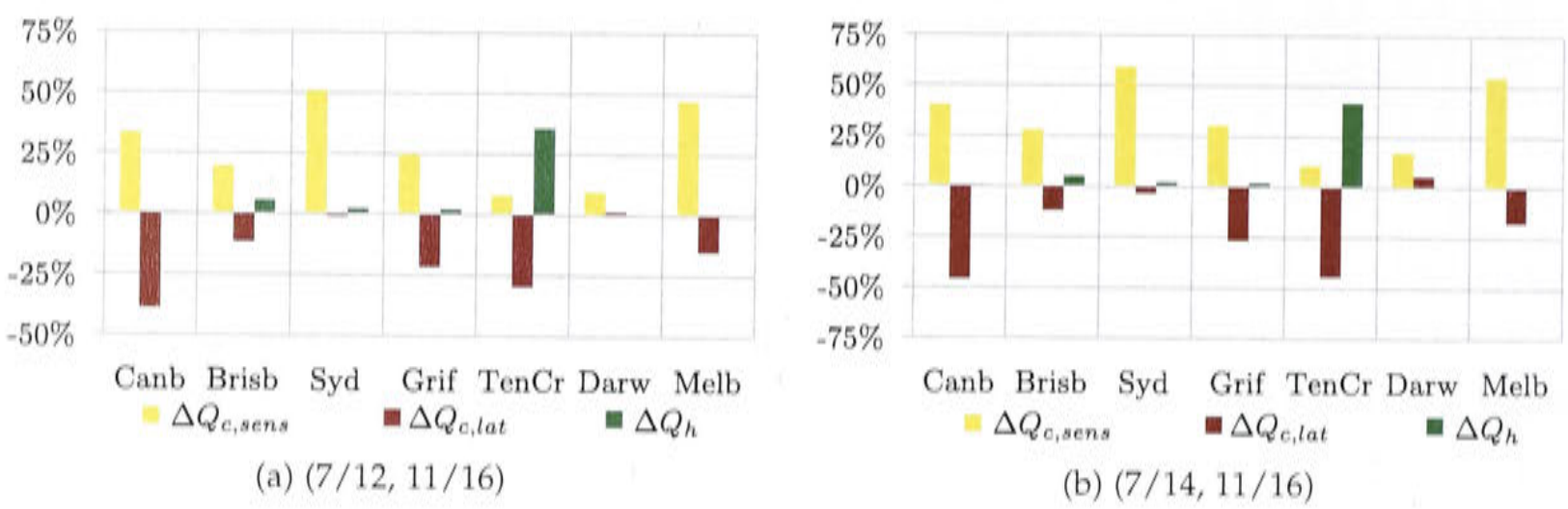

(a) (7/12, 11/16) (b) (7/14, 11/16)

Figure 9.24: Relative change of supplied sensible and latent cooling and heating, corresponding to Table 9.13 (scenario (7/14) is presented in Figure 9.12)

The comfort conditions are shown in Figure 9.25. Here the effects of changing the air outlet set point temperature are most pronounced. The comfort conditions are best met in case (7/14, 11/16), even though slightly less cooling energy was transferred to the rooms compared to case (7/14). The downside of discharging at higher set point temperatures is a increase in electricity consumption for the indoor fans (Table 9.15 and Figure 9.27).

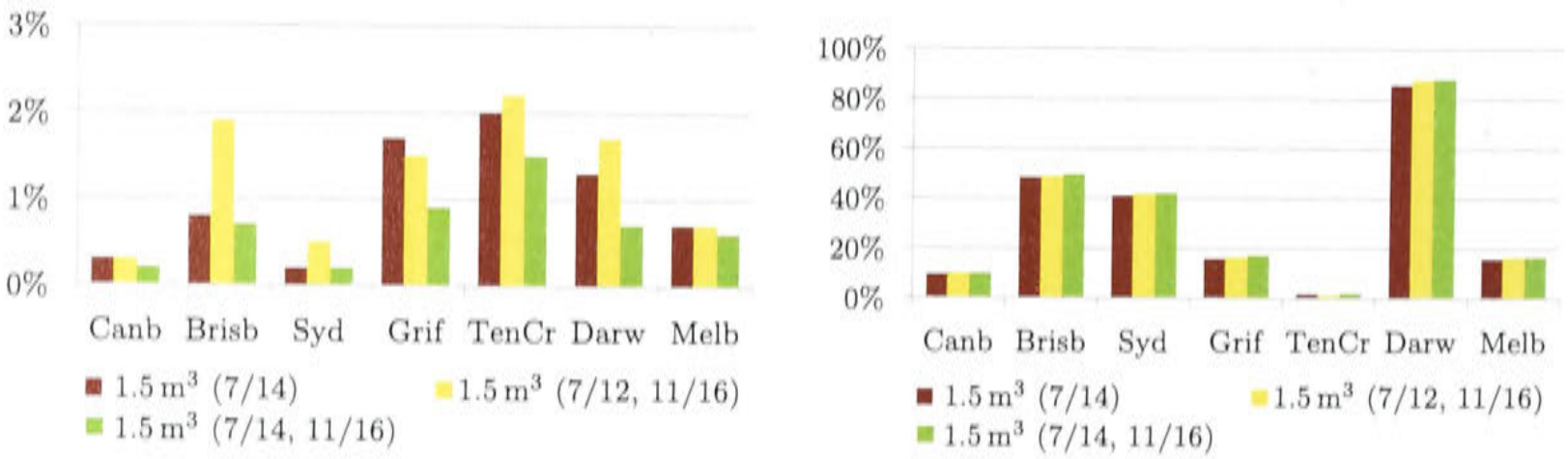

(a) $comf_T$ summer (b) $comf_{RH}$

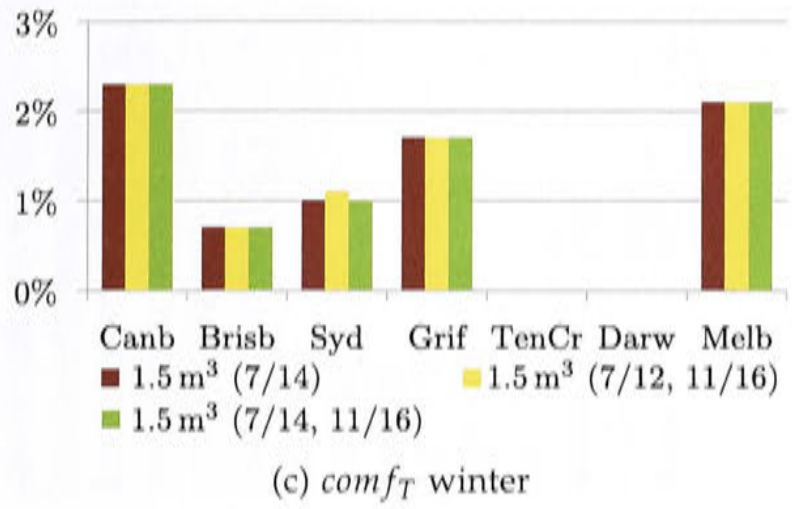

(c) $comf_T$ winter

Figure 9.25: Comfort conditions (latent CS and variable set points)

The details about the latent storage tank's status of charging can be found in the previous section Figure 9.16 and Table 9.9. A significant difference between the modes is only visible for Darwin, Griffith and Tennant Creek, where the frequency curve of varying charging and discharging set points is rather unsteady, compared to the case (7/14). This indicates that the tank is charged and discharged more frequently.

Figure 9.26 and Table 9.14 show how much of the supplied cooling is released from the cold storage tank. There is no significant difference between the set point modes noticeable.

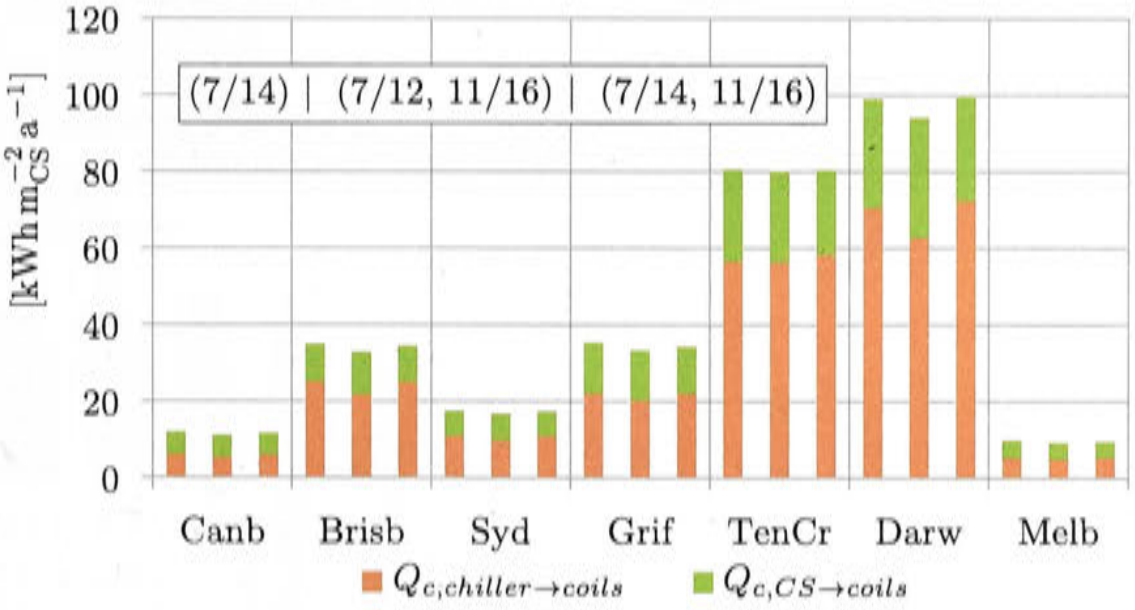

Figure 9.26: Cooling provided via cold storage tank (CS) and directly from the chiller (latent CS and variable set points)

Table 9.14: Percentage of cooling supplied by the cold storage tank (latent CS and variable set points)

	Canb	Brisb	Syd	Grif	TenCr	Darw	Melb
1.5 m³ (7/14)	48%	28%	37%	37%	30%	29%	44%
1.5 m³ (7/12, 11/16)	51%	34%	42%	39%	30%	33%	46%
1.5 m³ (7/14, 11/16)	47%	27%	37%	35%	27%	27%	43%

The cost specific to the amount of cooling and heating (and DHW) produced increases in all climates for all set point options, but least in case (7/14) (Figure 9.28).

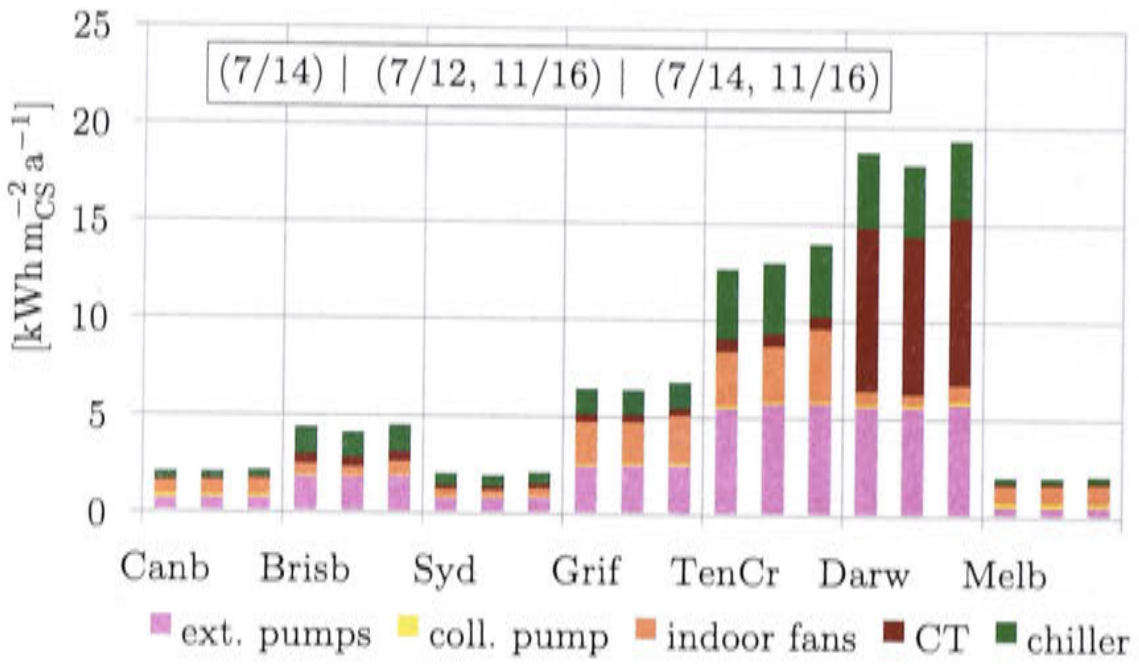

Figure 9.27: Electricity consumption of each individual consumer specific to the conditioned space compared to the base case. From left to right: base, 1.5 m^3 (7/14), 1.5 m^3 (7/12, 11/16), 1.5 m^3 (7/14, 11/16)

Table 9.15: Relative change of electricity consumption ΔE_{el} compared to the base case (latent CS and variable set points)

	Canb	Brisb	Syd	Grif	TenCr	Darw	Melb
1.5 m^3 (7/14)	11%	8%	17%	8%	3%	2%	12%
1.5 m^3 (7/12, 11/16)	12%	2%	13%	7%	6%	-1%	12%
1.5 m^3 (7/14, 11/16)	16%	11%	22%	14%	14%	5%	16%

The specific greenhouse gas emissions drop compared to the base case. However, the drop is insignificant in the colder climates of Canberra and Melbourne (Figure 9.29).

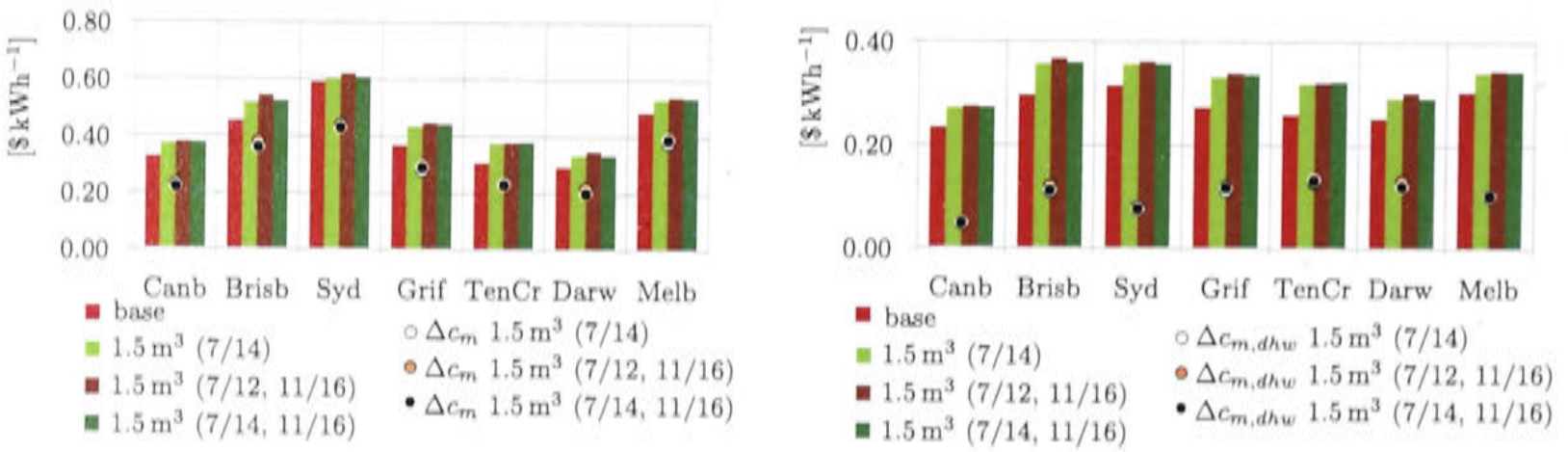

(a) c_m (b) $c_{m,dhw}$

Figure 9.28: Specific cost and cost difference compared to the reference case. $\Delta c_m = c_m - c_{m,ref}$.

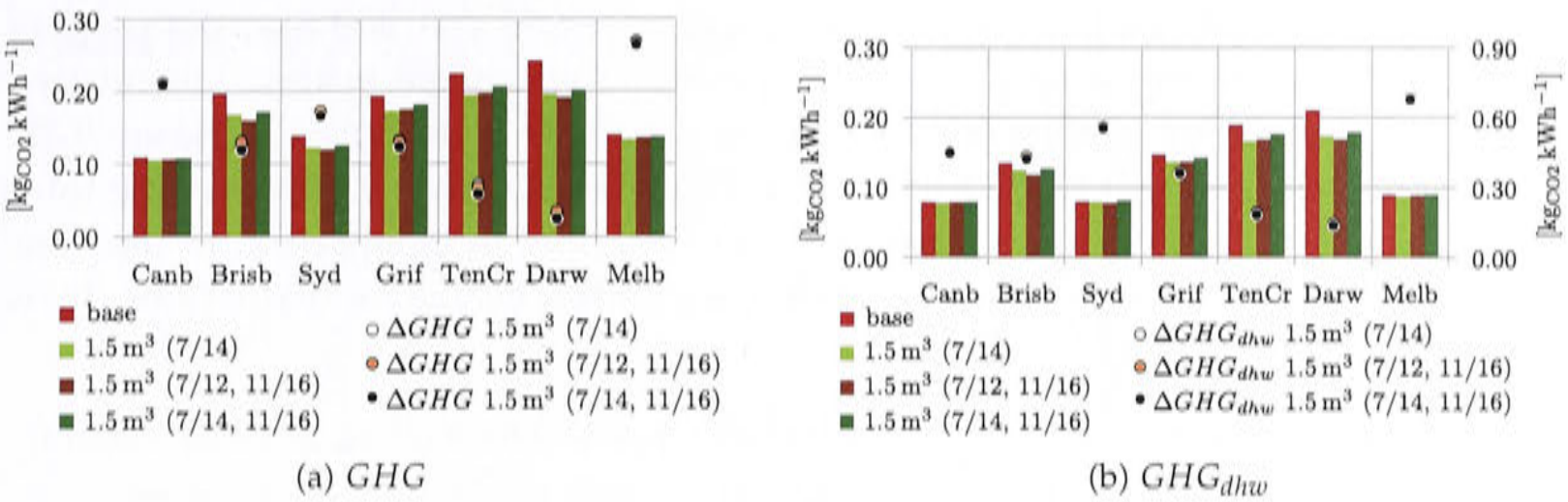

(a) GHG (b) GHG_{dhw}

Figure 9.29: Specific greenhouse gas emission and greenhouse gas savings compared to the reference case $\Delta GHG = GHG_{ref} - GHG$ (on right axis if included).

9.4.2 Latent storage tank and discharging via chilled beams (strategy 2)

The second strategy discharges the latent storage tank using chilled beams at a set point temperature of 18°C. The set point temperatures for the chilled water exiting the chiller ($T_{chw,set}$) and for the air leaving the fan coils ($T_{air,out,set}$) are 7°C and 14°C respectively.

In the following figures the cold storage tank of 1.5 m^3 with chilled beams for discharging (1.5 m^3 CS+beams) will be compared to the base case and to the cold storage tank scenario 1.5 m^3 CS (7/14).

The solar fraction (SF_{th}) in all climates has improved compared to the base case, but does not reach the solar fraction when discharging via fan coils only (Figure 9.30 and Table 9.16). The difference is especially pronounced in the cold climates. Only in Darwin the solar fraction (SF_{th}) is highest when using chilled beams for discharging.

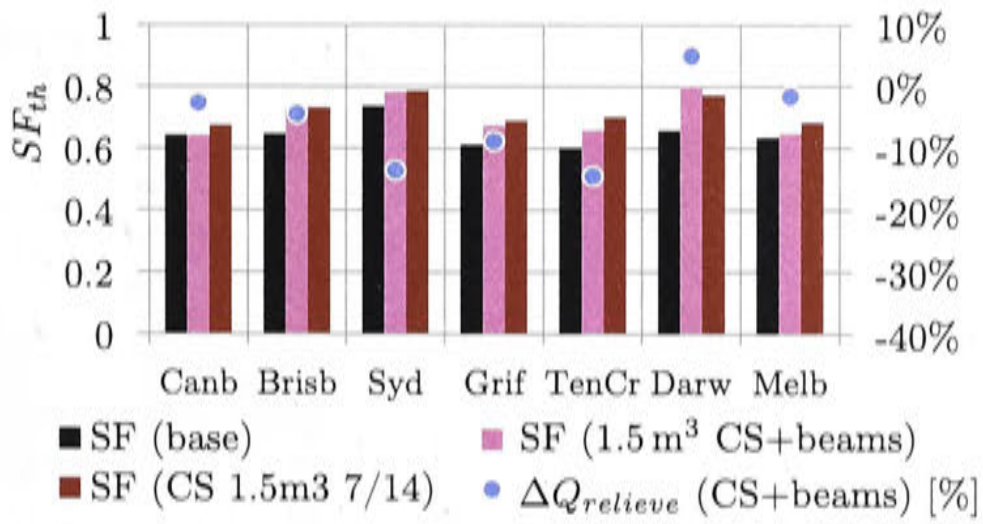

Figure 9.30: Solar fraction (left) and change of relieved heat compared to the base case (right).

Table 9.16: Change of solar fraction compared to the base case (latent CS + beams)

	Canb	Brisb	Syd	Grif	TenCr	Darw	Melb
1.5 m^3 CS+beams	0.2%	8.2%	4.9%	6.5%	5.9%	14.5%	1.5%
1.5 m^3 CS (7/14)	3.3%	8.7%	5.2%	7.9%	10.2%	11.8%	5.1%

The cooling and heating supplied is shown in Figure 9.31 and also the proportion of the total cooling supply, which is transferred via chilled beams. The relative changes of transferred cooling and heating via coils only is displayed in Figure 9.32. The latent cooling is reduced, which had to be expected. Table 9.17 shows the total change of cooling and heating supplied to the building in comparison to the base case. The cooling increase is much smaller using chilled beams for discharging, than discharging the tank via fan coils.

Table 9.17: Relative change in total cooling and heating supplied to the building (latent CS + beams)

		Canb	Brisb	Syd	Grif	TenCr	Darw	Melb
ΔQ_c	1.5 m^3 CS+beams	11.6%	4.0%	17.8%	3.5%	0.4%	-8.7%	12.4%
	1.5 m^3 CS (7/14)	30.1%	16.5%	41.0%	19.8%	3.9%	11.0%	37.6%
ΔQ_h	1.5 m^3 CS+beams	3.2%	2.7%	1.2%	4.3%	-18.4%	-	4.1%
	1.5 m^3 CS (7/14)	0.4%	4.0%	1.6%	1.8%	34.8%	-	0.4%

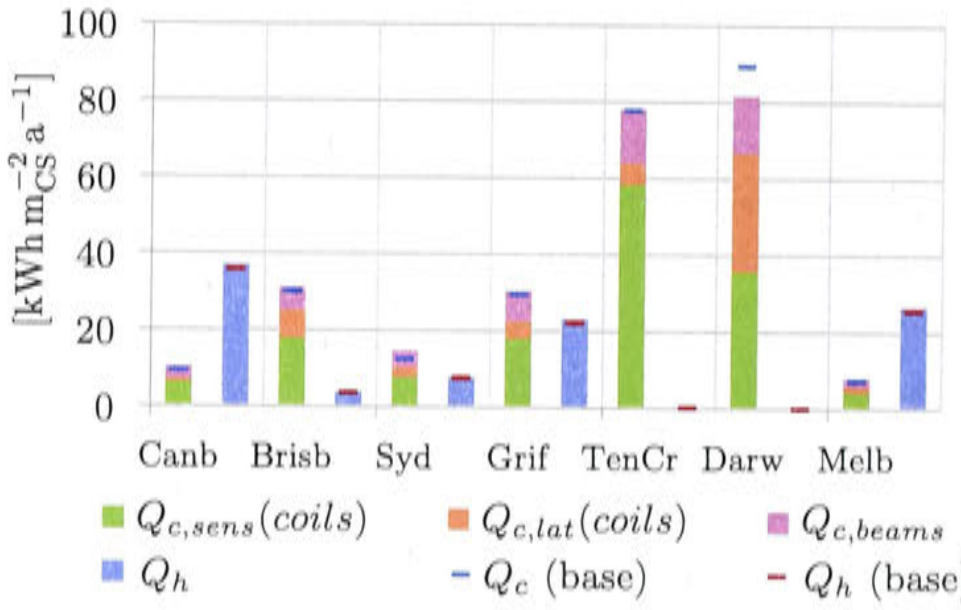

Figure 9.31: Specific cooling and heating energy supplied by cooling and heating coils and chilled beams. Comparison to base case.

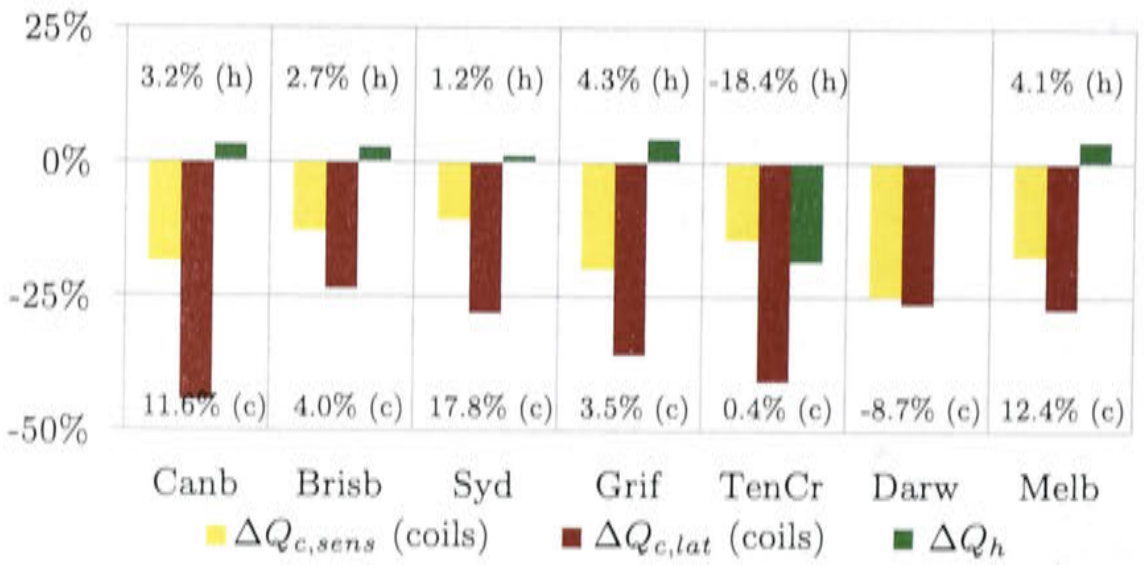

Figure 9.32: Relative change of sensible and latent cooling, and heating supplied by the fan coils.

The proportion of supplied cooling which is released from the cold storage tank is visible in Figure 9.33 and Table 9.18. Discharging the tank via chilled beams seems

to make less use of the latent storage medium.

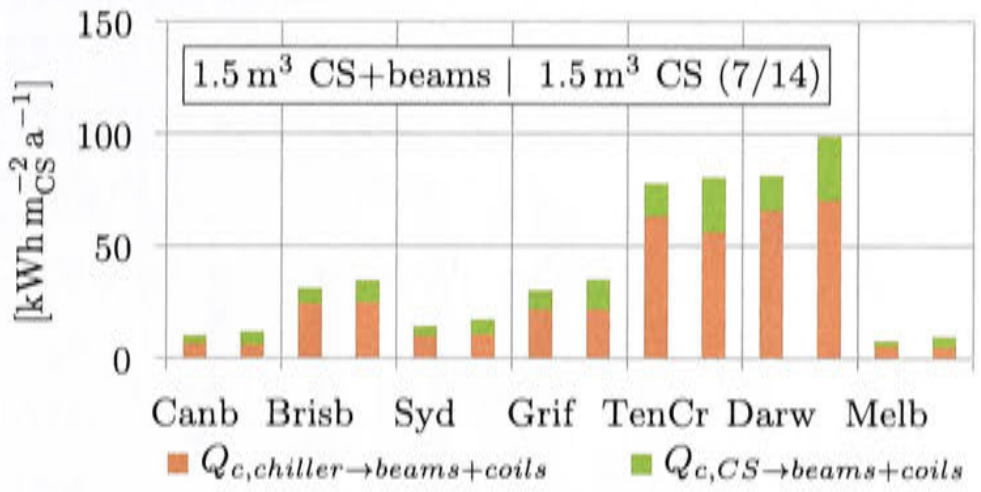

Figure 9.33: Cooling provided via cold storage tank and directly from the chiller (latent CS + beams)

Table 9.18: Percentage of cooling supplied by the cold storage tank

	Canb	Brisb	Syd	Grif	TenCr	Darw	Melb
1.5 m³ CS+beams	46.1%	25.7%	42.1%	37.3%	22.9%	23.4%	42.3%
1.5 m³ CS (7/14)	47.8%	27.7%	36.8%	37.4%	29.8%	28.7%	43.9%

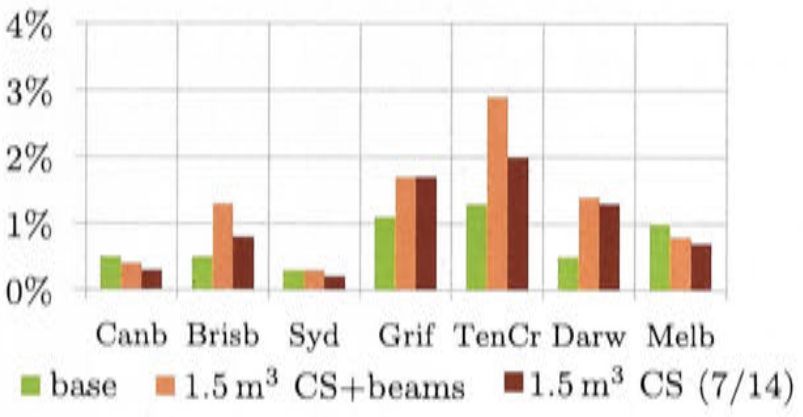

(a) $comf_T$ summer

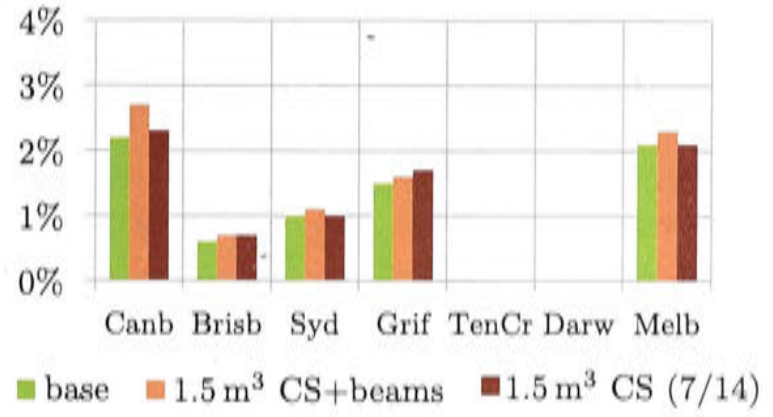

(b) $comf_T$ winter

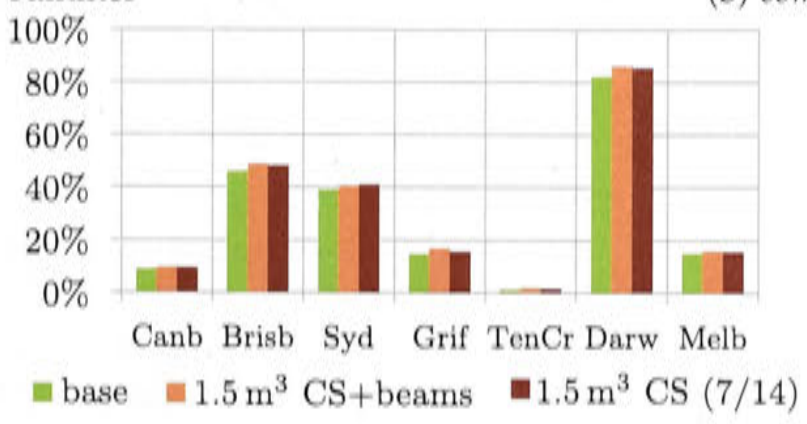

(c) $comf_{RH}$

Figure 9.34: Comfort conditions including chilled beams in the cold storage tank model

The effects on the comfort conditions are visible in Figure 9.34. The temperature comfort decreases even though in all climates, besides Darwin, the cooling input is increased. The effect is due to the different heat transfer characteristic of chilled beams as opposed to fan coils and was visible already in section 8.2.9.

The average air mass flow rates in Figure 9.35 increase but the operating hours of the fans vary only +/-30%. This is a large difference compared to figure 9.13, and it

shows the effect that discharging mode 2 is now accomplished by the chilled beams instead of the fan coils which formerly generated the cooling effect at minimum air flow.

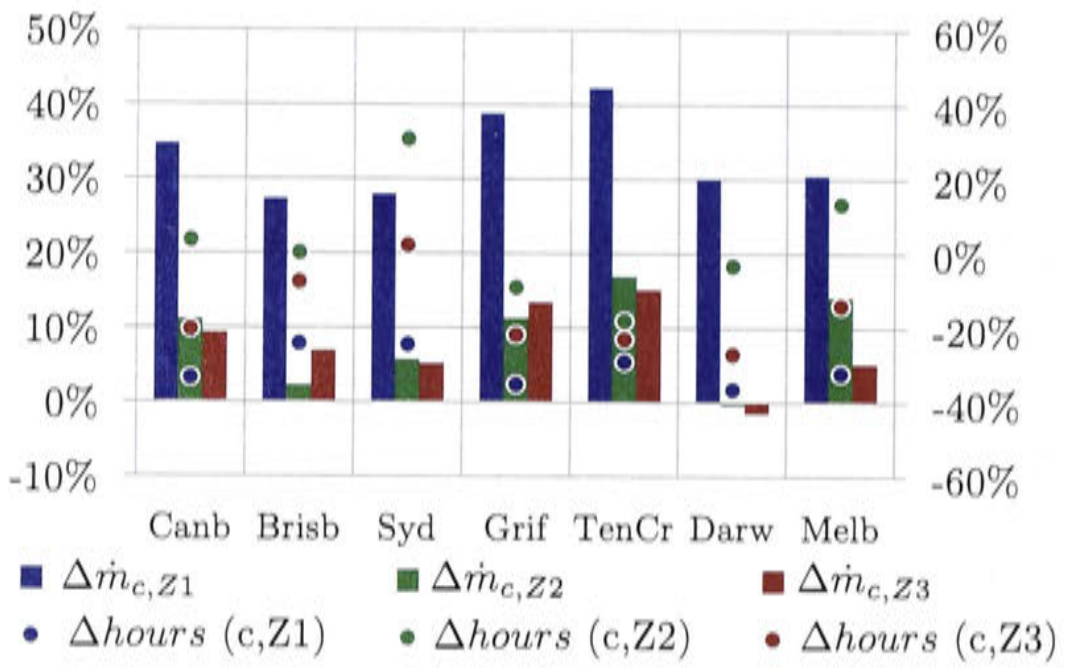

Figure 9.35: Average air flow (left) and fan operating hours (right) (latent CS + beams)

The frequency distribution of the latent storage tank's status of charging can be seen in Figure 9.36. Since discharging occurs always via chilled beams and the control strategy of discharging mode 1 essentially separates the chilled water circuits, it is not possible any longer that at low loads during discharging mode 1 the cold storage tank's inlet temperature could become lower than the cold storage medium temperature. Previously, it was possible that in such circumstances the mixed flow of load return and chiller supply could charge the tank in discharging mode 1. Hence, the liquid fraction could reach values smaller than 0.1 (Figure 9.16).

Table 9.19 shows the percentage of time the storage tank is depleted ($liqfrac = 1$) during the summer months. In all climates, besides Sydney, this occurs less often than when discharging using fan coils. Table 9.20 contains the percentage of time when there is a cooling demand, but the tank is empty and the auxiliary heater has to provide the heat to satisfy the cooling demand.

Table 9.19: Percentage of time during the summer months (September – April) when the latent storage tank is empty ($liqfrac = 1$)

	Canb	Brisb	Syd	Grif	TenCr	Darw	Melb
1.5 m^3 CS+beams	30%	45%	33%	22%	55%	44%	32%
1.5 m^3 CS (7/14)	55.4%	71.1%	72.3%	39.5%	50.8%	66.6%	68.4%

The electricity consumption specific to the conditioned space, for the case "CS+beams" can be seen in Figure 9.37. In all climates but in Darwin the electricity consumption increases. Darwin is the only climate on the other hand with a decrease in supplied cooling. The total change of electricity consumed compared to the base case is displayed in Table 9.21. The fan power consumption of the case CS+beams increases compared to the base case, because 14°C instead of 12°C is the air set point

Table 9.20: Percentage of time a cooling demand occurs but the cold storage tank is depleted and the auxiliary heater has to provide the heat demand for the absorption chiller

	Canb	Brisb	Syd	Grif	TenCr	Darw	Melb
1.5 m³ CS+beams	3.9%	25.0%	10.7%	15.7%	37.0%	22.4%	6.9%
1.5 m³ CS (7/14)	2.1%	15.3%	6.9%	7.5%	19.9%	18.0%	3.0%

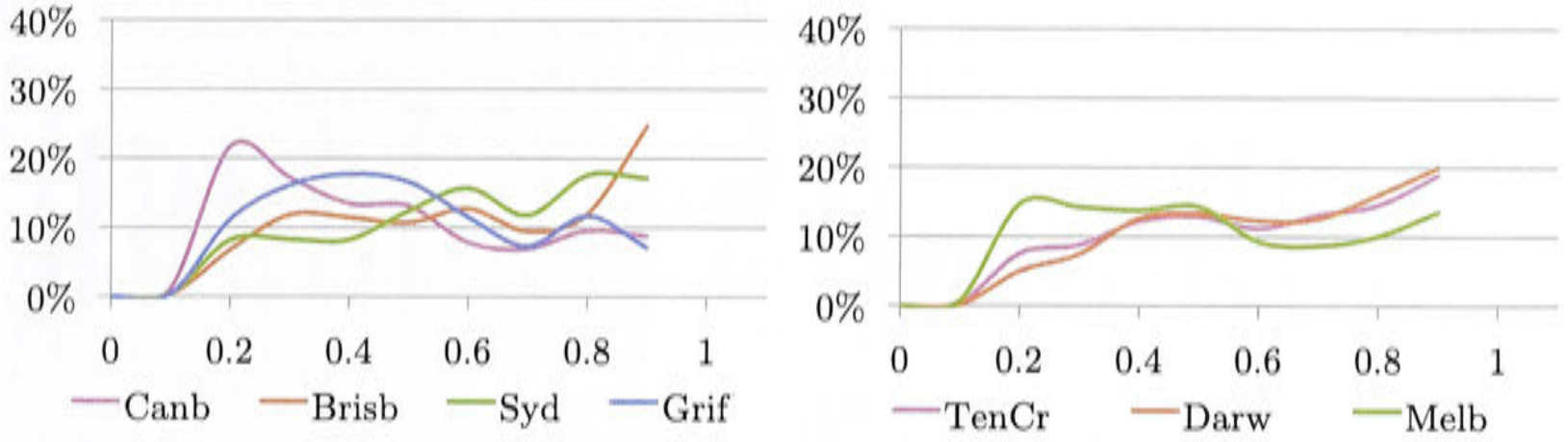

Figure 9.36: Percentage of time the cold storage tank is not empty and charged to a certain degree. The liquid fraction *liqfrac* is on the x-axis

temperature, in order to compare it to the case 1.5 m³ CS (7/14). Surprisingly, the indoor fan power consumption with chilled beams increases. This is unexpected and is linked most likely to the increase in average flow rate of the fans. Appendix F.2 shows in detail the change of electricity consumption compared to the base case of each electricity consumer. The change of the chiller's power consumption is directly proportional to the hours of chiller operation.

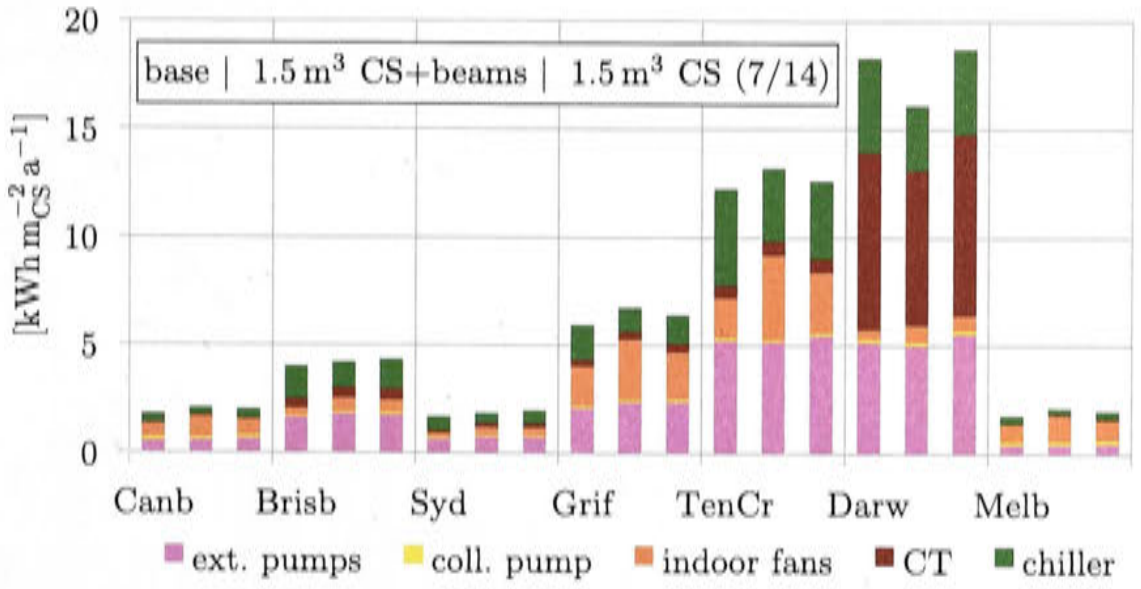

Figure 9.37: Electricity consumption of each individual consumer specific to the conditioned space compared to the base case (latent CS + beams)

The fraction of energy imbalance around the hot water system and around the chilled water circuit compared to the cold storage tank without chilled beams can be found in Figure 9.40. The fraction of imbalance around the hot water tank becomes smaller, but the energy imbalance around the chilled water circuit, especially for the humid and hot climates, increases. This may be linked to the reduction in supplied cooling, however, it stays below 5%, which is acceptable.

Table 9.21: Relative change of electricity consumption ΔE_{el} compared to the base case

	Canb	Brisb	Syd	Grif	TenCr	Darw	Melb
1.5 m^3 CS+beams	14.3%	4.5%	10.1%	13.5%	7.8%	-11.9%	19.7%
1.5 m^3 CS (7/14)	11.4%	8.2%	16.8%	7.8%	3.1%	2.2%	11.7%

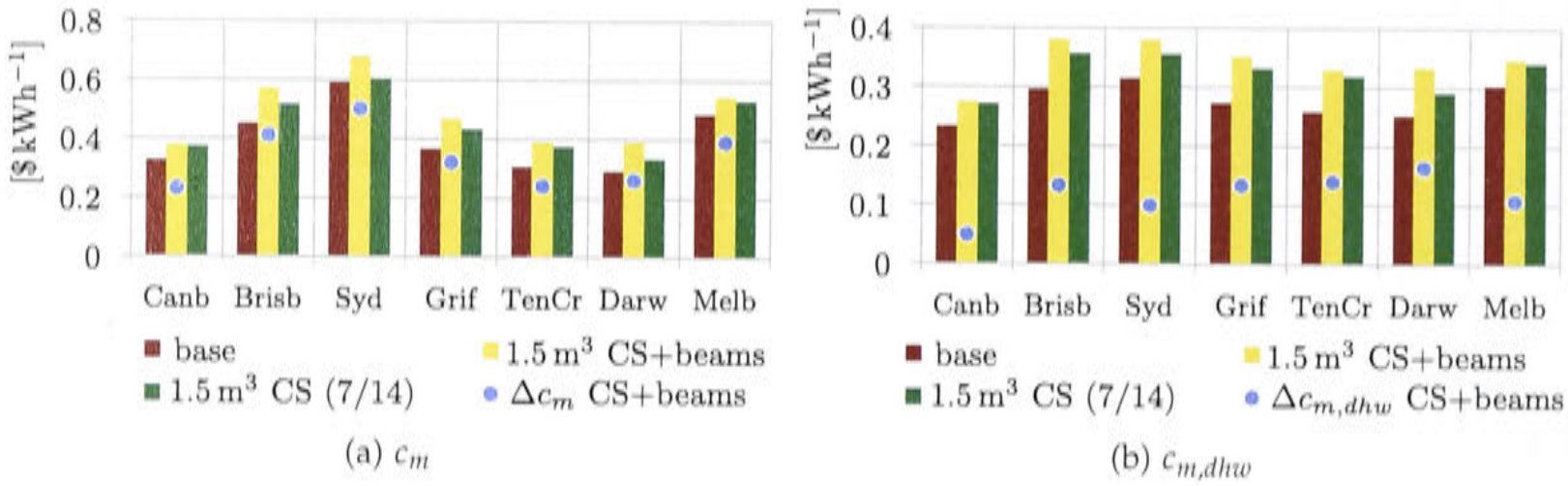

(a) c_m (b) $c_{m,dhw}$

Figure 9.38: Specific cost and cost difference compared to the reference case. $\Delta c_m = c_m - c_{m,ref}$.

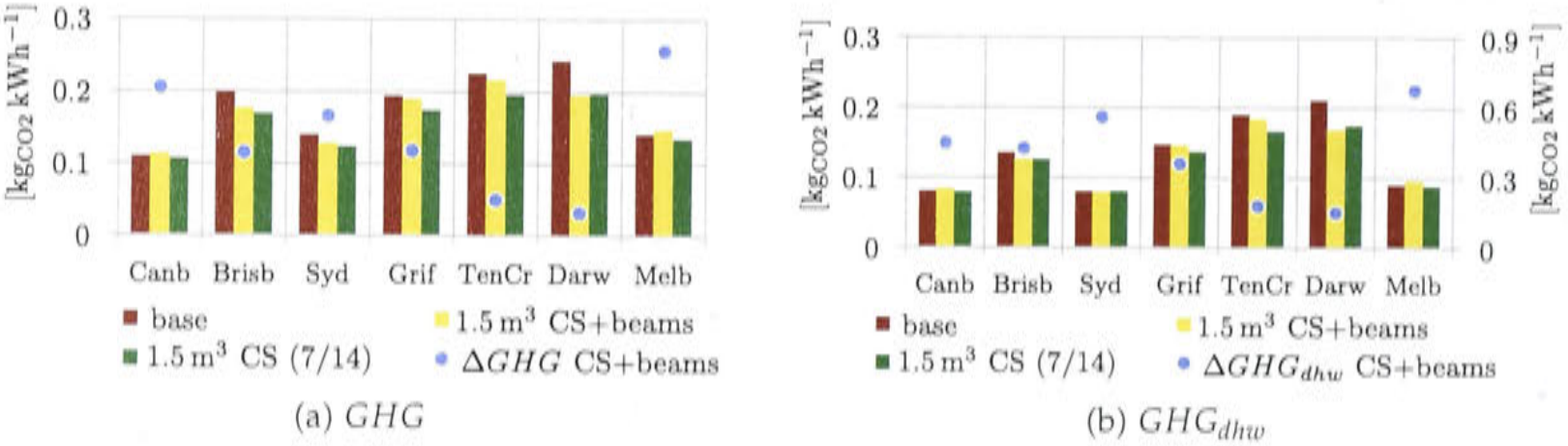

(a) GHG (b) GHG_{dhw}

Figure 9.39: Specific greenhouse gas emission and greenhouse gas savings compared to the reference case $\Delta GHG = GHG_{ref} - GHG$ (on right axis if included)

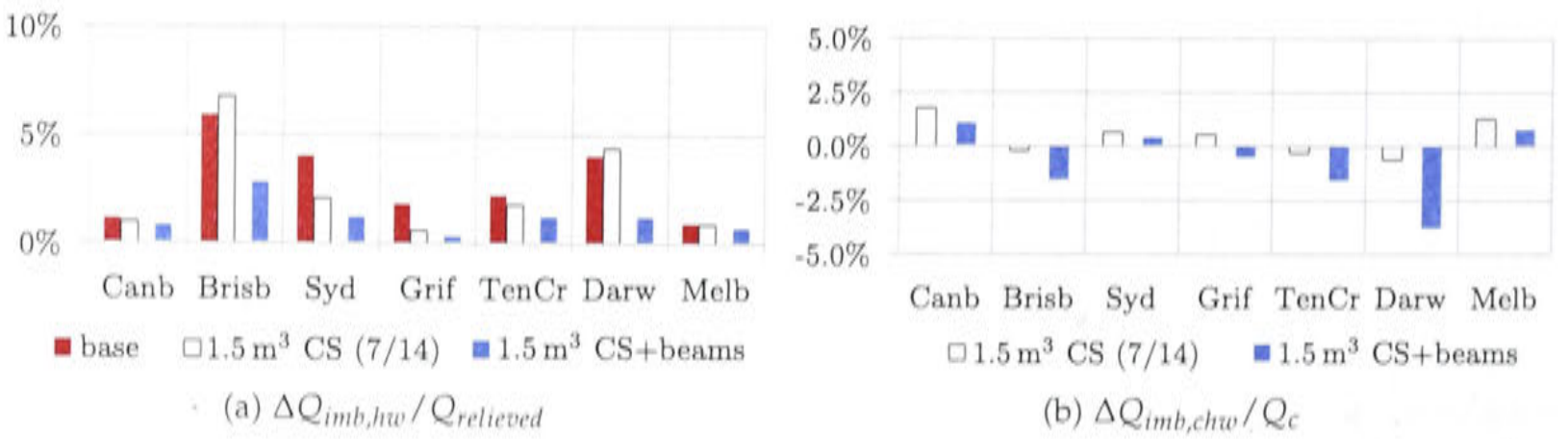

(a) $\Delta Q_{imb,hw}/Q_{relieved}$ (b) $\Delta Q_{imb,chw}/Q_c$

Figure 9.40: Energy imbalances around the hot water tank expressed as a fraction of the relieved heat and energy imbalance around the chilled water circuit expressed as a fraction of the total supplied cooling to the building

The specific greenhouse gas emissions and costs are shown in Figure 9.39 and 9.38. The specific costs are the highest compared to base case and the scenario 1.5 m^3 CS (7/14) using fan coil units. In all climates besides Darwin, Canberra and Melbourne the greenhouse gas emissions are lower than base case but higher than scenario 1.5 m^3 CS (7/14). In Darwin the greenhouse gas emissions are lowest of the three scenarios, but less cooling is provided. In the two coldest climates of Canberra and Melbourne the specific greenhouse gas emissions are slightly higher than the base case and the latent storage scenario with fan coil units instead of chilled beams.

9.4.3 Chilled water tank (strategy 3)

In this section the simulation results of the 2 m^3 chilled water tank are compared to the 1.5 m^3 PCM latent storage tank scenario CS (7/14) and to the base case without a cold storage tank.

The chilled water tanks for each climate are scaled using the *scalefactor* and equation 9.56.

$$V_{t,scaled} = 2\,\mathrm{m}^3 \cdot scalefactor \tag{9.56}$$

The solar fractions excluding DHW are displayed for each climate in Figure 9.41 and Table 9.22. The latent storage performs better than the chilled water tank in terms of solar fraction. However, the chilled water tank has a lower cooling capacity.

Table 9.22: Change of solar fraction compared to the base case (chilled water tank).

	Canb	Brisb	Syd	Grif	TenCr	Darw	Melb
2 m^3 chwtank	2.7%	8.3%	4.1%	7.2%	8.3%	7.8%	4.0%
1.5 m^3 CS (7/14)	3.3%	8.7%	5.2%	7.9%	10.2%	11.8%	5.1%

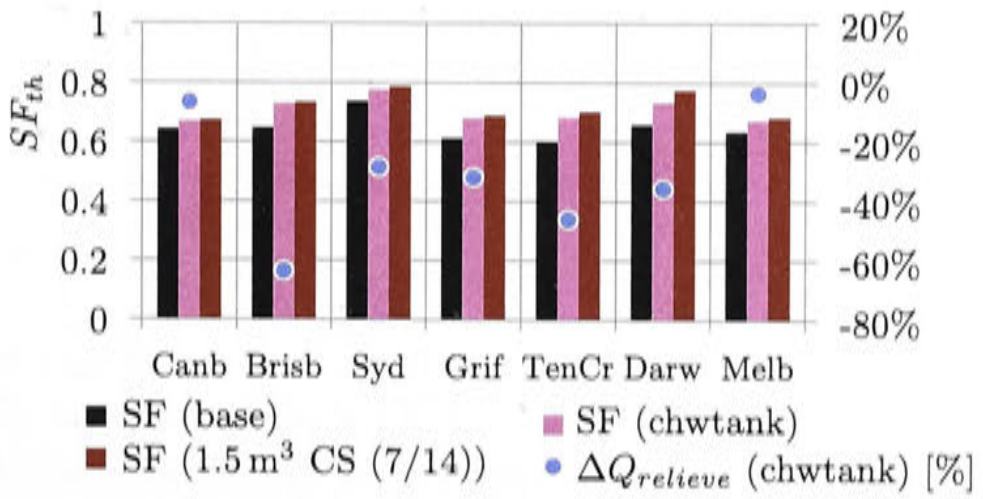

Figure 9.41: Solar fraction (left) and relieved heat comparing the chilled water tank to the latent storage and the base case.

The change of supplied cooling and heating can be seen in Figure 9.42. The increase of supplied cooling compared to the base case is in the range of 2/3 to 3/4

of the cooling increase of the latent storage tank.

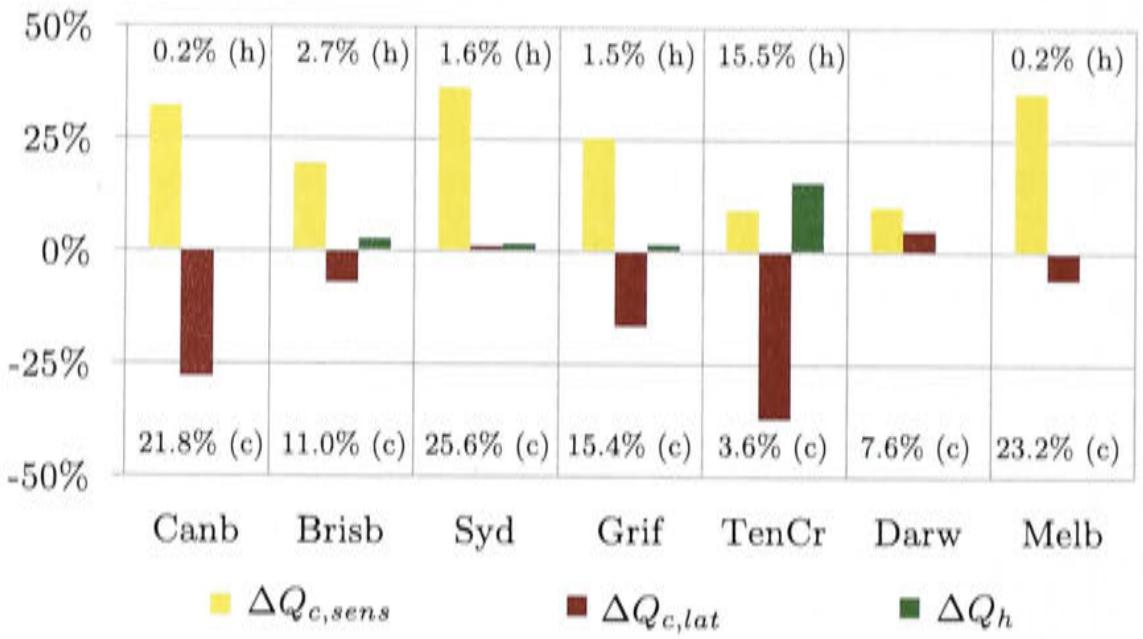

Figure 9.42: Relative change of supplied sensible and latent cooling, and heating compared to the base case.

The effect on the comfort conditions can be seen in Figure 9.43. Only in Griffith and Darwin the chilled water tank seems to provide more comfort than the latent storage tank. In Canberra and Tennant Creek the comfort is slightly worse compared to the latent storage, and in the other three climates (Brisbane, Sydney and Melbourne) no change is visible.

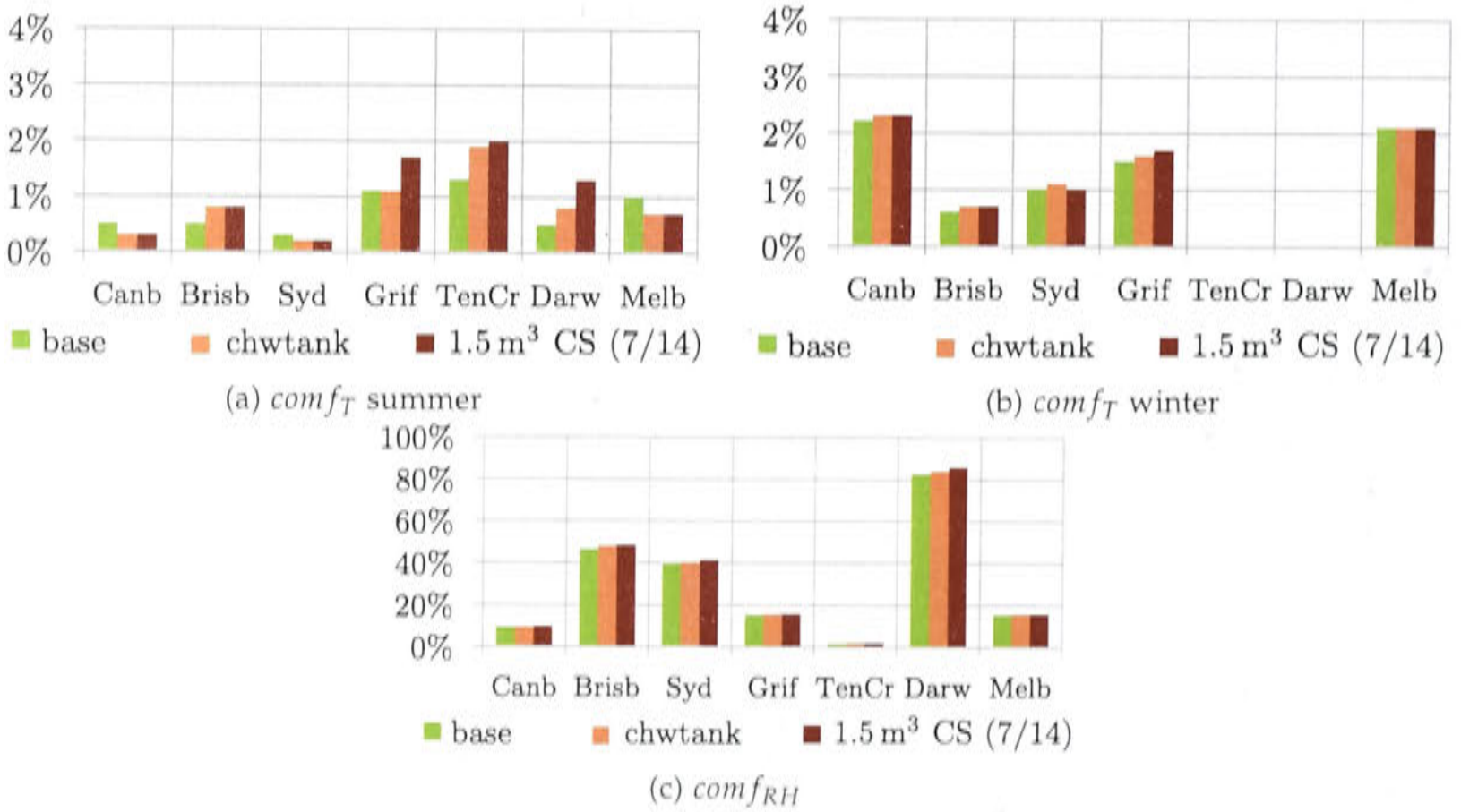

Figure 9.43: Comfort conditions comparing the base case to the chilled water and latent storage tanks.

The amount of cooling, which is supplied to the air-conditioning system from the chilled water tank, is shown in Table 9.44 and in Table 9.23. The chilled water tank supplies less cooling to the system than the latent storage tank. A larger tank having a higher storage capacity might provide more cooling to the system.

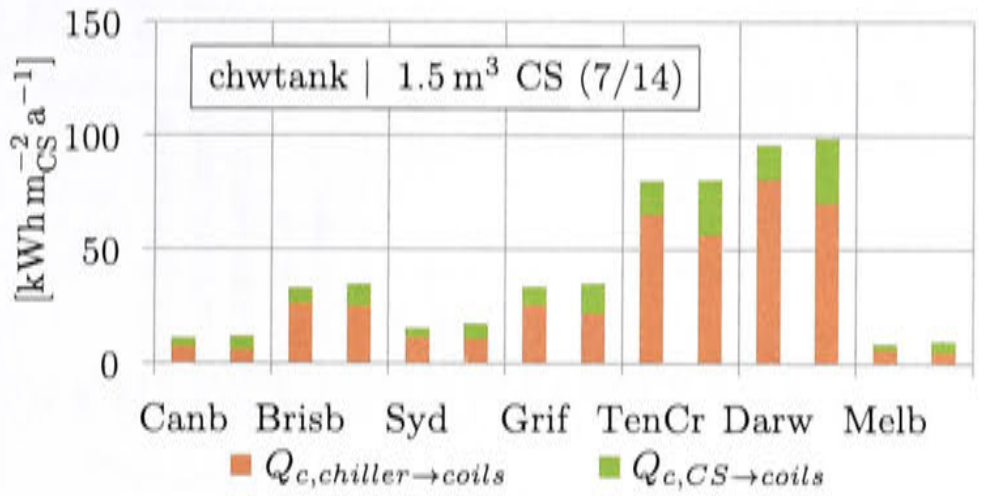

Figure 9.44: Cooling provided via cold storage tank (CS) and directly from chiller. Comparing latent to chilled water storage.

Table 9.23: Percentage of cooling supplied by the cold storage tank (chilled water tank compared to latent storage tank).

	Canb	Brisb	Syd	Grif	TenCr	Darw	Melb
2 m^3 chwtank	31.6%	19.7%	26.2%	24.2%	18.3%	15.7%	29.1%
1.5 m^3 CS (7/14)	47.8%	27.7%	36.8%	37.4%	29.8%	28.7%	43.9%

Comparing the indoor fan operating hours and the average mass flow rates for cooling in Figure 9.45 to the latent storage tank in figure 9.13, it becomes obvious that the average mass flow of air does not decrease as significantly and the indoor fan operating hours increase less, relative to the base case. This leads to the conclusion that discharging mode 2 is less often in effect.

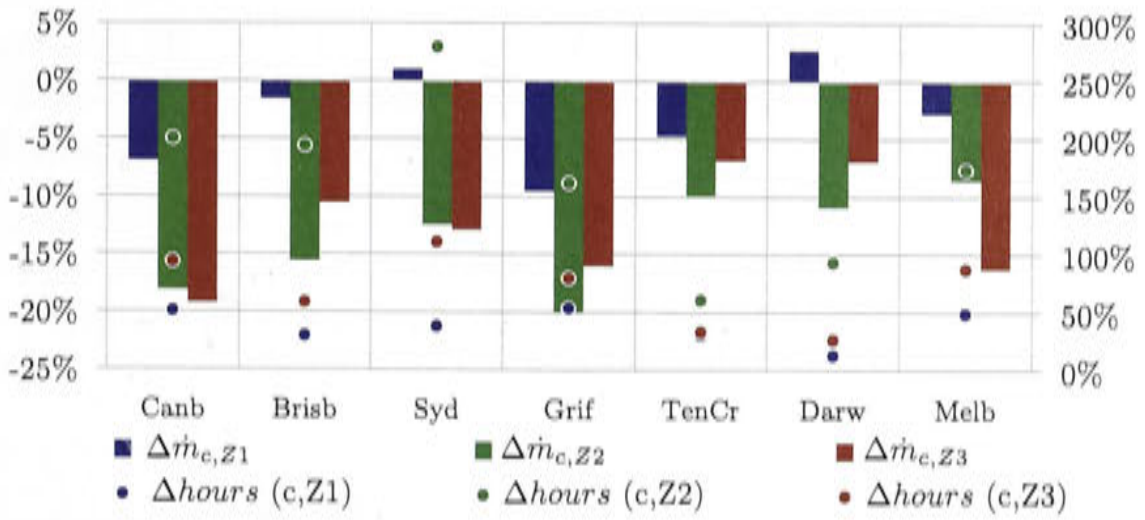

Figure 9.45: Average air flow (left) and fan operating hours (right) (chilled water tank)

The specific electricity consumption is compared in Figure 9.46 and the difference in electricity consumption compared to the base case is shown in Table 9.24.

In all climates besides Brisbane and Sydney the electricity consumption specific to the conditioned space is noticeably higher using a chilled water tank instead of a latent storage tank. When comparing the relative change in power consumption by each consumer compared to the base case (Table F.2), it can be seen that the external pumps use less electricity in the scenario with a chilled water tank, however, the chiller is operating longer hours.

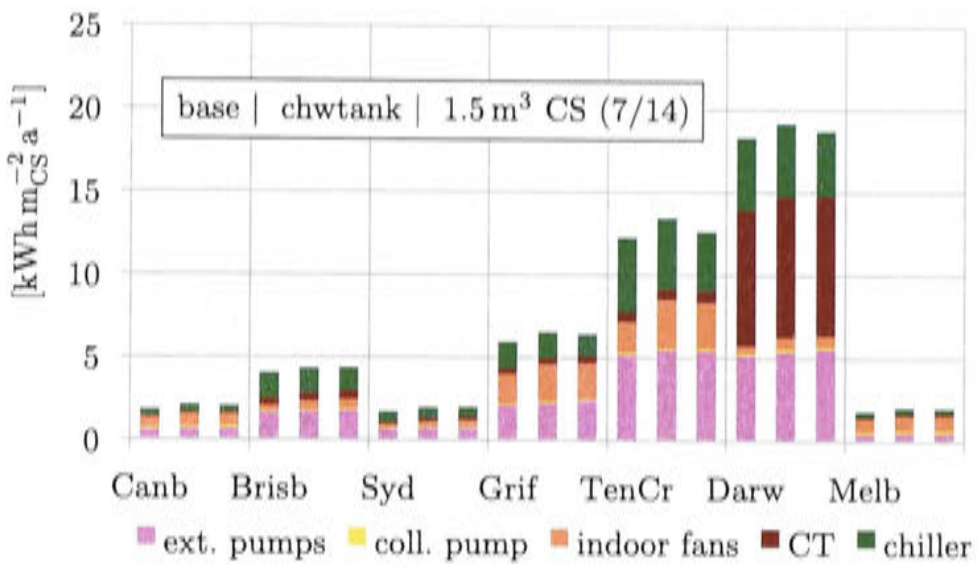

Figure 9.46: Electricity consumption of each individual consumer specific to the conditioned space compared to the base case (latent and chilled water CS). Total increase in Table 9.24

Table 9.24: Relative change of electricity consumption ΔE_{el} compared to the base case

	Canb	Brisb	Syd	Grif	TenCr	Darw	Melb
2 m³ chwtank	15.0%	7.3%	14.2%	9.9%	9.7%	4.7%	12.0%
1.5 m³ CS (7/14)	11.4%	8.2%	16.8%	7.8%	3.1%	2.2%	11.7%

Furthermore, in all climates, besides Darwin, the cooling tower seems to work less aggressively with the chilled water storage option, using less electricity. This can be explained by the capacity of the latent storage tank being more than double the size of the chilled water tank. The return chilled water temperature to the chiller might be relatively low more often than when charging the latent storage tank.

Figure 9.47 shows for each climate the distribution of charging stages during the months September to April, when the cold storage tank is not empty. Table 9.26 shows the proportion of time there is a cooling demand, but the tank is depleted and the auxiliary heater provides the heat to satisfy the cooling demand. Table 9.25 shows the percentage of time in the summer months the tank is empty, hence, the outlet temperature is 13°C. In all climates besides Tennant Creek and Darwin, the tank is fully charged between 15% and 30% of the time. In Tennant Creek and Darwin less than 13% of the time.

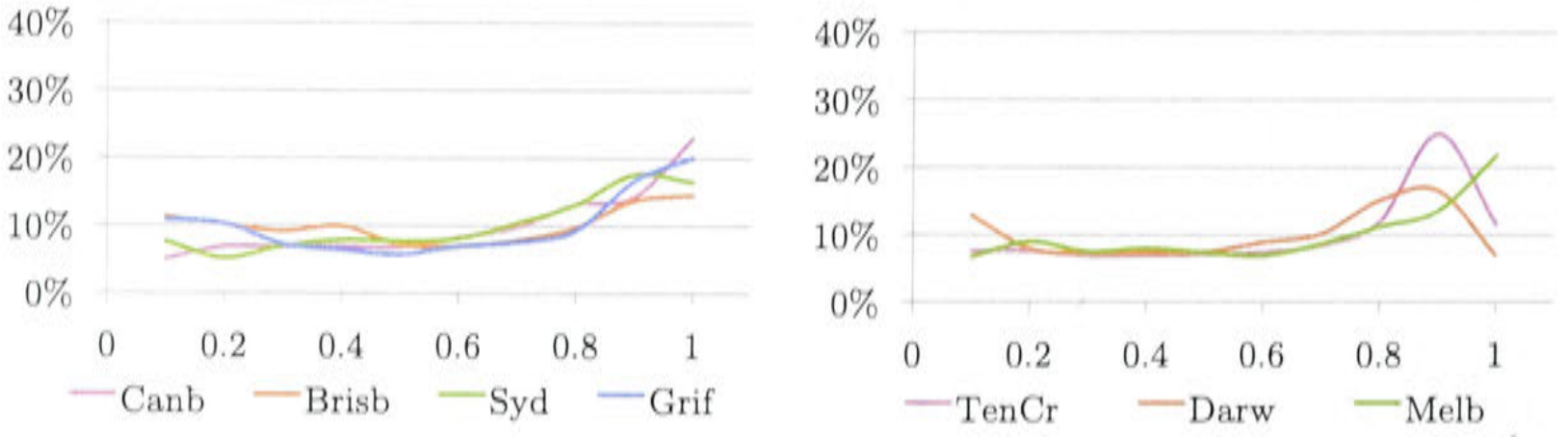

Figure 9.47: Percentage of time the chilled water tank is not empty and charged to a certain degree. 1 represents fully charged. $x = (13\,°\text{C} - T_{CS})/(13\,°\text{C} - 7\,°\text{C})$

Table 9.25: Percentage of summer time (September – April) the chilled water tank is empty

	Canb	Brisb	Syd	Grif	TenCr	Darw	Melb
2 m³ chwtank	59.1%	67.0%	72.8%	46.0%	48.2%	62.1%	71.3%
1.5 m³ CS (7/14)	55.4%	71.1%	72.3%	39.5%	50.8%	66.6%	68.4%

Table 9.26: Percentage of time a cooling demand occurs but the cold storage tank is depleted and the auxiliary heater has to provide the heat demand for the absorption chiller (chilled water tank)

	Canb	Brisb	Syd	Grif	TenCr	Darw	Melb
2 m³ chwtank	2.4%	17.2%	7.8%	9.5%	22.7%	23.1%	3.8%
1.5 m³ CS (7/14)	2.1%	15.3%	6.9%	7.5%	19.9%	18.0%	3.0%

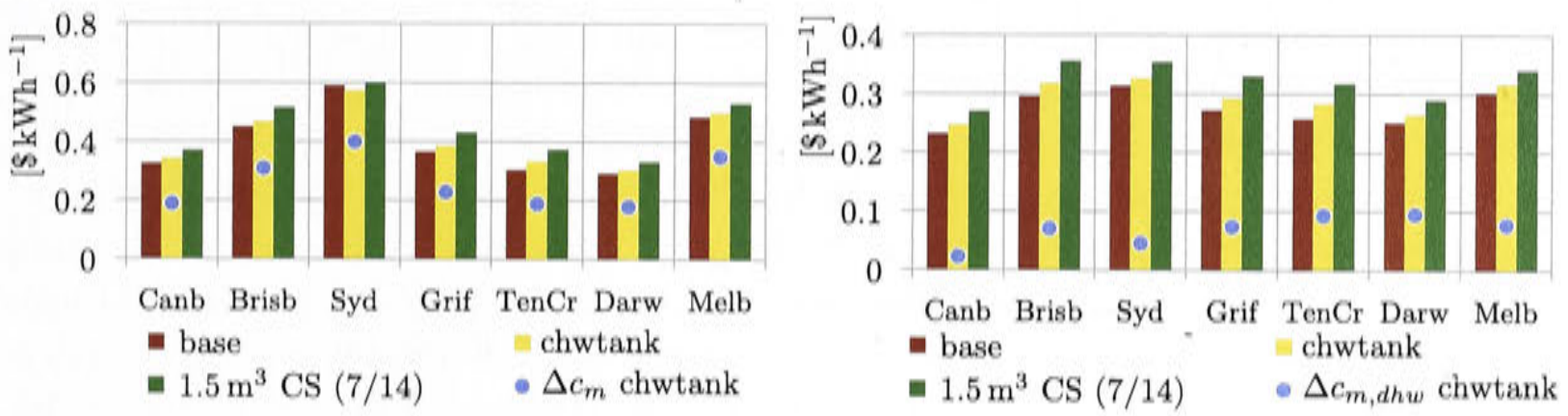

(a) c_m (b) $c_{m,dhw}$

Figure 9.48: Specific cost and cost difference compared to the reference case. $\Delta c_m = c_m - c_{m,ref}$.

The fraction of energy imbalances for the hot water tank and around the chilled water circuit are included in section 9.4.1.

In terms of greenhouse gas emissions and cost the results of the chilled water tank scenario are located in between the latent cold storage tank and base case without cold storage.

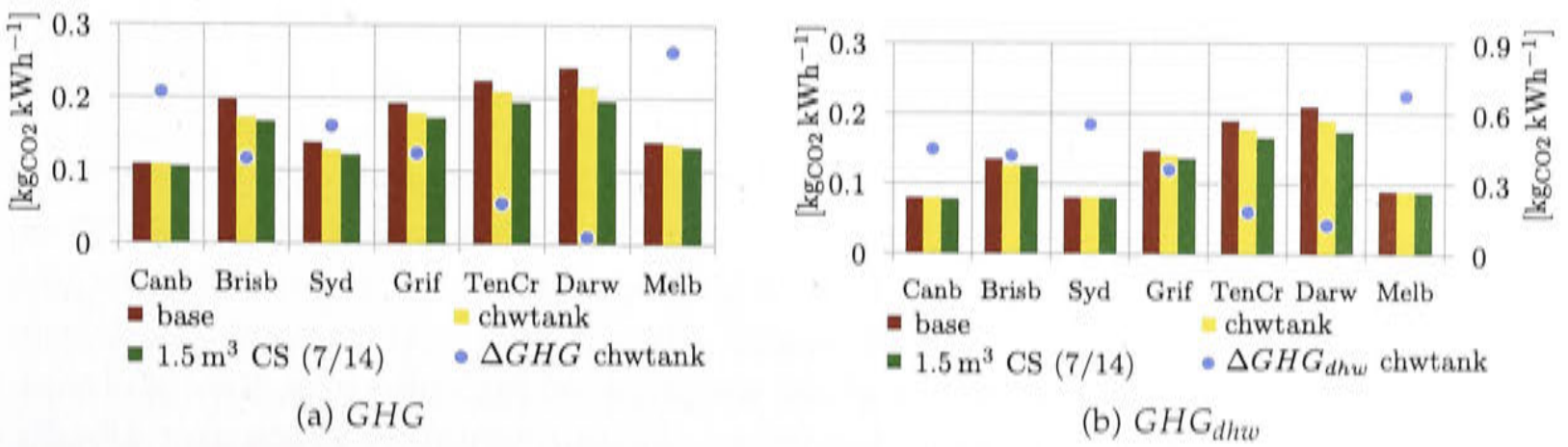

(a) GHG (b) GHG_{dhw}

Figure 9.49: Specific greenhouse gas emission and greenhouse gas savings compared to the reference case $\Delta GHG = GHG_{ref} - GHG$ (on right axis if included).

9.5 Direct coupling of the chiller and collector

The TRNSYS residential solar thermal models introduced in the last chapters were designed with a hot water storage tank, which is common practice. The hot water tank acts as a buffer between the chiller's heat demand and the solar supply. In this section a simplified steady state model is presented, connecting the chiller's generator directly to the collectors without the inclusion of a hot water buffer tank. The duration of the simulation is only two days and the effect of heat accumulation in the system is investigated. The motivation for this analysis originated from the idea to omit the hot water tank in order to save capital cost in large scale systems [S.O.L.I.D., 2014]. This section does not follow the same approach as all previous simulations, however, it shows the difficulty in omitting the hot water tank and was included for this purpose.

A VBA macro of a solar collector array coupled to the generator of an absorption chiller using a three way valve was developed to carry out a short sensitivity analysis on the feasibility of the absence of a hot water buffer tank. Figure 9.50 shows a schematic representation of the components. No tank heat losses are assumed and the ambient temperature is a constant 28°C. Only the heat transfer into the generator is modeled and not the entire absorption chiller.

The collector array area A_{coll} should be sized to design solar radiation conditions using equation 9.57. The parameters used in this equation are the cooling capacity of the chiller ($Q_{E,rated}$) and its coefficient of performance (COP_{rated}) at rated conditions. Collector efficiency ($\eta_{coll,design}$) and solar irradiation ($G_{tot,coll,design}$) are chosen at design conditions. If the maximum radiation is chosen as the design condition, the array is protected from overheating and stagnation. An alternative method is to install heat relief devices in the collector circuit. Systems sized to the maximum radiation usually cover the base cooling load and don't aim at covering full load at all times. They are meant to use all available solar heat but not follow the load [S.O.L.I.D., 2014]. This serves a key purpose: The solar collectors are generating useful heat most of the time and from a cost perspective it is better to oversize the chiller relative to the collector array than not use the expensive collectors.

$$A_{coll} = \frac{\dot{Q}_{E,rated}}{COP_{rated} \cdot \dot{G}_{tot,coll,design} \cdot \eta_{coll,design}} \tag{9.57}$$

One summer day from Singapore radiation data was chosen to obtain radiation data (Appendix F.1). The data was concatenated for two days and contains the global (total) radiation on the horizontal. For simplicity reasons it was assumed to be the total radiation normal to the collector's area. In reality the direct solar radiation normal to the collector is a function of the tilt angle of the collectors, the incidence angle of the sun, and the direct radiation on the horizontal. Diffuse and albedo radiation also have to be converted to the tilted collector area and are added to the direct radiation normal to the collector. However, this assumption is tolerable, keeping in mind that Singapore is close to the equator and solar collectors are to be

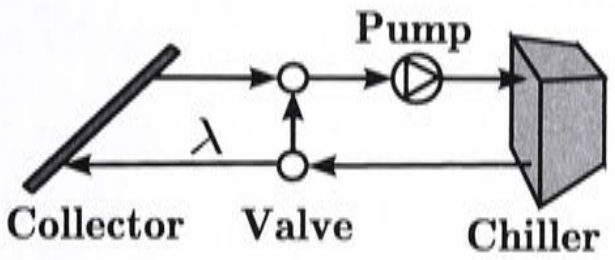

Figure 9.50: Direct coupling collector and tank

installed nearly flat on the ground for a high solar yield.

The collector efficiency curve seen in equation 9.58 from the HT collectors of the Austrian manufacturer Oekotech Solarkollektoren [2013] was chosen for the collector design. The design collector efficiency $\eta_{coll,design}$ was calculated with a design collector average temperature of $T_{coll,avg,design} = 80\,°C$ and an ambient temperature of $T_{amb} = 28\,°C$. Two thirds of the maximum radiation $\dot{G}_{tot,coll,max}$ is used for sizing the collector array.

As equation 9.58 uses the collector average temperature instead of the inlet temperature in order to calculate the collector efficiency, the collector average temperature and the collector outlet temperature, were calculated in an iterative way. A more accurate approach using transients would have been to include the thermal mass of the collector and solve a differential equation when calculating the collector outlet temperature. This approach is explained in detail in Eicker [2014, p. 245-247].

$$\eta_{coll} = 0.776 - 2.887\frac{(T_{coll,avg} - T_{amb})}{\dot{G}_{tot,coll}} - 0.006\frac{(T_{coll,avg} - T_{amb})^2}{\dot{G}_{tot,coll}} \tag{9.58}$$

Only the generator of the chiller was simulated using the properties in Table 9.27. The heat transfer within the chiller's generator $\dot{Q}_{hw}$ was calculated using the heat exchanger effectiveness method in equation 9.59. This equation is usually used for condensers or evaporators where one of the fluids is undergoing a phase change. The equation indicates that heat transfer strongly depends on the generator temperature T_G. In a real generator, the heat exchanger coils are immersed (at least partly) in a solution of refrigerant and absorbent. The mass (and energy) is increased by a solution rich in refrigerant coming from the absorber and it is decreased by a weak solution of low refrigerant concentration leaving the generator. The amount of refrigerant which can evaporate to the condenser is a function of the solution concentration and the generator temperature, hence, its vapor pressure. The vapor pressure for the refrigerant (here water) increases the richer the solution is (the more refrigerant it contains). The process is well explained in Eicker [2014, p. 304-342]. The more heat is added to the generator, the higher the generator temperature becomes and the more vapor is driven from the solution. Nevertheless, in this approach the temperature of the generator has been fixed at 65°C.

$$\dot{Q}_{hw} = (1 - e^{-NTU})\ \dot{m}_{hw}\ c_{p,hw}\ (T_{hw,in} - T_G) \tag{9.59}$$
$$NTU = \frac{UA_G}{c_{p,hw}\ \dot{m}_{hw}}$$

Table 9.27: Modeling assumptions (direct coupling)

Variable	Value	Unit	Source
$\dot{Q}_{E,rated}$	250	kW	scaled [ASHRAE, 2013, p. 2.18]
COP_{th}	0.7	-	
$\dot{m}_{hw,rated}$	8.7	$kg\,s^{-1}$	scaled [ASHRAE, 2013, p. 2.18]
T_G	65	°C	constant (assumption)
UA_G	17	$kW\,K^{-1}$	scaled [ASHRAE, 2013, p. 2.18]
$\dot{G}_{tot,coll,max}$	800	$W\,m^{-2}$	National University of Singapore (NUS) [2014]
A_{coll}	863	m^2	equation 9.57

In the model, two main parameters were varied. The valve position λ and the pump speed resulting in a variable collector water flow ($\dot{m}_{hw}$).

The valve position λ is used to adjust for a $\Delta T_{coll} = 20\,°C$ for the collector and it determines how much water flow $\dot{m}_{hw}$ is sent to the mixing valve through the collectors. The equation used to determine λ is shown below (equation 9.60). Since η_{coll} is calculated within the collector, depending on the average temperature, the efficiency of the previous time step is used. The time step is 1 hour.

$$\lambda = \min\left(0.2, \frac{\dot{G}_{tot,coll} \cdot \eta_{coll} \cdot A_{coll}}{c_p \cdot \Delta T_{coll}} / \dot{m}_{hw}\right) \tag{9.60}$$

Changing the pump speed varies the flow rate through the generator and the collectors, when a valve position is fixed. The speed is adjusted proportional to the radiation levels using equation 9.61, but a minimum flow rate of 30% of $\dot{m}_{hw,rated}$ is set for model stability reasons. The flow rate cannot exceed $\dot{m}_{hw,rated}$.

$$\dot{m}_{hw} = \dot{m}_{hw,rated} \cdot \min\left(0.3, \underbrace{\frac{COP_{th}}{\dot{Q}_{E,rated}}}_{1/\dot{Q}_{hw,rated}} \cdot \underbrace{\eta_{coll} \cdot \dot{G}_{tot,coll} \cdot A_{coll}}_{\dot{Q}_{hw}}\right) \tag{9.61}$$

The following cases will be compared:

- λ fixed and $\dot{m}_{hw}$ variable
- λ variable and $\dot{m}_{hw}$ fix at rated conditions
- λ variable and $\dot{m}_{hw}$ variable

There are three values which are used to evaluate the output of the two day simulation.

There's the ratio of the heat input to the generator (Q_{hw}) to the solar heat harvested through the collectors (Q_{sol}) ($\frac{Q_{hw}}{Q_{sol}}$). This ratio denotes how much of the collector's heat could actually be transferred into the chiller's generator and how much remaining heat accumulates in the water stream. It is in all cases 73%, but depends on the fixed generator temperature. It would be useful to harvest that accumulated energy below the generator's temperature when no cooling is required, for example to generate domestic hot water.

The second parameter is the percentage of time the collector outlet temperature rises above 100°C, indicating an overheating of the collector. This is shown in Figure 9.51 for various fixed λ positions and a variable $\dot{m}_{hw}$. For the other two cases, when λ is variable, the collector outlet temperature does not exceed 100°C at all. Of course, this is largely influenced by the size of the collector.

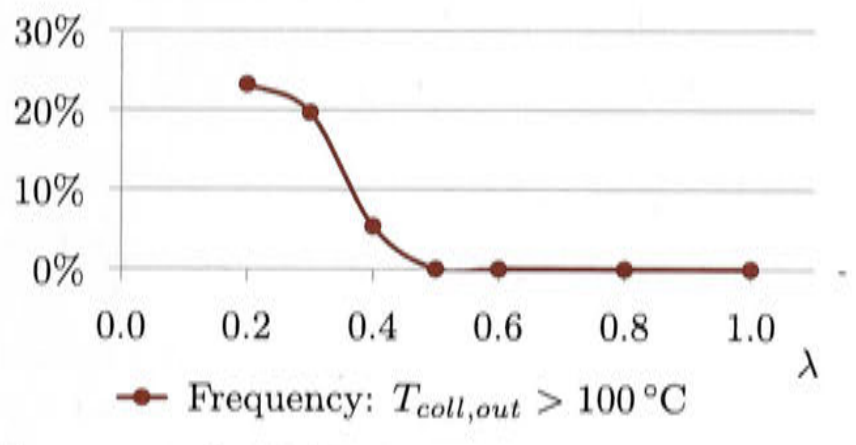

Figure 9.51: Frequency $T_{coll,out}$ exceeds 100 °C when $\dot{m}_{hw}$ is variable and λ is fixed at different levels.

As a third measure the average ΔT of collector and hot water circuits are examined. The ΔT_{hw} of absorption chillers is usually between 5°C and 10°C. The collector's ΔT_{coll} should be between 15°C and 25°C for large collector arrays. This allows for more stability when balancing the mass flows.

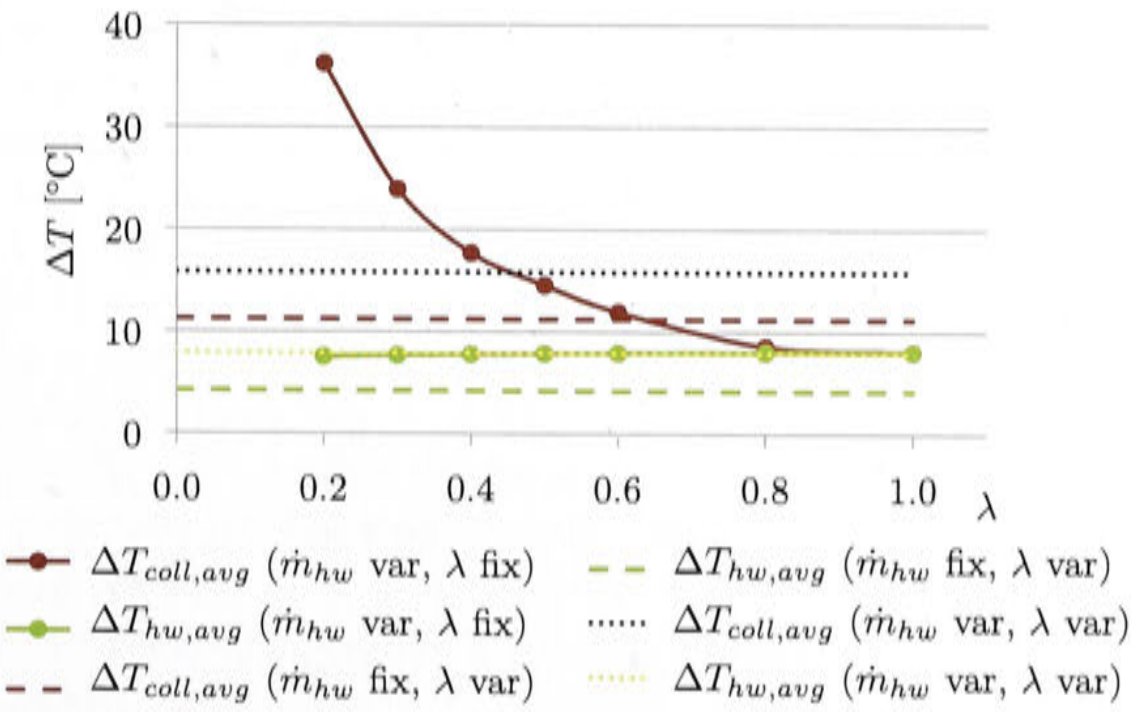

Figure 9.52: Average ΔT of collector and generator for the three different cases

In the results shown in figure 9.52 it became obvious that fixing λ between 0.4 and 0.5, whenever the collector is warm enough to supply the chiller with heat, seems best for keeping the collector ΔT around 15°C with minimal overheating.

The model did not include any collector heat losses or thermal masses, which would lead to a cooling down of the circuit over night, and to thermal lags. All the heat which can't be transferred to the chiller accumulates in the hot water circuit. Once the sun sets and no solar supply is available, the heat in the circuit can be transferred to the chiller until it reaches the generator temperature of 65°C.

The case of $\lambda = 1$ and $\dot{m}_{hw}$ at variable flow made the highest utilization of solar energy falling on the collectors ($Q_{sol} / G_{tot,coll}$).

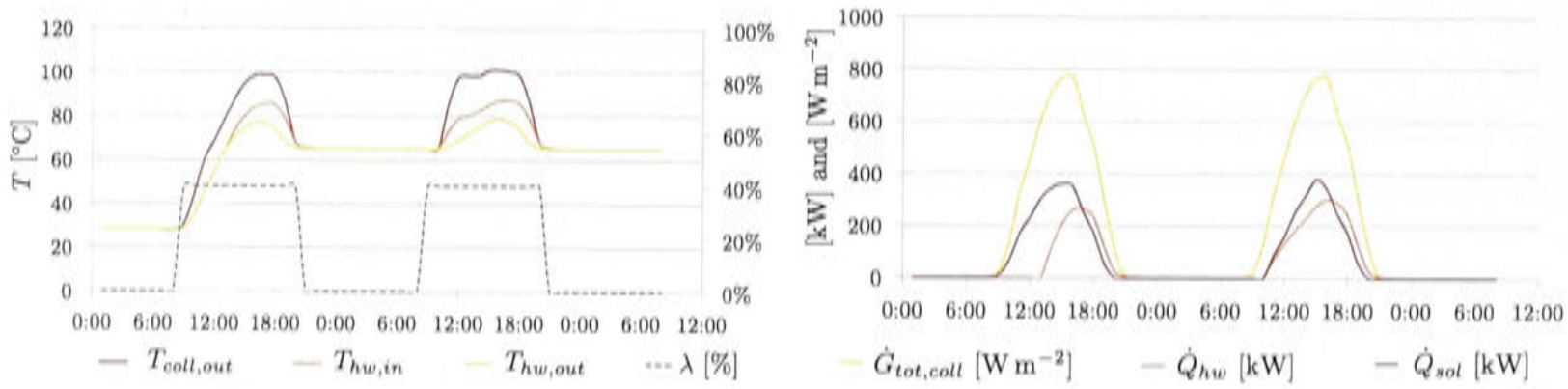

(a) Temperatures and λ

(b) Heat

Figure 9.53: $\lambda = 0.4$ fix and $\dot{m}_{hw}$ variable

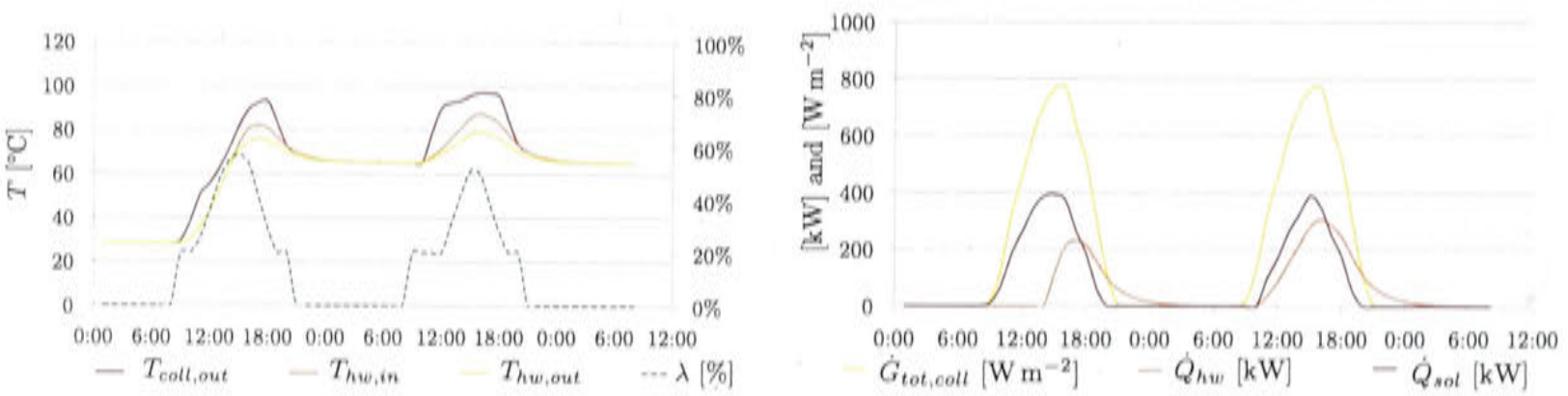

(a) Temperatures and λ

(b) Heat

Figure 9.54: λ variable and $\dot{m}_{hw}$ is fix at rated flow

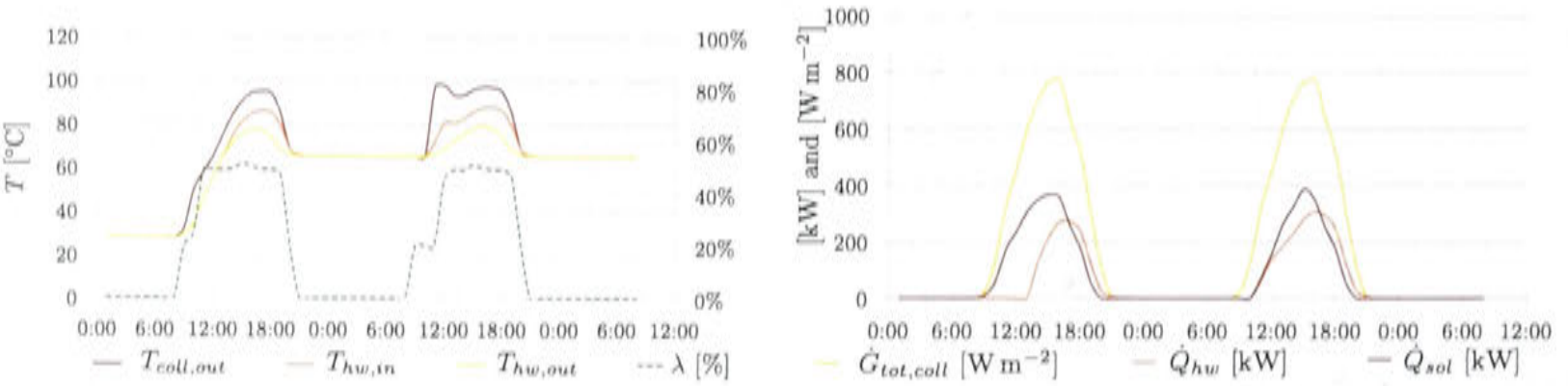

(a) Temperatures and λ

(b) Heat

Figure 9.55: λ variable and $\dot{m}_{hw}$ also variable

Figure 9.53 to 9.55 show the time shift between the heat intake of the generator

($\dot{Q}_{hw}$) and the heat into the water circuit from the collectors ($\dot{Q}_{sol}$). This shift occurred in all three cases. Furthermore, the figures show the variations of λ and the collector outlet and generator inlet and outlet temperatures throughout the two day simulation period.

If the heat below 65°C cannot be utilized it is recommended to keep $\lambda = 0$ at night times, and to bypass the collectors to prevent the accumulated energy from being lost via radiation heat loss towards the sky. In large scale systems long pipe runs can be used to store extra energy. These pipes should be well insulated to ensure the heat is contained as the ambient temperature drops[5].

Two major conclusions can be drawn from the results. There is a relatively large amount of accumulated energy in the system, which in reality would be lower due to heat losses. It is recommended to exchange the accumulated heat below 65°C in the evening for example with a domestic hot water system, even though this would lead to a longer chiller start up time in the morning. Furthermore, the collectors should be sized to prevent stagnation if no additional heat relief devices are utilized. To protect the chiller from excessive temperatures, the valve position λ could also be controlled by the chiller, to achieve a constant $T_{hw,in}$, instead of a constant ΔT_{coll}.

9.6 Conclusion solar thermal model including cold storage

The latent storage tank did increase the solar fraction in each climate between 4% and 12% points. This effect was especially strong in the hot climates where cooling demand is high. Reducing the amount of relieved heat in this model is an indicator for improved solar usage. The increase of solar fraction in the colder climates is lower because cooling is only a fraction of the collector heat consumption and the demand for heating in winter makes up the larger proportion.

The summer comfort increased in the cooler climates, but dropped in the hotter climates even though the provided cooling increased. The increase of cooling might be related to the strategy of discharging mode 2, which discharges the cold storage tank in the evening even when no cooling is required by the room thermostats or schedules. This strategy was implemented in order to pre-cool the buildings and to provide storage space for the next day's solar heat supply. The latent storage size specific to the installed chiller capacity was varied between $0.09\,m^3\,kW^{-1}$ and $0.18\,m^3\,kW^{-1}$. In the climates of Tennant Creek and Griffith the effect on the comfort conditions was significant and the larger storage tank improved the comfort conditions strongly, as opposed to the smaller tank. In the humid climates the sensitivity to the tank size was not significant. In all climates the comfort could be improved when discharging at different set point temperatures (11/16). The downside of higher air set point temperatures is a higher electricity consumption for the indoor fans.

In the colder climates of Canberra and Melbourne and Sydney the latent cold storage tank provided approximately 40% of the total cooling effect. In the hotter

[5]The water in the collectors and long pipe runs in the large scale system UWC in Singapore started circulating during the night due to heat losses and temperature differences.

climates it was 20% to 30%.

The increase of solar fraction goes hand in hand with the reduction of greenhouse gases, as long as the electricity consumption can be kept in check.

As a conclusion a latent cold storage tank is recommended for the thermal chillers from a greenhouse gas savings point of view. It can be most cost effectively implemented in the hotter climates. Table 9.28 show the expenses for each additionally saved kg_{CO2} for the different cold storage options compared to the base case without cold storage.

Table 9.28: Marginal cost for each additionally saved kg_{CO2} when employing one of the three cold storage tank options compared to the base case ($\Delta c_m / \Delta GHG$). Numbers in red indicate that cold storage tank option generates more greenhouse gases than the base case. Numbers in blue indicate that the specific cost of the cold storage option is lower than the base case.

	Canb	Brisb	Syd	Grif	TenCr	Darw	Melb
				[\$ kg_{CO2}^{-1}]			
2 m^3	19.67	3.27	2.27	4.30	2.77	1.12	9.59
1 m^3	12.82	1.24	-0.40	2.24	1.92	0.80	4.91
1.5 m^3 (7/14)	14.42	2.18	0.70	3.23	2.33	0.89	6.97
1.5 m^3 (7/12, 11/16)	23.59	2.39	1.49	4.26	2.72	1.08	12.71
1.5 m^3 (7/14, 11/16)	51.64	2.72	1.12	6.47	4.34	1.01	18.49
1.5 m^3 (CS+beams)	-15.50	5.38	7.13	20.51	10.13	2.09	-9.81
2 m^3 (chwtank)	144.02	0.73	-1.79	1.40	1.92	0.52	7.44

Chilled beams for discharging as in section 9.4.2 are not recommended as they increase the specific cost, provide less comfort if measured against the air temperature, and do not reduce the greenhouse gas emissions as strongly as fan coil units.

When examining cold storage using a chilled water tank there is an advantage of a lower pump power consumption and cost compared to the latent storage tank. Nevertheless, the total electricity consumption increases between 0.5% and 6.5% points. The highest increase occurs in Tennant Creek.

However, the chilled water storage's energy density is only 40% of that of the latent storage. The lower heat storage capacity in relation to the chilled water tank's volume leads to 7% to 12% points less cooling supplied from the tank as a fraction of the total air-conditioning cooling supplied.

General requirements on storage from Kohlenbach and Jakob [2014] are that they must have low thermal losses and be low in cost. Furthermore, they must have a high energy density and, if possible, a low weight. With a cold storage tank the thermal losses are relatively low compared to hot water storage and with latent storage tanks the energy density is 70% higher than for sensible storage tanks. However, costs at the current point of time are too high and in the suggested configuration not yet financial viable.

Chapter 10

Conclusions and future work

The following conclusions are an outcome of the extensive simulation work performed in this thesis. Furthermore, they are derived from case studies, participation in four solar cooling conferences (two in Australia and two in Europe) and while working for one of the world's most experienced solar cooling designer and installer SOLID.

10.1 Conclusions

Air-conditioning was identified as the main electricity price driver in Australia over the last 5 years, causing costly electricity network infrastructure upgrades worth over $60 billion. Furthermore, the international debate on greenhouse gas reduction offers a second strong motivation to reduce electricity consumption and to explore alternative cooling solutions. This work investigated into solar electric and solar thermal cooling, heating and domestic hot water (DHW) options with and without energy storage for the residential sector.

The installed capacity of photovoltaics in Australia reached 1.8 GW by the end of 2012 and this reduced peak electricity demand on average by 3%, depending on the state. Solar thermal systems are also able to reduce peak electricity consumption. The model conducted in this study suggests electricity savings of 0.05 kWh_{el} per kWh of cooling and heating are achievable during peak hours. This translates to a further peak electricity reduction of 3% under the assumption that an uptake of the modeled solar thermal system was equivalent to the penetration of photovoltaics.

Australia is a large continent, spanning a large range of latitudes and climate zones. This work uniquely includes analysis covering seven climate zones, including warm summers and cold winters and very hot or very humid summers without distinct winters. The modeling is also unique in that it considers representative residential buildings suited for each climate, normalized only by layout and floor area. The analysis considers annual environmental, economic and comfort related performance of a cooling, heating and domestic hot water system.

Solar-electric systems using photovoltaic modules to assist a conventional residential air-conditioner proved to be the most cost effective means to provide space heating and cooling. The recent removal of feed-in tariffs has incentivised self-

consumption of photovoltaic generation. A solar fraction of 60% can be achieved using photovoltaic collector areas of $3.6\,\mathrm{W\,m_{CS}^{-2}}$ to $9.0\,\mathrm{W\,m_{CS}^{-2}}$, depending on the climate. However, greenhouse gas savings are not as high as for systems with solar thermal collectors because photovoltaic systems use greenhouse intensive grid electricity as backup, unless battery storage is available. Furthermore, in a photovoltaic system the hot water tank is not charged with solar electricity unless hot water demand and solar electricity supply coincide.

The study showed that in most climates solar thermal systems save greenhouse gas emissions, hence fossil fuel sourced energy, but at increased cost compared to conventional systems. Furthermore, the motive heat for the absorption chiller must be rejected through the condenser, which is usually a wet cooling tower. Since water consumption is an issue in Australia, the high water consumption ($3.31\,\mathrm{kWh^{-1}}$ to $4.11\,\mathrm{kWh^{-1}}$ of cooling energy supplied) provides an additional obstacle for thermal cooling.

Since there is a large variation in the design and performance of the systems across each of the seven climates, climate specific recommendations have been listed in section 8.3.2. Table 10.1 summarizes the cost for greenhouse gas abatement with and without utilizing domestic hot water.

Table 10.1: Cost of greenhouse gas abatement for the chosen configuration of the base case

	excl. DHW			incl. DHW		
	Δc_m [$\$\,\mathrm{kWh^{-1}}$]	ΔGHG [$\$\,\mathrm{kg_{CO2}^{-1}}$]	$\frac{\Delta c_m}{\Delta GHG}$ [$\$\,\mathrm{kg_{CO2}^{-1}}$]	$\Delta c_{m,dhw}$ [$\$\,\mathrm{kWh^{-1}}$]	ΔGHG_{dhw} [$\$\,\mathrm{kg_{CO2}^{-1}}$]	$\frac{\Delta c_{m,dhw}}{\Delta GHG_{dhw}}$ [$\$\,\mathrm{kg_{CO2}^{-1}}$]
Canb (0.75 m³, 24 m²)	0.17	0.21	0.84	0.01	0.45	0.02
Brisb (0.4 m³, 12 m²)	0.29	0.09	3.15	0.05	0.41	0.12
Syd (0.4 m³, 12 m²)	0.42	0.15	2.73	0.03	0.56	0.06
Grif (0.4 m³, 18 m²)	0.21	0.11	1.93	0.05	0.36	0.15
TenCr (1.0 m³, 18 m²)	0.16	0.04	3.85	0.07	0.17	0.40
Darw (0.4 m³, 24 m²)	0.16	-0.02	-10.25	0.08	0.11	0.77
Melb (0.33 m³, 24 m²)	0.34	0.26	1.28	0.06	0.68	0.09

Across all climates, systems with a high high heating load perform best because they have a high collector utilization (e.g. Canberra, Melbourne and Griffith). The inclusion of domestic hot water in the delivered services improves the financial viability and the greenhouse gas savings of all climate zones, noting that most households in Australia still supply their domestic hot water via electricity. Manufacturers should consider solar thermal cooling applications for schools, hotels and other consumers with a high demand of hot water. For the very humid climate of Darwin a solar thermal cooling system does not provide a reasonable alternative as slightly more greenhouse gases are generated than in the base case.

Cold storage using phase change materials proved to be an effective way to increase the greenhouse gas savings, but imposed a cost penalty that rendered it futile. Furthermore, the use of a cold storage imposes heat exchange temperature losses on both charging and discharging that work to reduce the potential savings of this configuration. Direct sensible heat storage using chilled water is able to improve the

greenhouse gas savings and remain cost-effective.

Discharging of cooling effect via fan-coil units was the preferred method used in the modeling. The use of chilled beams allows the absorption chiller to operate at higher evaporator temperatures but does not provide performance or comfort benefits and is not recommended.

One of the major limitations of absorption chillers used in small scale residential applications is that the chiller must follow the building load. If coupled in this manner, without storage, auxiliary gas consumption and parasitic electricity consumption can be high. In larger commercial installations, the absorption chiller is usually the priority chiller amongst one or more conventional chillers. In this case, the absorption chiller is able to fully utilise the available solar energy and it's performance indicators are superior.

There is some pressure to phase-down or eliminate the use of HFC refrigerants. Indeed, Australia has set an HFC phase-down goal for 2030. The absorption chiller technology has an existing track record for operating with natural refrigerants. Should the price of electricity continue to rise, and a price be imposed upon carbon emissions, the absorption chiller is likely to be a contender. The work completed in this study provides a blueprint for rolling out absorption based air-conditioning systems in Australian conditions. Research effort and funding for energy efficient residential cooling, heating and domestic hot water should focus on the improvement of existing technologies while increasing efficiencies and also lowering the energy demand side of the buildings. A future of residential cooling with absorption chillers might be the development of chilled water networks supplied by a couple of large scale chillers, where the absorption chiller can operate in base load.

10.2 Future Work

Solar thermal cooling using absorption chillers

The heating demand is very dominant in the climates of Canberra and Melbourne. Instead of using the heat in the tank for fan coil units it might be more energy efficient to use a water-air heat pump with additional PV panels. The model could be extended to that alternative.

Since solar thermal cooling is most effective when the absorption chiller can be operated under constant full load only limited by the availability of the sun, residential solar thermal cooling should be designed in such a way. It would be possible to install a large district cooling network supplying multiple households by a couple of conventional chillers and one medium or large sized absorption chiller, which can operate under full load most of the time. In Australia the availability of roof space is a minor issue as much more exposed land is available to harness heat with solar thermal collectors, at least outside of the large cities.

For large scale applications it would be interesting to test chilled beams and operating the chiller as a base load device. The absorption chiller would only provide a small fraction of the cooling load and the remaining load, including latent cooling,

could be supplied by conventional chillers and fan coils. The chiller would operate under beneficial conditions with relatively high chilled water inlet temperatures. The advantage compared to large scale absorption chillers in series with conventional chillers, in order to pre-cool the chilled water, would be a strictly separated cold distribution system.

In General this study should be performed in a similar way for large scale commercial systems as a cost benefit can be expected.

Cold storage

The control strategy suggested for the model could be tested in reality for feasibility and the prediction function can be linked to the weather forecast.

Future work on the modeling side of the latent storage tank could be to test different trigger temperatures for the auxiliary gas heater. In this model the auxiliary heater switches on in case cooling is required, but the cold storage tank is empty and the hot water outlet temperature of the hot storage tank is lower than 75°C.

The hot water tank is already chosen relatively small, but it would be interesting to decrease the size of the hot water storage tank down to 0.1 m^3 or remove it completely. In case of complete removal, direct coupling obstacles as outlined in section 9.5 should be considered and the collector area should be sized so that the chiller can cope with the peak solar supply to avoid stagnation and overheating (unless heat relief devices are installed).

The scenario using a chilled water tank did not analyze different tank sizes as the volume was kept at the largest latent storage tank size. It would be interesting to see how effective a larger chilled water tank would perform.

The option of latent storage for heat rejection at night could also be analyzed in a full TRNSYS annual simulation. This way further savings might be achieved reducing fan power consumption at the cooling tower.

The potential of cold storage should be analyzed within a large scale systems with a constant chilled water outlet temperature of $T_{chw,set} = 11\,°C$, if the solar supply allows. With a melting temperature at 15°C chilled beams can be supplied by the storage tank and conventional chillers can allow for load adjustment and latent heat removal via fan coils.

Desiccant systems

Desiccant systems have not been analyzed in this thesis as the most common absorption chiller technology was chosen as the representative for thermal cooling systems. Nevertheless, desiccant systems have been included in the Australian standard AS 5389 TRNSYS model [Australian/ New Zealand Standard, 2013].

The effect of solar air-conditioning systems on the electricity grid

The electricity network of the NEM is currently upgraded to avoid black outs due to peaks in the electricity demand, widely understood to be caused by air-conditioning

systems.

The investigation into the potential of peak demand reduction of residential systems could be an extrapolation of thermal cooling systems throughout Australia. This study would investigate at what times electricity can be saved, and at what rates and times the auxiliary gas consumption increases. Would there be an additional peak in gas demand?

The potential of greenhouse gas reduction can be estimated. Greenhouse gas emissions change with a different mix of generators feeding power to the grid. In this thesis the simplification was used to set fix emissions factors for each state. It would be very interesting to model the hourly change in emission factors to achieve a more accurate estimation of greenhouse gas reduction.

It is possible to do such analyzes with historic weather or electricity market data retrospectively as has been done in Chapter 3. The results can give a good indication how much greenhouse gases could have been saved or how the electricity demand could have been reduced (in peak hours).

The implications of a reduced peak electricity demand on the historic demand patterns would lead to the questions on how an uptake of solar cooling could actually affect the electricity price in the future. In such a scenario the cooling demand prediction on the basis of weather forecasts should be taken into account, but also other impacts on the electricity supply side, for example the uptake of PV, the network upgrades or the electricity provider infrastructure in Australia.

Bibliography

AGEB AG Energiebilanzen e.V., 2014. Stromerzeugung. http://www.ag-energiebilanzen.de. Retrieved October 2014. (cited on page 19)

AIRAH, 2007. *Technical Handbook*. Australian Institute of Refrigeratio, Air Conditioning and Heating (AIRAH), Melbourne, 4 edn. (cited on pages 51, 118, and 119)

Albers, J., 2011. Dipl.-Ing. Jan Albers - Datenanalyse und Simulation (TRNSYS-Type 177). http://www.eta.tu-berlin.de/menue/mitarbeiter_innen/wimi/albers/. Retrieved December 2011. (cited on pages xxv, 111, and 231)

Albers, J. and Ziegler, F., 2011. Heat transfer calculation for absorption heat pumps under variable flow rate conditions. In *International Sorption Heat Pump Conference (ISHPC2011)*, 813–822. Italy, Padua. (cited on page 100)

ASHRAE, 2012. *ASHRAE Handbook - HVAC Systems and Equipment*. American Society of Heating, Refrigeration and Air-Conditioning Engineers. (cited on pages 116 and 234)

ASHRAE, 2013. *ASHRAE Handbook - Fundamentals*. American Society of Heating, Refrigeration and Air-Conditioning Engineers. (cited on pages 52, 233, 234, and 278)

Australian Building Codes Board, 2011. Building Code of Australia, Vol. 2. (cited on pages 4 and 50)

Australian Building Codes Board (ABCB), 2006. Protocol for house energy rating software. Technical report, Australian Building Codes Board. (cited on page 53)

Australian Bureau of Statistics (ABS), 2013. Environmental issues: energy use and conservation, March 2011. http://www.abs.gov.au. Retrieved February 2013. (cited on page 10)

Australian Bureau of Statistics (ABS), 2014. Household energy use and conservation. http://www.abs.gov.au/ausstats/abs@.nsf/mf/4602.0.55.001. Retrieved October 2014. (cited on pages 10 and 11)

Australian Energy Market Commission (AEMC), 2014. Final report 2013 residential electricity price trends. Technical report, Australian Energy Market Commission. (cited on pages 21 and 22)

Australian Energy Market Operator (AEMO), 2012. National electricity forecasting report 2014. Technical report, AEMO. http://www.aemo.com.au/Electricity/

Planning/Forecasting/National-Electricity-Forecasting-Report. (cited on pages 19, 20, and 33)

Australian Energy Market Operator (AEMO), 2013a. Aggregated price and demand: 2005 - 2012. http://www.aemo.com.au/Electricity/Data/Price-and-Demand. Retrieved February 2013. (cited on pages 24 and 25)

Australian Energy Market Operator (AEMO), 2013b. Forecasting methodology information paper. Technical report, AEMO. (cited on page 33)

Australian Energy Regulator (AER), 2012. State of the energy market 2012. (cited on pages 7, 20, 24, and 30)

Australian Energy Regulator (AER), 2014. Generation capacity and peak demand. https://www.aer.gov.au/node/9772. Retrieved October 2014. (cited on page 20)

Australian Institute of Petroleum (AIP), 2014a. Average weekly retail prices for diesel fuel. http://www.aip.com.au/pricing/retail/diesel/index.htm. Retrieved 27 May 2014. (cited on page 88)

Australian Institute of Petroleum (AIP), 2014b. Facts about prices in regional & country areas. http://www.aip.com.au/pricing/facts.htm. Retrieved 27 May 2014. (cited on page 89)

Australian/ New Zealand Standard, 2005. AS/NZS 4692.1:2005: Electric water heaters, performance and general requirements. (cited on page 124)

Australian/ New Zealand Standard, 2008. AS/NZS 4234:2008: Heated water systems - calculation of energy consumption. (cited on pages 5, 12, 36, 38, 48, 54, and 96)

Australian/ New Zealand Standard, 2012. AS/NZS 4755.3.1:2012 demand response capabilities and supporting technologies for electrical products-interaction of demand response enabling devices and electrical products - operational instructions and connections for air conditioners. (cited on page 13)

Australian/ New Zealand Standard, 2013. AS 5389(Int)-2013: Solar heating and cooling systems - calculation of energy consumption. (cited on pages 5, 12, 17, 58, 59, 107, and 286)

Australian Taxation Office (ATO), 2014. Fuel schemes - fuel tax credits if no GST registration requirement. https://www.ato.gov.au/Business/Fuel-schemes/In-detail/. Retrieved 27 May 2014. (cited on page 89)

Beitz, W. and Grote, K.-H. (Eds.), 1997. *Dubbel - Taschenbuch für den Maschienenbau*. Springer, 19 edn. (cited on pages 238 and 251)

Bettanini, E.; Gastaldello, A.; and Schibuola, L., 2003. Simplified models to simulate part load performances of air conditioning equipments. In *Eighth International IBPSA Conference*. (cited on pages 59 and 60)

Bourdoukan, P., 2009. Task 38 - description of simulation tools used in solar cooling (a technical report of subtask C, deliverable C2-A). (cited on page 35)

Broad Air Conditioning, 2008. Broad x absorption chiller - model selection & design manual. (cited on page 101)

Bureau of Meteorology (BOM), 2013a. Average daily solar exposure. http://www.bom.gov.au/jsp/ncc/climate_averages/solar-exposure/index.jsp. Retrieved 26 February 2013. (cited on page 31)

Bureau of Meteorology (BOM), 2013b. Climate classification Australia (temperature/ humidity zones). http://www.bom.gov.au/jsp/ncc/climate_averages/climate-classifications/index.jsp. Retrieved 8 May 2014. (cited on page 304)

Bureau of Resources and Energy Economics (BREE), 2014. 2013 Australian energy statistics. http://www.bree.gov.au/publications/australian-energy-statistics/2013-australian-energy-statistics-data. Retrieved 9 May 2014. (cited on pages 8, 10, 20, 21, and 40)

Che, N. and Pham, P., 2012. Economic analysis of end-use energy intensity in Australia. Technical report, Bureau of Resources and Energy Economics (BREE). (cited on page 10)

Christian Holter (CEO SOLID), 2014. Personal correspondence via e-mail . 4.11.2014. (cited on page 17)

Ciganda, J. L. C., 2007. *Modeling and Simulation of a 10 kW absorption chiller with cooling tower*. Ph.D. thesis, Process energy environmental systems engineering. (cited on page 117)

Clean Energy Council, 2011. cleanenergyaustralia report 2011. Technical report, Clean Energy Council. (cited on page 32)

Clean Energy Council, 2012. Clean energy Australia report 2012. Technical report, Clean Energy Council. (cited on pages 10, 12, and 14)

Clean Energy Council, 2013. Clean energy Australia report 2013. Technical report, Clean Energy Council. (cited on pages 10 and 32)

Cleland, A. and White, S., 2000. short course notes. In *Cost-effective refrigeration*. Massey University, New Zealand. (cited on page 59)

© Compaq Computer Corporation, 2000. Compaq visual fortran 6.6. Compiler to generate TRNSYS user .dll. (cited on pages 5 and 36)

Council of Australian Governments (COAG), 2009. National Strategy on Energy Efficiency. Technical report, Commonwealth of Australia. (cited on page 14)

Cramton, P. and Kerr, S., 2002. Tradeable carbon permit auctions: How and why to auction not grandfather. *Energy Policy*, 30 (2002). (cited on page 14)

CSIRO, 2010. AccuRate Australian Edition v 1.1.4.0 demonstration version. Haerne Scientific Software. Software program for Australian House Energy Rating Scheme. (cited on page 53)

CSIRO, 2013. Solar cooling. http://www.csiro.au/science/solar-cooling.html. Retrieved January 2013. (cited on page 2)

Dassault Systems, 2014. Dymola. http://www.3ds.com/products-services/catia/capabilities/systems-engineering/modelica-systems-simulation/dymola. Retrieved October 2014. (cited on page 36)

Department of Climate Change and Energy Efficiency, 2012. Australian national greenhouse accounts. (cited on pages 40 and 81)

Department of Employment, Economic Development and Innovation, 2011. Queensland energy management plan. Technical report, Queensland Government. (cited on page 21)

Department of Resources, Energy and Tourism, 2013. Energy in Australia 2013. Technical report, Department of Resources, Energy and Economics. (cited on pages 8 and 19)

Department of the Environment, 2014. Montreal protocol on substances that deplete the ozone layer. http://www.environment.gov.au/protection/ozone/montreal-protocol. Retrieved October 2014. (cited on page 9)

Dillon, M., 2011. Solar flair. *Ecolibrium*, (July 2011). (cited on page 3)

Doemland, I., 2014. Monitoring of the solar cooling installation UWC Singapore in 2013 and improvements based on TRNSYS simulation. In *Gleisdorf Solar 2014*. (cited on pages 149 and 181)

Doemland, I. and Albers, J., 2013. A non-linear absorption chiller model for TRNSYS with internal control algorithm. In *5th International Conference Solar Air-conditioning*. (cited on pages 6 and 99)

Doemland, I. and Dennis, M., 2011. Solar cooling in Australia - a review. In *4th International Conference on Solar Air-Conditioning*. (cited on page 5)

Doemland, I. and Dennis, M., 2013. Air conditioning, its effects on the summer peak electricity demand and the role of pv. In *Australian Solar Cooling 2013 Conference*. AIRAH & AusSCIG, Newcastle. (cited on pages 5 and 24)

EAW Energieanlagenbau GmbH Westenfeld, 2014. Product specification - Absorptionskälteanlage Wegracal SE 15 (2012). http://www.eaw-energieanlagenbau.de/index.php/akm-106.html. Retrieved October 2014. (cited on pages 111 and 231)

Eicker, U., 2014. *Energy Efficient Buildings with Solar and Geothermal Resources*. Wiley, 1 edn. (cited on pages 18, 35, and 277)

Energy Efficient Strategies (EES), 2008. Energy use in the australian residential sector 1986-2020. Technical report, Department of the Environment, Water, Heritage and the Arts (DEWHA). (cited on pages 9, 10, and 49)

Expertgroup, 2013. Cold hard facts 2. Technical report, Prepared for the Department of Sustainability, Environment, Water, Population and Communities. (cited on pages 8, 9, and 10)

FTF grop climate, 2014. X-wing passive "radiant" chilled beam. http://www.ftfgroup.us/products/passive-chilled-beams/x-wing-passive-chilled-beam.html. Retrieved July 2014. (cited on page 205)

German Institute for Standardization (DIN), 2007. DIN EN 15316-4-3:2007: Heating systems in buildings - method for calculation of system energy requirements and system efficiencies - part 4-3: heat generation systems, thermal solar systems. (cited on page 124)

Green Energy Market, 2012. Impact of market based measures on nem power consumption. Technical report, Green Energy Market. (cited on page 29)

Hellmann, H.-M.; Schweigler, C.; and Ziegler, F., 1999. The characteristic equations of absorption chillers. (cited on pages 99 and 100)

Henning, H.-M., 2007. *Solar-Assisted Air-Conditioning in Buildings - A Handbook for Planners*. Springer-Verlag Wien New York, Wien, second revised edn. (cited on pages 17 and 117)

Henning, H.-M., 2013a. *Solar Cooling Handbook - a guide to solar assisted cooling and dehumidification processes*. Ambra, Wien, third revised edn. (cited on pages 17, 120, 121, and 146)

Henning, H.-M., 2013b. *Solar Cooling Handbook, a guide to solar assisted cooling and dehumidification processes*. Solar heating and cooling programme, international energy agency. (cited on page 120)

Henze, G. P.; Krarti, M.; and Brandemuehl, M. J., 2001. Guidelines for improved performance of ice storage systems. *Energy and Buildings*, 35 (2001), 111–127. (cited on page 229)

Holman, J. P., 1997. *Heat transfer*. McGraw-Hill Companies, New Yor. (cited on page 233)

INSTITUTE FOR SUSTAINABLE FUTURES AND AIRAH, 2014. HVAC&R research summit - brief report. Technical report, University of technology (Sydney) and AIRAH. (cited on page 3)

INTERNATIONAL ENERGY AGENCY, 2014. Solar Heating and Cooling Programme - Projects (Tasks) by Number. http://www.iea-shc.org/tasks-number. Retrieved November 2014. (cited on page 18)

INTERNATIONAL ENERGY AGENCY (IEA), 2012. Technology roadmap - solar heating and cooling. Technical report, International Energy Agency (IEA). (cited on page 17)

INTERNATIONAL ENERGY AGENCY SOLAR HEATING AND COOLING PROJECT (IEA-SHC), 2011b. Task 38 - solar air-conditioning and refrigeration. (cited on page 14)

INVENSOR GMBH, 2014. Product specification - Adsorption chiller InvenSor HTC 18 plus. http://www.invensor.com/en/products/htc-high-temperature-chillers.htm. Retrieved October 2014. (cited on page 112)

ISO, 2005. ISO 7730:2005 - Ergonomics of the thermal environment - Analytical determination and interpretation of thermal comfort using calculation of the PMV and PPD indices and local thermal comfort criteria. (cited on pages 42 and 52)

KALOGIROU, S. A., 2009. *Solar energy engineering - processes and systems*. Elsevier. (cited on pages 120 and 303)

KINTNER-MEYER, M. AND EMERY, A., 1995. Optimal control of an HVAC system using cold storage building thermal capacitance. *Energy and Buildings*, 23, 1995 (1995), 19–31. (cited on page 229)

KOHLENBACH, P. AND DENNIS, M., 2010. Solar cooling in Australia: The future of air-conditioning. *Ecolibrium*, (December 2010). (cited on pages 3 and 136)

KOHLENBACH, P. AND JAKOB, U., 2014. *Solar cooling - the earthscan expert guide to solar cooling systems*. Routledge, 1 edn. (cited on pages 15, 17, 18, 230, and 282)

KOHLENBACH, P. AND ZIEGLER, F., 2008. A dynamic simulation model for transient absorption chiller performance. *International Journal of Refrigeration*, 31, issue 2 (2008), 217–225. (cited on page 99)

KONSTANTIN, P., 2009. *Praxisbuch Energiewirtschaft*. Springer, second edited and updated edn. (cited on page 43)

KUEHN, A. AND ZIEGLER, F., 2005. Operational results of a 10 kw absorption chiller and adaptation of the characteristic equation. (cited on pages 99 and 100)

METEOTEST; REMUND, J.; AND KUNZ, S., 2004. Meteonorm data (worldwide) - Australia-Oceania. Weatherfile in TMY2 format. (cited on pages 55, 56, and 180)

© Microsoft Corporation, 2007. Microsoft®office excel ®2007. Excel with visual basic for applications programming environment. (cited on page 5)

Mugnier, D., 2013. Quality assurance & support measures for solar cooling with iea shc task 48: overview and first results. (cited on page 14)

National University of Singapore (NUS), 2014. Geography weather station - archive. https://inetapps.nus.edu.sg/fas/geog/ajxdirList.aspx. Retrieved January 2014. (cited on pages xxviii, 278, and 341)

Oekotech Solarkollektoren, 2013. Website Oekotech Solarkollektoren. http://www.oekotech.biz/default.asp. Retrieved December 2013. (cited on page 277)

origin, 2014. Energy price fact sheets - residential electricity and natural gas prices. http://www.originenergy.com.au/962/Energy-price-fact-sheets. Retrieved November 2014. (cited on page 22)

Productivity Commission, 2013. Electricity network regulatory frameworks (no. 62). Technical report, Productivity Commission. (cited on pages 20, 21, and 25)

Puig-Arnavat, M.; Lopez-Villada, J.; Bruno, J. C.; and Coronas, A., 2009. Analysis and parameter identification for characteristic equations of single- and double-effect absorption chillers by means of multivariable regression. *International Journal of Refrigeration*, 33 (2009), 70–78. (cited on page 100)

Rehsler Kuehlsysteme GmbH, 2012. Kühltuerme Baureihe RAX aus GFK - technical specification. www.rehsler.de. Retrieved January 2012. (cited on page 117)

Renew, 2012a. Getting the lead out - alternatives to old battery technology. *Renew*, 121 (2012), 56–59. (cited on page 87)

Renew, 2012b. Taking care of your batteries - a regulator buyers guide. *Renew*, 121 (2012), 74–76. (cited on page 87)

Rowe, D.; White, S.; Mugnier, D.; and Nagidi, K., 2013. Deliverable M-C1.1 - Delivery report: review of relevant international standards rating and incentive schemes. Technical report, CSIRO and TECSOL SA and Energy Management Consulting Group. (cited on page 13)

SMA Solar Technology, 2014. Sunny boy 3000TL and 5000TL. http://www.sma-australia.com.au/en_AU.html. Retrieved April 2014. (cited on page 67)

Solar Energy Laboratory, Univ. of Wisconsin-Madison; TRNSOLAR Energietechnik GmbH; CSTB - Centre Scientifique et Technique du Batiment; and TESS - Thermal Energy Systems Specialists, 2007. TRNSYS 16 - volume 5 mathematical reference. (cited on page 116)

Solar Energy Laboratory, Univ. of Wisconsin-Madison; TRNSSOLAR Energietechnik GmbH; CSTB - Centre Scientifique et Technique du Batiment; and TESS - Thermal Energy Systems Specialists, 2012. TRNSYS 17 - volume 4 mathematical reference. (cited on page 183)

Solaranlagen-Portal, 2014. Marktübersicht Solarstromspeicher 2013. http://www.solaranlagen-portal.com/photovoltaik/stromspeicher/photovoltaik-speicher. Retrieved 16 May 2014. (cited on page 79)

solargis, 2014. Free download of solar radiation maps - GHI and DNI. http://solargis.info/doc/free-solar-radiation-maps-GHI. Retrieved November 2014. (cited on page 16)

S.O.L.I.D., 2014. S.O.L.I.D. Gesellschaft für Solarinstallation und Design mbH. http://www.solid.at/en/. Retrieved October 2014. (cited on pages 6, 104, 212, 226, and 276)

Sparber, W.; Napolitano, A.; Eckert, G.; and Preisler, A., 2009. State of the art on existing solar heating and cooling systems. Technical report, Institute for Renewable Energy, EURAC AIT Austrian Institute of Technology. (cited on page 124)

Specht, E., 2012. The best known packings of equal circles in a circle. http://hydra.nat.uni-magdeburg.de/packing/cci/. Complete up to N=1500 when retrieved 16 September 2013. (cited on page 236)

Sunpower, 2013. E19/318 solar panel. http://www.sunpower.com.au/. Retrieved January 2013 from a different website, but it used to be on the SUNPOWER website in 2010. (cited on page 67)

Systemair, 2013. Sysduct 21 & 22 - technical specification. www.systemair.com. Retrieved June 2013. (cited on page 125)

Tay, N.; Belusko, M.; and Bruno, F., 2011. Designing a PCM storage system using the effectiveness-number of transfer units method in low energy cooling of buildings. *Energy and Buildings*, 50, 2012 (2011), 234–242. (cited on pages 230, 232, and 233)

Thermal Energy System Specialists (TESS), 2007. TRNSYS 16.1.0003. http://sel.me.wisc.edu/trnsys/user-resources/index.html. Includes TESS libraries. (cited on pages 5 and 36)

Thermokey, 2013. power-line & power-j dry coolers. http://www.thermokey.com/Power_line_Dry_Coolers.aspx?LANG=ING. Retrieved June 2013. (cited on pages 184 and 185)

Umweltbundesamt, 2014. Klimaschutz- und Energiepolitik in Deutschland. http://www.umweltbundesamt.de/themen/klima-energie/

klimaschutz-energiepolitik-in-deutschland. Retrieved October 2014. (cited on page 13)

VELA SOLARIS, 2014. Polysun. http://www.velasolaris.com/produkt/produktuebersicht.html. Retrieved October 2014. (cited on page 35)

VIESSMANN, 2008. Planungshandbuch Solarthermie. (cited on pages 120 and 125)

VIESSMANN, 2013. Technical information on pressure drop of evacuated tubes collectors, personal communication on 16 april 2013. (cited on page 122)

WANG, S. K., 2000. *Handbook of air conditioning and refrigeration*. McGraw-Hill. (cited on pages 119 and 144)

WANG, X.; ZHAI, X.; WANG, T.; WANG, H.; AND YIN, Y., 2013. Performance of the capric and lauric acid mixture with additives as cold storage materials for high temperature cooling applications. *Applied Thermal Engineering*, 58 (2013), 252–260. (cited on page 230)

WENQI HUANG, T. Y., 2010. Global optimization method for finding dense packings of equal circles in a circle. *European journal of Operational Research*, 2010, 2011 (2010), 474–481. (cited on page 236)

Appendix A

The national electricity market

A.1 Wholesale electricity demand duration curves 2012

Figure A.1 and A.2 show the duration curves on the NEM.

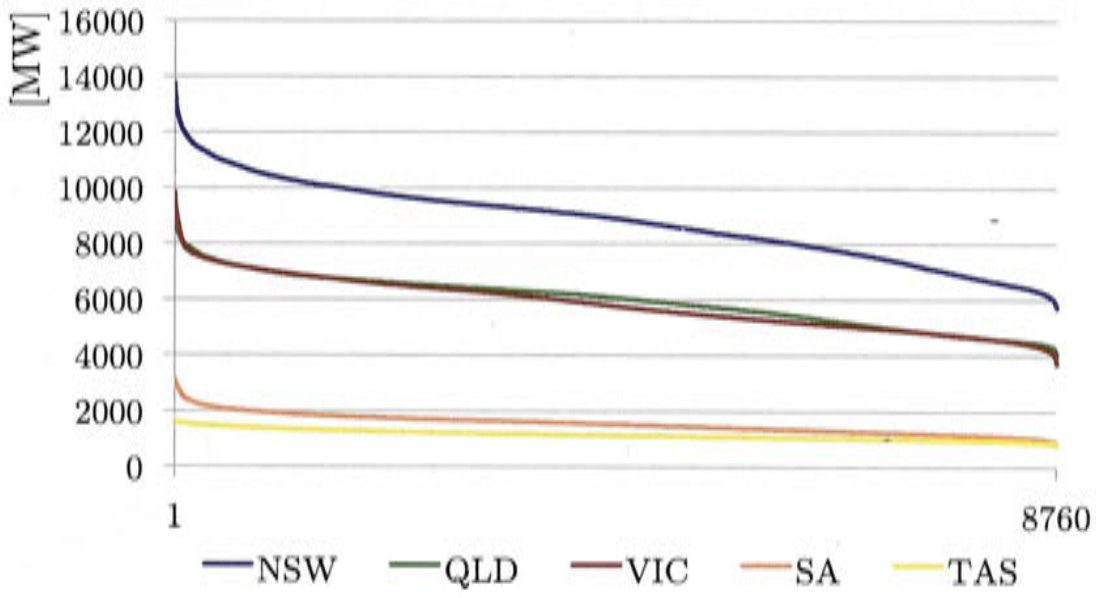

Figure A.1: Electricity demand duration curve on the NEM, 2012.

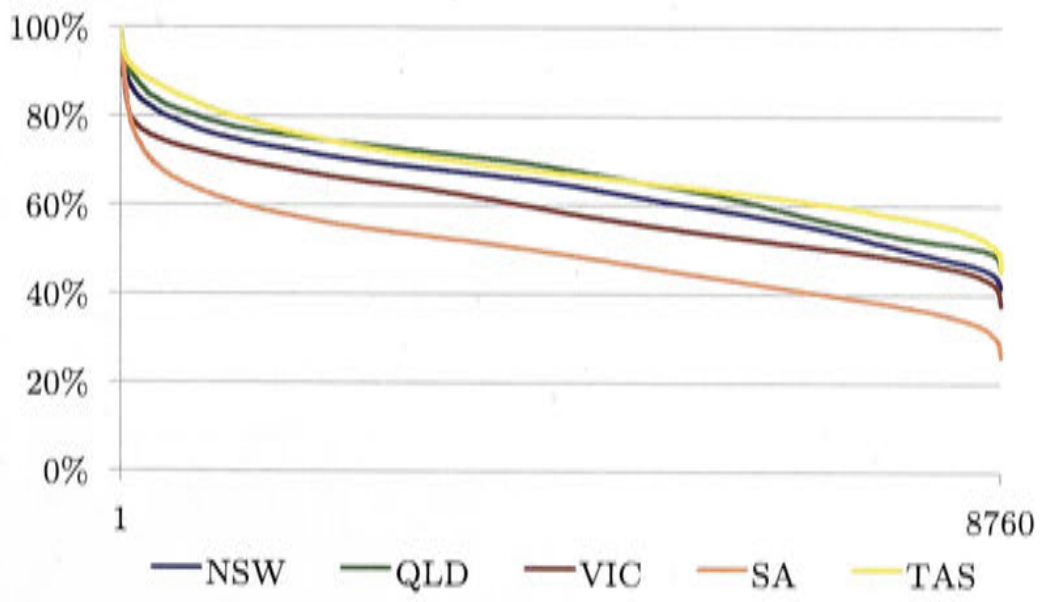

Figure A.2: Normalized electricity demand duration curve on the NEM, 2012.

A.2 Average monthly summer and winter electricity demand on the NEM

Figure A.3 and A.4 show the summer and winter average electricity demand.

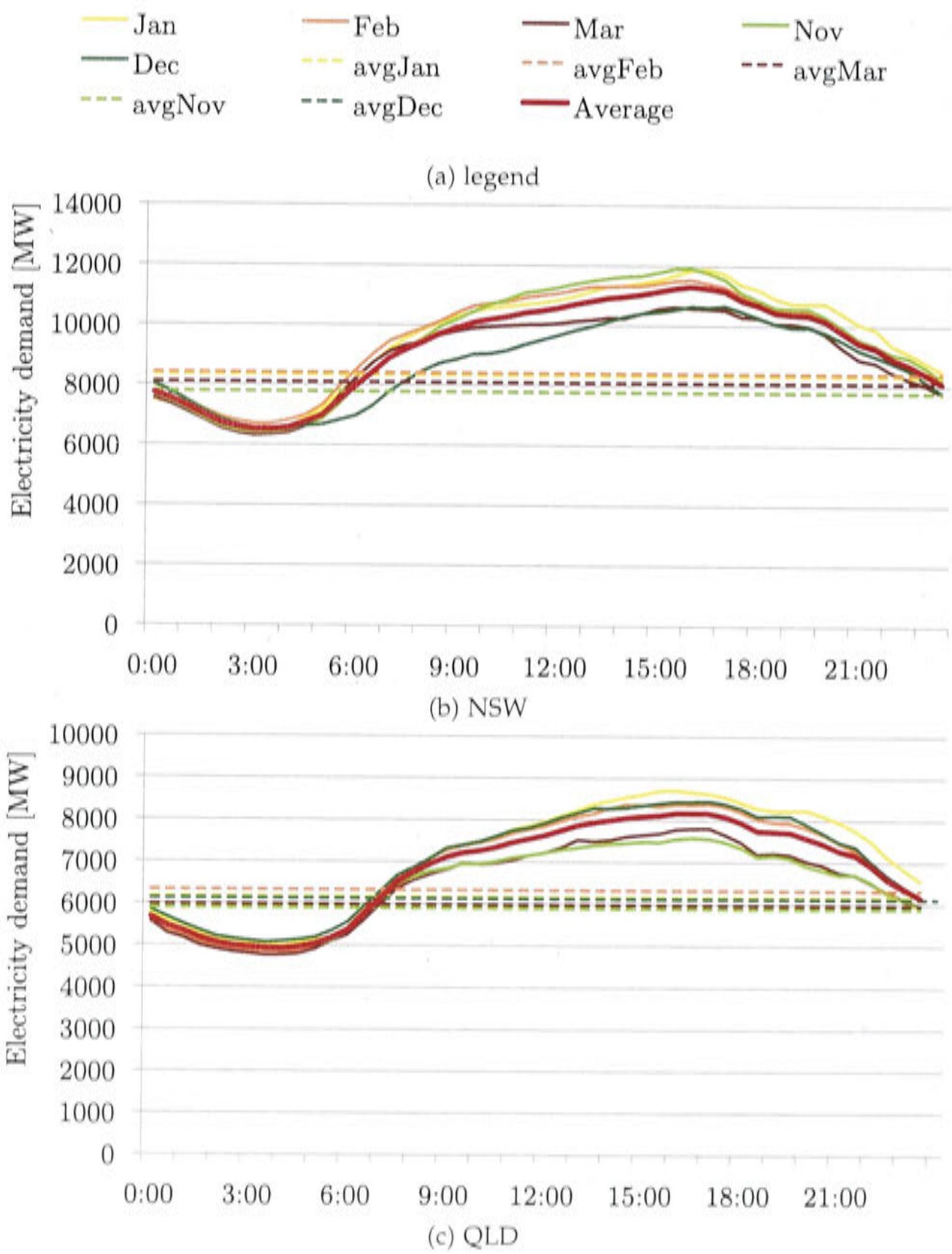

(a) legend

(b) NSW

(c) QLD

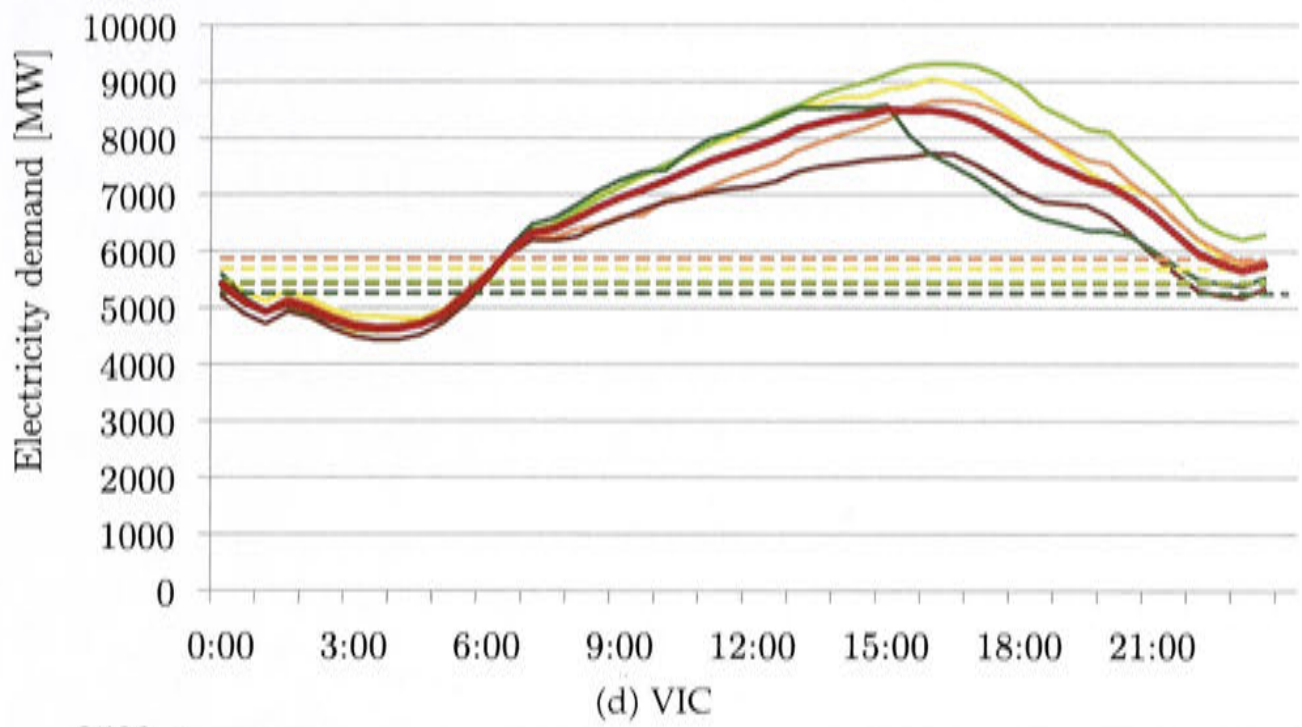

(d) VIC

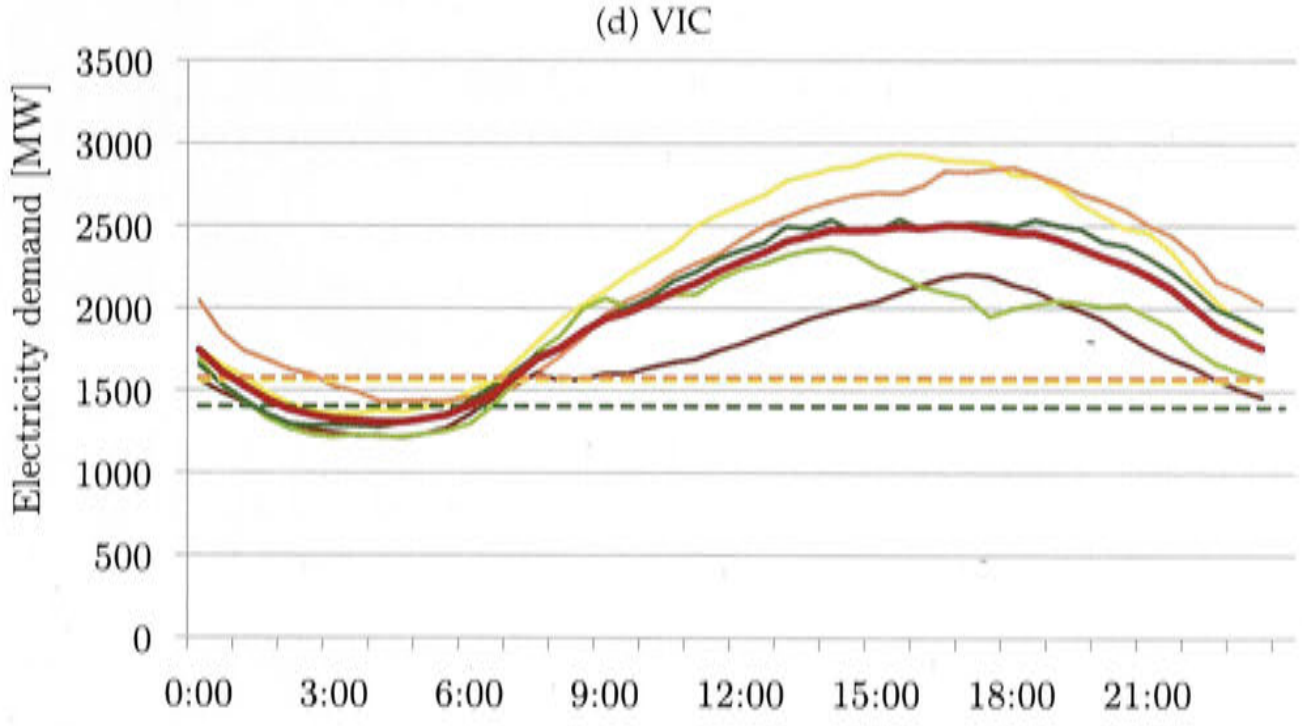

(e) SA

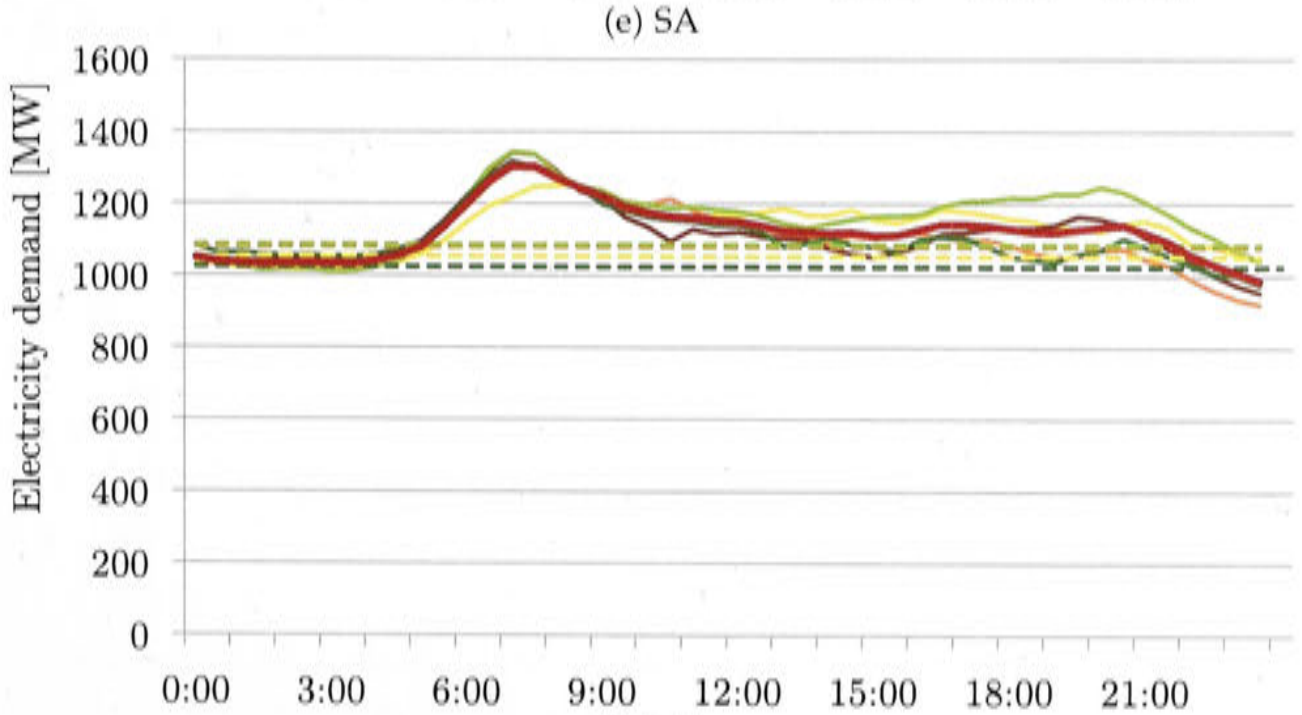

(f) TAS

Figure A.3: Average summer electricity demand in each state on the NEM (2012).

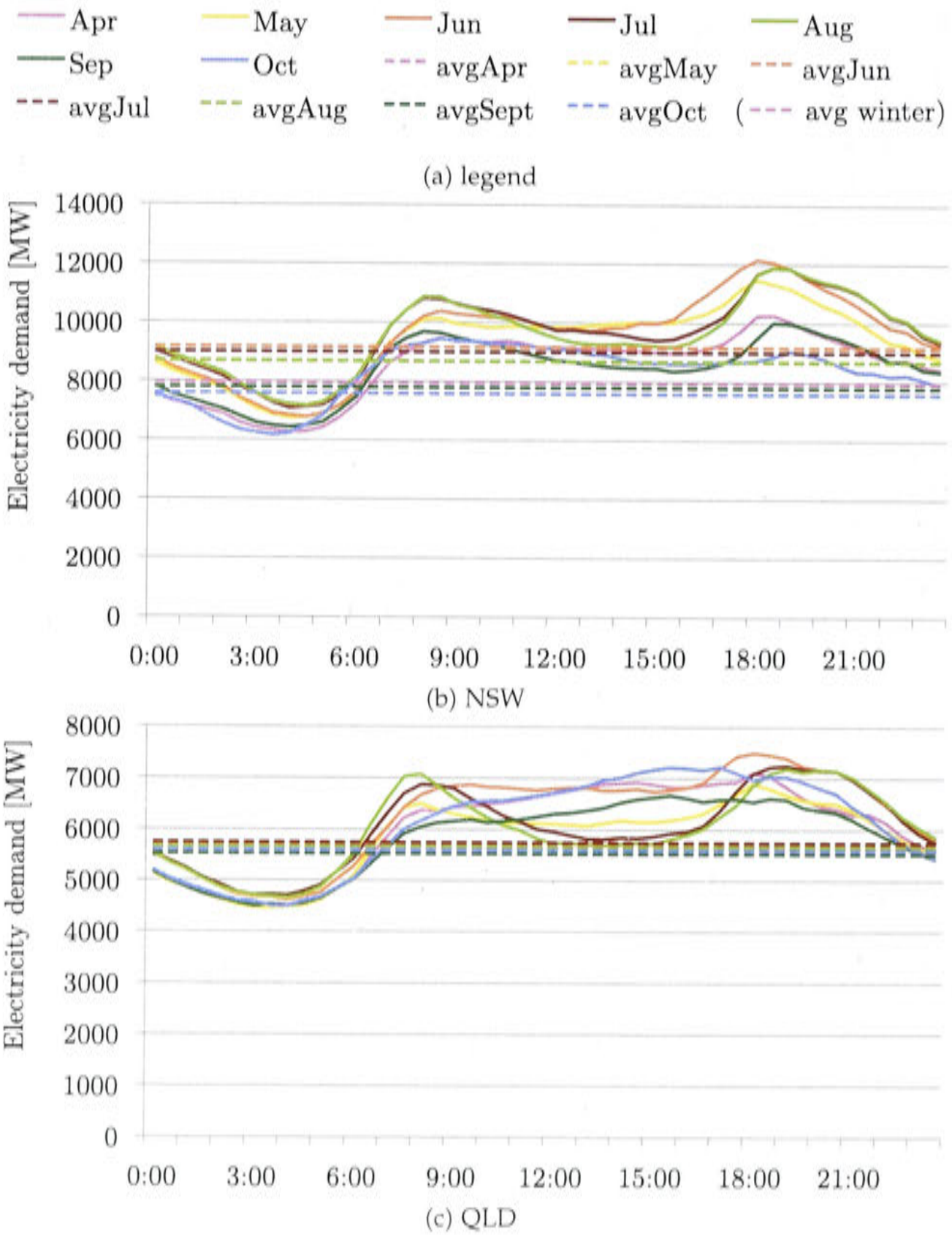

(a) legend

(b) NSW

(c) QLD

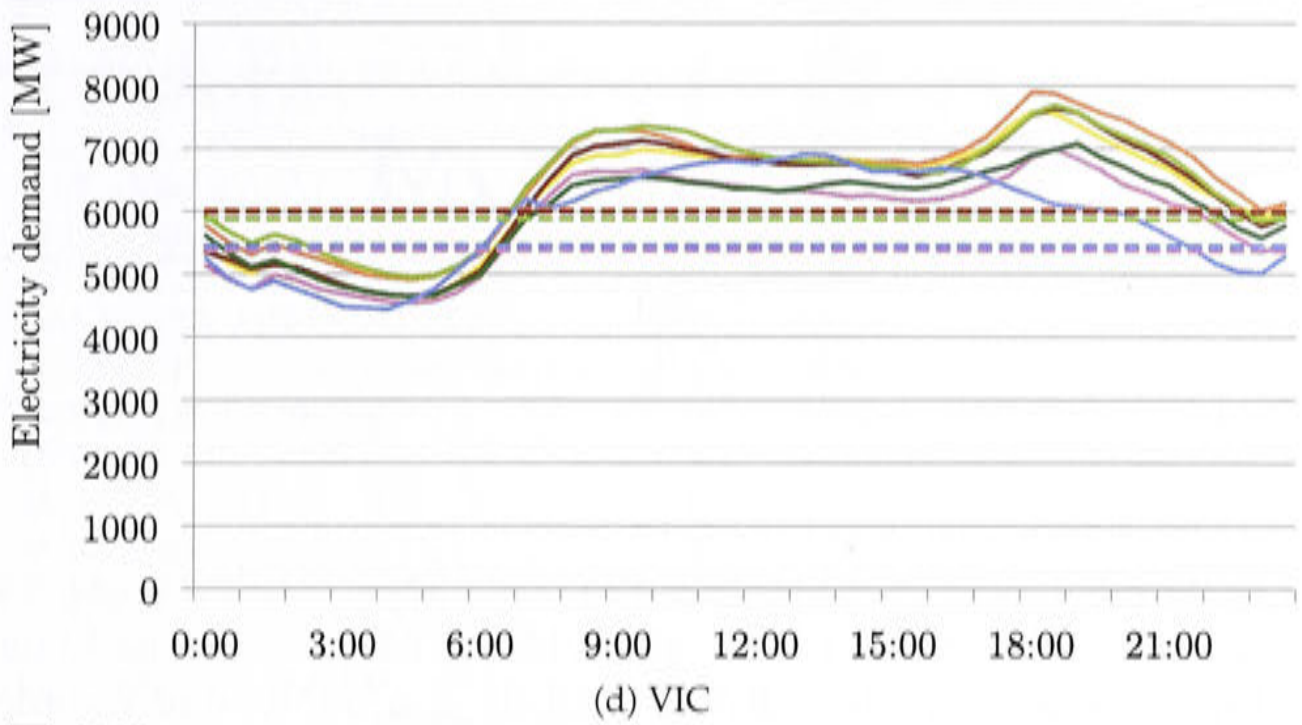

(d) VIC

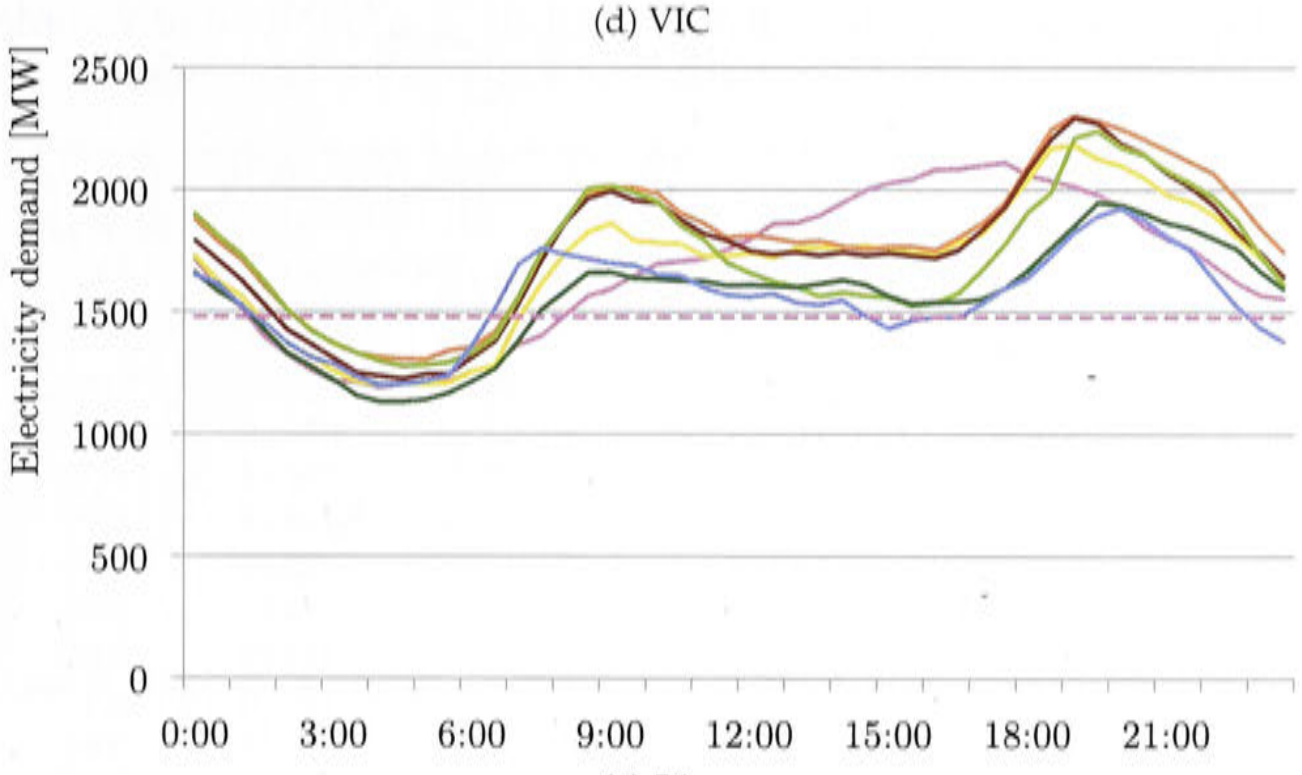

(e) SA

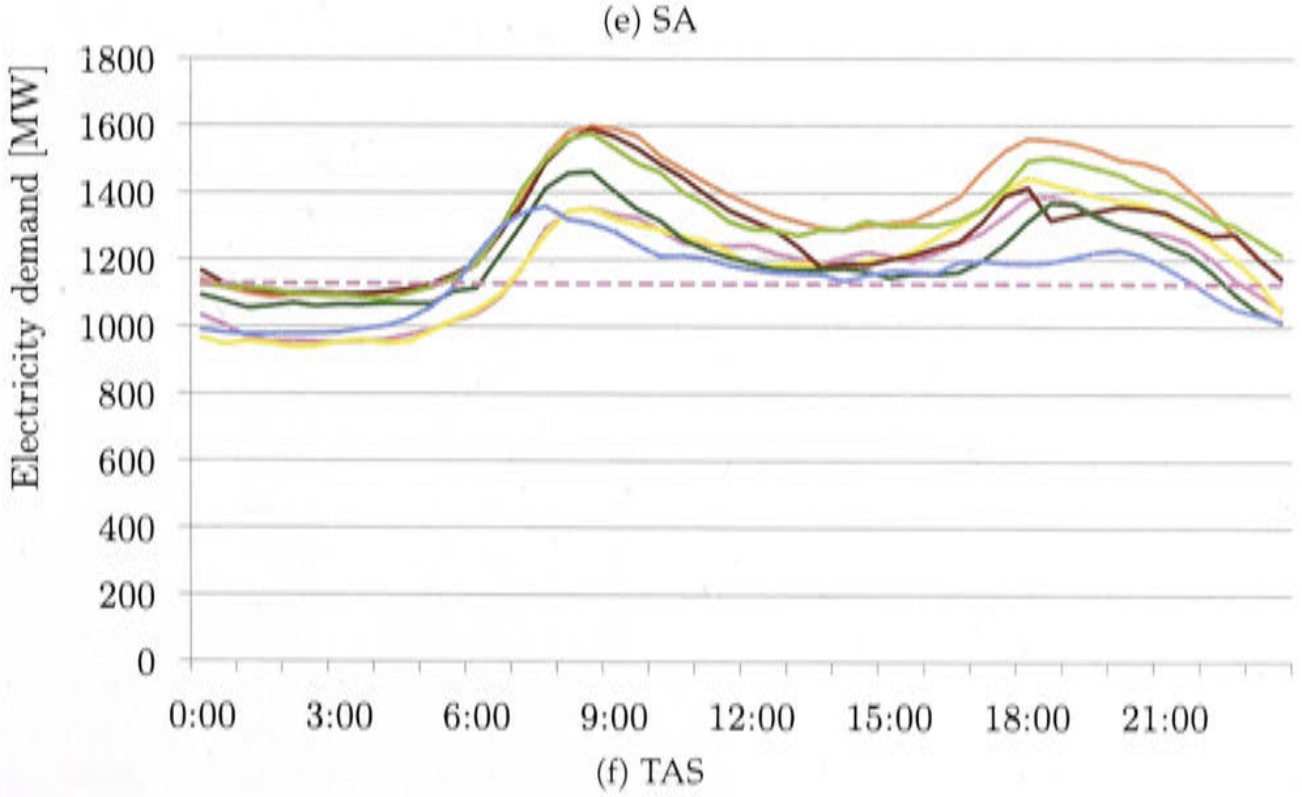

(f) TAS

Figure A.4: Average winter electricity demand in each state on the NEM (2012).

Weather data from BOM

Table B.1 shows all stations weather data files could be created from. Almost every station recorded hourly weather conditions including temperatures and humidities. The solar exposure data was recorded half-hourly and the type of recorded solar radiation varied. The variations are marked by flag 1 to 3 as explained in section 3.3.

location	flag	latitude	longitude	last year of record
HALLS CREEK APT (WA)	1	-18.23	-127.66	1980
FORREST AERO (WA)	1	-30.84	-128.11	1980
OODNADATTA APT (SA)	1	-27.56	-135.45	1980
LONGREACH AERO (QLD)	1	-23.44	-144.28	1980
WILLIAMTOWN RAAF (NSW)	1	-32.79	-151.84	1979
WILLIS ISLAND (QLD)	1	-16.29	-149.97	1979
BROOME AIRPORT (WA)	2	-17.95	-122.24	2012
LEARMONTH APT (WA)	2	-22.24	-114.10	2012
GERALDTON APT COMP. (WA)	2	-28.80	-114.70	2006
GERALDTON APT (WA)	2	-28.80	-114.70	2012
KALGOORLIE-BOULDER APT (WA)	2	-30.78	-121.45	2012
DARWIN APT (NT)	2	-12.42	-130.89	2012
TENNANT CREEK APT (NT)	2	-19.64	-134.18	2006
ALICE SPRINGS APT (NT)	2	-23.80	-133.89	2012
WOOMERA AERODROME (SA)	2	-31.16	-136.81	2012
ADELAIDE APT (SA)	2	-34.95	-138.52	2012
MOUNT GAMBIER AERO (SA)	2	-37.75	-140.77	2006
CAIRNS AERO (QLD)	2	-16.87	-145.75	2004
ROCKHAMPTON AERO (QLD)	2	-23.38	-150.48	2012
COBAR MO (NSW)	2	-31.48	-145.83	2012[1]
WAGGA WAGGA AMO (NSW)	2	-35.16	-147.46	2012
MILDURA APT (VIC)	2	-34.24	-142.09	2012
MELBOURNE APT (VIC)	2	-37.67	-144.83	2012
CAPE GRIM RADIATION (TAS)	2	-40.68	-144.69	2012[2]
COCOS ISLAND APT	2	-12.19	-96.83	2012
PORT HEDLAND APT (WA)	3	-20.37	-118.63	1980
CARNARVON APT (WA)	3	-24.89	-113.67	1995
MEEKATHARRA APT (WA)	3	-26.61	-118.54	1995
PERTH APT (WA)	3	-31.93	-115.98	1980

[1] only 2012

[2] no ambient conditions

location	flag	latitude	longitude	last year of record
PEARCE RAAF WA)	3	-31.67	-116.02	1975
ALBANY APT COMP (WA)	3	-34.94	-117.80	1980
ESPERANCE (WA)	3	-33.83	-121.89	1995
BRISBANE AERO (QLD)	3	-27.42	-153.11	1995
SYDNEY APT AMO (NSW)	3	-33.95	-151.17	1994
CANBERRA APT COMP (ACT)	3	-35.30	-149.20	1994
MELBOURNE REGIONAL OFF (VIC)	3	-37.81	-144.97	1980
LAVERTON RAAF (VIC)	3	-37.86	-144.76	1980
HOBART APT (TAS)	3	-42.83	-147.50	1980
MAWSON (SA)	3	-67.60	-62.88	1978
MACQUARIE ISLAND	3	-54.50	-158.94	1980
CASEY (THE TUNNEL) (?)	3	-66.28	-110.53	1977

Table B.1: Weather stations with recorded solar exposure data. APT=AIRPORT, COMP=COMPARISON, OFF=OFFICE

For locations marked with flag=3, the direct radiation on the horizontal ($G_{direct,hor}$) and the direct beam radiation (G_{direct}) had to be calculated from the total radiation on the horizontal ($G_{tot,hor}$) and from the diffuse radiation on the horizontal ($G_{diff,hor}$) using equations B.1 and B.2 with ϕ being the solar zenith angle.

$$G_{direct,hor} = G_{tot,hor} - G_{diff,hor} \tag{B.1}$$

$$G_{direct} = \frac{G_{direct,hor}}{\cos\phi} \tag{B.2}$$

The zenith angle was calculated as in equation B.3 by Kalogirou [2009].

$$\cos\phi = \sin l \sin\delta + \cos l \cos\delta \cos h \tag{B.3}$$

In equation B.3 l is the latitude (positive north, negative south), hr is the hour angle (equation B.5) and δ being the declination angle (equation B.4). The day of the year is represented by n and AST stands for the apparent solar time.

$$\delta = 23.45 \sin\left(\frac{360}{365}(284+n)\right) \tag{B.4}$$

$$hr = (AST - 12)15^\circ \tag{B.5}$$

Solar electric air-conditioning system

C.1 Population in the 6 climate zones of Australia

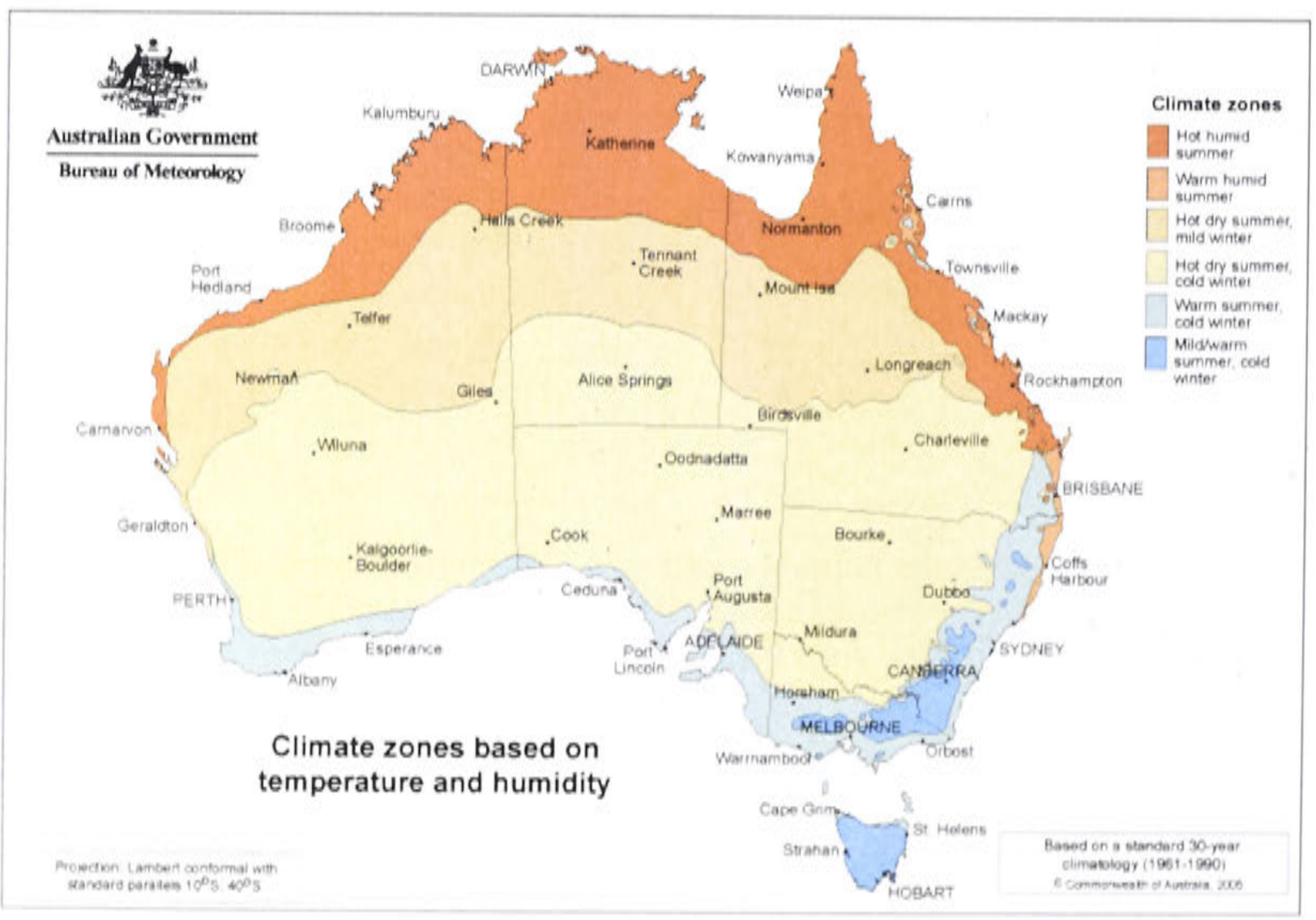

Figure C.1: Classification of climate zones Bureau of Meteorology (BOM) [2013b]

The Bureau of Meteorology divided Australia into zones characterized by temperatures and humidity. The cities or towns chosen for the simulation throughout the thesis are places from each climate zone. Air-conditioning systems were modeled for Melbourne and Canberra even though both lie in the same zone "mild/warm summer, cold winter". This is because Canberra is the Australian Capital and repre-

sents an own state. Furthermore, its climate differs from Melbourne having a larger diurnal temperature swing and being continental.

Table C.1 shows the population density in each climate zone. It consists of cities and towns with a population above 20 000 with the exception of Broome and Tennant Creek. The population in each climate zone is used to derive the weighing factors for the cost and greenhouse gas emission of a reference air-conditioning system (see chapter 5.3). Australia's population to date are 23 million people. Hence, approximately 83% of the total population are covered in this table.

Climate zone & city	Population per city	Population per climate zone
Hot humid summer		811,136
Darwin	131,678	
Broome	13,945	
Cairns	142,528	
Townsville	171,971	
Rockhampton	77,704	
Mackay	81,594	
Bundaberg	69,805	
Hervey Bay	50,431	
Gladstone - Tannum Sands	44,355	
Maryborough	27,125	
Warm humid summer		3,323,153
Brisbane	2,189,878	
Port Macquarie	43,587	
Gold Coast	590,889	
Sunshine Coast	285,169	
Coffs Harbour	66,610	
Lismore	29,443	
Taree	26,379	
Neslon Bay - Corlette	26,109	
Ballina	24,533	
Gymie	20,308	
Forster	20,248	
Hot dry summer, mild winter		61,728
Mount Isa	22,098	
Tennant Creek	1,600	
Geraldton	38,030	
Hot dry summer, cold winter		378,934
Alice Springs	28,517	
Mildura	48,783	
Dubbo	35,898	
Bendigo	89,666	
Griffith	18,700	
Shepparton	48,114	
Wagga	53,832	
Kalgoorlie - Boulder	32,787	
Wyalla	22,637	
Warm summer cold winter		9,244,374
Sydney	4,667,283	

Climate zone & city	Population per city	Population per climate zone
Toowoomba (QLD)	110,472	
Newcastle	418,958	
Wollongong	282,099	
Adelaide	1,277,174	
Perth	1,897,548	
Albury	84,982	
Bunbury (WA)	69,637	
Tamworth	40,832	
Orange	38,516	
Mittagong	36,402	
Nowra	34,798	
Bathurst	34,124	
Warnambool	33,204	
Ellenbrook	33,133	
Busselton	32,471	
Albany	31,978	
Mount Gambier	28,471	
Victor Harbor - Goolwa	24,635	
Armidale	23,665	
Morisset	22,718	
Cessnock	21,274	
Mild/warm summer, cold winter		4,689,707
Melbourne	4,246,345	
Melton	51,907	
Geelong	179,042	
Ballarat	95,007	
Traralgon - Morwell	40,602	
Warragul - Drouin	31,280	
Goulburn	22,429	
Ocean Grove	23,095	
Canberra	411,609	411,609
Australia		18,920,641

Table C.1: Population in each climate zone

C.2 Battery status

The following figures are histograms on the battery status supporting the photovoltaic solar array and the reference reverse cycle air-conditioning system in chapter 6.3. The states represent the percentage of full charge from 0% to 100% in 10% steps. Figure C.3 shows the frequency of the battery states when including DHW.

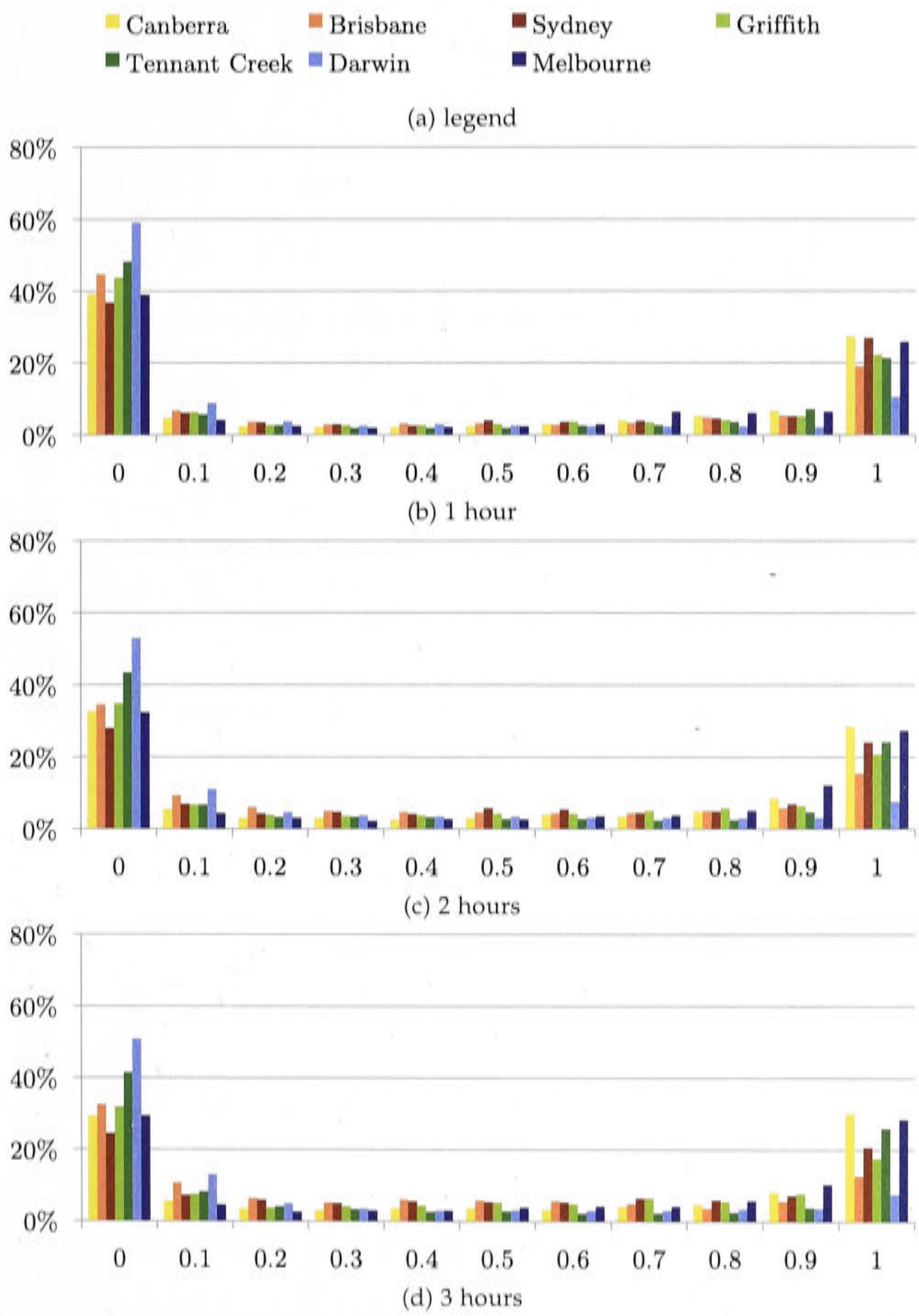

(a) legend

(b) 1 hour

(c) 2 hours

(d) 3 hours

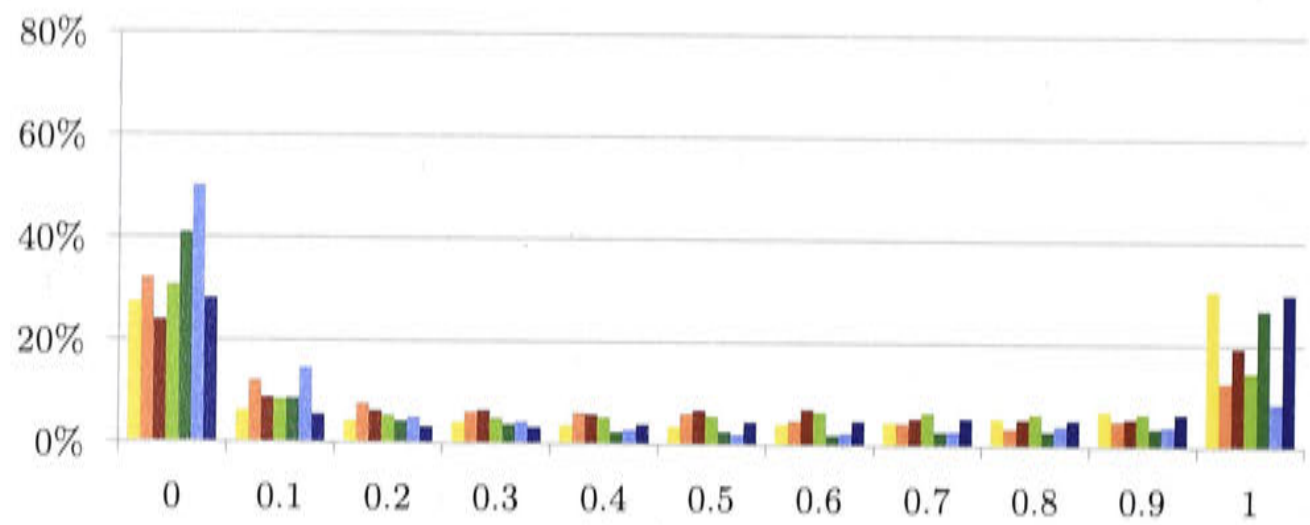

(e) 4 hours

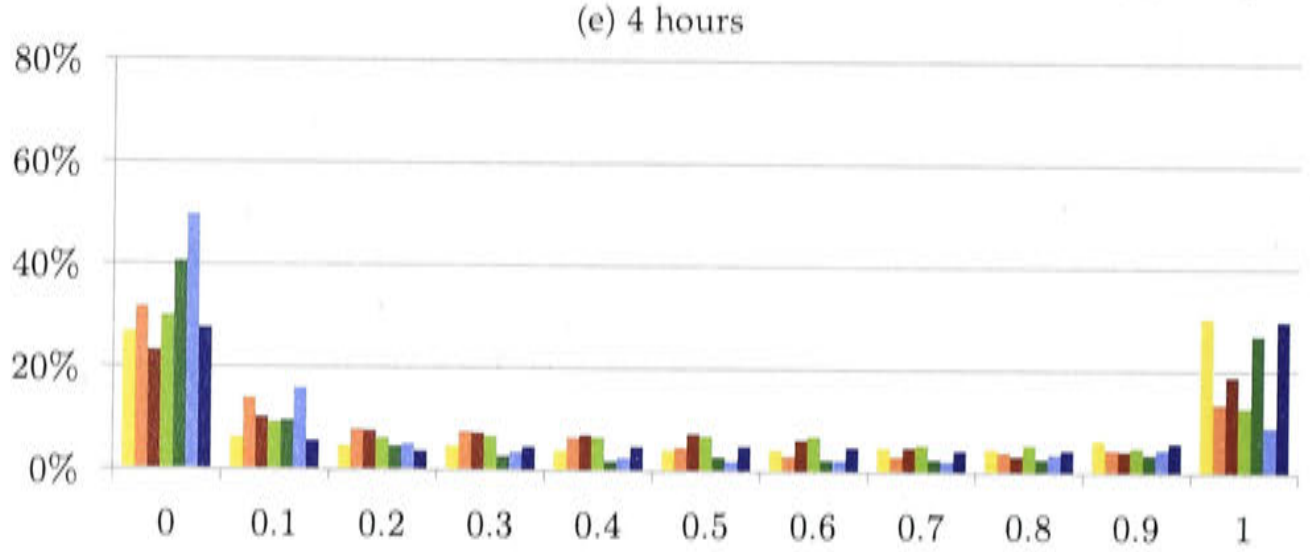

(f) 5 hours

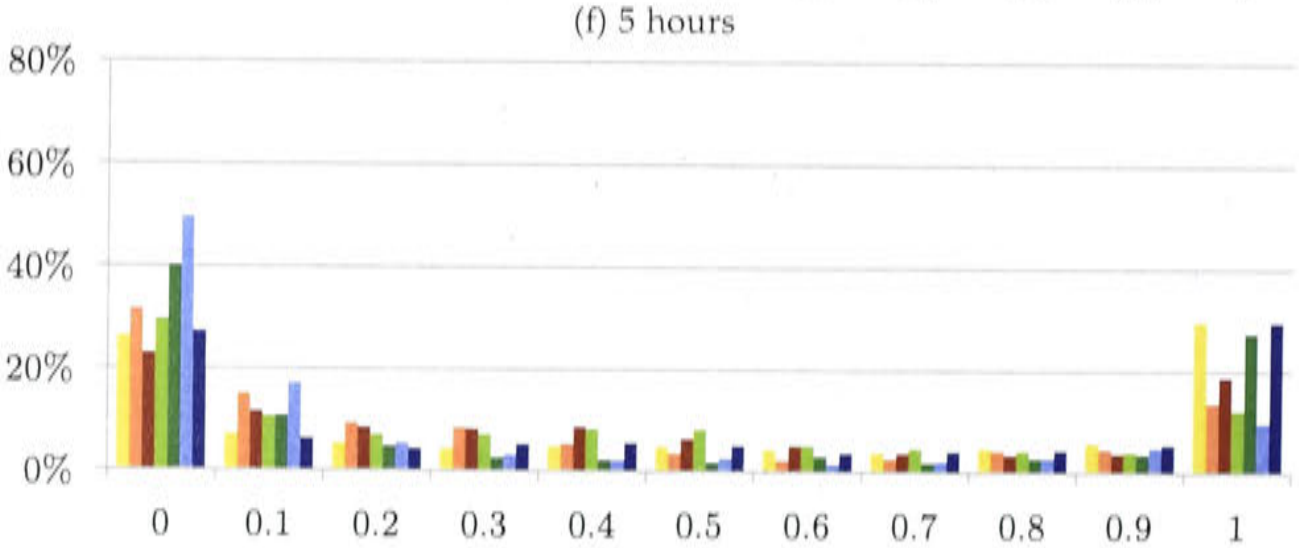

(g) 6 hours

Figure C.2: Frequency analysis of the battery's state of charge

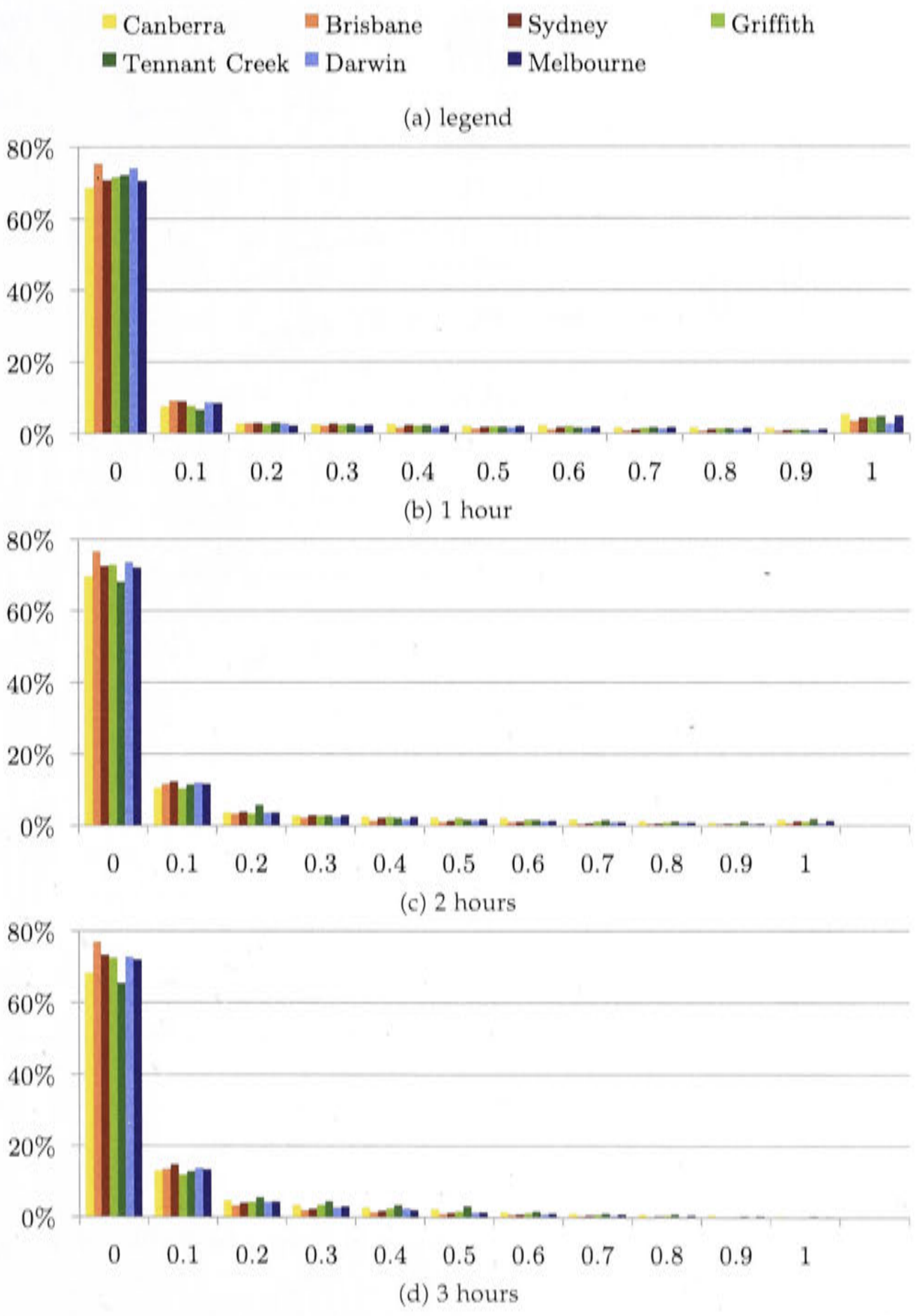

(a) legend

(b) 1 hour

(c) 2 hours

(d) 3 hours

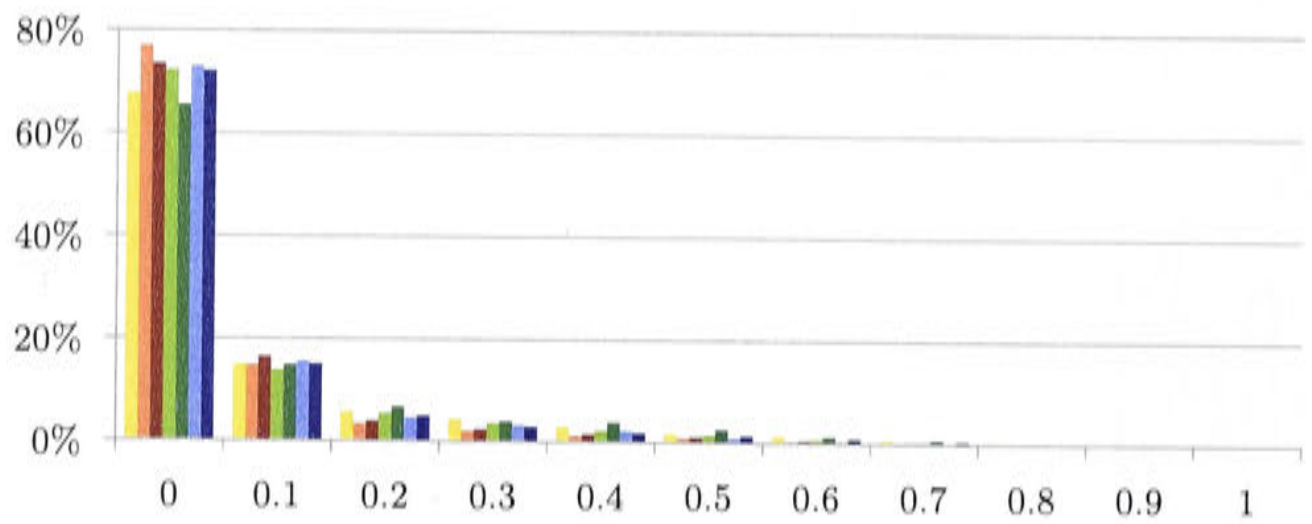

(e) 4 hours

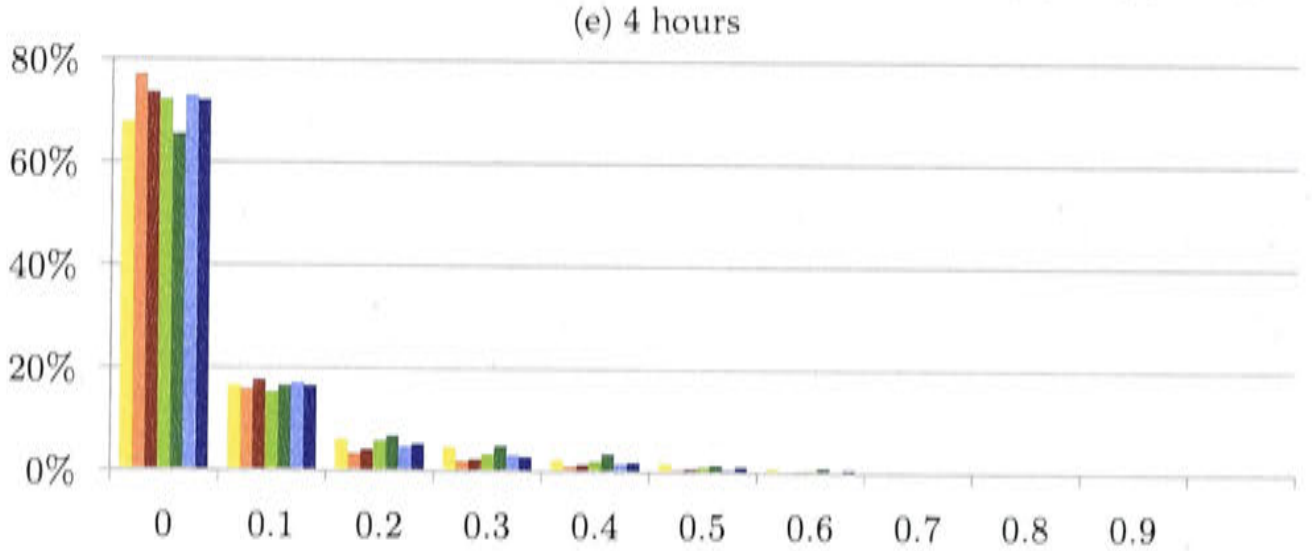

(f) 5 hours

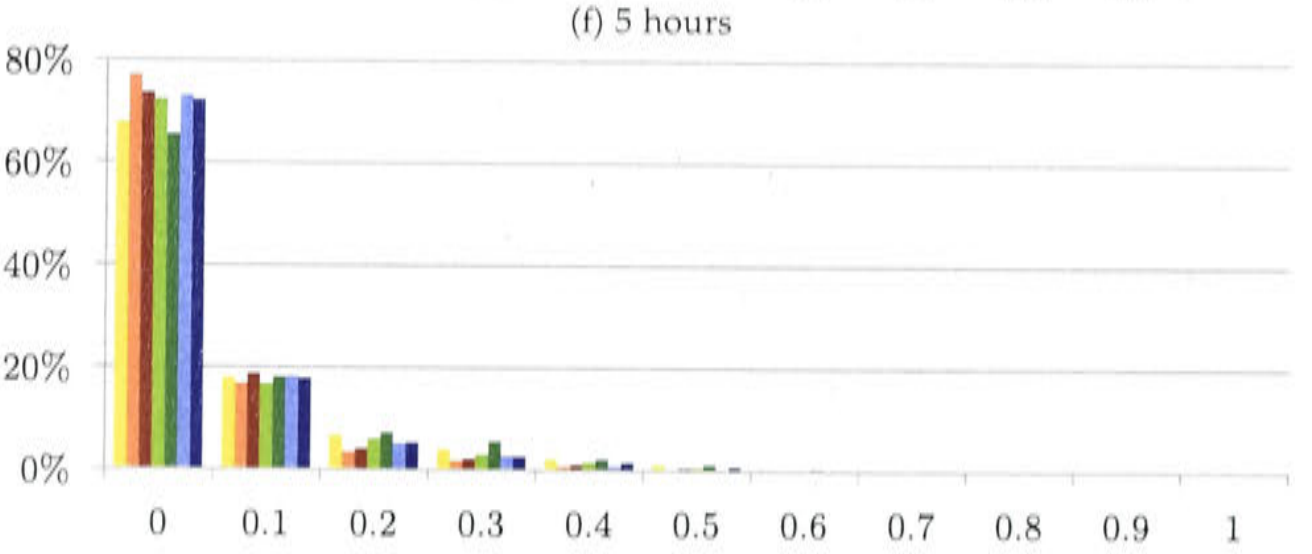

(g) 6 hours

Figure C.3: Frequency analysis of the battery's state of charge when DHW is included

C.3 Saved specific greenhouse gas emissions of the battery supported PV system

The following graphs show the saved specific greenhouse gas emissions of the battery supported PV and reverse cycle air conditioning system compared to the reference system without any renewable energy source from chapter 5. The back up electricity source here is either the electricity grid, if the system is grid connected, or a diesel generator.

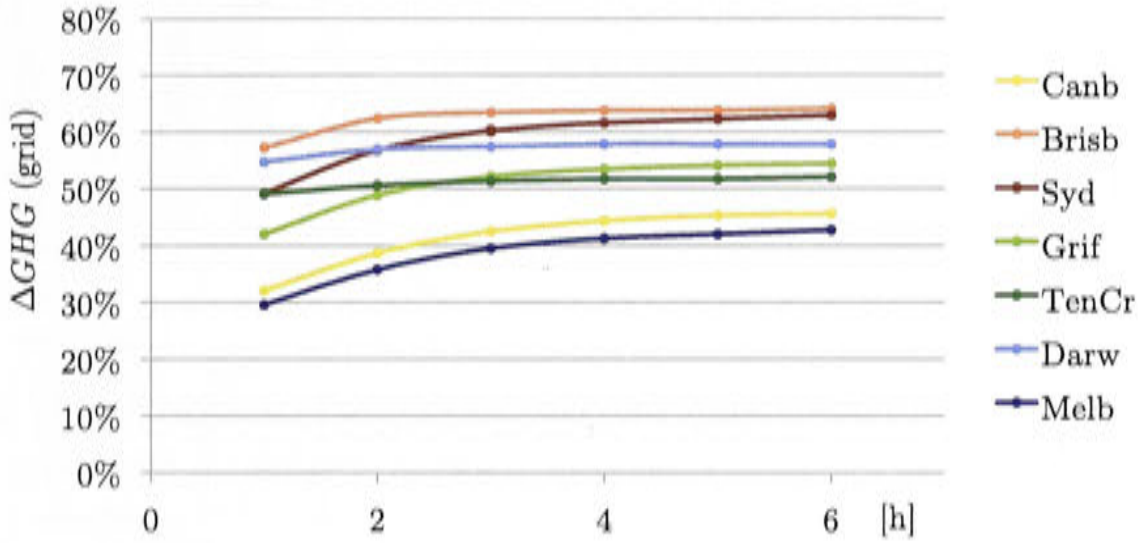

(a) backup grid

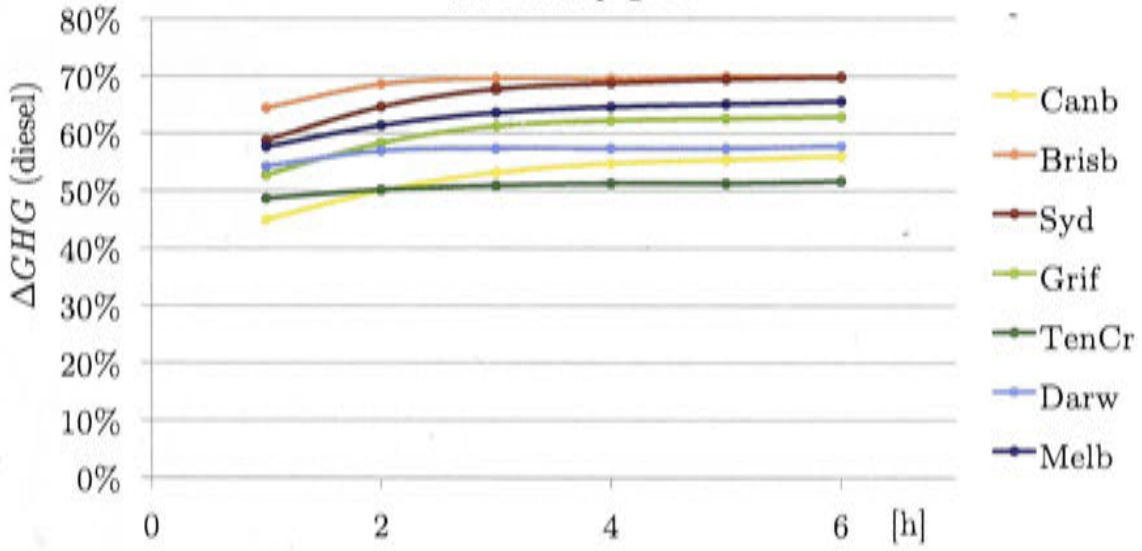

(b) backup diesel

Figure C.4: Saved specific greenhouse gas emissions ΔGHG.

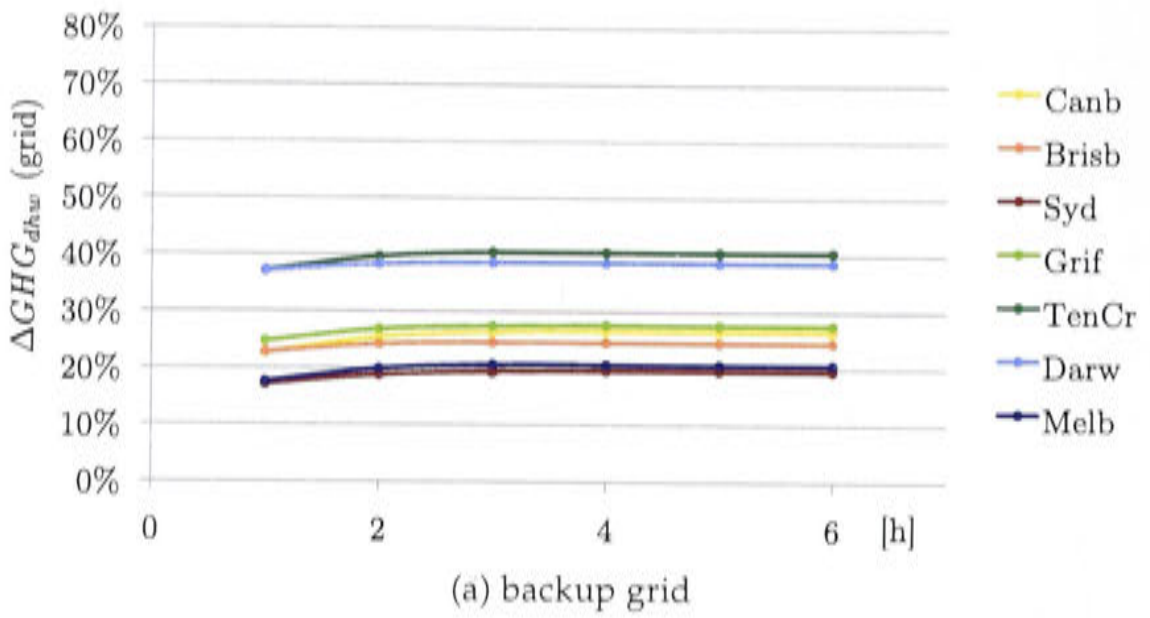

(a) backup grid

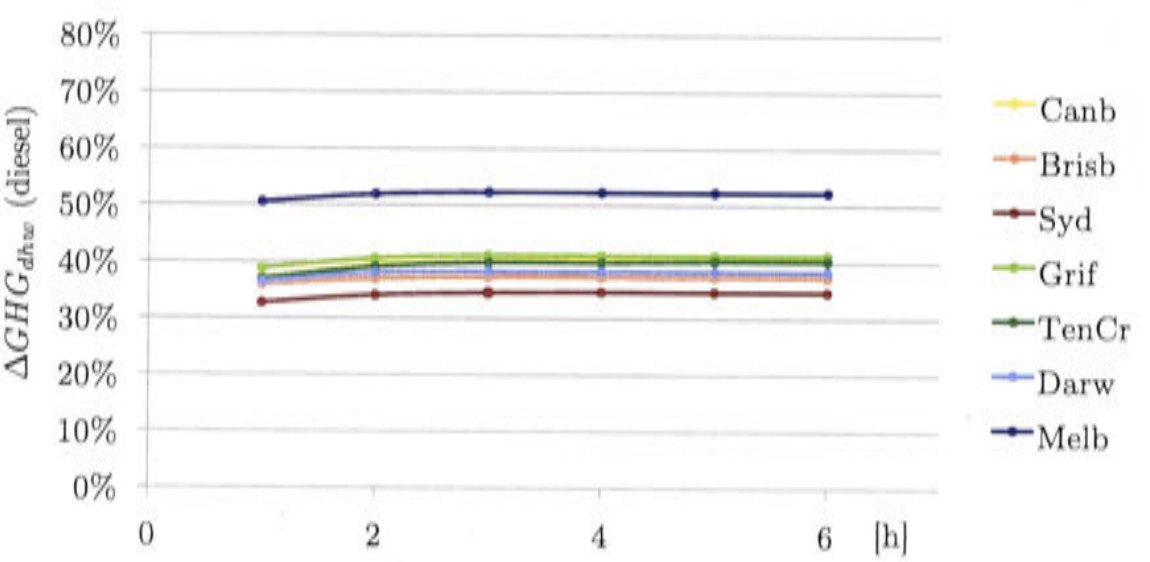

(b) backup diesel

Figure C.5: Saved specific greenhouse gas emissions ΔGHG_{dhw} including DHW.

C.4 The OPF for each climate of the battery supported PV system

These figures are included to understand what the OPF and OPF_{dhw} for the analyzed systems in section 6.3 is comprised of. The following figures split up the OPF in cost, GHG and comfort with and without DHW. Figures C.6 and C.7 include the electricity grid as a backup source, whereas C.8 and C.9 uses the diesel generator as backup electricity source.

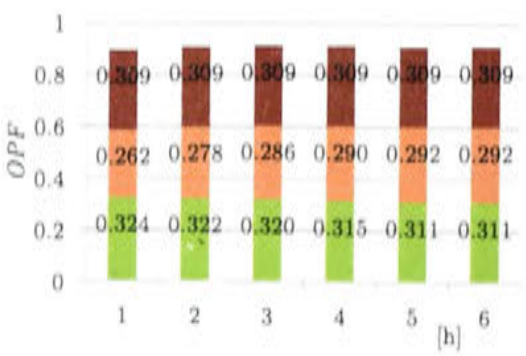

(a) Canberra

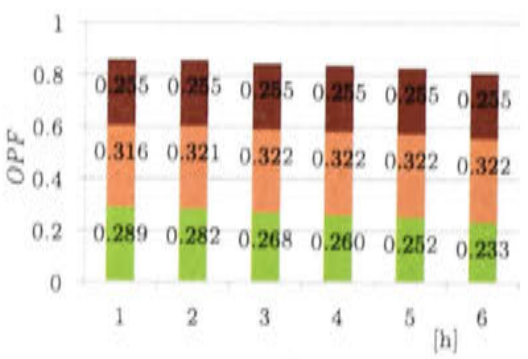

(b) Brisbane

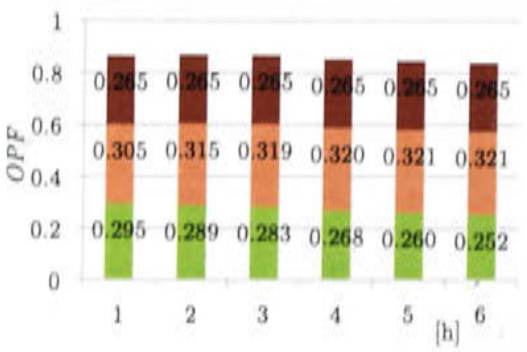

(c) Sydney

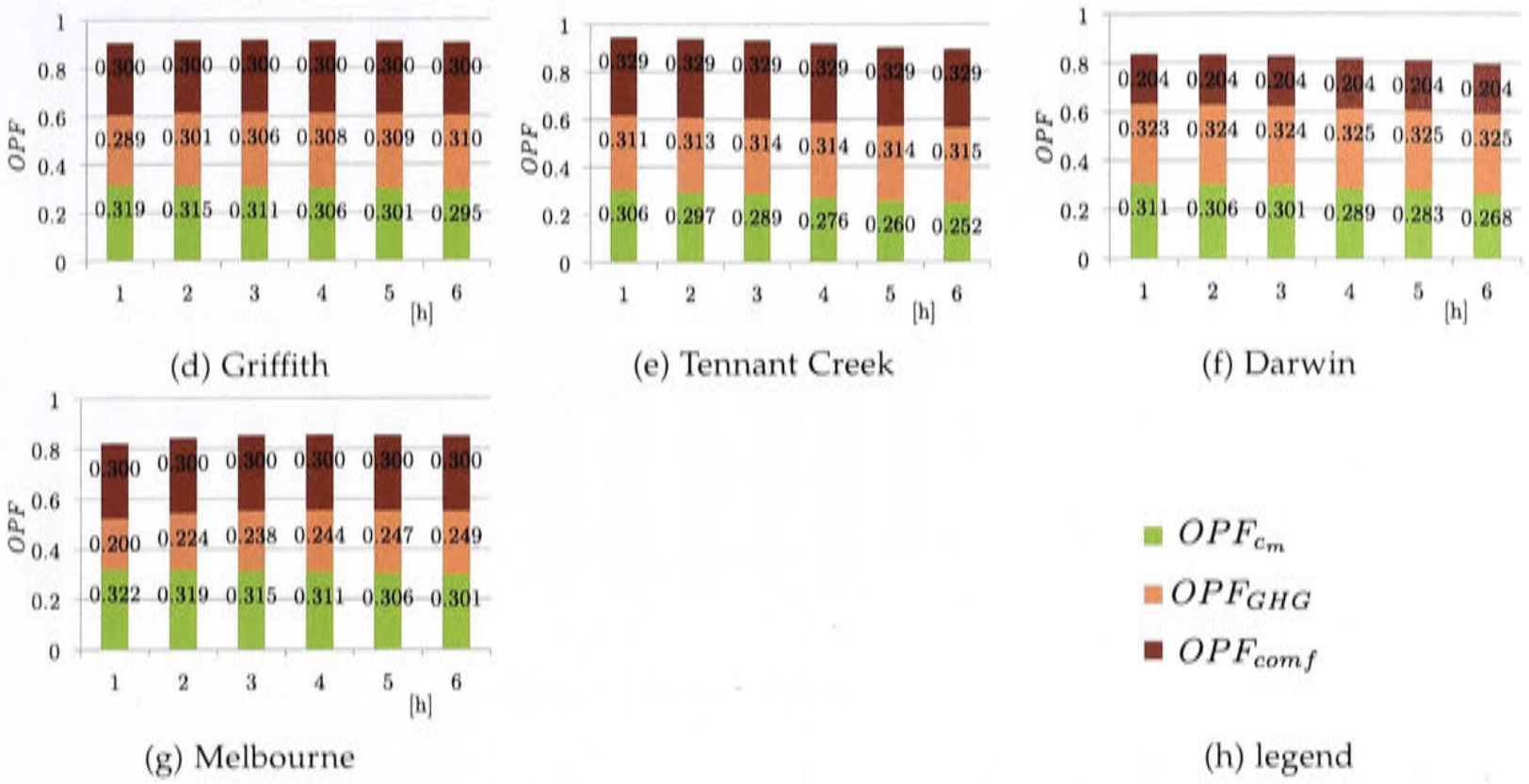

(d) Griffith (e) Tennant Creek (f) Darwin

(g) Melbourne (h) legend

Figure C.6: The OPF for the PV assisted system supported by a battery for each climate and storage capacity (electricity grid as backup source)

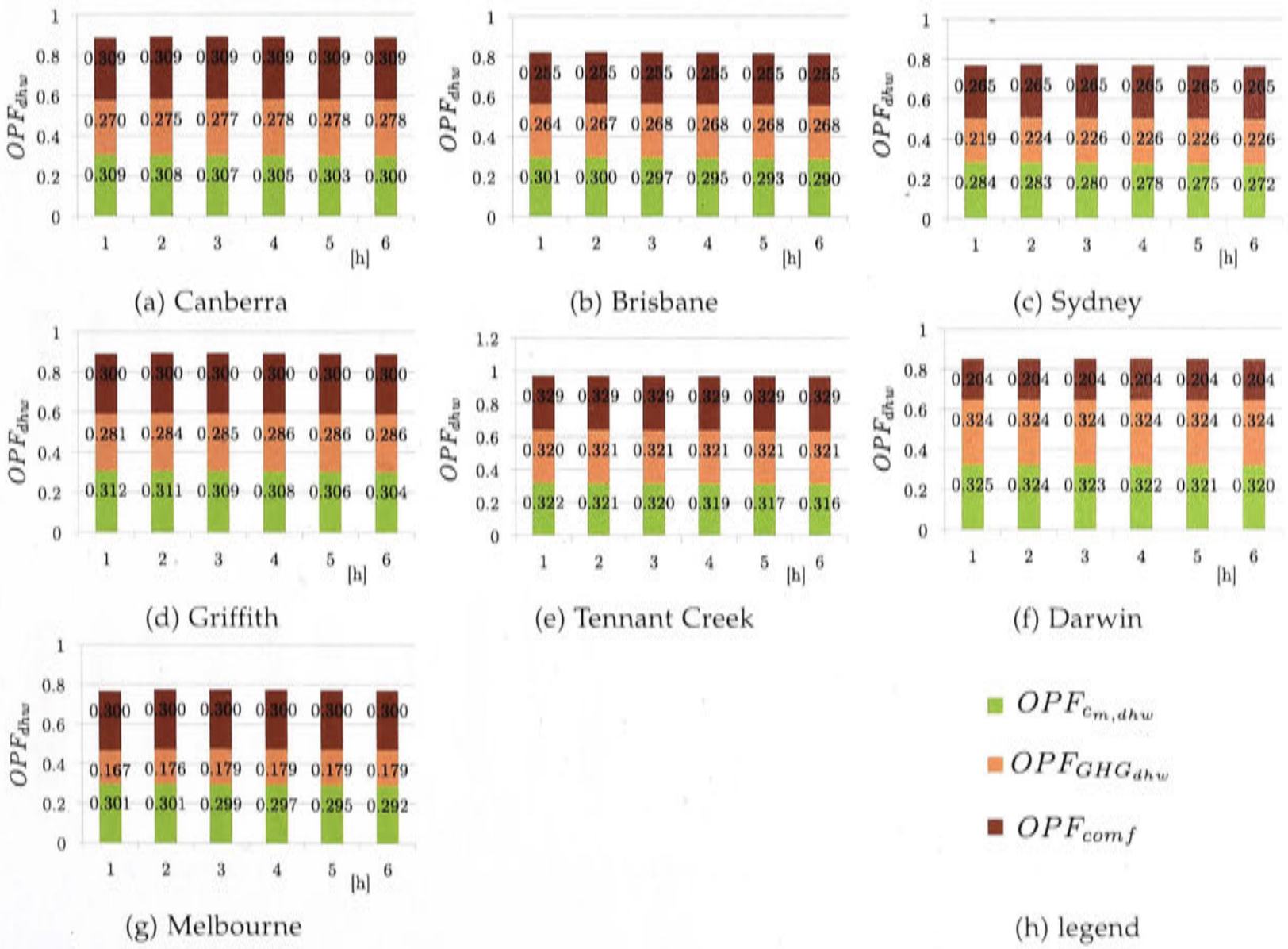

(a) Canberra (b) Brisbane (c) Sydney

(d) Griffith (e) Tennant Creek (f) Darwin

(g) Melbourne (h) legend

Figure C.7: The OPF for the PV assisted system supported by a battery for each climate and storage capacity including DHW (electricity grid as backup source)

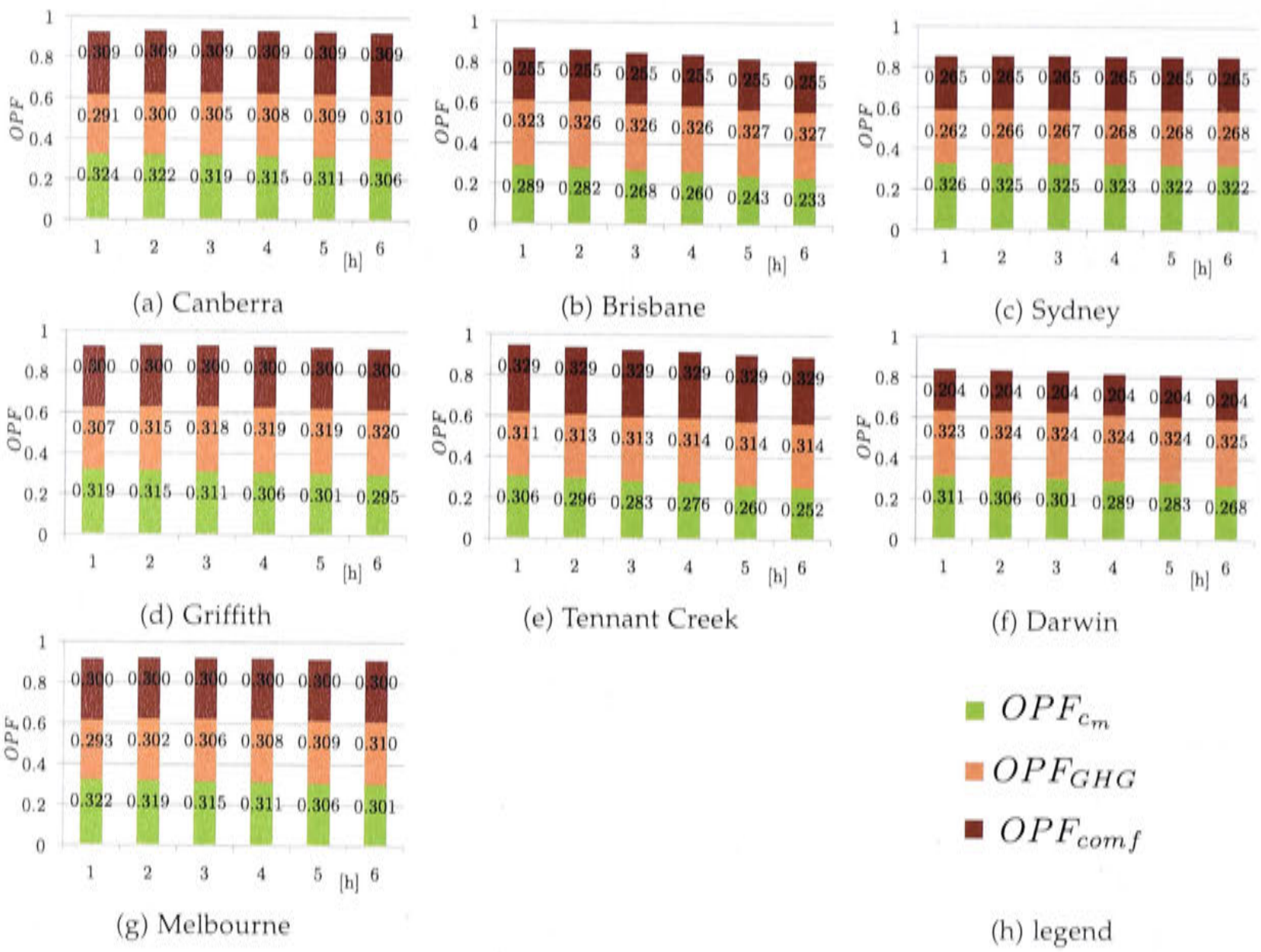

Figure C.8: The OPF for the PV assisted system supported by a battery for each climate and storage capacity (diesel generator as backup source)

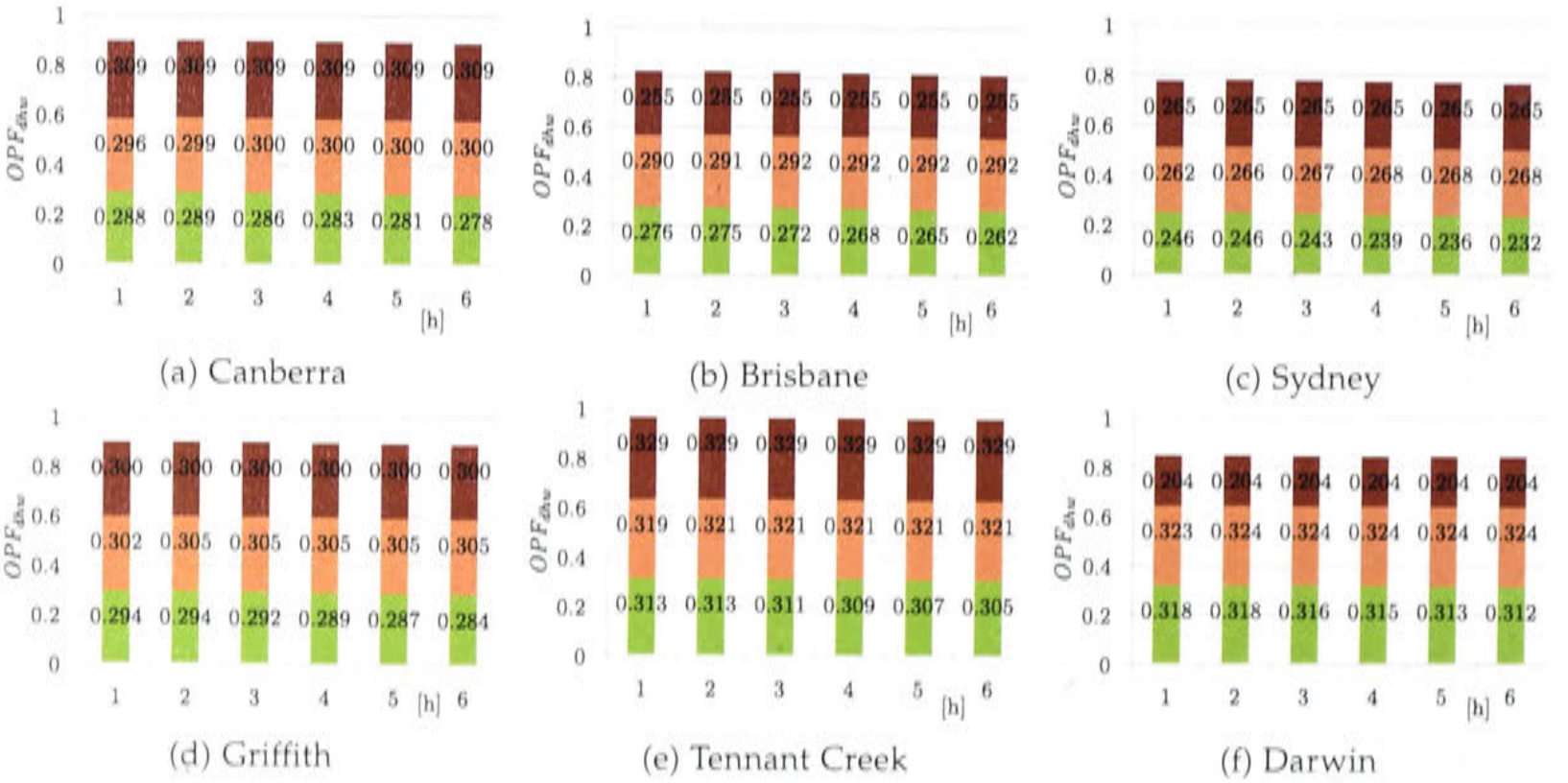

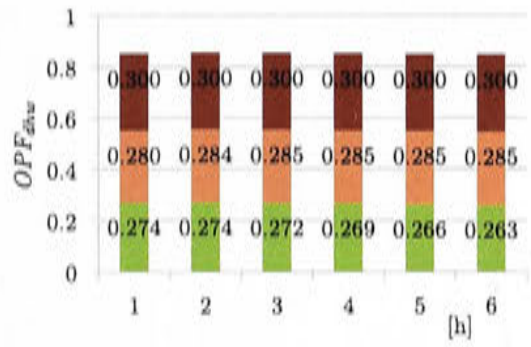

(g) Melbourne

(h) legend

Figure C.9: The OPF for the PV assisted system supported by a battery for each climate and storage capacity including DHW (diesel generator as backup source)

Solar thermal cooling, heating and DHW system - base case

D.1 Incidence angle modifiers evacuated tubes

For the incidence angle modifiers the following values are assumed (source: personal correspondence with Mike Dennis).

Table D.1: Incidence Angle modifiers (IAM)

		Transversal										
		0	10	20	30	40	50	60	70	80	85	90
Longitude	0	1	1	1	1	1	1	1	1	0.9	0.6	0
	10	1	1.05	1.14	1.24	1.35	1.46	2	1.98	0.9	0	0
	20	1	1.05	1.14	1.24	1.35	1.46	2	1.98	0.9	0	0
	30	0.99	1.04	1.13	1.23	1.34	1.45	1.98	1.96	0.89	0	0
	40	0.98	1.03	1.12	1.22	1.32	1.43	1.96	1.94	0.88	0	0
	50	0.96	1.01	1.09	1.19	1.3	1.4	1.92	1.9	0.86	0	0
	60	0.93	0.98	1.06	1.15	1.26	1.36	1.86	1.84	0.84	0	0
	70	0.87	0.91	0.99	1.08	1.17	1.27	1.74	1.72	0.78	0	0
	80	0.76	0.8	0.87	0.94	1.03	1.11	1.52	1.5	0.68	0	0
	85	0.5	0.53	0.57	0.62	0.68	0.73	1	0.99	0.45	0.12	0
	90	0	0	0	0	0	0	0	0	0	0	0

D.2 Excursion: results of milestone C

The regression coefficients of milestone C of the absorption chiller on the Singapore test rig are presented in the following figures.

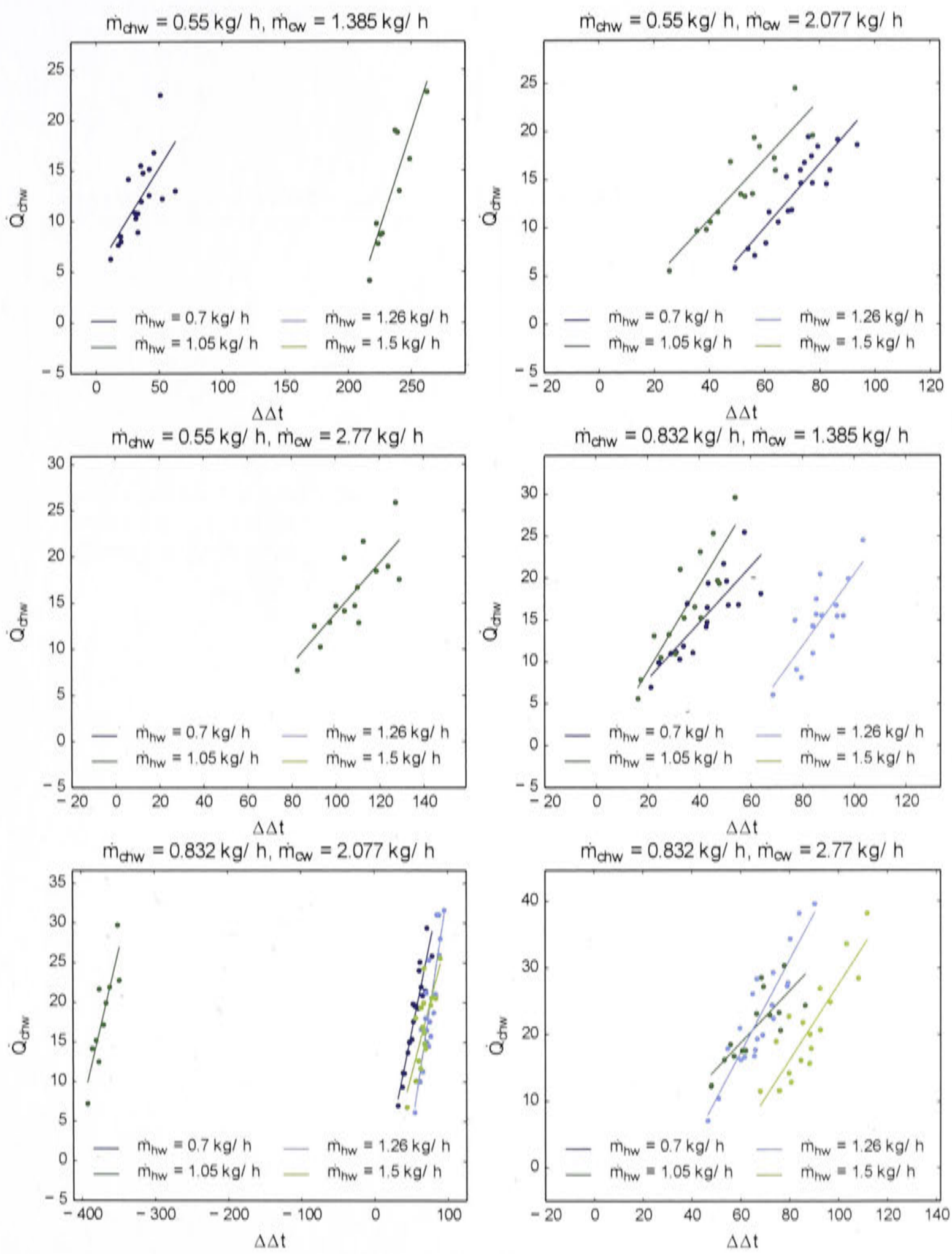
$\dot{m}_{chw}$ = 0.55 kg/ h, $\dot{m}_{cw}$ = 1.385 kg/ h
$\dot{m}_{chw}$ = 0.55 kg/ h, $\dot{m}_{cw}$ = 2.077 kg/ h
$\dot{m}_{chw}$ = 0.55 kg/ h, $\dot{m}_{cw}$ = 2.77 kg/ h
$\dot{m}_{chw}$ = 0.832 kg/ h, $\dot{m}_{cw}$ = 1.385 kg/ h
$\dot{m}_{chw}$ = 0.832 kg/ h, $\dot{m}_{cw}$ = 2.077 kg/ h
$\dot{m}_{chw}$ = 0.832 kg/ h, $\dot{m}_{cw}$ = 2.77 kg/ h
$\dot{Q}_{chw}$
ΔΔt
$\dot{m}_{hw}$ = 0.7 kg/ h
$\dot{m}_{hw}$ = 1.05 kg/ h
$\dot{m}_{hw}$ = 1.26 kg/ h
$\dot{m}_{hw}$ = 1.5 kg/ h

Figure D.1

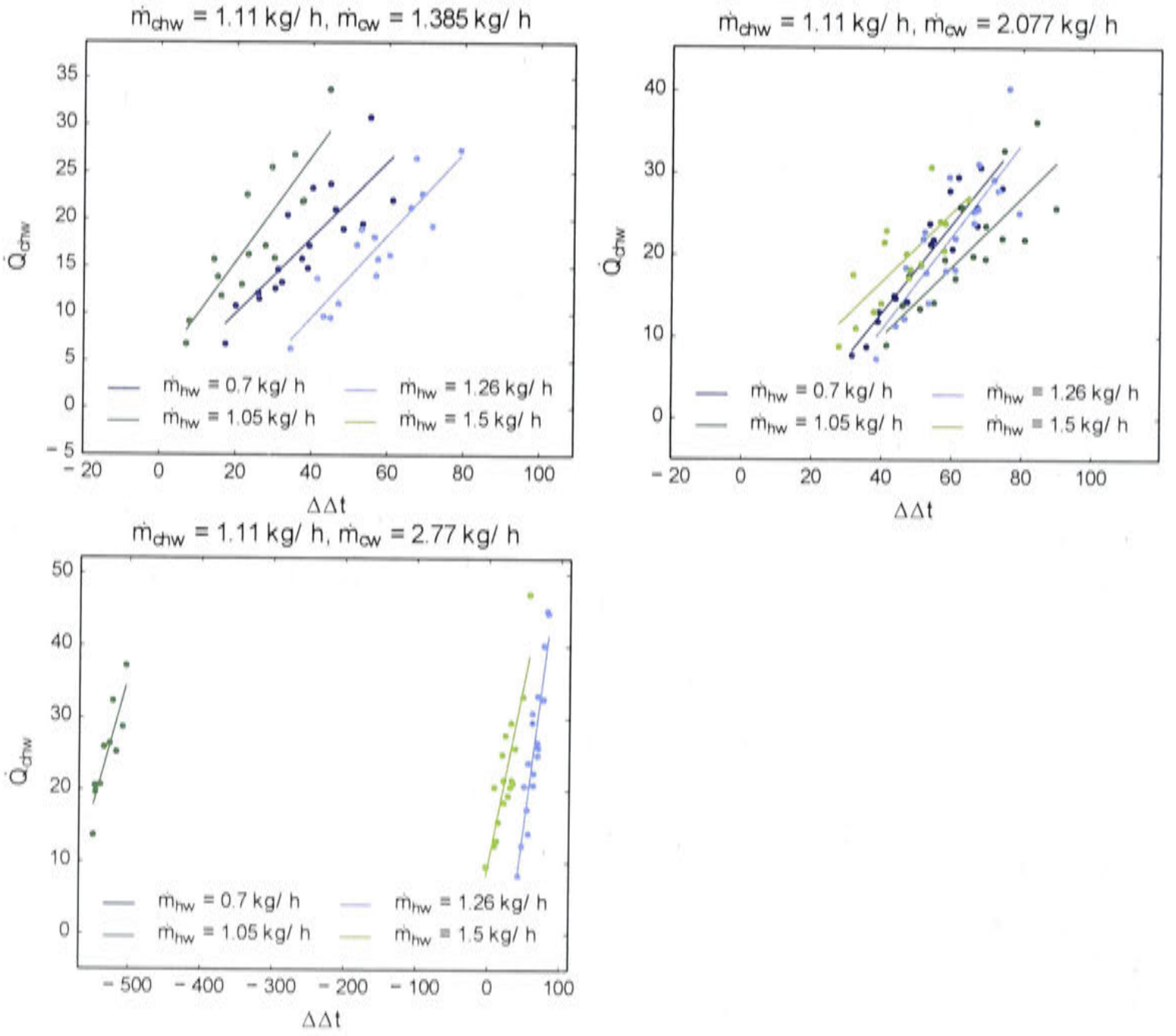

Figure D.1: Results $\dot{Q}_{chw}$ milestone C. x = chw or hw.

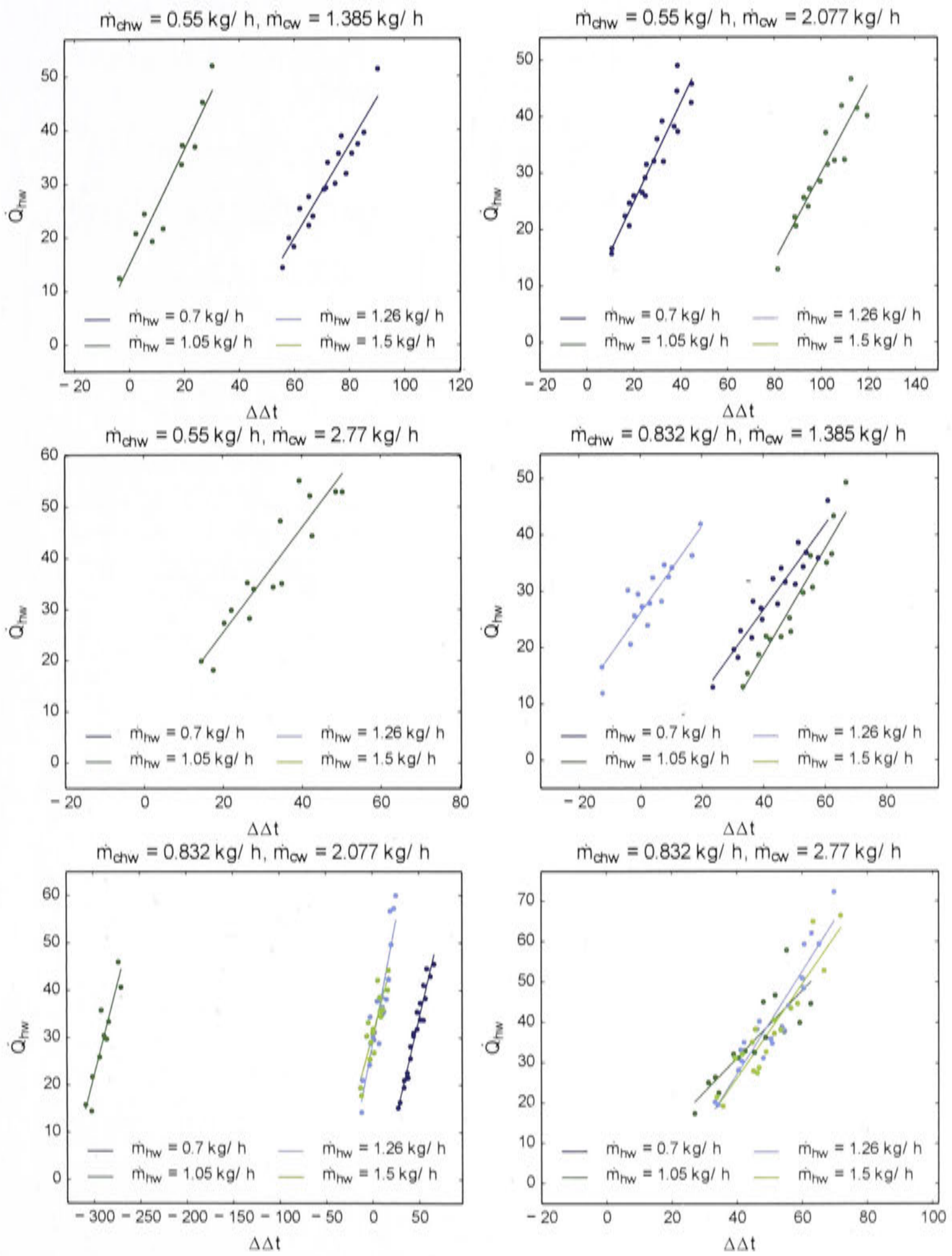
$\dot{m}_{chw}$ = 0.55 kg/ h, $\dot{m}_{cw}$ = 1.385 kg/ h
$\dot{m}_{chw}$ = 0.55 kg/ h, $\dot{m}_{cw}$ = 2.077 kg/ h
$\dot{m}_{chw}$ = 0.55 kg/ h, $\dot{m}_{cw}$ = 2.77 kg/ h
$\dot{m}_{chw}$ = 0.832 kg/ h, $\dot{m}_{cw}$ = 1.385 kg/ h
$\dot{m}_{chw}$ = 0.832 kg/ h, $\dot{m}_{cw}$ = 2.077 kg/ h
$\dot{m}_{chw}$ = 0.832 kg/ h, $\dot{m}_{cw}$ = 2.77 kg/ h
$\dot{Q}_{hw}$
ΔΔt
$\dot{m}_{hw}$ = 0.7 kg/ h
$\dot{m}_{hw}$ = 1.05 kg/ h
$\dot{m}_{hw}$ = 1.26 kg/ h
$\dot{m}_{hw}$ = 1.5 kg/ h

Figure D.2

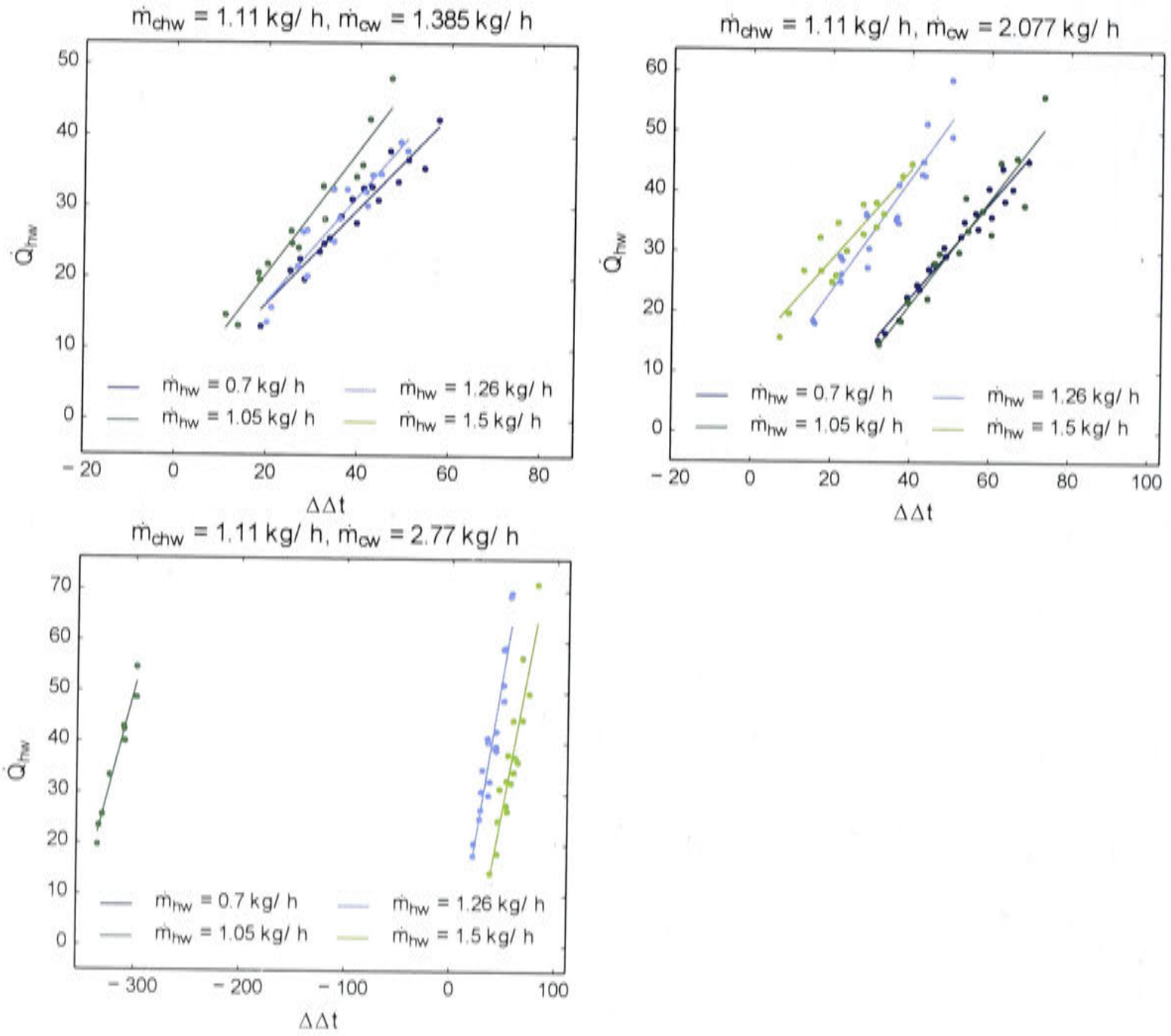

Figure D.2: Results $\dot{Q}_{hw}$ milestone C. x = chw or hw.

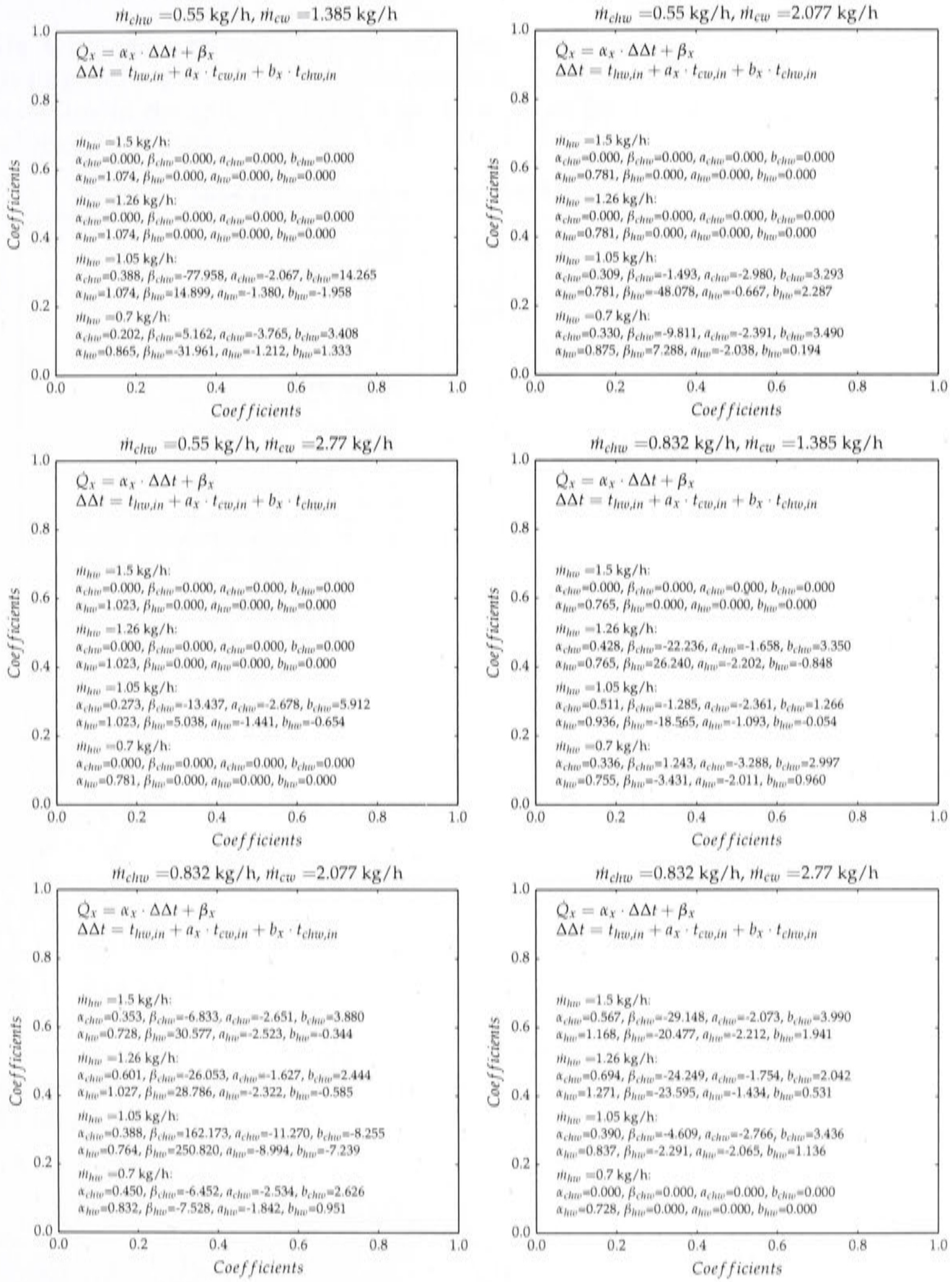
$\dot{m}_{chw}$ =0.55 kg/h, $\dot{m}_{cw}$ =1.385 kg/h
$\dot{Q}_X = \alpha_X \cdot \Delta\Delta t + \beta_X$
$\Delta\Delta t = t_{hw,in} + a_X \cdot t_{cw,in} + b_X \cdot t_{chw,in}$
$\dot{m}_{hw}$ =1.5 kg/h:
α_{chw}=0.000, β_{chw}=0.000, a_{chw}=0.000, b_{chw}=0.000
α_{hw}=1.074, β_{hw}=0.000, a_{hw}=0.000, b_{hw}=0.000
$\dot{m}_{hw}$ =1.26 kg/h:
α_{chw}=0.000, β_{chw}=0.000, a_{chw}=0.000, b_{chw}=0.000
α_{hw}=1.074, β_{hw}=0.000, a_{hw}=0.000, b_{hw}=0.000
$\dot{m}_{hw}$ =1.05 kg/h:
α_{chw}=0.388, β_{chw}=-77.958, a_{chw}=-2.067, b_{chw}=14.265
α_{hw}=1.074, β_{hw}=14.899, a_{hw}=-1.380, b_{hw}=-1.958
$\dot{m}_{hw}$ =0.7 kg/h:
α_{chw}=0.202, β_{chw}=5.162, a_{chw}=-3.765, b_{chw}=3.408
α_{hw}=0.865, β_{hw}=-31.961, a_{hw}=-1.212, b_{hw}=1.333
Coefficients
Coefficients
$\dot{m}_{chw}$ =0.55 kg/h, $\dot{m}_{cw}$ =2.077 kg/h
$\dot{Q}_X = \alpha_X \cdot \Delta\Delta t + \beta_X$
$\Delta\Delta t = t_{hw,in} + a_X \cdot t_{cw,in} + b_X \cdot t_{chw,in}$
$\dot{m}_{hw}$ =1.5 kg/h:
α_{chw}=0.000, β_{chw}=0.000, a_{chw}=0.000, b_{chw}=0.000
α_{hw}=0.781, β_{hw}=0.000, a_{hw}=0.000, b_{hw}=0.000
$\dot{m}_{hw}$ =1.26 kg/h:
α_{chw}=0.000, β_{chw}=0.000, a_{chw}=0.000, b_{chw}=0.000
α_{hw}=0.781, β_{hw}=0.000, a_{hw}=0.000, b_{hw}=0.000
$\dot{m}_{hw}$ =1.05 kg/h:
α_{chw}=0.309, β_{chw}=-1.493, a_{chw}=-2.980, b_{chw}=3.293
α_{hw}=0.781, β_{hw}=-48.078, a_{hw}=-0.667, b_{hw}=2.287
$\dot{m}_{hw}$ =0.7 kg/h:
α_{chw}=0.330, β_{chw}=-9.811, a_{chw}=-2.391, b_{chw}=3.490
α_{hw}=0.875, β_{hw}=7.288, a_{hw}=-2.038, b_{hw}=0.194
Coefficients
Coefficients
$\dot{m}_{chw}$ =0.55 kg/h, $\dot{m}_{cw}$ =2.77 kg/h
$\dot{Q}_X = \alpha_X \cdot \Delta\Delta t + \beta_X$
$\Delta\Delta t = t_{hw,in} + a_X \cdot t_{cw,in} + b_X \cdot t_{chw,in}$
$\dot{m}_{hw}$ =1.5 kg/h:
α_{chw}=0.000, β_{chw}=0.000, a_{chw}=0.000, b_{chw}=0.000
α_{hw}=1.023, β_{hw}=0.000, a_{hw}=0.000, b_{hw}=0.000
$\dot{m}_{hw}$ =1.26 kg/h:
α_{chw}=0.000, β_{chw}=0.000, a_{chw}=0.000, b_{chw}=0.000
α_{hw}=1.023, β_{hw}=0.000, a_{hw}=0.000, b_{hw}=0.000
$\dot{m}_{hw}$ =1.05 kg/h:
α_{chw}=0.273, β_{chw}=-13.437, a_{chw}=-2.678, b_{chw}=5.912
α_{hw}=1.023, β_{hw}=5.038, a_{hw}=-1.441, b_{hw}=-0.654
$\dot{m}_{hw}$ =0.7 kg/h:
α_{chw}=0.000, β_{chw}=0.000, a_{chw}=0.000, b_{chw}=0.000
α_{hw}=0.781, β_{hw}=0.000, a_{hw}=0.000, b_{hw}=0.000
Coefficients
Coefficients
$\dot{m}_{chw}$ =0.832 kg/h, $\dot{m}_{cw}$ =1.385 kg/h
$\dot{Q}_X = \alpha_X \cdot \Delta\Delta t + \beta_X$
$\Delta\Delta t = t_{hw,in} + a_X \cdot t_{cw,in} + b_X \cdot t_{chw,in}$
$\dot{m}_{hw}$ =1.5 kg/h:
α_{chw}=0.000, β_{chw}=0.000, a_{chw}=0.000, b_{chw}=0.000
α_{hw}=0.765, β_{hw}=0.000, a_{hw}=0.000, b_{hw}=0.000
$\dot{m}_{hw}$ =1.26 kg/h:
α_{chw}=0.428, β_{chw}=-22.236, a_{chw}=-1.658, b_{chw}=3.350
α_{hw}=0.765, β_{hw}=26.240, a_{hw}=-2.202, b_{hw}=-0.848
$\dot{m}_{hw}$ =1.05 kg/h:
α_{chw}=0.511, β_{chw}=-1.285, a_{chw}=-2.361, b_{chw}=1.266
α_{hw}=0.936, β_{hw}=-18.565, a_{hw}=-1.093, b_{hw}=-0.054
$\dot{m}_{hw}$ =0.7 kg/h:
α_{chw}=0.336, β_{chw}=1.243, a_{chw}=-3.288, b_{chw}=2.997
α_{hw}=0.755, β_{hw}=-3.431, a_{hw}=-2.011, b_{hw}=0.960
Coefficients
Coefficients
$\dot{m}_{chw}$ =0.832 kg/h, $\dot{m}_{cw}$ =2.077 kg/h
$\dot{Q}_X = \alpha_X \cdot \Delta\Delta t + \beta_X$
$\Delta\Delta t = t_{hw,in} + a_X \cdot t_{cw,in} + b_X \cdot t_{chw,in}$
$\dot{m}_{hw}$ =1.5 kg/h:
α_{chw}=0.353, β_{chw}=-6.833, a_{chw}=-2.651, b_{chw}=3.880
α_{hw}=0.728, β_{hw}=30.577, a_{hw}=-2.523, b_{hw}=-0.344
$\dot{m}_{hw}$ =1.26 kg/h:
α_{chw}=0.601, β_{chw}=-26.053, a_{chw}=-1.627, b_{chw}=2.444
α_{hw}=1.027, β_{hw}=28.786, a_{hw}=-2.322, b_{hw}=-0.585
$\dot{m}_{hw}$ =1.05 kg/h:
α_{chw}=0.388, β_{chw}=162.173, a_{chw}=-11.270, b_{chw}=-8.255
α_{hw}=0.764, β_{hw}=250.820, a_{hw}=-8.994, b_{hw}=-7.239
$\dot{m}_{hw}$ =0.7 kg/h:
α_{chw}=0.450, β_{chw}=-6.452, a_{chw}=-2.534, b_{chw}=2.626
α_{hw}=0.832, β_{hw}=-7.528, a_{hw}=-1.842, b_{hw}=0.951
Coefficients
Coefficients
$\dot{m}_{chw}$ =0.832 kg/h, $\dot{m}_{cw}$ =2.77 kg/h
$\dot{Q}_X = \alpha_X \cdot \Delta\Delta t + \beta_X$
$\Delta\Delta t = t_{hw,in} + a_X \cdot t_{cw,in} + b_X \cdot t_{chw,in}$
$\dot{m}_{hw}$ =1.5 kg/h:
α_{chw}=0.567, β_{chw}=-29.148, a_{chw}=-2.073, b_{chw}=3.990
α_{hw}=1.168, β_{hw}=-20.477, a_{hw}=-2.212, b_{hw}=1.941
$\dot{m}_{hw}$ =1.26 kg/h:
α_{chw}=0.694, β_{chw}=-24.249, a_{chw}=-1.754, b_{chw}=2.042
α_{hw}=1.271, β_{hw}=-23.595, a_{hw}=-1.434, b_{hw}=0.531
$\dot{m}_{hw}$ =1.05 kg/h:
α_{chw}=0.390, β_{chw}=-4.609, a_{chw}=-2.766, b_{chw}=3.436
α_{hw}=0.837, β_{hw}=-2.291, a_{hw}=-2.065, b_{hw}=1.136
$\dot{m}_{hw}$ =0.7 kg/h:
α_{chw}=0.000, β_{chw}=0.000, a_{chw}=0.000, b_{chw}=0.000
α_{hw}=0.728, β_{hw}=0.000, a_{hw}=0.000, b_{hw}=0.000
Coefficients
Coefficients

Figure D.3

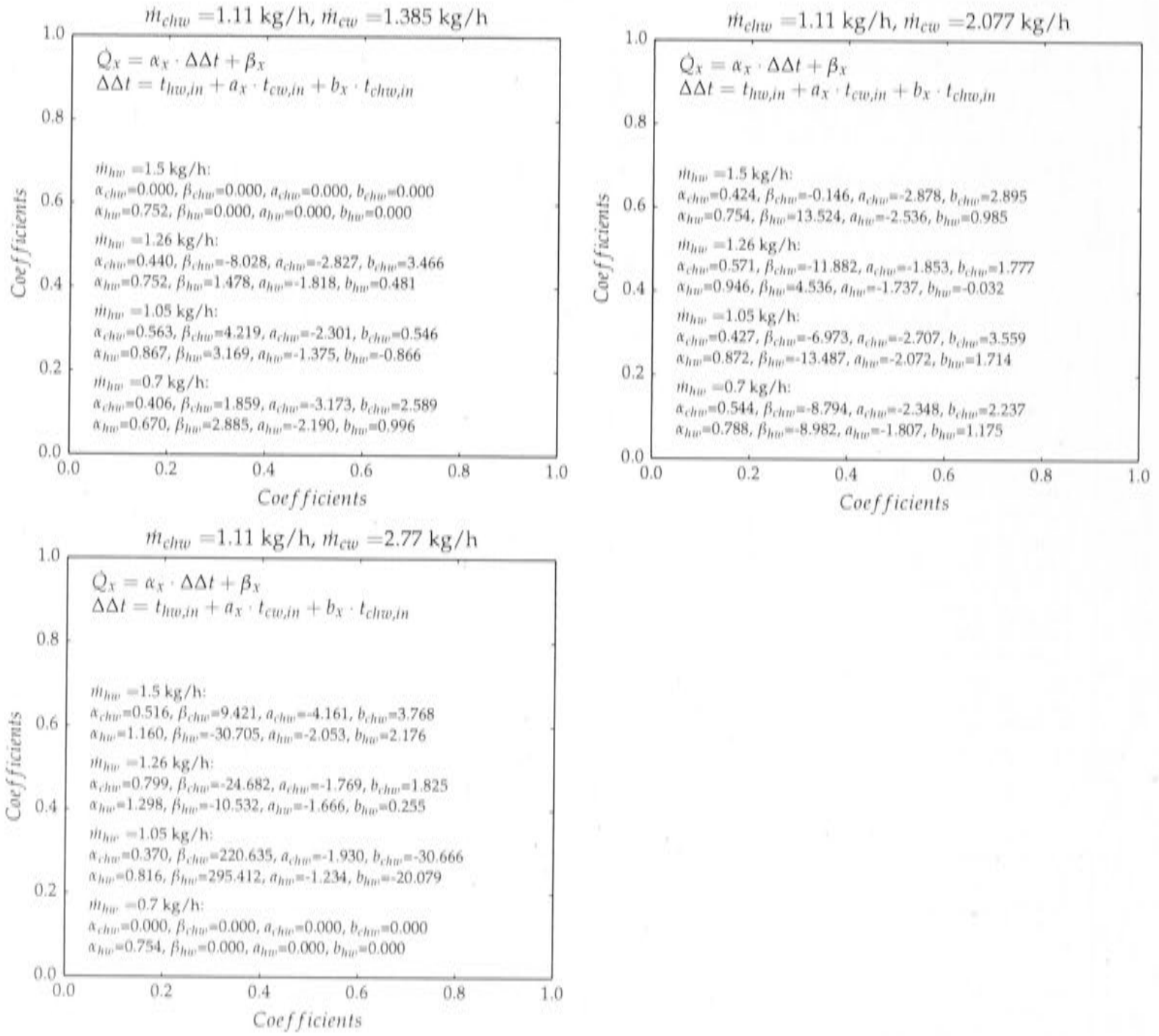

Figure D.3: Regression coefficients milestone C. In case all coefficients are zero, the particular $\dot{m}_{hw}$ was not tested.

D.3 Solar thermal cooling, heating and DHW model: Standard deviations base case

The following two tables D.2 and D.3 have been included to show how little the cooling, heating and DHW demand, comfort conditions and cooling water inlet temperatures to the chiller actually vary throughout the simulation runs of different collector and tank sizes.

Table D.2: Standard deviation for cooling, heating and DHW demand (base case)

	$\sigma\ \dot{Q}_c$	σ latent	$\sigma\ \dot{Q}_h$	$\sigma\ \dot{Q}_{dhw}$
Canb	2.72	0.00%	7.34	31.58
Brisb	2.89	0.00%	0	27.27
Syd	2.43	0.00%	0.01	22.03
Grif	0.94	0.00%	0.01	26.18
TenCr	0.61	0.00%	0	0.94
Darw	5.23	0.00%	0	0.75
Melb	2.85	0.00%	1.47	60.59

Table D.3: Standard deviation for comfort and cooling water set point conditions (base case)

	σ $T_{cw} > T_{cw,set} + 0.5\,^{\circ}C$	σ $T_{cw,set} < T_{wb} + 3\,^{\circ}C$	σ water consumption	σ $comf_T$	σ $comf_{RH}$
Canb	0.10%	0.00%	0.00%	0.00%	0.00%
Brisb	0.10%	0.00%	0.00%	0.00%	0.00%
Syd	0.10%	0.00%	0.00%	0.00%	0.00%
Grif	0.00%	0.00%	0.00%	0.00%	0.00%
TenCr	0.00%	0.00%	0.00%	0.00%	0.00%
Darw	0.00%	0.00%	0.00%	0.00%	0.00%
Melb	0.10%	0.00%	0.00%	0.00%	0.00%

D.4 Solar fraction from 50% to 80% for different collector areas and tank sizes

The following figure D.4 shows the required collector area in each climate to achieve solar fractions from 50% to 80%. Those figures are additional information to figure 8.3 in section 8.1.1.

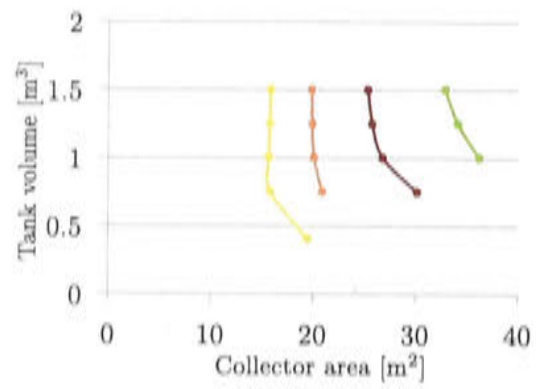

(a) Canberra

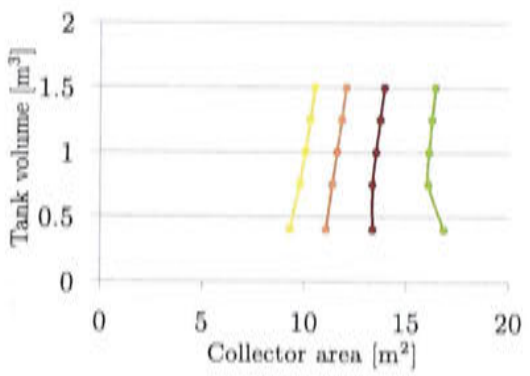

(b) Brisbane

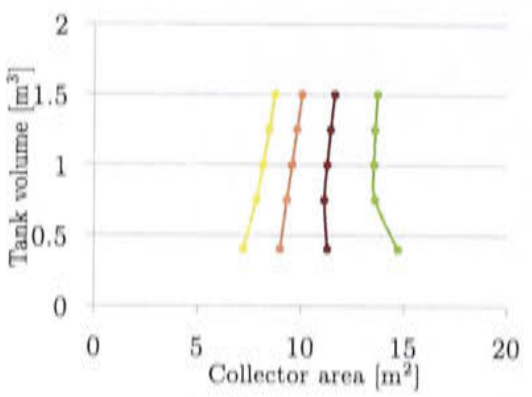

(c) Sydney

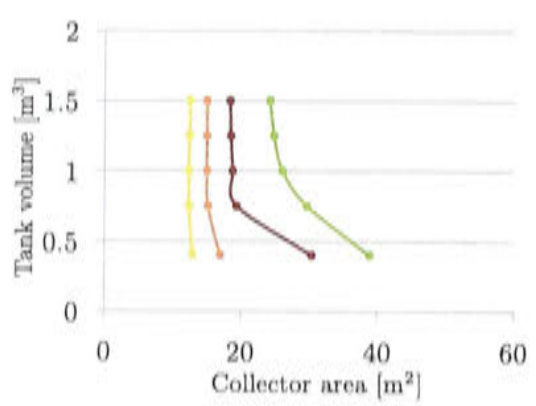

(d) Griffith

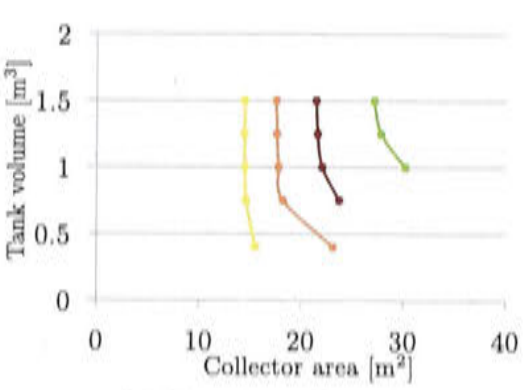

(e) Tennant Creek

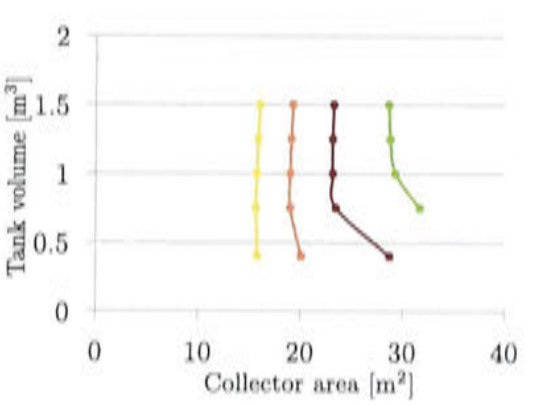

(f) Darwin

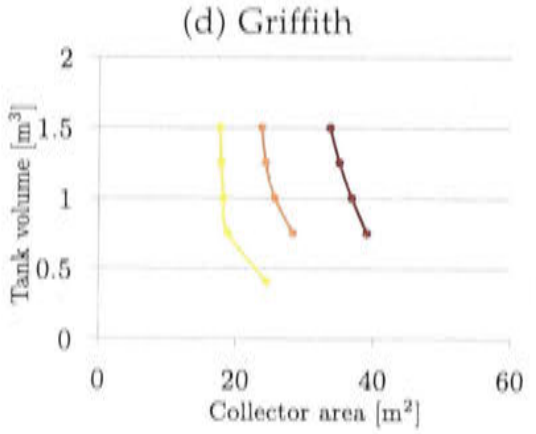

(g) Melbourne

(h) legend

Figure D.4: Tank and collector sizes to achieve a solar fraction SF_{th} from 50% to 80% in the 7 climates (base case)

D.5 Solar fraction versus greenhouse gas emission in each climate

The following graphs show the solar fraction and greenhouse gas emissions for three different tank sizes and all collector sizes in each climate.

(a) legend

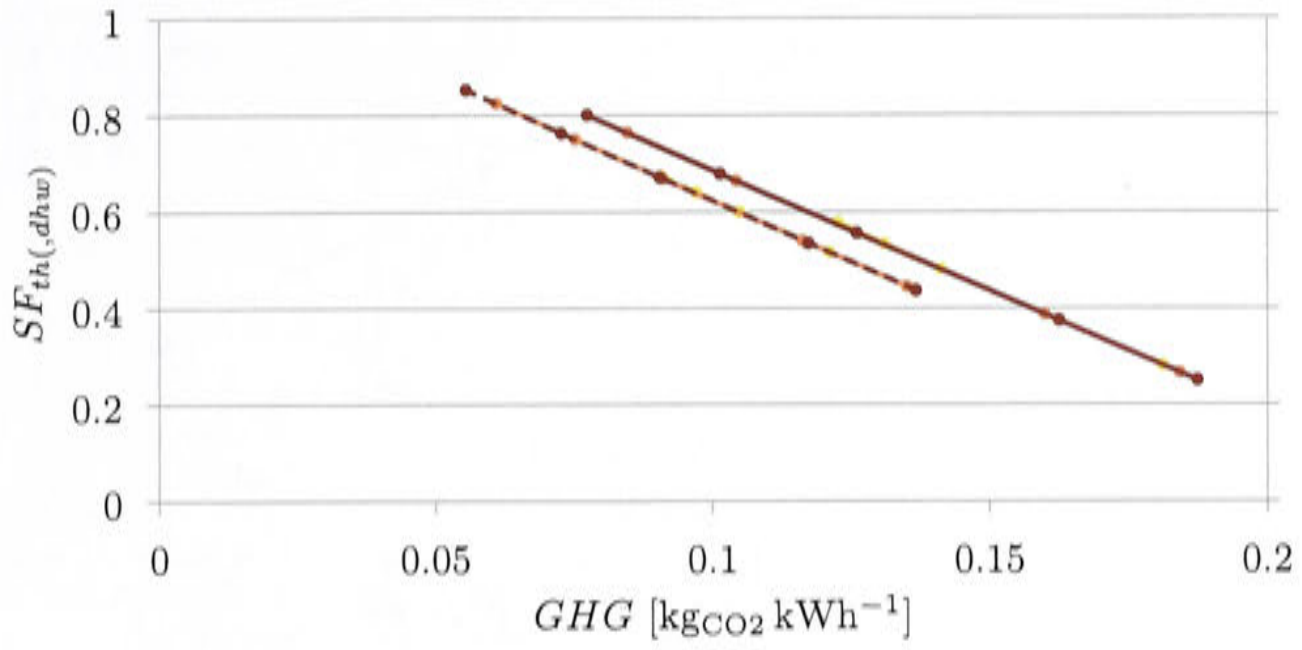

(b) Canberra

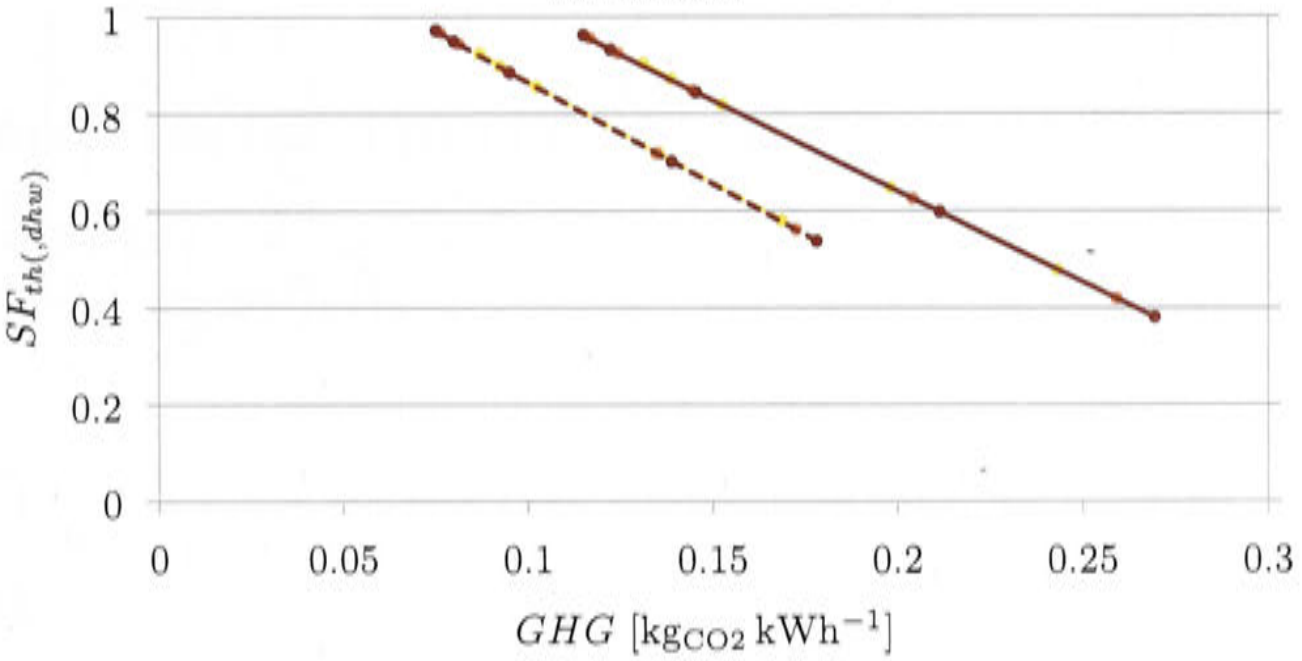

(c) Brisbane

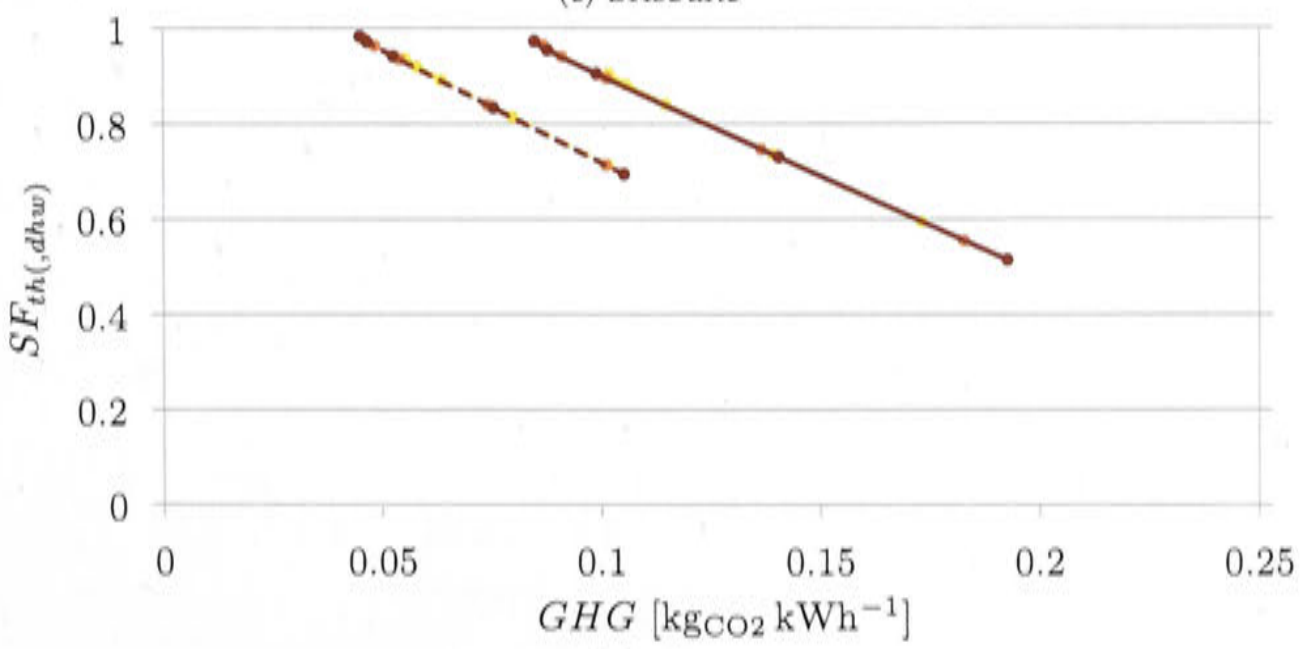

(d) Sydney

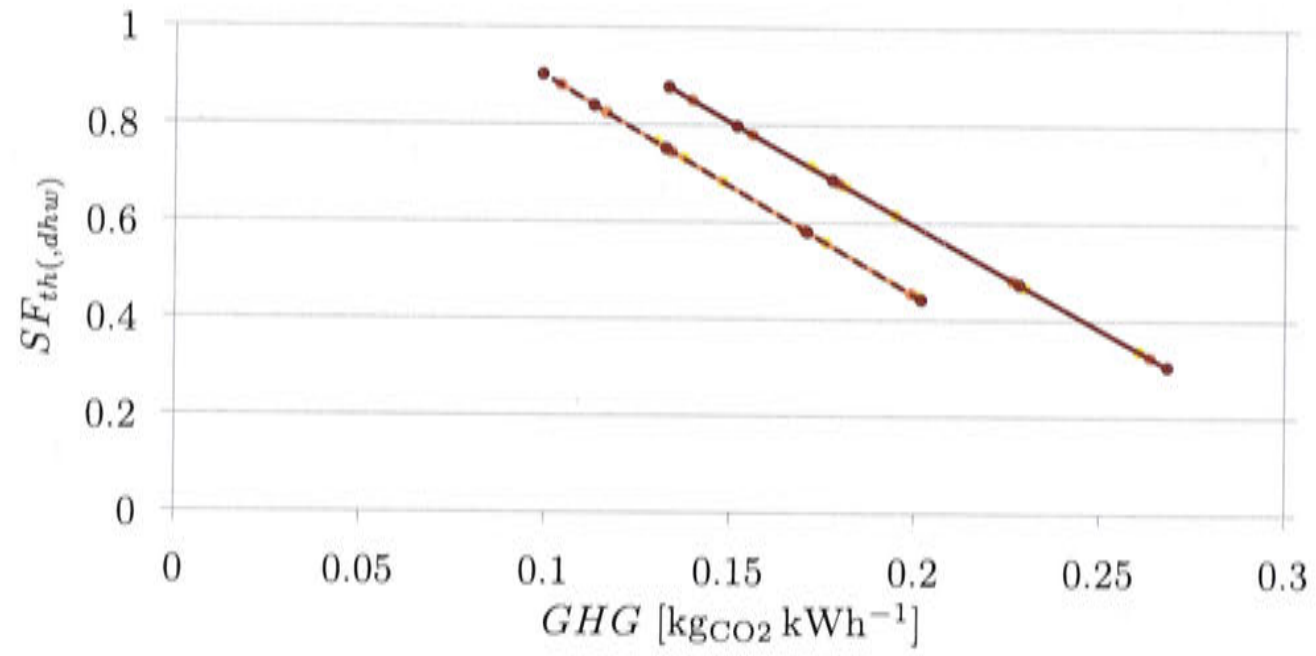

(e) Griffith

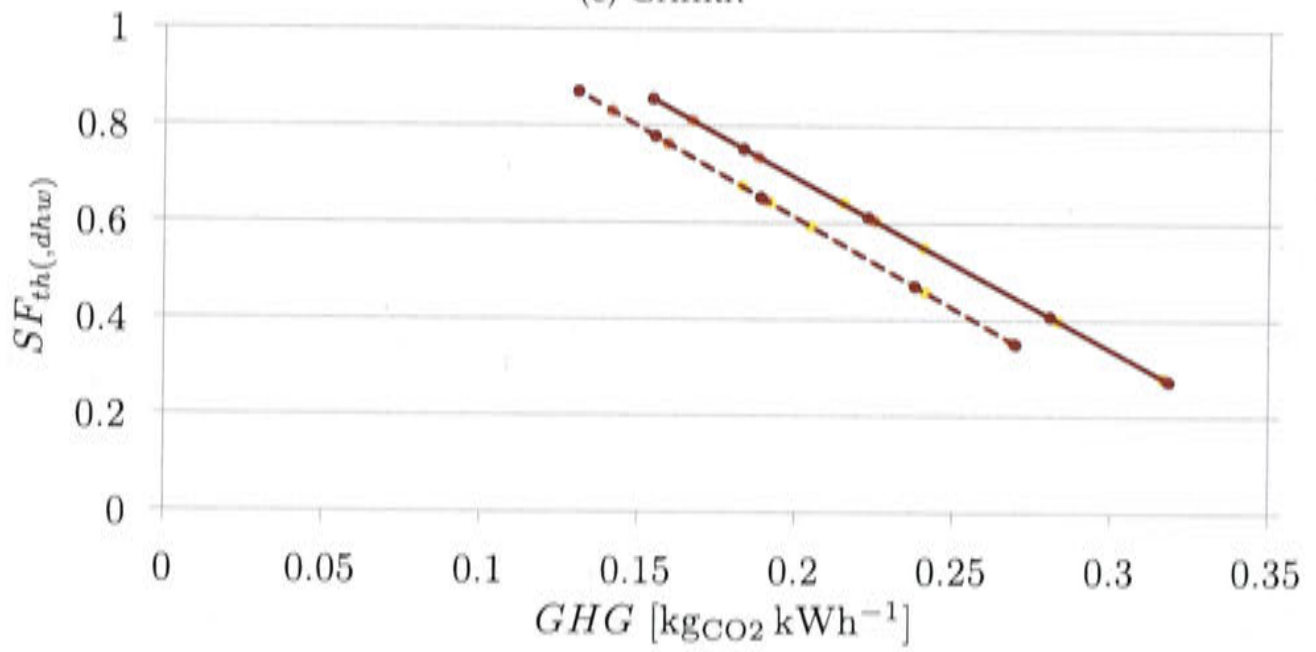

(f) Tennant Creek

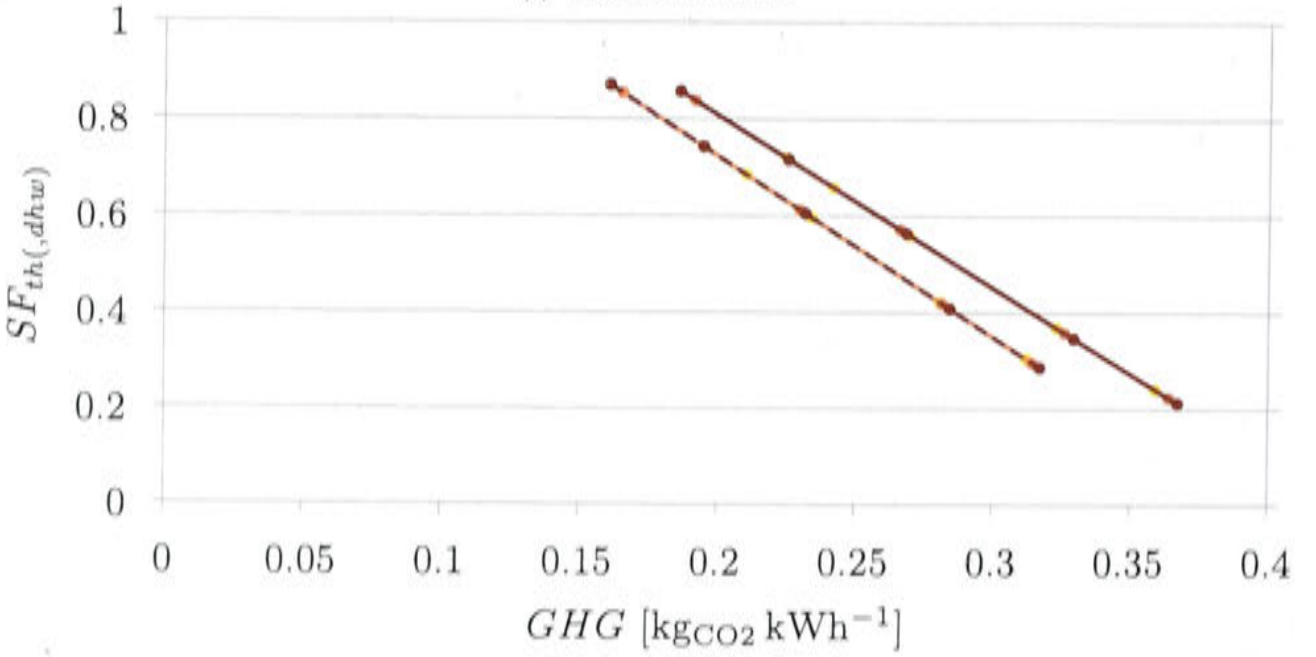

(g) Darwin

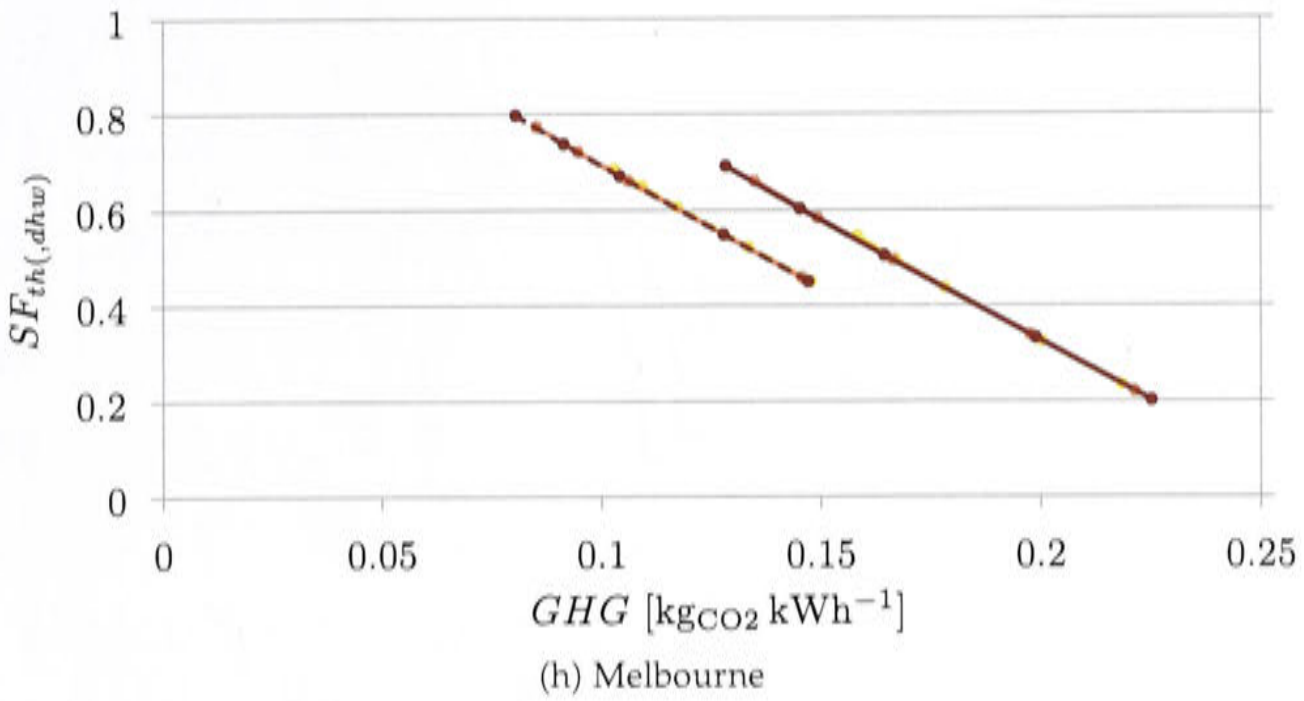

(h) Melbourne

Figure D.5: Solar fraction and greenhouse gas emissions for all collector sizes and three tank sizes, excluding DHW (solid —) or including DHW (dashed - -).

D.6 Solar fraction versus specific cost in each climate

The following graphs show the solar fraction and specific cost for three different tank sizes and all collector sizes in each climate.

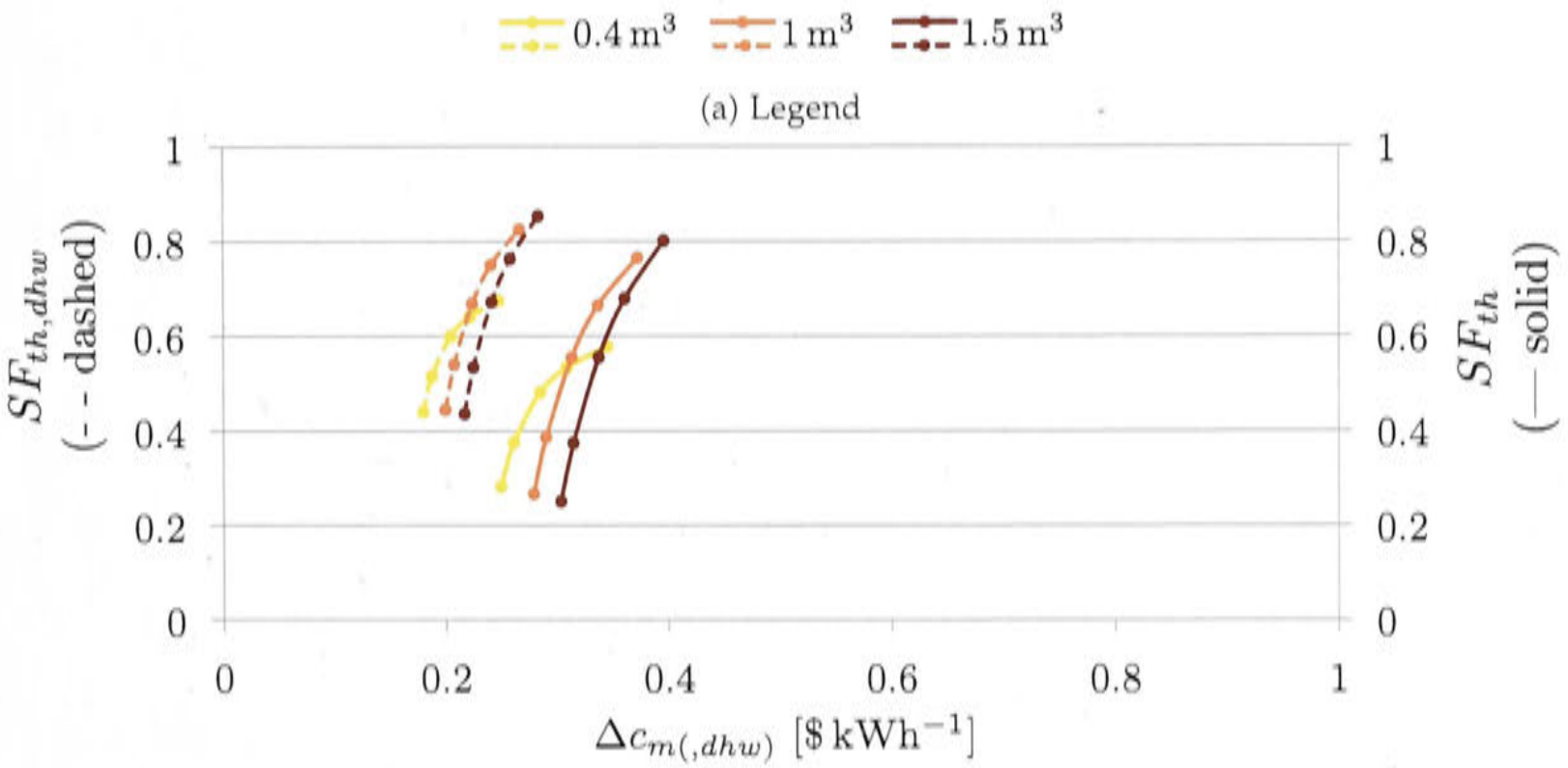

(a) Legend

(b) Canberra

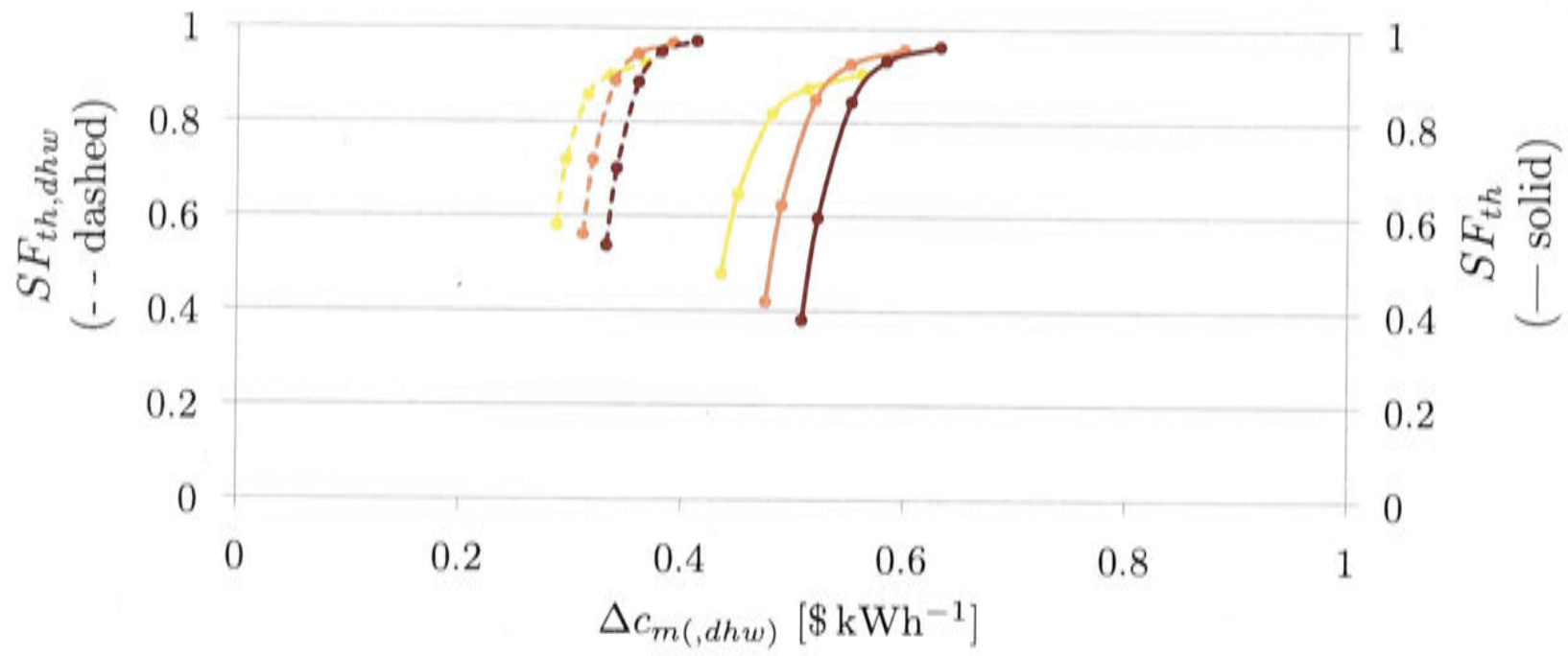

(c) Brisbane

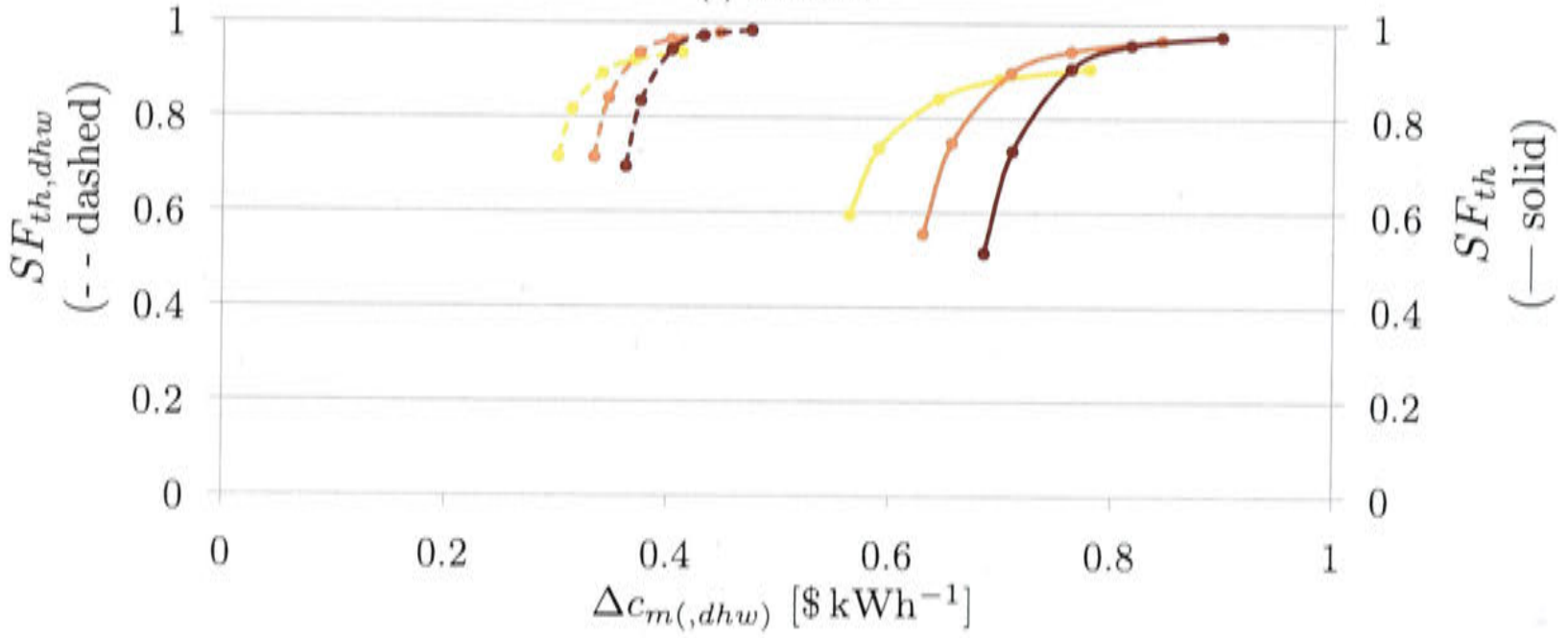

(d) Sydney

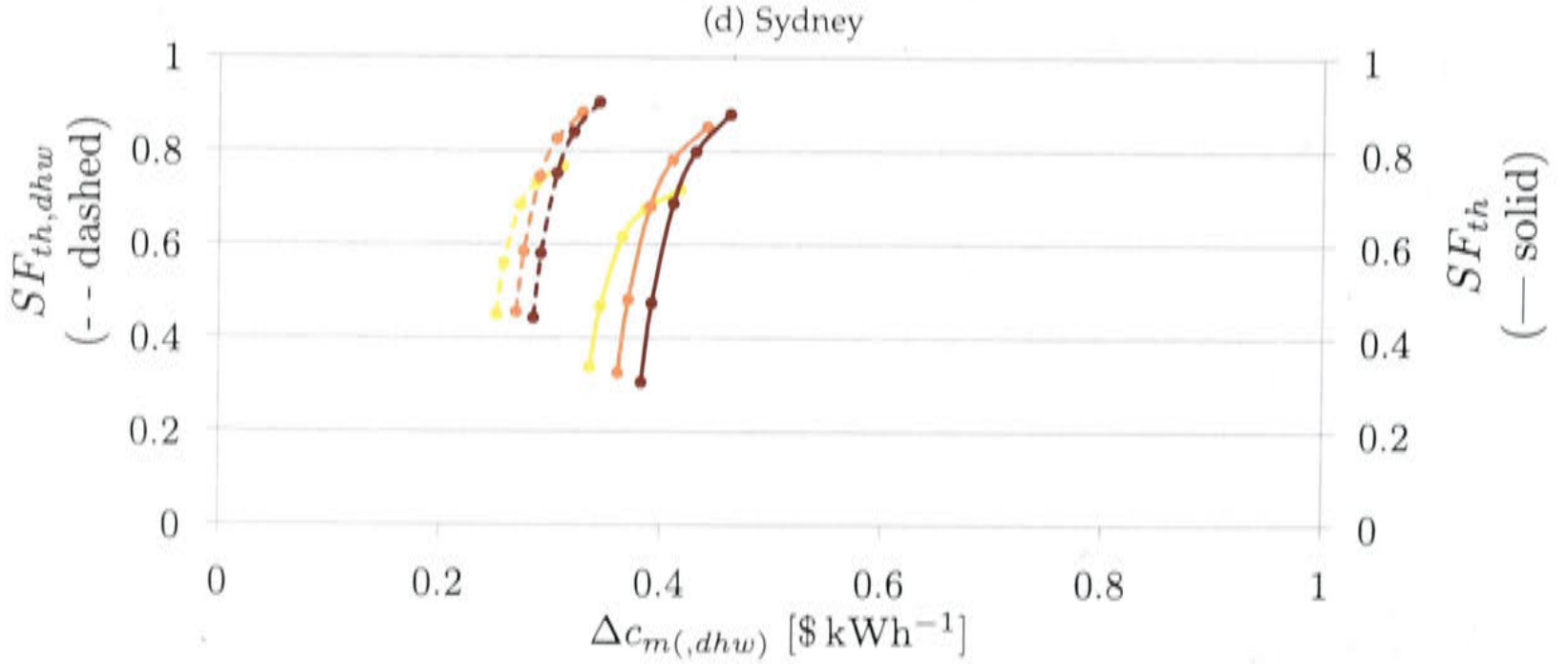

(e) Griffith

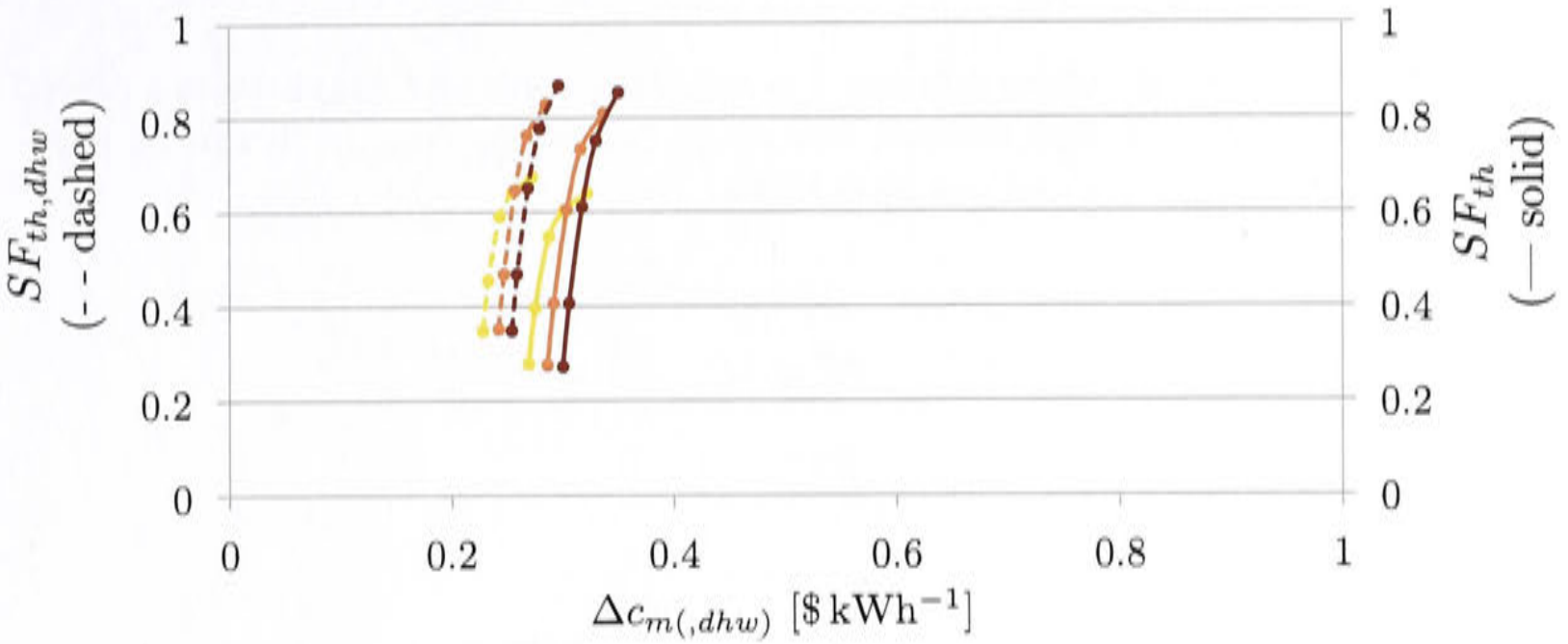

(f) Tennant Creek

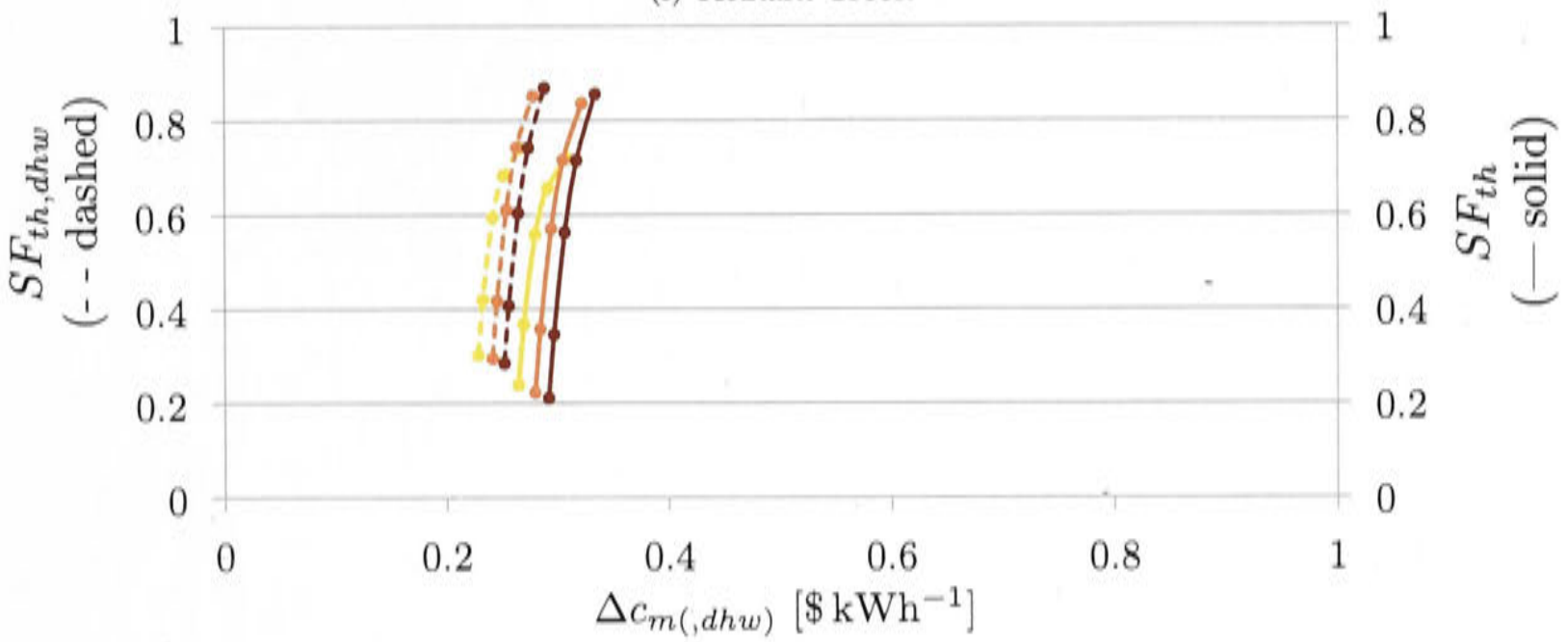

(g) Darwin

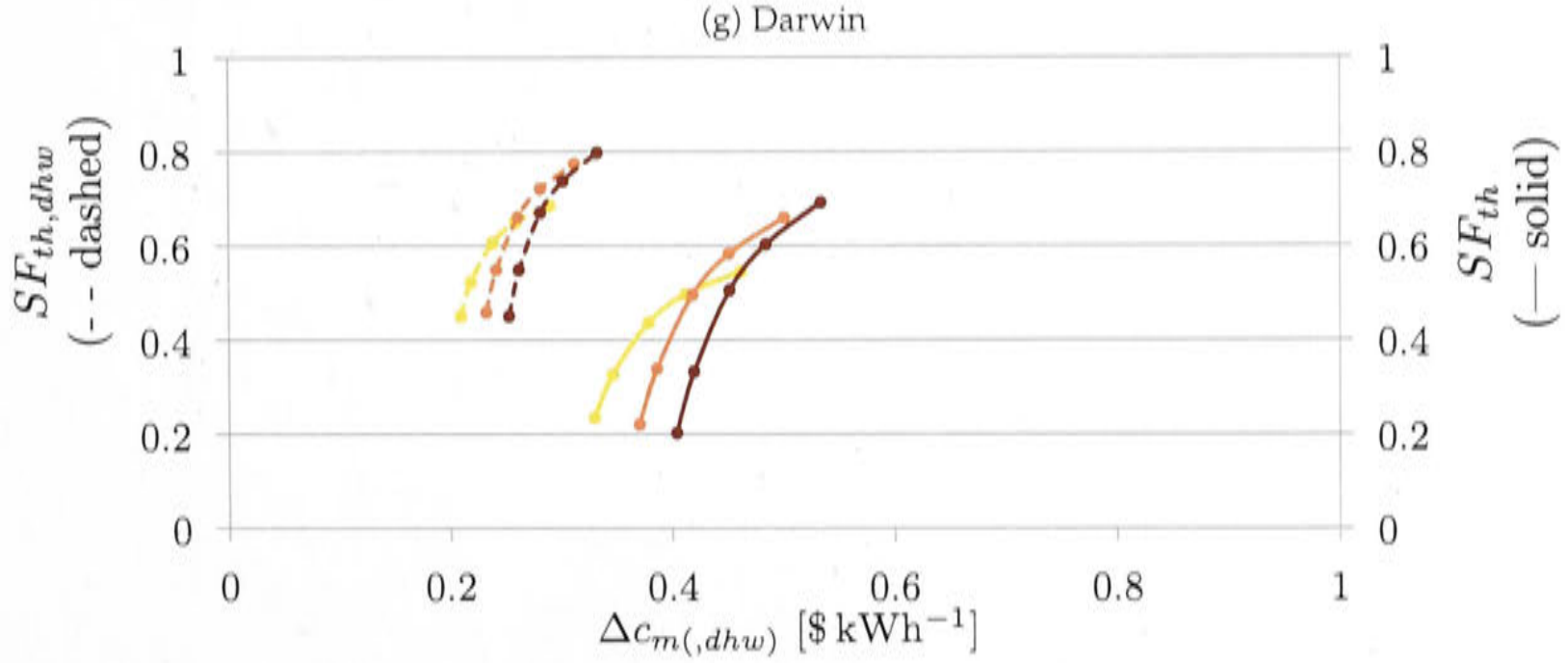

(h) Melbourne

Figure D.6: Solar fraction and specific cost for all collector sizes and three tank sizes

D.7 Greenhouse gas emission savings versus specific cost difference

The following graphs show the difference in specific greenhouse gas emissions $\Delta GHG = GHG_{ref} - GHG$ and the specific cost difference $\Delta c_m = c_m - c_{m,ref}$. It can be interpreted the cost for greenhouse gas abatement.

(a) legend

(b) Canberra

(c) Brisbane

(d) Sydney

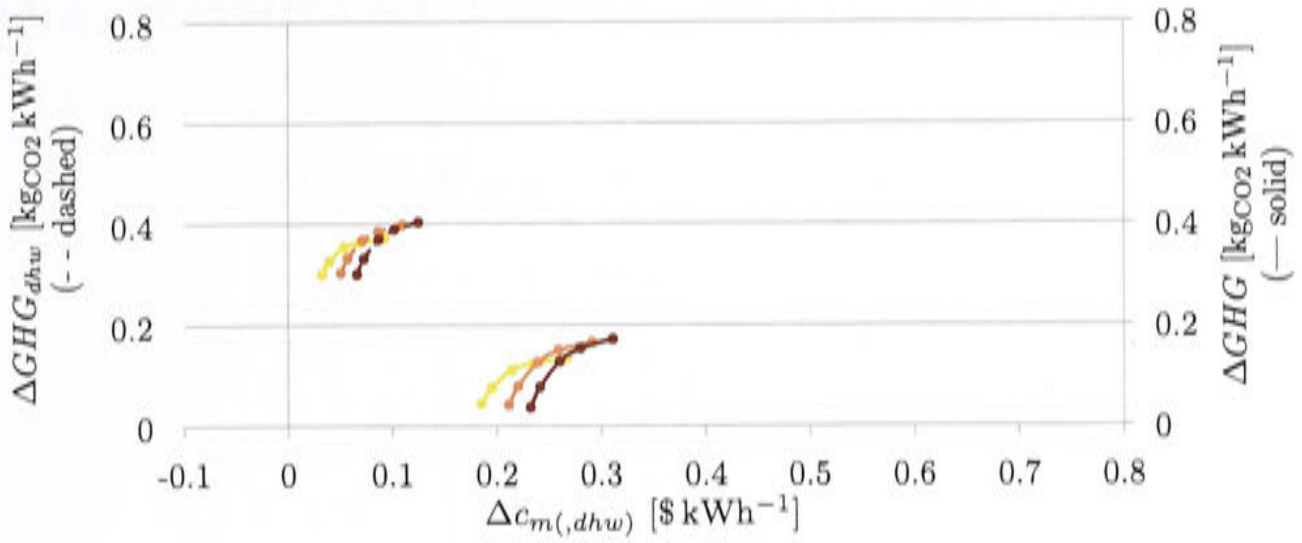

(e) Griffith

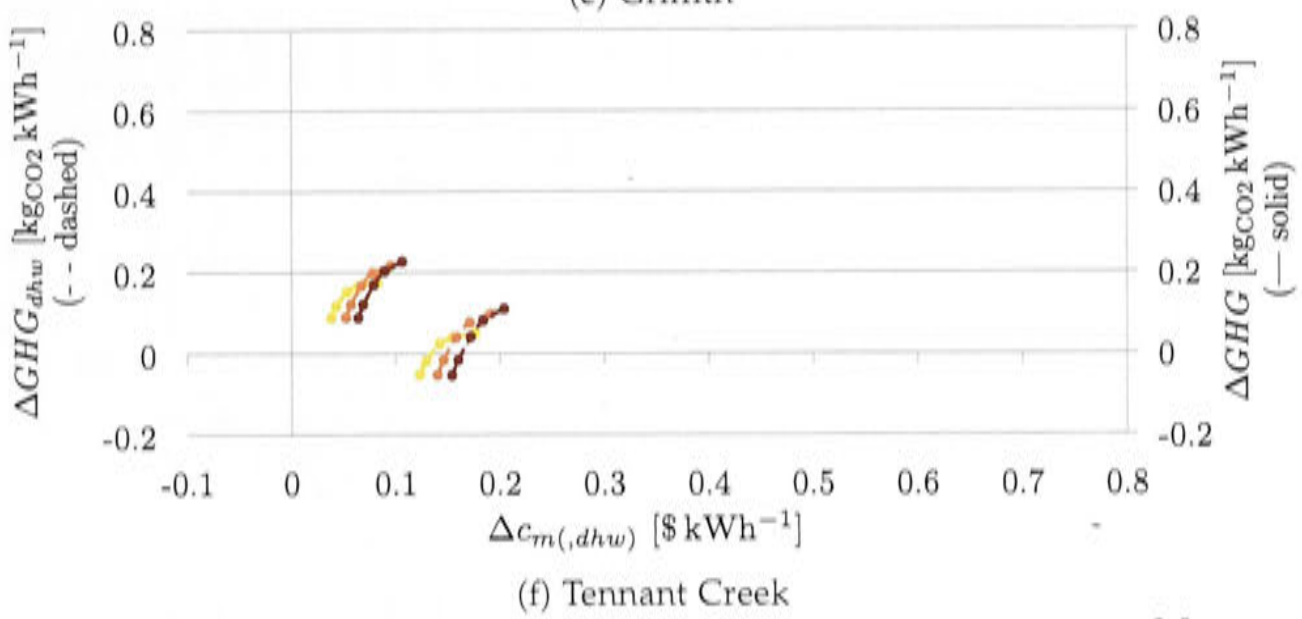

(f) Tennant Creek

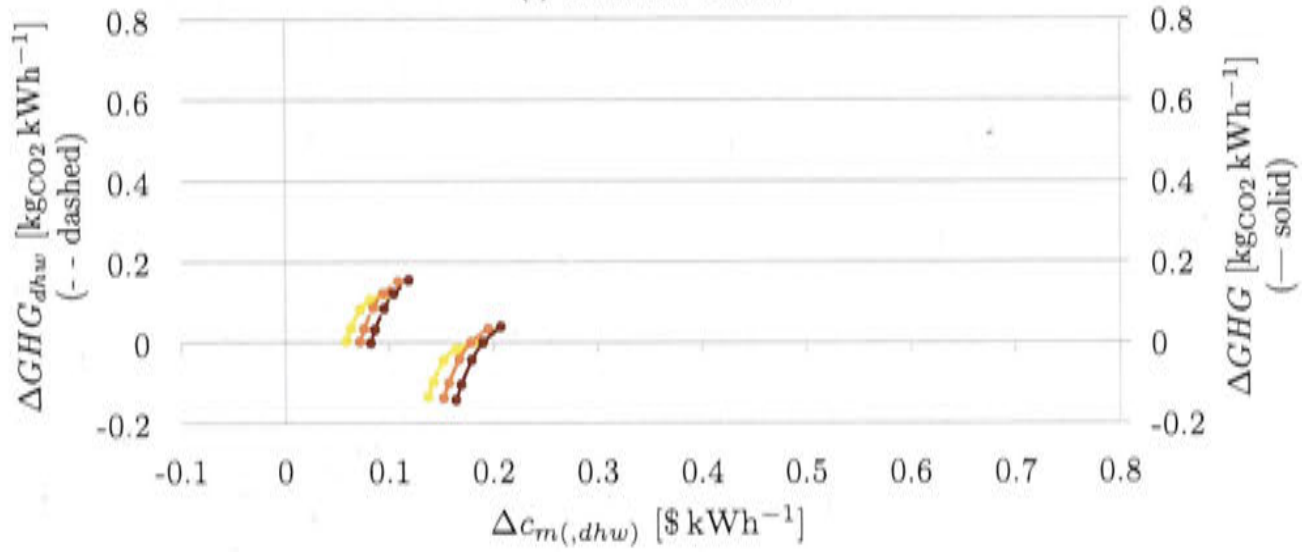

(g) Darwin

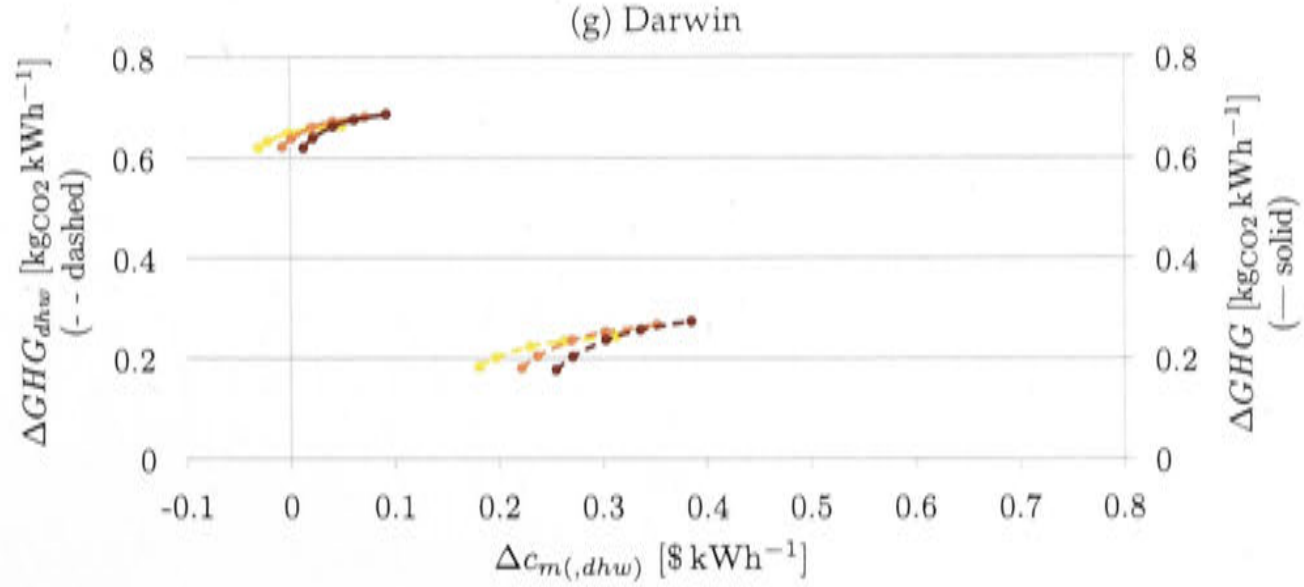

(h) Melbourne

Figure D.7: Solar fraction and greenhouse gas emissions for all collector sizes and three tank sizes

D.8 Temperature distribution around the collector and tank

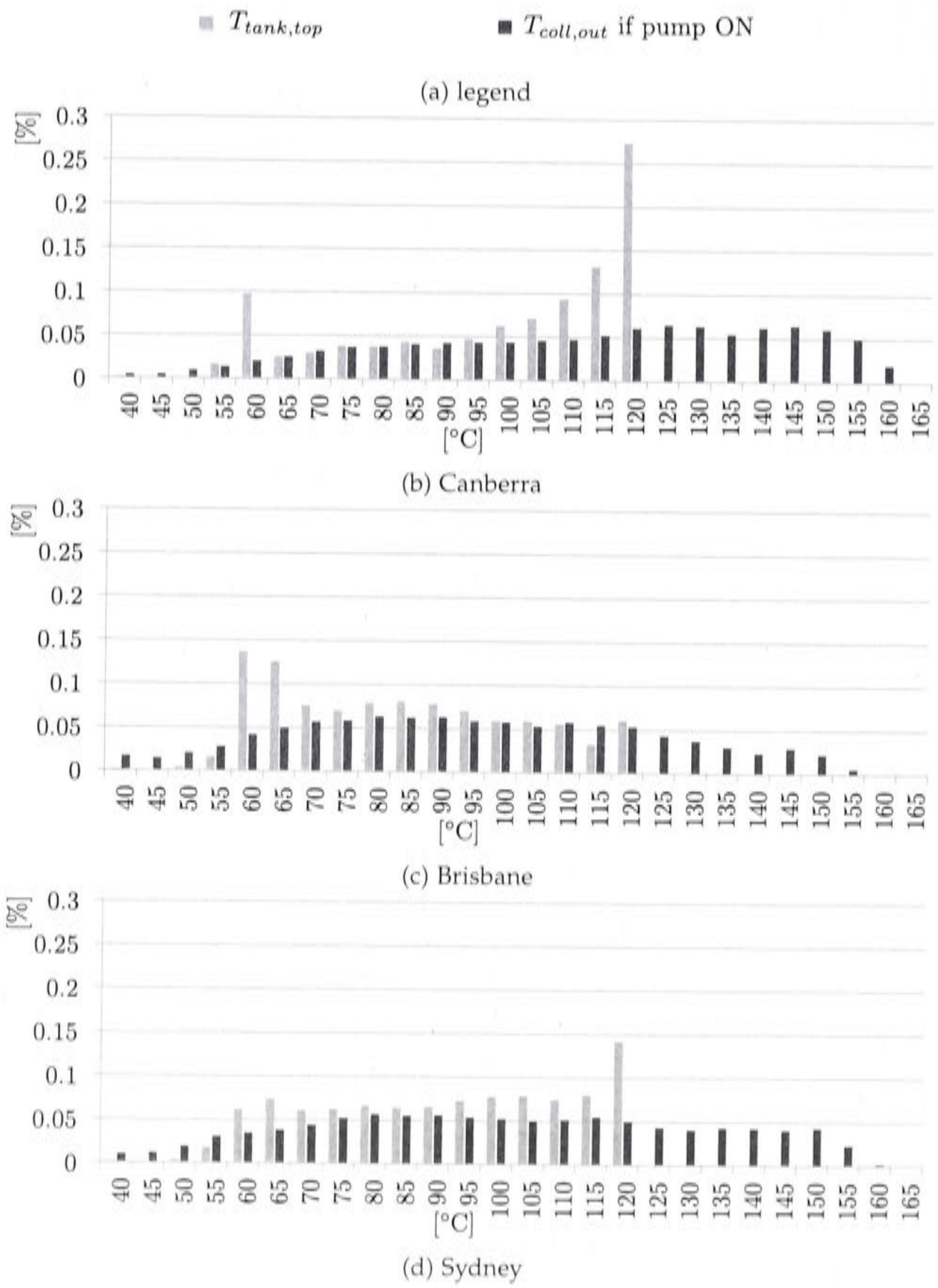

(a) legend

(b) Canberra

(c) Brisbane

(d) Sydney

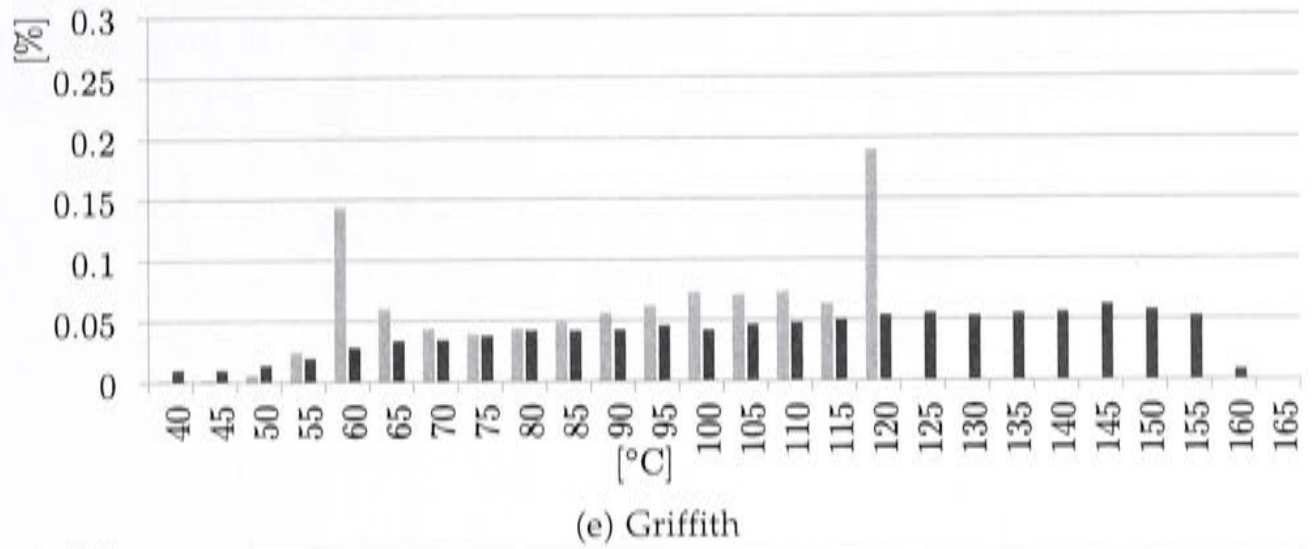

(e) Griffith

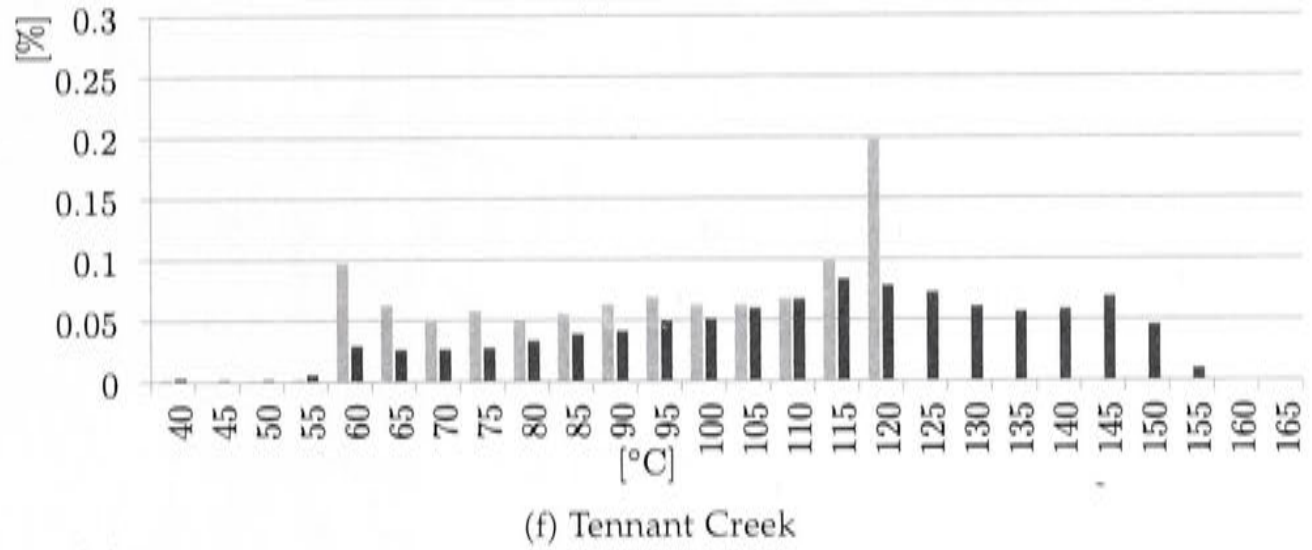

(f) Tennant Creek

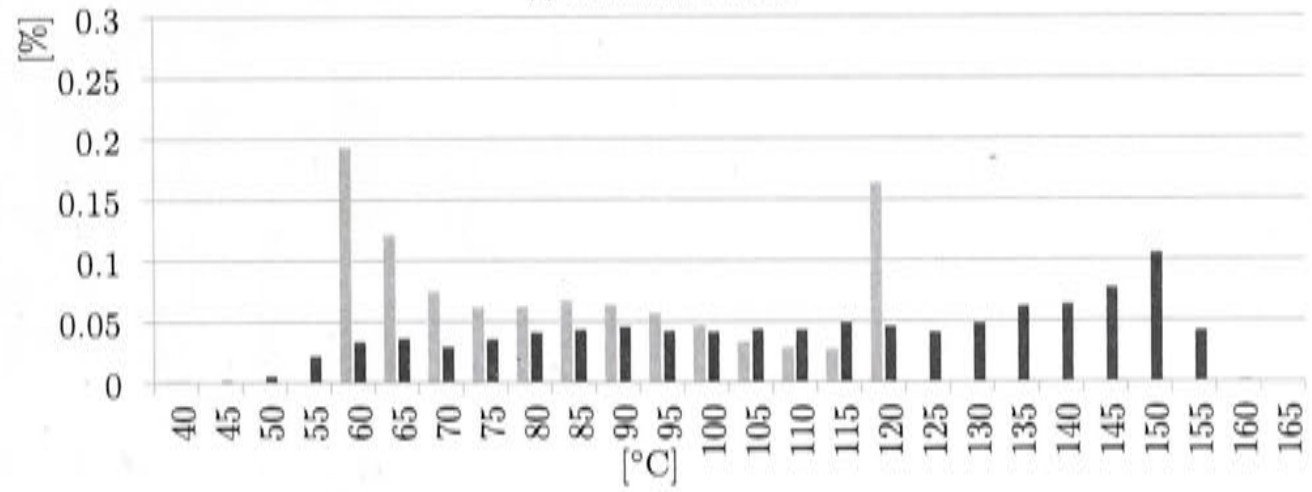

(g) Darwin

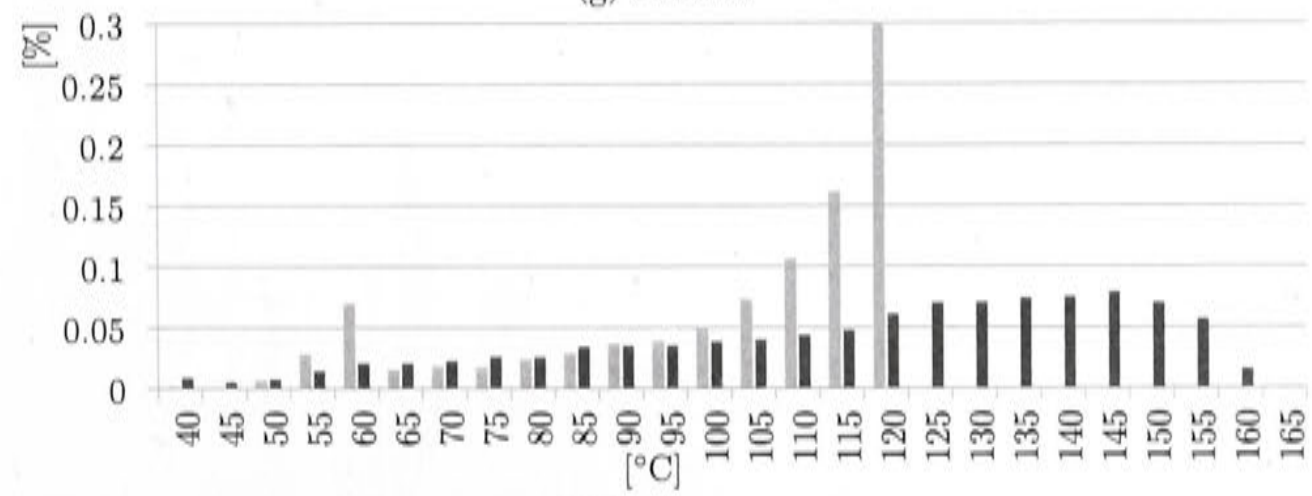

(h) Melbourne

Figure D.8: Temperature distribution (base case)

D.9 Distribution of air flow

The following figures show for each climate in heating and cooling mode the histogram of the air flows, given that the fan is in operation. Furthermore, it shows the average air flow in each zone.

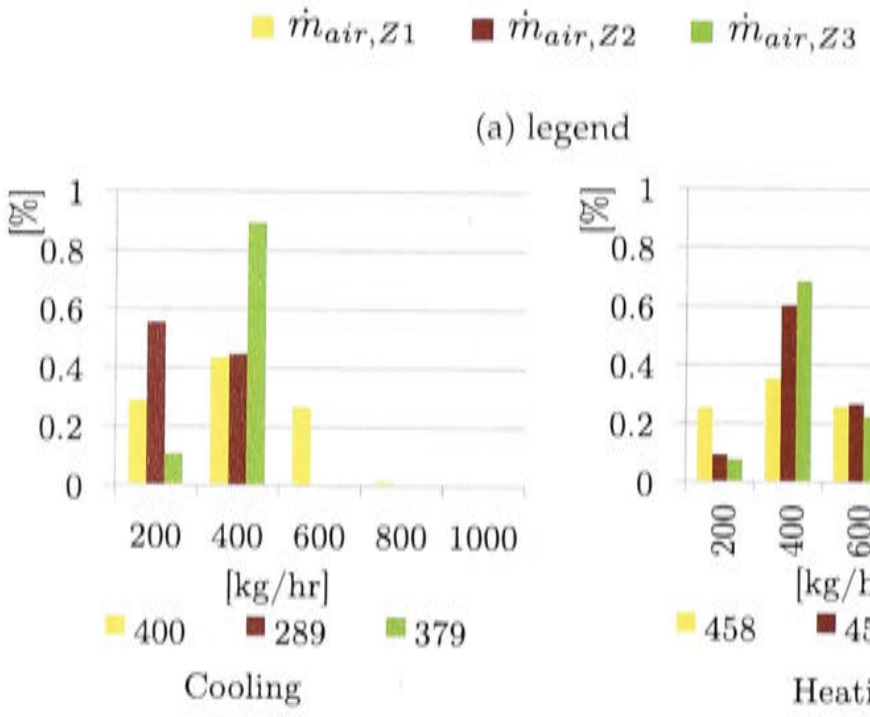

(a) legend

(b) Canberra

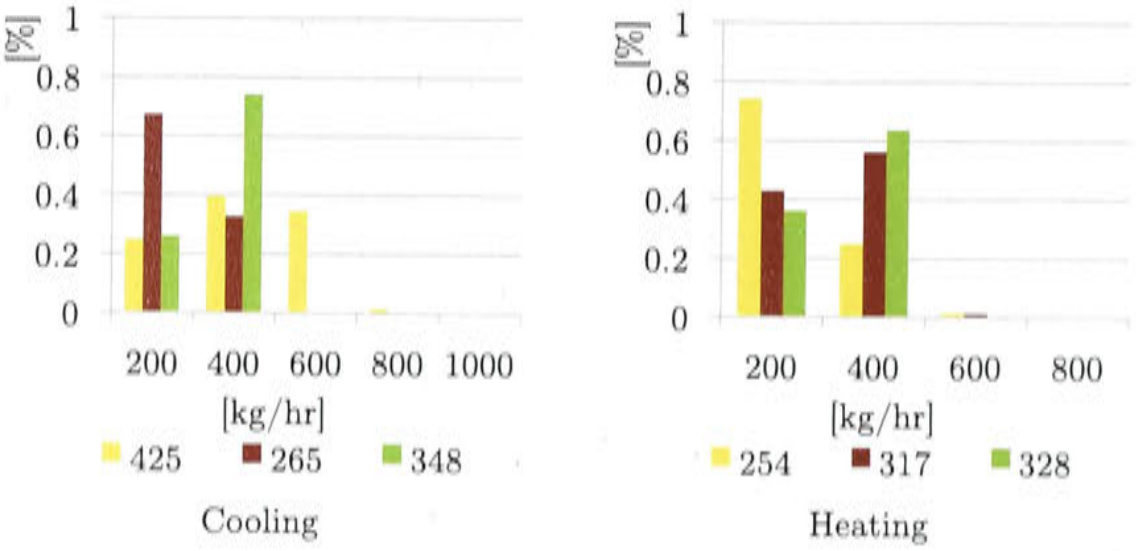

(c) Brisbane

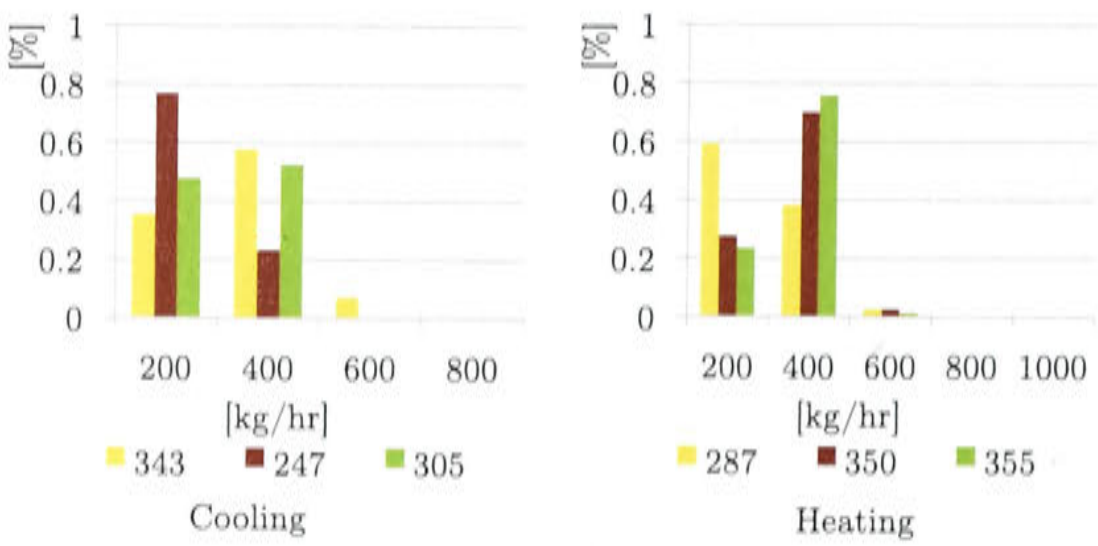

(d) Sydney

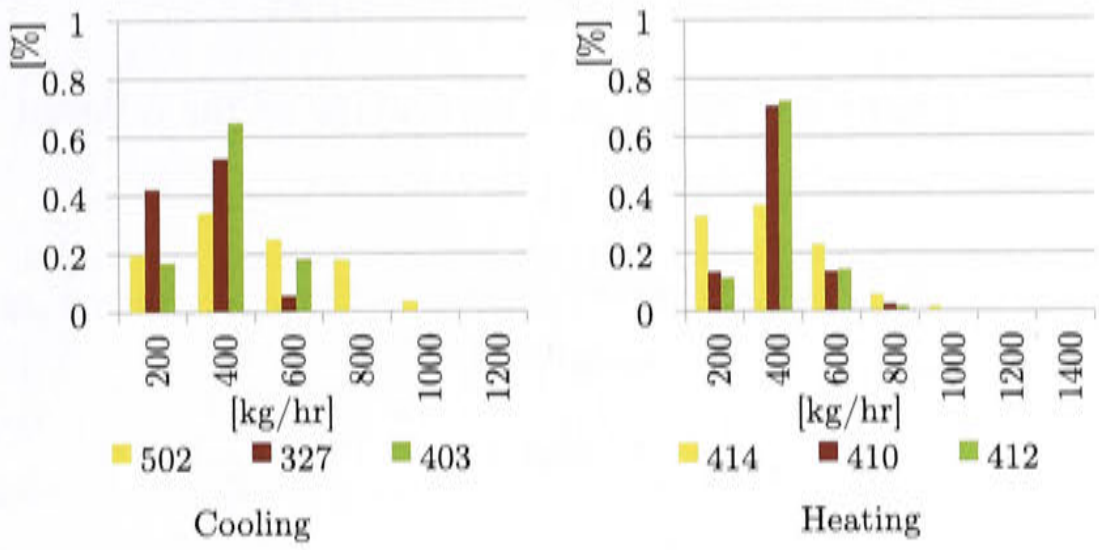

(e) Griffith

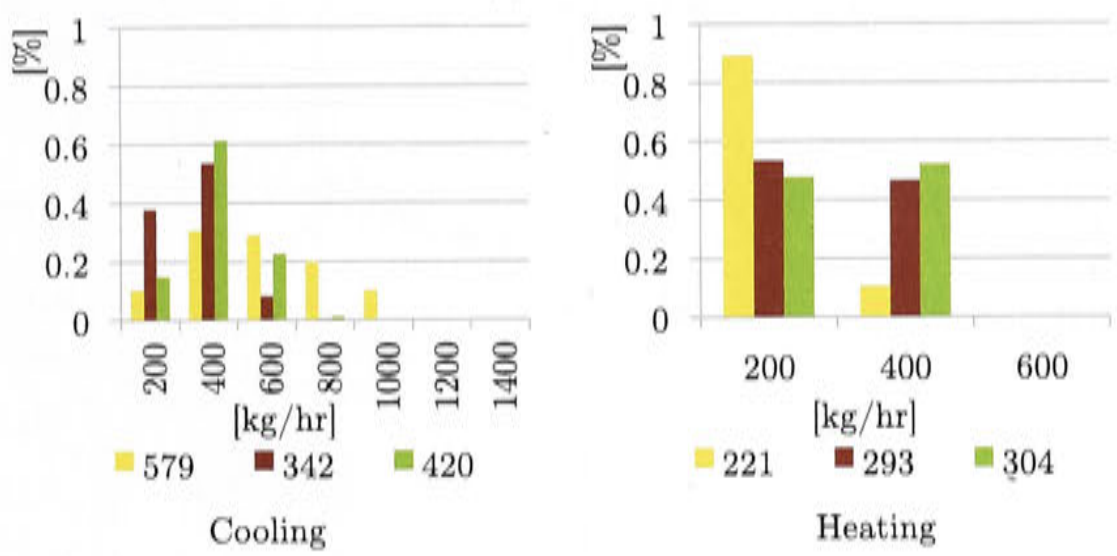

(f) Tennant Creek

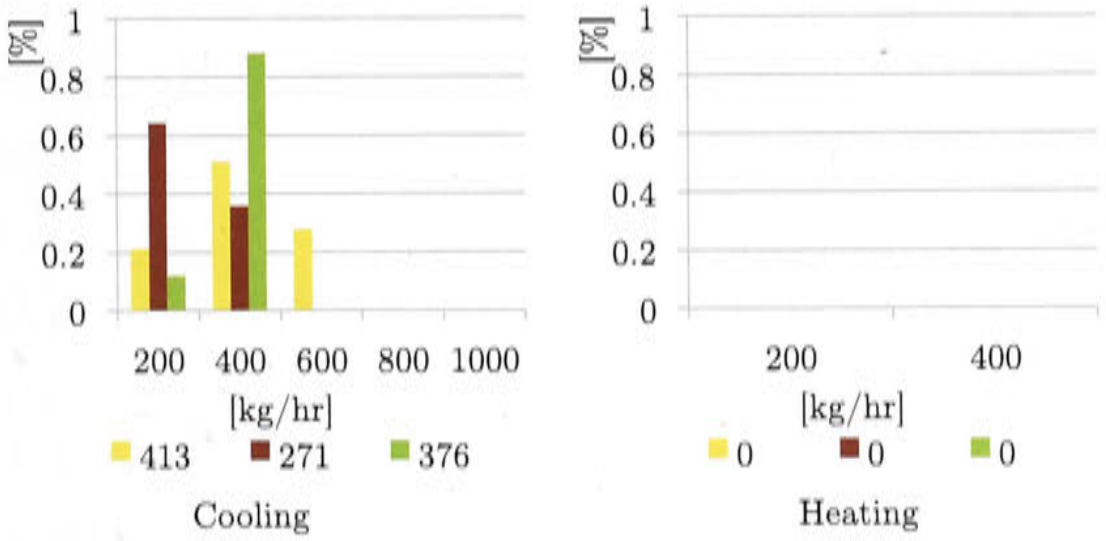

(g) Darwin

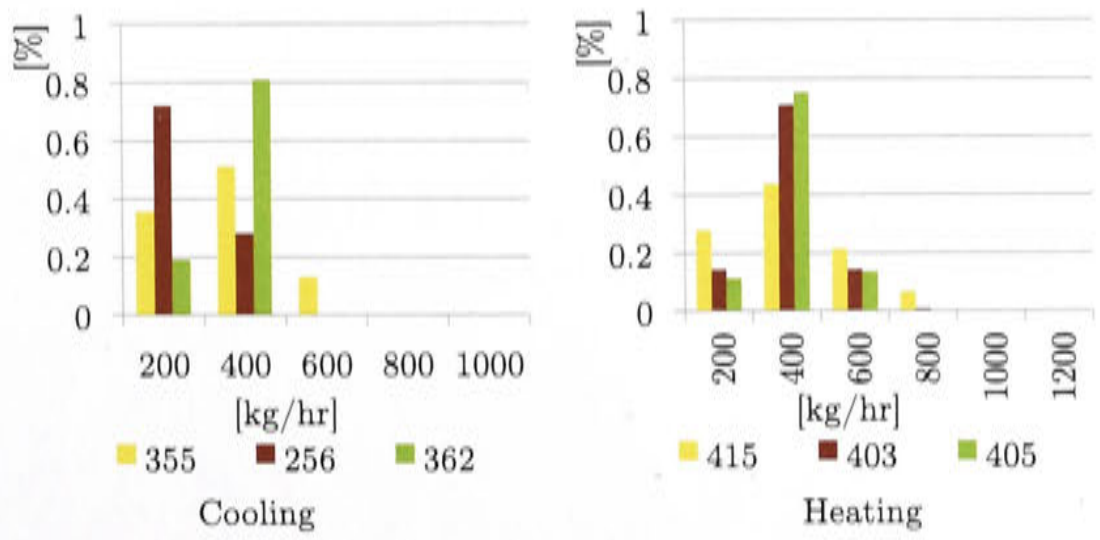

(h) Melbourne

Figure D.9: Distribution of air flow (base case)

D.10 Energy imbalance and relieved heat

The tables show the energy imbalance as a percentage of the relieved energy from the hot water tank.

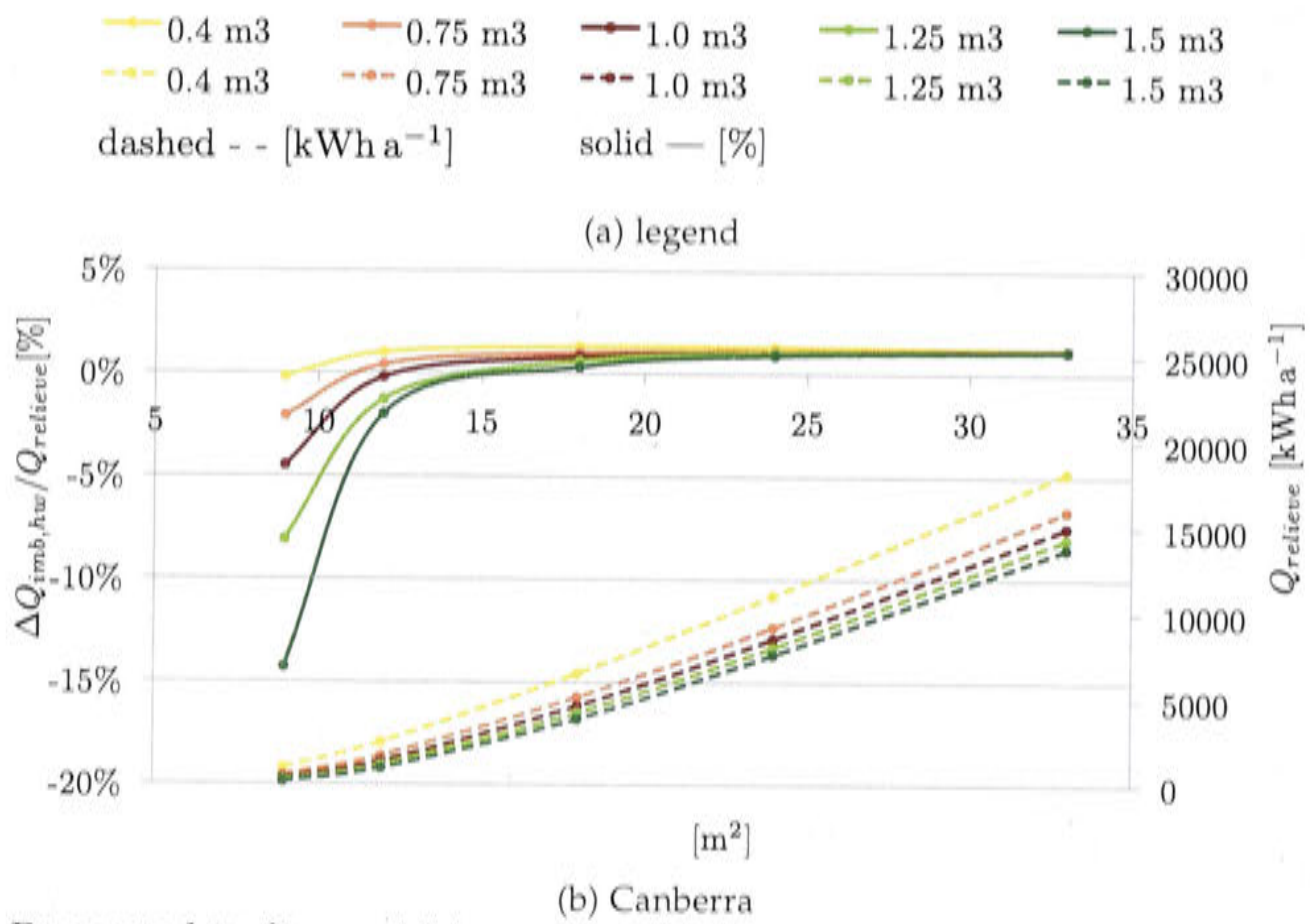

(a) legend

(b) Canberra

(c) Brisbane

(d) Sydney

Presented in figure 8.9 in section 8.1.5

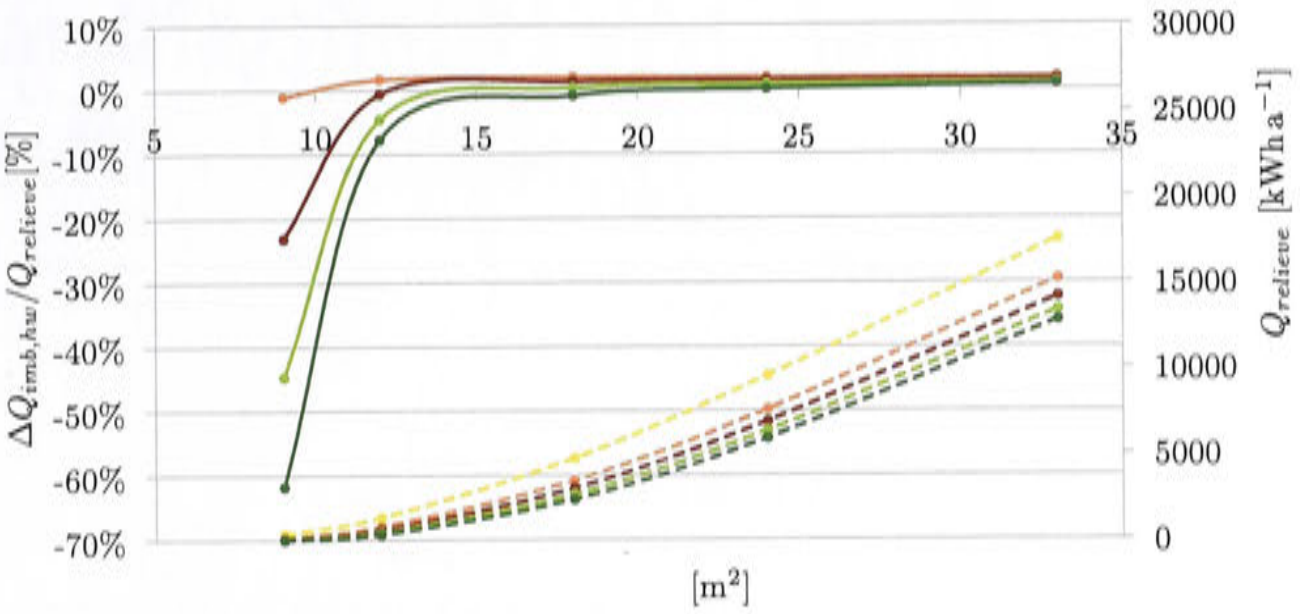

(e) Griffith

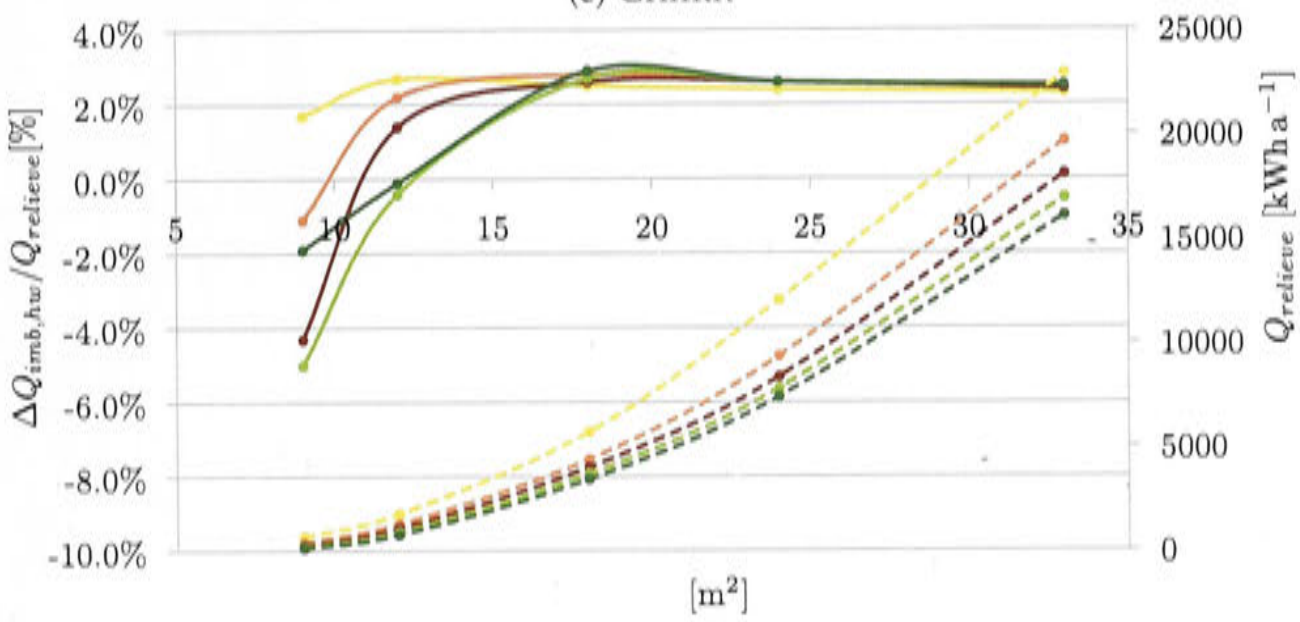

(f) Tennant Creek

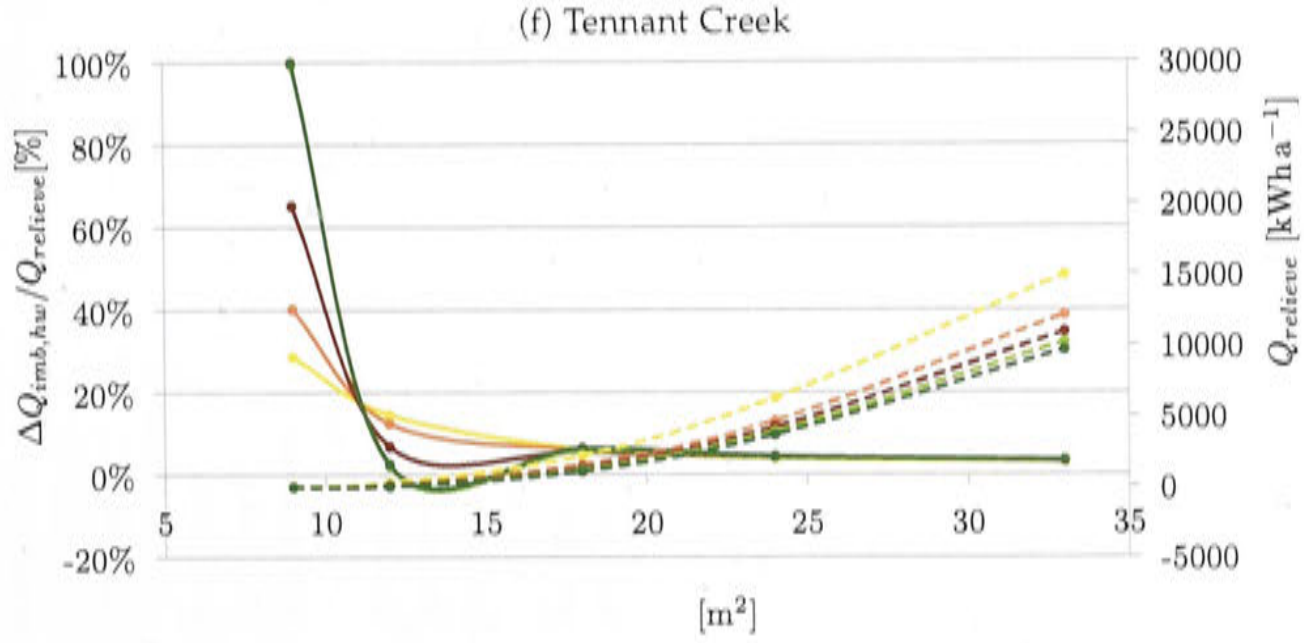

(g) Darwin

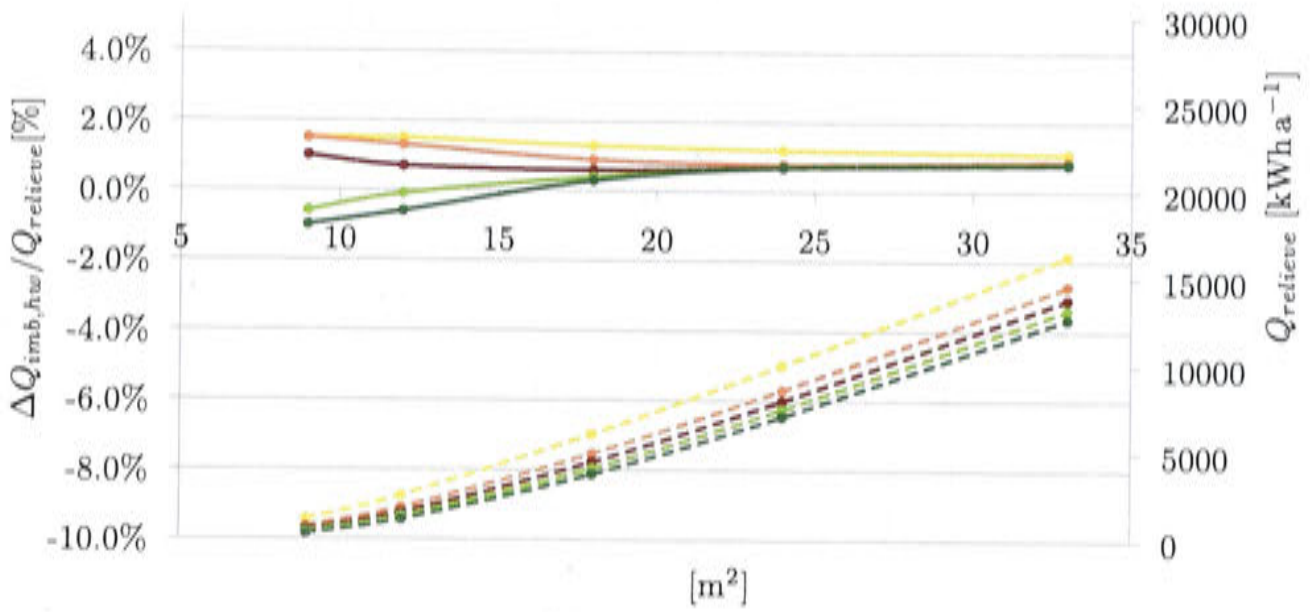

(h) Melbourne

Figure D.10: Energy imbalance (base case)

Solar thermal HVAC (and DHW) system - Variations

E.1 Average air mass flow rates dehumidification strategy II

The following three charts show the average air flow rates comparing the chosen configuration of the base case scenario to the dehumidification strategy II. Each chart represents a zone of the building model.

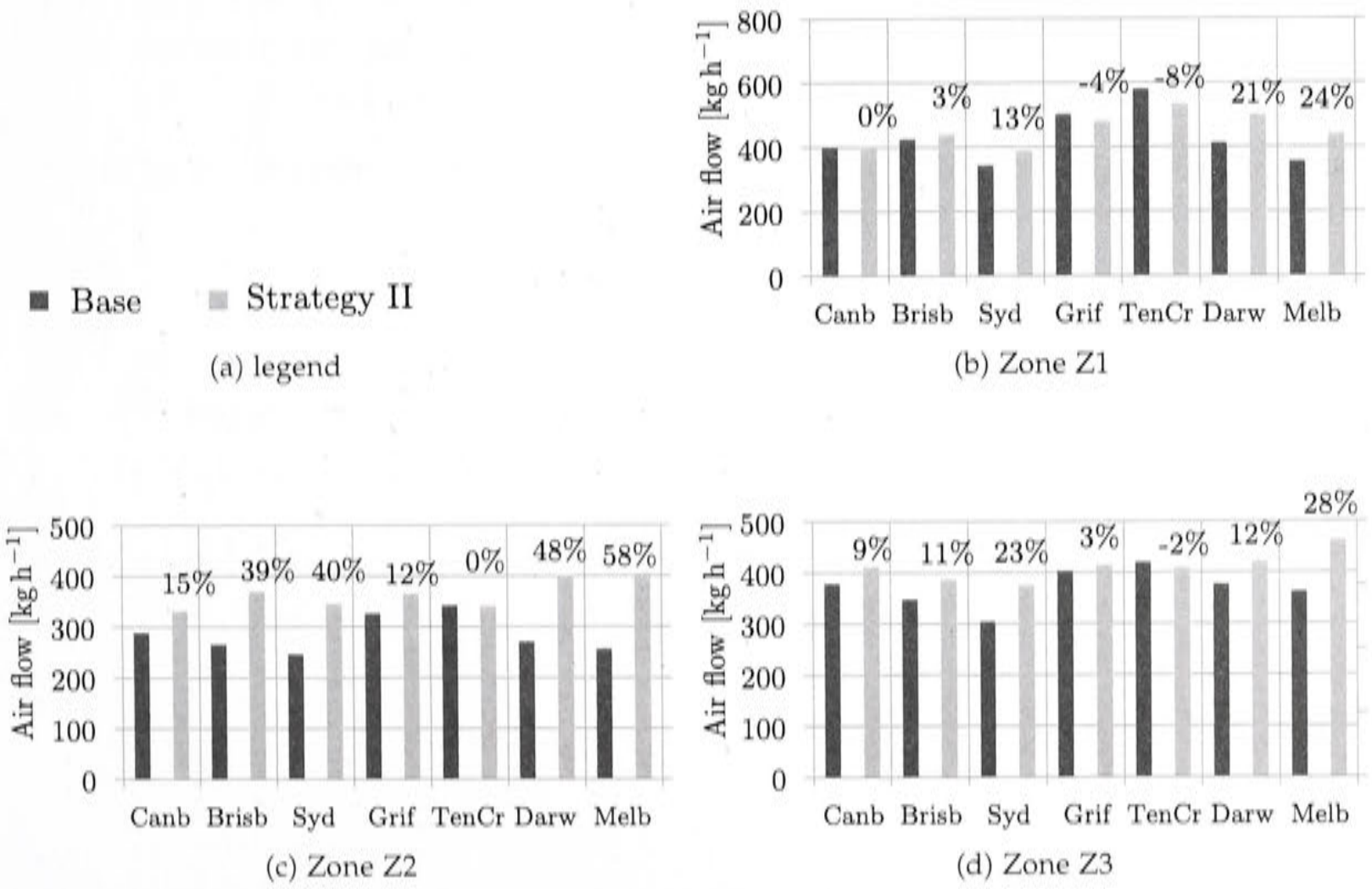

(a) legend

(b) Zone Z1

(c) Zone Z2

(d) Zone Z3

Figure E.1: Average air flow rate absolute and relative comparing dehumidification strategy II to the base case

E.2 Average air mass flow rates dehumidification strategy III

The following three charts show the average air flow rates comparing the chosen configuration of the base case scenario to the dehumidification strategy II. Each chart represents a zone of the building model.

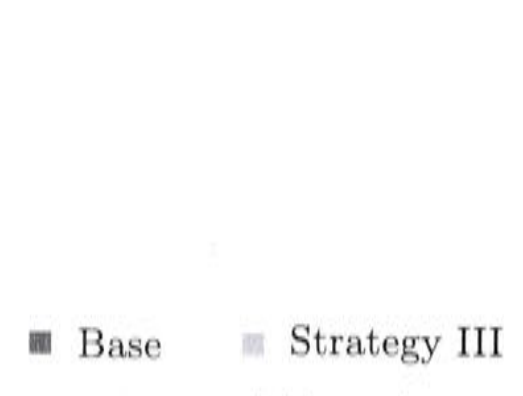

(a) legend

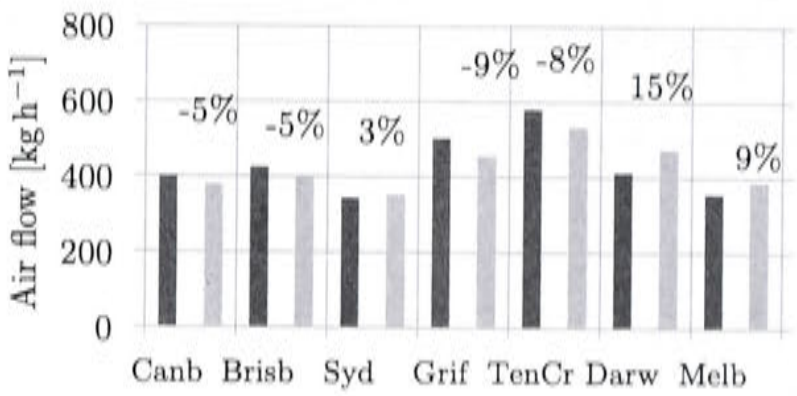

(b) Zone Z1

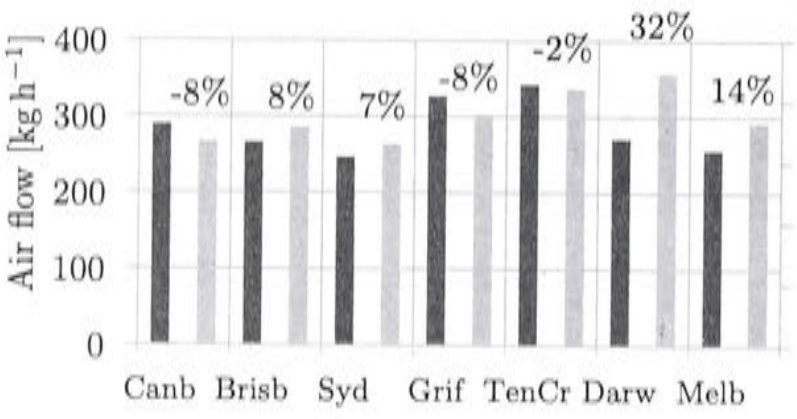

(c) Zone Z2

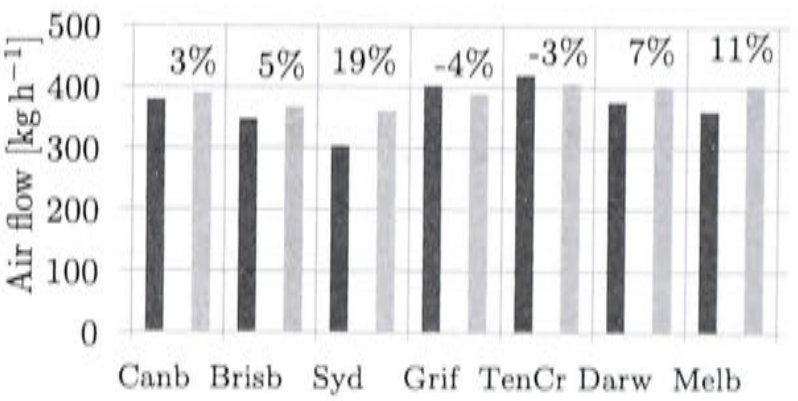

(d) Zone Z3

Figure E.2: Average air flow rate absolute and relative comparing dehumidification strategy III to the base case.

Including a cold storage tank

F.1 Direct coupling collectors and chiller

Table F.1: Hourly global radiation on the horizontal measured on the 26 January 2013, average over 5 minute measurements, National University of Singapore (NUS) [2014]

Time	$W\,m^{-2}$	Time	$W\,m^{-2}$
0:00	0.0	12:00	608.7
1:00	0.0	13:00	710.7
2:00	0.0	14:00	765.4
3:00	0.0	15:00	769.3
4:00	0.1	16:00	624.5
5:00	0.0	17:00	505.1
6:00	0.0	18:00	293.9
7:00	0.1	19:00	108.6
8:00	18.5	20:00	4.5
9:00	126.3	21:00	0.0
10:00	325.6	22:00	0.0
11:00	459.9	23:00	0.0

F.2 Change in electricity consumption comparing $1.5\,m^3$ CS (7/14) to CS+beams

The following table provides more detail to table 9.21. The change of electricity consumption by each consumer is shown compared to the base case.

Table F.2: Relative change of electricity consumption (ΔE_{el}) of each consumer, comparing the base case to the scenarios 1.5 m^3 CS (7/14), CS+beams and 2 m^3 chwtank

	ext. pumps	coll. pump	indoor fans	CT	chiller
	CS+beams				
Canb	2.7%	0.4%	53.4%	30.7%	-25.5%
Brisb	10.9%	2.9%	79.2%	13.2%	-22.7%
Syd	13.7%	2.1%	76.4%	35.5%	-22.7%
Grif	13.7%	1.9%	51.9%	10.8%	-30.0%
TenCr	-1.1%	1.3%	110.2%	14.8%	-25.0%
Darw	-2.7%	0.9%	72.6%	-12.5%	-31.0%
Melb	4.9%	0.7%	49.2%	23.7%	-25.0%
	1.5 m^3 CS (7/14)				
Brisb	8.7%	4.8%	65.8%	16.9%	-8.5%
Syd	12.7%	3.0%	71.3%	50.6%	-4.4%
Grif	14.9%	2.7%	19.7%	21.4%	-18.0%
TenCr	4.2%	1.5%	52.3%	13.5%	-20.0%
Darw	7.6%	2.2%	52.5%	2.9%	-10.7%
Melb	16.4%	0.5%	14.5%	35.8%	-2.5%
	2 m^3 chilled water tank (chwtank)				
Canb	14.7%	0.6%	20.0%	19.9%	10.6%
Brisb	3.5%	4.0%	62.6%	8.0%	-1.5%
Syd	7.5%	1.9%	63.9%	28.5%	1.7%
Grif	7.9%	1.2%	22.4%	8.5%	-1.2%
TenCr	4.3%	1.5%	60.1%	3.2%	-3.9%
Darw	4.6%	1.3%	59.1%	4.0%	0.4%
Melb	11.9%	0.2%	14.6%	18.6%	8.7%